CAMRAD/JA

A COMPREHENSIVE ANALYTICAL MODEL OF ROTORCRAFT AERODYNAMICS AND DYNAMICS

Johnson Aeronautics Version

Volume I : Theory Manual

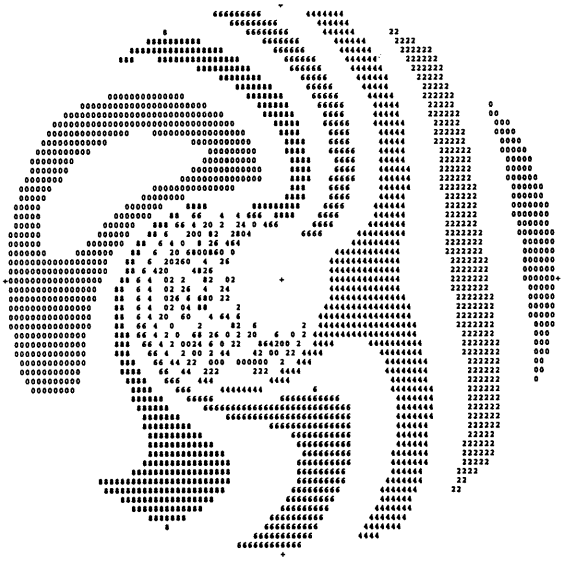

Wayne Johnson

Johnson Aeronautics
Palo Alto, California

Johnson Aeronautics
Palo Alto, California

CAMRAD/JA

A COMPREHENSIVE ANALYTICAL MODEL OF ROTORCRAFT AERODYNAMICS AND DYNAMICS

Johnson Aeronautics Version

Volume I: Theory Manual

Wayne Johnson

1988

Copyright 1988 Wayne Johnson

CAMRAD/JA

A COMPREHENSIVE ANALYTICAL MODEL OF ROTORCRAFT AERODYNAMICS AND DYNAMICS

Johnson Aeronautics Version

Volume I: Theory Manual

Wayne Johnson
Johnson Aeronautics
Palo Alto, California

SUMMARY

The development of a comprehensive analytical model of rotorcraft aerodynamics and dynamics is presented. This analysis is designed to calculate rotor performance, loads, and noise; helicopter vibration and gust response; flight dynamics and handling qualities; and system aeroelastic stability. The analysis is a combination of structural, inertial, and aerodynamic models that is applicable to a wide range of problems and a wide class of vehicles. The analysis is intended for use in the design, testing, and evaluation of rotors and rotorcraft, and to be a basis for further development of rotary wing theories. The analysis is implemented in a digital computer program, called CAMRAD/JA.

CONTENTS

1. Introduction 1

1.1 Objective 1
1.2 Comprehensive Analyses for Helicopters 2
1.3 Early Codes 5
1.4 Background of CAMRAD/JA Development 7
1.5 Description of CAMRAD/JA Models and Capabilities 8

1.5.1 Computational tasks 8
1.5.2 Trim solution 11
1.5.3 Configuration model 15
1.5.4 Rotor model 16
1.5.5 Wake model 17
1.5.6 Aircraft model 18

2. Rotor Model 21

2.1 Structural Analysis 21

2.1.1 Geometry 21
2.1.2 Description of the bending 24
2.1.3 Analysis of strain 27
2.1.4 Section moments 29
2.1.5 Vector formulation 33
2.1.6 Dyadic Notation 35

2.2 Inertia Analysis 36

2.2.1 Rotor geometry 38
2.2.2 Rotor motion 47
2.2.3 Coordinate frames 51
2.2.4 Blade acceleration 52
2.2.5 Aerodynamic forces 61
2.2.6 Force and moment equilibrium 62
2.2.7 Bending equation 65
2.2.8 Elastic torsion equation 70
2.2.9 Rigid pitch equation 74
2.2.10 Root force 78
2.2.11 Root moment 79
2.2.12 Gimbal equation 80
2.2.13 Teeter equation 81
2.2.14 Modal equations 82
2.2.15 Modal expansion 85
2.2.16 Lag damper 88
2.2.17 Gravitational forces 90
2.2.18 Equations of motion 91

2.2.19 Inertial constants 100
2.2.20 Aerodynamic spring and damping 111
2.2.21 Higher harmonic control 113

2.3 Blade Bending and Torsion Modes 115

2.3.1 Coupled bending modes of a rotating blade 116
2.3.2 Articulated blade modes 127
2.3.3 Torsion modes of a nonrotating blade 128
2.3.4 Kinematic pitch/bending coupling 131
2.3.5 Blade pitch definition 134

2.4 Aerodynamic Analysis 135

2.4.1 Section aerodynamic forces 137
2.4.2 Blade velocity 143
2.4.3 Induced velocity 148
2.4.4 Section aerodynamic characteristics 159
2.4.5 Tip flow corrections 170
2.4.6 Yawed flow and Reynolds number corrections 173
2.4.7 Dynamic stall model 179
2.4.8 Unsteady lift and moment 185
2.4.9 Circulation 188

2.5 Environment 188

2.6 Normalization Parameters 190

3. Rotor Wake Analysis 193

3.1 Nonuniform Wake-Induced Velocity 194

3.1.1 Rotor vortex wake 194
3.1.2 Wake and wing model 201
3.1.3 Geometry 214
3.1.4 Induced velocity calculation 233
3.1.5 Hover or vertical flight (axisymmetric geometry). 236
3.1.6 Computation Method 241
3.1.7 Finite length vortex line element 253
3.1.8 Vortex sheet element 263

3.2 Free Wake Geometry 276

3.3 CFD Interface 279

4. Aircraft Model 285

4.1 Aircraft Configuration Definition 286

4.1.1 Aircraft orientation: flight path and trim Euler angles 286
4.1.2 Rotor position and orientation 290
4.1.3 Wind tunnel case 293
4.1.4 Equations of motion 294
4.1.5 Aircraft description and auxiliary forces 295
4.1.6 Pilot's controls 299

4.2 Aircraft Analysis 303

4.2.1 Degrees of freedom 304
4.2.2 Hub motion 309
4.2.3 Pitch/mast-bending coupling 312
4.2.4 Equations of motion 312
4.2.5 Hub forces 315
4.2.6 Aircraft aerodynamic forces 316
4.2.7 Aircraft aerodynamics -- high frequency 328
4.2.8 Auxiliary forces 330
4.2.9 Airframe sensors 331

4.3 Transmission and Engine Analysis 334

4.3.1 Engine model 334
4.3.2 Equations of motion 337
4.3.3 Rotor speed governor 345

4.4 Airframe/Rotor Aerodynamic Interference 347

4.4.1 Interference velocities 347
4.4.2 Geometry 348
4.4.3 Wing-induced velocity 349
4.4.4 Straight dipole line segment 354
4.4.5 Nonlifting body-induced velocity 357

5. Solution for the Rotorcraft Motion 365

5.1 Rotor Motion and Airframe Vibration 371

5.1.1 Fourier series representation 371
5.1.2 Gimbal and teeter motion 373
5.1.3 Rigid pitch motion 379
5.1.4 Harmonic analysis solution 380
5.1.5 Motion evaluation 386
5.1.6 Rotor equations 396
5.1.7 Hub reactions 401
5.1.8 Aircraft equations 405
5.1.9 Transmission and engine equations 408
5.1.10 Static elastic deflection 412
5.1.11 Two-rotor aircraft 414

5.1.12 Circulation convergence 416
5.1.13 Calculation procedure 418

5.2 Rotor Performance, Loads, and Noise 421

5.2.1 Rotor performance 423
5.2.2 Section force 428
5.2.3 Section bending moment 435
5.2.4 Section torsion moment 441
5.2.5 Control load 445
5.2.6 Root forces and moments 446
5.2.7 Hub reactions 449
5.2.8 Airframe sensor vibratory response 451
5.2.9 Rotational noise 452

5.3 Steady State or Slowly Varying Aircraft Motion 461

5.3.1 Trim analysis 464
5.3.2 Transient analysis 471
5.3.3 Flight dynamics analysis 475
5.3.4 Transient gust and control 480
5.3.5 Calculation procedure 483

5.4 Self-Tuning Regulator 484

5.4.1 Rotorcraft model 486
5.4.2 Feedback control 487
5.4.3 T-matrix identification 489

6. Aeroelastic Stability 495

6.1 Rotor Model 495

6.1.1 Rotor degrees of freedom 495
6.1.2 Rotor equations and hub reactions 502
6.1.3 Inertial constants 508
6.1.4 Aerodynamic forces 510
6.1.5 Inflow dynamics 524
6.1.6 Rotor equations of motion 534
6.1.7 Constant coefficient approximation 542

6.2 Aircraft Model 546

6.2.1 Aircraft degrees of freedom 546
6.2.2 Aircraft equations of motion 548
6.2.3 Drive train equations of motion 550

6.3 Coupled Rotor and Aircraft 552

6.3.1 Coupled equations of motion 552
6.3.2 Quasistatic approximation 562
6.3.3 Symmetric aircraft 564

6.4 Matrices of Rotor Equations of Motion 566

6.4.1 Inertial matrices for rotor equations 566
6.4.2 Aerodynamic matrices for rotor equations in axial flow 577
6.4.3 Aerodynamic matrices for rotor equations in nonaxial flow 586
6.4.4 Inertial matrices for rotor with four or more blades 597
6.4.5 Aerodynamic matrices for rotor with four or more blades in axial flow 601
6.4.6 Inertial matrices for two-bladed rotor 602
6.4.7 Aerodynamic Matrices for two-bladed rotor 612

7. Linear System Analysis 623

7.1 State Variable Forum 623

7.2 Constant Coefficient System 625

7.2.1 Eigen-analysis 625
7.2.2 Static response 626
7.2.3 Frequency response 626
7.2.4 Zeros 626
7.2.5 Transient response 628
7.2.6 Rms gust response 629

7.3 Periodic Coefficient System 632

7.4 Aeroservoelasticity Analysis 634

7.4.1 Control system model 635
7.4.2 Stability evaluation 637
7.4.3 Closed-loop response 638

References 641

1. INTRODUCTION

1.1 Objective

In the design, testing, and evaluation of rotors and rotorcraft, it is necessary to predict and explain the rotor performance, loads, and noise; the helicopter vibration and gust response; the flight dynamics and handling qualities; and the system aeroelastic stability. This capability is required at several levels, including conceptual design; detailed design, development, and modification; and research. A comprehensive analysis makes it possible to perform these tasks with a consistent, balanced, yet high level of technology in a single code.

A comprehensive analysis for rotorcraft was published in 1980 (refs. 1-3). The digital computer program implementing the analysis has acquired the name CAMRAD (from the title of ref. 1, Comprehensive Analytical Model of Rotorcraft Aerodynamics and Dynamics). The origin, development, and structure of the analysis is described in references 4 and 5. In reference 6, the development, features, and capabilities of the code are summarized; and the history, status, and lessons of this comprehensive analysis are reviewed. This code has found application in both government and industry. Examples of the correlation of the computational results with experimental data, and other applications of the code, are given in references 4-6. Extensions of the code have been developed for research in several topics of helicopter technology (ref. 6).

Johnson Aeronautics has produced CAMRAD/JA, a new software implementation of the analysis, written utilizing a software tool that facilitates modifications, and incorporating major new capabilities. This report documents the theoretical basis for CAMRAD/JA. The use of CAMRAD/JA is described in volume II.

The analysis developed here is a consistent combination of structural, inertial, and aerodynamic models, applicable to a wide range

of problems and a wide class of vehicles. The present model is applicable to articulated, hingeless, gimballed, and teetering rotors with an arbitrary number of blades. The rotor degrees of freedom included are blade flap/lag bending, rigid pitch and elastic torsion, and optionally gimbal or teeter motion. This analysis is applicable to general two-rotor aircraft, including single main-rotor, coaxial, and tandem helicopter configurations, and side-by-side or tilting proprotor aircraft configurations. The case of a rotor or helicopter in a wind tunnel is also covered. The aircraft degrees of freedom included are the six rigid body motions, elastic airframe motions, and the rotor/engine speed perturbations. The trim operating conditions considered include level flight, steady climb or descent, and steady turns. The analysis of the rotor includes nonlinear inertial and aerodynamic models, applicable to large blade pitch angles and high inflow ratio. The rotor aerodynamic model is based on two-dimensional and unsteady flow effects, including a dynamic stall model. A detailed wake model for the rotor nonuniform inflow calculation is developed, with a lifting surface theory correction for vortex-induced loads. Available prescribed and free-wake-geometry models are used. The aeroelastic stability analysis derives linearized equations consistent with the nonlinear rotor model.

The solution of the equations of motion is separated into two parts, based on the different time scales involved in rotorcraft dynamics. The first part is the solution for the rotor motion and the airframe vibration. This motion is periodic, with fundamental frequency Ω for the rotor and $N\Omega$ for the airframe (Ω is the rotor rotational speed and N is the number of blades). The periodic motion is calculated by a harmonic analysis method. The second part is the solution for the steady state or slowly varying airframe motion (consisting of the aircraft rigid body and rotor speed perturbations, and the static elastic deflection of the airframe and drive train). The assumption that the aircraft motion is quasi-static (compared to the rotor speed)

allows the periodic rotor solution to be used for transient motions of the helicopter as well as for the trim calculations. Most importantly, by taking advantage of the frequency separation of the rotor and aircraft motions, an economical calculation procedure is realized.

The first computation task is the trim analysis, in which the control position and aircraft orientation are determined for the specified operating condition. The periodic blade motion is calculated, and then the rotor performance, loads, and noise can be evaluated. The rotor model in the trim solution can use uniform inflow, nonuniform inflow with a rigid wake geometry, and nonuniform inflow with a free wake geometry. The aeroelastic stability, flight dynamics, and transient analyses begin from the trim solution. The aeroelastic stability analysis sets up a set of linear differential equations describing the motion of the rotor and aircraft; the eigenvalues of these equations define the system stability. The flight dynamics analysis calculates the rotor and airframe stability derivatives, and sets up linear differential equations for the aircraft rigid body motions; the poles, zeros, and eigenvectors of these equations define the aircraft flying qualities. The transient analysis numerically integrates the rigid body equations of motion for a prescribed control or gust input.

In this analysis all quantities will be dimensionless, based on air density ρ, the rotor radius R, and the rotor rotational speed Ω.

1.2 Comprehensive Analyses for Helicopters

The word "comprehensive" takes on several meanings for helicopter analyses. It implies comprehensive technology: a code covering all disciplines, in a consistent and balanced fashion; dealing with the entire aircraft, with a concern for coupling of components and technology integration; incorporating a high technology level, and implementing recent advances.

It implies comprehensive modeling: the code must solve a wide range of problems in a single consistent analysis. The problems include performance and trim; blade motion and airloading; blade loads, control loads, vibration, and noise; aeroelastic stability; and handling qualities and response. The code must cover a wide range of configurations for both the rotor and the aircraft.

It implies comprehensive software: the flexibility to adapt or extend to new problems; and transportability for wide use throughout the government and in industry.

Helicopter problems are inherently complex and multidisciplinary, hence helicopter theory is ultimately driven toward a consideration of comprehensive modeling issues. What is desired in a comprehensive analysis is a practical tool, one that is reliable and accurate, efficient and economical; and good software, meaning good programming practice and documentation, for ease of test and maintenance. To obtain reliability and accuracy, it is necessary to devote resources to the checking, correcting, and proving of the codes, through extensive correlation and verification tasks. Efficiency and economy are also not automatically achieved, and require particular attention as the scope of an analysis expands. The software and documentation should not be assumed to be relatively unimportant because a code is intended for a single user. If the code is useful, it will grow in capability and acceptance, making the improvement of the programming and documentation even more difficult.

A comprehensive analysis involves a combination of elements from technology and disciplines, and a combination of components. Such a combination by itself goes beyond the state of the art, providing the opportunity to implement specialized developments for much wider practical use than in the original proof-of-method form. Moreover, the strong physical coupling of the modeled elements for a helicopter means that the solution capability is increased in a consistent combination of

technology; in original developments, the combination is likely to be unbalanced.

1.3 Early Codes

The intent here is to describe a particular comprehensive analysis for rotorcraft, not to consider all such analyses. Providing a summary of other analyses is useful, however, as a further definition of what the subject is, and to describe the background against which CAMRAD was developed. A number of representative codes are identified in Table 1-1.

Of the first generation codes, C81 is the classic example of a comprehensive analysis. The C81 code underwent at least six rounds of development, most sponsored by the U.S. Army. REXOR was developed for a four-bladed, hingeless rotor. The code G400 was initially developed for bearingless rotor stability. In many cases, for the first generation codes "comprehensive" refers specifically to a wide range or high level of technology. A number of generic limitations are present in these first generation codes. These codes cannot treat all problems or all configurations. Sometimes there are major restrictions, such as incomplete trim, incomplete body or rotor motion, uniform inflow, or lack of eigenanalysis capability. These codes are ten to fifteen years old (some have their roots in the early 1960s). Consequently, much of presently available technology is often not well or uniformly utilized in the first generation analyses. Some are derivative analyses, developed from narrow origins; some have been continuously updated, but without good software control. The first generation codes were typically developed for narrow purposes, with limited time and resources. They were developed and verified only for particular helicopter types or particular technical problems, reflecting the specific interest of the originating organization. Consequently, the codes frequently suffer from too little correlation and verification, too little reexamination of method and approach, and too narrow

Table 1-1. Representative Comprehensive Helicopter Analyses

First Generation (Roots in Early 1960s)		
Handling Qualities Origins		
	C81	Bell (late 1960s)
	REXOR	Lockheed (about 1971)
Loads and Stability Origins		
	C60	Boeing (about 1965)
	Normal Modes	Sikorsky (1968)
	G400	UTRC (1975)
Aerodynamics Origins		
	Piziali and Duwaldt	Cal (1962-1966)
	Miller and Scully	MIT (1962-1964, 1975)
	Landgrebe	UTRC (1969-1972)
Recent (Often Spurred by 2GCHAS)		
	RDYNE	Sikorsky
	CRAVA	Sikorsky
	COPTER	Bell
	DYSCO	Kaman
	CAMRAD	NASA Ames
Second Generation		
	2GCHAS	U.S. Army

application. Certainly each code does not have all of these problems, and most remain quite useful. A consensus exists, however, that these limitations are no longer acceptable. Hence there have been several recent major code developments.

The recent codes (Table 1-1) are characterized by an emphasis on the coupling of components. Often a substructure approach is used, and sometimes an automatic equation synthesis from a limited number of element types is used. The purpose of this emphasis is to obtain greater versatility than has been found in the first generation codes. The recent codes also show an increased concern about software, particularly the use of modular or structured software. Contemporary with the first generation comprehensive analyses there were also many special purpose codes, for individual subjects such as performance, flutter, and handling qualities. The use of special purpose codes is still apparent in recent developments.

The Second Generation Comprehensive Helicopter Analysis System (2GCHAS) is being developed by the U.S. Army and the helicopter industry. This analysis will emphasize the use of executive software for a flexible and unified structure, and the use of analysis options rather than a single technical basis (although the technical basis for the structural analysis will likely be finite element models).

1.4 Background of CAMRAD Development

The development of CAMRAD had it origins in a number of theoretical investigations, including an empirical dynamic stall model (1968-1969; refs. 7 and 8); vortex/blade interaction (1969-1970; refs. 9 and 10); nonuniform inflow (1968-1970; refs. 7 and 9); rotor/wing dynamic stability (1972-1975; refs. 11-13); and dynamic stability in free flight (1975-1976; refs. 14-16).

These aerodynamics investigations included the development of a rotor wake model, and the dynamic stall work (which required developing

a method of solving for the periodic motion of a rotor blade). The stability investigations produced linearized equations of motion for the rotor. Impetus for the stability investigations was provided by the requirement to analyze tilting proprotor aircraft (refs. 11-15). As a consequence, early consideration was given to high inflow and large angles in the aerodynamics model; to large pitch and twist in the dynamics model; to rotor and body dynamics coupled through shaft motion and hub forces; and to a drive train model.

The development of CAMRAD (1978-1980; refs. 1-3) was built upon these earlier investigations. The rotor and airframe model that was derived for the stability analysis was used, but in the nonlinear form. A new wake analysis was developed, incorporating additional modeling capability. Solution techniques were developed for the trim, motion, wake, and inflow problems. The free-wake geometry model of Scully (ref. 17) was incorporated; this was the only part of the code adapted from an outside source. The new wake model was a major justification for the development of CAMRAD, a fact reflected in the initial applications of the code. In addition, it was desired to obtain a solid basis for further development of rotary wing technology (reflected in more recent applications).

1.5 Description of CAMRAD/JA Models and Capabilities

1.5.1 Computational tasks.

Figure 1-1 shows an outline of the tasks and problems solved by CAMRAD/JA. The structure at this level emphasizes solving the dynamic equations of motion. The first task is the trim analysis; other tasks start from the trim solution. The rotorcraft in trim is in a steady state, unaccelerated flight condition; hence the rotor and airframe motion are periodic. The inverse problem, determining the control required for a specified flight condition, is being solved. The solution involves calculating the periodic rotor motion and the steady

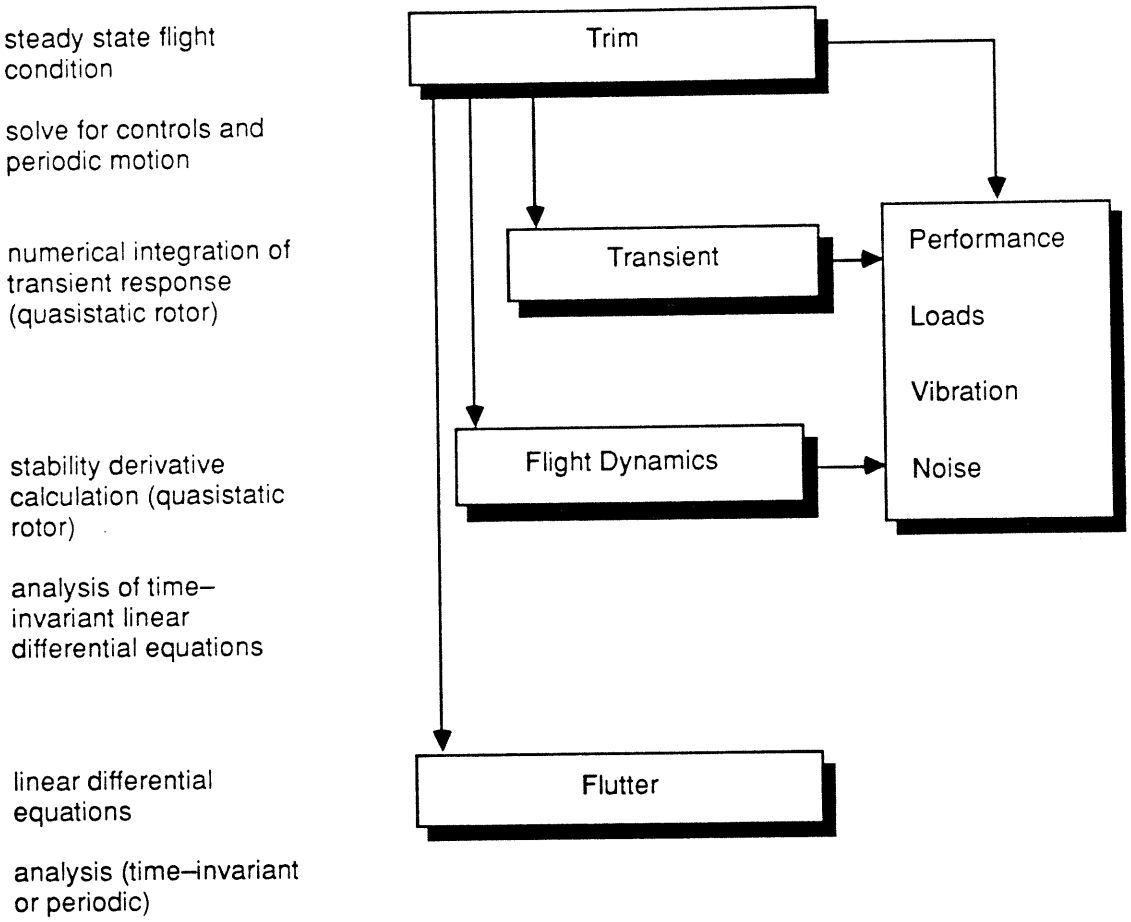

Figure 1-1. CAMRAD/JA tasks and solutions.

trim variables. After the calculation has converged, the performance, loads, and noise may be calculated. In CAMRAD/JA the blades of a rotor are assumed to be identical, with the same periodic motion. The assumption of periodicity (with a fundamental frequency equal to the rotor rotational speed) excludes a calculation of the vibratory dynamic and aerodynamic interaction between two rotors of unequal rotation rates, such as a main rotor and tail rotor; the static or mean interaction is always taken into account.

The flight dynamics analysis is based on a frequency separation of the motion of the rotor and body, allowing the use of a quasi-static rotor solution. Hence the rotor and airframe stability derivatives are calculated, using prescribed perturbations of the body motion and controls, in the same analysis that is used for the trim solution (where the motion is truly steady state). Time-invariant linear differential equations for the aircraft rigid-body motions are constructed. The poles, zeros, and eigenvectors of these equations define the aircraft flying qualities.

The transient analysis involves an integration in time to obtain the general vehicle response. For CAMRAD/JA, the only transients considered are those produced by rigid body dynamics, pilot inputs, and gusts, all of which are slow relative to the rotor rotational frequency. Hence a quasi-static rotor solution is sufficient, and again the rotor analysis is identical to that used for the trim solution. The rigid-body equations of motion are numerically integrated for prescribed control or gust inputs to calculate a nonequilibrium flight path.

The flutter analysis involves the construction of a set of linear differential equations describing the motion of the rotor and the aircraft (all variables). The eigenvalues of these equations define the system stability. The equations may be time-invariant (for axial flow), or may have periodic coefficients (solved using Floquet theory). A constant coefficient approximation for the periodic coefficient

equations, and various quasi-static reductions can be used (as implemented in CAMRAD/JA, neither is applicable for a two-bladed rotor).

1.5.2 Trim solution.

The structure of the solution of the trim task in CAMRAD/JA is outlined in Figures 1-2 and 1-3. The periodic motion in a steady-state, unaccelerated flight condition is required. The final converged solution, not intermediate transients, is desired. Hence following a strictly physical approach in the solution is not necessary. For efficiency and improved convergence, computationally intensive calculations are moved outside inner loops (if weak coupling allows this approach), and the major iteration loops are split into several levels.

The control required to achieve a specified flight condition is to be calculated (the inverse problem). Hence algebraic equations (for free flight obtained from equilibrium of forces and moments on the helicopter; for a wind tunnel case obtained by setting the thrust, tip-path-plane tilt, etc., equal to target values) are solved for the trim variables (rotor or pilot controls, and aircraft Euler angles). Differential equations are solved for the periodic rotor motion and airframe vibration.

The trim iteration is an outer loop (Figure 1-3). In CAMRAD/JA, the Newton-Raphson method (with a relaxation factor) is used to solve the algebraic equations. The periodic motion for fixed controls is calculated in an inner loop (Figure 1-3). In CAMRAD/JA a harmonic analysis method is used that is equivalent to an integration in time with a filter over the last revolution that forces the solution to be periodic. The analysis advances the rotor around the azimuth, calculating the forcing function in the time-domain and then updating the harmonics of the motion at each time step. The use of the frequency domain (a Fourier series representation) enforces periodicity, and allows the use of a large time step since numerical stability is separated from the physical stability of the system (which often has

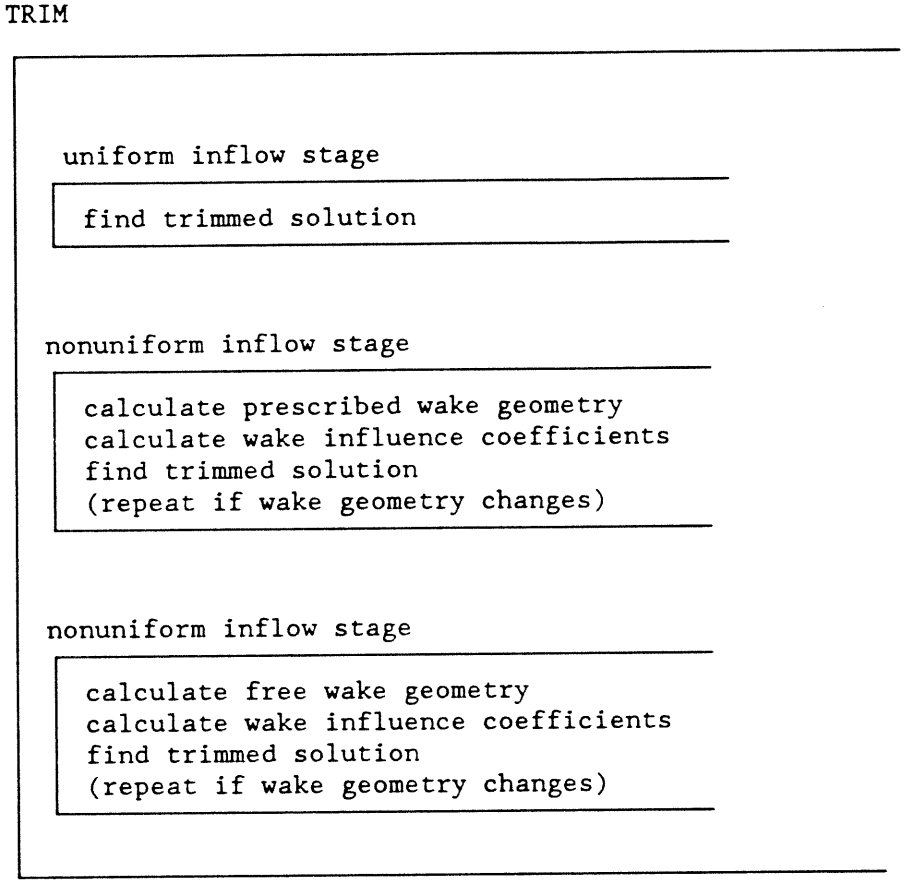

Figure 1-2. Solution of trim task: inflow analysis levels

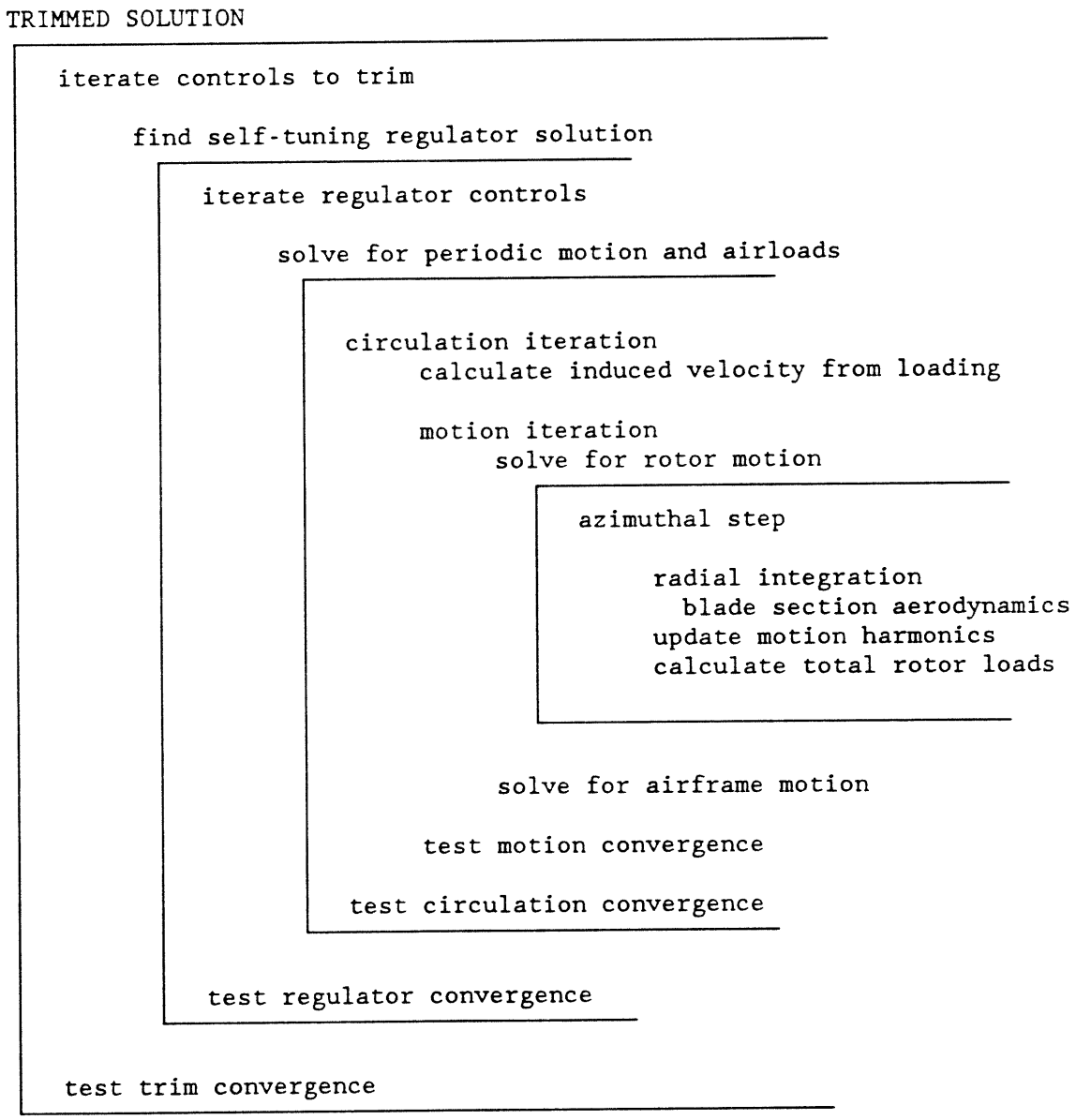

Figure 1-3. Solution of trim task: trim, regulator, circulation, and motion iterations.

low-damped or high-frequency modes). There are separate circulation and motion iterations (Figure 1-3). In the circulation loop, the uniform or nonuniform induced velocity is calculated from the circulation or aerodynamic loading; the motion is calculated for fixed induced velocity; the circulation is reevaluated; and the procedure is repeated until the circulation converges (a relaxation factor on the circulation is used to improve convergence). In the motion loop, there is an iteration between the calculation of the rotor motion and the airframe vibration, to avoid interharmonic coupling and to ensure proper filter of harmonics of the hub forces. A relaxation factor is also used in the motion loop to improve convergence. While the trim loop can be omitted (for a fixed controls solution), the circulation and motion iterations are always required.

The analysis includes a self-tuning regulator, that can automatically adjust controls selected from the rotor and aircraft primary controls, rotor higher harmonic controls, and higher harmonic auxiliary forces. The regulator forms a cost function (to be minimized) using selected rotor response quantities, including: flapping and power; airframe sensor vibratory response; hub and root loads; blade section loads; and rotor noise. For the trim analysis, an iteration to solve for the converged regulator state is introduced between the trim and circulation iterations.

The wake geometry and influence coefficient calculation are computationally expensive; they are therefore moved outside the trim iteration (Figure 1-2). The influence coefficients relate the induced velocity to the rotor blade bound circulation. This approach is possible because of the weak coupling of the influence coefficient calculation and the trim iteration, particularly when the rotor is trimmed to a specified thrust and tip-path-plane orientation. In CAMRAD/JA there are three levels of analysis: uniform inflow, nonuniform inflow with prescribed wake geometry, and nonuniform inflow with free wake geometry. Here "uniform inflow" refers to an empirical model based

on momentum theory, and actually includes a linear variation of the inflow over the rotor disk. For accuracy, it is necessary to use the bound circulation distribution from the nonuniform inflow calculation in the free wake geometry analysis. For efficiency, the nonuniform inflow calculation should originate from the trimmed uniform inflow solution. The wake influence coefficients and geometry (prescribed or free) depend on the rotor loading, so potentially an iteration between the influence coefficient calculation and trim solution is necessary (Figure 1-2). In practice, if the rotor is trimmed to a specified thrust and tip-path-plane orientation at each level, the remaining influence of the loading changes on the wake geometry is small, and hence iteration is seldom necessary. It is most efficient to execute each of the three levels once and only once to obtain a nonuniform, free wake solution.

It is possible to couple the CAMRAD/JA analysis with an external solution for the rotor airloads, typically from a computationally intensive CFD analysis. CAMRAD/JA can calculate a partial angle-of-attack (excluding wake elements that are inside the CFD domain) for use by the external analysis. By this means the effects of the rotor wake and blade motion can be included in the CFD analysis. Then CAMRAD/JA can read and use the externally calculated blade lift, drag, and moment coefficients. Since this new rotor loading will change the wake and motion solution, the process must generally be repeated. If the physical coupling between CAMRAD/JA and external analyses is weak, the iteration converges with a reasonably small number of executions of the CFD analysis.

1.5.3 Configuration model.

CAMRAD/JA analyzes a general two-rotor aircraft. The configurations considered are the single main-rotor and tail-rotor helicopter; tandem main-rotor helicopter; coaxial main-rotor helicopter; side-by-side main-rotor or tilting proprotor aircraft; and a rotor or aircraft in a wind tunnel. Auxiliary forces acting on the airframe can

be included. Articulated, hingeless, gimballed, and teetering rotors with an arbitrary number of blades can be analyzed.

1.5.4 Rotor model.

The rotor structural model is based on engineering beam theory for rotating wings with large pitch and twist. A single load path is assumed (multiple load-path, bearingless rotors cannot be analyzed). The rotor blade is assumed to have a straight, undeformed, elastic axis, with specific root geometry possibilities. The blade motion considered includes in-plane and out-of-plane bending, torsion, control system flexibility, flap/lag/gimbal/teeter hinges, and rotor rotational speed. The rotor shaft motion and hub forces are considered. The blade pitch input includes higher harmonic control, from either the rotating or nonrotating frame.

The blade motion is described by rotating, free-vibration modes, equivalent to a Galerkin analysis. The blade modes shapes can be calculated internally or obtained from an external analysis. Nonlinear terms are retained in the equations of motion based on established knowledge of certain important nonlinear effects, and the requirement of consistency in the derivation. A vector formulation of the blade structural dynamics is used. The vector combination of in-plane and out-of-plane moments and deflections eliminates the dependence on the coordinate system, with a simplification of the equations as a consequence.

The rotor aerodynamic model is based on lifting-line theory, using steady two-dimensional airfoil characteristics and a vortex wake. The analysis includes empirical dynamic stall models; yawed-flow and swept-blade corrections; and unsteady aerodynamic forces from thin airfoil theory. The aerodynamic model is applicable to axial and nonaxial flight, with high inflow and large angles. The induced velocity is obtained from momentum theory or a vortex wake model. The momentum theory model includes a mean term and terms that vary linearly

over the rotor disk (produced by forward flight or hub moments); rotor/rotor and rotor/airframe interference; and ground effect.

For the flutter analysis, multiblade coordinates and an inflow dynamics model to represent low-frequency, unsteady aerodynamics of the rotor can be used. In the inflow dynamics models, the uniform and linear induced-velocity components are related, by first-order differential equations, to the net aerodynamic thrust and hub moments on the rotor.

The rotor model is characterized by a section analysis, which follows from the assumption of high-aspect ratio: engineering beam theory for the structural model and lifting line theory for the aerodynamic model. The equations of motion are obtained from equilibrium of the inertial, aerodynamic, and elastic forces on the portion of blade outboard of a particular blade section. The interface between the aerodynamics and dynamics models is defined by the section aerodynamic forces and the section velocities.

1.5.5 Wake model.

The rotor wake model in CAMRAD/JA is usually based on a vortex lattice (straight-line segments) approximation for the wake. A small viscous core radius is used for the tip vortices. Vortex sheet elements can be used to represent the inboard wake, but usually it is sufficient (and more efficient) to approximate the sheets by line segments, with a large core radius to eliminate large velocities. Nonplanar, quadrilateral sheet elements are available if needed. The wake influence coefficients are calculated for incompressible flow. Rotor/rotor interference can be calculated (but only the mean velocities at the hub for the single main rotor and tail rotor case). The mean interference velocities at the airframe can be calculated.

The wake roll-up process is modeled. Eventually the tip vortex has the strength of the peak bound circulation at the azimuth where the wake element was trailed. The possibility of two bound circulation peaks,

inboard and outboard peaks of opposite sign, is included in the rolled-up wake model. A number of prescribed parameters allow the tip vortex to have only a fraction of this peak strength when it encounters the following blade. The radial location of the tip vortex at the generating blade is also prescribed.

Blade-vortex interaction loading is calculated using either second-order, lifting-line theory (three-quarter-chord collocation point), or using a lifting-surface theory correction. Simply using a artificially large vortex core size is a third possibility. A large core radius can be used for the velocity induced on the inboard part of the blade, in order to suppress the blade-vortex interactions there (as observed in experiment).

The wake geometry models in CAMRAD/JA include simple undistorted models; hover prescribed wake models based on experimental measurements; and a calculated free wake. The free wake analysis used (from ref. 17) calculates the distorted tip vortex geometry for a single rotor in forward flight. This free-wake analysis is very efficient, and has modeling features that are consistent with the CAMRAD/JA wake model. The influence of aircraft turn rate on the undistorted wake convection is included.

1.5.6 Aircraft model.

The aircraft model in CAMRAD/JA allows for two rotors on a body having both rigid and elastic motion. A wind tunnel configuration (no rigid body motion) is also considered. The elastic airframe modes must be obtained from an external analysis (such as NASTRAN). CAMRAD/JA includes a drive train model, with the engine, governor, shaft flexibility, and rotor rotational speed degrees-of-freedom represented. The airframe auxiliary forces include trim, perturbation, and higher harmonic terms. Airframe sensors available include accelerometers, airframe angular rate and motion measurements, and air velocity

measurements. For the frequency-domain aeroservoelasticity analysis, a control system consisting of several scalar loops can be defined.

The airframe aerodynamic loads are a combination of nonlinear and linearized forces (only the nonlinear forces are considered for trim). The nonlinear terms are obtained from tables and simple equations. The interference velocities produced by the airframe at the rotor position can be calculated for a collection of wings (horseshoe vortices and doublet lines) and non-lifting bodies (ellipsoids and airfoil-shaped bodies of revolution). The interference velocities can also be obtained from an external analysis.

2. ROTOR MODEL

2.1 Structural Analysis

The structural model of the rotor is based on engineering beam theory (i.e., the Bernouli-Euler theory of bending) for the coupled flap-lag bending and torsion of a blade with large pitch and twist. The basic assumption is that the structural elements of the blade have a high aspect ratio. This assumption is normally well satisfied for rotor blades, although engineering beam theory may be suspect at the root for hingeless rotors. It is also assumed that the blade has a single load path at the root, with a pitch bearing; the analysis is not applicable to bearingless blades. The objective is to relate the bending moments at the section, and the torsion moment, to the blade deflection and elastic torsion at that section.

The analysis follows the work of reference 18. The structural model includes only the lowest order terms; nonlinear effects are accounted for in the inertial and aerodynamic forces. Hence it is only necessary to assume that the elastic motion is small; a more precise definition of the order of various quantities is not necessary.

2.1.1 Geometry.

The basic assumptions are that an elastic axis exists, and the undeformed elastic axis is a straight line; and that the blade has a high aspect ratio (of the structural elements) so engineering beam theory applies. Figure 2-1 shows the geometry of the undeformed blade. The span variable r is measured from the center of rotation along the straight elastic axis. The section coordinates x and z are the principal axes of the section, with origin at the elastic axis. Then by definition, $\int(xz)dA = 0$. Really this integral is over the tension carrying elements, i.e., a modulus weighted integral: $\int xzEdA = 0$. This remark

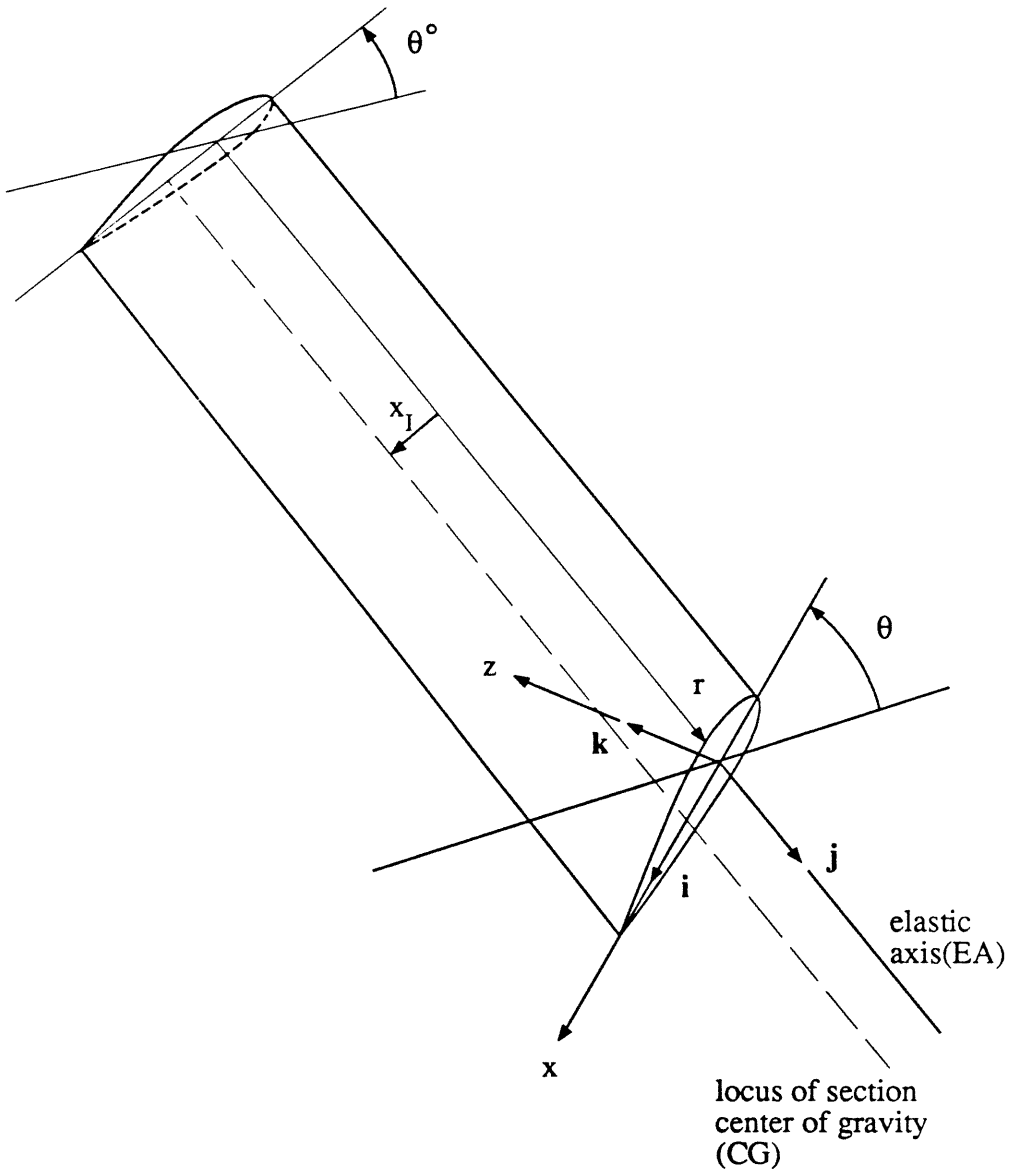

Figure 2-1. Geometry of the undeformed blade.

holds for all the section integrals in the structural analysis. The tension center (modulus weighted centroid) is on the x axis, at a distance x_C aft of the elastic axis: $\int x dA = x_C A$ and $\int z dA = 0$. Again, these are modulus weighted integrals. If E is uniform over the section, then x_C is the area centroid; and if the section mass distribution is the same as the E distribution, then the tension center coincides with the section center of gravity.

The angle of the major principal axis (the x axis) with respect to the hub plane is θ. The existence of the elastic axis means that twist about the elastic axis occurs without bending. In general, the elastic torsion deflection will be included in θ. The blade pitch bearing is at the radial station r_{FA}. The blade pitch is described by root pitch θ^o (rigid pitch about the feathering axis, including that due to the elastic distortion of the control system), built-in twist θ_{tw}, and elastic torsion about the elastic axis θ_e. So $\theta = \theta^o + \theta_{tw} + \theta_e$, where $\theta^o(\psi)$ is the root pitch, $\theta(r_{FA}) = \theta^o$; $\theta_{tw}(r)$ is the built-in twist, $\theta_{tw}(r_{FA}) = 0$; and $\theta_e(r,\psi)$ is the elastic torsion, $\theta_e(r_{FA},\psi) = 0$. There is shear stress in the blade due to θ_e only. It is assumed that θ_e is small, but θ^o and θ_{tw} are allowed to be large angles.

The unit vectors in the rotating hub plane axis system are $\vec{i}_B$, $\vec{j}_B$, and $\vec{k}_B$ (Fig. 2-1). The unit vectors for the principal axes of the section (x, r, z) are $\vec{i}$, $\vec{j}$, and $\vec{k}$; these are for no bending, but include the elastic torsion in the pitch angle θ. So the principal unit vectors are rotated by θ from the hub plane:

$$\vec{i} = \vec{i}_B \cos\theta - \vec{k}_B \sin\theta$$

$$\vec{j} = \vec{j}_B$$

$$\vec{k} = \vec{i}_B \sin\theta + \vec{k}_B \cos\theta$$

2.1.2 Description of the bending.

Now the engineering beam theory assumption is introduced: plane sections perpendicular to the elastic axis remain so after the bending of the blade. Figure 2-2 shows the geometry of the deformed section. The deformation of the blade is described by (a) deflection of the elastic axis, x_o, r_o, and z_o; (b) rotation of the section due to bending, by ϕ_x and ϕ_z; and (c) twist about the elastic axis by θ_e, which is implicit in $\mathbf{i}$ and $\mathbf{k}$. The quantities x_o, r_o, z_o, ψ_x, ϕ_z, and θ_e are assumed to be small.

The unit vectors of the unbent cross section are $\vec{i}$, $\vec{j}$, $\vec{k}$. The unit vectors of the deformed cross section are $\vec{i}_{xs}$, $\vec{j}_{xs}$, and $\vec{k}_{xs}$, where $\vec{i}_{xs}$ and $\vec{k}_{xs}$ are the principal axes of the section, and $\vec{j}_{xs}$ is tangent to the deformed elastic axis. It follows that

$$\vec{i}_{xs} = \vec{i} + \phi_z \vec{j}$$
$$\vec{j}_{xs} = \vec{j} - \phi_z \vec{i} + \phi_x \vec{k}$$
$$\vec{k}_{xs} = \vec{k} - \phi_x \vec{j}$$

Now by definition, $\vec{j}_{xs} = d\vec{r}/ds$, where $\vec{r} = x_o\vec{i} + (r + r_o)\vec{j} + z_o\vec{k}$ and s is the arc length along the deformed elastic axis. Hence to first order

$$\vec{j}_{xs} = \vec{j} + (x_o\vec{i} + z_o\vec{k})'$$
$$= \vec{j} + (x_o' + z_o\theta')\vec{i} + (z_o' - x_o\theta')\vec{k}$$

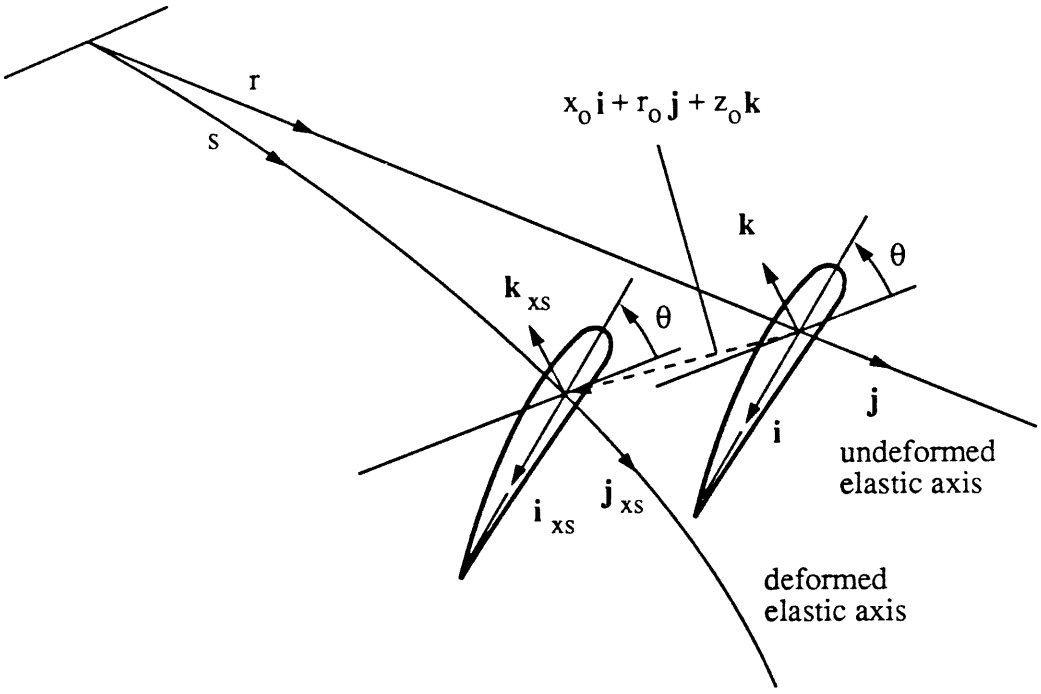

Figure 2-2. Geometry of the deformed blade.

It follows the rotation of the section is

$$-\phi_z = x_o' + z_o\theta'$$
$$\phi_x = z_o' - x_o\theta'$$

or

$$\phi_x\vec{i} + \phi_z\vec{k} = (z_o\vec{i} - x_o\vec{k})'$$

The undeflected position of the blade element is $\vec{r} = x\vec{i} + r\vec{j} + z\vec{k}$, and the deflected position is

$$\vec{r} = (r + r_o)\vec{j} + x_o\vec{i} + z_o\vec{k} + x\vec{i}_{xs} + z\vec{k}_{xs}$$
$$= r\vec{j} + x_o\vec{i} + z_o\vec{k} + (r_o + x\phi_z - z\phi_x)\vec{j} + x\vec{i} + z\vec{k}$$

The first term in the deflected position is the radial station; the next three terms are the deflection of the elastic axis; the next term is the rotation of the section; and the final two terms are the location of the point on the cross section. For now the elastic extension r_o will be neglected. The strain analysis is simplified since then to first order, $s = r$; r_o gives a uniform strain over the section, which may be reintroduced later.

2.1.3 Analysis of strain.

The fundamental metric tensor g_{mn} of the undistorted blade is defined by:

$$(ds)^2 = d\vec{r} \cdot d\vec{r}$$
$$= \left(\frac{\partial \vec{r}}{\partial x_m} dx_m \right) \cdot \left(\frac{\partial \vec{r}}{\partial x_n} dx_n \right)$$
$$= g_{mn} dx_m dx_n$$

Where ds is the differential length in the material, and x_m are general curvilinear coordinates. Similarly, the metric tensor G_{mn} of the deformed blade is

$$(ds')^2 = d\vec{r} \cdot d\vec{r}$$
$$= \left(\frac{\partial \vec{r}}{\partial x_m} dx_m \right) \cdot \left(\frac{\partial \vec{r}}{\partial x_n} dx_n \right)$$
$$= G_{mn} dx_m dx_n$$

Then the strain tensor γ_{mn} is defined by the differential length increment

$$2\gamma_{mn} dx_m dx_n = (ds')^2 - (ds)^2$$

or

$$\gamma_{mn} = \frac{1}{2} (G_{mn} - g_{mn})$$

For engineering beam theory, only the axial components of the strain and stress are required. For a full exposition of the analysis of strain, the reader is directed to reference 19.

The metric of the undeformed blade (no bending, and no torsion so $\theta' = \theta_{tw}'$) is obtained from the undistorted position vector $\vec{r} = x\vec{i} + r\vec{j} + z\vec{k}$, giving

$$g_{rr} = \frac{\partial \vec{r}}{\partial r} \cdot \frac{\partial \vec{r}}{\partial r} = 1 + \theta_{tw}'^2 (x^2 + z^2)$$

The metric of the deformed blade, including bending and torsion, is similarly obtained from the position vector $\vec{r} = (x + x_o)\vec{i} + (r + x\phi_z - z\phi_x)\vec{j} + (z + z_o)\vec{k}$:

$$G_{rr} = \frac{\partial \vec{r}}{\partial r} \cdot \frac{\partial \vec{r}}{\partial r}$$

$$= (1 + x\phi_z' - z\phi_x')^2 + (x_o' + \theta'(z + z_o))^2 + (z_o' - \theta'(x + x_o))^2$$

Then the axial component of the strain tensor is

$$\gamma_{rr} = \frac{1}{2}(G_{rr} - g_{rr})$$

$$= \frac{1}{2}\left[(1 + x\phi_z' - z\phi_x')^2 - 1 + (x_o' + \theta'(z + z_o))^2 - \theta_{tw}'^2 z^2 + (z_o' - \theta'(x + x_o))^2 - \theta_{tw}'^2 x^2\right]$$

The linear strain (for small x_o, z_o, θ_e, ϕ_x, and ϕ_z) is

$$\gamma_{rr} \cong \epsilon_{rr} = x\phi_z' - z\phi_x' + \theta_{tw}'^2 (xx_0 + zz_0) + \theta_{tw}' (zx_0' - xz_0' + \theta_e' (x^2 + z^2))$$

The strain due to the blade tension, ϵ_T, is a constant such that the tension is given by the integral over the blade section:

$$T = \int E \epsilon_{rr} dA = \epsilon_T \int E dA$$

Substituting for ϵ_{rr} and using the results $\int z da = 0$, $\int x da = x_c A$, and $\int (x^2 + z^2) dA = I_p = k_p^2 A$ (where k_p is the modulus weighted radius of gyration about the elastic axis), gives

$$\epsilon_T = \frac{T}{EA} = \phi_z' x_c + \theta_{tw}'^2 x_0 x_c - \theta_{tw}' z_0' x_c + \theta_{tw}' \theta_e' k_p^2 + r_0'$$

In this expression, the strain due to the blade extension r_o has been included. It follows that the strain may be written as

$$\epsilon_{rr} = \epsilon_T + (x - x_c)(\phi_z' - \theta_{tw}' \phi_x) - z(\phi_x' + \theta_{tw}' \phi_z) + \theta_{tw}' \theta_e' (x^2 + z^2 - k_p^2)$$

2.1.4 Section moments.

To find the moments on the section, the second engineering beam theory assumption is introduced: that all stresses except σ_{rr} are

negligible. The axial stress is given by $\sigma_{rr} = E\epsilon_{rr}$. The direction of σ_{rr} is assumed to be given by the vector

$$\hat{e} = \frac{\partial \vec{r}}{\partial r} \Big/ \left| \frac{\partial \vec{r}}{\partial r} \right|$$

(which does not give the torsion moment caused by tension quite correctly, but the error is not usually important for rotor blades).

The moment on the deformed cross section (Fig. 2-3) is $\vec{M} = M_x \vec{i}_{xs} + M_r \vec{j}_{xs} + M_z \vec{k}_{xs}$. The moment about the elastic axis due to the elemented force $\sigma_{rr} dA$ on the cross section is

$$d\vec{M} = (x\vec{i}_{xs} + z\vec{k}_{xs}) \times (\sigma_{rr}\hat{e})\, dA$$

$$= \left[-z\vec{i}_{xs} + x\vec{k}_{xs} + \theta'(x^2+z^2)\vec{j}_{xs}\right] \sigma_{rr}\, dA$$

Integrating over the blade section, there follows the result for the total moments due to bending and elastic torsion:

$$(M_x)_{EA} = -\int z\sigma_{rr}\, dA$$

$$(M_z)_{EA} = \int x\sigma_{rr}\, dA$$

$$M_r = GJ\theta_e' + \int (x^2+z^2)\theta'\sigma_{rr}\, dA$$

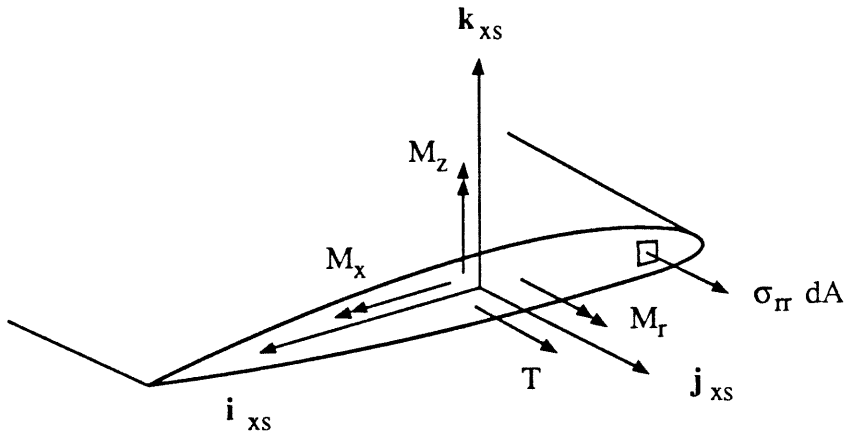

Figure 2-3. Bending and torsion moments on the blade section.

To M_r has been added the torsion moment $GJ\theta_e'$, due to shear stresses produced by elastic torsion. These moments are about the elastic axis. For bending it is more convenient to work with moments about the tension center at x_C:

$$M_x = -\int z\,\sigma_{rr}\,dA$$

$$M_z = \int (x - x_c)\,\sigma_{rr}\,dA$$

Substituting for σ_{rr} and integrating, the moments are

$$M_x = EI_{zz}(\phi_x' + \theta'\phi_z) - \theta_{tw}'\theta_e' EI_{zp}$$

$$M_z = EI_{xx}(\phi_z' - \theta'\phi_x) + \theta_{tw}'\theta_e' EI_{xp}$$

$$M_r = (GJ + k_p^2 T + \theta_{tw}'^2 EI_{pp})\theta_e' + \theta_{tw}' k_p^2 T + \theta_{tw}'\left[EI_{xp}(\phi_z' - \theta'\phi_x) - EI_{zp}(\phi_x' + \theta'\phi_z)\right]$$

where

$$I_{zz} = \int z^2\,dA$$

$$I_{xx} = \int (x - x_c)^2\,dA$$

$$I_p = \int (x^2 + z^2)\,dA = k_p^2 A$$

$$I_{xp} = \int (x - x_c)(x^2 + z^2)\, dA$$

$$I_{zp} = \int z\,(x^2 + z^2)\, dA$$

$$I_{pp} = \int (x^2 + z^2 - k_p^2)^2\, dA$$

The integrals are all over the tension carrying elements (i.e., modulus weighted). The tension T acts at the tension center at x_C; hence the bending moments about the elastic axis may be obtained from those about the tension center by $(M_z)_{EA} = M_z + x_C T$ and $(M_x)_{EA} = M_x$.

2.1.5 Vector formulation.

Define the section bending moment vector $\vec{M}_E^{(2)}$, and the flap/lag deflection $\vec{w}$ as follows:

$$\vec{M}_E^{(2)} = M_x \vec{i} + M_z \vec{k}$$

$$\vec{w} = z_o \vec{i} - x_o \vec{k}$$

($\vec{M}_E^{(2)}$ is not quite the moment on the section, because M_x and M_z are really the $\vec{i}_{xs}$ and $\vec{k}_{xs}$ components of the moment.) The derivatives of $\vec{w}$ are

$$(z_o \vec{i} - x_o \vec{k})' = (z_o' - x_o \theta')\vec{i} - (x_o' + z_o \theta')\vec{k}$$

$$= \phi_x \vec{i} + \phi_z \vec{k}$$

$$(z_o \vec{i} - x_o \vec{k})'' = (\phi_x' + \theta' \phi_z)\vec{i} + (\phi_z' - \theta' \phi_x)\vec{k}$$

Then the result for the bending and torsion moments can be written as follows:

$$\vec{M}_E^{(2)} = (EI_{zz}\vec{i}\vec{i} + EI_{xx}\vec{k}\vec{k}) \cdot (z_0\vec{i} - x_0\vec{k})'' + \theta_{tw}'\theta_e' (EI_{xp}\vec{k} - EI_{zp}\vec{i})$$

$$M_r = (GJ + k_p^2 T + \theta_{tw}'^2 EI_{pp})\theta_e' + \theta_{tw}' k_p^2 T + \theta_{tw}' (EI_{xp}\vec{k} - EI_{zp}\vec{i}) \cdot (z_0\vec{i} - x_0\vec{k})''$$

This is the result sought, the relation between the structural moments and deflections of the rotor blade.

Writing the bending stiffness dyadic as $EI = EI_{zz}\vec{i}\vec{i} + EI_{xx}\vec{k}\vec{k}$, and for the purposes of this paragraph neglecting the EI_{XP} and EI_{ZP} coupling terms, gives

$$\vec{M}_E^{(2)} = EI\,\vec{w}''$$

$$M_r = GJ_{eff}\,\theta_e' + k_p^2 T \theta_{tw}'$$

In this form the result appears as a simple extension of the engineering beam theory result for uncoupled bending and torsion (the $\theta_{tw}' = 0$ case). The vector form allows a simultaneous treatment of the coupled in-plane and out-of-plane bending of the blade, with considerable simplification of the equations as a consequence.

This relation between the moments and deflections is a linearized result. Thus, the vectors $\vec{i}$ and $\vec{k}$ appearing in EI and in $\vec{w}$ are based on the trim pitch angle $\theta = \theta^{o} + \theta_{tw}$. The net torsion modulus is

$$GJ_{eff} = GJ + k_p^2 T + \theta_{tw}'^2 EI_{pp}$$

where $T = \Omega^2 \int_r^1 \rho m d\rho$ is the centrifugal tension in the blade. For the elastic torsion stiffness characteristic of rotor blades, the GJ term usually dominates. The $k_p^2 T$ term is only important near the root for blades which are very soft torsionally. The $\theta_{tw}'^2 EI_{pp}$ term is only important for very soft, highly twisted blades.

2.1.6 Dyadic notation.

The previous section introduces dyadic notation, which will be used in the following equations as well. A dyadic D is a sum of terms of the form

$$(c\,\vec{a}\,\vec{b})$$

where $\vec{a}$ and $\vec{b}$ are vectors and c is a scalar. Then the operation of a dyadic on a vector $\vec{x}$ is defined by

$$D \cdot \vec{x} = (c\,\vec{a}\,\vec{b}) \cdot \vec{x} = c\,\vec{a}\,(\vec{b} \cdot \vec{x})$$

using the conventional vector dot product.

2.2 Inertial Analysis

An integrated Newtonian approach is used to derive the partial differential equations describing the motion of the rotor blade. The same or equivalent equations could be obtained by Lagrangian or differential Newtonian techniques. A modal representation is used to transform the partial differential equations to ordinary differential equations (in time) for the degrees of freedom. The approach used is equivalent to a Galerkin analysis, based on the orthogonal modes of free vibration for the rotating blade. A formal modal derivation is most convenient, and gives the same results as the Galerkin approach. A true orthogonal mode analysis is not possible, however, since it cannot handle the boundary conditions correctly (particularly those associated with the lag damper moment and the pitch control moment at the blade root).

The selection of modes affects the efficiency of the solution procedure. The modal representation separates the solution for the spatial variation and the time variation of the rotor motion. Certain forces that couple aspects of the motion can be put in either half of the solution. The modes should be chosen such that as few as possible are needed to accurately represent the forced response of the structure, which suggests including as many forces as possible in the modal solution. However, the increase in complexity of the modal computation is not compensated by any significant simplification of the equations of motion, so it is desirable to limit what is included in the modal solution as far as possible. In the present analysis, separate modes are used for the bending and torsion motion of the blade. The differential equations for the bending and torsion modes are of a different order. Also, for most blades the coupling between bending and torsion is primarily produced by aerodynamic and nonlinear dynamic forces. Coupled flap-lag bending modes are used (including the rigid flap and lag modes for an articulated blade). The coupling of the

in-plane and out-of-plane blade motion by the structural and inertial forces is significant, especially at large pitch angles or with large twist. Separate rigid body modes are used for the gimbal pitch and roll motion, or the teeter motion of a two-bladed rotor. Representing the motion of the blade on a gimballed or teetering rotor by a rigid flap mode plus K elastic modes with a cantilever root boundary conditions is equivalent to modeling the blade by K elastic modes with a pinned root boundary condition, although K + 1 degrees of freedom are used. Hence, the model for a gimballed or teetering rotor will be somewhat inefficient. The alternative, however, would be to calculate modes for the entire rotor, not just for a single blade. A separate rigid body mode is used for the blade pitch motion allowed by control system flexibility. Again there is some inefficiency involved in combining this mode with the elastic torsion modes of the blade. However, it is simpler to handle the pitch control input and the root boundary conditions by working directly with the rigid pitch mode (since the equation of motion is obtained directly from equilibrium of moments about the pitch axis). Also, the rigid pitch mode is usually more important than the elastic torsion motion.

There have been numerous investigations of rotor and helicopter dynamics, with much of the work in recent years focused on hingeless rotor characteristics. The models developed in these investigations generally are restricted to uniform blade properties or no shaft motion, or involve other limitations on the geometry or degrees of freedom that preclude their use here. Consequently, the equations of motion were independently derived for the present analysis. While recent investigations have tended to deal with the mathematics of the problem rather than the physics, certain nonlinear effects are known to be required for an adequate representation of rotor dynamics, particularly the Coriolis forces and the equivalent pitch-flap and pitch-lag coupling. The inertial analysis used here includes nonlinear accelerations and forces to some extent. The rotor blade and shaft

motion are assumed to be small, but no formal ordering scheme is introduced to derive the equations of motion (hence no precise definition of what small means is required). The retention of nonlinear terms in the equations is based generally on established knowledge of certain important nonlinear effects and the requirement of consistency in the derivation. The structure of the resulting equations is described at the end of this section. Basically, the equations are linearized about the time-averaged bending deflection of the blade. It has been found that this model gives results that are in good agreement with calculations based on independently developed models for an isolated blade in hover.

This section derives the inertia forces of a helicopter rotor blade. The blade motion considered includes coupled flap/lag bending (including the rigid modes if the blade is articulated), rigid pitch and elastic torsion, gimbal pitch and roll (which are dropped from the model for articulated and hingeless rotors) or teeter motion (for two-bladed rotors only), and the rotational speed perturbation. The geometric model of the blade and hub includes precone, droop, and sweep; pitch bearing radial offset; feathering axis droop and sweep; and torque offset and gimbal undersling.

2.2.1 Rotor geometry.

Consider an N-bladed rotor, rotating at speed Ω (Fig. 2-4). The mth blade (m = 1 to N) is at the azimuth location $\psi_m = \psi + m\Delta\psi$, where $\Delta\psi = 2\pi/N$ and $\psi = \Omega t$ is the dimensionless time variable. Because for steady flight the blade motion is periodic, it is only necessary to calculate the motion and forces of one of the blades. For this reference blade we choose that identified by m = N. The S coordinate system ($\vec{i}_S$, $\vec{j}_S$, $\vec{k}_S$) is a nonrotating, inertial reference frame (Fig. 2-4). The S system coordinates are the rotor shaft axes when there is no hub motion. When the shaft moves, however, due to the motion of the helicopter or the wind tunnel support, the S system remains fixed in

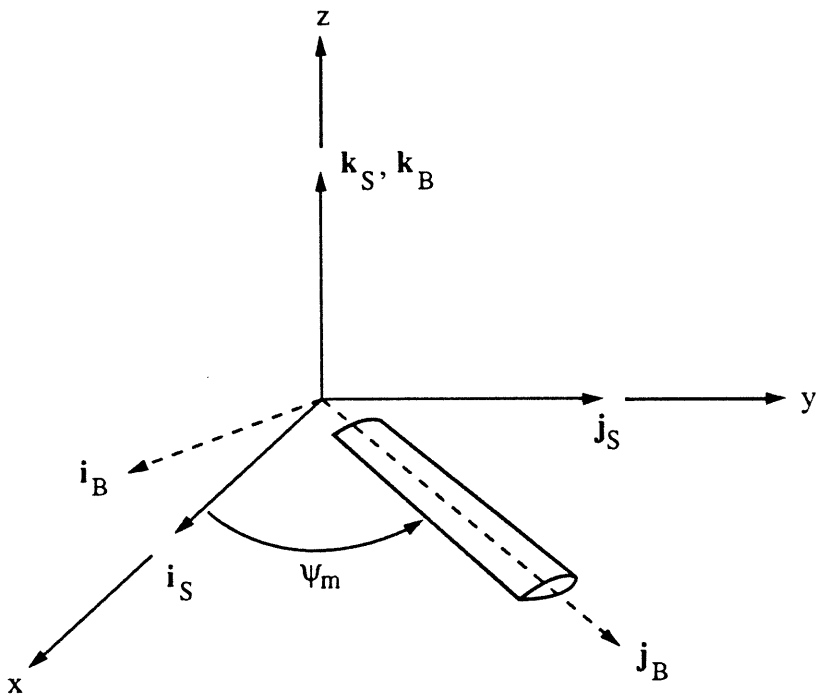

Figure 2-4. Hub frame coordinate systems: shaft axes and blade axes (nonrotating and rotating frames).

space. The B system ($\vec{i}_B$, $\vec{j}_B$, $\vec{k}_B$) is a coordinate frame rotating with the mth blade. The acceleration, angular velocity, and angular acceleration of the hub, and the forces and moments exerted by the rotor on the hub are defined in the nonrotating frame (the S system). Figure 2-5(a) shows the definition of the linear and angular motion of the rotor hub, and Figure 2-5(b) shows the definition of the rotor forces and moments acting on the hub. The rotor blade equations of motion will be derived in the rotating frame.

Figures 2-6 and 2-7 show the blade hub and root geometry considered. The origin of the B and S system is the location of the gimbal (or teeter hinge). For articulated or hingeless rotors, where there is no gimbal, this is simply the point where the shaft motion and hub forces are evaluated. The hub of the rotor is a distance z_{ZA} below the gimbal (gimbal undersling, which is not shown in Fig. 2-6). The torque offset x_{FA} is positive in the $-\vec{i}_B$ direction. The azimuth ψ_m is measured to the feathering axis line (its projection in the hub plane), so the feathering axis is parallel to the $\vec{j}_B$ axis, and offset x_{FA} from the center of rotation. The precone angle δ_{FA_1} gives the orientation of the blade elastic axis inboard of the pitch bearing with respect to the hub plane; δ_{FA_1} is positive upward, and is assumed to be a small angle. The pitch bearing is offset radially from the center of rotation by r_{FA}. The rigid pitch rotation of the blade about the feathering axis occurs at r_{FA}. The droop angle δ_{FA_2} and sweep angle δ_{FA_3} occur at r_{FA}, just outboard of the pitch bearing; δ_{FA_2} and δ_{FA_3} give the orientation of the elastic axis of the blade outboard of the pitch bearing, with respect to the precone. Both δ_{FA_2} and δ_{FA_3} are assumed to be small angles; δ_{FA_2} is positive downward, and δ_{FA_3} is positive aft. Feathering axis droop δ_{FA_4} and sweep δ_{FA_5} define the orientation of the feathering axis with respect to the precone; δ_{FA_4} is positive downward, δ_{FA_5} is positive aft, and both are small angles. If $\delta_{FA_4} = \delta_{FA_5} = 0$, then the feathering axis orientation is just given by the precone; if $\delta_{FA_4} = \delta_{FA_2}$ and $\delta_{FA_5} = \delta_{FA_3}$, then the orientation is the same as the outboard elastic axis.

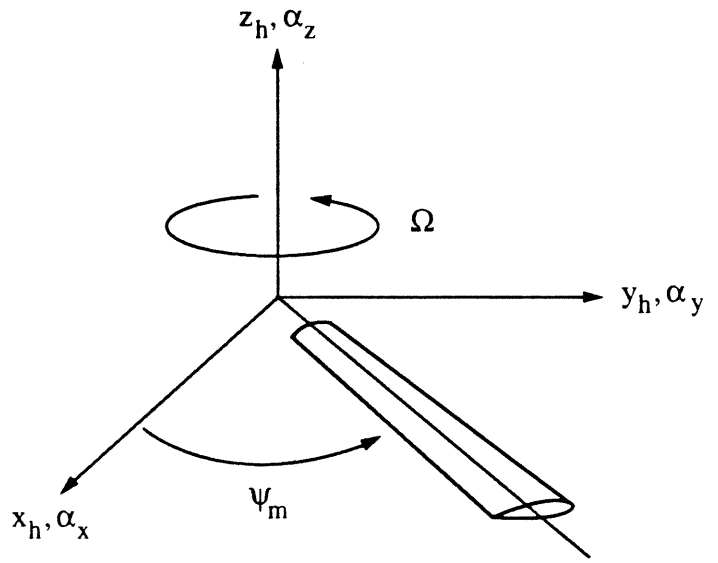

(a) shaft motion

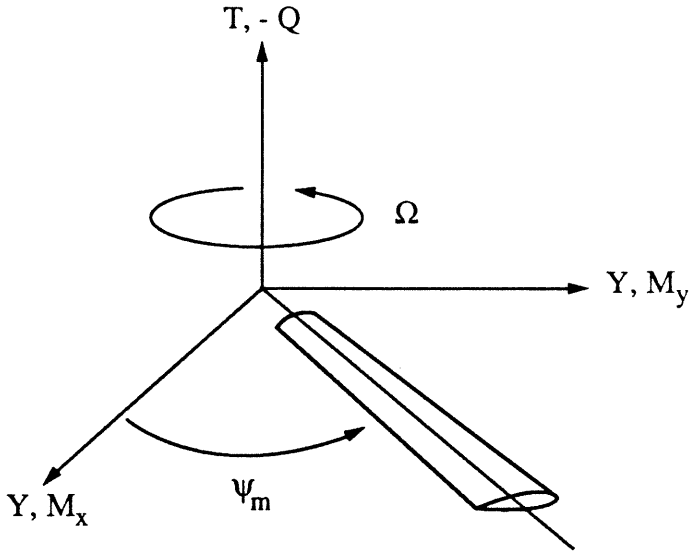

(b) hub reactions

Figure 2-5. Notation and sign conventions for the linear and angular shaft motion, and the forces and moments acting on the rotor hub.

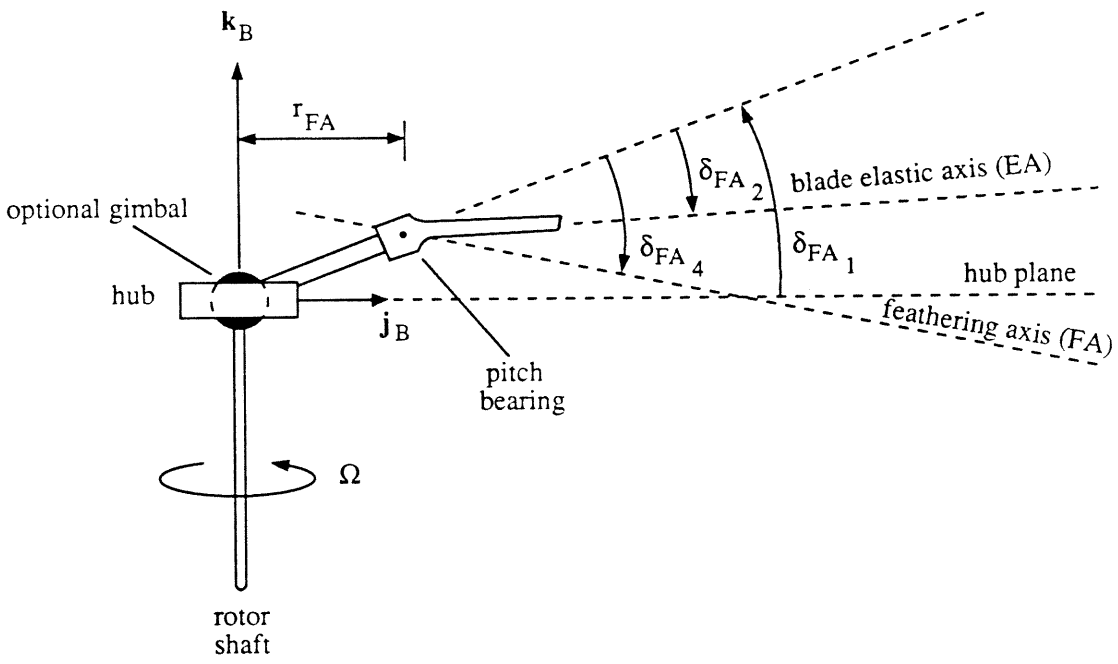

Figure 2-6. Schematic of the rotor hub and root geometry (side view). Only a single, undistorted blade is shown, without the gimbal undersling. The gimbal is omitted from the model for articulated and hingeless rotors.

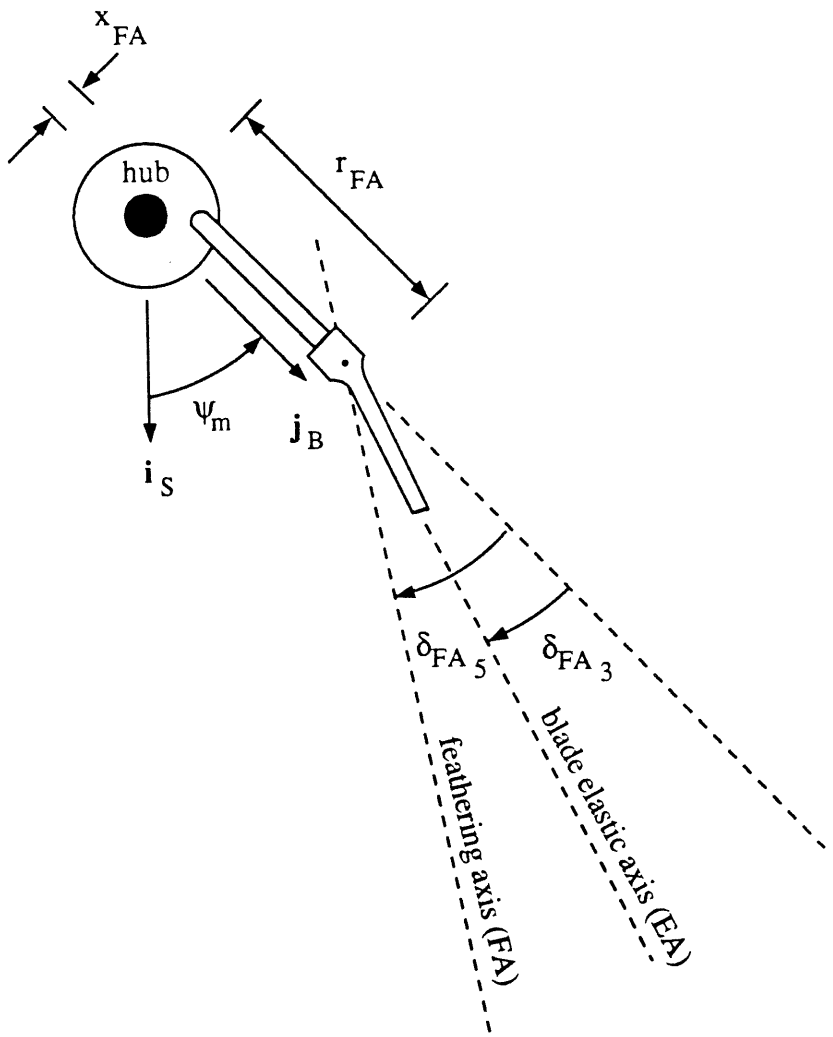

Figure 2-7. Schematic of the rotor hub and root geometry (top view). Only a single, undistorted blade is shown, without the gimbal undersling. The gimbal is omitted from the model for articulated and hingeless rotors.

From the root to the pitch bearing (at $r = r_{FA}$), the undistorted elastic axis is a straight line at the precone angle to the hub plane. The blade outboard of the pitch bearing has a straight undistorted elastic axis, with small droop and sweep angles. The feathering axis also has small droop and sweep with respect to the precone. The entire blade is flexible in bending. The portion of the blade outboard of the pitch bearing is flexible in torsion as well. The rotation of the blade about the pitch bearing takes place about the local direction of the feathering axis. Incorporation of bending flexibility of the blade inboard of the pitch bearing allows consideration of an articulated rotor with the feathering axis inboard or outboard of the hinges, or a cantilever blade with or without flexibility inboard of the pitch bearing.

Figure 2-8 shows the undeformed geometry of the blade. The description of the blade for the inertial analysis parallels that for the structural analysis (see Fig. 2-1 and section 2.1.1). It is assumed that an elastic axis exists, and that the undeformed elastic axis is a straight line; and that the blade has a high aspect ratio. Here x_I is the locus of the section center of gravity, x_A is the locus of the section aerodynamic center, and x_C is the locus of the section tension center. The distances x_I, x_A, and x_C are positive aft, measured from the elastic axis; in general, they are a function of r. The corresponding z displacements are neglected.

The $\vec{i}$, $\vec{j}$, and $\vec{k}$ coordinate system is the elastic axis/principal axis system of the section. The direction of the elastic axis is $\vec{j}$; $\vec{i}$ and $\vec{k}$ are the direction of the local principal axes of the section. The spanwise variable is r, measured from the center of rotation. This variable is dimensionless, so $r = 1$ at the blade tip. The section coordinates x and z are mass principal axes, with origin at the elastic axis. It is assumed that the direction of the mass principal axes and the modulus principal axes is the same. The center of gravity is at $z = 0$ and $x = x_I$. The section mass, center of gravity position, and section

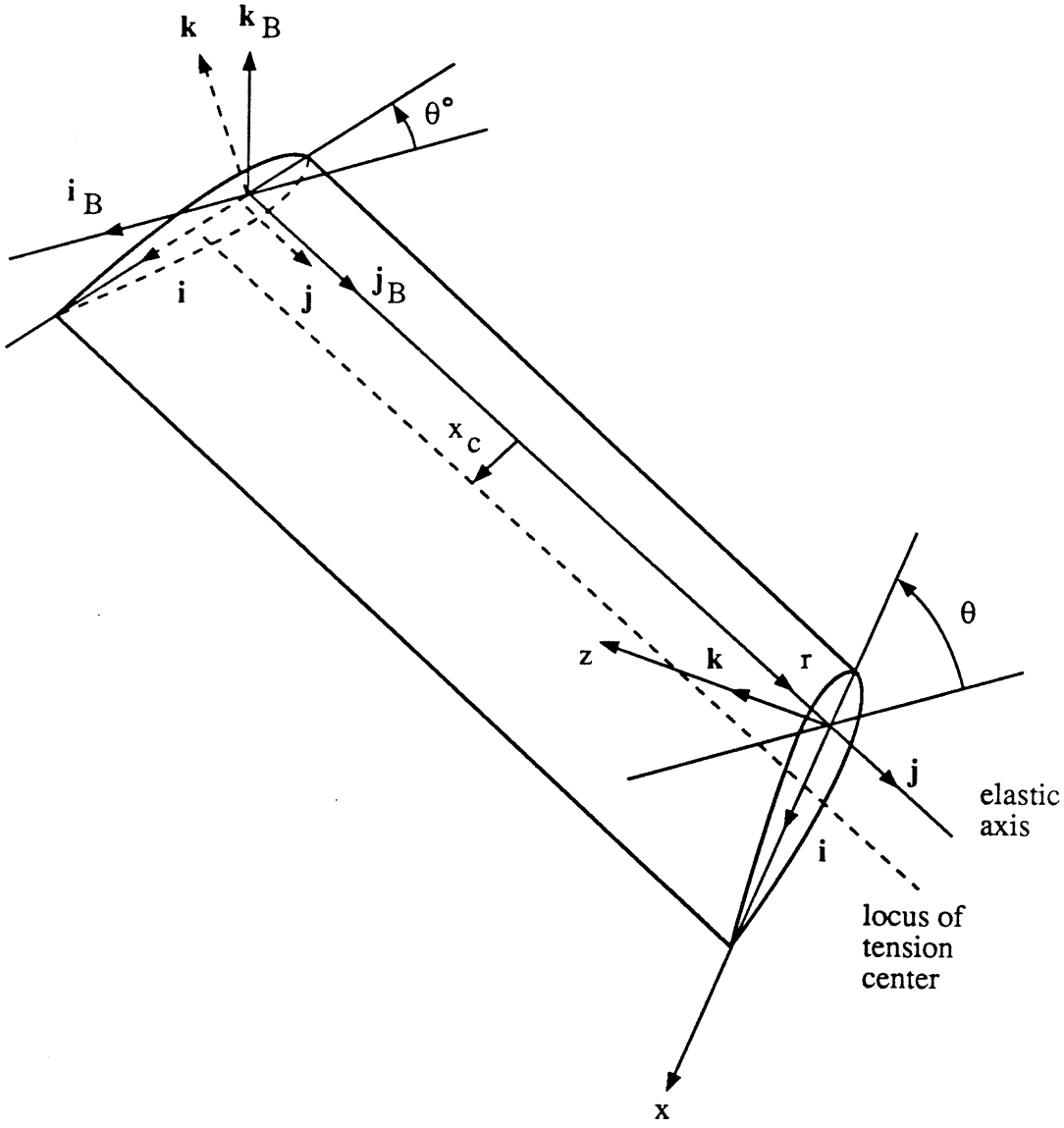

Figure 2-8. Geometry of the undeformed blade.

polar moment of inertia (about the elastic axis) are by definition then as follows:

$$\int dm = m$$

$$\int z\,dm = 0$$

$$\int xz\,dm = 0$$

$$\int x\,dm = x_I m$$

$$\int (x^2 + z^2)\,dm = I_\theta$$

where the integrals are over the blade cross section.

The droop and sweep of the blade elastic axis are defined with respect to hub plane axes, so it follows that unless the feathering axis is parallel to the outboard elastic axis, these angles vary with the pitch of the blade. Let $\delta_{FA_2}{}^*$ and $\delta_{FA_3}{}^*$ be the droop and sweep of the blade when the pitch angle at 75% radius is zero. Then the following relation can be obtained from the root geometry:

$$\delta_{FA_2} = \delta_{FA_4} + (\delta^*_{FA_2} - \delta_{FA_4}) \cos\theta_{75} + (\delta^*_{FA_3} - \delta_{FA_5}) \sin\theta_{75}$$

$$\delta_{FA_3} = \delta_{FA_5} - (\delta^*_{FA_2} - \delta_{FA_4}) \sin\theta_{75} + (\delta^*_{FA_3} - \delta_{FA_5}) \cos\theta_{75}$$

where θ_{75} is the blade pitch at 75% radius.

2.2.2 Rotor motion.

The rotor blade motion is described by the following degrees of freedom:

(a) Gimbal pitch and roll motion of the rotor disk (omitted for articulated and hingeless rotors), or teeter motion of the blade (for two-bladed rotors only).

(b) Rotor speed perturbation.

(c) Rigid pitch motion about the feathering axis and torsion about the elastic axis.

(d) Bending deflection of the elastic axis, including rigid flap and lag motion of the blade is articulated.

Figure 2-9(a) shows the gimbal motion and rotor speed perturbation in the nonrotating frame. The gimbal degrees of freedom are β_{GC} and β_{GS}, respectively pitch and roll of the rotor disk. The rotor rotational speed perturbation is ψ_s. Figure 2-9(b) shows the gimbal motion in the rotating frame. The degrees of freedom are β_G and θ_G, given by

$$\beta_G = \beta_{GC} \cos\psi_m + \beta_{GS} \sin\psi_m$$

$$\theta_G = -\beta_{GC} \sin\psi_m + \beta_{GS} \cos\psi_m$$

The blade pitch θ is defined with respect to the hub plane, so only the blade inboard of the pitch bearing sees the pitch rotation due to θ_G. For two-bladed rotors, the teetering degree of freedom β_T may be included. The teetering motion is defined in the rotating frame, hence $\beta_G = \beta_T(-1)^m$ and $\theta_G = 0$ for this case.

Figure 2-2 showed the geometry of the deformed blade. The blade deformation is described by twist θ about the elastic axis, bending

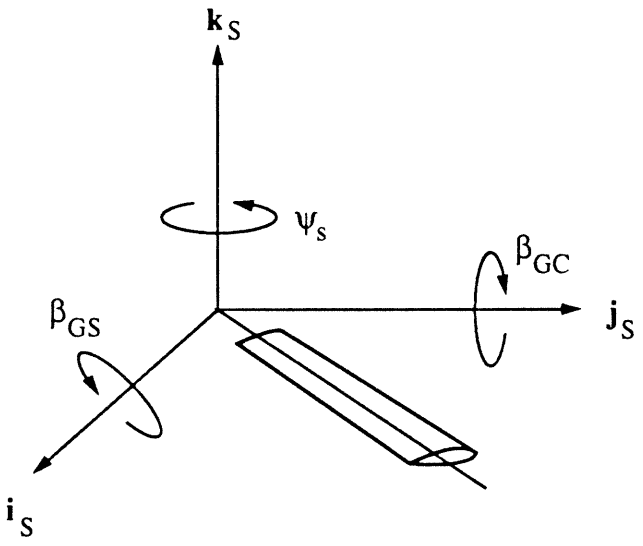

(a) nonrotating frame

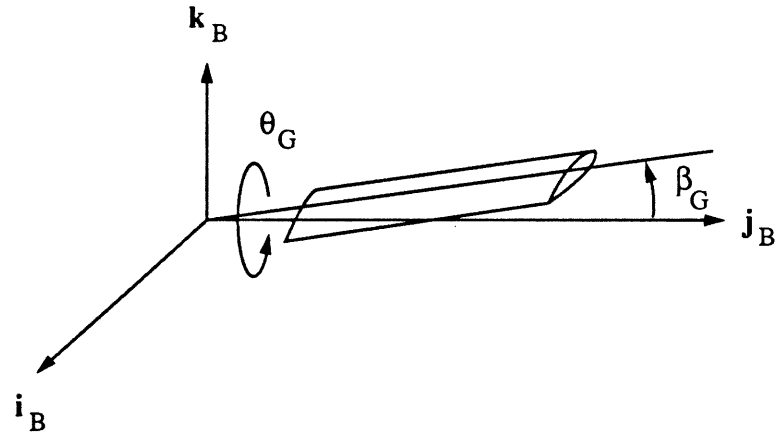

(b) rotating frame

Figure 2-9. Notation and sign conventions for the gimbal motion and the rotor speed perturbation.

deflection x_o and z_o of the elastic axis; and rotations of the section by ϕ_x and ϕ_z due to the bending (see section 2.1.2).

The blade pitch angle θ is measured from the hub plane to the section major principal axis (the x axis). The undeformed pitch angle consists of the collective pitch θ_{coll} plus the built-in twist θ_{tw}. We define θ_{coll} as the pitch at r_{FA}, so $\theta_{tw}(r_{FA}) = 0$. The rotation by θ_{coll} is not present inboard of the pitch bearing, but there can be pitch if the local principal axes with respect to the hub plane, which is included in θ_{tw} for $r < r_{FA}$. The pitch of the deformed blade is composed of the root pitch $\theta^o(\psi)$ (the blade angle at the pitch bearing, $r = r_{FA}$, due to control commands, control system flexibility, and kinematic coupling); the built-in twist $\theta_{tw}(r)$; and torsion about the elastic axis $\theta_e(r,\psi)$ (where $\theta_e(r_{FA},\psi) = 0$, and only θ_e produces shear stress in the blade). Thus the blade pitch is

$$\theta = \theta^o + \theta_{tw} + \theta_e$$

The commanded root pitch angle is defined as $\theta^c = \theta_{coll} + \theta_{con}$. Here θ_{coll} is the trim value of the collective pitch, which may be large but is steady in time; and θ_{con} is the perturbation control input (including the cyclic control required to trim the rotor), which is time dependent but is assumed to be a small angle. The blade root pitch commanded by the control system is θ^c, while θ^o is the actual root pitch. The difference $(\theta^o - \theta^c)$ is the rigid pitch motion due to control system flexibility or kinematic coupling in the control system. Hence, the blade pitch may be written as

$$\theta = (\theta_{coll} + \theta_{tw}) + (\theta^{\circ} - \theta^{c}) + \theta_{con} + \theta_{e}$$

The pitch angle may now be separated into trim and perturbation terms, $\theta = \theta_m + \tilde{\theta}$, where the trim term is

$$\theta_m = \theta_{coll} + \theta_{tw}$$

and the perturbation is

$$\tilde{\theta} = (\theta^{\circ} - \theta^{c}) + \theta_{con} + \theta_{e}$$

The trim pitch θ_m is a large, steady angle; the perturbation pitch $\tilde{\theta}$ is small angle since all the components are small. The pitch at the blade root ($r = r_{FA}$) is then

$$\theta(r_{FA}) = \theta^{\circ} = \theta_{coll} + (\theta^{\circ} - \theta^{c}) + \theta_{con}$$
$$= \theta_m^{\circ} + \tilde{\theta}^{\circ}$$

For the rigid pitch motion the notation p_o is used:

$$p_o = \tilde{\theta}^{\circ} = (\theta^{\circ} - \theta^{c}) + \theta_{con}$$

(This notation is consistent with that for the modal expansion of the elastic torsion θ_e, as described below.) Note that p_o is the total rigid pitch motion of the blade, including the control angle θ_{con}.

2.2.3 Coordinate frames.

The rotating hub plane coordinate frame is obtained from the nonrotating hub plane frame by rotating about the z-axis:

$$\vec{i}_B = \sin\psi_m \vec{i}_s - \cos\psi_m \vec{j}_s$$
$$\vec{j}_B = \cos\psi_m \vec{i}_s + \sin\psi_m \vec{j}_s$$
$$\vec{k}_B = \vec{k}_s$$

The blade coordinate frame is obtained by rotating by the angle $\beta_G + \delta_{FA_1} - \delta_{FA_2}$ about the x-axis, by the angle $\psi_s - \delta_{FA_3}$ about the z-axis, and by the angle θ about the y-axis:

$$\vec{i} = \cos\theta \vec{i}_B - \sin\theta \vec{k}_B + \vec{j}_B \left[(\beta_G + \delta_{FA_1} - \delta_{FA_2}) \sin\theta + (\psi_s - \delta_{FA_3}) \cos\theta \right]$$

$$\vec{j} = \vec{j}_B - (\psi_s - \delta_{FA_3}) \vec{i}_B + (\beta_G + \delta_{FA_1} - \delta_{FA_2}) \vec{k}_B$$

$$\vec{k} = \sin\theta \vec{i}_B + \cos\theta \vec{k}_B + \vec{j}_B \left[-(\beta_G + \delta_{FA_1} - \delta_{FA_2}) \cos\theta + (\psi_s - \delta_{FA_3}) \sin\theta \right]$$

The cross section principal axes for the deformed blade are then

$$\vec{i}_{xs} = \vec{i} + \phi_z \vec{j}$$

$$\vec{j}_{xs} = \vec{j} - \phi_z \vec{i} + \phi_x \vec{k} = \vec{j} + (x_0' \vec{i} + z_0' \vec{k})'$$

$$\vec{k}_{xs} = \vec{k} - \phi_x \vec{j}$$

The vector $\vec{j}_{xs}$ is tangent to the deformed elastic axis.

2.2.4 Blade acceleration.

Based on this model, the distance, velocity, and acceleration are expressed as linear functions of the degrees of freedom, except that the coefficients of the blade torsion degrees of freedom depend on the bending deflection (since torsion of a bent blade produces in-plane and out-of-plane motion of the elastic axis). The distance from the rotor hub to the center of gravity of the blade section is:

$$
\begin{aligned}
\vec{r} = {} & \vec{\imath}_B \left[-x_{FA} - (r - r_{FA})\,\delta_{FA_3} - r\psi_S - z_{FA}\,\theta_G \right] \\
& + \vec{k}_B \left[-z_{FA} - (r - r_{FA})\,\delta_{FA_2} + r(\beta_G + \delta_{FA_1}) \right] \\
& + \vec{\jmath}_B \left[r + z_{FA}\,\beta_G - x_{FA}\,\psi_S \right] \\
& + (x_o \vec{\imath} + z_o \vec{k}) + x_I \vec{\imath} \\
& - \tilde{\theta}\, x_I \vec{k} + \int_{r_{FA}}^{r} \theta_e \, (z_o \vec{\imath} - x_o \vec{k})'' (r - \rho)\, d\rho \\
& + \tilde{\theta}^{\circ} \left[(z_o \vec{\imath} - x_o \vec{k}) - (z_o \vec{\imath} - x_o \vec{k})\big|_{r_{FA}} \right. \\
& \qquad - (z_o \vec{\imath} - x_o \vec{k})'\big|_{r_{FA}} (r - r_{FA}) \\
& \qquad \left. - \left((\delta_{FA_2} - \delta_{FA_4})\vec{\imath}_B + (\delta_{FA_3} - \delta_{FA_5})\vec{k}_B \right)(r - r_{FA}) \right]
\end{aligned}
$$

$$
\begin{aligned}
= {} & \vec{\imath}_B \left[-x_{FA} - (r - r_{FA})\,\delta_{FA_3} - r\psi_S - z_{FA}\,\theta_G \right] \\
& + \vec{k}_B \left[-z_{FA} - (r - r_{FA})\,\delta_{FA_2} + r(\beta_G + \delta_{FA_1}) \right] \\
& + \vec{\jmath}_B \left[r + z_{FA}\,\beta_G - x_{FA}\,\psi_S \right] \\
& + (x_o \vec{\imath} + z_o \vec{k}) + x_I \vec{\imath} \\
& - \sum_{k=0}^{\infty} \vec{X}_k\, P_k
\end{aligned}
$$

where

$$
\vec{X}_k = \xi_k x_I \vec{k} - \int_{r_{FA}}^{r} \xi_k \, (z_o \vec{\imath} - x_o \vec{k})'' (r - \rho)\, d\rho
$$

for elastic torsion ($k \geq 1$) and

$$\vec{X}_0 = -(z_0\vec{i} - x_0\vec{k} - x_I\vec{k}) + (z_0\vec{i} - x_0\vec{k})|_{r_{FA}} + (z_0\vec{i} - x_0\vec{k})'|_{r_{FA}}(r - r_{FA}) + \left((\delta_{FA_2} - \delta_{FA_4})\vec{i}_B + (\delta_{FA_3} - \delta_{FA_5})\vec{k}_B\right)(r - r_{FA})$$

for rigid pitch. These terms ($\vec{X}_k$) are the displacement produced by torsion of the bent blade. The torsion increment $d\theta = \theta' d\rho$ at ρ produces an in-plane motion if the blade has an out-of-plane deflection z:

$$d\Delta x = d\theta\,(z(r) - z(\rho) - (r - \rho)z'(\rho))$$

so

$$\Delta x = \int_{r_{FA}}^{r} \theta'\,(z(r) - z - (r - \rho)z')\,d\rho$$

$$= \int_{r_{FA}}^{r} \theta\, z''\,(r - \rho)\,d\rho$$

Including the corresponding out-of-plane motion when the blade has an in-plane deflection gives the above results for $\vec{X}_k$. For rigid pitch motion θ^o at r_{FA}, the in-plane motion is

$$\Delta x = \tilde{\theta}^{\circ}\left(z(r) - z(r_{FA}) - (r - r_{FA})z'(r_{FA})\right)$$

which, with the corresponding out-of-plane motion, gives the above result for $\vec{X}_o$.

Then the velocity of the blade section, relative to the rotating frame, is:

$$\begin{aligned}\vec{v}_r &= \left(\frac{d}{dt}\vec{r}\right)_B \\ &= -\vec{\imath}_B\left(r\dot{\psi}_s + z_{FA}\dot{\theta}_G\right) + \vec{k}_B\, r\dot{\beta}_G \\ &\quad + \vec{\jmath}_B\left(z_{FA}\dot{\beta}_G - x_{FA}\dot{\psi}_s\right) \\ &\quad + \left(x_o\vec{\imath} + z_o\vec{k}\right)^{\cdot} - \sum_{k=0}^{\infty}\vec{X}_k\,\dot{p}_k\end{aligned}$$

Neglecting the squares of velocities, the acceleration relative to the rotating frame is

$$\begin{aligned}\vec{a}_r &= \left(\frac{d}{dt}\vec{v}_r\right)_B \\ &= -\vec{\imath}_B\left(r\ddot{\psi}_s + z_{FA}\ddot{\theta}_G\right) + \vec{k}_B\, r\ddot{\beta}_G \\ &\quad + \vec{\jmath}_B\left(z_{FA}\ddot{\beta}_G - x_{FA}\ddot{\psi}_s\right) \\ &\quad + \left(x_o\vec{\imath} + z_o\vec{k}\right)^{\cdot\cdot} - \sum_{k=0}^{\infty}\vec{X}_k\,\ddot{p}_k\end{aligned}$$

For the blade Coriolis acceleration the radial velocity component $\vec{j} \cdot \vec{v}_r$ is required, including the effect of the change in the radial position of the section due to bending:

$$\Delta\vec{r} = -\vec{j}_B \frac{1}{2} \int_0^r \left[(x_0\vec{i} + z_0\vec{k} + x_I\vec{i})' - (\psi_s - \delta_{FA_3})\vec{i}_B + (\beta_G + \delta_{FA_1} - \delta_{FA_2})\vec{k}_B \right]^2 d\eta$$

then

$$\vec{j}\cdot\vec{v}_r = -\int_0^r (z_0\vec{i} - x_0\vec{k})' \cdot (z_0\vec{i} - x_0\vec{k} - x_I\vec{k})' d\eta$$
$$- (z_0\vec{i} - x_0\vec{k})' \cdot ((\delta_{FA_1} - \delta_{FA_2})\vec{i}_B - \delta_{FA_3}\vec{k}_B)$$
$$- \dot{\beta}_G \left[-z_{FA} + r\delta_{FA_1} - (r - r_{FA})\delta_{FA_2} + \vec{i}_B \cdot (z_0\vec{i} - x_0\vec{k} - x_I\vec{k}) \right]$$
$$- \dot{\psi}_s \left[x_{FA} - (r - r_{FA})\delta_{FA_3} + \vec{k}_B \cdot (z_0\vec{i} - x_0\vec{k} - x_I\vec{k}) \right]$$

The acceleration of the blade is required with respect to an inertial frame, specifically the S system. The B coordinate frame rotates at a constant angular velocity $\vec{\Omega} = \Omega\vec{k}_B$ with respect to the S frame. The shaft motion is composed of linear and angular displacement

of the origin of the S frame. The acceleration, angular velocity, and angular acceleration of the S system have the following components in the nonrotating, inertial frame:

$$\vec{a}_o = \ddot{x}_h \vec{i}_s + \ddot{y}_h \vec{j}_s + \ddot{z}_h \vec{k}_s$$

$$\vec{\omega}_o = \dot{\alpha}_x \vec{i}_s + \dot{\alpha}_y \vec{j}_s + \dot{\alpha}_z \vec{k}_s$$

$$\dot{\vec{\omega}}_o = \ddot{\alpha}_x \vec{i}_s + \ddot{\alpha}_y \vec{j}_s + \ddot{\alpha}_z \vec{k}_s$$

It is assumed that a_o, ω_o and $\dot{\omega}_o$ are all small quantities.

The acceleration ($\vec{a}_r$) and velocity ($\vec{v}_r$) of the blade relative to the B frame have been derived above. Now the acceleration of a blade point in inertial space will be derived, in terms of the motion of the shaft, the rotation of the rotor, and the blade motion in the B frame. From the result for the acceleration in the rotating coordinate frame (the S frame, rotating at rate $\vec{\omega}_o$), there follows:

$$\vec{a} = \vec{a}_o + \vec{a}_{r,s} + 2\vec{\omega}_o \times \vec{v}_{r,s} + \vec{\omega}_o \times (\vec{\omega}_o \times \vec{r}) + \dot{\vec{\omega}}_o \times \vec{r}$$

where $\vec{a}_{r,s}$ and $\vec{v}_{r,s}$ are the acceleration and velocity relative to the S frame. The B system rotates at angular velocity $\vec{\Omega} = \Omega \vec{k}_B$ with respect to the S frame. Hence with Ω constant and no angular or linear acceleration of the B frame with respect to the S frame, there follows:

$$\vec{a}_{r,s} = \vec{a}_r + 2\vec{\Omega} \times \vec{v}_r + \vec{\Omega} \times (\vec{\Omega} \times \vec{r})$$

$$\vec{v}_{r,s} = \vec{v}_r + \vec{\Omega} \times \vec{r}$$

where $\vec{a}_r$ and $\vec{v}_r$ are the acceleration and velocity relative to the B frame. Thus:

$$\vec{a} = \vec{a}_0 + \vec{a}_r + 2\vec{\Omega} \times \vec{v}_r + \vec{\Omega} \times (\vec{\Omega} \times \vec{r})$$
$$+ 2\vec{\omega}_0 \times \vec{r} + 2\vec{\omega}_0 \times (\vec{\Omega} \times \vec{r})$$
$$+ \vec{\omega}_0 \times (\vec{\omega}_0 \times \vec{r}) + \dot{\vec{\omega}}_0 \times \vec{r}$$

To first order in the velocity and angular velocity, this becomes finally:

$$\vec{a} \cong \vec{a}_0 + 2\vec{\omega}_0 \times (\vec{\Omega} \times \vec{r}) + \dot{\vec{\omega}}_0 \times \vec{r}$$
$$+ \vec{a}_r + 2\vec{\Omega} \times \vec{v}_r + \vec{\Omega} \times (\vec{\Omega} \times \vec{r})$$

or in dyadic operator form, with $\vec{\Omega} = \Omega \vec{k}_B$:

$$\vec{a} = \vec{a}_0 + 2\Omega(\vec{k}_B \vec{r} - \vec{r}\,\vec{k}_B)\vec{\omega}_0 - (\vec{r}\times)\dot{\vec{\omega}}_0$$
$$+ \vec{a}_r + 2\Omega(\vec{j}_B \vec{i}_B - \vec{i}_B \vec{j}_B)\vec{v}_r$$
$$- \Omega^2 (\vec{i}_B \vec{i}_B + \vec{j}_B \vec{j}_B)\vec{r}$$

The approximation $\vec{r} \simeq r\vec{j}_B$ will be used to evaluate the hub motion terms. The six terms in $\vec{a}$ are, respectively, the acceleration of the origin, the Coriolis acceleration due to the angular velocity of the origin, the angular acceleration of the origin, the relative acceleration in the rotating frame, the relative Coriolis acceleration, and the centrifugal acceleration.

For the blade bending and torsion equations, the following components of the acceleration will be required:

$$\vec{j}\cdot\vec{a} = -\Omega^2 r - 2\Omega\left(r\dot{\psi}_s + \vec{k}_B\cdot(z_0\vec{i} - x_0\vec{k})^{\cdot}\right) + \ddot{x}_h\cos\psi + \ddot{y}_h\sin\psi - 2\Omega r\dot{\alpha}_z$$

$$\vec{j}\times\vec{a} = (z_0\vec{i} - x_0\vec{k})^{\cdot\cdot} + r\ddot{\psi}_s\vec{k}_B + r\ddot{\beta}_G\vec{i}_B + z_{FA}\ddot{\theta}_G\vec{k}_B - \sum_{k=0}^{\infty}(\vec{j}\times\vec{X}_k)\ddot{p}_k$$

$$+ \Omega^2\vec{k}_B\left[\vec{i}_B\cdot(x_0\vec{i} + z_0\vec{k} + x_1\vec{i}) - x_{FA} - r_{FA}\delta_{FA_3}\right] + \Omega^2\vec{i}_B r\left(\beta_G + \delta_{FA_1} - \delta_{FA_2}\right) - \Omega^2\vec{k}_B\sum_{k=0}^{\infty}\vec{i}_B\cdot\vec{X}_k\,p_k$$

$$+ 2\Omega\vec{k}_B\,\vec{j}\cdot\vec{v}_r + 2\Omega\left[(\delta_{FA_1} - \delta_{FA_2})\vec{i}_B - \delta_{FA_3}\vec{k}_B\right]\left(r\dot{\psi}_s + \vec{k}_B\cdot(z_0\vec{i} - x_0\vec{k})^{\cdot}\right)$$

$$+ \vec{i}_B\ddot{z}_h - \vec{k}_B\left(\ddot{x}_h\sin\psi - \ddot{y}_h\cos\psi\right) + 2\Omega r\vec{i}_B\left(\dot{\alpha}_x\cos\psi + \dot{\alpha}_y\sin\psi\right) + r\left(\vec{i}_B\left(\ddot{\alpha}_x\sin\psi - \ddot{\alpha}_y\cos\psi\right) + \vec{k}_B\ddot{\alpha}_z\right)$$

For the hub moment the angular acceleration is required:

$$\vec{r}\times\vec{a} = r^2\ddot{\psi}_s\vec{k}_B + r^2\ddot{\beta}_G\vec{i}_B + r(z_0\vec{i} - x_0\vec{k})^{\cdot\cdot} + r z_{FA}\ddot{\theta}_G\vec{k}_B - \sum_{k=0}^{\infty}(\vec{j}\times\vec{X}_k)\,r\ddot{p}_k$$

$$+ \Omega^2 r\vec{i}_B\left[-z_{FA} + r\delta_{FA_1} - (r - r_{FA})\delta_{FA_2} + r\beta_G + \vec{k}_B\cdot(x_0\vec{i} + z_0\vec{k} + x_1\vec{i}) - \sum_{k=0}^{\infty}\vec{k}_B\cdot\vec{X}_k\,p_k\right]$$

$$+ 2\Omega\left(r\dot{\Psi}_s + \vec{k}_B\cdot(z_0\vec{\imath} - x_0\vec{k})^{\cdot}\right)\left[-\vec{\imath}_B\left(-x_{FA} + (r - r_{FA})\delta_{FA_3}\right)\right.$$
$$+ \vec{\imath}_B\left(-z_{FA} + r\delta_{FA_1} - (r - r_{FA})\delta_{FA_2}\right)$$
$$\left. + (z_0\vec{\imath} - x_0\vec{k}) - x_I\vec{k}\right]$$
$$+ 2\Omega r\,\vec{k}_B\,\vec{\jmath}\cdot\vec{v}_r$$
$$+ \vec{\imath}_B\, r\ddot{z}_h - \vec{k}_B\, r\left(\ddot{x}_h\sin\Psi - \ddot{y}_h\cos\Psi\right)$$
$$+ 2\Omega r^2\,\vec{\imath}_B\left(\dot{\alpha}_x\cos\Psi + \dot{\alpha}_y\sin\Psi\right)$$
$$+ r^2\left(\vec{\imath}_B\left(\ddot{\alpha}_x\sin\Psi - \ddot{\alpha}_y\cos\Psi\right) + \vec{k}_B\,\ddot{\alpha}_z\right)$$

and for the hub force we can use

$$\vec{a} = -r\ddot{\Psi}_s\vec{\imath}_B + r\ddot{\beta}_G\vec{k}_B + (x_0\vec{\imath} + z_0\vec{k})^{\cdot\cdot}$$
$$- 2\Omega\vec{\jmath}_B\left(r\dot{\Psi}_s + \vec{k}_B\cdot(z_0\vec{\imath} - x_0\vec{k})^{\cdot}\right)$$
$$- \Omega^2\left[\vec{\imath}_B\,\vec{\imath}_B\cdot(x_0\vec{\imath} + z_0\vec{k} + x_I\vec{\imath}) + \vec{\jmath}_B\, r\right.$$
$$\left. + \vec{\imath}_B\left(-x_{FA} + (r - r_{FA})\delta_{FA_3} - r\Psi_s\right)\right]$$
$$+ \vec{\imath}_B\left(\ddot{x}_h\sin\Psi - \ddot{y}_h\cos\Psi\right) + \vec{k}_B\,\ddot{z}_h$$
$$+ \vec{\jmath}_B\left(\ddot{x}_h\cos\Psi + \ddot{y}_h\sin\Psi\right)$$
$$+ 2\Omega r\left(\vec{k}_B\left(\dot{\alpha}_x\cos\Psi + \dot{\alpha}_y\sin\Psi\right) - \vec{\jmath}_B\dot{\alpha}_z\right)$$
$$+ r\left(\vec{k}_B\left(\ddot{\alpha}_x\sin\Psi - \ddot{\alpha}_y\cos\Psi\right) - \vec{\imath}_B\ddot{\alpha}_z\right)$$

The approximation $\vec{r} \simeq r\vec{j}_B$ has been used in all cases to evaluate the hub motion terms.

2.2.5 Aerodynamic forces.

The aerodynamic forces acting on the blade section at the elastic axis are F_z, F_x, and F_r (see Fig. 2-11 in section 2.4). These are the components of the aerodynamic lift and drag forces in the hub plane axis system (the B frame). F_x is in the hub plane, positive in the drag direction; F_z is normal to the hub plane, positive upward; and F_r is the radial force, positive outward. There are also radial components of F_x and F_z due to the tilt of the section by blade bending; here F_r is just the radial drag force. Thus, the aerodynamic force acting on the section at the deformed elastic axis is:

$$\vec{F}_{aero} = F_x \vec{i}_B + F_z \vec{k}_B - \vec{j}_B \vec{j}_{xs} \cdot (F_x \vec{i}_B + F_z \vec{k}_B) + F_r \vec{j}_{xs}$$

$$\simeq F_x \vec{i}_B + F_z \vec{k}_B + \tilde{F}_r \vec{j}_B$$

where

$$\tilde{F}_r = F_r - F_z (\beta_G + \delta_{FA_1} - \delta_{FA_2} + \vec{k}_B \cdot (x_0 \vec{i} + z_0 \vec{k})') - F_x (-\psi_s + \delta_{FA_3} + \vec{i}_B \cdot (x_0 \vec{i} + z_0 \vec{k})')$$

The section aerodynamic moment about the elastic axis is M_a, positive nose upward (so $\vec{M}_{aero} = M_a \vec{j}_{xs}$). These section aerodynamic loads are integrated over the blade span to obtain the total forces and moments.

2.2.6 Force and moment equilibrium.

The equations of motion for elastic bending, torsion, and rigid pitch of the blade are obtained from equilibrium of inertial, aerodynamic, and elastic moments on the portion of the blade outboard of r:

$$-\vec{M}_E + \vec{M}_A = \vec{M}_I$$

Where M_E is the structural moment on the inboard face of the deformed cross section (so $-M_E$ is the external force on the outboard face); M_A is the total aerodynamic moment on the blade surface outboard of r; and M_I is the total inertial moment on the blade surface outboard of r. The structural moment M_E is obtained from the engineering beam theory for bending and torsion (section 2.1.5), from the control system flexibility for rigid pitch, or from the hub spring for gimbal or teeter motion. Alternatively, M_E may be viewed as the force or moment on the hub due to the rotor (so $-M_E$ is the force on the rotor). M_I is the inertial moment of the blade outboard of r, about the point $\vec{r}_o(r)$, obtained by integrating the acceleration times the blade density ($dm d\rho$) over the volume of the blade:

$$\vec{M}_I = \int_r^1 \int_{section} (\vec{r}(\rho) - \vec{r}_o(r)) \times \vec{a} \, dm \, d\rho$$

The aerodynamic moment M_A is obtained by integrating the section aerodynamic forces over the length of the blade:

$$\vec{M}_A = \int_r^1 (\vec{r}(\eta) - \vec{r}_o(r)) \times \vec{F}_{aero}\, d\eta + \int_r^1 M_a \vec{j}_{xs}\, d\eta$$

For bending of the blade, engineering beam theory gives

$$\vec{M}_E^{(2)} = M_x \vec{i} + M_z \vec{k} = (\vec{i}\vec{i}_{xs} + \vec{k}\vec{k}_{xs})\vec{M}_E$$

Therefore, the operator $(\vec{i}\vec{i}_{xs} + \vec{k}\vec{k}_{xs})$ is applied to $\vec{M}_I$ and $\vec{M}_A$ also. For bending, moments about the tension center ($x = x_C$) are required. Then, the desired partial differential equation for bending is obtained from $\partial^2\vec{M}^{(2)}/\partial^2 r$. The ordinary differential equation for the kth bending mode of one blade is obtained by operating with $\int_o^1 \vec{\eta}_k \cdot (\ldots) dr$, where $\vec{\eta}_k$ is the flap/lag bending mode shape (see section 2.2.15). For elastic torsion, engineering beam theory gives $M_r = \vec{j}_{xs} \cdot \vec{M}_E$. So this same operator is applied to $\vec{M}_I$ and $\vec{M}_A$. For torsion, moments about the section elastic axis ($x = 0$) at r are required; also, elastic torsion involves only the blade outboard of r_{FA}. The desired partial differential equation for torsion is then obtained from $\partial M_r/\partial r$. The ordinary differential equation for the kth torsion mode is obtained by operating with $\int_o^1 \xi_k (\ldots) dr$, where ξ_k is the elastic torsion mode shape (see section 2.2.15). The equation of motion for the rigid pitch degree of freedom p_o is obtained from equilibrium of moments about the feathering axis, $M_{FA} = \hat{e}_{FA} \cdot \vec{M}(r_{FA})$. There $\vec{M}$ is the moment about the

feathering axis ($x = 0$) at $r = r_{FA}$, and $\hat{e}_{FA}$ is the direction of the feathering axis, including perturbations due to blade bending:

$$\hat{e}_{FA} = \vec{j}_{FA} + (x_0\vec{i} + z_0\vec{k})'\Big|_{r_{FA}} - \delta_{FA_4}\vec{k}_B + \delta_{FA_5}\vec{i}_B$$

The elastic restraint from the control system flexibility gives the restoring moment about the feathering axis, completing the desired equation of motion.

The total rotor force and moment on the hub (at the gimbal point) are obtained from a sum over the N blades of $\vec{F}^{(m)}$ and $\vec{M}^{(m)}$, the force and moment due to the mth blade:

$$\vec{F} = \sum_{m=1}^{N} \vec{F}^{(m)}$$

$$\vec{M} = \sum_{m=1}^{N} \vec{M}^{(m)}$$

Since $-\vec{F}^{(m)}$ and $-\vec{M}^{(m)}$ are the forces on the blade, from force and moment equilibrium of the entire blade it follows that

$$\vec{F}^{(m)} = \vec{F}_A - \vec{F}_I$$

$$\vec{M}^{(m)} = \vec{M}_A - \vec{M}_I$$

The hub force and moment are required in the nonrotating hub plane frame (the S system), with components defined as follows:

$$\vec{F} = H\vec{i}_S + Y\vec{j}_S + T\vec{k}_S$$

$$\vec{M} = M_x\vec{i}_S + M_y\vec{j}_S - Q\vec{k}_S$$

(see Fig. 2-5).

The equations of motion for the gimbal degrees of freedom β_{GC} and β_{GS} are obtained from equilibrium of moments about the gimbal, $M_x = \vec{i}_S \cdot \vec{M}$ and $M_y = \vec{j}_S \cdot \vec{M}$, where $\vec{M}$ is the total moment (from all N blades) about the gimbal point, in the nonrotating frame. The equation of motion for the teeter degree of freedom β_T is obtained from equilibrium of the moments about the teeter hinge from both blades, in the rotating frame. The equation of motion for the rotor speed perturbation ψ_s is obtained from equilibrium of the shaft torque moments, $Q = -M_z = \vec{k}_S \cdot \vec{M}$. The drive train couples the torque perturbations of both the rotors, hence this degree of freedom is best considered with the other motions of the helicopter body.

2.2.7 Bending equation.

The equation of motion for blade bending is obtained from

$$\int_0^1 \vec{\eta}_x \cdot \frac{\partial^2 \vec{M}_I(z)}{\partial r^2}\,dr + \int_0^1 \vec{\eta}_x \cdot \frac{\partial^2 \vec{M}_E(z)}{\partial r^2}\,dr = \int_0^1 \vec{\eta}_x \cdot \frac{\partial^2 \vec{M}_A(z)}{\partial r^2}\,dr$$

where $\vec{M}$ is the moment about the tension center ($x = x_C$) at r, and

$$\vec{M}^{(2)} = (\vec{i}\vec{i}_{xs} + \vec{k}\vec{k}_{xs})\vec{M} = (\vec{i}\vec{i} + \vec{k}\vec{k} - (x_0\vec{i} + z_0\vec{k})'\vec{j})\vec{M}$$

Considering first the blade outboard of r_{FA}, the inertia moment is

$$\vec{M}_I = \int_r \int_{section} (\vec{r}|_{gxz} - \vec{r}|_{rx_{c0}}) \times \vec{a}\, dm\, dy$$

$$= \int_r^1 \left[\begin{array}{l} (y-r)\vec{j} + (x_0+x_I)\vec{i} + z_0\vec{k} \\ -((x_0+x_c)\vec{i} + z_0\vec{k})|_r \end{array} \right] \times \vec{a}\, m\, dy$$

so

$$\frac{\partial \vec{M}}{\partial r} = -(\vec{j} + (x_0\vec{i} + z_0\vec{k} + x_c\vec{i})') \times \int_r^1 \vec{a}\, m\, dy$$
$$- (x_I - x_c)\vec{i} \times \vec{a}\, m$$

$$\frac{\partial^2 \vec{M}}{\partial r^2} = \vec{j} \times \vec{a}\, m - \left[(x_0\vec{i} + z_0\vec{k} + x_c\vec{i})' \times \int_r^1 \vec{a}\, m\, dy \right]'$$
$$- \left[(x_I - x_c)\vec{i} \times \vec{a}\, m \right]'$$

$$\vec{j} \cdot \vec{M} = \int_r^1 \left[z_0\vec{i} - (x_0 + x_I)\vec{k} - (z_0\vec{i} - x_0\vec{k} - x_c\vec{k})|_r \right] \cdot \vec{a}\, m\, dy$$

Finally:

$$\frac{\partial^2 \vec{M}_I^{(2)}}{\partial r^2} = (\hat{\imath}\hat{\imath} + \hat{k}\hat{k}) \frac{\partial^2 \vec{M}_I}{\partial r^2} - \left[(x_0\hat{\imath} + z_0\hat{k})' \vec{J} \cdot \vec{M}_I\right]''$$

$$= \vec{J} \times \vec{a}\, m + \left[(x_c - x_I)\hat{k}\, \vec{J} \cdot \vec{a}\, m\right]'$$

$$+ \left[(z_0\hat{\imath} - x_0\hat{k} - x_c\hat{k})' \int_r^1 \vec{J} \cdot \vec{a}\, m\, d\eta\right]'$$

$$- \left\{(x_0\hat{\imath} + z_0\hat{k})' \int_r^1 \left[z_0\hat{\imath} - x_0\hat{k} - x_I\hat{k} - (z_0\hat{\imath} - x_0\hat{k} - x_c\hat{k})\big|_r\right] \cdot \vec{a}\, m\, d\eta\right\}''$$

The last term in this result will be neglected since it is order $(c/R)^2$ smaller than the first term. Including the case $r < r_{FA}$, which only introduces an effect of the droop and sweep, the result is

$$\frac{\partial^2}{\partial r^2} \vec{M}_I^{(2)} = \vec{J} \times \vec{a}\, m + \left[(x_c - x_I)\hat{k}\, \vec{J} \cdot \vec{a}\, m\right]'$$

$$+ \left[(z_0\hat{\imath} - x_0\hat{k} - x_c\hat{k})' \int_r^1 \vec{J} \cdot \vec{a}\, m\, d\eta\right]'$$

$$- \delta(r - r_{FA})(\delta_{FA_2}\hat{\imath}_B + \delta_{FA_3}\hat{k}_B) \int_{r_{FA}}^1 \vec{J} \cdot \vec{a}\, m\, dr$$

where $\delta(r)$ is the delta function (an impulse at $r = 0$). Operating with $\int_0^1 \vec{\eta}_k \cdot (\ldots) dr$ and integrating the second and third terms by parts gives:

$$\int_0^1 \vec{\eta}_k \cdot \frac{\partial^2 \vec{M}_I^{(2)}}{\partial r^2}\, dr = \int_0^1 \vec{\eta}_k \cdot (\ddot{y} \times \vec{a})\, m\, dr$$
$$+ \int_0^1 \vec{\eta}_k \cdot \left[(x_c - x_z)\vec{k}\, \ddot{y} \cdot \vec{a}\, m \right]' dr$$
$$+ \int_0^1 \vec{\eta}_k \cdot \left[(z_0\vec{i} - x_0\vec{k} - x_c\vec{k})' \int_r^1 \ddot{y} \cdot \vec{a}\, m\, d\xi \right]' dr$$
$$- \vec{\eta}_k(r_{FA}) \cdot (\delta_{FA_2}\vec{i}_B + \delta_{FA_3}\vec{k}_B) \int_{r_{FA}}^1 \ddot{y} \cdot \vec{a}\, m\, dr$$

$$= \int_0^1 \vec{\eta}_k \cdot (\ddot{y} \times \vec{a})\, m\, dr$$
$$+ \left[\vec{\eta}_k \cdot \vec{k}\, (x_c - x_z)\, \ddot{y} \cdot \vec{a}\, m \right]\Big|_{r=1}$$
$$- \int_0^1 \vec{\eta}_k' \cdot \vec{k}\, (x_c - x_z)\, \ddot{y} \cdot \vec{a}\, m\, dr$$
$$- \int_0^1 \vec{\eta}_k' \cdot (z_0\vec{i} - x_0\vec{k} - x_c\vec{k})' \int_r^1 \ddot{y} \cdot \vec{a}\, m\, d\xi\, dr$$
$$- \vec{\eta}_k(r_{FA}) \cdot (\delta_{FA_2}\vec{i}_B + \delta_{FA_3}\vec{k}_B) \int_{r_{FA}}^1 \ddot{y} \cdot \vec{a}\, m\, dr$$

Finally, the torsion terms are introduced; the inertia and centrifugal forces directly due to the blade bending motion are extracted; and the fourth term above is again integrated by parts. Thus, the inertia force is:

$$\int_0^1 \vec{\eta}_k \cdot \frac{\partial^2 \vec{M}_I^{(2)}}{\partial r^2}\, dr =$$

$$\int_0^1 \vec{\eta}_k \cdot (z_0\vec{\imath} - x_0\vec{k})'' m\, dr \quad - \Omega^2 \int_0^1 \vec{\eta}_k \cdot \left[\int_r^1 \rho m\, d\rho\, (z_0\vec{\imath} - x_0\vec{k})'\right]' dr$$

$$- \int_0^1 \vec{\eta}_k \cdot \vec{\Omega}\, m\, \vec{\Omega} \cdot (z_0\vec{\imath} - x_0\vec{k})\, m\, dr$$

$$+ \int_0^1 \vec{\eta}_k \cdot \left[\vec{\jmath} \times \vec{a} - (z_0\vec{\imath} - x_0\vec{k})'' - \Omega^2 \vec{k}_B \vec{\imath}_B \cdot (x_0\vec{\imath} + z_0\vec{k})\right] m\, dr$$

$$+ \left[\vec{\eta}_k \cdot \vec{k}\, (x_c - x_I)\, \vec{\jmath} \cdot \vec{a}\, m\right]\Big|_{r=1}$$

$$- \int_0^1 \vec{\eta}_k' \cdot \vec{k}\, (x_c - x_I)\, \vec{\jmath} \cdot \vec{a}\, m\, dr - \left[\vec{\eta}_k' \cdot \vec{k}\, x_c\right]\Big|_{r=0} \int_0^1 \vec{\jmath} \cdot \vec{a}\, m\, dr$$

$$- 2\Omega \int_0^1 (z_0\vec{\imath} - x_0\vec{k} - x_c\vec{k}) \cdot \left\{\vec{\eta}_k'' \int_r^1 (\dot{\Psi}_s \rho + \vec{k}_B \cdot (z_0\vec{\imath} - x_0\vec{k})^{\cdot})\, m\, d\rho \right.$$

$$\left. - \vec{\eta}_k' (\dot{\Psi}_s r + \vec{k}_B \cdot (z_0\vec{\imath} - x_0\vec{k})^{\cdot})\, m \right\} dr$$

$$+ \Omega^2 \int_0^1 x_c \vec{k} \cdot \left\{\vec{\eta}_k'' \int_r^1 \rho m\, d\rho - \vec{\eta}_k' r m\right\} dr$$

$$- \vec{\eta}_k(r_{FA}) \cdot (b_{FA_2} \vec{\imath}_B + b_{FA_3} \vec{k}_B) \int_{r_{FA}}^1 \vec{\jmath} \cdot \vec{a}\, m\, dr$$

$$- \Omega^2 \left[\vec{\eta}_k \cdot \vec{\imath}\, \tilde{\Theta}\, (x_c - x_I)\, m\right]\Big|_{r=1}$$

$$+ \Omega^2 \int_0^1 \vec{\eta}_k' \cdot \vec{\imath}\, \tilde{\Theta}\, (x_c - x_I)\, r m\, dr + \Omega^2 \left[\vec{\eta}_k \cdot \vec{\imath}\, \tilde{\Theta}\, x_c\right]\Big|_{r=0} \int_0^1 r m\, dr$$

$$+ \Omega^2 \int_0^1 \sum_{k=0}^{\tilde{k}} \rho_k (\vec{\jmath} \times \vec{X}_k) \cdot \left\{\vec{\eta}_k'' \int_r^1 \rho m\, d\rho - \vec{\eta}_k' r m\right\} dr$$

The structural moment (from section 2.1.5) is

$$\int_0^1 \vec{\eta}_k \cdot \frac{\partial^2 \vec{M}_E^{(2)}}{\partial r^2}\, dr =$$

$$\int_0^1 \vec{\eta}_k \cdot \left[\left(EI_{zz}\vec{\imath}\vec{\imath} + EI_{xx}\vec{k}\vec{k} \right) \left(z_0\vec{\imath} - x_0\vec{k} \right)'' \right]'' dr$$

$$+ \int_0^1 \vec{\eta}_k \cdot \left[\left(EI_{xp}\vec{k} - EI_{zp}\vec{\imath} \right) \theta_{tw}' \theta_e' \right]'' dr$$

The aerodynamic moment about the tension center ($x = x_C$) at r, due to the blade loading at the elastic axis at station ρ is

$$\vec{M}_A = \int_r^1 \left(\vec{r}\big|_{\rho x_{c_0}} - \vec{r}\big|_{r x_{c_0}} \right) \times \vec{F}_{aero}\, d\rho$$

$$\cong \int_r^1 (\rho - r) \left(F_z \vec{\imath}_B - F_x \vec{k}_B \right) d\rho$$

so

$$\int_0^1 \vec{\eta}_k \cdot \frac{\partial^2 \vec{M}_A^{(2)}}{\partial r^2}\, dr = \int_0^1 \vec{\eta}_k \cdot \left(F_z \vec{\imath}_B - F_x \vec{k}_B \right) dr$$

2.2.8 Elastic torsion equation.

The equation of motion for elastic torsion is obtained from

$$-\int_0^1 \xi_k \frac{\partial M_{r_I}}{\partial r}\, dr - \int_0^1 \xi_k \frac{\partial M_{r_E}}{\partial r}\, dr = -\int_0^1 \xi_k \frac{\partial M_{r_A}}{\partial r}\, dr$$

where $\vec{M}$ is the moment about the elastic axis at r, and

$$\frac{\partial}{\partial r} M_r = \frac{\partial}{\partial r} \vec{f}_{xs} \cdot \vec{M} = \vec{f} \cdot \frac{\partial \vec{M}}{\partial r} + \left[(x_0 \vec{\imath} + z_0 \vec{k})' \cdot \vec{M} \right]'$$

The inertial moment is

$$\vec{M}_I = \int_r^1 \int_{\text{section}} (\vec{r}|_{\rho x z} - \vec{r}|_{r 0 0}) \times \vec{a} \, dm \, d\rho$$

$$= \int_r^1 \int \left[\begin{matrix} (\rho - r)\vec{f} + (x_0 + x)\vec{\imath} + (z_0 + z)\vec{k} \\ - (x_0 \vec{\imath} + z_0 \vec{k})|_r \end{matrix} \right] \times \vec{a} \, dm \, d\rho$$

so

$$\frac{\partial \vec{M}}{\partial r} = -(\vec{f} + (x_0 \vec{\imath} + z_0 \vec{k})') \times \int_r^1 \vec{a} \, dm \, d\rho$$

$$- \int (x \vec{\imath} + z \vec{k}) \times \vec{a} \, dm$$

$$\frac{\partial M_{rI}}{\partial r} = \int (x \vec{k} - z \vec{\imath}) \cdot \vec{a} \, dm - (z_0 \vec{\imath} - x_0 \vec{k})'' \cdot \int_r^1 (\rho - r) \vec{a} \, dm \, d\rho$$

$$- (x_0 \vec{\imath} + z_0 \vec{k})' \cdot (x_1 \vec{k}) \, \vec{f} \cdot \vec{a} \, m$$

$$- (x_0 \vec{\imath} + z_0 \vec{k})'' \cdot \int_r^1 \left[z_0 \vec{\imath} - x_0 \vec{k} - x_1 \vec{k} \right.$$

$$\left. - (z_0 \vec{\imath} - x_0 \vec{k})|_r \right] \vec{f} \cdot \vec{a} \, m \, d\rho$$

Operating with $\int_{r_{FA}}^1 \xi_k(\ldots) dr$ and changing the order of the ρ and r integrations in the second term gives

$$\int_{r_{FA}}^{1} \xi_k \frac{\partial M_{rx}}{\partial r}\, dr = \int_{r_{FA}}^{1} \vec{X}_k \cdot \vec{a}\, m\, dr$$
$$+ \int_{r_{FA}}^{1} \int \xi_k (x\vec{k} - z\vec{i} - x_I\vec{k}) \cdot \vec{a}\, dm\, dr$$
$$- \int_{r_{FA}}^{1} \xi_k (x_o\vec{i} + z_o\vec{k})' \cdot (x_I\vec{k}) \vec{j} \cdot \vec{a}\, m\, dr$$
$$- \int_{r_{FA}}^{1} \xi_k (x_o\vec{i} + z_o\vec{k})'' \cdot \int_r^1 [z_o\vec{i} - x_o\vec{k} - x_I\vec{k}$$
$$- (z_o\vec{i} - x_o\vec{k})|_r] \vec{j} \cdot \vec{a}\, m\, d\rho\, dr$$

where

$$\vec{X}_k = \xi_k x_I \vec{k} - \int_{r_{FA}}^{r} \xi_k (z_o\vec{i} - x_o\vec{k})'' (r - \rho)\, d\rho$$

Finally, introducing the torsion terms by expanding the unit vectors, the inertia force is:

$$-\int_{r_{FA}}^{1} \xi_k \frac{\partial M_{rx}}{\partial r}\, dr = \int_{r_{FA}}^{1} \xi_k \ddot{\theta} I_\theta\, dr + \Omega^2 \int_{r_{FA}}^{1} \xi_k I_\theta \cos\theta \sin\theta\, dr$$
$$+ \Omega^2 \int_{r_{FA}}^{1} \xi_k I_\theta \tilde{\theta} (\cos^2\theta - \sin^2\theta)\, dr$$
$$- \int_{r_{FA}}^{1} \vec{X}_k \cdot \vec{a}\, m\, dr$$
$$- \Omega^2 \int_{r_{FA}}^{1} \xi_k (x_o\vec{i} + z_o\vec{k})' \cdot (x_I\vec{k}) r m\, dr$$
$$- \Omega^2 \int_{r_{FA}}^{1} \xi_k (x_o\vec{i} + z_o\vec{k})'' \cdot \int_r^1 [z_o\vec{i} - x_o\vec{k} - x_I\vec{k}$$
$$- (z_o\vec{i} - x_o\vec{k})|_r] \rho m\, d\rho\, dr$$

Where $I_\theta = \int(x^2 + z^2)dm$ is the section pitch moment of inertia, about the elastic axis. In the centrifugal acceleration we have neglected a number of terms due to the blade torsion motion which are the same order as the propeller moment, but which are normally much smaller than the structural moment.

With the centrifugal tension $T = \Omega^2\int_r^1 \rho m d\rho$, the structural moment (from section 2.1.5) is :

$$
\begin{aligned}
-\int_{r_{FA}}^{1} \xi_k \frac{\partial M_{r_E}}{\partial r}\,dr = & -\int_{r_{FA}}^{1} \xi_k (GJ\theta_e')'\,dr \\
& + \int_{r_{FA}}^{1} \xi_k' k_p^2 \Omega^2 \int_r^1 \rho m\, d\rho\,(\theta_{tw}' + \theta_e')\,dr \\
& - \int_{r_{FA}}^{1} \xi_k \left[\theta_{tw}'^2 EI_{pp}\theta_e'\right]'\,dr \\
& - \int_{r_{FA}}^{1} \xi_k \left[\theta_{tw}'(EI_{xp}\vec{k} - EI_{zp}\vec{i})\cdot \right. \\
& \qquad \left. (z_0\vec{i} - x_0\vec{k})''\right]'\,dr
\end{aligned}
$$

Finally, the aerodynamic moment about the elastic axis at r is

$$
\begin{aligned}
\vec{M}_A = & \int_r^1 M_a \vec{j}\, x_s\, d\rho \\
& + \int_r^1 \left[(\rho - r)\vec{j} + (x_0\vec{i} + z_0\vec{k}) - (x_0\vec{i} + z_0\vec{k})|_r\right] \times \vec{F}_{aero}\, d\rho
\end{aligned}
$$

so

$$\frac{\partial \vec{M}_A}{\partial r} = -M_a \vec{\jmath}_{xs} - \vec{\jmath}_{xs} \times \int_r^1 (F_x \vec{i}_B + F_z \vec{k}_B)\, d\rho$$

$$\frac{\partial M_{rA}}{\partial r} = \vec{\jmath}_{xs} \cdot \frac{\partial \vec{M}_A}{\partial r} + (x_o \vec{i} + z_o \vec{k})'' \cdot \vec{M}_A$$

$$= -M_a - (z_o \vec{i} - x_o \vec{k})'' \cdot \int_r^1 (\rho - r)(F_x \vec{i}_B + F_z \vec{k}_B)\, d\rho$$

Hence

$$-\int_{r_{FA}}^1 \xi_k \frac{\partial M_{rA}}{\partial r}\, dr = \int_{r_{FA}}^1 \xi_k M_a\, dr - \int_{r_{FA}}^1 \vec{X}_{A_k} \cdot (F_x \vec{i}_B + F_z \vec{k}_B)\, dr$$

where

$$\vec{X}_{A_k} = -\int_{r_{FA}}^r \xi_k (z_o \vec{i} - x_o \vec{k})'' (r - \rho)\, d\rho$$

2.2.9 Rigid pitch equation.

The equation of motion for rigid pitch is obtained from $M_{FA_I} + M_{FA_E} - M_{FA_A}$, where

$$M_{FA} = \hat{e}_{FA} \cdot \vec{M} = \left[\vec{\jmath}_{FA} + (x_o \vec{i} + z_o \vec{k})'\big|_{r_{FA}} - \delta_{FA_4} \vec{k}_B + \delta_{FA_5} \vec{i}_B\right] \cdot \vec{M}$$

and M is the moment about the feathering axis at $r = r_{FA}$. The inertia moment is

$$\vec{M}_I = \int_{r_{FA}}^{l} \int_{section} (\vec{r}|_{rxz} - \vec{r}|_{r_{FA}00}) \times \vec{a}\, dm\, dr$$

$$= \int_{r_{FA}}^{l} \int \left[\begin{array}{c} (r-r_{FA})\vec{j} + (x_0+x)\vec{i} + (z_0+z)\vec{k} \\ - (x_0\vec{i} + z_0\vec{k})|_{r_{FA}} \end{array} \right] \times \vec{a}\, dm\, dr$$

So

$$M_{FA_I} = -\int_{r_{FA}}^{l} \vec{X}_0 \cdot \vec{a}\, m\, dr - \int_{r_{FA}}^{l} \int (x\vec{i} - x_I\vec{i} - z\vec{k}) \cdot \vec{a}\, dm\, dr$$

$$+ \int_{r_{FA}}^{l} \Big[\big(-(x_0\vec{i} + z_0\vec{k})'|_{r_{FA}} - \delta_{FA_5}\vec{i}_B + \delta_{FA_4}\vec{k}_B \big) \cdot$$

$$\big(z_0\vec{i} - x_0\vec{k} - x_I\vec{k} - (z_0\vec{i} - x_0\vec{k})|_{r_{FA}} \big)$$

$$+ \big(\delta_{FA_3}\vec{i}_B - \delta_{FA_2}\vec{k}_B \big) \cdot$$

$$\big(z_0\vec{i} - x_0\vec{k} - x_I\vec{k} \big) \Big] \vec{j} \cdot \vec{a}\, m\, dr$$

where

$$\vec{X}_0 = -\big(z_0\vec{i} - x_0\vec{k} - x_I\vec{k} \big) \cdot$$

$$+ \big((\delta_{FA_2} - \delta_{FA_4})\vec{i}_B + (\delta_{FA_3} - \delta_{FA_5})\vec{k}_B \big)(r - r_{FA})$$

$$+ (z_0\vec{i} - x_0\vec{k})|_{r_{FA}} + (z_0\vec{i} - x_0\vec{k})'|_{r_{FA}} (r - r_{FA})$$

Introducing the torsion terms by expanding the unit vectors, the inertia force is

$$M_{FA_I} = \int_{r_{FA}}^{1} \ddot{\theta} I_\theta \, dr + \Omega^2 \int_{r_{FA}}^{1} I_\theta \sin\theta \cos\theta \, dr$$
$$+ \Omega^2 \int_{r_{FA}}^{1} I_\theta \tilde{\theta} (\cos^2\theta - \sin^2\theta) dr - \int_{r_{FA}}^{1} \vec{X}_0 \cdot \vec{a}\, m \, dr$$
$$- \Omega^2 \int_{r_{FA}}^{1} \Big[\left(-(x_0\vec{i} + z_0\vec{k})'\big|_{r_{FA}} - \delta_{FA_5}\vec{i}_B + \delta_{FA_4}\vec{k}_B\right) \cdot$$
$$(z_0\vec{i} - x_0\vec{k} - x_I\vec{k} - (z_0\vec{i} - x_0\vec{k})|_{r_{FA}})$$
$$+ (\delta_{FA_3}\vec{i}_B - \delta_{FA_2}\vec{k}_B) \cdot$$
$$(z_0\vec{i} - x_0\vec{k} - x_I\vec{k}) \Big] r\, m \, dr$$

The aerodynamic moment about the feathering axis at r_{FA} is

$$\vec{M}_A = \int_{r_{FA}}^{1} M_a \vec{j}_{x_5} dr + \int_{r_{FA}}^{1} \Big[(r - r_{FA})\vec{j} + (x_0\vec{i} + z_0\vec{k})$$
$$- (x_0\vec{i} + z_0\vec{k})|_{r_{FA}} \Big] \times \vec{F}_{aero} \, dr$$

So

$$M_{FA_A} = \int_{r_{FA}}^{1} M_a \, dr - \int_{r_{FA}}^{1} (F_x\vec{i}_B + F_z\vec{k}_B) \cdot \vec{X}_{A_0} \, dr$$

where

$$\vec{X}_{A_0} = \vec{X}_0 - x_I\vec{k}$$

The aerodynamic and inertial moments about the feathering axis are reacted by moments due to the deformation of the control system. The

restoring moment acting on the blade, about the feathering axis, is $-M_{con}$. It is given by the product of the elastic deformation in the control system, and the control system stiffness K_θ:

$$M_{con} = K_\theta (p_o - p_r)$$

where the rigid pitch p_r consists of the kinematic coupling and the blade commanded pitch angle:

$$p_r = \theta_{1c}\cos\psi_m + \theta_{1s}\sin\psi_m + \Delta\theta_{govr} + \Delta\theta_{\substack{mast \\ bend}} - \sum_i K_{p_i} q_i - K_{p_G}\beta_G + (\theta_{1s}\cos\psi_m - \theta_{1c}\sin\psi_m)\psi_s + \theta_{HHC}$$

The first two terms are the lateral and longitudinal cyclic pitch control inputs; the next terms are feedback from the governor, and kinematic coupling due to the rotor mast bending. The term $-K_{p_i} q_i$ is the kinematic pitch/bending coupling due to the control system and blade root geometry, where q_i is the ith bending degree of freedom (introduced below). Similarly, Kp_G is the pitch/flap coupling for the gimbal or teeter motion. For the rigid flap motion of the blade, this coupling is usually expressed in terms of a delta-three (δ_3) angle, such that $K_p = \tan\delta_3$. Finally, the ψ_s term is the pitch change due to the rotor azimuth perturbation with a fixed swashplate. For rigid control system (K_θ very large) the rigid pitch equation of motion reduces to $p_o = p_r$. The higher harmonic control input, θ_{HHC}, is described in section 2.2.21.

Including control system damping in the restoring moment gives

$$M_{con} = K_\theta (\beta_0 - \beta_r) + C_\theta (\dot{\beta}_0 - \dot{\beta}_r)$$

where C_θ is the viscous damping coefficient. For consistency with the elastic torsion equations, the control system stiffness can be written in terms of the nonrotating natural frequency of the blade rigid pitch motion, ω_0:

$$K_\theta = \omega_0^2 \int_{r_{FA}}^1 I_\theta \, dr$$

and the damping coefficient in terms of a structural damping coefficient g_s:

$$C_\theta = g_s \omega_0 \int_{r_{FA}}^1 I_\theta \, dr$$

Then the structural pitch moment is

$$M_{FA_E} = \left(\int_{r_{FA}}^1 I_\theta \, dr \right) \left(\omega_0^2 (\beta_0 - \beta_r) + g_s \omega_0 (\dot{\beta}_0 - \dot{\beta}_r) \right)$$

2.2.10 Root force.

The net force of the mth blade acting on the hub is $\vec{F}^{(m)} - \vec{F}_A - \vec{F}_I$. The inertial force is

$$\vec{F}_I = \int_0^1 \vec{a} \, m \, dr$$

and the aerodynamic force is

$$\vec{F}_A = \int_0^1 (F_x \vec{i}_B + F_z \vec{k}_B + \tilde{F}_r \vec{j}_B)\, dr$$

The components of the total hub force in the nonrotating frame are

$$\vec{F} = \sum_{m=1}^{N} \vec{F}^{(m)} = H\vec{i}_s + Y\vec{j}_s + T\vec{k}_s$$

2.2.11 Root moment.

The net moment of the mth blade acting on the rotor hub is

$$\vec{M}^{(m)} = \vec{M}_A - \vec{M}_I$$

The inertial moment is

$$\vec{M}_I = \int_0^1 \vec{r} \times \vec{a}\, m\, dr$$

and the aerodynamic moment is

$$\vec{M}_A = \int_0^1 (F_z \vec{i}_B - F_x \vec{k}_B)\, r\, dr$$

The components of the total hub moment in the nonrotating frame are

$$\vec{M} = \sum_{m=1}^{N} \vec{M}^{(m)} = M_x \vec{i}_S + M_y \vec{j}_S - Q \vec{k}_S$$

Note that the $\vec{j}_B$ (torsion) component of the root moment in the rotating frame is neglected compared to the $\vec{i}_B$ (flap) and $\vec{k}_B$ (lag) components.

The flapwise root moment in the rotating frame gives the pitch and roll moments on the gimbal:

$$M_y = \sum_{m=1}^{N} \vec{j}_S \cdot \vec{M}^{(m)} = - \sum_{m=1}^{N} \cos\psi_m \, \vec{i}_B \cdot \vec{M}^{(m)}$$

$$M_x = \sum_{m=1}^{N} \vec{i}_S \cdot \vec{M}^{(m)} = \sum_{m=1}^{N} \sin\psi_m \, \vec{i}_B \cdot \vec{M}^{(m)}$$

The inertial moment is

$$\vec{i}_B \cdot \vec{M}_I = \int_0^1 \vec{i}_B \cdot (\vec{r} \times \vec{a}) \, m \, dr$$

and the aerodynamic moment is

$$\vec{i}_B \cdot \vec{M}_A = \int_0^1 F_z \, r \, dr$$

2.2.12 Gimbal equation.

The equations of motion for the gimbal degrees of freedom are obtained from the pitch and roll components of the total rotor hub

force. Allowing for a gimbal spring and damper in the nonrotating frame reacting the rotor moments, the equations of motion are

$$M_y + C_G \dot{\beta}_{GC} + K_G \beta_{GC} = 0$$

$$-M_x + C_G \dot{\beta}_{GS} + K_G \beta_{GS} = 0$$

The gimbal hub spring and damper constants can be written

$$K_G = \frac{2}{2} I_o \Omega^2 (\nu_G^2 - 1)$$

$$C_G = \frac{2}{2} I_b \Omega C_G^*$$

Where $I_o = \int_o^R r^2 m dr$ and I_b is a characteristic inertia of the blade, and ν_G is the rotating natural frequency of the gimbal flap motion. To allow for different longitudinal and lateral hub spring rates, ν_{GC} and ν_{GS} can be used for the β_{GC} and β_{GS} equations.

2.2.13 Teeter equation.

The equation of motion for the teeter degree of freedom of a two-bladed rotor is obtained from equilibrium of flap moments about the teeter hinge. Allowing for a teeter spring and damper in the rotating frame, the equation of motion is

$$-2M_T + C_T \dot{\beta}_T + K_T \beta_T = 0$$

C_T and K_T are the damper and spring constants about the teeter hinge. In terms of the natural frequency and damping coefficient, we may write

$$C_T = 2 I_b \Omega C_T^*$$

$$K_T = 2 I_b \Omega^2 (\nu_T^2 - 1)$$

where $I_o = \int_o^R r^2 m dr$.

The teetering moment M_T is the root flapwise moment from the two blades:

$$2 M_T = \sum_{m=1}^{2} (-1)^m \vec{i}_B \cdot \vec{M}^{(m)}$$

where again

$$\vec{i}_B \cdot \vec{M}_I = \int_0^1 \vec{i}_B \cdot (\vec{r} \times \vec{a}) m dr$$

$$\vec{i}_B \cdot \vec{M}_A = \int_0^1 F_z r dr$$

2.2.14 Modal equations.

Consider the equilibrium of the elastic, inertial, and centrifugal bending moments. From the results of section 2.2.7 these terms give the following homogenous equation for bending of the blade:

$$\left[\left(EI_{zz}\hat{i}\hat{i} + EI_{xx}\hat{k}\hat{k}\right)\left(z_0\hat{i} - x_0\hat{k}\right)''\right]''$$
$$- \Omega^2\left[\int_r^1 \rho m\, dq\, \left(z_0\hat{i} - x_0\hat{k}\right)'\right]'$$
$$- \vec{\Omega} m \vec{\Omega} \cdot \left(z_0\hat{i} - x_0\hat{k}\right)$$
$$+ m\left(z_0\hat{i} - x_0\hat{k}\right)'' = 0$$

This equation may be solved by the method of separation of variables. Writing

$$\left(z_0\hat{i} - x_0\hat{k}\right) = \vec{\eta}(r)\, e^{i\nu t}$$

it becomes

$$\left(EI\vec{\eta}''\right)'' - \Omega^2\left[\int_r^1 \rho m\, dq\, \vec{\eta}'\right]' - \vec{\Omega} m \vec{\Omega} \cdot \vec{\eta} - m\nu^2\vec{\eta} = 0$$

This is the modal equation for coupled flap/lag bending of the rotating blade. It is an ordinary differential equation for the mode shape $\eta(r)$; this mode may be interpreted as the free vibration of the rotating beam at natural frequency ν.

This modal equation, with the appropriate boundary conditions for a cantilever or hinged blade, is a proper Sturm-Liouville eigenvalue problem. It follows that there exists a series of eigensolutions $\vec{\eta}_k(r)$ of this equation, with corresponding eigenvalues ν_k^2. The eigensolutions or modes are orthogonal with weighting function m; so if $i \neq k$,

$$\int_0^1 \vec{\eta}_i \cdot \vec{\eta}_k \, m \, dr = 0$$

These modes form a complete series, so it is possible to expand the rotor blade bending as a series in the modes:

$$z_0 \vec{i} - x_0 \vec{k} = \sum_{i=1}^{\infty} q_i(t) \vec{\eta}_i(r)$$

The bending modes are normalized to unit amplitude (dimensionless) at the tip: $|\vec{\eta}(1)| = 1$.

Consider the homogenous equation for the elastic torsion motion of the nonrotating blade, i.e., the balance of structural and inertial torsion moments. The results of section 2.2.8 give

$$-(GJ\theta_e')' + I_\vartheta \ddot{\theta}_e = 0$$

The equation for the torsion motion of a rotating blade, including centrifugal forces and some additional structural torsion moments could be used instead. For the torsional stiffness typical of rotor blades these terms have little effect however, and the nonrotating torsion modes are an accurate representation of the blade motion. Solving this equation by separation of variables, we write $\theta_e = \xi(r)e^{i\omega t}$, so

$$(GJ\xi')' + I_\vartheta \omega^2 \xi = 0$$

This equation is a proper Sturm-Liouville eigenvalue problem, from which it follows that there exists a series of eigensolutions $\xi_k(r)$, and corresponding eigenvalues ω_k^2 ($k = 1 \ldots \infty$). The modes are orthogonal with weighting function I_θ, so if $i \neq k$

$$\int_{r_{FA}}^{1} \xi_k \xi_i I_\theta \, dr = 0$$

The modes form a complete set, so the elastic torsion of the blade may be expanded as a series in the modes:

$$\theta_e = \sum_{i=1}^{\infty} p_i(t) \xi_i(r)$$

These modes are the free vibration shape of the nonrotating blade in torsion, at natural frequency ω_k. The torsion modes are normalized to unity at the tip, $\xi_k(1) = 1$.

2.2.15 Modal expansion.

The bending and torsion motion of the blade is expanded as series in the normal modes. By this means the partial differential equations for the motion (in r and t) are converted to ordinary differential equations (in time only) for the degrees of freedom.

For the bending we write:

$$(z_0 \vec{\tau} - x_0 \vec{k}) = \sum_{i=1}^{\infty} q_i(t) \vec{\eta}_i(r)$$

where $\vec{\eta}_i$ are the rotating, coupled flap/lag bending modes defined above. These modes are orthogonal and satisfy the modal equation given above. The variables q_i are the degrees of freedom for the bending motion of the blade.

For the blade elastic torsion we write

$$\theta_e = \sum_{i=1}^{\infty} p_i(t)\,\xi_i(r)$$

where ξ_i are the nonrotating elastic torsion modes. These modes are orthogonal, and satisfy the modal equation given above. The variables p_i ($i \geq 1$) are the degrees of freedom for the elastic torsion motion of the blade. The degree of freedom for rigid pitch motion is $p_o = \tilde{\theta}^o = (\theta^o - \theta^c) + \theta_{con}$. For rigid rotation about the feathering axis, the mode shape is simply $\xi_o = 1$. Thus the total blade pitch perturbation is expanded as the series:

$$\tilde{\theta} = \sum_{i=0}^{\infty} p_i(t)\,\xi_i(r)$$

The total blade pitch θ (mean and perturbation) is then:

$$\theta = \theta_m + \tilde{\theta} = (\theta_{coll} + \theta_{tw}) + \sum_{i=0}^{\infty} p_i(t)\,\xi_i(r)$$

The partial differential equation for bending of the blade is obtained from $\partial^2\vec{M}^{(2)}/\partial r^2$. The ordinary differential equation for the kth bending mode (the q_k equation) is then obtained by operating with $\int_o^1 \vec{\eta}_k \cdot (\ldots)dr$ (which has already been done in section 2.2.7). The

modal equation is used to introduce the bending mode natural frequency into the equation, replacing the structural and centrifugal stiffness terms, and the orthogonality of the bending modes decouples the inertial and spring terms as follows:

$$\int_0^1 \vec{\eta}_k \cdot (z_0\vec{\imath} - x_0\vec{k})'' \, m \, dr - \Omega^2 \int_0^1 \vec{\eta}_k \cdot \left[\int_r^1 \int_0^r m \, dr \, dr \, (z_0\vec{\imath} - x_0\vec{k})' \right]' dr$$
$$- \int_0^1 \vec{\eta}_k \cdot \vec{\Omega} \, m \, \vec{\Omega} \cdot (z_0\vec{\imath} - x_0\vec{k}) \, dr$$
$$+ \int_0^1 \vec{\eta}_k \cdot \left[(EI_{xx}\vec{\imath}\vec{\imath} + EI_{zz}\vec{k}\vec{k})(z_0\vec{\imath} - x_0\vec{k})'' \right]'' dr$$

$$= \sum_{i=1}^{\infty} \ddot{q}_i \int_0^1 \vec{\eta}_k \cdot \vec{\eta}_i \, m \, dr$$
$$+ \sum_{i=1}^{\infty} q_i \int_0^1 \vec{\eta}_k \cdot \left[(EI\vec{\eta}_i'')'' - \Omega^2 \left(\int_r^1 \int_0^r m \, dr \, dr \, \vec{\eta}_i' \right)' \right.$$
$$\left. - \vec{\Omega} \, m \, \vec{\Omega} \cdot \vec{\eta}_i \right] dr$$

$$= \sum_{i=1}^{\infty} \ddot{q}_i \int_0^1 \vec{\eta}_k \cdot \vec{\eta}_i \, m \, dr + \sum_{i=1}^{\infty} q_i \nu_i^2 \int_0^1 \vec{\eta}_k \cdot \vec{\eta}_i \, m \, dr$$

$$= I_{q_k} (\ddot{q}_k + \nu_k^2 q_k)$$

where

$$I_{q_k} = \int_0^1 \eta_k^2 \, m \, dr$$

The partial differential equation for torsion of the blade is obtained from $\partial M_r / \partial r$. The ordinary differential equation for the kth torsion mode (the p_k equation is then obtained by operating with

$\int_{r_{FA}}^{1} \xi_k(\ldots)dr$ (which has already been done in section 2.2.8). The modal equation is used to replace the structural stiffness term with the torsion mode natural frequency, and the orthogonality of the modes decouples the inertial and spring terms as follows:

$$\int_{r_{FA}}^{1} \xi_k \ddot{\theta}_e I_\theta \, dr - \int_{r_{FA}}^{1} \xi_k (GJ\theta_e')' \, dr$$

$$= \sum_{i=1}^{\infty} \ddot{p}_i \int_{r_{FA}}^{1} \xi_k \xi_i I_\theta \, dr - \sum_{i=1}^{\infty} p_i \int_{r_{FA}}^{1} \xi_k (GJ\xi_i')' \, dr$$

$$= \sum_{i=1}^{\infty} \ddot{p}_i \int_{r_{FA}}^{1} \xi_k \xi_i I_\theta \, dr + \sum_{i=1}^{\infty} p_i \omega_i^2 \int_{r_{FA}}^{1} \xi_k \xi_i I_\theta \, dr$$

$$= I_{p_k} (\ddot{p}_k + \omega_k^2 p_k)$$

where

$$I_{p_k} = \int_{r_{FA}}^{1} \xi_k^2 I_\theta \, dr$$

2.2.16 Lag damper.

Articulated rotors usually have a lag damper, which has an important influence on the blade loads. Therefore a lag damping term is added to the blade bending equation of motion as follows:

$$I_{q_k}\left(\ddot{q}_k + g_s \nu_k \dot{q}_k + \nu_k^2 q_k\right) + I_b \sum_{i=1}^{\infty} g_{lag}\, \vec{k}_B \cdot \vec{\eta}_k'(e)\, \vec{k}_B \cdot \vec{\eta}_i'(e)\, \dot{q}_i + \cdots$$

where $g_{lag} = C_\zeta / I_b \Omega$ and C_ζ is the lag damping coefficient (I_b is a characteristic inertia of the blade, used to normalize the inertial constants as described in the next section). The quantity $\vec{k}_B \cdot \vec{\eta}_k'(e)$ is the slope of the kth bending mode in the lagwise direction, just outboard of the lag hinge. The manner in which the lag damping enters the equation of motion is obtained by a Galerkin or Rayleigh-Ritz analysis. The lag damper results in a bending moment at the lag hinge. Thus it is necessary to evaluate moments at the blade root by integrating along the span, which has in fact been our practice.

Note that structural damping has also been included in the bending equation, modeled as equivalent viscous damping. The structural damping coefficient g_s (equal to twice the equivalent damping ratio) in general is different for each degree of freedom. Structural damping is included in the torsion equations in a similar manner.

Consider also a nonlinear lag damper, for which the lag moment opposing the motion is proportional to $\dot{\zeta}^2$ at low lag velocity (hydraulic damping) and constant at M_{LD} for lag velocity above $\dot{\zeta}_{LD}$ (friction damping):

$$M_{lag} = \frac{M_{LD}}{I_b \Omega^2} (\operatorname{sign} \dot{\zeta}) \min\left(1, (\dot{\zeta}/\dot{\zeta}_{LD})^2\right)$$

where

$$\dot{\zeta} = \sum_{i=1}^{\infty} \vec{k}_B \cdot \vec{\eta}_i'(e)\, \dot{q}_i$$

Hence the term

$$I_b \vec{k}_B \cdot \vec{\eta}_k'(e)\,(g e_{ag} \dot{\zeta} - M_{lag})$$

is added to the right-hand side of the bending equation. Here linear damping is included on the left-hand side still, but only to improve the convergence of the solution; so the $C_\zeta \dot{\zeta}$ term must be subtracted from M_{lag}.

2.2.17 Gravitational forces.

The acceleration due to gravity is $\vec{g} = g\vec{k}_E = gR_{SF}\vec{k}_E$, where g is the gravitational constant, $\vec{k}_E$ is the vertical vector, and R_{SF} is the coordinate transformation matrix between the rotor shaft axes (S frame) and the aircraft body axes (F frame, see section 4.1.2). In terms of the aircraft trim pitch and roll angles, the vertical vector is

$$\vec{k}_E = -\sin\theta_{FT}\,\vec{i}_F + \cos\theta_{FT}\sin\phi_{FT}\,\vec{j}_F + \cos\theta_{FT}\cos\phi_{FT}\,\vec{k}_F$$

(see section 4.1). The gravitational forces acting on the rotor blades may be accounted for by substituting $\vec{a}_o - \vec{g}$ for $\vec{a}_o$, the hub linear acceleration. Thus the components of $\vec{g}$ in the S frame are subtracted from the components of the hub acceleration in the nonrotating shaft axes:

$$\vec{a}_o = \ddot{x}_{eq}\,\vec{i}_s + \ddot{y}_{eq}\,\vec{j}_s + \ddot{z}_{eq}\,\vec{k}_s$$

2.2.18 Equations of motion.

The rotor blade equations of motion are now obtained by substituting for the expansion of the bending and torsion motion as series in the modes of free vibration. Names are given to all the inertial constants. Also, the equations of motion, hub forces and moments, and inertia constants are normalized at this point in the analysis, using the characteristic blade inertia I_b, and the blade Lock number $\gamma = \rho acR^4/I_b$ is introduced. (A good choice for this characteristic inertia is $I_b = \int_o^R r^2 m dr$. Here a is the two-dimensional lift curve slope, usually taken as 5.7; and c is the blade mean chord. Both a and c are just normalization quantities; while physically appropriate values should be used, they have no effect on the actual dimensional results.) The inertia constants are divided by I_b, with this normalization denoted by a superscript "*." The blade equations of motion are divided by I_b. The hub forces and moments are divided by NI_b, so they appear in rotor coefficient form. The equations of motion for blade coupled flap/lag bending and for rigid pitch/elastic torsion take the form

$$M\begin{pmatrix}\ddot{q}_k\\ \ddot{p}_k\end{pmatrix} + C\begin{pmatrix}\dot{q}_k\\ \dot{p}_k\end{pmatrix} + K\begin{pmatrix}q_k\\ p_k\end{pmatrix} = F + \frac{\gamma}{ac}\begin{pmatrix}M_{q_k}\\ M_{p_k}\end{pmatrix}_{aero}$$

The coefficient matrices M, C, and K contain terms that are functions of the blade bending deflection q_j. The generalized force F is a linear function of the gimbal and rotational speed degrees of

freedom, and of the shaft motion components. Some coefficients of the terms in F are functions of the blade bending deflection. In addition, F contains the nonlinear lag damper moment in the bending equation, and the control moment (produced by p_r) in the pitch equation. The time-average of the bending deflection is used in the coefficient matrices, so the inertia terms in these equations are nonlinear but time-invariant (except for the shaft motion terms, where the transformation from the nonrotating to the rotating frame introduces $\sin\psi_m$ and $\cos\psi_m$ factors). The aerodynamic forces produce periodic coefficients in forward flight. In detail, the equations of motion are thus:

$$
\begin{aligned}
&-I^*_{q_k}\left(\ddot{q}_k + g_s \nu_k \dot{q}_k + \nu_k^2 q_k\right) \\
&\quad + 2\sum_i \left(I^*_{q_k \dot{q}_i} + \sum_j I^*_{q_k \dot{q}_i q_j}\, q_j\right)\dot{q}_i \\
&\quad + \sum_i g_{ey}\, \vec{k}_B \cdot \vec{\eta}'_k(e)\, \vec{k}_B \cdot \vec{\eta}'_i(e)\, \dot{q}_i \\
&- \sum_i \left(S^*_{q_k \ddot{\beta}_i} + \sum_j S^*_{q_k \ddot{\beta}_i q_j}\, q_j\right)\ddot{\beta}_i - \sum_i \left(S^*_{q_k \beta_i} + \sum_j S^*_{q_k \beta_i q_j}\, q_j\right)\beta_i \\
&+ I^*_{q_k \alpha} \cdot \vec{k}_B \left(\ddot{\psi}_s + \ddot{\alpha}_z\right) + I^*_{q_k \alpha} \cdot \vec{i}_B \left(\ddot{\beta}_G + \beta_G\right) \\
&\quad + 2\left(I^*_{q_k \dot{\psi}} + \sum_j I^*_{q_k \dot{\psi} q_j}\, q_j\right)\left(\dot{\psi}_s + \dot{\alpha}_z\right) \\
&\quad - \left(I^*_{q_k \dot{\beta}} + \sum_j I^*_{q_k \dot{\beta} q_j}\, q_j\right)\left(\ddot{\theta}_G - \theta_G + 2\dot{\beta}_G\right) \\
&\quad + S^*_{q_k} \cdot \vec{i}_B\, \ddot{z}_h - S^*_{q_k} \cdot \vec{k}_B \left(\ddot{x}_h \sin\psi_m - \ddot{y}_h \cos\psi_m\right) \\
&\quad + I^*_{q_k \alpha} \cdot \vec{i}_B \left(\left(\ddot{\alpha}_x + 2\dot{\alpha}_y\right)\sin\psi_m - \left(\ddot{\alpha}_y - 2\dot{\alpha}_x\right)\cos\psi_m\right) \\
&= I^*_{q_{k0}} + \vec{k}_B \cdot \vec{\eta}'_k(e)\left(g_{ey}\zeta - M_{ey}\right) + \gamma \frac{M_{q_k}^{aero}}{ac}
\end{aligned}
$$

$$I^*_{\rho_K}\left(\ddot{\rho}_K + q_S\omega_K\dot{\rho}_K + \omega_K^2\rho_K\right) + \sum_i I^*_{\rho_K\rho_i}\rho_i + \sum_i I^*_{\rho_K\ddot{\rho}_i}\ddot{\rho}_i$$
$$- \sum_i\left(S^*_{\rho_K\ddot{q}_i} + \sum_j S^*_{\rho_K\ddot{q}_i q_j}q_j\right)\ddot{q}_i - \sum_i\left(S^*_{\rho_K q_i} + \sum_j S^*_{\rho_K q_i q_j}q_j\right)q_i$$
$$+ \left(I^*_{\rho_K\alpha} + \sum_j I^*_{\rho_K\alpha q_j}q_j\right)\cdot\left[\vec{\iota}_B\left(\ddot{\psi}_S + \ddot{\alpha}_z\right) - \vec{k}_B\left(\ddot{\beta}_G + \beta_G\right)\right.$$
$$\left. - \vec{k}_B\left(\left(\ddot{\alpha}_x + 2\dot{\alpha}_y\right)\sin\psi_m - \left(\ddot{\alpha}_y - 2\dot{\alpha}_x\right)\cos\psi_m\right)\right]$$
$$+ \left(S^*_{\rho_K} + \sum_j S^*_{\rho_K q_j}q_j\right)\cdot\left[-\vec{k}_B\ddot{z}_h - \vec{\iota}_B\left(\ddot{x}_h\sin\psi_m - \ddot{y}_h\cos\psi_m\right)\right]$$
$$= I^*_{\rho_K o} + I^*_{\rho o}\xi_K(r_{FA})\left(\omega_o^2\rho_r + \omega_o q_S\dot{\rho}_r\right) + \gamma\frac{M_{\rho_K aero}}{ac}$$

where

$$\beta_G = \beta_{oc}\cos\psi + \beta_{os}\sin\psi + \beta_T$$
$$\ddot{\beta}_G - \beta_G + 2\dot{\beta}_G = -\ddot{\beta}_{oc}\sin\psi + \ddot{\beta}_{os}\cos\psi + 2\dot{\beta}_T$$

The inertia constants are defined in section 2.2.19.

In rotor coefficient form, the rotor hub force and moment are

$$\frac{\vec{F}}{\rho\Omega^2 R_b} = \gamma\left(\frac{C_H}{\sigma a}\vec{\iota}_S + \frac{C_Y}{\sigma a}\vec{\jmath}_S + \frac{C_T}{\sigma a}\vec{k}_S\right)$$
$$= \frac{1}{2}\sum_{m=1}^{2}\frac{\vec{F}^{(m)}}{R_b}$$
$$= \frac{1}{2}\sum_{m=1}^{2}\gamma\left(\frac{C_{fx}}{\sigma a}\vec{\iota}_B + \frac{C_{fy}}{\sigma a}\vec{\jmath}_B + \frac{C_{fz}}{\sigma a}\vec{k}_B\right)$$

$$\frac{\vec{M}}{2H_b} = \gamma\left(\frac{C_{mx}}{\sigma a}\vec{i}_s + \frac{C_{my}}{\sigma a}\vec{j}_s - \frac{C_Q}{\sigma a}\vec{k}_s\right)$$

$$= \frac{1}{2}\sum_{m=1}^{2N}\frac{\vec{M}^{(m)}}{H_b}$$

$$= \frac{1}{2}\sum_{m=1}^{2N}\gamma\left(\frac{C_{mx}}{\sigma a}\vec{i}_B - \frac{C_{mz}}{\sigma a}\vec{k}_B\right)$$

or

$$\begin{bmatrix} \gamma\frac{H_{1c}}{\sigma a} \\ \gamma\frac{H_{1s}}{\sigma a} \\ \gamma\frac{C_T}{\sigma a} \\ \gamma\frac{C_{Mx}}{\sigma a} \\ \gamma\frac{C_{My}}{\sigma a} \\ -\gamma\frac{C_Q}{\sigma a} \end{bmatrix} = \frac{1}{2}\sum_{m=1}^{2N}\begin{bmatrix} \sin\psi_m\ \gamma\frac{C_{fx}}{\sigma a} + \cos\psi_m\ \gamma\frac{C_{fz}}{\sigma a} \\ -\cos\psi_m\ \gamma\frac{C_{fx}}{\sigma a} + \sin\psi_m\ \gamma\frac{C_{fz}}{\sigma a} \\ \gamma\frac{C_{fz}}{\sigma a} \\ \sin\psi_m\ \gamma\frac{C_{mx}}{\sigma a} \\ -\cos\psi_m\ \gamma\frac{C_{mx}}{\sigma a} \\ -\gamma\frac{C_{mz}}{\sigma a} \end{bmatrix}$$

So the blade root force and moment are resolved in the nonrotating frame, and then filtered by the hub operator $\frac{1}{N}\sum_{m=1}^{N}$. The harmonics of the forces in the nonrotating frame can be related directly to the harmonics of the rotating forces; the solution of the support equations of motion requires, however, the hub forces and moment in the time domain.

The components of the blade root force and moment in the rotating frame are as follows:

$$\gamma \frac{C_{fx}}{\sigma a} = \left(\gamma \frac{C_{fx}}{\sigma a}\right)_{aero} - M_b^* \left(\ddot{x}_m \sin\psi_m - \ddot{y}_m \cos\psi_m\right) + S_b^* \left(\ddot{\alpha}_z + \ddot{\psi}_s\right) - S_b^* \psi_s + \sum_i S_{fi}^* \cdot \vec{E}_B \left(\ddot{q}_i - q_i\right) + I_{fx}^*$$

$$\gamma \frac{C_{fr}}{\sigma a} = \left(\gamma \frac{C_{fr}}{\sigma a}\right)_{aero} - M_b^* \left(\ddot{x}_m \cos\psi_m + \ddot{y}_m \sin\psi_m\right) + 2 S_b^* \left(\dot{\alpha}_z + \dot{\psi}_s\right) + \sum_i 2 S_{qi}^* \cdot \vec{E}_B \dot{q}_i + S_b^*$$

$$\gamma \frac{C_{fz}}{\sigma a} = \left(\gamma \frac{C_{fz}}{\sigma a}\right)_{aero} - M_b^* \ddot{z}_m - S_b^* \left(\left(\ddot{\alpha}_x + 2\dot{\alpha}_y\right)\sin\psi_m - \left(\ddot{\alpha}_y - 2\dot{\alpha}_x\right)\cos\psi_m\right) - S_b^* \ddot{\beta}_G - \sum_i S_{qi}^* \cdot \vec{E}_B \ddot{q}_i$$

$$\gamma \frac{C_{m_x}}{\sigma a} = \left(\gamma \frac{C_{m_x}}{\sigma a}\right)_{aero} - S_b^* \ddot{z}_B$$
$$- I_0^* \left((\ddot{\alpha}_x + 2\dot{\alpha}_y)\sin\Psi_m - (\ddot{\alpha}_y - 2\dot{\alpha}_x)\cos\Psi_m\right)$$
$$- I_0^* (\ddot{\beta}_G + \beta_G) - \sum_i I_{q_i \alpha}^* \cdot \vec{r}_B (\ddot{q}_i + q_i)$$
$$- 2 \sum_i \left(I_{q_i \dot{q}_i}^* + \sum_j I_{q_i \dot{q}_i q_j}^* q_j\right) \cdot \vec{r}_B \dot{q}_i$$
$$- 2 \left(I_{q_i \dot{\psi}}^* + \sum_j I_{q_i \dot{\psi} q_j}^* q_j\right)(\dot{\psi}_s + \dot{\alpha}_z)$$
$$+ \sum_i \left(S_{q_i \ddot{\rho}_i}^* + \sum_j S_{q_i \ddot{\rho}_i q_j}^* q_j\right) \cdot \vec{r}_B (\ddot{\rho}_i + \rho_i)$$
$$- I_{m_x 0}^*$$

$$\gamma \frac{C_{m_z}}{\sigma a} = \left(\gamma \frac{C_{m_z}}{\sigma a}\right)_{aero} - S_b^* (\ddot{x}_B \sin\Psi_m - \ddot{y}_B \cos\Psi_m)$$
$$+ I_0^* (\ddot{\alpha}_z + \ddot{\psi}_s) + \sum_i I_{q_i \alpha}^* \cdot \vec{r}_B \ddot{q}_i$$
$$+ 2 \sum_i \left(I_{q_i \dot{q}_i}^* + \sum_j I_{q_i \dot{q}_i q_j}^* q_j\right) \cdot \vec{r}_B \dot{q}_i$$
$$- \left(I_{q_i \dot{\beta}}^* + \sum_j I_{q_i \dot{\beta} q_j}^* q_j\right)(\ddot{\theta}_G - \theta_G + 2\dot{\beta}_G)$$
$$- \sum_i \left(S_{q_i \dot{\rho}_i}^* + \sum_j S_{q_i \dot{\rho}_i q_j}^* q_j\right) \cdot \vec{r}_B \ddot{\rho}_i$$

The inertia constants are defined in section 2.2.19. So the blade root forces take the form

$$\frac{\gamma}{\sigma a}\begin{pmatrix} C_t \\ C_m \end{pmatrix} = G + \frac{\gamma}{ac}\begin{pmatrix} C_f \\ C_m \end{pmatrix}_{aero}$$

The inertia term G is a linear function of the blade bending, torsion, gimbal, and rotational speed degrees of freedom; and of the shaft motion components. Some of the coefficients in G are functions of the blade bending deflections (nonlinear terms).

Note that the total hub forces due to the rotor linear acceleration are simply

$$\Delta\begin{pmatrix} \gamma \frac{C_H}{\sigma a} \\ \gamma \frac{C_Y}{\sigma a} \\ \gamma \frac{C_T}{\sigma a} \end{pmatrix} = \frac{1}{2}\sum_{m=1}^{2} M_b^* \begin{pmatrix} -\ddot{x}_h \\ -\ddot{y}_h \\ -\ddot{z}_h \end{pmatrix}$$

where M_b^* is the normalized mass of a blade. Since the rotor mass is included in the aircraft mass, these hub linear acceleration terms should be omitted when C_{fx}, C_{fr}, and C_{fz} are evaluated for the aircraft equations of motion. These terms should be retained, however, when evaluating the actual blade root forces.

Similarly, since the rotor weight is included in the aircraft weight, the corresponding gravitational force terms are omitted.

Dividing by $(1/2)NI_b$, the gimbal equations of motion are

$$\gamma \frac{2C_{My}}{\sigma a} + C_G^* \dot{\beta}_{GC} + I_0^* (\nu_{GC}^2 - 1)\beta_{GC} = 0$$

$$-\gamma \frac{2C_{Mx}}{\sigma a} + C_G^* \dot{\beta}_{GS} + I_0^* (\nu_{GS}^2 - 1)\beta_{GS} = 0$$

where

$$\gamma \frac{2C_{My}}{\sigma a} = -\frac{1}{2} \sum_{m=1}^{2} 2 \cos\psi_m \gamma \frac{C_{mx}}{\sigma a}$$

$$\gamma \frac{2C_{Mx}}{\sigma a} = \frac{1}{2} \sum_{m=1}^{2} 2 \sin\psi_m \gamma \frac{C_{mx}}{\sigma a}$$

Dividing by NI_b, the teetering equation of motion is

$$-\gamma \frac{C_{MT}}{\sigma a} + C_T^* \dot{\beta}_T + I_0^* (\nu_T^2 - 1)\beta_T = 0$$

where

$$\gamma \frac{C_{MT}}{\sigma a} = \frac{1}{2} \sum_{m=1}^{2} (-1)^m \gamma \frac{C_{mx}}{\sigma a}$$

The equation of motion for the rotor speed perturbation $\dot{\psi}_s$ is obtained from equilibrium of the rotor torque. The speed perturbations of the two rotors are coupled by the helicopter transmission, so the equation of motion for $\dot{\psi}_s$ is best derived with the body equations.

Finally, the aerodynamic forces required for the blade equations of motion and the rotor hub reactions are as follows:

$$\frac{M_{\beta_k}^{aero}}{ac} = \int_0^1 \vec{\eta}_k \cdot \left(\frac{F_z}{ac} \vec{i}_B - \frac{F_x}{ac} \vec{k}_B \right) dr$$

$$\frac{M_{\rho_k}^{aero}}{ac} = \int_{r_{FA}}^1 \eta_k \frac{M_a}{ac} dr - \int_{r_{FA}}^1 \vec{X}_{A_k} \cdot \left(\frac{F_x}{ac} \vec{i}_B + \frac{F_z}{ac} \vec{k}_B \right) dr$$

$$\left(\frac{C_{mx}}{\sigma a} \right)_{aero} = \int_0^1 \frac{F_z}{ac} r \, dr$$

$$\left(\frac{C_{mz}}{\sigma a} \right)_{aero} = \int_0^1 \frac{F_x}{ac} r \, dr$$

$$\left(\frac{C_{fx}}{\sigma a} \right)_{aero} = \int_0^1 \frac{F_x}{ac} \, dr$$

$$\left(\frac{C_{fr}}{\sigma a} \right)_{aero} = \int_0^1 \frac{\tilde{F}_r}{ac} \, dr$$

$$\left(\frac{C_{fz}}{ac} \right)_{aero} = \int_0^1 \frac{f_z}{ac} \, dr$$

2.2.19 Inertial constants.

The normalized inertial constants required for the blade equations of motions and the hub reactions given above are defined as follows:

$$M_b^* = \frac{1}{I_b}\int_0^1 m\,dr$$

$$S_b^* = \frac{1}{I_b}\int_0^1 r\,m\,dr$$

$$I_b^* = \frac{1}{I_b}\int_0^1 r^2\,m\,dr$$

$$I_{q_k}^* = \frac{1}{I_b}\int_0^1 \eta_k^2\,m\,dr$$

$$S_{q_k}^* = \frac{1}{I_b}\int_0^1 \vec{\eta}_k\,m\,dr$$

$$I_{q_k}^*\alpha = \frac{1}{I_b}\int_0^1 \vec{\eta}_k\,r\,m\,dr$$

$$I_{q_k\dot{q}_i}^* = \frac{1}{I_b}\Bigg\{ \int_0^1 \vec{\eta}_k\cdot(\vec{\jmath}\times\vec{\eta}_i)(\delta_{FA_1}-\delta_{FA_2})\,m\,dr$$
$$-\vec{\eta}_k\cdot\vec{k}\,(x_c-x_I)\vec{k}_B\cdot\vec{\eta}_i\,m\,|_{r=1}$$
$$+\int_0^1 \vec{\eta}_k'\cdot\vec{k}\,(-x_I)\vec{k}_B\cdot\vec{\eta}_i\,m\,dr$$
$$+\vec{\eta}_k'\cdot\vec{k}\,x_c|_{r=e}\int_0^1 \vec{k}_B\cdot\vec{\eta}_i\,m\,dr$$
$$+\int_0^1 x_c\vec{k}\cdot\Big(\vec{\eta}_k''\int_r^1 \vec{k}_B\cdot\vec{\eta}_i\,m\,d\xi\Big)\,dr$$
$$+\vec{\eta}_k(r_{FA})\cdot(\delta_{FA_2}\vec{i}_B+\delta_{FA_3}\vec{k}_B)\int_{r_{FA}}^1 \vec{k}_B\cdot\vec{\eta}_i\,m\,dr$$
$$-\vec{\eta}_i'\cdot\vec{k}\,x_I|_{r=e}\int_0^1 \vec{k}_B\cdot\vec{\eta}_k\,m\,dr$$
$$-\int_0^1 x_I\vec{k}\cdot\Big(\vec{\eta}_i''\int_r^1 \vec{k}_B\cdot\vec{\eta}_k\,m\,d\xi-\vec{\eta}_i'\vec{k}_B\cdot\vec{\eta}_k\,m\Big)\,dr$$

$$I^*_{q_k \dot{q}_i \dot{q}_j} = \frac{1}{I_b} \begin{cases} -\int_0^1 \vec{\eta}_k \cdot \vec{i}_B \int_0^r \vec{\eta}_i' \cdot \vec{\eta}_j' \, d\xi \, m \, dr \\ +\int_0^1 \vec{\eta}_i \cdot \vec{i}_B \int_0^r \vec{\eta}_k' \cdot \vec{\eta}_j' \, d\xi \, m \, dr \end{cases}$$

$$I^*_{q_k \dot{\psi}} = \frac{1}{I_b} \begin{cases} \int_0^1 \vec{\eta}_k \cdot [\vec{i}_B \, r(\delta_{FA_1} - \delta_{FA_2}) \\ \qquad -\vec{k}_B (x_{FA} + r_{FA}\delta_{FA_3} - x_I \cos\theta)] m \, dr \\ -\vec{\eta}_k \cdot \vec{k} \, (x_c - x_I) m \big|_{r=1} \\ +\int_0^1 \vec{\eta}_k' \cdot \vec{k} \, (-x_I) r \, m \, dr \\ +\vec{\eta}_k' \cdot \vec{k} \, x_c \big|_{r=e} \int_0^1 r m \, dr \\ +\int_0^1 x_c \vec{k} \cdot (\vec{\eta}_k'' \int_r^1 \xi m \, d\xi) \, dr \\ +\vec{\eta}_k(r_{FA}) \cdot (\delta_{FA_2} \vec{i}_B + \delta_{FA_3} \vec{k}_B) \int_{r_{FA}}^1 r m \, dr \end{cases}$$

$$I^*_{q_k \dot{\psi} \dot{q}_j} = \frac{1}{I_b} \begin{cases} -\int_0^1 \vec{\eta}_k \cdot \vec{i}_B \, \vec{\eta}_j \cdot \vec{k}_B \, m \, dr \\ +\int_0^1 r \int_0^r \vec{\eta}_k' \cdot \vec{\eta}_j' \, d\xi \, m \, dr \end{cases}$$

$$I^*_{q_k \dot{\beta}} = \frac{1}{I_b} \int_0^1 \vec{\eta}_k \cdot \vec{i}_B \, (-z_{FA} + r\delta_{FA_1} - (r - r_{FA})\delta_{FA_2} - x_I \delta_{m\theta}) m \, dr$$

$$I^*_{q_k \dot{\beta} \dot{q}_j} = \frac{1}{I_b} \int_0^1 \vec{\eta}_k \cdot \vec{k}_B \, \vec{\eta}_j \cdot \vec{i}_B \, m \, dr$$

$$S^{*}_{q_k \ddot{p}_i} = \frac{1}{I_b} \int_{r_{FA}}^{1} \vec{\eta}_k \cdot [\xi_i x_I \vec{\tau} + \xi_i(r_{FA})(r - r_{FA})(\vec{\tau}_B(\delta_{FA_3} - \delta_{FA_5}) - \vec{k}_B(\delta_{FA_2} - \delta_{FA_4}))] m \, dr$$

$$S^{*}_{q_k \ddot{p}_i q_j} = \frac{1}{I_b} \int_{r_{FA}}^{1} \vec{\eta}_k \cdot (\vec{\jmath} \times \vec{X}_{ij}) m \, dr$$

$$S^{*}_{q_k p_i} = \frac{1}{I_b} \left\{ \begin{aligned} & - \int_0^1 \vec{\eta}_k \cdot [(EI_{xp}\vec{k} - EI_{zp}\vec{\tau})\Theta_{tw}' \xi_i']'' \, dr \\ & + \int_{r_{FA}}^{1} \vec{\eta}_k \cdot \vec{k}_B [\xi_i x_I \sin\theta + \xi_i(r_{FA})(r - r_{FA})(\delta_{FA_2} - \delta_{FA_4})] m \, dr \\ & - \int_{r_{FA}}^{1} \xi_i(r_{FA})(r - r_{FA})[\vec{\tau}_B(\delta_{FA_3} - \delta_{FA_5}) - \vec{k}_B(\delta_{FA_2} - \delta_{FA_4})] \cdot \\ & \quad [\vec{\eta}_k'' \int_r^1 \rho m \, d\rho - \vec{\eta}_k' r m] \, dr \\ & + \vec{\eta}_k \cdot \vec{\tau} \, \xi_i (x_c - x_I) m \big|_{r=1} \\ & - \int_{r_{FA}}^{1} \vec{\eta}_k \cdot \vec{\tau} \, \xi_i (-x_I) r m \, dr \\ & - (\xi_i \vec{\eta}_k' \cdot \vec{\tau} \, x_c)\big|_{r=r_{FA}} \int_{r_{FA}}^{1} r m \, dr \\ & - \int_{r_{FA}}^{1} \xi_i x_c \vec{\tau} \cdot (\vec{\eta}_k'' \int_r^1 \rho m \, d\rho) \, dr \end{aligned} \right.$$

$$S^{*}_{q_k p_i q_j} = \frac{1}{I_b} \left\{ \begin{aligned} & \int_{r_{FA}}^{1} \vec{\eta}_k \cdot \vec{k}_B \, \vec{\tau}_B \cdot \vec{X}_{ij} \, m \, dr \\ & - \int_{r_{FA}}^{1} (\vec{\jmath} \times \vec{X}_{ij}) \cdot (\vec{\eta}_k'' \int_r^1 \rho m \, d\rho - \vec{\eta}_k' r m) \, dr \end{aligned} \right.$$

$$I^*_{q_k o} = \frac{1}{I_b}\Bigg\{ -\int_0^1 \vec{\eta}_k \cdot \Big[\vec{k}_B\,(-x_{FA} - r_{FA}\delta_{FA_3} + x_I\cos\theta) + \vec{\imath}_B\, r\,(\delta_{FA_1} - \delta_{FA_2})\Big] m\,dr$$
$$+ \vec{\eta}_k \cdot \vec{k}\,(x_c - x_I) m\big|_{r=1}$$
$$- \int_0^1 \vec{\eta}_k' \cdot \vec{k}\,(-x_I)\, r m\,dr$$
$$- \vec{\eta}_k' \cdot \vec{k}\, x_c\big|_{r=c} \int_0^1 r m\,dr$$
$$- \int_0^1 x_c \vec{k} \cdot \Big(\vec{\eta}_k'' \int_r^1 \rho m\,d\rho\Big)\,dr$$
$$- \vec{\eta}_k(r_{FA}) \cdot (\delta_{FA_2}\vec{\imath}_B + \delta_{FA_3}\vec{k}_B) \int_{r_{FA}}^1 r m\,dr$$

$$I^*_{q_o \dot{q}_i} = \frac{1}{I_b}\Bigg\{ \vec{\imath}_B \int_0^1 \vec{k}_B \cdot \vec{\eta}_i\,(-z_{FA} + r\delta_{FA_1} - (r - r_{FA})\delta_{FA_2} - x_I\sin\theta) m\,dr$$
$$+ \vec{k}_B \int_0^1 \vec{k}_B \cdot \vec{\eta}_i\,(x_{FA} + r_{FA}\delta_{FA_3} - x_I\cos\theta) m\,dr$$
$$- \vec{k}_B \int_0^1 r\,\vec{\eta}_i \cdot \vec{\imath}_B\,(\delta_{FA_1} - \delta_{FA_2}) m\,dr$$
$$- \vec{k}_B\,\vec{\eta}_i' \cdot \vec{k}\, x_I\big|_{r=c} \int_0^1 r m\,dr$$
$$- \vec{k}_B \int_0^1 x_I \vec{k} \cdot \Big(\vec{\eta}_i'' \int_r^1 \rho m\,d\rho - \vec{\eta}_i' r m\Big)\,dr$$

$$I^*_{q_o \dot{q}_i \dot{q}_j} = \frac{1}{I_b}\int_0^1 \Big[\vec{k}_B \cdot \vec{\eta}_i\,\vec{\eta}_j\, m + \vec{k}_B\,\vec{\eta}_j \cdot \Big(\vec{\eta}_i'' \int_r^1 \rho m\,d\rho - \vec{\eta}_i' r m\Big)\Big] dr$$

$$I^*_{q_o \dot{\psi}} = \frac{1}{I_b}\int_0^1 r(-z_{FA} + r\delta_{FA_1} - (r - r_{FA})\delta_{FA_2} - x_I\delta\sin\theta) m\,dr$$

$$I^*_{q_o \dot{\psi} q_j} = \frac{1}{I_b}\int_0^1 r\,\vec{\imath}_B \cdot \vec{\eta}_j\, m\,dr$$

$$I^*_{q_0\dot{\beta}} = \frac{1}{I_b}\int_0^1 r\left(-z_{FA}+r\delta_{FA_1}-(r-r_{FA})\delta_{FA_2}-x_I\delta_{m\theta}\right)m\,dr$$

$$I^*_{q_0\dot{\beta}q_j} = \frac{1}{I_b}\int_0^1 r\,\vec{\tau}_B\cdot\vec{\eta}_j\,m\,dr$$

$$S^*_{q_0\ddot{\beta}_i} = \frac{1}{I_b}\int_{r_{FA}}^1\left[\xi_i x_I\vec{\tau}+\xi_i(r_{FA})(r-r_{FA})\left[\vec{\tau}_B(\delta_{FA_3}-\delta_{FA_5})-\vec{k}_B(\delta_{FA_2}-\delta_{FA_4})\right]\right]r\,m\,dr$$

$$S^*_{q_0\ddot{\beta}_iq_i} = \frac{1}{I_b}\int_{r_{FA}}^1 \vec{J}\times\vec{X}_{ij}\,r\,m\,dr$$

$$I^*_{f_{x^0}} = \frac{1}{I_b}\int_0^1\left(-x_{FA}+(r-r_{FA})\delta_{FA_3}+x_I\cos\theta\right)m\,dr$$

$$I^*_{m_{x^0}} = \frac{1}{I_b}\int_0^1 r\left(-z_{FA}+r\delta_{FA_1}-(r-r_{FA})\delta_{FA_2}-x_I\sin\theta\right)m\,dr$$

$$I^*_{\rho_k} = \frac{1}{I_b}\int_{r_{FA}}^1 \xi_k^2\,I_\theta\,dr$$

$$I^*_{\rho_k\alpha} = \frac{1}{I_b}\int_{r_{FA}}^1\left[\xi_k x_I\vec{k}+\xi_k(r_{FA})(r-r_{FA})\left(\vec{\tau}_B(\delta_{FA_2}-\delta_{FA_4})+\vec{k}_B(\delta_{FA_3}-\delta_{FA_5})\right)\right]r\,m\,dr$$

$$I^*_{\rho_k\alpha q_j} = \frac{1}{I_b}\int_{r_{FA}}^1 \vec{X}_{kj}\,r\,m\,dr$$

$$S^*_{\rho_k} = \frac{1}{I_b}\int_{r_{FA}}^1\left[\xi_k x_I\vec{k}+\xi_k(r_{FA})(r-r_{FA})\left(\vec{\tau}_B(\delta_{FA_2}-\delta_{FA_4})+\vec{k}_B(\delta_{FA_3}-\delta_{FA_5})\right)\right]m\,dr$$

$$S^*_{\rho_kq_j} = \frac{1}{I_b}\int_{r_{FA}}^1 \vec{X}_{kj}\,m\,dr$$

$$I^*_{p_k \ddot{p}_i} = \frac{1}{I_b} \int_{r_{FA}}^{1} \Big[(\xi_k - \xi_k(r_{FA}))\,\xi_i(r_{FA}) + (\xi_i - \xi_i(r_{FA}))\,\xi_k(r_{FA}) \Big] I_\theta \, dr$$

$$I^*_{p_k p_i} = \frac{1}{I_b} \left\{ \begin{array}{l} \int_{r_{FA}}^{1} \xi_k \xi_i \, I_\theta (\cos^2\theta - \sin^2\theta)\, dr \\ + \int_{r_{FA}}^{1} \xi_k' k_p^2 \int_r^1 \rho m \, dr \, \xi_i \, dr \\ - \int_{r_{FA}}^{1} (\xi_k - \xi_k(r_{FA})) \left[\theta_{tw}'^2 E I_{pp} \xi_i' \right]' dr \end{array} \right.$$

$$S^*_{p_k \ddot{q}_i} = \frac{1}{I_b} \int_{r_{FA}}^{1} \vec{\eta}_i \cdot \Big[\xi_k x_I \vec{L} + \xi_k(r_{FA})(r - r_{FA}) \big(\vec{L}_B (\delta_{FA_3} - \delta_{FA_5}) - (\delta_{FA_2} - \delta_{FA_4}) \vec{L}_B \big) \Big] m \, dr$$

$$S^*_{p_k \ddot{q}_i q_j} = \frac{1}{I_b} \int_{r_{FA}}^{1} \vec{X}_{kj} \cdot (-\vec{J} \times \vec{\eta}_i)\, m \, dr$$

$$I^*_{p_k 0} = \frac{1}{I_b} \left\{ \begin{array}{l} - \int_{r_{FA}}^{1} \xi_k I_\theta \cos\theta \sin\theta \, dr \\ + \int_{r_{FA}}^{1} \xi_k x_I \cos\theta \, r (\delta_{FA_1} - \delta_{FA_2}) m \, dr \\ - \int_{r_{FA}}^{1} \xi_k' k_p^2 \int_r^1 \rho m \, dr \, \theta_{tw}' \, dr \end{array} \right.$$

$$S^{*}_{pkqi} = \frac{1}{H_b}\left\{\begin{array}{l}
\int_{r_{FA}}^{1} \xi_k \left[\theta'_{tw}\left(EI_{xp}\vec{k} - EI_{zp}\vec{\tau}\right)\cdot\vec{\eta}_i''\right]' dr \\
+ \int_{r_{FA}}^{1} \xi_k \vec{\eta}_i' \cdot \vec{\tau}\, x_I\, r\, m\, dr \\
- \int_{r_{FA}}^{1} \xi_k \vec{\eta}_i'' \cdot \int_r^1 x_I\left(\vec{\tau}_B r\cos\theta - \vec{k}_B \rho \sin\theta\right) m\, d\rho\, dr \\
+ \int_{r_{FA}}^{1} \xi_k\, x_I \sin\theta\, \vec{k}_B \cdot \vec{\eta}_i\, m\, dr \\
- \int_{r_{FA}}^{1} \xi_k \vec{\eta}_i'' \cdot \int_r^1 \left(\vec{\tau}_B\left(x_{FA} + r_{FA}\delta_{FA_3}\right)\right. \\
\qquad \left. + \vec{k}_B \rho\left(\delta_{FA_1} - \delta_{FA_2}\right)\right)(\rho - r) m\, d\rho\, dr
\end{array}\right.$$

$$S^{*}_{pkqiqj} = \frac{1}{H_b}\left\{\begin{array}{l}
\int_{r_{FA}}^{1} \xi_k \vec{\eta}_i'' \cdot \vec{\tau}_B \int_r^1 \left(r\vec{k}_B \cdot \vec{\eta}_j\right. \\
\qquad \left. - \rho\, \vec{k}_B \cdot \vec{\eta}_j(r)\right) m\, d\rho\, dr \\
- \int_{r_{FA}}^{1} \xi_k \vec{\eta}_i'' \cdot \vec{k}_B \int_r^1 \left(\vec{\tau}_B \cdot \vec{\eta}_j\right. \\
\qquad \left. - \vec{\tau}_B \cdot \vec{\eta}_j(r)\right) \rho m\, d\rho\, dr
\end{array}\right.$$

$$
\begin{aligned}
S^{*}_{p_o q_i} = \frac{1}{I_b} \Bigg\{ & \int_{r_{FA}}^{1} \vec{\iota} \cdot \vec{\eta}_i'(r_{FA})\, x_I\, r\, m\, dr \\
& + \int_{r_{FA}}^{1} \vec{k}_B \cdot \vec{\eta}_i \; x_I \sin\theta \; m\, dr \\
& + \int_{r_{FA}}^{1} \vec{\iota}_B \cdot \vec{\eta}_i \; (\delta_{FA_3} - \delta_{FA_5})\, r\, m\, dr \\
& - \int_{r_{FA}}^{1} \vec{k}_B \cdot \vec{\eta}_i \; (\delta_{FA_2} - \delta_{FA_4})\, r_{FA}\, m\, dr \\
& - \int_{r_{FA}}^{1} (\delta_{FA_4} \vec{k}_B - \delta_{FA_5} \vec{\iota}_B) \cdot \vec{\eta}_i(r_{FA})\, r\, m\, dr \\
& + \int_{r_{FA}}^{1} \Big[(-\vec{\eta}_i + \vec{\eta}_i(r_{FA}) + \vec{\eta}_i'(r_{FA})(r - r_{FA})) \cdot \\
& \qquad (\vec{\iota}_B (x_{FA} + r_{FA}\delta_{FA_3} - x_I \cos\theta) \\
& \qquad + \vec{k}_B (\delta_{FA_1} - \delta_{FA_2})\, r) \Big]\, m\, dr
\end{aligned}
$$

$$
\begin{aligned}
S^{*}_{p_o q_i q_j} = \frac{1}{I_b} \Bigg\{ & \int_{r_{FA}}^{1} \vec{\iota}_B \cdot (-\vec{\eta}_i + \vec{\eta}_i(r_{FA}) - \vec{\eta}_i'(r_{FA})\, r_{FA}) \\
& \qquad \vec{k}_B \cdot \vec{\eta}_j \; m\, dr \\
& + \int_{r_{FA}}^{1} \vec{\iota}_B \cdot \vec{\eta}_i'(r_{FA})\, \vec{k}_B \cdot \vec{\eta}_j(r_{FA})\, r\, m\, dr \\
& + \int_{r_{FA}}^{1} \vec{k}_B \cdot \vec{\eta}_i'(r_{FA}) (\vec{\iota}_B \cdot \vec{\eta}_j \\
& \qquad - \vec{\iota}_B \cdot \vec{\eta}_j(r_{FA}))\, r\, m\, dr
\end{aligned}
$$

Note that $S^{*}_{p_k q_i q_j}$ and $S^{*}_{p_o q_i q_j}$ are evaluated in symmetric form.

We have used the relation

$$\vec{X}_k = \xi_k x_I \vec{k} - \int_{r_{FA}}^{r} \xi_k (z_o \vec{\imath} - x_o \vec{k})'' (r-\rho)\, d\rho$$

$$= \xi_k x_I \vec{k} - \sum_j q_j \int_{r_{FA}}^{r} \xi_k \vec{\eta}_j'' (r-\rho)\, d\rho$$

$$= \xi_k x_I \vec{k} - \sum_j q_j \left[\xi_k \vec{\eta}_j - \int_{r_{FA}}^{r} \xi_k' (\vec{\eta}_j + \vec{\eta}_j' (r-\rho))\, d\rho \right]$$

for elastic torsion ($k \geq 1$), and

$$\vec{X}_o = -(z_o \vec{\imath} - x_o \vec{k} - x_I \vec{k})$$
$$+ ((\delta_{FA_2} - \delta_{FA_4}) \vec{\imath}_B + (\delta_{FA_3} - \delta_{FA_5}) \vec{k}_B)(r - r_{FA})$$
$$+ (z_o \vec{\imath} - x_o \vec{k})|_{r_{FA}} + (z_o \vec{\imath} - x_o \vec{k})'|_{r_{FA}} (r - r_{FA})$$

$$= x_I \vec{k} + ((\delta_{FA_2} - \delta_{FA_4}) \vec{\imath}_B + (\delta_{FA_3} - \delta_{FA_5}) \vec{k}_B)(r - r_{FA})$$
$$- \sum_j q_j \left[\vec{\eta}_j - \vec{\eta}_j (r_{FA}) - \vec{\eta}_j' (r_{FA})(r - r_{FA}) \right]$$

for rigid pitch ($k = 0$); or for $k \geq 0$

$$\vec{X}_k = \xi_k x_I \vec{k} + \xi_k (r_{FA}) ((\delta_{FA_2} - \delta_{FA_4}) \vec{\imath}_B + (\delta_{FA_3} - \delta_{FA_5}) \vec{k}_B)(r - r_{FA})$$
$$+ \sum_j \vec{X}_{kj} q_j$$

where

$$\vec{\chi}_{kj} = \begin{cases} -\xi_k \vec{\eta}_j + \int_{r_{FA}}^{r} \xi_k' \left(\vec{\eta}_j + \vec{\eta}_j' (r-\rho) \right) d\rho & k \geq 1 \\ -\vec{\eta}_j + \vec{\eta}_j (r_{FA}) + \vec{\eta}_j'(r_{FA})(r-r_{FA}) & k = 0 \end{cases}$$

Also then,

$$\vec{\chi}_{Ak} = \xi_k(r_{FA}) \left((\delta_{FA_2} - \delta_{FA_4}) \vec{i}_B + (\delta_{FA_3} - \delta_{FA_5}) \vec{k}_B \right) (r - r_{FA}) + \sum_j \vec{\chi}_{kj} q_j$$

for the aerodynamic coefficients.

The blade inertial and structural properties (m, x_I, x_C, EI, I_θ, GJ, etc.) will be defined at a series of radial stations, r_i, with linear variation between.

The blade bending and torsion mode shapes will be evaluated at M+1 equidistant radial stations: $r = 0, \Delta r, \ldots M\Delta r$ where $\Delta r = 1/M$. The inertial coefficients are then calculated by numerical integration (using the trapezoidal rule) over these radial stations.

A concentrated mass at the blade tip ($r = 1$) will be allowed, with a corresponding center of gravity offset. This tip mass contributes an equivalent distributed mass, as follows:

$$m_e(1) = m(1) + M_{tip} \frac{2}{\Delta r R}$$

$$x_{Ie}(1) = \frac{1}{m_e(1)} \left(x_I(1) m(1) + x_{I_{tip}} M_{tip} \frac{2}{\Delta r R} \right)$$

$$I_{\theta e}(1) = I_\theta(1) + x^2_{I_{tip}} M_{tip} \frac{2R}{\Delta r}$$

where Δr is the segment length for numeral integration. Alternatively, the tip mass can be included in the distributed mass directly (to avoid difficulties with the $(x_C - x_I)m$ terms evaluated at $r = 1$).

The total mass of the blade can be specified, so

$$M_b^* = \frac{R^2}{I_b} M_{blade}$$

Alternatively, a point mass can be added at $r = 0$ to account for the weight of the hub.

The inertial coefficients have been integrated by parts as required to eliminate radial derivatives of x_I and x_C. This operation introduces terms proportional to x_I and x_C evaluated at $r = 1$ (for example, in $I^*_{q_k o}$), which appear as point loads at the blade tip. These terms can be a source of incorrect blade motion and loads, attributed to the lack of validity of beam theory at the tip. The difficulty is handled in the analysis by setting x_C equal to x_I at the tip. A linear transition is introduced between the actual x_C (used inboard of $r = .94$), and $x_C = x_I$ (used outboard of $r = .98$).

2.2.20 Aerodynamic spring and damping.

To improve the convergence of the solution for the blade motion, spring and damping forces should be included on the left-hand side of the equations of motion. The required perturbation aerodynamic forces are:

$$\Delta \frac{M_{q_k}}{ac}_{aero} = \sum_i M_{q_k \dot{q}_i} \dot{q}_i + M_{q_k \dot{\beta}} \dot{\beta}_G + \sum_i M_{q_k p_i} p_i$$

$$\Delta \frac{M_{p_k}}{ac}_{aero} = \sum_i M_{p_k \dot{q}_i} \dot{q}_i + M_{p_k \dot{\beta}} \dot{\beta}_G + \sum_i M_{p_k \dot{p}_i} \dot{p}_i + \sum_i M_{p_k p_i} p_i$$

$$\Delta \left(\frac{C_{mx}}{\sigma a}\right)_{aero} = \sum_i M_{\dot{q}_i} \dot{q}_i + M_{\dot{\beta}} \dot{\beta}_G + \sum_i M_{p_i} p_i$$

$$\Delta \left(\frac{C_\omega}{\sigma a}\right)_{aero} = Q_\zeta \ddot{\psi}_s + Q_\theta \Delta\theta_{gov}$$

These terms will be added to both sides of the equations of motion, so they need not be exact values of the damping and spring forces, but only close enough to achieve good convergence (see section 5.1). The damping terms are needed to avoid unrealistic resonant amplification of the harmonics near the natural frequency, and the spring terms help obtain the correct phase of the response quickly. Following the aeroelastic analysis (section 6.1.4), the following expressions are used for the aerodynamic coefficients.

$$M_{q_k \dot{q}_i} = \int_0^1 \Big\{ \vec{\eta}_k \cdot \vec{\iota}_B \; \vec{\eta}_i \cdot \vec{\iota}_B \left[-\tfrac{1}{2} \tfrac{r^2}{U} \right] + \vec{\eta}_k \cdot \vec{\iota}_B \; \vec{\eta}_i \cdot \vec{k}_B \left[\tfrac{r}{U} \left(\tfrac{\lambda}{2} + r \tfrac{6C_T}{\sigma a} \right) \right]$$
$$+ \vec{\eta}_k \cdot \vec{k}_B \; \vec{\eta}_i \cdot \vec{\iota}_B \left[\tfrac{r}{U} \left(\tfrac{\lambda}{2} - \tfrac{r}{2} \tfrac{6C_T}{\sigma a} \right) \right]$$
$$- \vec{\eta}_k \cdot \vec{k}_B \; \vec{\eta}_i \cdot \vec{k}_B \left[\tfrac{1}{2} \tfrac{\lambda}{U} \left(\lambda + r \tfrac{6C_T}{\sigma a} \right) + \tfrac{C_d}{a} r \right] \Big\} \tfrac{c}{c_m} dr$$

$$M_{q_k \dot{\beta}} = \int_0^1 r \Big\{ \vec{\eta}_k \cdot \vec{\iota}_B \left[-\tfrac{1}{2} \tfrac{r^2}{U} \right]$$
$$+ \vec{\eta}_k \cdot \vec{k}_B \left[\tfrac{r}{U} \left(\tfrac{\lambda}{2} - \tfrac{r}{2} \tfrac{6C_T}{\sigma a} \right) \right] \Big\} \tfrac{c}{c_m} dr$$

$$M_{q_k \beta_i} = \int_0^1 \xi_i \Big\{ \vec{\eta}_k \cdot \vec{\iota}_B \left[\tfrac{1}{2} U r \right] - \vec{\eta}_k \cdot \vec{k}_B \left[\tfrac{1}{2} U \lambda \right] \Big\} \tfrac{c}{c_m} dr$$

$$M_{\dot{q}_i} = \int_0^1 r \Big\{ \vec{\eta}_i \cdot \vec{\iota}_B \left[-\tfrac{1}{2} \tfrac{r^2}{U} \right]$$
$$+ \vec{\eta}_i \cdot \vec{k}_B \left[\tfrac{r}{U} \left(\tfrac{\lambda}{2} + r \tfrac{6C_T}{\sigma a} \right) \right] \Big\} \tfrac{c}{c_m} dr$$

$$M_{\dot{\beta}} = \int_0^1 \left[-\tfrac{1}{2} \tfrac{r^4}{U} \right] \tfrac{c}{c_m} dr$$

$$M_{\beta_i} = \int_0^1 \xi_i \, r \left[\tfrac{1}{2} U r \right] \tfrac{c}{c_m} dr$$

$$Q_\xi = \int_0^1 \left[\tfrac{1}{2} \tfrac{\lambda}{U} \left(\lambda + r \tfrac{6C_T}{\sigma a} \right) + \tfrac{C_d}{a} r \right] r^2 \tfrac{c}{c_m} dr$$

$$Q_\theta = \int_0^1 \tfrac{1}{2} U \lambda r \tfrac{c}{c_m} dr$$

$$M_{p_k \dot{q}_i} = \int_{r_{FA}}^1 x_A \xi_k \Big\{ \vec{\eta}_i \cdot \vec{\iota}_B \left[\tfrac{1}{2} r \right] - \vec{\eta}_i \cdot \vec{k}_B \left[\tfrac{\lambda}{2} + r \tfrac{6C_T}{\sigma a} \right] \Big\} \tfrac{c}{c_m} dr$$

$$M_{p_k \dot{\beta}} = \int_{r_{FA}}^1 x_A \xi_k \left\{ \tfrac{1}{2} r^2 \right\} \tfrac{c}{c_m} dr$$

$$M_{P_K \dot{P}_i} = -\int_{c_{FA}}^{1} \zeta_k \zeta_i \frac{c^2}{16} r \left[1 + 6\frac{x_A}{c} + 8\left(\frac{x_A}{c}\right)^2\right] \frac{c}{c_m} dr$$

$$M_{P_K P_i} = -\int_{c_{FA}}^{1} \zeta_k \zeta_i \left[x_A \frac{1}{2} U^2\right] \frac{c}{c_m} dr$$

where

$$U = (r^2 + \lambda^2)^{\frac{1}{2}}$$

$$\lambda = \lambda_i + \mu_z$$

2.2.21 Higher harmonic control.

Higher harmonic control is included in the commanded blade pitch (see section 2.2.9). Both rotating and nonrotating frame input are considered. The rotating frame input consists of sine and cosine components of n/rev harmonics (n greater than or equal to 2; the 1/rev input is not used, as it is equivalent to existing cyclic control). The nonrotating frame input consists of sine and cosine components of pN/rev collective, longitudinal cyclic, and lateral cyclic controls (p greater than or equal to 1, N = number of blades). With three blades, the same rotating frame blade pitch motion can be produced using either rotating frame or nonrotating frame input. The HHC input is a steady state, prescribed control.

For rotating frame HHC input, the blade pitch increment (in the rotating frame) is:

$$\theta_{HHC} = \theta_{nc}\, C + \theta_{ns}\, S$$

where $C = \cos n(\psi + \psi_s)$ and $S = \sin n(\psi + \psi_s)$. The corresponding rates of change are then:

$$\dot{\theta}_{HHC} = (-\theta_{nc}\, S + \theta_{ns}\, C)\, n\, (1 + \dot{\psi}_s)$$

$$\ddot{\theta}_{HHC} = (-\theta_{nc}\, C - \theta_{ns}\, S)\, n^2\, (1 + \dot{\psi}_s)^2 + (-\theta_{nc}\, S + \theta_{ns}\, C)\, n\, \ddot{\psi}_s$$

For nonrotating frame HHC input, the blade pitch increment is:

$$\begin{aligned}\theta_{HHC} &= (\theta_{0pc} + \theta_{cpc}\, C + \theta_{spc}\, S)\, C_p \\ &\quad + (\theta_{0ps} + \theta_{cps}\, C + \theta_{sps}\, S)\, S_p \\ &= \theta_c\, C_p + \theta_s\, S_p\end{aligned}$$

where $C = \cos(\psi + \psi_s)$ and $S = \sin(\psi + \psi_s)$; $C_p = \cos pN(\psi + \psi_s)$ and $S_p = \sin pN(\psi + \psi_s)$. The corresponding rates of change are:

$$\dot{\theta}_{HHC} = (-\theta_c\, S + \theta_s\, C)\, pN\, (1 + \dot{\psi}_s) + (\dot{\theta}_c\, C + \dot{\theta}_s\, S)$$

$$\ddot{\theta}_{HHC} = (-\theta_c C - \theta_s S)(pN)^2 (1 + \dot{\psi}_s)^2 + (-\theta_c S + \theta_s C)\, pN \ddot{\psi}_s + (-\dot{\theta}_c S + \dot{\theta}_s C)\, 2pN (1 + \dot{\psi}_s) + (\ddot{\theta}_c C + \ddot{\theta}_s S)$$

$$\dot{\theta}_c = (-\theta_{cpc} S + \theta_{spc} C)(1 + \dot{\psi}_s)$$

$$\dot{\theta}_s = (-\theta_{cps} S + \theta_{sps} C)(1 + \dot{\psi}_s)$$

$$\ddot{\theta}_c = (-\theta_{cpc} C - \theta_{spc} S)(1 + \dot{\psi}_s)^2 + (-\theta_{cpc} S + \theta_{spc} C)\ddot{\psi}_s$$

$$\ddot{\theta}_s = (-\theta_{cps} C - \theta_{sps} S)(1 + \dot{\psi}_s) + (-\theta_{cps} S + \theta_{sps} C)\ddot{\psi}_s$$

2.3 Blade Bending and Torsion Modes

The requirements for the blade mode calculation procedure are that it be numerically efficient, and that it work well for blades with rapid radial variations in mass and stiffness distributions. There are numerous satisfactory mode shape calculation methods available. In the present analysis the modal equations are solved by a modified Galerkin method (ref. 20) that works better for large radial variations of the blade properties than does the Rayleigh-Ritz method in standard form.

The option to read the bending modes from an external source is also available in the analysis. These modes would be calculated by some other program, for the required collective and rotor speed. If this option is used, care must be taken that the modes used are consistent with the present analysis; specifically, the bending modes are the solution of the linear equation for coupled flap/lag bending (torsion

modes are separate). Because of collective pitch variations during trim, requiring updates of the bending modes, it is best to use the internal calculation if possible.

2.3.1 Coupled bending modes of a rotating blade.

Equilibrium of the elastic, inertial, and centrifugal bending moments on the blade gives the differential equation for the coupled flap/lag bending of the rotating blade (see section 2.2.14). For free vibration--the homogenous equation with harmonic motion at the natural frequency ν--we obtain the modal equation for bending of the blade:

$$(EI\vec{\eta}'')'' - \Omega^2\left(\int_r^R \rho m\, d\xi\, \vec{\eta}'\right)' - m\vec{\Omega}\,\vec{\Omega}\cdot\vec{\eta} - m\nu^2\vec{\eta} = 0$$

Here $\vec{\eta}(r) = z_o\vec{i} - x_o\vec{k}$ is the bending deflection (mode shape),

$$\begin{aligned} EI &= EI_{zz}\,\vec{\tau}\vec{\tau} + EI_{xx}\,\vec{k}\vec{k} \\ &= (EI_{zz}\cos^2\theta + EI_{xx}\sin^2\theta)\,\vec{\tau}_B\vec{\tau}_B \\ &\quad + (EI_{zz}\sin^2\theta + EI_{xx}\cos^2\theta)\,\vec{k}_B\vec{k}_B \\ &\quad + (EI_{xx} - EI_{zz})\sin\theta\cos\theta\,(\vec{\tau}_B\vec{k}_B + \vec{k}_B\vec{\tau}_B) \end{aligned}$$

is the bending stiffness dyadic, $\vec{\Omega} = \Omega\vec{k}_B$ is the rotor rotational speed, and ν is the natural frequency of the mode. The boundary conditions are as follows:

(a) at the tip (r = R): $EI\vec{\eta}'' = (EI\vec{\eta}'')' = 0$

(b) and at the root (r = e): $\vec{\eta} = \vec{\eta}' = 0$ for a cantilever blade; $\vec{\eta} = 0$ and $EI\vec{\eta}'' = K_s\vec{\eta}'$ for an articulated blade.

The root boundary condition is applied at the offset r = e to allow for hinge offset of an articulated rotor, or a very stiff hub of a hingeless rotor. Different offsets can be used for the out-of-plane and in-plane motion (e_f and e_l). With the hinges at an angle θ_h from the hub plane, the hinge spring dyadic is

$$k_s = K_F \vec{\imath}_h \vec{\imath}_h + K_L \vec{k}_h \vec{k}_h$$

where $\vec{\imath}_h = \vec{\imath}_B \cos\theta_h - \vec{k}_B \sin\theta_h$, and $\vec{k}_h = \vec{\imath}_B \sin\theta_h + \vec{k}_B \cos\theta_h$; K_F is the flap spring constant; and K_L is the lag spring constant.

It can be desirable to be able to use for the pitch angle of the structural principal axes the effective angle $\theta_e = \Re\theta$. The parameter $\Re$ is zero for no structural coupling of the in-plane and out-of-plane blade motion; and $\Re = 1$ for complete coupling. For the hinge spring pitch angle θ_h, an input value can be used; or $\Re\theta_{75}$ can be used; or more generally $\theta_h = \Re\theta_{75} + \theta_{ho}$.

Four possible root boundary conditions will be considered:

(a) cantilever in flap and lag;

(b) hinged in flap and lag;

(c) hinged in flap and cantilever in lag (coning hub); and

(d) cantilever in flap and hinged in lag (lagging hub).

The last two cases could be simulated using a very stiff lag or flap spring, but such an approach can lead to numerical problems. These four cases are accommodated by selecting Galerkin functions with the appropriate boundary conditions. Note that for the hinged blade options (b, c, and d above), the flap and/or lag hinges are rotated by the angle θ_h relative to the hub plane.

This differential equation is an eigenvalue problem for the mode shapes η and the natural frequencies ν. The equation and boundary conditions constitute a proper Sturm-Liouville problem. It follows that

a series of eigensolutions or modes $\eta_i(r)$ exists with corresponding natural frequencies ν_i; and that the modes are orthogonal with weight m. Hence if $i \neq k$,

$$\int_0^R \vec{\eta}_i \cdot \vec{\eta}_k \, m \, dr = 0$$

The frequencies satisfy the energy balance relation:

$$\nu^2 = \frac{\vec{\eta}'(e) K_s \vec{\eta}'(e) + \int_e^R \left[\vec{\eta}'' EI \vec{\eta}'' + \Omega^2 \int_r^R \rho m \, dr \, \eta'^2 - m (\vec{\Omega} \cdot \vec{\eta})^2 \right] dr}{\int_e^R \eta^2 m \, dr}$$

The modal equation will be solved by a modified Galerkin method following reference 20. This approach works better for large radial variations in the bending stiffness than does the Rayleigh-Ritz method in standard form. Write the differential equation as

$$\vec{M}'' - \left(\int_r^1 \rho m \, dr \, \vec{\eta}' \right)' - m \vec{k}_B \vec{k}_B \cdot \vec{\eta} - m \nu^2 \vec{\eta} = 0$$

$$\vec{\eta}'' - \left(\frac{EI}{\Omega^2 R^4} \right)^{-1} \vec{M} = 0$$

with boundary conditions $\vec{M} = \vec{M}' = 0$ at r = 1, and $\vec{\eta} = 0$ and $\vec{M} = K_s \vec{\eta}'$ at r = e. The deflection and moment are expanded as finite series in the functions $\vec{f}_i$ and $\vec{g}_i$

$$\vec{\gamma} = \sum c_i \vec{f}_i(r)$$

$$\vec{M} = \sum d_i \vec{g}_i(r)$$

It is required that each of the functions $\vec{f}_i$ and $\vec{g}_i$ satisfy the boundary conditions; then, the sum automatically does. Since a finite series is required for numerical calculations, this will be an approximate solution. For best numerical accuracy, the functions $\vec{f}_i$ and $\vec{g}_i$ must be chosen so that the lower frequency modes can be well represented by the truncated series. Substituting these series into the differential equations and operating with

$$\int_e^1 \vec{f}_k \cdot (\cdots)\, dr \quad \text{and} \quad \int_e^1 \vec{g}_k \cdot (\cdots)\, dr$$

gives

$$\sum d_i \int_e^1 \vec{f}_k \vec{g}_i''\, dr$$

$$- \sum c_i \int_e^1 \left[\left(\int_r^1 \rho m \vec{f}_i' \right)' \cdot \vec{f}_k + m \vec{k}_B \cdot \vec{f}_i \vec{k}_B \cdot \vec{f}_k + m\nu^2 \vec{f}_k \cdot \vec{f}_i \right] dr = 0$$

$$\sum c_i \int_e^1 \vec{g}_k \cdot \vec{f}_i''\, dr - \sum d_i \int_e^1 \vec{g}_k \left(\frac{EI}{\Omega^2 R^4} \right)^{-1} \vec{g}_i\, dr = 0$$

Integrating by parts and applying the boundary conditions gives

$$\int_e^1 \left(\int_r^1 \rho m \vec{f}_i' \right)' \cdot \vec{f}_k\, dr = - \int_e^1 \int_r^1 \rho m \vec{f}_i' \cdot \vec{f}_k'\, dr$$

$$\int_e^1 \vec{f}_k \cdot \vec{M}'' \, dr = \vec{f}_k \cdot \vec{M}' \Big|_e^1 - \vec{f}_k' \cdot \vec{M} \Big|_e^1 + \int_e^1 \vec{f}_k'' \cdot \vec{M} \, dr$$

$$= \vec{f}_k \cdot \frac{k_s}{\Omega^2 R^3} \vec{\eta}' \Big|_e + \int_e^1 \vec{f}_k'' \cdot \vec{M} \, dr$$

so the first equation becomes

$$\varepsilon d_i \int_e^1 \vec{f}_k'' \cdot \vec{g}_i \, dr + \varepsilon c_i \left(\vec{f}_k' \frac{k_s}{\Omega^2 R^3} \vec{f}_i' \right) \Big|_e$$

$$+ \varepsilon c_i \int_e^1 \left[\int_r^1 \rho m \, dr \, \vec{f}_i' \cdot \vec{f}_k' - m \vec{r}_B \cdot \vec{f}_k \vec{r}_B \cdot \vec{f}_i - m \nu^2 \vec{f}_k \cdot \vec{f}_i \right] dr$$

$$= 0$$

Hence the problem reduces to a set of algebraic equations for $\vec{c} = [c_i]$ and $\vec{d} = [d_i]$

$$C \vec{d} + D \vec{c} - \nu^2 B \vec{c} = 0$$

$$C^T \vec{c} - A \vec{d} = 0$$

or

$$(C A^{-1} C^T + D - \nu^2 B) \vec{c} = 0$$

For simplicity the functions used for the moment expansion are $\vec{g}_i = \vec{f}_i''$. Then, the coefficients of the matrices are

$$A_{ki} = \int_e \vec{f}_k'' \left(\frac{EI}{\Omega^2 R^4}\right)^{-1} \vec{f}_i'' \, dr$$

$$B_{ki} = \int_e m \vec{f}_k \cdot \vec{f}_i \, dr$$

$$C_{ki} = \int_e \vec{f}_k'' \cdot \vec{f}_i'' \, dr$$

$$D_{ki} = \vec{f}_k'(e) \frac{k_s}{\Omega^2 R^3} \vec{f}_i'(e) + \int_e \left[\int_r^1 \rho m \, dq \; \vec{f}_i' \cdot \vec{f}_k' - m \vec{r}_B \cdot \vec{f}_k \, \vec{r}_B \cdot \vec{f}_i \right] dr$$

Note that using $\vec{g}_i = EI\vec{f}_i''$ would give $C = C^T = A$, hence $\vec{d} = \vec{c}$, and this solution would reduce to the standard Galerkin form. For the rigid function of a hinged blade ($f'' = 0$), the corresponding row and column of A (and C) are zero; hence the diagonal element of A is set to 1.0 for this function, in order to invert A without first deleting the zero row and column.

The eigenvalues of the matrix $B^{-1}(CA^{-1}C^T + D)$ are the natural frequencies ν^2 of the coupled bending vibration of the blade; and the corresponding eigenvectors $\vec{c}$ give the mode shape $\vec{\eta}$. As a final step, the modes are normalized to unity at the tip: $|\vec{\eta}(1)| = 1$. This modified Galerkin approach equivalently replaces the Rayleigh energy expression for the natural frequency (given above) by

$$\nu^2 = \frac{\vec{\eta}'(e) K_s \vec{\eta}'(e) + \int_e^R \left[2\vec{\eta}'' \cdot \vec{M} - \vec{M} E I^{-1} \vec{M} + \Omega^2 \int_r^R \rho m \, dy \, \eta'^2 - m(\vec{\Omega} \cdot \vec{\eta})^2 \right] dr}{\int_e^R \eta^2 m \, dr}$$

The blade nonrotating modes and frequencies can be obtained using

$$A_{ki} = \int_e^1 \vec{f}_k'' \left(\frac{EI}{R^4} \right)^{-1} \vec{f}_i'' \, dr$$

$$D_{ki} = \vec{f}_k(e) \frac{K_s}{R^3} \vec{f}_i(e)$$

A convenient set of functions for $\vec{f}_i$ are the bending mode shapes of a nonrotating, uniform beam. Such functions will satisfy the required boundary conditions, and furthermore are orthogonal (necessary for good numerical conditioning of the Galerkin solution). Let w_n be the series of eigensolutions of the differential equation $d^4w/dx^4 = a^4w$ with appropriate boundary conditions. Using these functions for both out-of-plane and in-plane deflections gives

$$\vec{f}_1(r) = w_1(x) \vec{\iota}_R$$

$$\vec{f}_2(r) = w_1(x) \vec{\kappa}_R$$

$$\vec{f}_3(r) = w_2(x) \vec{\iota}_R$$

$$\vec{f}_4(r) = w_2(x) \vec{\kappa}_R$$

etc., where $x = (r - e)/(1 - e)$. Hence in the sum $\vec{\eta} = \Sigma c_i \vec{f}_i$, the out-of-plane ($\vec{i}_h$) displacement comes from $\vec{f}_i$ with i odd, and the in-plane ($\vec{k}_h$) displacement comes from $\vec{f}_i$ with i even. Note that these functions are defined relative to the hinge axes, which are rotated by the angle θ_h from the hub plane (B axes). Then, $\vec{f}_k \cdot \vec{f}_i$ (and so the elements of the B and C matrices, and the centrifugal stiffening part of the D matrix) is nonzero only if k + i is even, i.e., if both k and i are odd or both are even. The products involving the stiffness dyadic, $\vec{f}_k "E \vec{f}_i"$ (the elements of the A matrix), take the form:

$$\vec{f}_k'' \begin{bmatrix} E_{11} & E_{12} \\ E_{21} & E_{22} \end{bmatrix} \vec{f}_i'' = f_k'' f_i'' E_{mn}$$

where m = 1 (or 2) if k is odd (or even), and n = 1 (or 2) if i is odd (or even). The spring stiffening part of the D matrix has a flap spring contribution if both k and i are odd, or a lag spring contribution if both k and i are even. The derivatives of f are obtained using

$$\frac{d}{dr} = \frac{1}{1-e} \frac{d}{dx}$$

Care must be taken in evaluating x, since the slope of a hinged blade (or curvature of a cantilever blade) is nonzero at the hinge (x = 0), but zero inboard.

For a uniform hinged blade, the nonrotating mode shapes are:

$$w = \frac{\sinh a \sin ax + \sin a \sinh ax}{2 \sin a \sinh a}$$

where a is the solution of

$$\tan a = \tanh a$$

(so a approaches $(n - 3/4)\pi$ for large n). The first mode (a = 0) is w = x. For a uniform cantilever blade, the nonrotating mode shapes are

$$w = \frac{(\sin a - \sinh a)(\sinh ax - \sin ax)}{2 \sin a \sinh a} + \frac{(\cos a + \cosh a)(\cosh ax - \cos ax)}{2 \sin a \sinh a}$$

where a is the solution of

$$\cos a \cosh a = -1$$

(so a approaches $(n - \frac{1}{2})\pi$ for large n). The values of a for the lowest modes are given in the table below.

Mode	Hinged	Cantilever
1	0	1.875104069
2	3.926602313	4.694091134
3	7.068582747	7.854757439
4	10.21017612	10.99554074
5	13.35176878	14.13716839
6	16.49336143	17.27875953
7	19.63495409	20.42035225
8	22.77654674	23.56194490
9	25.91813940	26.70353756
10	29.05973205	29.84513021

The uniform hinged blade modes are then

$$w = A \sinh ax + B \sin ax$$

where $w(0) = w''(0) = w''(1) = 0$, $w(1) = 1$, and the hinge slope is $w'(0) = a(A + B)$. The constants are given in the table below.

Mode	A	B	w'(0)
1			1.0
2	-.7073812	.01971819	-2.700181
3	.7071073	8.514396E-4	5.004265
4	-.7071068	3.679399E-5	-7.219309
5	.7071068	1.590012E-6	9.441147
6	-.7071068	6.871066E-8	-11.66257
7	.7071068	2.969257E-9	13.88401
8	-.7071068	1.283132E-10	-16.10545
9	.7071068	5.544917E-12	18.32689
10	-.7071068	2.396176E-13	-20.54833

The uniform cantilever blade modes are

$$w = C(\sinh ax - \sin ax) + D(\cosh ax - \cos ax)$$

where $w(0) = w'(0) = w''(1) = 0$, $w(1) = 1$, and the root curvature is $w''(0) = a^2(2D)$. The constants are given in the table below.

Mode	C	D
1	-.3670478	.5
2	.5092337	-.5
3	-.4996123	.5
4	.5000168	-.5
5	-.4999993	.5
6	.5	-.5
7	-.5	.5
8	.5	-.5
9	-.5	.5
10	.5	-.5

The centrifugal force is required for the bending mode calculation. With the section mass defined at radial stations r_i (i = 1 to M), the centrifugal force is

$$\int_r^1 \rho m \, dy = \int_r^{r_I} \rho m \, dy + \sum_{i=I+1}^{M} \int_{r_{i-1}}^{r_i} \rho m \, dy$$

where $r_{I-1} \le r < r_I$. Then for linear variation of the section mass between the stations r_i, the integrals can be evaluated as follows:

$$\int_r^1 \zeta m \, d\zeta = \frac{1}{r_I - r_{I-1}} \left[m_{I-1} \frac{1}{6} (r - r_I)^2 (2r + r_I) - m_I \frac{1}{6} (r - r_{I-1})^2 (2r + r_{I-1}) \right] + \sum_{i=I}^{M-1} m_i \left[f(r_i, r_{i-1}) - f(r_i, r_{i+1}) \right] + m_M f(r_M, r_{M-1})$$

where

$$f(x,y) = \int_y^x \frac{\zeta - y}{x - y} \zeta \, d\zeta = \frac{1}{6} (x - y)(2x + y)$$

2.3.2 Articulated blade modes.

For an articulated blade the modal differential equation need not be solved if the higher bending modes are not required. Rigid flap and lag motion about the hinges gives the two lowest frequency modes:

$$\vec{\eta}_1 = \vec{\eta}_{lag} = - \left(\frac{r - e_l}{1 - e_l} \right) \vec{k}_B$$

$$\vec{\eta}_2 = \vec{\eta}_{flap} = \left(\frac{r - e_f}{1 - e_f} \right) \vec{k}_B$$

Note that separate hinge offsets may be used for flap and lag motion. The natural frequencies are obtained directly from the energy relation, as follows:

$$\nu_{lag}^2 = \frac{e_l \int_{e_l}^1 \eta m \, dr + k_L / \Omega^2 R^3}{(1-e_l) \int_{e_l}^1 \eta^2 m \, dr}$$

$$\nu_{flap}^2 = 1 + \frac{e_f \int_{e_f}^1 \eta m \, dr + k_F / \Omega^2 R^3}{(1-e_f) \int_{e_f}^1 \eta^2 m \, dr}$$

2.3.3 Torsion modes of a nonrotating blade.

Equilibrium of the elastic and inertial torsion moments (see section 2.2.14) gives the modal equation

$$(GJ\}')' + I_\theta \omega^2 \} = 0$$

with the boundary conditions $\xi' = 0$ at the tip ($r = R$) and $\xi = 0$ at the root ($r = r_{FA}$). The modes are orthogonal with weight I_θ, so if $i \neq k$

$$\int_{r_{FA}}^R \}_i \}_k I_\theta \, dr = 0$$

The frequencies satisfy the relation

$$\omega^2 = \frac{\int_{r_{FA}}^R GJ \}'^2 \, dr}{\int_{r_{FA}}^R I_\theta \}^2 \, dr}$$

These are the nonrotating torsion modes, so the solution is independent of the rotor speed or collective pitch.

The equation is solved by the modified Galerkin method, as described in detail above for the bending modes. Write the differential equation as

$$-T' - I_\theta \omega^2 \zeta$$

$$\zeta' - \left(\frac{GJ}{\Omega^2 R^2}\right)^{-1} T = 0$$

Expand the torsion deflection and torsion moment as series:

$$\zeta = \sum c_i f_i(r)$$

$$T = \sum d_i g_i(r)$$

where the functions f_i and g_i satisfy the boundary conditions on ζ and T. Substitute these series in the equations, operate with

$$\int_{r_{FA}}^{1} f_k(\ldots)\,dr \quad \text{and} \quad \int_{r_{FA}}^{1} g_k(\ldots)\,dr$$

integrate by parts and use the boundary conditions

$$\int_{r_{FA}}^{1} f_k T'\,dr = f_k T\Big|_{r_{FA}}^{1} - \int_{r_{FA}}^{1} f_k' T\,dr$$

$$= -\int_{r_{FA}}^{1} f_k' T\,dr$$

to obtain

$$\sum d_i \int_{r_{FA}}^{1} f_k' g_i \, dr - \omega^2 \sum c_i \int_{r_{FA}}^{1} I_\theta f_k f_i \, dr = 0$$

$$\sum c_i \int_{r_{FA}}^{1} g_k f_i' \, dr - \sum d_i \int_{r_{FA}}^{1} g_k \left(\frac{GJ}{\Omega^2 R^2}\right)^{-1} g_i \, dr = 0$$

Hence the problem reduces to a set of algebraic equations for $\vec{c} = [c_i]$ and $\vec{d} = [d_i]$

$$C \vec{d} - \omega^2 B \vec{c} = 0$$

$$C^T \vec{c} - A \vec{d} = 0$$

or

$$(C A^{-1} C^T - \omega^2 B) \vec{c} = 0$$

For simplicity, the functions used for the torsion moment at $g_i = f_i'$. Then, the coefficients of the matrices are

$$A_{ki} = \int_{r_{FA}}^{1} f_k' \left(\frac{GJ}{\Omega^2 R^2}\right)^{-1} f_i' \, dr$$

$$B_{ki} = \int_{r_{FA}}^{1} I_\theta f_k f_i \, dr$$

$$C_{ki} = \int_{r_{FA}}^{1} f_k' f_i' \, dr$$

(Note using $g_i = GJf_i'$ would give the standard Galerkin result.)

The eigenvalues of the matrix $B^{-1}(CA^{-1}C^T)$ give the natural frequencies of the torsion vibration, and the corresponding eigenvectors for c give the modes. Finally, the torsion modes are normalized to unity at the tip, $\xi(1) = 1$.

A convenient set of functions to use for f_i is the solution for the torsion modes of a uniform beam:

$$w_n = \sin\left[\left(n - \tfrac{1}{2}\right)\pi \frac{r - r_{FA}}{1 - r_{FA}}\right]$$

These functions satisfy the boundary conditions, and will often be close to the true mode shapes.

2.3.4 Kinematic pitch/bending coupling.

The kinematic pitch/bending coupling K_{Pi} and the pitch/gimbal coupling K_{PG} have a significant role in the rotor dynamic behavior. The definition of K_{Pi} is the rigid pitch motion due to a unit deflection of the ith bending mode: $K_{Pi} = -d\theta/dq_i$. For an articulated rotor, the first "bending" modes are rigid lag and flap motion about the hinges. The pitch/flap coupling is often defined in terms of the delta-three angle: $K_p = \tan \delta_3$. It is possible to simply input these kinematic coupling parameters to the dynamics analysis, if values are available from either measurements or some other analysis. It is also desirable to be able to calculate the coupling from a model of the blade root geometry.

Figure 2-10 is a schematic of the blade root and control system geometry considered, showing the position of the feather bearing, pitch horn, and pitch link for no bending deflection of the blade. The radial locations of the feather bearing and pitch link are r_{PB} and r_{PH},

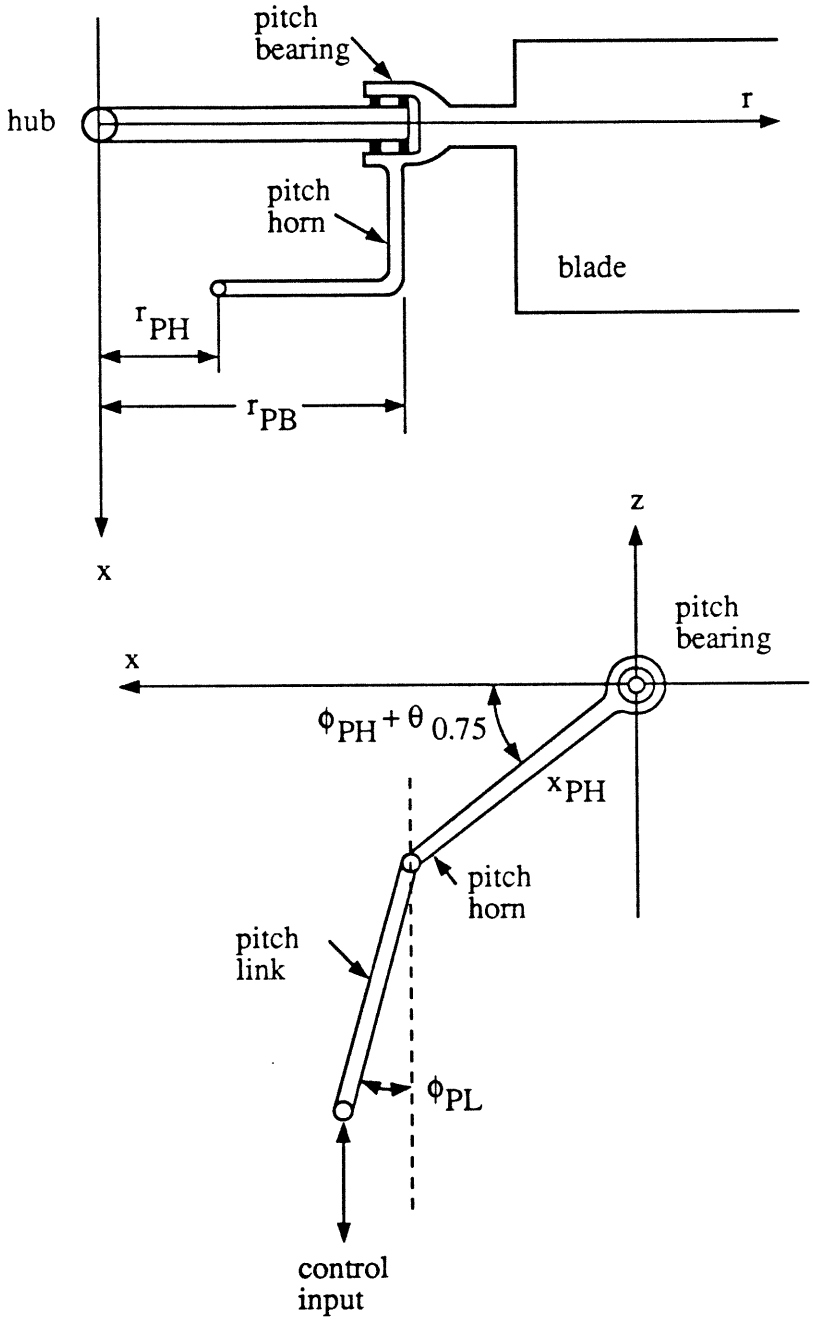

Figure 2-10. Schematic of blade root and control system geometry for calculating the kinematic pitch-bending coupling.

respectively; the length of the pitch horn is x_{PH}. The orientation of the pitch horn and pitch link are given by the angles $\phi_{PH} + \theta_{75}$ and ϕ_{PL}. Control input produces a vertical motion of the bottom of the pitch link, and hence a feathering motion of the blade about the pitch axis. Bending motion of the blade, with either structural flexibility or an actual hinge inboard of the pitch bearing, produces an in-plane or out-of-plane deflection of the pitch bearing. With the bottom of the pitch link fixed in space, a pitch change of the blade results. The vertical and in-plane displacements of the pitch horn (the end at r_{PH}) due to bending of the blade in the ith mode are:

$$\Delta z = q_i \vec{i}_B \cdot \left(\vec{\eta}_i(r_{PB}) - \vec{\eta}_i'(r_{PB})(r_{PB} - r_{PH}) \right)$$

$$\Delta x = -q_i \vec{k}_B \cdot \left(\vec{\eta}_i(r_{PB}) - \vec{\eta}_i'(r_{PB})(r_{PB} - r_{PH}) \right)$$

The kinematic pitch/bending coupling is derived from the geometric constraint that the lengths of the pitch horn and pitch link are fixed. The result is:

$$K_{P_i} = \frac{(\cos\phi_{PL}\vec{i}_B + \sin\phi_{PL}\vec{k}_B) \cdot (\vec{\eta}_i(r_{PB}) - \vec{\eta}_i'(r_{PB})(r_{PB} - r_{PH}))}{-x_{PH}\cos(\phi_{PH} + \theta_{75} + \phi_{PL})}$$

Similarly, for a gimballed (or teetering) rotor the pitch/flap coupling is:

$$K_{P_G} = \frac{-(r_{PH}/x_{PH})\cos\phi_{PL}}{\cos(\phi_{PH} + \theta_{75} + \phi_{PL})}$$

$$= \frac{(K_{PG})_{\text{pitch horn level}}}{\cos(\phi_{PH} + \theta_{75} + \phi_{PL})}$$

Note that for a hinged blade, the pitch/bending coupling K_{Pi} is zero if pitch horn radial station equals the hinge offset, $r_{PH} = e$. Also, for this root geometry the pitch link load is obtained from the feathering axis moment using:

$$F_{PL} = \frac{M_{FA}}{r_{PH}\cos(\theta_{75} + \phi_{PH} + \phi_{PL})}$$

2.3.5 Blade pitch definition.

Outboard of r_{FA}, the trim pitch angle is given by the collective and twist angles, while inboard of r_{FA} it is given by just the twist angle:

$$\theta = \begin{cases} \theta_{coll} + \theta_{tw}(r) & r > r_{FA} \\ \theta_{tw}(r) & r < r_{FA} \end{cases}$$

(see section 2.2.2). It is convenient to use the collective pitch value at 75% radius, θ_{75}. Then,

$$\theta = \begin{cases} \theta_{75} + \theta_{tw}(r) & r > r_{FA} \\ \theta_{tw}(r) & r < r_{FA} \end{cases}$$

which requires $\theta_{tw}(r = .75) = 0$ (but no change to θ_{tw} for $r < r_{FA}$). For the structural and inertial analysis, the pitch angle is multiplied by the structural coupling parameter $\mathfrak{K}$.

The twist distribution $\theta_{tw}(r)$ is required at the radial stations for which the inertial and structural properties are defined; and at the radial stations at which the aerodynamic forces are calculated. The aerodynamic twist definition can include the zero lift axis pitch θ_{ZL} (see section 2.4.1). Frequently, a linear twist distribution is used, for which

$$\theta_{tw} = \theta_{\underset{\text{twist}}{\text{linear}}} (r - .75)$$

2.4 Aerodynamic Analysis

The rotor blade aerodynamic loading is calculated using lifting line theory and steady, two-dimensional airfoil characteristics, with corrections for unsteady and three-dimensional flow effects. The model is applicable to rotors operating in low or high inflow, and in axial or nonaxial flight. The assumptions of lifting line theory are generally well satisfied for helicopter rotor blades: that the wing has a high aspect ratio, or more correctly that spanwise variations of the aerodynamic environment are small. In addition, for the rotary wing it is essential to have the capability to treat compressible and viscous flow effects, which are present to some degree in almost all helicopter operating conditions. These effects are included in lifting line theory by using experimental data for the two-dimensional airfoil characteristics. Lifting surface theory models offer more accuracy in the treatment of three-dimensional and perhaps compressible flow effects at low angles of attack, but are no more accurate and cause more difficulties than lifting line theory when calculating the loading at

high angles of attack. Computational fluid dynamics (CFD) methods are just beginning to be applied to the type of flows encountered on helicopter rotors. Finally, lifting line theory is far more efficient than lifting surface theory or CFD methods, to the extent that with current computers lifting line theory is probably the only practical approach for the comprehensive analysis of the rotary wing in forward flight.

Lifting line theory is not accurate at the tip of a wing or for a close vortex-blade interaction. The calculation of the loading at the blade tip is corrected for three-dimensional effects by using a tip loss factor in the conventional manner of rotor analyses. The calculation of the loading induced by a vortex passing close to the blade is corrected by using the solution for a model problem, obtained from linear lifting surface theory (described further below). The steady section aerodynamic characteristics must be corrected to account for unsteady flow effects. For low angles of attack, thin airfoil theory results are used to calculate the unsteady aerodynamic loading. For high angles of attack an empirical dynamic stall model is used. The dynamic stall model must be based on the steady, two-dimensional airfoil characteristics in order to be widely applicable. Two such models are implemented in the present analysis. The section aerodynamic characteristics are also corrected for the effects of yawed flow.

The aerodynamic loading is determined by the air velocity at the blade section. Only the lowest order contribution of each degree of freedom to the velocity is considered here. To include higher order terms would not be consistent since the basic elements of the aerodynamic model are obtained from first order theories (lifting line theory and thin airfoil theory). Nonlinear effects, such as stall, are included when they have a first order influence on the loading. Both momentum theory and vortex theory induced velocity models are included in the present analysis. The momentum theory model has empirical corrections for nonideal induced power losses, rotor-rotor interference,

and ground effect, and a linear variation of the induced velocity over the rotor disk caused by forward flight or aerodynamic moments on the rotor. Such a model is efficient, and as an empirical model, is reliable when used within its limits. A detailed wake model for a nonuniform inflow calculation is also developed for the analysis, using available prescribed and free wake geometry models.

In this section the aerodynamic forces and moments on the rotor blade are derived. The general case of a rotor in high or low inflow, axial or nonaxial flight is considered, including the effects of reverse flow and large angles. Lifting line theory (i.e., strip theory or blade element theory) is used to calculate the section loading from the airfoil two-dimensional aerodynamic characteristics, with corrections for yawed and three-dimensional flow effects required. The unsteady aerodynamic lift and moment are obtained from this airfoil theory, and a dynamic stall model accounts for the unsteady aerodynamic phenomena at large angles of attack.

2.4.1 Section aerodynamic forces.

A hub plane reference frame is used for the aerodynamic forces. All forces and velocities are resolved in the hub plane (i.e., the B coordinate system). The hub plane reference frame is fixed with respect to the shaft, hence it is tilted and displaced by the shaft motion. Figure 2-11 illustrates the forces and velocities of the blade section aerodynamics. The blade pitch angle is θ, measured from the reference plane. The velocity of the air as seen by the moving blade has components u_T, u_P, and u_R, resolved with respect to the reference frame; $U = (u_T^2 + u_P^2)^{1/2}$ is the resultant air velocity in the plane of the section; and $\phi = \tan^{-1} u_P/u_T$ is the induced angle. The section angle of attack is

$$\alpha = \theta + \theta_{TL} - \phi$$

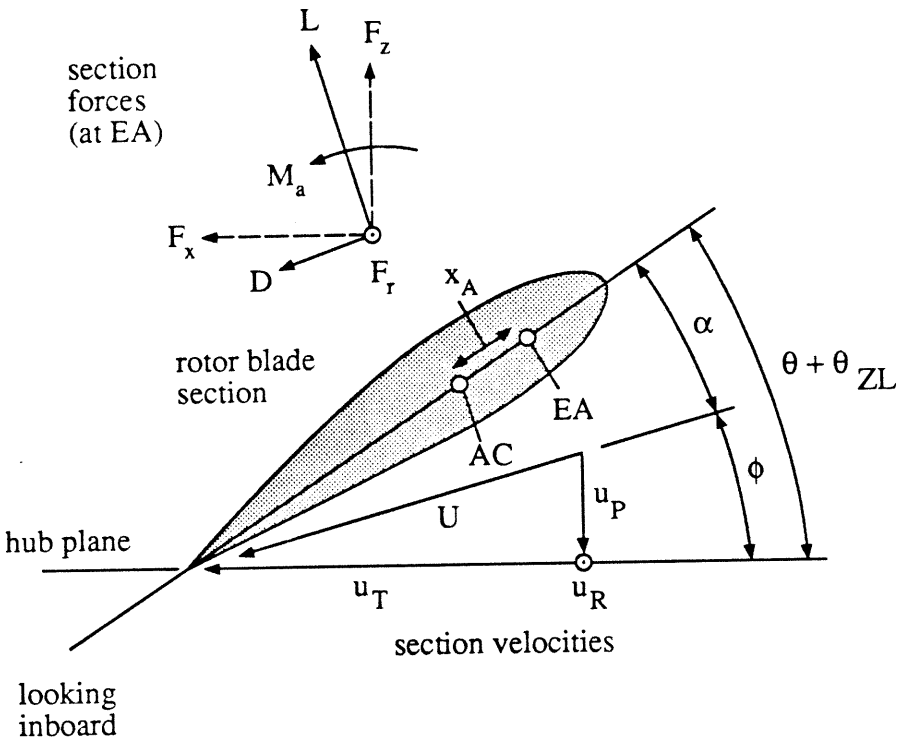

Figure 2-11. Rotor blade section aerodynamics.

where θ_{ZL} is the pitch of the aerodynamic zero-lift axis of the section relative to the structural/inertial principal axis at pitch angle θ (θ_{ZL} may vary along the span, and should not, therefore, be included in the definition of the section aerodynamic coefficients as a function of α; θ_{ZL} can, however, be included in the aerodynamic twist distribution, if θ_{tw} is defined separately for the inertial/structural pitch and for the aerodynamic pitch). The velocity u_T is in the hub plane, positive in the blade drag direction; u_R is in the hub plane, positive radially outward along the blade; and u_P is normal to the hub plane, positive down through the rotor disk. The aerodynamic forces and moment on the section, at the elastic axis, are defined as follows: L and D are the aerodynamic lift and drag forces on the section, respectively, normal and parallel to the resultant velocity U; F_Z and F_X are the components of the total aerodynamic force on the section resolved with respect to the hub plane, normal to and in the plane of the rotor; F_r is the radial drag force on the blade, positive outward (the same direction as positive u_R); and M_a is the section aerodynamic moment about the elastic axis, positive nose up. The radial forces due to the tilt of F_Z and F_X are considered separately, hence F_r consists only of the radial drag forces.

The section lift and drag are

$$L = \frac{1}{2}\rho U^2 c c_\ell + L_{us}$$

$$D = \frac{1}{2}\rho U^2 c c_d$$

where U is the resultant velocity at the section, ρ is the air density, and c is the chord of the blade. (The air density can be dropped since all quantities are actually dimensionless, based on ρ, Ω, and R.) The section lift and drag coefficients, c_l and c_d, are functions of the section angle of attack and Mach number:

$$\alpha = \theta + \theta_{TL} - \phi = \theta + \theta_{TL} - \tan^{-1}\frac{u_P}{u_T}$$

$$M = M_{TIP}\, U$$

where M_{TIP} is the tip Mach number (the rotor tip speed ΩR divided by the speed of sound). L_{us} is the unsteady aerodynamic lift force. The radial drag force is

$$F_r = (u_R/U)\, D = \tfrac{1}{2}\rho U u_R c_d$$

This radial drag force is based on the assumption that the viscous drag force on the section has the same sweep angle as the local section velocity. The moment about the elastic axis is

$$M_a = -x_A L + M_{AC} + M_{us}$$

$$= -x_A \tfrac{1}{2}\rho U^2 c c_l + \tfrac{1}{2}\rho U^2 c^2 c_m + M_{us}$$

where x_A is the distance the aerodynamic center is behind the elastic axis, c_m is the section moment about the aerodynamic center (positive nose up), and M_{us} is the unsteady aerodynamic moment.

The components of the section aerodynamic forces relative to the hub plane axes are then

$$F_z = L\cos\phi - D\sin\phi = (L u_T - D u_P)/U$$

$$F_x = L\sin\phi + D\cos\phi = (L u_P + D u_T)/U$$

Substituting for L and D, and dividing by a, the two-dimensional lift-curve slope, and by c_m, the mean section chord (which enter the Lock number γ also), we obtain:

$$\frac{F_z}{ac} = \left[U\left(u_T \frac{c_l}{2a} - u_P \frac{c_d}{2a}\right) + \frac{u_T}{U}\frac{L_{us}}{ac}\right]\frac{c}{c_m}$$

$$\frac{F_x}{ac} = \left[U\left(u_P \frac{c_l}{2a} + u_T \frac{c_d}{2a}\right) + \frac{u_P}{U}\frac{L_{us}}{ac}\right]\frac{c}{c_m}$$

$$\frac{F_r}{ac} = \left[U u_R \frac{c_d}{2a}\right]\frac{c}{c_m}$$

$$\frac{M_a}{ac} = \left[-x_A U^2 \frac{c_l}{2a} + U^2 c \frac{c_m}{2a} + \frac{M_{us}}{ac}\right]\frac{c}{c_m}$$

The net rotor forces required are obtained by integration of these section forces over the span of the blade:

$$\frac{M_{q_k}}{ac}^{aero} = \int_0^1 \vec{r}_k \cdot \left(\frac{F_z}{ac}\vec{k}_B - \frac{F_x}{ac}\vec{i}_B\right) dr$$

$$\frac{M_{p_k}}{ac}^{aero} = \int_{r_{FA}}^1 \xi_k \frac{M_a}{ac}\, dr - \int_{r_{FA}}^1 \vec{x}_{A_k} \cdot \left(\frac{F_x}{ac}\vec{k}_B + \frac{F_z}{ac}\vec{i}_B\right) dr$$

$$\left(\frac{C_{mx}}{\sigma a}\right)_{aero} = \int_0^1 \frac{F_z}{ac}\, r\, dr$$

$$\left(\frac{C_{mz}}{\sigma a}\right)_{aero} = \int_0^1 \frac{F_x}{ac}\, r\, dr$$

$$\left(\frac{C_{fx}}{\sigma a}\right)_{aero} = \int_0^1 \frac{F_x}{ac}\, dr$$

$$\left(\frac{C_{fz}}{\sigma a}\right)_{aero} = \int_0^1 \frac{F_z}{ac}\, dr$$

$$\left(\frac{C_{fr}}{\sigma a}\right)_{aero} = \int_0^1 \frac{\tilde{F}_r}{ac}\, dr$$

where X_{Ak} is essentially the moment arm about the elastic axis at r, produced by the blade bending deflection; and the radial force in shaft axes is

$$\tilde{F}_r = F_r - F_z\left(\beta_G + \delta_{FA_1} - \delta_{FA_2}\right) - F_x\left(-\psi_s + \delta_{FA_3}\right) - \sum_i q_i \left(F_z \vec{r}_B - F_x \vec{r}_B\right) \cdot \vec{\eta}_i'$$

The section forces are divided by the two-dimensional lift-curve slope a, and by the mean chord c_{mean}; these are the quantities used to define the Lock number.

To numerically integrate the aerodynamic loads over the blade span, define K radial segments by the boundaries

$$r_0, r_1, r_2, \ldots r_{k-1}, r_k, \ldots, r_K$$

where $r_K = 1$. For the kth segment, the airloads are calculated at the center:

$$r = \frac{1}{2}\left(r_k + r_{k-1}\right)$$

Then the spanwise integration is approximated by a summation over all segments:

$$\int_0^1 f(r)\,dr \cong \sum_{k=1}^{K} f\left(\frac{r_k + r_{k-1}}{2}\right)\Delta r_k$$

where

$$\Delta r_k = \left(r_k - r_{k-1}\right)$$

In summary, the rotor blade aerodynamic forces are evaluated as follows. First the section velocity components and pitch angle are evaluated, and then the angle of attack and Mach number. Next the section aerodynamic coefficients are obtained (see section 2.4.4), and from them the section force components and moment. Finally, the section forces are integrated over the rotor radius to obtain the required generalized forces.

2.4.2 Blade velocity.

The air velocity seen by the blade section is due to the rotor rotation, the helicopter forward speed, the rotor and shaft motion, and the wake induced velocity. The rotor is rotating at speed Ω. The velocity of the air as seen by the rotor disk has the following dimensionless components in the shaft axis system: μ_x, positive aft; μ_y, positive from the right; and μ_z, positive down through the disk:

$$\vec{\mu} = -\frac{V}{\Omega R}\vec{i}_w = \mu_x \vec{i}_s - \mu_y \vec{j}_s - \mu_z \vec{k}_s$$

Often the lateral velocity component $\mu_y = -\vec{j}_s \cdot \vec{\mu}$ is assumed to be zero in the rotor aerodynamic analysis, and indeed it is small for most flight conditions. An exception is the case of sideward flight. An alternative to including μ_y is to rotate the shaft axes until $\vec{j}_s \cdot \vec{\mu} = 0$, but that would imply a redefinition of the rotor zero azimuth position for every flight state. Such a redefinition of ψ is not desirable since it changes the values of parameters such as the control system phasing, and even changes the definition of the harmonics of the rotor motion. Hence it is preferable to directly include the effects of the lateral velocity in the analysis.

The rotor wake-induced velocity is $\lambda_i = v_i/\Omega R$, normal to the rotor disk and positive downward. A simple model may be used, such as a uniform or linear variation over the disk, or calculated nonuniform induced velocities may be used. For the latter case, all three components of the wake induced velocity (in shaft axes) will be considered:

$$\vec{\lambda}_i = \lambda_x \vec{i}_s - \lambda_y \vec{j}_s - \lambda_z \vec{k}_s$$

The rotor advance ratio μ and inflow ratio λ as conventionally defined are here

$$\mu = \sqrt{\mu_x^2 + \mu_y^2}$$

$$\lambda = \lambda_i + \mu_z$$

These are the dimensionless in-plane and normal components of the total velocity seen by the rotor disk. The hub plane angle of attack and yaw angle are then

$$\alpha_{HP} = \tan^{-1} \frac{\mu_z}{\sqrt{\mu_x^2 + \mu_y^2}}$$

$$\psi_{HP} = \tan^{-1} \frac{\mu_y}{\mu_x}$$

so

$$\mu = \frac{V \cos \alpha_{HP}}{\Omega R}$$

$$\lambda = \frac{v_i + V \sin \alpha_{HP}}{\Omega R} = \frac{v_i}{\Omega R} + \mu \tan \alpha_{HP}$$

Here V is the helicopter velocity, with angle of attack α_{HP} relative to the hub plane (α_{HP} is positive for forward tilt of the rotor disk). The advance ratio μ is zero for hover and axial flow, and $\mu > 0$ for helicopter forward flight.

The aerodynamic gust velocity has components u_G, v_G, and w_G in the shaft axis system, normalized by dividing by the tip speed ΩR. The longitudinal gust u_G is positive from the front, the lateral gust v_G is positive from the right, and the vertical gust w_G is positive upward ($\vec{V}_{gust} = u_G \vec{i}_s - v_G \vec{j}_s + w_G \vec{k}_s$ relative to the rotor). This gust velocity is evaluated at azimuth angle ψ and radial station r on the rotor disk

(at $r = r\vec{j}_B = r(\cos\psi\vec{i}_s + \sin\psi\vec{j}_s)$ relative to the hub). The quasisteady shaft motion and the gust velocity at the rotor hub will be included in the advance ratio components μ_x, μ_y, and μ_z (see section 4.1.2).

The blade and shaft motion have been defined in the inertial analysis (section 2.2). Define

$$u_{T_o} = r + (\mu_x + \lambda_x)\sin\Psi + (\mu_y + \lambda_y)\cos\Psi + \Delta u_T$$

$$u_{R_o} = (\mu_x + \lambda_x)\cos\Psi - (\mu_y + \lambda_y)\sin\Psi + \Delta u_R$$

$$u_{T_o} = \mu_z + \lambda_z + \Delta u_T$$

where Δu_T, Δu_R, and Δu_P are the velocities produced by the airframe aerodynamic interference, in the rotating shaft axes and divided by the tip speed of this rotor (see section 4.4). The resulting velocity components in the rotor shaft axes are thus:

$$\begin{aligned} u_T = u_{T_o} &- u_{R_o}\left(\delta_{FA_3} - \vec{k}_B\cdot(z_o\vec{i} - x_o\vec{k})'\right) \\ &+ \vec{k}_B\cdot(z_o\vec{i} - x_o\vec{k})^{\cdot} \\ &+ (\mu_z\alpha_x + \dot{y}_{cm} + v_G)\cos\Psi \\ &+ (\mu_z\alpha_y - \dot{x}_{cm} + u_G)\sin\Psi \\ &+ (\mu_x\cos\Psi - \mu_y\sin\Psi)(\alpha_z + \Psi_s) \\ &+ r(\dot{\alpha}_z + \dot{\Psi}_s) \end{aligned}$$

$$\begin{aligned} u_R = u_{R_o} &+ x_{FA} - (r - r_{FA})\delta_{FA_3} + \vec{k}_B\cdot(z_o\vec{i} - x_o\vec{k}) \\ &+ u_{T_o}\left(\delta_{FA_3} - \vec{k}_B\cdot(z_o\vec{i} - x_o\vec{k})'\right) \\ &- u_{P_o}\left(\delta_{FA_1} - \delta_{FA_2} + \beta_G + \vec{i}_B\cdot(z_o\vec{i} - x_o\vec{k})'\right) \end{aligned}$$

$$
\begin{aligned}
&- (\mu_z \alpha_x + \dot{\gamma}_H + v_G) \sin\psi \\
&+ (\mu_z \alpha_y - \dot{x}_H + u_G) \cos\psi \\
&- (\mu_x \sin\psi + \mu_y \cos\psi)(\alpha_z + \psi_s)
\end{aligned}
$$

$$
\begin{aligned}
u_P = u_{P_0} &+ r\dot{\beta}_G + \vec{r}_B \cdot (z_0 \vec{i} - x_0 \vec{k})^{\cdot} \\
&+ u_{R_0} (\delta_{FA_1} - \delta_{FA_2} + \beta_G + \vec{r}_B \cdot (z_0 \vec{i} - x_0 \vec{k})') \\
&+ (\dot{z}_H - w_G - \mu_x \alpha_y - \mu_y \alpha_x) \\
&+ r(\dot{\alpha}_x \sin\psi - \dot{\alpha}_y \cos\psi)
\end{aligned}
$$

and the pitch angle is

$$
\theta = \theta_{coll} + \theta_{tw} + \sum_{i=0}^{\infty} A_i \zeta_i
$$

In body axes, the trim velocity vector is fixed with the reference frame, and would therefore tilt with it. With inertial axes, however, a tilt of the rotor by the shaft motion results in a small change in the directions of the components of μ as seen in the reference frame. All the $\mu\alpha$ terms in the expressions above for u_T, u_P, and u_R result from such tilt of the inertial axes relative to the trim velocity vector. The aircraft body yaw, pitch, and roll will be defined as body axis motion however. Hence the body Euler angles are not to be included in the evaluation of α_x, α_y, and α_z for the blade velocities.

2.4.3 Induced velocity.

For the case of uniform inflow, the rotor wake-induced velocity is obtained from the momentum theory result

$$\lambda_i = \frac{C_T}{2\sqrt{\lambda^2/\kappa_h^4 + \mu^2/\kappa_f^2}}$$

where $\lambda = \mu_z + \lambda_i$ and $\mu^2 = \mu_x^2 + \mu_y^2$. Empirical correction factors κ_h and κ_f are included for the effects of nonuniform inflow, tip losses, swirl, blockage, etc., in hover and forward flight. An iterative solution of this equation for λ_i is necessary:

$$(\lambda_i)_{n+1} = \left[\frac{\frac{C_T}{2}\left(\lambda(\lambda+\lambda_i)/\kappa_h^4 + \mu^2/\kappa_f^2\right)}{C + \frac{C_T}{2}\lambda/\kappa_h^4} \right]_n$$

$$C = \left(\lambda^2/\kappa_h^4 + \mu^2/\kappa_f^2\right)^{3/2}$$

with

$$\lambda_i \cong \frac{C_T}{2\sqrt{C_T/2\kappa_h^2 + \mu^2/\kappa_f^2}}$$

to start the solution; 3 or 4 iterations are usually sufficient. For the vortex ring and turbulent wake states this momentum theory result is not applicable. Thus is

$$\mu^2 + (2\mu_z + 3\lambda_h)^2 < \lambda_h^2$$

the following expression is used instead:

$$\lambda = \mu_z + k_h \mu_z \left[\frac{.373\mu_z^2 + .598\mu^2}{\lambda_h^2} - 1.991 \right]$$

where

$$\lambda_h = \sqrt{C_T/2}$$

As discussed in section 5.1.12, the circulation iteration will not converge with the above expressions for the case of a hovering rotor at zero thrust. For such cases, the induced velocity can be calculated instead from the following equation:

$$\lambda_i = \frac{C_T}{2\sqrt{\lambda_0^2/k_h^4 + \mu^2/k_t^2}}$$

where

$$\lambda_0 = \mu_z + \lambda_{i0}$$

$$\lambda_{i0} = k_h \sqrt{C_{T_0}/2}$$

and C_{To} is a fixed, nominal value of the rotor thrust. Fixing the denominator in this fashion is equivalent to fixing the wake geometry. The resulting induced velocity is not accurate, but it is acceptable for cases of small thrust, and the circulation iteration will converge.

The wake-induced velocity is reduced when the rotor disk is in the proximity of the ground plane. The effect of the ground will be accounted for using the following approximate expression (from reference 21) for the ratio of the induced velocities in and out of ground effect:

$$\frac{v_\infty}{v} = \frac{T}{T_\infty} = \frac{1}{1 - (4z/\cos\epsilon)^{-2}}$$

where z is the height of the rotor hub above ground level, normalized by the rotor radius; and ϵ is the angle between the ground and the rotor wake ($\epsilon = 0$ for hover and ϵ approaches 90° in forward flight), which accounts for the effect of forward speed. Note that ground effect is essentially negligible for altitudes greater than the rotor diameter ($z > 2$) or at forward speeds $\mu > 2(C_T/2)^{\frac{1}{2}}$. This expression compares well with test results, down to an altitude of about one-half rotor radius (see reference 21). The rotor wake-induced velocity in ground effect is thus

$$(\lambda_i)_{IGE} = \left(1 - \frac{\cos^2\epsilon}{16z^2}\right)(\lambda_i)_{OGE}$$

Let h_{AGL} be the height of the helicopter center of gravity above ground level; and (x_R, y_R, z_R) be the components of the rotor hub position relative to the center of gravity, in a body axis system (the F frame, see section 4.1.5). Then the altitude of the rotor hub above ground level is

$$z = \frac{1}{R}\left[h_{AGL} - R_{rotor\#1}\left(x_R \vec{i}_F + y_R \vec{j}_F + z_R \vec{k}_F\right)\cdot \vec{k}_E \right]$$

The vertical (k_E) is defined relative to the body axes by the trim pitch and roll Euler angles (θ_{FT} and ϕ_{FT}, see section 4.1.1). The angle between the rotor wake and the vertical is

$$\cos\epsilon = \frac{\left(\mu_x \vec{i}_S - \mu_y \vec{j}_S - \lambda \vec{k}_S\right)\cdot \vec{k}_E}{\sqrt{\mu_x^2 + \mu_y^2 + \lambda^2}}$$

$$= \frac{1}{\sqrt{\mu_x^2+\mu_y^2+\lambda^2}} \begin{pmatrix} \mu_x \\ -\mu_y \\ -\lambda \end{pmatrix}^T R_{SF} \begin{pmatrix} -\sin\theta_{FT} \\ \cos\theta_{FT}\sin\phi_{FT} \\ \cos\theta_{FT}\cos\phi_{FT} \end{pmatrix}$$

where R_{SF} is the transformation matrix between the shaft and fuselage axis coordinate frames.

As a first approximation to the rotor nonuniform induced velocity distribution in forward flight, a linear variation over the disk is considered:

$$\Delta\lambda = \lambda_i \left(\kappa_x r\cos\Psi + \kappa_y r \sin\Psi\right)$$

where λ_i is the mean value of the induced velocity, calculated as described above. Typically κ_x is positive, roughly 1 at high speed; and κ_y is smaller in magnitude and negative. Both κ_x and κ_y must be zero in hover. Based on references 22-25, the following models are considered:

a) Coleman and Feingold

$$k_{x_0} = \frac{15\pi}{32} \tan\chi/2 = \frac{15\pi}{32} \frac{\mu}{\sqrt{\mu^2+\lambda^2} + |\lambda|}$$

$$k_{y_0} = -2\mu$$

b) White and Blake

$$k_{x_0} = \sqrt{2} \sin\chi = \sqrt{2} \frac{\mu}{\sqrt{\mu^2+\lambda^2}}$$

$$k_{y_0} = -2\mu$$

where $\tan\chi = |\lambda|/\mu$. Accounting for the sideward velocity gives

$$\Delta\lambda = \lambda_i r \left[k_{x_0} \cos(\Psi+\Psi_0) + k_{y_0} \sin(\Psi+\Psi_0) \right]$$

$$= \lambda_i r \left[(k_{x_0}\cos\Psi_0 + k_{y_0}\sin\Psi_0)\cos\Psi + (-k_{x_0}\sin\Psi_0 + k_{y_0}\cos\Psi_0)\sin\Psi \right]$$

where $\cos\psi_0 = \mu_x/\mu$ and $\sin\psi_0 = \mu_y/\mu$. Hence the two models give:

a) Coleman and Feingold

$$k_x = f_x \frac{15\pi}{32} \frac{\mu_x}{\sqrt{\mu^2+\lambda^2} + |\lambda|} - f_y 2\mu_y$$

$$k_y = -f_x \frac{15\pi}{32} \frac{\mu_y}{\sqrt{\mu^2+\lambda^2} + |\lambda|} - f_y 2\mu_x$$

b) White and Blake

$$k_x = f_x \sqrt{2} \frac{\mu_x}{\sqrt{\mu^2+\lambda^2}} - f_y 2\mu_y$$

$$k_y = -f_x \sqrt{2} \frac{\mu_y}{\sqrt{\mu^2+\lambda^2}} - f_y 2\mu_x$$

For flexibility, the empirical factors f_x and f_y have been introduced (values of 1.0 give the baseline model). Other options are to input κ_x and κ_y directly; or to omit these terms.

There will also be an inflow variation produced by any net aerodynamic moment on the rotor disk. A differential form of momentum theory gives:

$$\Delta\lambda = \frac{f_m(-2C_{My}r\cos\psi + 2C_{Mx}r\sin\psi)}{\sqrt{\mu^2/k_f^2 + \lambda^2/k_\ell^4}}$$

including an empirical factor f_m. Note that the denominator is zero for a hovering rotor at zero thrust; hence this inflow contribution should not be used for cases of low or zero speed and low thrust.

With twin-rotor aircraft it is also necessary to account for the rotor-rotor aerodynamic interference in the wake-induced inflow velocities. The induced velocity at each rotor will be expressed as a

linear combination of the isolated rotor induced velocity. Let λ_{i1} and λ_{i2} be the trim induced velocities of the two isolated rotors, calculated as above. Then the trim inflow ratios are:

$$\lambda_1 = \mu_{z_1} + \lambda_{i1} + k_{12} \frac{(\Omega R)_2}{(\Omega R)_1} \lambda_{i2}$$

$$\lambda_2 = \mu_{z_2} + \lambda_{i2} + k_{21} \frac{(\Omega R)_1}{(\Omega R)_2} \lambda_{i1}$$

Here κ_{12} and κ_{21} are the rotor-rotor aerodynamic interference factors. Separate values are used for the interference factors in hover and forward flight, with a linear variation from $\mu = 0.05$ to 0.10.

In summary, the isolated rotor mean induced velocity is calculated from the advance ratio and thrust,

$$\lambda_i = f_{GE}\, \lambda_{i_{OGE}}(\vec{\mu}, C_T)$$

where $f_{GE} = 1$ out of ground effect. Including the rotor-rotor interference and the linearly varying induced velocity components, the inflow ratios are then

$$\lambda_1 = \mu_{z_1} + \lambda_{i_1} + k_{12} \frac{(\Omega R)_2}{(\Omega R)_1} \lambda_{i2} + (\lambda_{i_1} k_x r \cos\psi + \lambda_{i_1} k_y r \sin\psi) + \frac{f_m(-2C_{M_y} r\cos\psi + 2C_{M_x} r \sin\psi)}{\sqrt{\mu^2/k_x^2 + \lambda^2/k_m^4}}$$

$$\lambda_2 = \mu_{z_2} + \lambda_{i_2} + k_{21} \frac{(\Omega R)_1}{(\Omega R)_2} \lambda_{i_1}$$

$$+ (\lambda_{i_2} k_x r \cos\Psi + \lambda_{i_2} k_y r \sin\Psi)$$

$$+ \frac{\zeta_m (-2C_{M_y} r \cos\Psi + 2C_{M_x} r \sin\Psi)}{\sqrt{\mu^2/k_f^2 + \lambda^2/k_{2m}^2}}$$

for rotor #1 and rotor #2, respectively.

The aerodynamic interference of the rotor on the airframe is included in the airframe aerodynamic model (section 4.2.6). As a simple model for the aerodynamic interference, the rotor-induced velocities at the wing/body, horizontal tail, and vertical tail can be obtained as a linear combination of the mean induced velocity at the two rotors:

$$\vec{\lambda} = K_1 C_1 \lambda_{i1} R_{SF}^T (-\vec{k}_s) + K_2 C_2 \lambda_{i2} R_{SF}^T (-\vec{k}_s)$$

assuming that the induced velocity is normal to the disk plane ($-k_s$ direction). The K factors account for the maximum fraction of the aerodynamic surface which is affected by the wake, and the fraction of the fully developed wake velocity which is achieved. Typical values would be K = 1.5 to 1.8 (or zero for no interference). The C

multiplicative factors account for the decrease in the wake induced velocity away from the wake surface, using the following expression:

$$C = \frac{1}{\max(1, 1+l)}$$

where l is the perpendicular distance from the aerodynamic surface to the nearest wake boundary ($l < 0$ if the surface is inside the rotor wake cylinder). Consider the geometry sketched in Figure 2-12. The aerodynamic surface is located at $(\vec{r} - \vec{r}_R)$ relative to the rotor hub. The unit vector along the wake center-line is

$$\vec{e} = \frac{\mu_x \vec{i}_s - \mu_y \vec{j}_s - \lambda \vec{k}_s}{\sqrt{\mu_x^2 + \mu_y^2 + \lambda^2}}$$

and we write

$$\vec{e} \times (\vec{r} - \vec{r}_R) = (\vec{e} \times) R_{sf} (\vec{r} - \vec{r}_R) = x\vec{i}_s + y\vec{j}_s + z\vec{k}_s$$

(times R_1/R_2 for rotor #2). Now the unit vector in the $\vec{e}/(\vec{r} - \vec{r}_R)$ plane, perpendicular to $\vec{e}$ is

$$\vec{d} = \frac{(\vec{e} \times (\vec{r} - \vec{r}_R)) \times \vec{e}}{|\vec{e} \times (\vec{r} - \vec{r}_R)|}$$

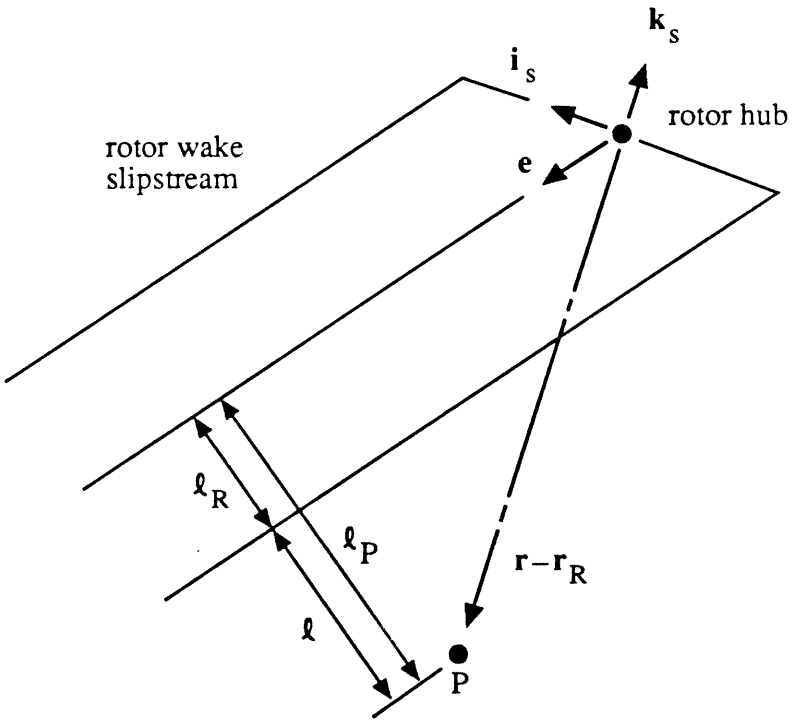

Figure 2-12. Model for rotor/airframe aerodynamic interference.

So the distance from P to the wake center-line is

$$\ell_P = (\vec{r} - \vec{r}_R) \cdot \vec{d} = |\vec{e} \times (\vec{r} - \vec{r}_R)|$$

A point on the edge of the rotor disk is a unit vector perpendicular to $\vec{k}_s$; the point also in the $\vec{e}/(\vec{r} - \vec{r}_R)$ plane (perpendicular to $\vec{e} \times (\vec{r} - \vec{r}_R)$) is then

$$\vec{f} = \frac{\vec{k}_s \times (\vec{e} \times (\vec{r} - \vec{r}_R))}{|\vec{k}_s \times (\vec{e} \times (\vec{r} - \vec{r}_R))|}$$

The distance of the wake edge to the wake center-line is thus

$$\ell_R = \vec{f} \cdot \vec{d} = -\vec{e} \cdot \vec{k}_s \frac{|\vec{e} \times (\vec{r} - \vec{r}_R)|}{|\vec{k}_s \times (\vec{e} \times (\vec{r} - \vec{r}_R))|}$$

So the distance from P to the wake boundary is

$$\begin{aligned} \ell &= \ell_P - \ell_R \\ &= |\vec{e} \times (\vec{r} - \vec{r}_R)| \left(1 - \frac{|\vec{e} \cdot \vec{k}_s|}{|\vec{k}_s \times (\vec{e} \times (\vec{r} - \vec{r}_R))|}\right) \\ &= \sqrt{x^2 + y^2 + z^2} \left(1 - \frac{|\vec{e} \cdot \vec{k}_s|}{\sqrt{x^2 + y^2}}\right) \end{aligned}$$

2.4.4 Section aerodynamic characteristics.

The section aerodynamic characteristics required are the static lift, drag, and moment coefficients as a function of angle of attack and Mach number: $c_l(\alpha, M)$, $c_d(\alpha, M)$, and $c_m(\alpha, M)$. Most often rotor loads analyses use two-dimensional airfoil test data in tabular form. The aerodynamic description of the blade also requires θ_{ZL}, the zero lift angle of the section relative to the structural/inertial principal axis at pitch angle θ; and x_A, the distance the aerodynamic center (in normal flow) is behind the elastic axis. The strict definition of θ_{ZL} is actually the pitch of the axis corresponding to $\alpha = 0$ in the airfoil data used. Similarly the strict definition of x_A is simply the location of the axis about which the moment data c_m are given. It is convenient to use the zero lift axis and the aerodynamic center, but the most important consideration is that the definitions of θ_{ZL} and x_A be consistent with the zero angle of attack and moment axis definitions in the airfoil data used.

The angle of attack α is defined in the range -180 to 180, with the same sense as θ. The lift, drag, and moment as a function of angle of attack are defined as in two-dimensional airfoil tests, where α is varied by pitching the airfoil; and the lift is always positive vertically; the drag is positive in the direction of the free stream; and the moment is positive nose up. For the rotor blade in reverse flow then ($u_T < 0$), a positive pitch θ or positive (down) normal velocity u_P gives an angle of attack near -180; which gives positive c_l and c_d; which are down lift L and forward acting drag D. The section moment is given about a fixed axis of the section. In reverse flow the aerodynamic center shifts to near the three-quarter chord (from near the quarter chord in normal flow) so it is expected that the c_m data will show a nose up moment contribution of $\Delta M = \frac{c}{2}L$ or $\Delta c_m = \frac{1}{2}c_l$ in reverse flow (see Figure 2-13).

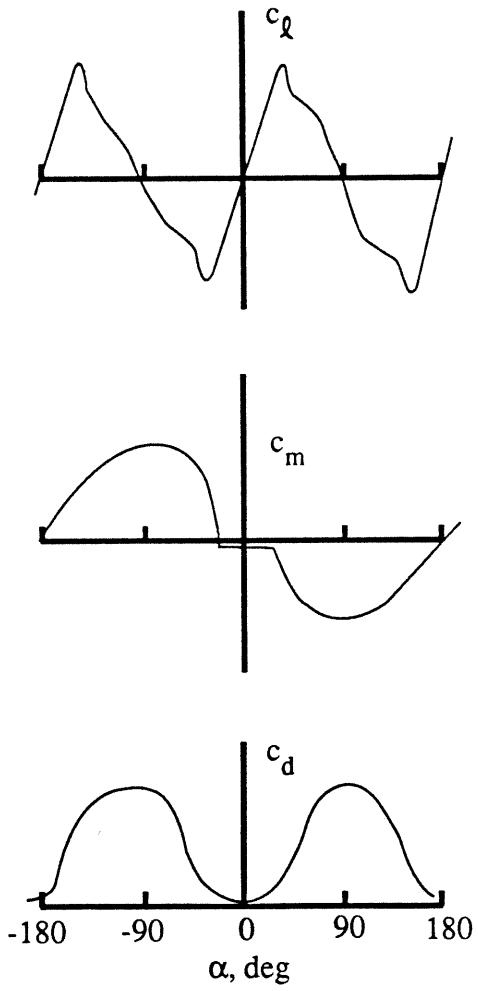

Figure 2-13. Sketch of section aerodynamic characteristics.

Incremental values of the drag and moment coefficients (as a function of rotor radius) can optionally be added to the values obtained from the airfoil tables. This is a common technique, typically used to account for Reynolds number effects.

The steady, two dimensional airfoil data (c_l, c_d, and c_m as a function of α, M, and r) are usually obtained in tables from wind tunnel test data. If test data are not available, approximate tables might be synthesized from generalized airfoil equations. For use by this analysis, the tables will be translated to the following form. The data will be defined at a finite set of angle of attack points. To facilitate interpolation, these points will consist of several groups, with the same angle of attack increment within each group. Then the set of angle of attack points are completely specified by the α at the boundaries between the groups, and the indices of these points: N_a, α_{n_1} to $\alpha_{n_{Na}}$, and n_1 to n_{Na} (for N_a - 1 groups). The organization is illustrated below.

++++++++++++++++++++++++++++++++							angle of attack points
+	+	+	+	+		+	boundaries of groups
1	2	3	4	5	...	N_a	boundary index
n_1	n_2	n_3	n_4	n_5	...	n_{Na}	angle of attack index at boundary
α_1	α_2	α_3	α_4	α_5	...	α_{Na}	angle of attack at boundary

Note that n_k is a count of all the angle of attack points (not just the boundary points). So n_{Na} is the total number of values in the table. The angle of attack range in the table should be from -180 to 180 degrees (the interpolation routine does not extrapolate if asked for data from outside the domain of the table). With this organization, the interpolation is most efficient: it is only necessary to search the table in terms of the groups; interpolation within a group requires only numerical operations. The reduction in search operations will be significant if a large number of points can be divided into a small

number of groups. The organization is similar for the variation with Mach number.

For the radial variation, the blade is divided into segments with the same section, defined by r at the boundaries: N_r, and r_1 to r_{N_r+1} for N_r segments. Hence the data set for the lift coefficient has the form

N_a, n_k ($k = 1$ to N_a), α_k ($k = 1$ to N_a)

N_m, n_k ($k = 1$ to N_m), M_k ($k = 1$ to N_m)

N_r, r_k ($k = 1$ to N_r+1)

$c_l(i)$ for $i = (j_r-1)n_{N_a}n_{N_m} + (j_m-1)n_{N_a} + j_a$

$(((j_a = 1$ to $n_{N_a})$, $j_m = 1$ to $n_{N_m})$, $j_r = 1$ to $N_r)$

and similarly for the drag and moment coefficient data sets.

The data will be linearly interpolated over angle of attack and Mach number. The boundary point definitions determine the values of α and M for all points in the data set. Consider the angle of attack variation. The boundary point definition of α_{n_i} for $i = 1$ to N_a implies that the angles of attack for points between the boundaries α_{n_i} and $\alpha_{n_{i+1}}$ are

$$\alpha_{n_i+j} = \alpha_{n_i} + j \frac{\alpha_{n_{i+1}} - \alpha_{n_i}}{n_{i+1} - n_i}$$

for $j = 0$ to $(n_{i+1} - n_i)$. Hence given α, we search for i such that

$$\alpha_{n_i} \leq \alpha \leq \alpha_{n_{i+1}}$$

It follows immediately that

$$\alpha_j \leq \alpha \leq \alpha_{j+1}$$

where

$$j_\alpha = n_i + \left[\frac{\alpha - \alpha_{n_i}}{\Delta\alpha} \right]$$

$$\alpha_j = \alpha_{n_i} + (j_\alpha - n_i)\Delta\alpha$$

$$\Delta\alpha = \frac{\alpha_{n_{i+1}} - \alpha_{n_i}}{n_{i+1} - n_i}$$

([a] means the greatest integer in a; i.e., integer arithmetic). With a function c defined at α_j and at α_{j+1}, linear interpolation then gives

$$c = a_j c_{j_\alpha} + a_{j+1} c_{j_\alpha+1}$$

where

$$a_{j+1} = \frac{\alpha - \alpha_j}{\alpha_{j+1} - \alpha_j} = \frac{1}{\Delta\alpha}(\alpha - \alpha_j) = \frac{1}{\Delta\alpha}(\alpha - \alpha_{n_i}) - (j_\alpha - n_i)$$

$$= \frac{\alpha - \alpha_{n_i}}{\Delta\alpha} - \left[\frac{\alpha - \alpha_{n_i}}{\Delta\alpha} \right]$$

and

$$a_j = \frac{\alpha_{j+1} - \alpha}{\alpha_{j+1} - \alpha_j} = \frac{\alpha_j + \Delta\alpha - \alpha}{\Delta\alpha} = 1 - a_{j+1}$$

If $\alpha < \alpha_1$, set $j_a = 1$ and $a_{j+1} = 0$; if $\alpha > \alpha_{n_{Na}}$, set $j_a = n_{N_a} - 1$ and $a_{j+1} = 1$. Similarly, for a given Mach number M search for k such that

$$M_{n_k} \leq M \leq M_{n_{k+1}}$$

then calculate

$$j_m = n_k + \left[\frac{M - M_{n_k}}{\Delta M} \right]$$

$$\Delta M = \frac{M_{n_{k+1}} - M_{n_k}}{n_{k+1} - n_k}$$

$$m_{j+1} = \frac{M - M_{n_k}}{\Delta M} - \left[\frac{M - M_{n_k}}{\Delta M} \right]$$

$$m_j = 1 - m_{j+1}$$

If $M < M_1$, set $j_m = 1$ and $m_{j+1} = 0$; if $M > M_{n_{Nm}}$, set $j_m = n_{N_m} - 1$ and $m_{j+1} = 1$. The appropriate radial station is determined by searching for j_r such that

$$r_{j_r} < r \leq r_{j_r+1}$$

The aerodynamic coefficient is evaluated at the four corners, and then the interpolated value is

$$C = a_j m_j C(j_a, j_m, j_r) + a_j m_{j+1} C(j_a, j_m+1, j_r)$$
$$+ a_{j+1} m_j C(j_a+1, j_m, j_r) + a_{j+1} m_{j+1} C(j_a+1, j_m+1, j_r)$$

Experimental airfoil characteristics are normally available in the form of two-parameter tables, the coefficients defined at a discrete set of angle of attack and Mach number points (not necessarily the same for lift, drag, and moment): $c(j,k)$, $\alpha(j)$, $M(k)$ for $j = 1$ to N_a, $k = 1$ to N_m. These data will be linearly interpolated as required to translate the table into the form required for the present analysis. Hence given an angle of attack α, the list is searched for j such that

$$\alpha_j \leq \alpha \leq \alpha_{j+1}$$

Then

$$a_j = \frac{\alpha_{j+1} - \alpha}{\alpha_{j+1} - \alpha_j} = 1 - a_{j+1}$$

The procedure is similar for the Mach number. Hence the interpolated coefficient is:

$$c = a_j m_k c(j,k) + a_j m_{k+1} c(j,k+1) + a_{j+1} m_k c(j+1,k) + a_{j+1} m_{k+1} c(j+1,k+1)$$

If α or M lie outside the range of the original table, the nearest values are used; the data are not extrapolated beyond the table domain.

It is best to use airfoil tables based on two-dimensional measurements of the section loads. For cases when such measurements are not available, and cannot be approximated by data for similar airfoils, the tables can be synthesized from equations that represent typical airfoil characteristics. The airfoil data preparation used here includes the option to use the following expressions (illustrated in Figures 2-14 and 2-15).

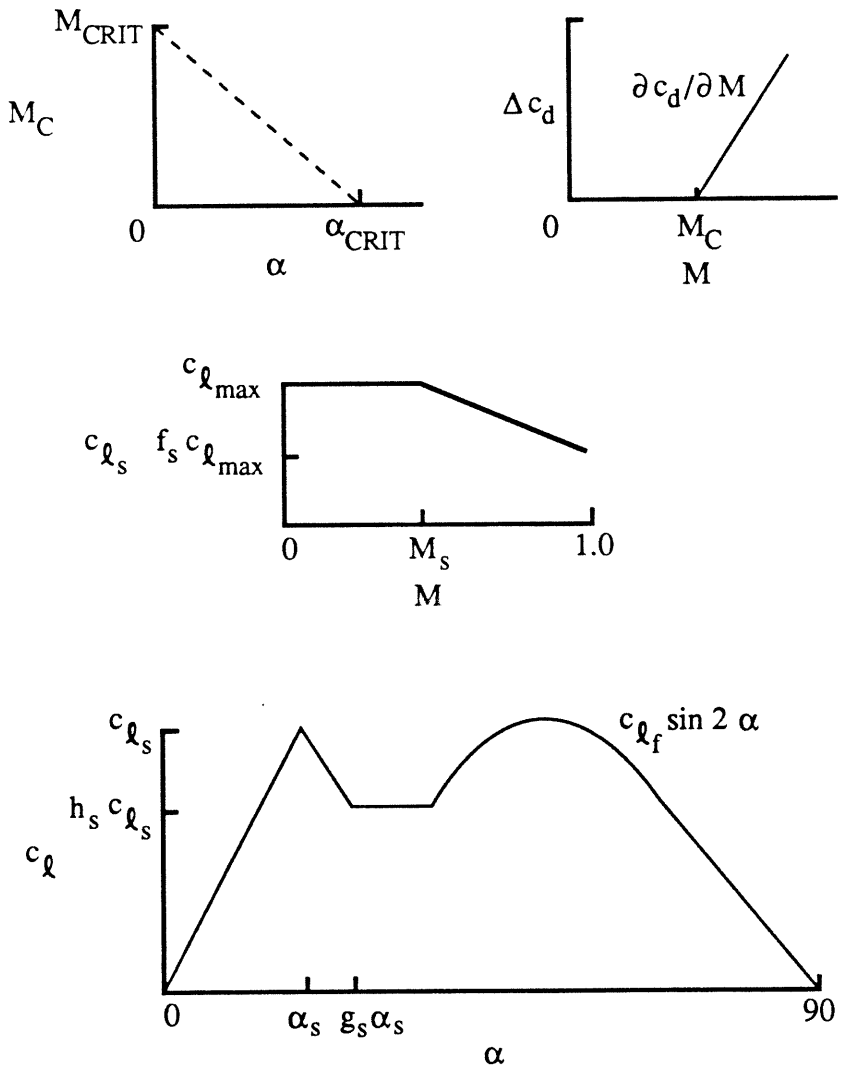

Figure 2-14. Airfoil characteristics--lift and drag coefficients.

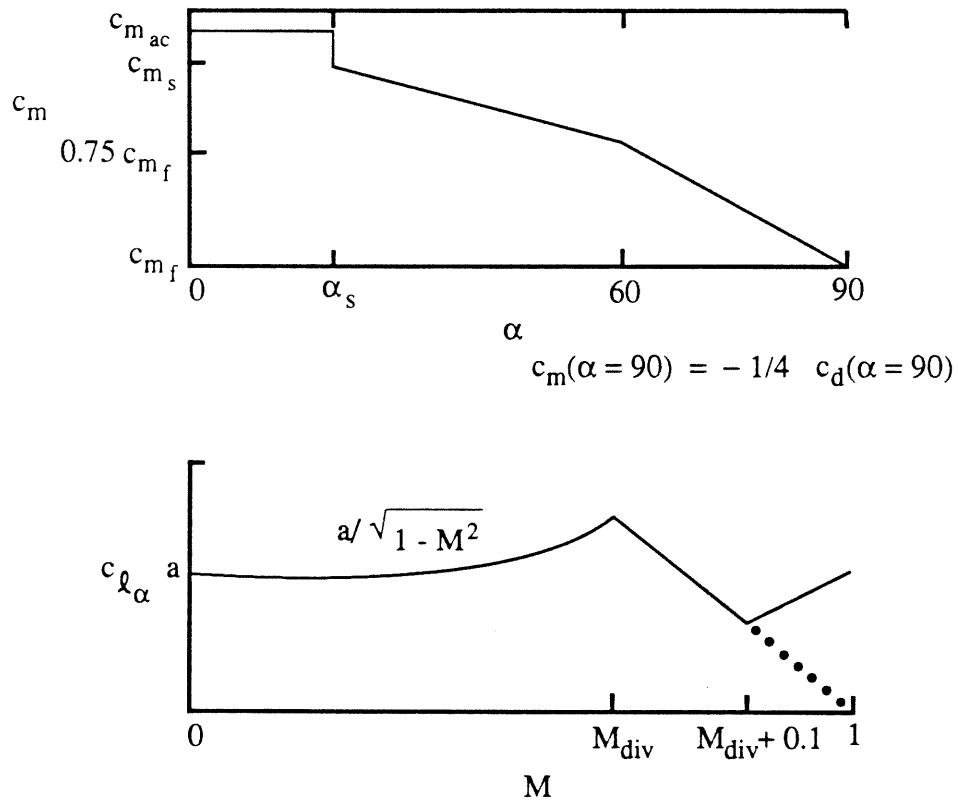

Figure 2-15. Airfoil characteristics--moment coefficient and lift-curve slope.

A) Below stall

$$c_{\ell_\alpha} = \begin{cases} a/\sqrt{1-M^2} & M < M_{div} \\ a(1-M)/((1-M_{div})\sqrt{1-M_{div}^2}) & M_{div} < M < M_{div}+.1 \\ a\left[(1-M)/((1-M_{div})\sqrt{1-M_{div}^2}\right. & M \geq M_{div}+.1 \\ \qquad \left. + (M-M_{div}-.1)/(1-M_{div}-.1)\right] & \end{cases}$$

$$c_\ell = c_{\ell_\alpha} \alpha$$

$$c_m = c_{m_{ac}}$$

$$c_d = \delta_0 + \delta_1 \alpha + \delta_2 \alpha^2 + \Delta c_d$$

$$\Delta c_d = \max\left(0,\ \partial c_d / \partial M\ (M-M_c)\right)$$

$$M_c = \max\left(0,\ M_{crit}\ (1 - |\alpha|/\alpha_{crit})\right)$$

B) Stall angle

$$c_{\ell_s} = c_{\ell_{max}} \min\left(1,\ \frac{(1-M) + f_s(M-M_s)}{1-M_s}\right)$$

$$\alpha_s = c_{\ell_s} / c_{\ell_\alpha}$$

c) Stalled lift ($|\alpha| > \alpha_s$)

$$c_\ell = \text{sign}(\alpha)\ \max\left[\frac{(g_s \alpha_s - |\alpha|)c_{\ell_s} + (|\alpha| - \alpha_s)h_s c_{\ell_s}}{g_s \alpha_s - \alpha_s},\right.$$
$$\left. \max\left(h_s c_{\ell_s},\ c_{\ell_f} \sin 2|\alpha|\right)\right]$$

$$c_\ell = c_{\ell_f} \sin 2\alpha \qquad \text{if} \quad |\alpha| > 45^\circ$$

D) Stalled moment ($|\alpha| > \alpha_s$)

$$c_m = \begin{cases} \text{sign}(\alpha) \dfrac{(60 - |\alpha|)c_{m_s} + (|\alpha| - \alpha_s).75c_{m_f}}{60 - \alpha_s} & |\alpha| < 60^\circ \\ \text{sign}(\alpha) \dfrac{(90 - |\alpha|).75c_{m_f} + (|\alpha| - 60)c_{m_f}}{30} & |\alpha| > 60^\circ \end{cases}$$

$$c_{m_f} = -\tfrac{1}{4}c_d(\alpha = 90) = -\tfrac{1}{4}(c_d(\alpha = \alpha_d) + c_{d_f})$$

E) Stalled drag ($|\alpha| > \alpha_d$)

$$c_d = c_d(\alpha = \alpha_d) + c_{d_f} \sin\left(\frac{|\alpha| - \alpha_d}{90 - \alpha_d} 90\right)$$

F) Reverse flow ($|\alpha| > 90$)

use effective angle of attack and account for moment axis shift

$$\alpha_e = \alpha - \pi \, \text{sign}\alpha$$

$$c_m = c_m + (\tfrac{1}{2}\cos\alpha_e)c_{\ell} + (\tfrac{1}{2}\sin\alpha_e)c_d$$

2.4.5 Tip flow corrections.

Three-dimensional flow effects at the blade tips significantly alter the wing loading. Principally it is necessary to correct the blade element theory section loading calculation for the lift reduction and compressibility relief near the tip. The standard tip loss correction assumes that the blade has drag but no lift outboard of

radial station r = B. Hence for a radial segment extending from r_i to r_{i+1}, the lift coefficient is multiplied by the factor

$$\max\left(0, \min\left(1, \frac{B - r_i}{r_{i+1} - r_i}\right)\right)$$

The moment and drag coefficients are not altered. For the tip loss factor B = .97 can be used, or

$$B = 1 - \frac{\sqrt{2C_T}}{N}$$

Alternatively, the tip losses can be accounted for by multiplying the blade element theory lift by the Prandtl function:

$$F = \frac{2}{\pi} \cos^{-1} e^{(r-1)N/2\lambda_0}$$

An effective tip loss factor can be evaluated from this function:

$$B = 1 - \frac{\lambda_0}{N} 2\ln 2$$

hence

$$F = \frac{2}{\pi} \cos^{-1} e^{-\ln 2\,(1-r)/(1-B)}$$

$$= \frac{2}{\pi} \cos^{-1} \left(\frac{1}{2}\right)^{(1-r)/(1-B)}$$

This tip loss factor takes on different roles for nonuniform inflow and uniform inflow analyses (and so different input parameters will be used to define the tip loss for the two analyses). Lifting line theory in integral form (as used here) will correctly produce zero loading at the wing tip. Hence for the nonuniform inflow analysis, which calculates the induced velocity from the discrete vortex wake, the tip loss factor just represents the radial station of the tip vortex roll up at the blade trailing edge (see section 3.1.2). The use of momentum theory, however, produces an approximation to lifting line theory, in which the blade lift will not go to zero at the tip. Hence for the uniform inflow analysis, which uses an empirical inflow model based on momentum theory, the tip loss factor accounts for the reduction of the loading at the tip by the actual discrete vortex wake. In this case the loading is typically set to zero over the outer 2-3.5% of the blade radius.

The three-dimensional flow at the blade tip increases the critical Mach number of the tip sections, compared to the two-dimensional flow characteristics. This compressible tip relief may be accounted for by reducing the effective section Mach number by the factor f_M, which must be specified at each blade station, for the lift, drag, and moment coefficients. If the blade quarter-chord line is swept at an angle ϵ relative to the reference span line, then the section normal Mach number equals the Mach number calculated from the resultant velocity U, times the sweep factor $f_\epsilon = \cos(\Lambda + \epsilon)/\cos\Lambda$, where Λ is the sweep angle of the flow relative to the span line (see section 2.4.6). Hence the effective Mach number

$$M_{eff} = f_t f_m M$$

is used to evaluate the lift, drag, and moment coefficients from the airfoil tables.

Swept and tapered tip platforms are defined in the present analysis by the blade chord, sweep, aerodynamic center, pitch angle and zero lift angle, center of gravity distributions along the span (c, ϵ, x_A, θ and θ_{ZL}, and x_I). Any sweep of the blade elastic axis at the tip is neglected, however. The tip platform should also be considered in choosing the tip loss factor and the compressible tip relief factors for the rotor blade.

2.4.6 Yawed flow and Reynolds number corrections.

Yawed flow over the blade section may be accounted for using the equivalence assumption for swept wings: that the yawed section drag coefficient is given by two-dimensional airfoil characteristics, and the normal section lift coefficient is not influenced by yawed flow below stall. Since the wing viewed in a frame moving spanwise at a velocity $V\sin\Lambda$ (where V is the wing velocity, yawed at angle Λ) is equivalent to an unyawed wing with free stream velocity $V\cos\Lambda$, except for changes in the boundary layer, there should then be no effect of spanwise flow on the loading below stall. It is also assumed that the total wing drag force is in the direction of the yawed flow. Accounting for the effective dynamic pressure and angle-of-attack of the yawed section relative to the normal section leads to

$$c_\ell(\alpha) = c_{\ell_{2D}}(\alpha\cos^2\Lambda)/\cos^2\Lambda$$

$$c_d(\alpha) = c_{d_{2D}}(\alpha\cos\Lambda)/\cos\Lambda$$

$$c_m(\alpha) = c_{m_{2D}}(\alpha\cos^2\Lambda)/\cos^2\Lambda$$

for the section aerodynamic coefficients in terms of two-dimensional airfoil characteristics. These results are largely verified by the experimental data for yawed wings. The section yaw angle is given by

$$\cos\Lambda = \sqrt{\frac{u_T^2 + u_P^2}{u_T^2 + u_P^2 + u_R^2}}$$

(Λ is positive for u_T and u_R positive; $|\Lambda|$ is less than 90°, so $\cos\Lambda$ is always positive).

Next consider a wing with both yaw Λ of the free stream and sweep ϵ of the wing quarter-chord relative to a reference span line (Figure 2-16). The rotor blade sweep ϵ is positive for aft sweep of the tip. Hence the total sweep angle of the free stream relative to the quarter chord is $(\Lambda + \epsilon)$. The swept wing equivalence assumption relates the aerodynamics of the wing normal and yawed sections. Here the aerodynamic analysis is conducted for blade sections perpendicular to the reference span line. For this analysis section, the aerodynamic coefficients are:

$$c_\ell(\alpha) = c_{\ell_{2D}}(\alpha f_\epsilon \cos^2\Lambda) / \cos^2\Lambda$$

$$c_d(\alpha) = c_{d_{2D}}(\alpha \cos\Lambda) / \cos\Lambda$$

$$c_m(\alpha) = c_{m_{2D}}(\alpha f_\epsilon \cos^2\Lambda) / \cos^2\Lambda$$

The sweep of the wing by ϵ introduces the factor

$$f_\epsilon = \frac{\cos(\Lambda + \epsilon)}{\cos\Lambda} = \cos\epsilon - \sin\epsilon \tan\Lambda$$

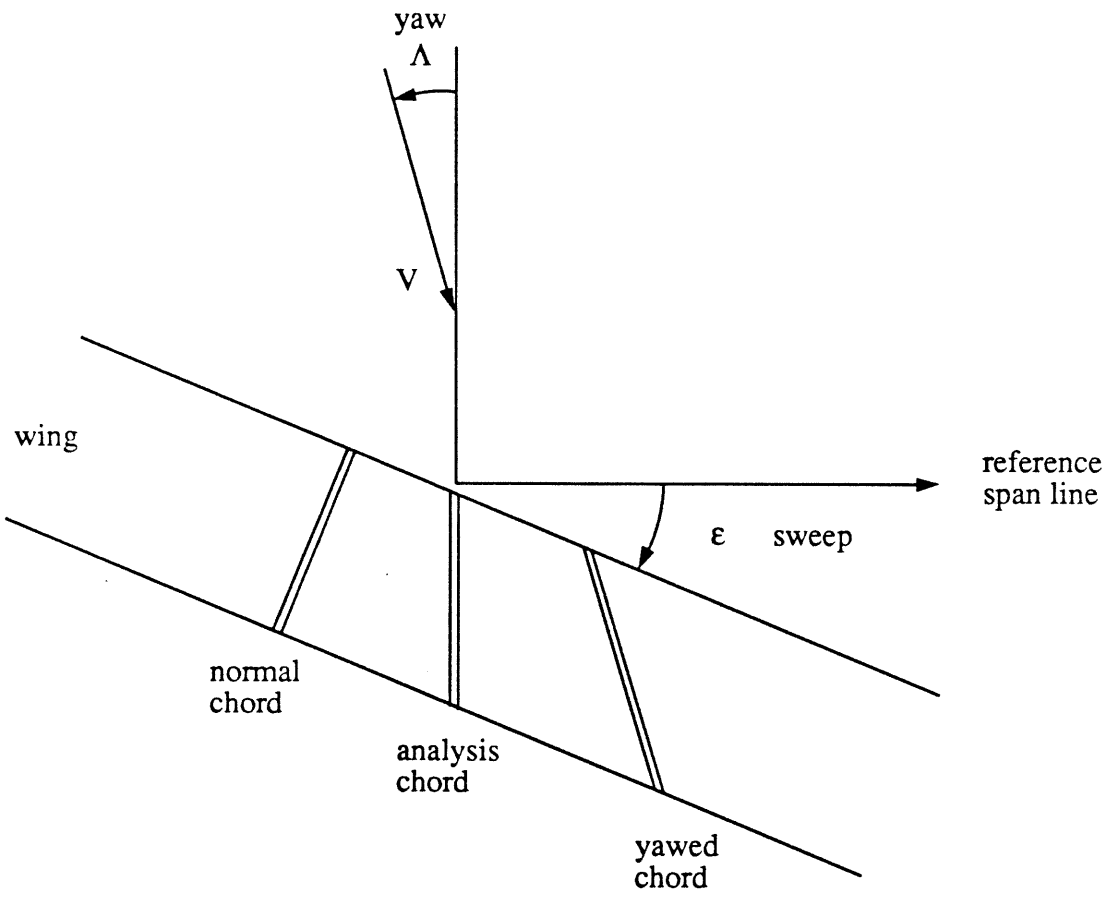

Figure 2-16. Swept and yawed wing aerodynamics.

hence

$$f_t = \begin{cases} \cos\epsilon - (u_R/u)\sin\epsilon & \text{normal flow} \\ \cos\epsilon + (u_R/u)\sin\epsilon & \text{reverse flow} \end{cases}$$

Without yawed flow, $f_\epsilon = \cos\epsilon$, so sweep of the wing reduces the lift-curve-slope of the swept (analysis) section.

The compressibility effects on the swept wing depend on the normal section Mach number:

$$M_n = \frac{\cos(\Lambda+\epsilon)}{\cos\Lambda} M = f_t M$$

This correction has been included in section 2.4.5.

If the Reynolds number Re of the rotor section does not equal the Reynolds number Re_t of the airfoil table, the drag and lift coefficients may be corrected as follows (reference 26):

$$c_d = \frac{1}{K_D} c_{d_t}$$

$$c_\ell = K_L c_{\ell_t} (\alpha/K_L)$$

where $K = (Re/Re_t)^n$. Experimental data for turbulent flow suggests n = 0.125 to 0.2 for the exponent; n = 0.2 is the 1/5th power law for a turbulent flat plate boundary layer. If the Reynolds number is larger for the airfoil than for the table, then K > 1, and the above corrections will reduce the drag coefficient and increase the maximum

lift coefficient. The table Reynolds number can be defined in terms of the Reynolds number corresponding to Mach number = 1:

$$Re_t = M Re_{t1} = \frac{u}{\Omega R} M_{tip} \cos\epsilon \, f_M \, Re_{t1} \left(\frac{f_t}{\cos\epsilon}\right)$$

The actual Reynolds number, for the yawed section, is:

$$Re = V_y c_y / \nu = \frac{u}{\Omega R} \frac{c}{c_m} Re_o \left(\frac{\cos\epsilon}{f_t \cos^2\Lambda}\right)$$

where Re_o is based on the mean chord and rotor tip speed. Hence:

$$\frac{Re}{Re_t} = \left(\frac{Re_o}{Re_{t1}} \frac{c}{c_m} \frac{1}{M_{tip} \cos\epsilon \, f_M}\right) \left(\frac{\cos\epsilon}{f_t \cos\Lambda}\right)^2$$

where the first factor depends only on the blade radial station, not on the flow; and the last factor is the yawed flow effect. Note also that the analysis includes drag and moment coefficient increments (section 2.4.4), which are an alternative means for introducing a Reynolds number correction.

The analysis must combine the yawed flow and Reynolds number corrections, and consider the case of large angle of attack. The correction in reverse flow (for angles of attack near $\pm 180^o$) is analogous to that in normal flow (for angles of attack near 0). The correction will be washed out for angles of attack near $\pm 90^o$ (so $\alpha_e = \alpha$ at $\pm 90^o$), using linear interpolation over a range of $\pm \alpha_o$. Hence the following effective angle of attack is used:

$$\alpha_e = \begin{cases} (\alpha+180)C - 180 & \alpha < -90 - \alpha_0 \\ (\alpha+90)\left[(1-90/\alpha_0)C + 90/\alpha_0\right] - 90 & -90-\alpha_0 < \alpha < -90+\alpha_0 \\ \alpha C & -90+\alpha_0 < \alpha < 90-\alpha_0 \\ (\alpha-90)\left[(1-90/\alpha_0)C + 90/\alpha_0\right] + 90 & 90-\alpha_0 < \alpha < 90+\alpha_0 \\ (\alpha-180)C + 180 & 90+\alpha_0 < \alpha \end{cases}$$

where

$$C = \begin{cases} f_t \cos^2\Lambda / K_L & \text{lift} \\ \cos\Lambda & \text{drag} \\ f_t \cos^2\Lambda & \text{moment} \end{cases}$$

and $\alpha_0 = 30$ is used. In the lift coefficient correction, the case of nonzero lift at zero angle of attack must be considered, as well as reverse flow. Hence:

$$c_d = \frac{1}{K_D \cos\Lambda} c_{d_{2D}}(\alpha_e) + \Delta c_d$$

$$c_m = \frac{1}{\cos^2\Lambda} c_{m_{2D}}(\alpha_e) + \Delta c_m$$

$$c_\ell = \begin{cases} \dfrac{(\alpha+180)f_t}{(\alpha_e+180)}\left[c_{\ell_{2D}}(\alpha_e) - c_{\ell_{2D}}(180)\right] + c_{\ell_{2D}}(180) + \Delta c_\ell & \alpha < -90 \\ \dfrac{\alpha f_t}{\alpha_e}\left[c_{\ell_{2D}}(\alpha_e) - c_{\ell_{2D}}(0)\right] + c_{\ell_{2D}}(0) + \Delta c_\ell & -90 < \alpha < 90 \\ \dfrac{(\alpha-180)f_t}{(\alpha_e-180)}\left[c_{\ell_{2D}}(\alpha_e) - c_{\ell_{2D}}(180)\right] + c_{\ell_{2D}}(180) + \Delta c_\ell & 90 < \alpha \end{cases}$$

The Δc's are increments defined by the dynamic stall model (see section 2.4.7). The form of the lift coefficient correction ensures that the lift-curve slope below stall is unchanged, except for the f_ϵ factor associated with sweep. The drag and moment correction factors will be washed out by using

$$1 + (F-1)\,\frac{|\,|\alpha|-90\,|}{\alpha_0}$$

in the place of the factor F, if α is within $\pm\,\alpha_0$ of $\pm\,90^\circ$.

2.4.7 Dynamic stall model.

Dynamic stall is characterized by a delay in the occurrence of separated flow produced by the blade motion, and high transient loads induced by a vortex shed from the leading edge when stall does occur. These features are modeled by the following procedure, adapted from reference 27. McCroskey (reference 28) and Beddoes (reference 29) have found that the dynamic stall delay correlates fairly well in terms of

the normalized time constant $\tau = \Delta t\ V/c$. Their results for lift and moment stall are:

	τ_L	τ_M
McCroskey	4.3 ± 0.5	2.8 ± 0.2
Beddoes	5.4 ± 0.6	2.45 ± 0.5

or approximately $\tau_L = 4.8$ and $\tau_M = 2.7$ (a time constant τ_D is also required for the drag stall delay). Hence the section lift will be evaluated at the delayed angle of attack

$$\alpha_d = \alpha(\Psi - \Delta\Psi_L) \cong \alpha - \Delta\Psi_L \dot{\alpha}$$

where $\Delta\psi_L = \Omega\Delta t_L = \tau_L c/|U_T|$ (radians). A maximum value of the angle increment should be specified in order to avoid difficulties at small values of u_T. Thus:

$$\alpha_d = \alpha - \min\left(\tau_L \left|\frac{\dot{\alpha} c}{u_T}\right|, \Delta\alpha_{\substack{max \\ delay}}\right) \text{sign}\,\dot{\alpha}$$

is the delayed angle of attack associated with dynamic stall. This delay accounts for hysteresis effects around stall. Similar delayed angles of attack are used for the drag and moment. Hence α_d is used instead of α in the equations for the effective angle of attack α_e (section 2.4.6). Note, however, that α_d does not replace α in the lift coefficient correction factor. Note that the equations for the coefficients include the increments Δc_l, Δc_d, and Δc_m, which are produced by the leading edge vortex.

When the blade section angle of attack reaches the dynamic stall angle α_{ds}, a leading edge vortex is shed. As this vortex passes aft

over the airfoil upper surface it induces large transient loads. The experimental data of reference 30 show that the peak incremental aerodynamic coefficients depend on the pitch rate at the instant of stall, $\dot{\alpha}c/V$, approximately as follows:

$$\Delta c_l = \begin{cases} \Delta c_{l_{ds}} (20\, \dot{\alpha}c/V) & \dot{\alpha}c/V < .05 \\ \Delta c_{l_{ds}} & \dot{\alpha}c/V > .05 \end{cases}$$

$$\Delta c_m = \begin{cases} 0 & \dot{\alpha}c/V < .02 \\ \Delta c_{m_{ds}} (33.3\, \dot{\alpha}c/V - .667) & .02 < \dot{\alpha}c/V < .05 \\ \Delta c_{m_{ds}} & \dot{\alpha}c/V > .05 \end{cases}$$

$$\Delta c_d = \begin{cases} \Delta c_{d_{ds}} (20\, \dot{\alpha}c/V) & \dot{\alpha}c/V < .05 \\ \Delta c_{d_{ds}} & \dot{\alpha}c/V > .05 \end{cases}$$

with $\Delta c_{l_{ds}} = 2.0$ and $\Delta c_{m_{ds}} = -.65$. In the present model of the dynamic stall loads it is assumed that the incremental coefficients due to the shed vortex (Δc_l, Δc_m, and Δc_d) rise linearly to the above peak values in the small azimuth increment $\Delta\psi_{ds}$ (typically 10° to 15°), and then fall linearly to zero in the time $\Delta\psi_{ds}$ again. Hence the model involves impulsive lift and nose down moment increases when dynamic stall occurs, which produce the blade motion and loads characteristic of rotor stall. After these transient loads decay, the blade section is assumed to be in deep stall, and dynamic stall is not allowed to occur again until the flow has reattached. Flow reattachment takes place when the angle of attack drops below the angle α_{re}. Generally a dynamic stall angle about

three degrees above the static stall angle gives good results. Different values of α_{ds}, $\Delta\psi_{ds}$, and α_{re} can be used for the lift, drag, and moment characteristic if necessary to adequately model the dynamic stall of an airfoil. The calculation of the vortex induced lift in dynamic stall is outlined in Figure 2-17.

Note that the parameter STATE in Figure 2-17 takes the following values:

(a) STATE = 0 for attached flow.

(b) STATE = 1 at dynamic stall (when α first exceeds α_{ds}).

(c) STATE increases by 1 with every azimuth step until reattachment (hence is a count of azimuth steps since dynamic stall occurred).

(d) STATE = $\Delta\psi_{ds}/\Delta\psi$ at peak vortex-induced loads, $2\Delta\psi_{ds}/\Delta\psi$ when vortex-induced loads zero again.

(e) STATE set to 1000 when the reverse flow boundary is crossed (since 1000 is greater than $2\Delta\psi_{ds}/\Delta\psi$), so the calculation of vortex-induced loads is not applied across the reverse flow boundary.

The drag and moment are calculated in a similar fashion, except that the drag is not multiplied by sign of (α (90 - $|\alpha|$)); and $\frac{1}{2}\Delta c_l$ is added to the moment in reverse flow.

As an alternative dynamic stall model, consider that developed in references 31 to 33. They introduce an effective angle of attack of the form

$$\alpha_{dyn} = \alpha - \min\left(\tau_L \sqrt{\left|\frac{\dot{\alpha} c}{\mu_T}\right|}, \Delta\alpha_{\substack{max \\ delay}}\right) \operatorname{sign} \dot{\alpha}$$

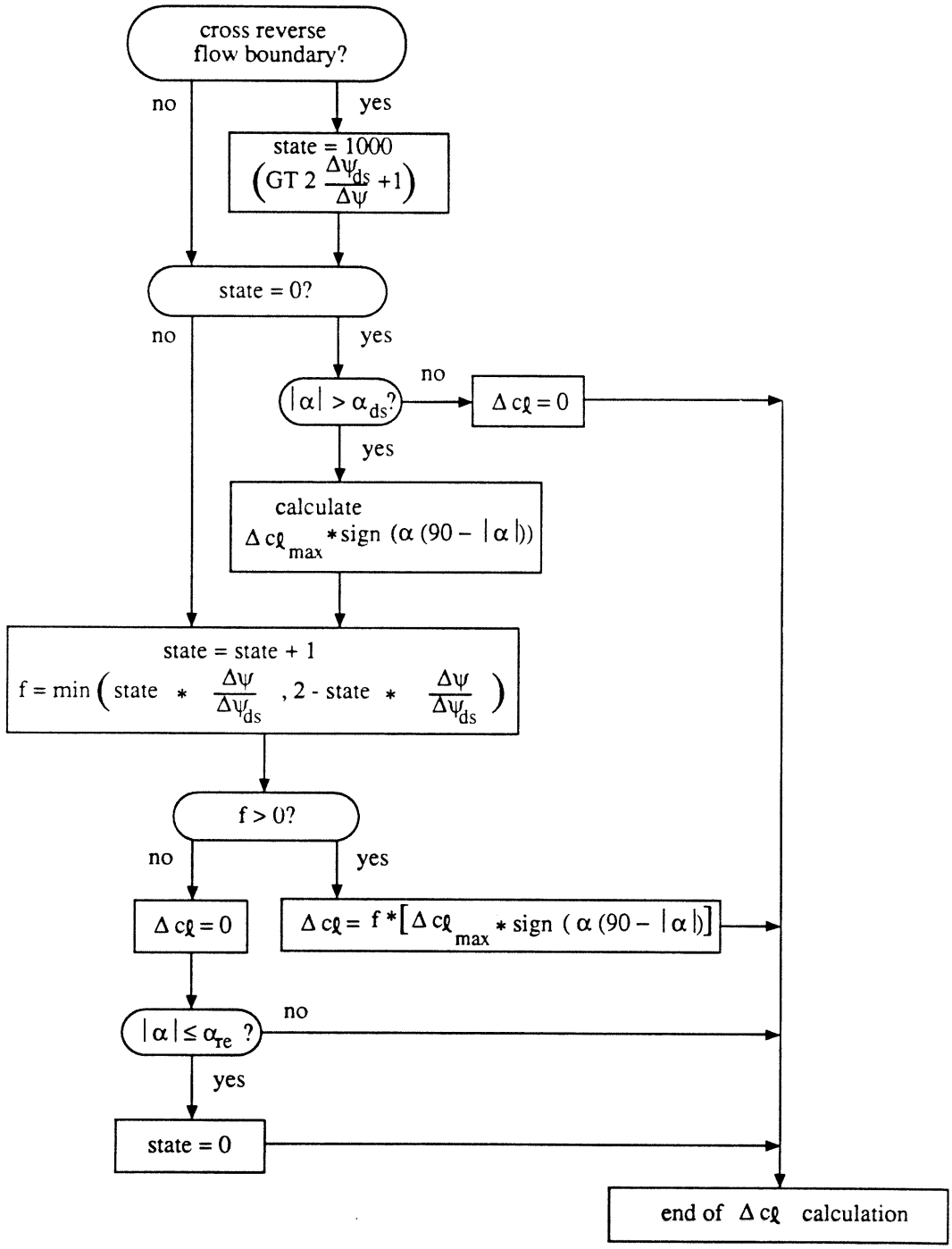

Figure 2-17. Outline of calculation of dynamic stall vortex-induced lift coefficient.

where τ_L is a function of Mach number and the airfoil section obtained from oscillating airfoil tests. This angle α_{dyn} can be used in place of α in the expression for c_l given above, with $\Delta c_l = 0$. Similar corrected angles of attack are calculated for the moment and drag coefficients, using appropriate factors τ_M and τ_D. For an NACA 0012 airfoil, reference 33 gives

$$\tau_L = \max(0, \min(1.71, 2.16 - 2.81 M))$$

$$\tau_M = \tau_D = \max(0, \min(1.12, 1.71 - 2.98 M))$$

(in radians).

A no-stall model can be implemented by using for α_d the smaller of the actual angle of attack α and a maximum angle of attack α_{max} in the linear range (say 10°):

$$\alpha_d = \begin{cases} \min(|\alpha|, \alpha_{max}) \operatorname{sign}\alpha & |\alpha| < 90^\circ \\ \max(|\alpha|, 180^\circ - \alpha_{max}) \operatorname{sign}\alpha & |\alpha| > 90^\circ \end{cases}$$

The incremental coefficients (Δc_l, Δc_m, and Δc_d) should be set to zero as well.

In summary, the following procedure is used to calculate the section aerodynamic coefficients. First, the Mach number corrections are applied to obtain M_{eff}: first the yawed/delayed effective angle of attack is calculated; then c_{l2D}, c_{d2D} and c_{m2D} for α_{eff} and M_{eff} are obtained from two-dimensional steady airfoil tables; c_{l2D} at $\alpha = 0$ or 180° is also required; finally the section coefficients are evaluated. Next the dynamic stall vortex loads Δc_l, Δc_d, and Δc_m are evaluated from α and $\dot{\alpha}$. Finally the tip loss correction is applied to the lift coefficient.

The aeroelastic analysis (see section 6.1.4) requires the derivatives of the section coefficients with respect to angle of attack and Mach number. These derivatives are evaluated by applying the above procedure with small increments in α and M (not M_{eff}). For the purpose of evaluating these derivatives, $\dot{\alpha}$, Λ, and the dynamic stall vortex loads are held constant.

2.4.8 Unsteady lift and moment.

The thin airfoil theory result for the unsteady aerodynamic lift and moment about the pitch axis for the rotary wing is

$$\frac{L_{us}}{ac} = \pm \frac{c}{4} V B \left(1 + 2\frac{x_{Ae}}{c}\right) \pm \frac{c}{8}\left(\dot{w} + u_R w'\right)$$

$$\frac{M_{us}}{ac} = \mp \frac{c^2}{32} V B \left(1 + 4\frac{x_{Ae}}{c}\right)^2 \mp \frac{c^2}{32}\left(\dot{w} + u_R w'\right)\left(1 + 4\frac{x_{Ae}}{c}\right)$$

where x_{Ae} is the distance between the aerodynamic center and the elastic axis:

$$x_{Ae} = \begin{cases} x_{AC} & \text{normal flow} \\ -\left(x_{AC} + \frac{c}{2}\right) & \text{reverse flow} \end{cases}$$

(here x_{AC} must in fact be the position of the aerodynamic center); and in the double sign the upper one is for normal flow and the lower one for reverse flow, $\pm$ = sign (V). Here $w = u_T \sin\theta - u_p \cos\theta$ is the upwash velocity normal to the blade surface (with no order c terms); $B = dw/dx$ is the gradient of the upwash along the chord, as due to a pitch rate; and $V = u_T \cos\theta + u_p \sin\theta$.

In this result the order c^2 lift and order c^3 moment terms have been neglected. The virtual mass terms (aerodynamic forces due to the section pitch and heave acceleration) can also be neglected. The sign changes in reverse flow have been accounted for in this result. Radial flow effects are included in the slender body pressure terms (from the radial derivative w') and in the contributions to the upwash w. The time derivative $\dot{w}$ includes terms due to the time varying free stream. Corrections for real flow effects on the lift-curve slope and aerodynamic center have been included (thin airfoil theory gives $a = 2\pi$ and the aerodynamic center at the quarter chord).

For stalled flow, these unsteady aerodynamic forces can be set to zero ($L_{us} = M_{us} = 0$). The unsteady forces at high angle of attack are accounted for in the dynamic stall model for c_l, c_d, and c_m.

Finally, the velocities required for these unsteady aerodynamic forces are as follows:

$$V = u_T \cos\theta + u_P \sin\theta$$

$$\beta = \dot{\theta} + \beta_G + \vec{\iota}_B \cdot (z_o\vec{\imath} - x_o\vec{k})' + u_R\theta'$$

and from $w = u_T\sin\theta - u_P\cos\theta$, $u_P = \dot{z} + u_R z' + u_{Po}$, and $u_T = u_{To} + \dot{x} + u_R x'$, there follows

$$\dot{w} + u_R w' = V\dot{\theta} + \dot{u}_T \sin\theta - \dot{u}_P \cos\theta + u_R(V\theta' + u_T' \sin\theta - u_P' \cos\theta)$$

$$= V(\dot{\theta} + u_R\theta') + (\dot{u}_T + u_R u_T')\sin\theta - (\dot{u}_P + u_R u_P')\cos\theta$$

$$= V(\dot{\theta} + u_R\theta') + \sin\theta\,(u_R + u_R\dot{x}' + \dot{u}_R x' + \ddot{x} + u_R + u_R\dot{x}' + u_R^2 x'') - \cos\theta\,(u_R\dot{z}' + \dot{u}_R z' + \ddot{z} + u_R\dot{z}' + u_R^2 z'')$$

$$= V(\dot{\theta} + u_R\theta') + 2u_R\sin\theta + (\ddot{x} + 2u_R\dot{x}' + \dot{u}_R x' + u_R^2 x'')\sin\theta - (\ddot{z} + 2u_R\dot{z}' + \dot{u}_R z' + u_R^2 z'')\cos\theta$$

$$= V(\dot{\theta} + u_R\theta') + 2u_R\sin\theta + 2u_R\sin\theta\,(\dot{\alpha}_z + \dot{\psi}_s) + \dot{u}_R\sin\theta\,(\alpha_z + \psi_s) - 2u_R\cos\theta\,\dot{\beta}_G - \dot{u}_R\cos\theta\,\beta_G - 2u_R\vec{\tau}\cdot(z_o\vec{\tau} - x_o\vec{k})' - \dot{u}_R\vec{\tau}\cdot(z_o\vec{\tau} - x_o\vec{k}) - u_R^2\vec{\tau}\cdot(z_o\vec{\tau} - x_o\vec{k}) + r\sin\theta\,(\ddot{\alpha}_z + \ddot{\psi}_s) - r\cos\theta\,\ddot{\beta}_G - \vec{\tau}\cdot(z_o\vec{\tau} - x_o\vec{k})''$$

with $u_R = \mu_x\cos\psi - \mu_y\sin\psi$, and using

$$z' = \beta_G + \vec{\tau}_B\cdot(z_o\vec{\tau} - x_o\vec{k})'$$

$$x' = \alpha_z + \psi_s + \vec{k}_B\cdot(z_o\vec{\tau} - x_o\vec{k})'$$

2.4.9 Circulation.

The blade bound circulation is required for the wake induced velocity calculation:

$$\Gamma = \frac{1}{2} U c c_l + \Gamma_{us}$$

Thin airfoil theory gives for the unsteady circulation (below stall)

$$\frac{\Gamma_{us}}{ac} = \frac{c}{4} B \left(1 + 2 \frac{x_{AC}}{c}\right)$$

(see section 2.4.8).

2.5 Environment

The aerodynamic environment of the helicopter is defined by the speed of sound c_s, the air density ratio to sea level standard ρ/ρ_o, and the kinematic viscosity $\nu = \mu/\rho$. These parameters can be calculated from the altitude h for a standard day; from the pressure altitude and temperature τ; or from the density and temperature.

For a standard day (with constant temperature lapse rate) or for input temperature, the density ratio, speed of sound, and viscosity are obtained from the following expressions.

$$\frac{T_s}{T} = 1 - \frac{h}{T_0/\beta}$$

$$\frac{T}{T_0} = \begin{cases} T_s/T_0 & \text{standard day} \\ (T_1+\tau)/T_0 & \text{input temperature} \end{cases}$$

$$\frac{\rho}{\rho_0} = \left(\frac{T_s}{T_0}\right)^{g/\beta R} \left(\frac{T}{T_0}\right)^{-1}$$

$$c_s = c_{s_0} \left(\frac{T}{T_0}\right)^{\frac{1}{2}}$$

$$\mu = \mu_0 \frac{(T/T_0)^{3/2}}{0.723\,(T/T_0) + 0.277}$$

For the case of temperature and altitude specified, the density altitude is

$$h_d = \frac{T_0}{\beta}\left(1 - \left(\frac{\rho}{\rho_0}\right)^{\frac{1}{g/\beta R - 1}}\right)$$

Alternatively, the air density and temperature can be specified directly. Then the equivalent altitude can be obtained from

$$h_e = \frac{T_0}{\beta}\left(1 - \left(\frac{\rho}{\rho_0}\frac{T}{T_0}\right)^{\frac{1}{g/\beta R}}\right)$$

The required constants are given in the table below.

Constants	English units		SI units
dimension h	ft		m
dimension τ	^{o}F		^{o}C
$g/\xi R$		5.256115	
$(g/\xi R-1)^{-1}$		0.234956	
T_0/ξ	145442 ft		44330.8 m
T_0	518.67 ^{o}R		288.15 ^{o}K
T_1	459.67 ^{o}R		273.15 ^{o}K
c_{s_o}	1116.45 ft/sec		340.294 m/sec
g	32.17405 ft/sec^2		9.80665 m/sec^2
ρ_o	.002378 slug/ft^3		1.225 kg/m^3
$(g/\xi R)^{-1}$		0.190255	
μ_o	3.7373E-7 slug/ft-sec		1.7894E-5 kg/m-sec

2.6 Normalization Parameters

It has been the practice here to deal with dimensionless quantities based on the air density, rotor speed, and rotor radius (ρ, Ω, and R). In addition, the equations of motion, the inertial coefficients, and the aerodynamic forces have been normalized using the following parameters: I_b, a characteristic moment of inertia of the blade; c_m, the blade mean chord; and a, the blade two-dimensional lift-curve slope. The rotor coefficients are often divided by the solidity, σ. The values of these parameters have no influence on the numerical problem and its dimensional solution; they only affect the values of normalized, dimensionless quantities. The rotor solidity is taken as the primary (input) parameter; then the mean chord is $c_m = (\pi\sigma R)/N$. The characteristic inertia used is the moment of inertia of the blade about the center of rotation:

$$I_b = \int_0^R r^2 m \, dr$$

calculated from the input blade mass distribution. For normalization, the value a = 5.7 is used. From these parameters, the blade Lock number can be calculated:

$$\gamma = \rho a c_m R^4 / I_b$$

which is also used to normalize certain quantities.

With the section mass defined at radial stations r_i (i = 1 to M) the characteristic moment of inertia is:

$$\int_0^1 r^2 m \, dr = \sum_{i=2}^{M} \int_{r_{i-1}}^{r_i} r^2 \, \frac{m_{i-1}(r_i - r) + m_i (r - r_{i-1})}{r_i - r_{i-1}} \, dr$$

$$= \sum_{i=2}^{M} m_{i-1} f(r_i, r_{i-1}) - m_i f(r_{i-1}, r_i)$$

where

$$f(x,y) = \int_y^x r^2 \, \frac{x-r}{x-y} \, dr = \frac{1}{12}(x^3 + x^2 y + x y^2 - 3y^3)$$

3. ROTOR WAKE ANALYSIS

The rotor nonuniform inflow is calculated using a vortex wake model developed for this analysis. The wake analysis involves two tasks: calculation of the wake-induced velocities and calculation of the resulting aerodynamic loading on the rotor blade. The blade loading is calculated using lifting line theory. The induced velocity calculation depends on the strength and geometry of the vorticity in the rotor wake. An existing free wake geometry analysis, which efficiently calculates the distorted geometry of the tip vortices of the rotor in forward flight, has been incorporated. This free wake geometry analysis is not applicable in hover.

Available empirical models are used for the wake geometry in hover. These models generally define well (compared with experiment) the radial and vertical position of the tip vortex when it first encounters the following blade. This position has a major role in determining the radial distribution of the loading. The far wake vertical convection determines the density of the circumferential vorticity in the wake, hence it controls the value of the mean induced velocity at the rotor disk. Typically fine tuning of the far wake vertical convection rate is needed to obtain a reasonable power calculation. Such tuning can be done for individual cases, but it is preferable to correlate the analysis with hover performance for a wide range of rotors. It is the nature of such empirical models that they must be adjusted, within the scope of the original data, to give good results with a particular wing analysis.

The tip vortex roll-up process is not calculated in the present analysis. Several details of the roll up have a major influence on the solution: the effect of the vortex roll up on the tip loading of the generating blade; the strength of the tip vortex when it encounters the following blade; and the core radius when the vortex is fully rolled up. The key features are modeled, not calculated, primarily because the

techniques are not well developed to calculate them accurately and efficiently. As a result, the model for the rolled up wake is quite simple (and hence efficient), emphasizing the properties of the tip vortex, which is in fact the most important component in the rotor wake. The loads produced by close blade-vortex interaction may be calculated using a second order lifting line theory, using a lifting surface theory correction, or using an empirical vortex core radius.

3.1 Nonuniform Wake-Induced Velocity

3.1.1 Rotor vortex wake.

Conservation of vorticity on a three-dimensional wing requires that the bound circulation is trailed into the wake from the blade tip and root. Radial variation of the bound circulation produces trailed vorticity in the wake, parallel to the local free stream direction at the instant it leaves the blade. Azimuthal variation of the bound circulation will produce shed vorticity, oriented radially in the wake. The strength of the trailed and shed vorticity is determined by the radial and azimuthal derivatives of the bound circulation at the time the wake element left the blade. The lift and circulation are concentrated at the tip of the rotating wing, due to the larger dynamic pressure there. Consequently, the trailed vorticity strength is high at the outer edge of the rotor wake, and the vortex sheet quickly rolls up into a concentrated tip vortex. The formation of this tip vortex is influenced by the blade tip geometry. With square tips, much of the roll up has occurred by the time the vortex leaves the trailing edge. The rolled up tip vortex quickly attains a strength nearly equal to the maximum bound circulation of the blade. The tip vortex has a small core radius, depending on the blade geometry and loading. The vorticity in the tip vortex is distributed over a small but finite region, called the vortex core, due to the viscosity of the fluid. The vortex core radius is defined at the maximum tangential velocity. The vortex core is an

important factor in the wake-induced velocity, since it limits the maximum velocity induced near a tip vortex. Only a limited amount of data on the vortex core radius is available, particularly for rotary wings. There is an inboard vortex sheet of trailed vorticity in the wake, with opposite sign as the tip vortex. Since the gradient of the bound circulation is low on the inboard portion of the blade, the root vortex is generally much weaker and more diffuse than the tip vortex.

On a lifting rotor in hover or low speed forward flight, the bound circulation Γ is positive along the entire span of the blade. There may be local minima or maxima from blade-vortex interaction, but generally Γ monotonically increases and decreases, with a peak at a radial station near the tip. In high speed forward flight however, the bound circulation can be negative at the blade tip in the second quadrant of the rotor disk. This negative loading is a consequence of moment balance on a flapping rotor, especially with large negative twist. Over much of the disk Γ is still positive all along the blade span, but in a range of azimuths on the advancing side, the bound circulation has a negative peak near the tip, and a positive peak inboard. So, in this region the tip vortex will be formed with negative strength, and there will be a sheet of positive trailed vorticity created from the inboard positive peak to the outboard negative peak. This sheet probably rolls up to some extent, but the peaks are usually widely separated (implying a small gradient), so the roll up will not be as extreme as for the tip vortices of the rotor.

There are other cases with major positive and negative bound circulation peaks. For example, a tiltrotor in cruise (propeller operation, with twist less than optimum for the flight speed) will have negative loading inboard and positive loading outboard on the blade. A highly twisted blade, such as on a tiltrotor or even some helicopter rotors, can encounter negative loading at the tip even in edgewise flight at moderate speeds. Local minima and maxima in bound circulation can also be expected, such as from strong blade-vortex interaction or

from reverse flow in high speed forward flight. In this analysis, the wake roll up will be modeled rather than calculated, so only the two major cases are considered: (1) Γ vs. r with a single peak (all the same sign at a given ψ); and (2) Γ vs. r with dual peaks, from one region of positive Γ and one region of negative Γ. More complicated radial distributions of bound circulation can be encountered, but in such cases the roll up should be calculated in more detail.

The trailed and shed vorticity of the rotor wake is created in the flow field as the blades rotate, and then convected with the local velocity of the fluid. This local velocity consists of the free stream velocity, and the wake self-induced velocity. The wake is transported downward, normal to the disk plane, by a combination of the mean wake-induced velocity and the free stream velocity. The wake is transported aft of the rotor disk by the in-plane component of the free stream velocity. The self-induced velocity of the wake also produces substantial distortion of the vortex filaments as they are convected with the local flow. Thus, the wake geometry basically consists of distorted interlocking helices, one behind each blade, skewed aft in forward flight.

The strong concentrated tip vortices trailed in helices from each blade are the dominant feature of the rotor wake. Due to its rotation, a rotor blade encounters the tip vortex from the preceding blade in both hover and forward flight. These tip vortices produce a highly nonuniform flow field through which the blades must pass. In hover the tip vortex is convected downward only slightly until after it encounters the next blade. The vortex produces a large variation in the tip loading on the following blade, therefore, with a substantial influence on the rotor hover performance. In forward flight the rotor wake is convected downstream, so the tip vortices are swept past the entire rotor disk instead of remaining in the tip region. The close vortex/blade encounters occur primarily on the sides of the disk, where the blades sweep over the vortices. The resulting large azimuthal

variation in the induced velocity produces a large higher harmonic content of the blade loading. Nonuniform inflow is thus an important factor in the vibration, loads, and noise of the rotor in forward flight. In a tandem helicopter, the rear rotor also encounters the wake of the front rotor.

For close vortex-blade encounters, the induced loading varies rapidly along the blade span. First-order lifting-line theory overpredicts such loading, particularly if the radial or azimuthal resolution is not small enough. The analysis incorporates three approaches to improve the calculation of blade-vortex loads: (1) use of second-order lifting-line theory; (2) use of a lifting-surface theory correction; and (3) use of an empirical vortex core radius. Second-order lifting-line theory (three-quarter-chord collocation point) is also required if the lifting-line is not straight, as with a swept tip. As an alternative to second-order lifting-line theory, a lifting-surface correction can be applied, as a factor reducing the vortex-induced velocity as required to obtain the correct loading. This factor is the ratio of the lifting-surface loading to the lifting-line loading, for an infinite aspect-ratio, nonrotating wing encountering a straight, infinite, constant-strength free vortex. (Note that with this approach the actual blade angle-of-attack at blade-vortex interactions will be larger than calculated for the lifting-line theory loading solution.) The simplest option is to increase the tip vortex core radius, thereby reducing the induced loading to simulate the lifting-surface effect. Even when the second-order lifting-line theory or the lifting-surface theory correction is used, the core radius may have to be larger than the true physical value, in order to compensate for the radial or azimuthal resolution being too large.

An examination of measured rotor airloads indicates that the vortex-induced loading is generally high when the blade first encounters a vortex, but decreases as the blade sweeps over the vortex. There is evidently some phenomenon limiting the loads (see references 34 to 36).

Local flow separation due to the high vortex-induced radial pressure gradients on the blade may be responsible for the reduction in loading after the initial encounter. Bursting of the vortex core induced by the blade is also a possibility. Another possibility is that the vortex interacts with the trailed wake it induces behind the blade, with the effect of diffusing the vorticity. Note that the latter two phenomena, involving a change in the tip vortex itself, will also influence the loading when the vortex encounters yet another blade of the rotor. The phenomenon limiting vortex-induced loads after the initial encounter will be modeled by increasing the core radius of a vortex segment for inboard collocation points on the blade. An increase in core size is a convenient means to reduce the influence of the vortex; the exact physical explanation for this phenomenon is at present speculative.

A possible model for the tip vortex viscous core is solid body rotation, which implies that all the vorticity is concentrated within the core radius r_c (defined at the point of maximum tangential velocity). Measured vortex velocity distributions show that the maximum tangential velocity is much less then $\Gamma/2\pi r_c$, implying that a substantial fraction of the vorticity is outside the core radius. Reference 35 suggests using a circulation distribution

$$\gamma = \Gamma \frac{r^2}{r^2 + r_c^2}$$

based on measured velocity distributions of vortices from nonrotating wings; the corresponding vorticity distribution is

$$\zeta = \frac{\Gamma}{\pi r_c^2} \left(\frac{r_c^2}{r^2 + r_c^2} \right)^2$$

where r is the distance from the vortex line. In this case half the vorticity is outside the core radius. Along a line at right angles to the vortex and a distance h above it (as in a blade/vortex intersection), this vorticity distribution produces a downwash with peak value

$$w_{max} = \frac{\Gamma}{4\pi\sqrt{h^2 + r_c^2}}$$

a distance $(h^2 + r_c^2)^{\frac{1}{2}}$ either side of the intersection; compared to $w_{max} = \Gamma/4\pi h$ at a distance h from the intersection for a vortex with no core. (Note that as far as the downwash velocity is concerned, this core effect is equivalent to moving the vortex away from the blade, to an effective distance $h_e = (h^2 + r_c^2)^{\frac{1}{2}}$; such a simple interpretation will be useful in the lifting-surface correction.) The peak tangential velocity with this vorticity distribution is $\Gamma/4\pi r_c$, half the value obtained with all the vorticity concentrated within the core radius.

There are many factors that determine the magnitude of vortex-induced loading on a rotor blade: the tip vortex strength; extent of the tip vortex roll up; the viscous core radius; local vortex geometry distortions; lifting-surface effects on the induced blade loading; and possibly vortex bursting or vortex-induced stall on the blade. In addition to such physical phenomena, the calculated peak loading can also depend on the radial and azimuth resolution in the discretized wake. In the absence of theoretical or experimental information to guide the modeling of these phenomena, the vortex core radius is a convenient parameter with which to account for their cumulative influence on the rotor blade loading.

The rotor wake induced velocity is calculated by integrating the Biot-Savart law over the vortex elements in the rotor wake. The wake strength is determined by the radial and azimuthal variation of the bound circulation. For the wake geometry a simple assumed model, experimental measurements, or a calculated geometry can be used. With the helical geometry of the rotary wing wake, it is not possible to analytically evaluate the induced velocity, even if the self-induced distortion of the wake is neglected. A direct numerical integration of the Biot-Savart law is not satisfactory either, because the large variations in the induced velocity at close vortex/blade encounters requires a small integration step size for accurate results. It is most accurate and most efficient to calculate the rotor nonuniform inflow with the wake modeled using a set of discrete vortex elements. For each vortex element in the wake the induced velocity at a point in the flow field is evaluated by analytical expression, and the total induced velocity is obtained by summing contributions from all elements. The tip vortex is well represented by a connected series of straight-line vortex segments. The inboard trailed and shed vorticity can be modeled using vortex sheets, or a lattice of discrete straight-line vortex segments (with a large effective core to limit the induced velocity close to individual line segments). A large core vortex line element might in some cases be a better model than a sheet for the inboard trailing vorticity, if the inboard wake has partially rolled up to form a root vortex. The inboard wake is less important to the nonuniform inflow calculation than the tip vortices, so a more approximate model may be used. The approximations involved in modeling the rotor wake using a set of discrete vortex elements include replacing the curvilinear geometry by a series of straight-line or planar segments; a simplified distribution of vorticity over the individual wake elements (linear variation, or even constant strength); and perhaps physical approximations such as the use of line elements to represent the inboard

vortex sheet. The development of a practical model involves a balance between the accuracy and efficiency resulting from such approximations.

3.1.2 Wake and wing model.

The rotor aerodynamic analysis is based on lifting-line theory (ref. 37), which separates the problem into wing and wake models, coupled by the induced velocity and bound circulation. Guided by the results of perturbation theory, a practical implementation is as follows. The outer problem consists of an incompressible vortex wake from a lifting-line, with distorted wake geometry. The trailed wake arises from the bound vortex at the quarter-chord (an approximation for the second-order wing loading). The shed wake is created a quarter-chord aft of the collocation point on the wing (a lifting-line approximation for unsteady aerodynamics; see ref. 38). The three components of induced velocity are evaluated at the wing collocation points from the wake vorticity, excluding the bound vortex. The collocation points are at the wing three-quarter-chord, in the direction of the local flow (an approximation for the second-order induced velocity). The inner problem consists of unsteady, compressible, viscous flow about an infinite aspect-ratio, yawed wing. This wing is in a uniform flow consisting of the yawed free stream and the three components of wake-induced velocity. The inner problem is split into two-dimensional, steady, compressible, viscous flow (airfoil tables); with corrections for unsteady aerodynamics (linear noncirculatory loads, but with no shed wake), dynamic stall, and yawed flow (based on the swept wing equivalence assumption). This model is described in section 2.4.

This lifting-line analysis is generally second-order (in the inverse of the aspect-ratio) accurate for lift, including the effects of sweep and yaw, but less accurate for pitch moments. With the wing collocation point at the quarter-chord, a first-order lifting-line theory is obtained. For typical blade-vortex separations, second-order

lifting-line theory (collocation points at three-quarter chord) is often as accurate as lifting-surface theory. First-order lifting-line theory (collocation points at quarter chord) will, however, overpredict the peak blade-vortex interaction loads, perhaps by 20-30% for very small separation. A lifting-surface correction is available for the first-order lifting-line theory blade-vortex interactions (section 3.1.7).

The wing geometry is defined by the quarter-chord position and the chord (x_A and c, as a function of r), measured perpendicular to a straight reference span axis. The inner problem, then, is an infinite aspect-ratio wing with the local chord, sweep, and yaw.

The blade bound circulation will be calculated at discrete points on the rotor disk radially and azimuthally. Assuming a linear variation of the bound circulation between these known points results in a wake model consisting of vortex sheet panels (see Fig. 3-1). Assume that the blade bound circulation $\Gamma(r, \psi)$ is given at the radial stations r_i (i = 1 to M) and at the azimuthal stations $\psi_j = j\Delta\psi$ (j = 1 to J, $\Delta\psi = 2\pi/J$). Let ϕ be the age of vortex elements in the wake ($\phi_k = k\Delta\psi$, k = 0 to ∞). The strength of the trailed and shed vorticity of a wake element is determined by the bound circulation of the blade at the time the vorticity was created. Consider a wake panel of age $\phi = \phi_k$ to ϕ_{k+1}, arising from the blade between radial stations r_i and r_{i+1} (Fig. 3-2). The strength of the vorticity in this panel is determined by the bound circulation at the time it was created, which is known at the four corners. The bound circulation corresponding to the panel leading edge is that at time $\psi - \phi_k$, where ψ is the current blade position (dimensionless time) and $\phi_k = k\Delta\psi$ is the age of the panel at the leading edge. The bound circulation corresponding to the panel trailing edge is that at $\psi - \phi_{k+1}$, $\Delta\psi$ earlier than the leading edge. The difference between the bound circulation at r_i and r_{i+1} defines the trailed vorticity strength δ, which is constant radially along the panel assuming a linear variation of the bound circulation from r_i to r_{i+1}.

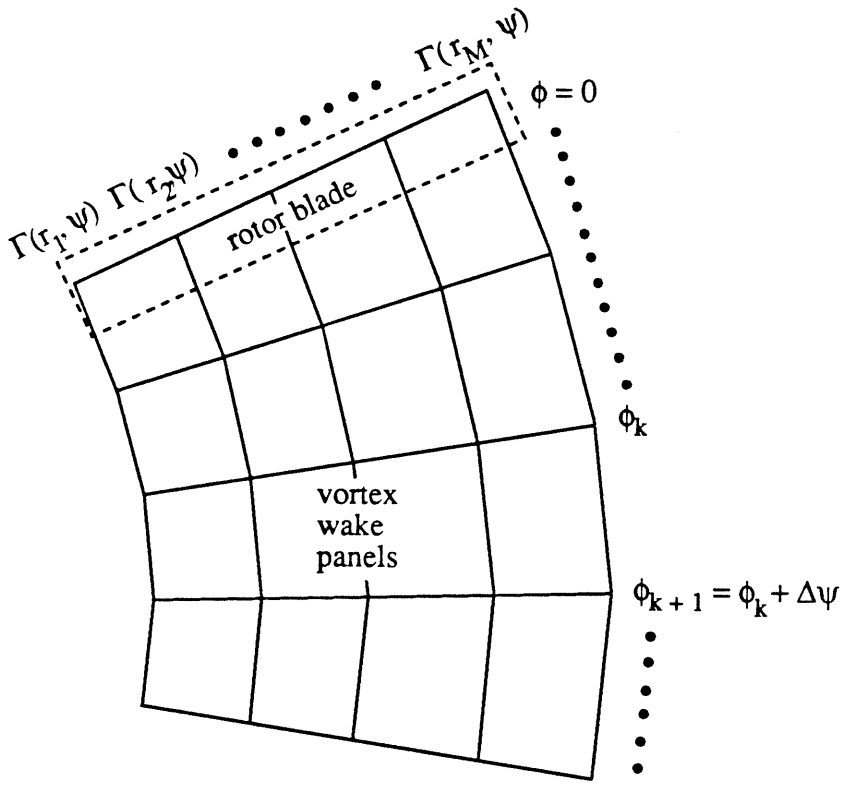

Figure 3-1. Wake model with bound circulation calculated at discrete points on rotor disk.

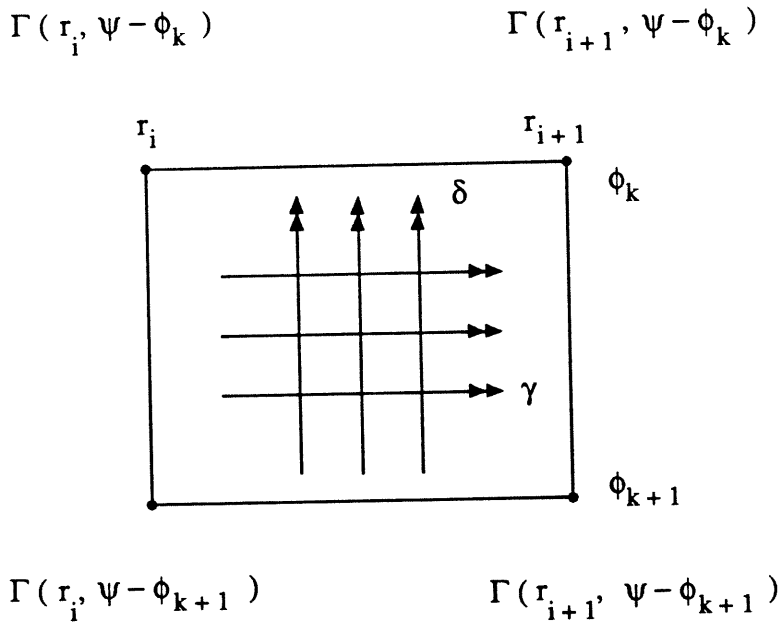

Figure 3-2. Vortex wake panel.

When the bound circulation varies azimuthally, however, the trailed vorticity strength δ is different at the panel leading and trailing edges; a linear variation of δ in the direction of the trailed vorticity will be used. Similarly, the difference between the bound circulation at $\psi - \phi_k$ and $\psi - \phi_{k+1}$ defines the shed vorticity strength γ, which is constant azimuthally along the panel (for a linear azimuthal variation of the bound circulation) but varies linearly from the left to the right panel edges.

A vortex sheet panel in the wake may be economically approximated by shed and trailed line vortices located in the middle of the panel, with a large core to avoid the induced velocity singularity near a vortex line. A vortex lattice model of the rotor wake is produced by collapsing all the wake panels to such finite strength line segments. Since the line segments are in the center of the sheets, the points at which the induced velocity and bound circulation are evaluated lie at the midpoints of the vortex lattice grid, both radially and azimuthally. Positioning the collocation points midway between the trailed vortex elements (radially) is a standard practice of wing theory utilizing the vortex lattice wake model, in order to avoid the singularities at the lines; positioning the collocation points midway azimuthally is required to correctly obtain the unsteady aerodynamic effects of the shed wake (see ref. 39). Simply collapsing the shed and trailed vorticity in the wake panels to lines, the strength of the line segments will vary along their length as described above. The shed and trailed line segments will cross in the middle of the panel. As a further approximation, a stepped (piecewise constant) variation of strength can be used instead of the linear variation, with the jump in strength occurring at the center of the segment where it crosses the other vortex line. Such a vortex lattice wake model with constant-strength line segments corresponds to a stepped distribution of the blade bound circulation, azimuthally and radially (with the jumps occurring midway between the points where the circulation is evaluated).

The rotor vortex wake quickly rolls up at the outer edge to form a concentrated tip vortex. Because of the dominant role of the tip vortex in the wake flow field, it is important to model these rolled up tip vortices in the induced velocity calculation. The lesser role of the inboard wake vorticity also allows a more approximate model to be used for it. Consider first the case with a single bound circulation peak (Γ entirely of the same sign, positive or negative, radially along the blade at a given azimuth). Let $\Gamma_{max}(\psi)$ be the radial maximum of the blade bound circulation. It is assumed that in the far wake, where the roll-up process is complete, that all of the bound circulation Γ_{max} is concentrated in the tip vortex. The tip vortex will be modeled by a vortex line segment with a small but finite core radius. When Γ_{max} varies azimuthally, the tip vortex strength varies along its length. Furthermore, the inboard portion of the wake will be modeled by a single sheet panel, with trailed and shed vorticity as described above. Since an analysis of the roll up is not attempted here, the actual vorticity distribution over the inboard sheet is not known. Hence an approximation involving constant strength determined by the known maximum bound circulation is appropriate. This far wake model may be viewed as corresponding to the circulation distribution sketched in Figure 3-3. The linear variation from $\Gamma = 0$ at the root to $\Gamma = \Gamma_{max}$ at the tip defines the single inboard sheet, and the sharp drop from Γ_{max} to zero at the tip defines the tip vortex line. (This circulation distribution should not be associated with the actual bound circulation at the rotor blade. Rather it is an approximate representation of the vorticity distribution in the far wake, which is determined by the roll-up process.) This far wake model is computationally efficient, since it depends only on the maximum bound circulation Γ_{max}.

The roll-up process may not be complete by the time the tip vortex encounters the following blade. The induced loads will be significantly lower if the tip vortex has strength less than the maximum bound circulation. Therefore, the tip vortex roll-up will be included in the

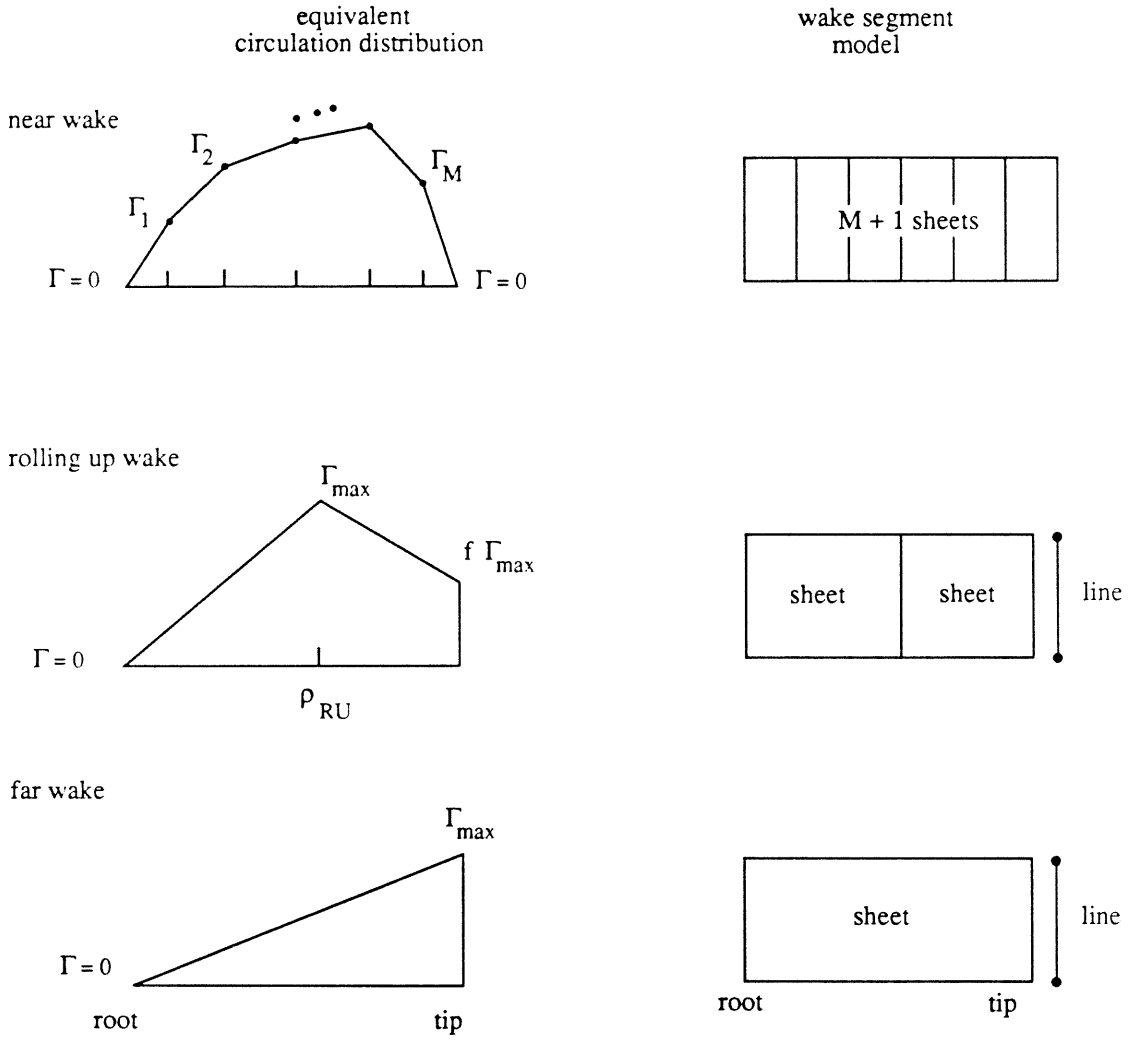

Figure 3-3. Equivalent circulation distribution and resulting wake segment models.

wake model. Figure 3-3 sketches the radial circulation distribution assumed, which produces the model for the rolling up wake. The circulation goes from zero at the root to Γ_{max} at radial station ρ_{RU}; to $f\Gamma_{max}$ at the tip. Thus there is a line tip vortex of strength $f\Gamma_{max}$, and two inboard wake panels. The roll-up process will take place over the wake from $\phi = 0$ to $\phi = \phi_{RU}$. The position of the maximum circulation and the roll-up fraction will vary linearly from r_{RU} and f_{RU} at $\phi = 0$, to $\rho = 1$ and $f = 1$ at $\phi = \phi_{RU}$. An analysis of the roll-up process is not part of the present work, so the parameters ϕ_{RU}, r_{RU}, and f_{RU} will be prescribed inputs to the calculation procedure. Note that the velocity induced by the rolling up wake will also depend only on the single bound circulation value Γ_{max}.

Consider now the case of a radial distribution of bound circulation with two peaks of opposite sign. Let $\Gamma_O(\psi)$ be the outboard peak (positive or negative) and $\Gamma_I(\psi)$ the inboard peak, located at radial stations r_{GO} and r_{GI}, respectively. The most important requirement of the wake analysis is that the rotor tip vortices be well modeled. If the single peak wake model based on Γ_{max} (Figure 3-3) is applied to a dual peak loading case, the tip vortex will have the correct strength and sign only if Γ_{max} is the most outboard peak. In the case of a helicopter rotor in forward flight, however, typically there is a small negative bound circulation at the tip, and a large positive bound circulation inboard; in this case the tip vortex $\Gamma_{max} = \Gamma_I$ will have the wrong sign, and a magnitude too large as well. Retaining the single peak wake model, the tip vortex will at least be correct if Γ_O is used instead of Γ_{max}.

To improve the modeling of the inboard wake vorticity, a dual peak wake configuration can be used. Figure 3-4 shows the wake model and equivalent circulation distribution for the far wake and rolling up wake. In the rolled up far wake it is assumed that the outboard peak Γ_O produces the tip vortex; and that the inboard peak Γ_I, located at ρ_{GI}, breaks the inboard sheet into two elements, in each of which the trailed

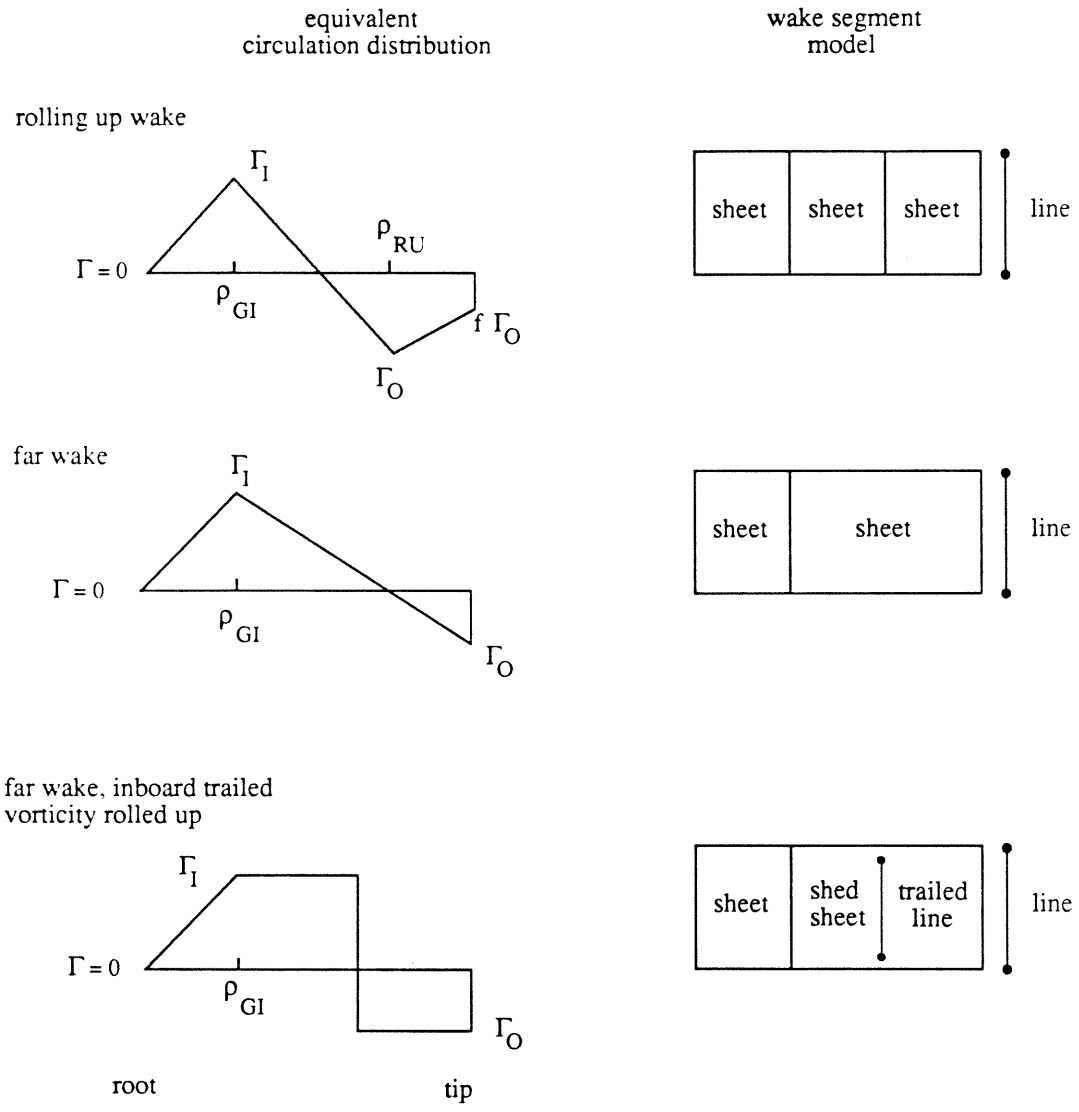

Figure 3-4. Dual peak model: equivalent circulation distribution and resulting wake segment models.

vorticity has constant strength radially. Similarly, the rolling up wake now has three elements for the inboard sheet. Typically the slope from Γ_I to Γ_0 is small, so strong roll up inboard is unlikely. Hence the resulting trailed vorticity (from ρ_{GI} to the tip) can optionally be represented by either a sheet or a rolled up line. The line segment will be placed in the middle of the panel and will have a core radius, probably much larger than the core radius of the tip vortex. (It is possible to use line segments as an efficient approximation for a sheet element; here the line is intended as a physical model of the roll up, with the actual core size.)

The wake geometry specification for the dual peak model requires the parameter $\rho_I(\psi)$, which may be input or obtained from the calculated location of Γ_I (using the latest available solution). Consistency between the value of ρ_{GI} used for the wake geometry (and hence for the influence coefficients) and the current value of r_{GI} in the circulation solution must be a concern. The solution method (see section 5.3.5) includes an iteration on the influence coefficient calculation, for cases where the wake geometry depends significantly on the loading solution. Often this iteration is not required when the rotor is trimmed to a specified thrust and tip-path-plane angle of attack. The effect of ρ_{GI} may require the iteration now. The possibility that the inboard peak is absent in the wake geometry (ρ_{GI}) is treated by using the single peak model for azimuths where that occurs. Then any inboard peak in the circulation solution will be ignored in evaluating the induced velocity, since the corresponding influence coefficient will be zero. The possibility that the inboard peak is absent in the circulation solution (r_{GI}) is treated by interpolating between $\Gamma = 0$ and Γ_0 to define Γ_I. Then the dual peak wake model will give the single peak result.

In summary, two wake configuration models are considered for the far wake and rolling up wake: single peak and dual peak. For the single peak configuration, either Γ_{max} or Γ_0 can be used (the influence

coefficients are the same); using Γ_0 is best in general. For the dual peak configuration, the inboard trailed vorticity from (Γ_I - Γ_0) can be rolled up or not. The single peak model based on Γ_0 is the most efficient configuration that meets the objective of modeling the tip vortex correctly. It is assumed that there is only one zero crossing of $\Gamma(r)$. The influences on the roll up of two or more zero crossings, and of local peaks from blade-vortex interactions, are not dealt with here. For such complicated configurations the roll up should be calculated rather than modeled.

Just behind the reference blade (where the induced velocity is being calculated), it is the detailed radial and azimuthal variation of the wake vorticity that is important, not the roll-up process. Hence for the near wake of the reference blade, the full vortex panel representation is retained. Figure 3-3 illustrates the circulation distribution for the near wake model, which in this case is the actual bound circulation distribution. The bound circulation is calculated at the aerodynamic radial stations, where the induced velocity is being calculated. Again, a piecewise linear variation of Γ implies a vortex sheet panel, with the trailed and shed vorticity strength varying linearly along their direction (Figure 3-1). A vortex lattice approximation then places the trailed and shed lines in the middle of the sheets, still with linearly varying strength.

The geometry of the near wake will be defined in terms of these sheet panels. However, vortex sheet elements will not be used, since the discretization of the wake is better behaved using line segments. Some difficulties with sheets elements arise from the edge and corner singularities, and the fact that only a planar-rectangular element can be integrated analytically. Also, the most important case of the induced velocity from the two sheet panels adjoining the collocation point requires a higher order element. Hence a vortex lattice model of the near wake is always used here.

The panel geometry is given by the locations of the corners: radially at the root, tip, and aerodynamic stations; azimuthally at $\psi - \phi_k$ (leading edge) and $\psi - \phi_{k+1}$ (trailing edge). The panel edges are straight lines joining the corners. The trailed lines are placed in the middle of the panel (interpolated from the corner position), or at the root and tip for the most inboard and most outboard panels respectively. Specifically, the end points of a trailed line are on the panel leading edge and trailing edge, at the radial stations of the aerodynamic panel boundaries (see section 2.4.1). Then the collocation points at the aerodynamic radial stations are equidistant from the nearest trailed lines. The shed lines are placed in the middle ($\phi_k + \Delta\psi/2$) of the panels (interpolated from the corner position), and moved aft by 3c/4 (c/4 if the collocation points are on the quarter chord). Specifically, the end points of a shed line are on the panel side edges, 3c/4 aft of the midpoints. The collocation points are on the three-quarter-chord position at the aerodynamic radial stations (or optionally on the quarter-chord, for a first-order lifting-line theory). Specifically, the collocation points are on the side edges of the first wake panels, c/2 aft of the leading edge (so the geometry of the wake is used to obtain the local flow direction).

The geometry of this discretization of the shed and trailed vorticity and the collocation points is well controlled. Note that in defining the lifting-line (bound vortex) at the quarter-chord, reverse flow is being ignored (for the wake geometry only; the loads are properly applied on the blade). With a vortex lattice model and the distorted helical geometry of the rotor wake, the possibility of the collocation points being too near a line segment is a concern (especially near the reverse flow boundary). A solid-body rotation core is used to avoid singular velocities near the near wake lines, with a radius equal to one-fifth the panel width. So, in normal configurations this core will have no influence on the induced velocity.

The tip vortex is rolled up substantially by the time it reaches the blade trailing edge, even with a highly tapered tip. Many of the effects of such roll up cannot be obtained with lifting-line theory, but it is important to include the radial station r_{TV} of the roll up in the near wake model. Typically for rectangular plan for blades the vortex rolls up 1-1.5% radius inboard of the tip. With all the bound circulation in the trailed vorticity, there can be no lift outboard of this station. The near wake model has trailed lines from the aerodynamic segment boundaries and the tip (replacing the sheets shown in Figure 3-3). Hence the bound circulation can be forced to be trailed at r_{TV} by using the factor

$$\max\left(0, \min\left(1, \frac{r_{TV} - r_i}{r_{i+1} - r_i}\right)\right)$$

on the lift coefficient at aerodynamic station $r_{Ai} = \frac{1}{2}(r_{i+1} - r_i)$ (where r_i are the aerodynamic segment boundaries; see section 2.4.1). Note that if r_{TV} is placed exactly at one of the aerodynamic segment boundaries, then there will be exactly zero bound circulation outboard of r_{TV}, and so zero wake strength. This factor is calculated and used just as is the tip-loss factor for uniform inflow (section 2.4.5), but r_{TV} is the physical roll-up position, while the tip loss B is an empirical correction.

For computing the induced velocity, the tip vortices will be represented by a connected series of straight vortex line segments, with a small viscous core radius. Normally a linear variation of the strength along each segment will be used; a piecewise constant variation corresponding to a stepped bound circulation distribution is also possible. The inboard wake panels will be represented by vortex sheets,

with shed and trailed vorticity varying linearly along their length. For computational economy, the vortex sheets can be replaced by line segments in the middle of the sheets, with a large core radius (which in this case does not have physical significance, rather a viscous core is a convenient means for eliminating the singularity near a line used to represent a sheet element).

The complete model of the rotor wake is sketched in Figure 3-5, which shows the tip vortex and inboard sheets of the various wake regions. For the dual circulation peak configuration, there will be an additional sheet panel in the rolling up wake and far wake. The near wake is used only behind the reference blade. Figure 3-6 shows the corresponding line segment models, always used for the near wake, and available as an option for the rolling up and far wake inboard sheets. When calculating the induced velocity at points off the rotor blade, as at another rotor or for the airframe aerodynamics, the near wake model is not used. Calculating the induced velocity away from the rotor may require a consideration of more wake spirals than are needed for points on the rotor disk.

3.1.3 Geometry.

A nonrotating tip path plane coordinate frame with origin at the rotor hub will be used for the induced velocity calculation. The solution process will iterate between the induced velocity calculation, and the harmonic blade motion and helicopter trim solution (using uniform inflow to start the cycle). Thus the hub plane orientation (S system) will be updated based on a new induced velocity estimate. In contrast, the tip path plane orientation is well defined by the helicopter or rotor trim, hence is less sensitive to changes in the induced velocity estimate. Also, the rotor wake geometry is simplest when defined relative to the tip path plane. The tip path plane tilt relative to the hub plane is given by the first harmonics of the tip deflection $z_{TIP} = \beta_G + \Sigma_i q_i \vec{i}_B \cdot \vec{\eta}_i(1)$:

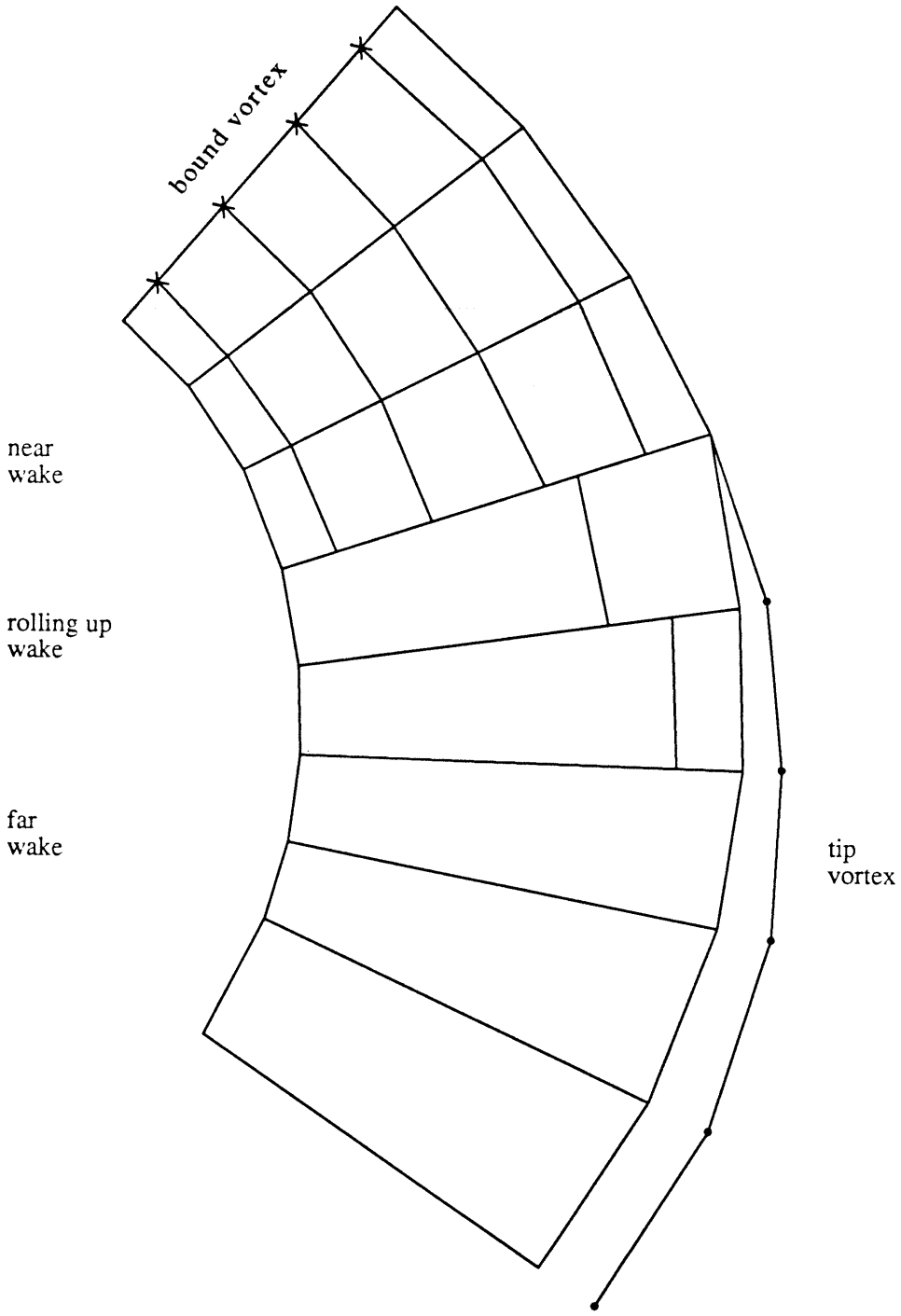

Figure 3-5. Sketch of wake model for nonuniform induced velocity calculation.

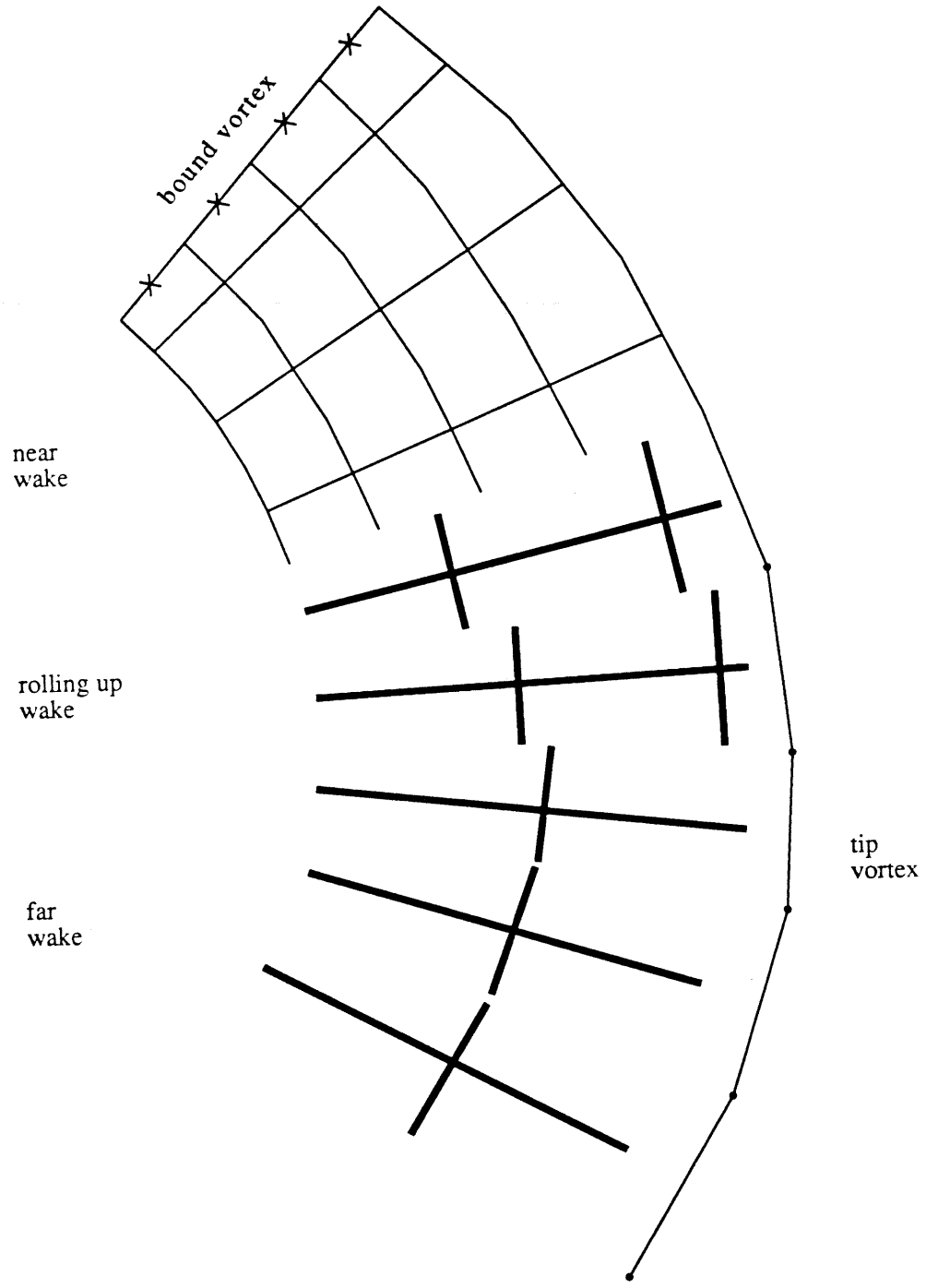

Figure 3-6. Sketch of wake model, showing actual near wake model and possible far wake model using vortex line segments.

$$\beta_c = (\beta_G)_{1c} + \sum_i \beta_{1c}^{(i)} \vec{i}_B \cdot \vec{\eta}_i \quad (1)$$

$$\beta_s = (\beta_G)_{1s} + \sum_i \beta_{1s}^{(i)} \vec{i}_B \cdot \vec{\eta}_i \quad (1)$$

The rotation matrix

$$R_{TS} = \begin{bmatrix} 1 & 0 & \beta_c \\ 0 & 1 & \beta_s \\ -\beta_c & -\beta_s & 1 \end{bmatrix}$$

will transform position and velocity vectors from the shaft axes (S system) to the tip-path-plane axes (T system).

The induced velocity is required at the radial station r_n along the rotor blade. These points, together with the root and tip locations, also define the starting position of the wake geometry. From the section 2.2.4, the position vector of the rotor blade is:

$$\vec{r}_b = \vec{i}_B \left[-x_{FA} + (r - r_{FA})\delta_{FA_3} - r\psi_s - \vec{k}_B \cdot (z_0 \vec{i} - x_0 \vec{k}) + x_A \cos\theta \right]$$

$$+ \vec{j}_B r$$

$$+ \vec{k}_B \left[-z_{FA} - (r - r_{FA})\delta_{FA_2} + r(\beta_G + \delta_{FA_1}) + \vec{i}_B \cdot (z_0 \vec{i} - x_0 \vec{k}) - x_A \sin\theta \right]$$

where $\vec{i}_B = (\sin\psi\vec{i}_s - \cos\psi\vec{j}_s)$, $\vec{j}_B = (\cos\psi\vec{i}_s + \sin\psi\vec{j}_s)$, and $\vec{k}_B = \vec{k}_s$. The pitch is $\theta = (\theta_{coll} + \theta_{tw})$, neglecting perturbations as higher order. Transforming to the tip patch plane (neglecting second-order terms) gives then:

$$\vec{r}_b = \vec{i}_T \left\{ \sin\Psi \left[-x_{FA} + (r - r_{FA})\delta_{FA_3} - r\Psi_s - \vec{k}_B \cdot (z_0\vec{i} - x_0\vec{k}) + x_A \cos\theta \right] + r\cos\Psi \right\}$$

$$+ \vec{j}_T \left\{ -\cos\Psi \left[-x_{FA} + (r - r_{FA})\delta_{FA_3} - r\Psi_s - \vec{k}_B \cdot (z_0\vec{i} - x_0\vec{k}) + x_A \cos\theta \right] + r\sin\Psi \right\}$$

$$+ \vec{k}_T \left\{ -z_{FA} - (r - r_{FA})\delta_{FA_2} + r(\beta_0 + \delta_{FA_1}) + \vec{i}_B \cdot (z_0\vec{i} - x_0\vec{k}) - x_A \sin\theta - r(\beta_c \cos\Psi + \beta_s \sin\Psi) \right\}$$

The lifting-line is defined at the quarter-chord, hence at the chord position x_A aft of the reference axis (ignoring the c/2 shift of the aerodynamic center in reverse flow). For the root station, x_A and θ_{tw} of the most inboard aerodynamic radial station is used. For the tip station, x_A and θ_{tw} are extrapolated from the two most outboard aerodynamic stations to r = 1. Optionally, a straight lifting-line can be used, by omitting the x_A terms. It is useful in the computation of $\vec{r}_b$ to have the option to suppress the in-plane deflection; to suppress all the harmonics except the mean; to linearly interpolate the geometry between the root and the tip; or to suppress the twist angles in the x_A terms.

The wake induced velocity is also required at points in the flow field off the rotor disk:

(a) at the wing/body, horizontal tail, and vertical tail for the rotor/airframe aerodynamic interference;

(b) at the other rotor hub for rotor/rotor aerodynamic interference;

(c) at an arbitrary point in the flow field; and

(d) at the reference blade of the other rotor, for detailed rotor/rotor aerodynamic interference.

For the first two, only the mean value of the induced velocity will be used in the present analysis. The induced velocity distribution over the disk of the other rotor can be used in the present analysis only if the two rotors have the same rotational speed (see section 5.1.11); so for the single main rotor and tail rotor configuration, the rotor/rotor interference can be accounted for only in terms of the induced velocity at the rotor hub. The position vector of the wing/body is

$$R_{TS} R_{SF} \left(-\vec{r}_R + \vec{r}_{WB} \right)$$

where $\vec{r}_R$ and $\vec{r}_{WB}$ are the position of the rotor hub and the wing/body center of action, in the body axes (F system). The vectors for the horizontal tail, vertical tail, and other rotor hub are similar. For the induced velocity of rotor #2, these vectors must be multiplied by R_1/R_2. For the induced velocity at the disk of rotor #2 due to the wake of rotor #1, the position vector is

$$\vec{r}_{z/1} = \left(R_{TS} R_{SF}\right)_1 \left[-\vec{r}_{R1} + \vec{r}_{R2} + \frac{R_2}{R_1} \left(R_{TS} R_{SF}\right)_2^T \vec{r}_{bz}\left(r_{n2}, \Psi + \Delta\Psi_{21}\right) \right]$$

$$= \vec{r}_{\substack{\text{other} \\ \text{hub}}} + R_{z1} \vec{r}_{bz}\left(r_{n2}, \Psi + \Delta\Psi_{21}\right)$$

where $\Delta\psi_{21}$ is the azimuth angle of the reference blade of rotor #2 when $\psi = 0$ for rotor #1 (see section 5.1.5) and

$$R_{21} = (R_{TS}R_{SF})_{\substack{\text{this}\\\text{rotor}}} (R_{TS}R_{SF})^T_{\substack{\text{other}\\\text{rotor}}} \quad \frac{R_{\text{other rotor}}}{R_{\text{this rotor}}}$$

The position vector for the induced velocity at the disk of rotor #1 due to the wake of rotor #2 is

$$\vec{r}_{12} = \frac{R_1}{R_2} (R_{TS}R_{SF})_2 \left[-\vec{r}_{R2} + \vec{r}_{R1} + (R_{TS}R_{SF})_1^T \vec{r}_{b1}(r_{n1}, \psi - \Delta\psi_{21})\right]$$

$$= \vec{r}_{\substack{\text{other}\\\text{hub}}} + R_{21}\vec{r}_{b1}(r_{n1}, \psi - \Delta\psi_{21})$$

If the rotor rotates clockwise, it is necessary to change the sign of the $\vec{j}_s$ component of $\vec{r}$ (between the R_{TS} and R_{SF} rotation matrices).

The geometry of the tip vortex behind the reference blade will be defined by the vector $\vec{r}_w(\psi,\phi)$, where ψ is the present azimuth angle of the blade and ϕ is the age of the vortex element. The wake geometry is required at the discrete azimuth positions $\psi_l = l\Delta\psi$ and wake ages $\phi_k = k\Delta\psi$, where l ranges from 1 to J (one revolution of the blade, with $\Delta\psi = 2\pi/J$) and k ranges from zero to the specified number of wake spirals for the induced velocity calculation. The tip vortex geometry behind the other blades of the rotor can be obtained for $\vec{r}_w$ at the appropriate azimuth angle. The tip vortex elements are created at the blade tip ($\vec{r}_b$ at radial station r = 1), convected with the free stream velocity $\vec{\mu}$, and distorted by the self-induced velocity in the wake. The rotation of the

wing together with convection by the free stream velocity produces the basic helical geometry of the rotor wake. As at the rotor disk, the induced velocity throughout the wake is highly nonuniform. The actual position of the wake elements, determined by the integral of the local convection velocity, is thus highly distorted from the basic helical form. The resulting wake geometry is

$$\vec{r}_w(\psi,\phi) = \vec{r}_b(\psi-\phi) + \phi\vec{\mu} + \vec{D}(\psi,\phi)$$

where $\vec{D}(\psi,\phi)$ is the distortion due to the wake self-induced velocity (note $\vec{D}(\psi,0) = 0$) and the free stream convection velocity is

$$\vec{\mu} = R_{TS}\begin{pmatrix}\mu_x\\-\mu_y\\-\mu_z\end{pmatrix} = \begin{pmatrix}\mu_x - \beta_c\mu_z\\-\mu_y - \beta_s\mu_z\\-\mu_z - \beta_c\mu_x + \beta_s\mu_y\end{pmatrix}$$

relative to the tip path plane.

In a steady turn, the motion of the rotorcraft relative to the air produces additional convection terms. In E axes, the location of the center of the turn is

$$\vec{r}_c = \begin{pmatrix}R_t \sin\psi_{FP}\\-R_t\cos\psi_{FP}\\-Vt\sin\theta_{FP}\end{pmatrix}$$

with the turn radius $R_t = (V\cos\theta_{FP})/\dot{\psi}_F$ (see section 4.1.1 for the definition of the parameters in these expressions). The orientation of the E axes relative to a fixed frame is

$$R_{EC} = Z_{\psi_F}$$

where $\psi_F = \dot{\psi}_F t - \psi_{FP}$. Then the position $\vec{r}_W$ of a wake element (created at the blade portion, at time $\psi - \phi$), relative the current hub position (tip-path-plane axes, at time ψ) is

$$\vec{r}_w = R_{TC}(\psi) R_{CT}(\psi-\phi)\left[\vec{r}_b(\psi-\phi) + R_{TF}\vec{r}_R + R_{TE}\vec{c}\,(\psi-\phi)\right] - \left[R_{TF}\vec{r}_R + R_{TE}\vec{c}\,(\psi)\right]$$

Now $R_{TC}(\psi)R_{CT}(\psi - \phi) = R_{TE}Z_{\dot{\psi}_F\phi}R_{ET}$; and

$$Z_{\dot{\psi}_F\phi} = \begin{bmatrix} \cos\dot{\psi}_F\phi & \sin\dot{\psi}_F\phi & 0 \\ -\sin\dot{\psi}_F\phi & \cos\dot{\psi}_F\phi & 0 \\ 0 & 0 & 1 \end{bmatrix}$$

$$= \begin{bmatrix} 1 & 0 & 0 \\ 0 & 1 & 0 \\ 0 & 0 & 1 \end{bmatrix} + \Delta Z_1$$

$$= \begin{bmatrix} 1 & \dot{\psi}_F\phi & 0 \\ -\dot{\psi}_F\phi & 1 & 0 \\ 0 & 0 & 1 \end{bmatrix} + \Delta Z_2$$

So

$$\vec{r}_w = \vec{r}_b(\psi-\phi) + R_{TE}\,\Delta z_1\,R_{ET}\left[\vec{r}_b(\psi-\phi) + R_{TF}\,\vec{r}_R\right] + R_{TE}\,\Delta z_2\,\vec{r}_c(\psi-\phi) + R_{TE}\begin{vmatrix} -R_t\dot{\psi}_F\cos\psi_{FP} \\ -R_t\dot{\psi}_F\sin\psi_{FP} \\ V\sin\theta_{FP}\end{vmatrix}\phi$$

$$= \vec{r}_b(\psi-\phi) + \phi\,\vec{\mu} + \vec{D}(\psi,\phi) + R_{TE}\,\Delta z_1\,R_{ET}\,\vec{r}_b(\psi-\phi) + R_{TE}\left[\Delta z_1\,R_{EF}\,\vec{r}_R + \Delta z_2\,\vec{r}_c\right]$$

where the distortion $\vec{D}$ has been introduced in the last step. The effect of the turn rate on the self-induced distortion (prescribed or calculated) is not considered. The turn rate produces an order $\dot{\psi}_F/\Omega$ change in the geometry. Since the pitch component of the turn rate relative the banked aircraft axes ($\dot{\psi}_F\sin\phi_{FT}$) is normally positive (nose up), a principal effect of the turn rate is to reduce the rotor-wake separation on the rear of the disk, and increase it on the front.

Similarly the geometry of the inboard wake sheet will be defined at the root and tip edges, trailing from the blade position $\vec{r}_b$ at radial stations $r = r_{root}$ and $r = 1$, respectively; and at the aerodynamic radial stations. The distortion D will be different for the tip vortex and the inboard sheet. Because of the dominant role of the tip vortices, the most important information in the wake geometry is the tip vortex position, and a less accurate definition of the inboard sheet geometry is often acceptable. The distortion D will be evaluated for the root and tip edges of the inboard sheet, and then interpolated to the aerodynamic radial stations:

$$\vec{D} = \frac{\vec{D}_{root}(1 - r_{A_i}) + \vec{D}_{tip}(r_{A_i} - r_{root})}{1 - r_{root}}$$

The induced velocity calculation may require the wake geometry beyond the point where the stored distortion ends. For this portion of the wake rigid geometry will be used. Consider the distortion $\vec{D}(\psi,\phi)$ when the age ϕ is greater than the age of the last element in the known distortion, $\phi_{last} = K_{WG}\Delta\psi$. The wake geometry will be extrapolated from ϕ_{last} to ϕ, using only vertical convection produced by the mean induced velocity:

$$\vec{D}(\psi,\phi) = \vec{D}(\psi - (\phi - \phi_{last}), \phi_{last}) - (\phi - \phi_{last}) K_2 \vec{k}$$

with K_2 defined below. Note that the azimuth angle of the blade at the time the wake element was created, $\psi - \phi$, has been held constant.

For the self-induced distortion of the rotor wake geometry, the following models are considered: (a) rigid or prescribed wake; and (b) calculated free wake geometry (see section 3.2). The prescribed wake geometry is defined by two-stage vertical convection and exponential radial contraction:

$$\vec{D} = \begin{pmatrix} D_r \cos(\psi - \phi) \\ D_r \sin(\psi - \phi) \\ D_z \end{pmatrix}$$

where the convection and contraction are independent of ψ:

$$\Delta z = \begin{cases} -K_1 \phi & \phi < 2\pi/N \\ -K_1 \frac{2\pi}{N} - K_2 \left(\phi - \frac{2\pi}{N}\right) & \phi > 2\pi/N \end{cases}$$

$$\Delta r = -\left(1 - e^{-K_3 \phi}\right)\left(1 - K_4\right) r_i$$

Here $r_i = 1$ for the tip vortex and the outside edge of the inboard shed, and $r_i = r_{root}$ for the inside edge. Note that K_4 is then the radial location of the contracted tip vortex in the far wake. The constants K_1, K_2, K_3, K_4 may be obtained in several ways.

For a rigid wake geometry, it is assumed that all the elements in the wake are convected downward by the mean induced velocity at the rotor disk, giving $K_1 = K_2 = \lambda_i$. The convection velocity λ_i is the mean induced velocity at the rotor disk, including ground effect, rotor/rotor interference, and rotor/body interference. A more general rigid wake geometry will be used here:

$$K_1 = f_1 \lambda_i$$

$$K_2 = f_2 \lambda_i$$

where f_1 and f_2 are constant factors. This model is defined by the input parameters f_1, f_2, K_3, and K_4, which may be different for the tip

vortex and inboard sheet. Alternatively, the constants K_1 and K_2 can be specified directly, instead of f_1 and f_2.

For fixed collective trim, C_T and hence λ_i are not known in advance, and it is necessary to iterate the nonuniform inflow calculation until the wake geometry converges. In hover, the iteration will not converge without a relaxation factor on the geometry: $\bar{\lambda}_n = f\lambda_n + (1 - f)\bar{\lambda}_{n-1}$. Representing the nonuniform inflow solution as the operation $\lambda_{n+1} = A(\bar{\lambda}_n)$, and requiring that the solution be converged ($\lambda_{n+1} - \bar{\lambda}_n = A(\bar{\lambda}_n) - \bar{\lambda}_n = 0$) defines a nonlinear function of $\bar{\lambda}_n$ with the Newton-Raphson solution $\bar{\lambda}_n = (A(\bar{\lambda}_{n-1}) - A'\bar{\lambda}_{n-1})/(1 - A') = (\lambda_n - A'\bar{\lambda}_{n-1})/(1 - A')$, or $f = 1/(1 - A')$. In hover, momentum theory gives $A(\lambda) = \kappa C_T/2\lambda$, so $A' = -\kappa C_T/2\lambda^2 = -1$ and $f = 1/2$. Hence to improve convergence,

$$\bar{\lambda} = \frac{1}{2}\left(\lambda_i + \bar{\lambda}_{old}\right)$$

is used in place of λ_i in the above wake geometry model (for the second and succeeding cycles in the iteration).

Landgrebe (ref. 40) developed a prescribed wake geometry model for a hovering rotor from experimental model rotor flow visualization data. The model consists of contraction and two-stage convection as defined above, with the constants as follows:

a. tip vortex

$$K_1 = .25\left(C_T/\sigma + .001\,\theta_{tw}\right)$$

$$K_2 = f_{K2}\left(1 + .01\,\theta_{tw}\right)\sqrt{C_T}$$

b. sheet tip edge

$$k_1 = 1.55\sqrt{C_T}$$

$$k_2 = 1.9\sqrt{C_T}$$

c. sheet root edge

$$k_1 = 0$$

$$k_2 = -(.0025\,\theta_{tw}^2 + .099\,\theta_{tw})\sqrt{C_T}$$

d. radial contraction

$$k_3 = .143 + 27\,C_T$$

$$k_4 = .78$$

where θ_{tw} is here the blade linear twist rate in degrees. Kocurek and Tangler (ref. 41) revised the tip vortex geometry based on experimental data for low aspect-ratio two-bladed rotors, obtaining

$$k_1 = B + C\,(C_T/N^n)^m$$

$$k_2 = f_{k2}\left[C_T - N^n(-B/C)^{1/m}\right]^{\frac{1}{2}}$$

$$k_3 = 4.0\sqrt{C_T}$$

with

$$B = 0.000729\theta_{tw}$$
$$C = 2.3 - 0.206\theta_{tw}$$
$$m = 1.0 - 0.25e^{.04\theta_{tw}}$$
$$n = 0.5 - 0.0172\theta_{tw}$$

These two prescribed wake geometry models are based on flow visualization results, in which typically only four spirals of the wake are observed. Hence such experiments do not determine the tip vortex vertical convection in the far wake, which has a significant influence on the calculated rotor performance. It is therefore necessary to calibrate the wake model, in terms of measured and calculated power. For this purpose, a factor f_{K2} has been introduced in the tip vortex K_2. Limited correlation of the present analysis (for example, reference 42) suggests that $f_{K2} = 0.9$ at normal to high thrust levels.

In reference 43 it was found that the prediction of measured rotor hover performance was improved when the wake geometry was prescribed based on the blade maximum bound circulation rather than C_T as above. Hence as an alternate model, the prescribed wake geometry can be obtained from an equivalent C_T:

$$C_{T_{eq}} = f_\Gamma \frac{N\Gamma_{max}}{8}$$

where Γ_{max} is in general the average over the rotor azimuth. The factor 1/8 is a typical value; it would be replaced by $1/2\pi$ for a constant spanwise bound circulation, or by $1/3\pi$ for a bound circulation proportional to the blade radius. In general, the relation between the equivalent C_{Teq} and Γ_{max} must be established through correlation, for which purpose the factor f_Γ has been included.

The wake geometry arrays will be organized as follows. The rigid or prescribed wake geometry is defined by D_z and D_r at $\phi = k\Delta\psi$, k = 1 to K_{RWG} (independent of ψ). So the structure of the array is

D(k), for k = 1 to K_{RWG}

for D_z and D_r, for the tip vortex and the two inboard sheet edges. The convection rate K_2 is also required, for extrapolation of the geometry beyond $\phi = K_{RWG}\Delta\psi$. The free wake geometry is defined by $D(\psi,\phi)$. The first subscript in the array will be the age $\phi = k\Delta\psi$ for k = 1 to K_{FWG}; the second subscript will be the blade azimuth angle $\psi = l\Delta\psi$, l = 1 to J. So the structure of the array is

D(k,l), for k = 1 to K_{FWG}, l = 1 to J

The free wake geometry will be used for the tip vortex only (see section 3.2).

In the far wake and the rolling up wake, the position of a panel corner at an arbitrary radial station ρ is required ($r_{root} \le \rho \le 1$). Linear interpolation between the root and tip edges of the inboard sheet gives

$$\vec{r}_w = \frac{\vec{r}_{w_{root}} (1-\rho) + \vec{r}_{w_{tip}} (\rho - r_{root})}{1 - r_{root}}$$

The positions required are ρ_{GI} and ρ_{RU}. The radial station of the inboard peak, $r_{GI}(\psi)$, can be an input value, or the calculated location of Γ_I can be used (from the latest circulation solution). Then ρ_{GI} will be the average of the values of r_{GI} at the panel leading and trailing edges:

$$\rho_{GI} = \frac{1}{2}\left(r_{GI}(\psi_m - \phi_k) + r_{GI}(\psi_m - \phi_{k+1})\right)$$

If the inboard peak exists for neither the leading edge nor the trailing edge, then the single peak model will be used. If the inboard peak exists for one, then $\rho_{GI} = \frac{1}{2}(r_{GI} + r_{root})$. It will be required that $r_{root} \leq \rho_{GI} \leq 1$. The rolling up wake requires

$$\rho_{RU} = r_{RU} + (1 - r_{RU})(\phi / \phi_{RU})$$

(using ϕ at the panel leading edge). The strength factor for the tip vortex in the rolling up wake is interpolated in the same manner:

$$\rho = \rho_{RU} + (1 - \rho_{RU})(\phi / \phi_{RU})$$

It will be required that $(r_{root} + .05) \leq \rho_{RU} \leq 1$ for a single peak model, or $(.95\rho_{GI} + .05) \leq \rho_{RU} \leq 1$ for a dual peak model. When a line segment is used for the rolled up inboard trailing wake, it is placed at $\rho = \frac{1}{2}(\rho_{GI} + 1)$, by using the line segment option described in section 3.1.8.

In the near wake, the geometry is defined by the vectors to the four corners of the ith panel, i = 1 to M + 1 (Figure 3-7), where r_{Ai} are the aerodynamic radial stations, except at the root ($r_{A0} = r_{SI}$ at r_{root}) and at the tip ($r_{A_{M+1}} = r_{SO}$ at r = 1). The end points of the trailed lines are on the panel leading edge and trailing edge, interpolated to the aerodynamic segment boundaries r_i:

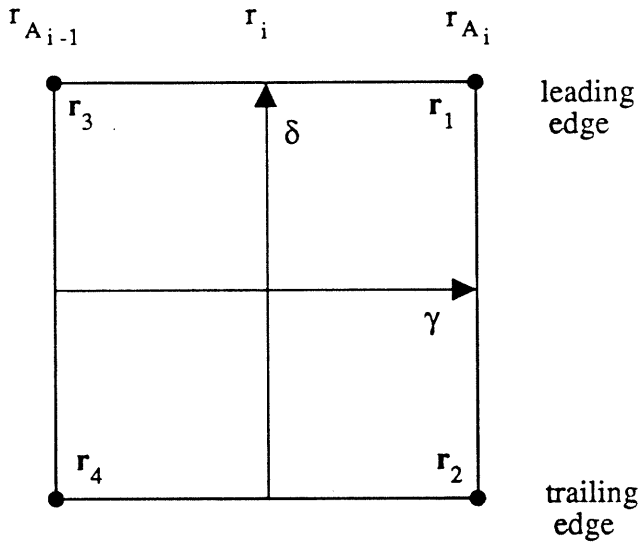

Figure 3-7. Geometry of near wake panel.

$$\vec{r}_{\ell 2} = \frac{(r_i - r_{Ai-1})\,\vec{r}_1 + (r_{Ai} - r_i)\,\vec{r}_3}{r_{Ai} - r_{Ai-1}}$$

$$\vec{r}_{\ell 1} = \frac{(r_i - r_{Ai-1})\,\vec{r}_2 + (r_{Ai} - r_i)\,\vec{r}_4}{r_{Ai} - r_{Ai-1}}$$

except $\vec{r}_1 = \vec{r}_{SI}$ for i = 1, and $\vec{r}_1 = \vec{r}_{SO}$ for i = M + 1. The end points of the shed line are on the middle of the panel side edges, and moved c/4 aft of the collocation point:

$$\vec{r}_{\ell 2} = \frac{1}{2}(\vec{r}_1 + \vec{r}_2) + \frac{\vec{r}_2 - \vec{r}_1}{|\vec{r}_2 - \vec{r}_1|}\, d_i$$

$$\vec{r}_{\ell 1} = \frac{1}{2}(\vec{r}_3 + \vec{r}_4) + \frac{\vec{r}_4 - \vec{r}_3}{|\vec{r}_4 - \vec{r}_3|}\, d_{i-1}$$

where $d_i = 3c_i/4$ ($d_i = c_i/4$ if the collocation points are at the quarter-chord rather than the three-quarter-chord).

The blade collocation points, where the induced velocity is calculated, are located on the r_{Ai} side edges of the first near wake panels behind the blade ($\phi_{le} = 0$, so $\vec{r}_1 = \vec{r}_b$). The vector to the three-quarter-chord point is

$$\vec{r}_p = \vec{r}_1 + \frac{\vec{r}_2 - \vec{r}_1}{|\vec{r}_2 - \vec{r}_1|} d_i$$

where $d_i = c_i/2$. If the collocation points are on the quarter-chord, $d_i = 0$ is used. For induced velocities from either the other rotor or the airframe, the collocation points are at the quarter-chord.

3.1.4 Induced velocity calculation.

The blade bound circulation is calculated at discrete points on the rotor disk: $\Gamma_{ij} = \Gamma(r_i, \psi_j)$. The solution is periodic, so the azimuthal points cover one revolution of the blade: $\psi_j = j\Delta\psi$ for j = 1 to J ($\Delta\psi = 2\pi/J$). The radial stations r_i (i = 1 to M) are the aerodynamic loading stations. Except for the near wake, the vorticity strength in the present wake model depends only on the peak values of the blade bound circulation: Γ_{Ij}, Γ_{Oj}, and Γ_{maxj} at azimuth ψ_j. These peaks are identified as follows. The circulation Γ_{ij} is searched at a given azimuth over the radial stations $r_{Gmax} \le r_i \le r_{TV}$. The inboard limit is an input parameter. The outboard limit is the position of the tip vortex (outboard of Γ_{TV}, the tip loss factor is zero; any small negative circulation there should not be considered an outboard peak). The peak negative and peak positive circulation values are found, with their radial stations, and appropriately assigned to the inboard and outboard peaks. Then Γ_{max} is the peak with largest magnitude. If no inboard peak is found, but an inboard peak (at r_{GI}) was used in the wake geometry for this azimuth, then a linear circulation distribution from $\Gamma = 0$ to Γ_O is interpolated to give

$$\Gamma_I = \left(\frac{r_{GI} - r_{root}}{1 - r_{root}} \right) \Gamma_O$$

so that the dual peak model will give the single peak result (approximately, since actually the values of r_{GI} at both the leading edge and trailing edge of a wake panel affect the induced velocity produced by the circulation at both the leading edge and trailing edge).

Summing the contributions from all vortex elements in the wake gives the induced velocity as the product of the blade bound circulation and influence coefficients:

$$\vec{v} = \sum_{j=1}^{J} \Gamma_{0j} \vec{C}_{0j} + \sum_{j=1}^{J} \Gamma_{Ij} \vec{C}_{Ij} + \sum_{j=\ell-K_{NW}}^{\ell} \sum_{i=1}^{M} \Gamma_{ij} \vec{C}_{NW\,ij}$$

A set of influence coefficients is obtained for each point in the flow field at which the induced velocity is calculated: at points distributed radially and azimuthally over the rotor disk, and at points off the rotor disk (see section 3.1.3). The last term is produced by the near wake, extending from $\phi = 0$ to $\phi = K_{NW}\Delta\psi$ behind the reference blade at azimuth angle $\psi_1 = 1\Delta\psi$. The wake configuration options lead to the following cases:

(a) single peak model based on Γ_{max} (Γ_{max} in first term of **v**, second term absent);

(b) single peak model based on Γ_0 (second term of **v** absent);

(c) dual peak model, from Γ_0 and Γ_I.

Correspondingly, the prescribed wake geometry (section 3.1.3) or free wake geometry (section 3.2) should be based on Γ_{max} or Γ_0; and the convergence test for the circulation iteration (section 5.1.12) should use Γ_{max}, Γ_0, or Γ_0 and Γ_I.

For a given wake geometry, the influence coefficients are calculated by the procedure described in section 3.1.6. Then, from a circulation estimate at some stage in the blade motion and helicopter trim solution, the induced velocity $\vec{v}$ can be evaluated. The vector $\vec{v}$ is at the aerodynamic radial station, in the tip-path-plane coordinate frame. The aerodynamic analysis requires the induced velocity in the hub plane coordinate frame. Transforming to the S system gives

$$\vec{\lambda} = \begin{pmatrix} \lambda_x \\ -\lambda_y \\ -\lambda_z \end{pmatrix} = R_{TS}^T \vec{v}$$

using the current values of the tip-path-plane tilt angles (β_c and β_s).

The induced velocity for the rotor/airframe aerodynamic interference (at the wing/body, horizontal tail, vertical tail, or an arbitrary point) is required in the body axis system (the F frame):

$$\begin{pmatrix} \lambda_x \\ \lambda_y \\ \lambda_z \end{pmatrix} = (R_{TS} R_{SF})^T \vec{v}$$

For the induced velocity from rotor #2, a factor $\Omega R_2/\Omega R_1$ is required as well. The induced velocity for the rotor/rotor interference (at the hub or over the disk) is required in the shaft axis system of the other rotor. The interference velocity at rotor #2 due to the loading of rotor #1 is then

$$\begin{pmatrix} \lambda_x \\ -\lambda_y \\ -\lambda_z \end{pmatrix}_{2/1} = \frac{\Omega R_1}{\Omega R_2} (R_{SF})_2 (R_{TS} R_{SF})_1^T \vec{v}_{2/1}$$

and at rotor #1 due to rotor #2

$$\begin{pmatrix} \lambda_x \\ -\lambda_y \\ -\lambda_z \end{pmatrix}_{1/2} = \frac{\Omega R_2}{\Omega R_1} (R_{SF})_1 (R_{TS} R_{SF})_2^T \vec{v}_{1/2}$$

These coordinate rotations normally should not be included in the influence coefficients because the updated values of the tip path plane tilt angles are to be used in the matrix R_{TS} (although the rotation of the induced velocity by the small angles β_c and β_s should not be important). The factor $\Omega R_1/\Omega R_2$ can be incorporated in the influence coefficients, however. For a clockwise rotating rotor, the sign of the j_s component of the induced velocity must be changed (between the R_{TS} and R_{SF} rotation matrices).

The interference induced velocity due to rotor #1 is calculated at rotor #2 for the azimuth angles $\psi = l\Delta\psi + \Delta\psi_{21}$ (l = 1 to J). When $\Delta\psi_{21} \neq 0$ it will be necessary to linearly interpolate the velocity to the azimuth angles $\psi = k\Delta\psi$ (k = 1 to J). Similarly, the induced velocity due to rotor #2 at rotor #1 must be interpolated from $\psi = l\Delta\psi - \Delta\psi_{21}$ to $\psi = k\Delta\psi$. The velocity moved off the rotor disk by rotor #2 is also calculated for $\psi = l\Delta\psi - \Delta\psi_{21}$, and must be interpolated to $\psi = k\Delta\psi$.

3.1.5 Hover or vertical flight (axisymmetric geometry).

The nonuniform inflow calculation can be simplified in hover due to the axisymmetry of the wake geometry. For the hover case, the influence

coefficients will be the same for the induced velocity at all azimuth angles, except for an azimuth shift and axis rotation:

$$\vec{C}_j\,(\psi = \ell\,\Delta\psi) =$$

$$\begin{bmatrix} \cos(\psi-\Delta\psi) & -\sin(\psi-\Delta\psi) & 0 \\ \sin(\psi-\Delta\psi) & \cos(\psi-\Delta\psi) & 0 \\ 0 & 0 & 1 \end{bmatrix} \vec{C}_{j-\ell+1} \quad (\psi = \Delta\psi)$$

Even in hover the rotor may have a net pitch or roll moment if the center of gravity is offset from the shaft (with offset hinges or a hingeless rotor). Hence, in general, the hover case will not involve induced velocity and bound circulation independent of azimuth angle. These considerations apply to the general vertical flight case as well.

An accurate calculation of the induced velocity of a rotor in axial flight usually requires consideration of the wake very far from the rotor disk. The detailed wake model described above is required only close to the disk, however. Very far from the disk a more approximate and more efficient model will be used, obtained by spreading the vorticity vertically over the distance h between successive sheets, as sketched in Figure 3-8. The axial convection velocity in the far wake is taken from the prescribed wake model:

$$v = -\vec{k} \cdot \vec{\mu}_{\text{tpp}} + (k_z)_{\text{tip vortex}}$$

giving for the spiral axial spacing

$$h = 2\pi v$$

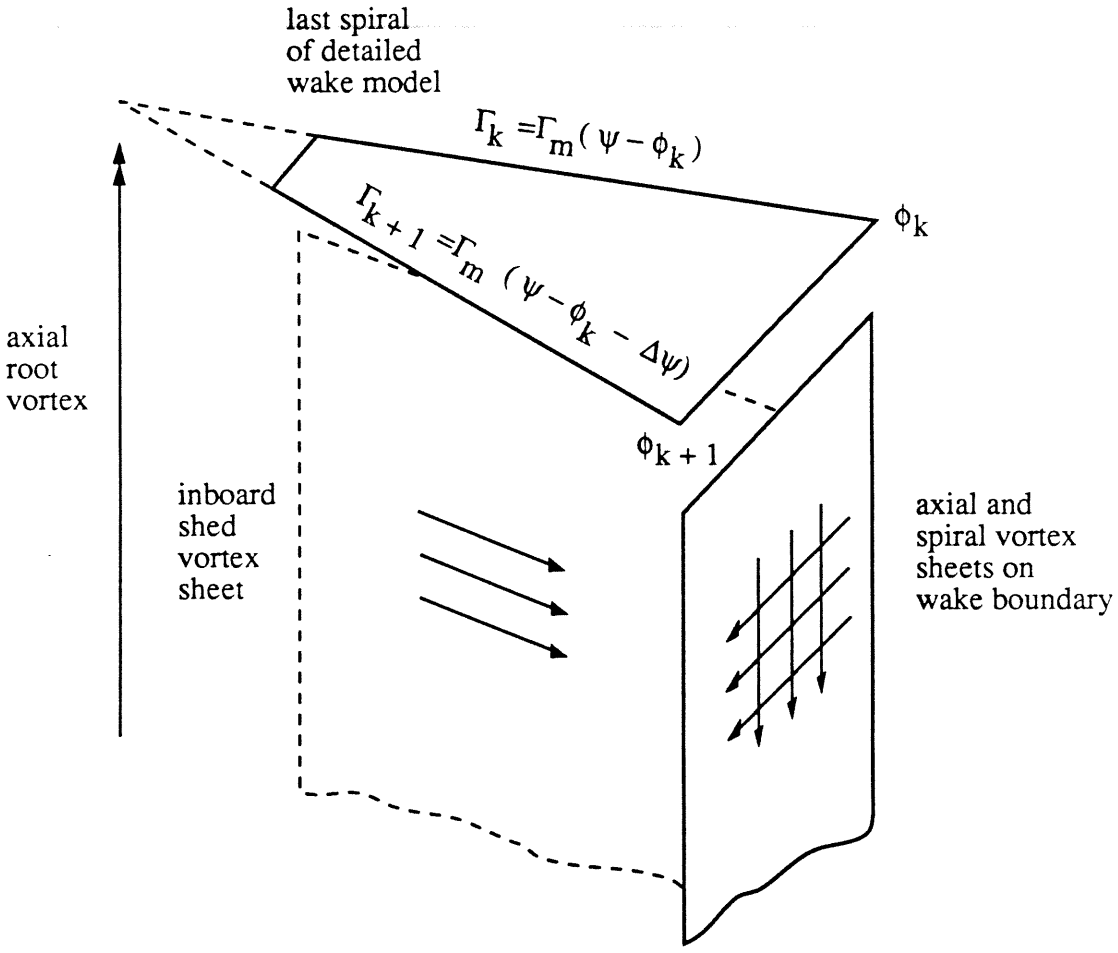

Figure 3-8. Far wake model for hover or vertical flight.

The tip vortex elements are spread vertically to form a vortex sheet with axial and spiral components. There is a corresponding axial root vortex from the inboard trailing vorticity. The shed vorticity is spread vertically to form a vortex sheet. This wake model extends L turns (an axial distance Lh) beyond the last spiral of the detailed wake model from each blade.

The influence coefficients of this very far wake model are calculated as follows. For a panel in the last spiral in the wake, the geometry is specified by the location of the ends of the tip vortex line segment, and the corners of the inboard panel. The wake strength is determined by the bound circulation corresponding to the panel leading and trailing edges:

$$\Gamma_k = \Gamma_{max}(\psi_m - \phi_k)$$

$$\Gamma_{k+1} = \Gamma_{max}(\psi_m - \phi_k - \Delta\psi)$$

The geometry of the sheet vorticity on the wake boundary is obtained from the position of the tip vortex segment, $\vec{r}_k$ and $\vec{r}_{k+1}$ (vectors to the segment ends). The vectors to the sheet vector are then

$$\vec{r}_1 = \vec{r}_k - \tfrac{1}{2} h \vec{k}$$

$$\vec{r}_2 = \vec{r}_1 - L h \vec{k}$$

$$\vec{r}_3 = \vec{r}_{k+1} - \vec{r}_{k+1} \cdot \vec{k}\, \vec{k} + \vec{r}_1 \cdot \vec{k}\, \vec{k}$$

$$\vec{r}_4 = \vec{r}_3 - L h \vec{k}$$

The induced velocity of the tip axial vorticity is given by the trailed sheet vorticity solution with

$$\Gamma_1 = \Gamma_2 = -\Gamma_k$$

$$\Gamma_3 = \Gamma_4 = -\Gamma_{k+1}$$

(see section 3.1.8). The induced velocity of the tip spiral vorticity is given by the shed sheet vorticity solution with

$$\Gamma_1 = L\Gamma_k$$

$$\Gamma_2 = 0$$

$$\Gamma_3 = L\Gamma_{k+1}$$

$$\Gamma_4 = 0$$

Let $\vec{r}_i$ and $\vec{r}_o$ be the position vectors of the inboard wake panel (the inside and outside edges, respectively, at $\phi_k + \Delta\phi/2$). Then the vectors to the inboard shed vortex sheet are:

$$\vec{r}_1 = \vec{r}_o - \tfrac{1}{2}\ell\vec{k}$$

$$\vec{r}_2 = \vec{r}_1 - L\ell\vec{k}$$

$$\vec{r}_3 = \vec{r}_i - \vec{r}_i\cdot\vec{k}\,\vec{k} + \vec{r}_1\cdot\vec{k}\,\vec{k}$$

$$\vec{r}_4 = \vec{r}_3 - L\ell\vec{k}$$

and the induced velocity is given by the shed sheet vorticity with

$$\Gamma_1 = L\Gamma_k$$
$$\Gamma_2 = L\Gamma_{k+1}$$
$$\Gamma_3 = L\Gamma_k$$
$$\Gamma_4 = L\Gamma_{k+1}$$

(see section 3.1.8). Finally, the vectors to the ends of the root axial vortex are

$$\vec{r}_2 = \vec{r}_i \cdot \vec{k}\,\vec{k} - \tfrac{1}{2} h \vec{k}$$
$$\vec{r}_1 = \vec{r}_2 - Lh\vec{k}$$

and the induced velocity is given by the line vortex solution with

$$\Gamma_1 = \Gamma_2 = \Gamma_k - \Gamma_{k+1}$$

(see section 3.1.7).

3.1.6 Computation method.

This section describes the method used to evaluate the wake influence coefficients. The azimuthal increment is $\Delta\psi = 2\pi/J$, where J is the number of azimuth stations in one revolution. The number of blades is N; it is required that J be a multiple of N. The blade bound circulation is calculated at discrete points on the rotor disk: Γ_{ij} =

$\Gamma(r_i,\psi_j)$. The azimuth stations are equally spaced over one revolution: $\psi_j = j\Delta\psi$ for j = 1 to J. The radial stations are the aerodynamic loading points: r_i for i = 1 to M_A (see section 2.4.1). The corresponding bound circulation peak values are $\Gamma_{Oj} = \Gamma_O(\psi_j)$ and $\Gamma_{Ij} = \Gamma_I(\psi_j)$. The induced velocity is calculated at azimuth stations $\psi_l = l\Delta\psi$ for l = 1 to J, and at a set of field points r_k for k = 1 to M_R. The field points may include the aerodynamic radial stations on this rotor; the aerodynamic radial stations on the other rotor, or the hub of the other rotor; the centers of action of the wing/body, horizontal tail, and vertical tail forces; and arbitrary points in space (fixed relative to the airframe). The influence coefficients relate the velocity to the circulation:

$$\vec{v}_{kl} = \sum_{j=1}^{J} \Gamma_{Oj}\, \vec{C}_O(j,k,l) + \sum_{j=1}^{J} \Gamma_{Ij}\, \vec{C}_I(j,k,l)$$

$$+ \sum_{j_{NW}=1}^{K_{NW}+1} \sum_{i=1}^{M_L} \Gamma_{ij}\, \vec{C}_{NW}(i,j_{NW},k,l)$$

For C_O and C_I the field point and circulation indices are

l = 1 to J	(ψ_l)
k = 1 to M_R	(r_k)
j = 1 to J	(ψ_j)

In the near wake, the field points are restricted to this rotor, and the azimuthal extent is $K_{NW}\Delta\psi$ behind the blade position. So for C_{NW}, the field point and circulation indices are

l = 1 to J	(ψ_l)
k = 1 to M_L	(r_k)

$j = 1 - K_{NW}$ to 1 (ψ_j)

$i = 1$ to M_L (r_i)

with $j_{NW} = j - 1 + (K_{NW} + 1)$, so

$j_{NW} = 1$ to $(K_{NW} + 1)$

With the reference blade at azimuth ψ_1, the mth blade is at azimuth angle $\psi_m = \psi_1 + m2\pi/N$ ($\psi_m = l_m\Delta\psi$, $l_m = 1 + mJ/N$; $m = 0$ to $N - 1$, $m = 0$ the reference blade). The wake spiral behind each blade is defined by the age $\phi = k\Delta\psi$, for $k = 0$ at the blade to $k = K_{max}$ (maximum extent of the far wake, which may be different when calculating velocities at points on or off the rotor disk).

The blade specification plus the wake age determines the vortex panel being considered, extending from ϕ to $\phi + \Delta\psi$ behind the mth blade. The wake strength is determined from the bound circulation as follows:

(a) panel leading edge: $\Gamma(\psi_m - \phi)$, so $j_{le} = l_m - k$

(b) panel trailing edge: $\Gamma(\psi_m - \phi - \Delta\psi)$, so $j_{te} = l_m - k - 1$

(see Figure 3-2). These values of j (hence ψ_j) define to which influence coefficients the induced velocity of this panel contributes.

Each wake panel consists of a number of line and sheet elements. The convention for describing the vortex elements is shown in Figure 3-9. The geometry is defined by vectors to each of the numbered points (r_1, r_2, r_3, r_4) and a vector to the field point where the velocity is calculated (r_p). Associated with each numbered point is the blade bound circulation when the wake point was created (Γ_1, Γ_2, Γ_3, Γ_4). Then the velocity induced by a vortex line segment is

$$\Delta v = \Gamma_1 \Delta v_1 + \Gamma_2 \Delta v_2$$

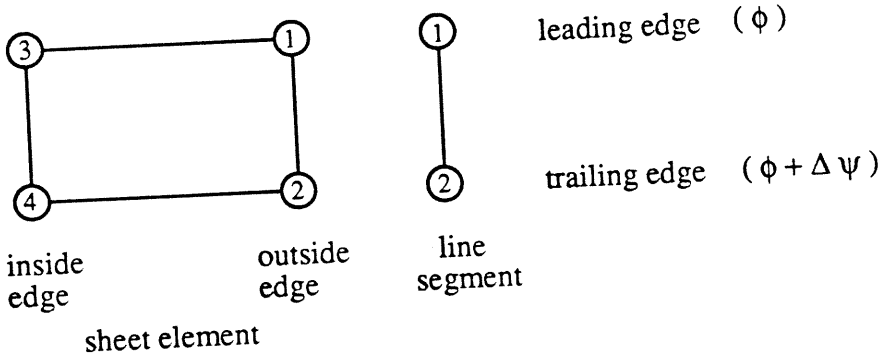

Figure 3-9. Description of vortex line and sheet elements.

The velocity induced by a vortex sheet element is

$$\Delta v = \Gamma_1 \Delta v_{t_1} + \Gamma_2 \Delta v_{t_2} + \Gamma_3 \Delta v_{t_3} + \Gamma_4 \Delta v_{t_4}$$

with

$$\Delta v_{t_3} = - \Delta v_{t_1}$$
$$\Delta v_{t_4} = - \Delta v_{t_2}$$

for the trailed vorticity, and

$$\Delta v = \Gamma_1 \Delta v_{s_1} + \Gamma_2 \Delta v_{s_2} + \Gamma_3 \Delta v_{s_3} + \Gamma_4 \Delta v_{s_4}$$

with

$$\Delta v_{s_2} = - \Delta v_{s_1}$$
$$\Delta v_{s_4} = - \Delta v_{s_3}$$

for the shed vorticity. The velocity increments are evaluated in sections 3.1.7 and 3.1.8.

The wake consists of several regions, defined in terms of the wake age: the near wake, the rolling up wake, and the far wake. The wake model in each region was described in section 3.1.2 (see Figures 3-3 and 3-4). Figures 3-10 and 3-11 show these wake models in terms of the sheet and line element conventions. In the far wake and rolling up

bound vortex

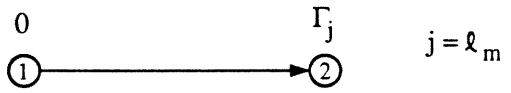

near wake

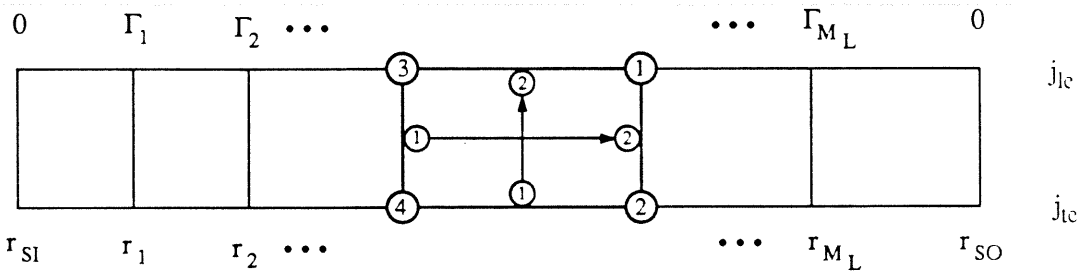

rolling up wake (single peak)

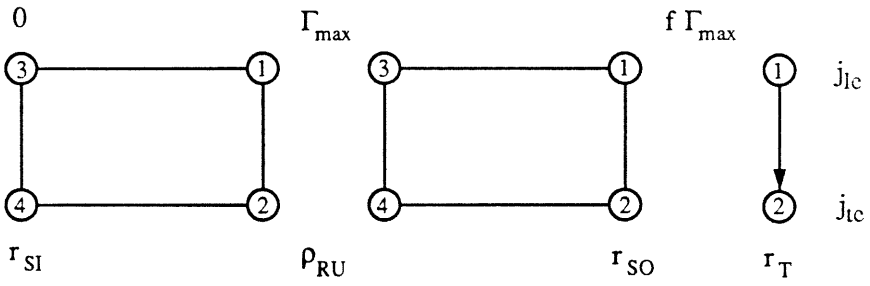

far wake (single peak)

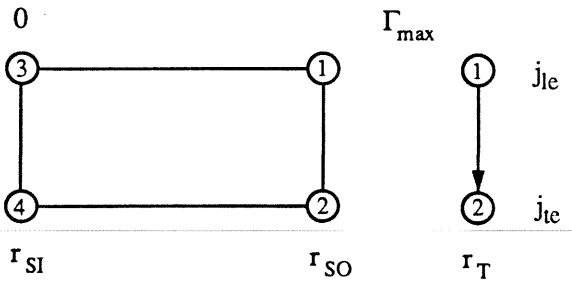

Figure 3-10. Description of wake panels.

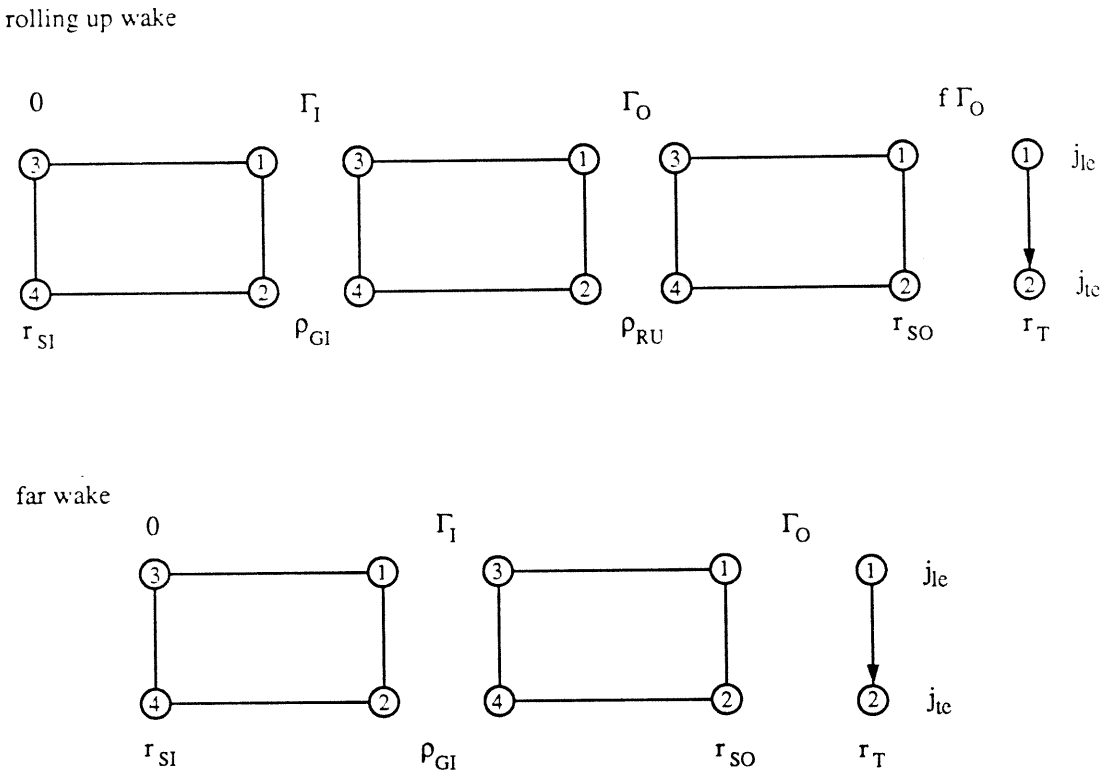

Figure 3-11. Description of wake panels, dual peak model.

wake, the geometry is defined in terms of the tip vortex (r_T) and the inside and outside edges of the inboard sheet (r_{SI} and r_{SO}). The panel geometry at ρ_{RU} and ρ_{GI} is obtained by interpolation between r_{SI} and r_{SO}. In the near wake, the geometry is defined in terms of the aerodynamic loading stations (r_i, i = 1 to M_L), and the inboard sheet edges (r_{SI} and r_{SO}). The equivalent circulation varies linearly between the values shown.

The near wake model consists of M_L + 1 panels, defined by the root, tip, and M_L aerodynamic radial stations. Each panel has a trailed vortex line segment and a shed vortex line segment (Figure 3-10). The near wake is used only behind the reference blade (extending to $\phi = K_{NW}\Delta\psi$), and only for the inflow field points on the reference blade.

The rolling up wake model consists of a tip vortex line segment of strength $f\Gamma_{max}$, and an inboard wake sheet divided into two elements at radial station ρ_{RU} (three elements for the dual peak model, divided at ρ_{GI} and ρ_{RU}). The values of f and ρ_{RU} are interpolated between f_{RU} and r_{RU} at the blade, and unity at the wake age ϕ_{RU} (based on ϕ of the panel leading edge). If $\phi > \phi_{RU}$ but $\phi < (K_{RU} - 1)\Delta\psi$ (maximum extent of rolling up wake), then the far wake model is used (with rolling up model parameters).

The far wake model consists of a tip vortex line segment, and an inboard vortex sheet consisting of one element (two elements for the dual peak model, divided at ρ_{GI}). The far wake parameters (such as the core radius, and various modeling options) can be different for the induced velocity calculated on and off this rotor. The wake extent is $K_{FW}\Delta\psi$ for points on this rotor and $K_{DW}\Delta\psi$ for points off this rotor.

For the dual peak model, ρ_{GI} is calculated as described in section 3.1.3. If no inboard peak location is identified, then the single peak model is used for this wake age. The trailed vorticity from ρ_{GI} to the tip can optionally be modeled as a sheet (not rolled up) or as a line segment with a core (rolled up).

The induced velocity contribution of the bound vortex of each blade is also calculated. For this purpose the blade bound vorticity is represented by a straight line segment extending from the root to the tip, at azimuth angle ψ_m. This model is not accurate very close to the blade, although a core radius equal to 25% of the mean chord is used to avoid excessive velocities. The contribution of the bound vortex of the reference blade to the induced velocities at the reference blade is not included.

The induced velocity expressions for vortex line and sheet elements give the contributions to the influence coefficients for each of these models:

(a) bound vortex: $\Delta C_0(l_m, k_r, l) = \Delta v_2$

(b) near wake panels, $i_r = 1$ to $M_L + 1$

(i) except $i_r = M_L + 1$:

$$\Delta C_{NW}(i_r, j_{NWle}, k_r, l) = \Delta v_{t1} + \Delta v_{s1}$$

$$\Delta C_{NW}(i_r, j_{NWte}, k_r, l) = \Delta v_{t2} - \Delta v_{s1}$$

(ii) except $i_r = 1$:

$$\Delta C_{NW}(i_r - 1, j_{NWle}, k_r, l) = -\Delta v_{t1} + \Delta v_{s3}$$

$$\Delta C_{NW}(i_r - 1, j_{NWte}, k_r, l) = -\Delta v_{t2} - \Delta v_{s3}$$

(c) rolling up wake

(i) tip vortex:

$$\Delta C_0(j_{le}, k_r, l) = f\Delta v_1$$

$$\Delta C_0(j_{te}, k_r, l) = f\Delta v_2$$

(ii) outboard sheet (ρ_{RU} to 1):

$$\Delta C_0(j_{le}, k_r, l) = (f - 1)\Delta v_{t1} + f\Delta v_{s1} + \Delta v_{s3}$$

$$\Delta C_0(j_{te}, k_r, l) = (f - 1)\Delta v_{t2} - f\Delta v_{s1} - \Delta v_{s3}$$

(iii) middle or inboard sheet (0 to ρ_{RU}, or ρ_{GI} to ρ_{RU}):

$$\Delta C_0(j_{le}, k_r, l) = \Delta v_{t1} + \Delta v_{s1}$$

$$\Delta C_0(j_{te}, k_r, l) = \Delta v_{t2} - \Delta v_{s1}$$

and dual peak model only:

$$\Delta C_I(j_{le}, k_r, l) = -\Delta v_{t1} + \Delta v_{s3}$$

$$\Delta C_I(j_{te},k_r,1) = -\Delta v_{t2} - \Delta v_{s3}$$

(iv) dual peak model only, inboard sheet (0 to ρ_{GI}):

$$\Delta C_I(j_{le},k_r,1) = \Delta v_{t1} + \Delta v_{s1}$$

$$\Delta C_I(j_{te},k_r,1) = \Delta v_{t2} - \Delta v_{s1}$$

(d) far wake

(i) tip vortex:

$$\Delta C_O(j_{le},k_r,1) = \Delta v_1$$

$$\Delta C_O(j_{te},k_r,1) = \Delta v_2$$

(ii) sheet or outboard sheet (0 to 1, or ρ_{GI} to 1):

$$\Delta C_O(j_{le},k_r,1) = \Delta v_{t1} + \Delta v_{s1}$$

$$\Delta C_O(j_{te},k_r,1) = \Delta v_{t2} - \Delta v_{s1}$$

and dual peak model only:

$$\Delta C_I(j_{le},k_r,1) = -\Delta v_{t1} + \Delta v_{s3}$$

$$\Delta C_I(j_{te},k_r,1) = -\Delta v_{t2} - \Delta v_{s3}$$

(iii) dual peak model only, inboard sheet (0 to ρ_{GI}):

$$\Delta C_I(j_{le},k_r,1) = \Delta v_{t1} + \Delta v_{s1}$$

$$\Delta C_I(j_{te},k_r,1) = \Delta v_{t2} - \Delta v_{s1}$$

Using line segments for the near wake, it follows that $\Delta v_{t1} = \Delta v_2$, $\Delta v_{t2} = \Delta v_1$, and $\Delta v_{s1} = -\Delta v_2$, $\Delta v_{s3} = -\Delta v_1$. The influence coefficient contributions from the axisymmetric far wake model (section 3.1.5) are:

(i) wake boundary (ring/shed, axial/trailed):

$$\Delta C_O(j_{le},k_r,1) = -(\Delta v_{t1} + \Delta v_{t2}) + L\Delta v_{s1}$$

$$\Delta C_O(j_{te},k_r,1) = (\Delta v_{t1} + \Delta v_{t2}) + L\Delta v_{s3}$$

(ii) shed wake (interior):

$$\Delta C_O(j_{le},k_r,1) = L(\Delta v_{s1} + \Delta v_{s3})$$

$$\Delta C_O(j_{te},k_r,1) = -L(\Delta v_{s1} + \Delta v_{s3})$$

(iii) root vortex:

$$\Delta C_O(j_{le},k_r,1) = (\Delta v_1 + \Delta v_2)$$

$$\Delta C_O(j_{te},k_r,1) = -(\Delta v_1 + \Delta v_2)$$

For the case of axisymmetric geometry, the influence coefficients are calculated only for $l = 1$ ($\psi_l = \Delta\psi$). Then the influence coefficients for other azimuths are obtained from:

$$C_O(j,k,l) = TC_O(j - l + 1,k,1)$$
$$C_I(j,k,l) = TC_I(j - l + 1,k,1)$$
$$C_{NW}(i,j_{NW},k,l) = TC_{NW}(i,j_{NW},k,1)$$

with the matrix $T(\psi_l)$ defined in section 3.1.5.

The procedure to calculate the influence coefficients is outlined below.

A. azimuth loop: azimuth angle of reference blade (dimensionless time) $\psi_l = l\Delta\psi$, $l = 1$ to J; only $l = 1$ for axisymmetric geometry
   (1) calculate position vector at induced velocity field points (on reference blade of this or other rotor at ψ_l, or off rotors); total number M_R, with M_L on this rotor

B. blade loop: m = 0 to N - 1 (m = 0 is reference blade)
   (1) $l_m = l + mJ/N$ ($l_m = l_m - J$ if $l_m > J$); $\psi_m = l_m\Delta\psi$
   (2) evaluate wake geometry r_{te} at blade (at ψ_m and $\phi = 0$)
   (3) bound vortices
      a. field point: $k_r = 1$ to M_R
         (i) skip if m = 0 and $k_r \le M_L$ (wake of reference blade and induced velocity on reference blade)
         (ii) ΔC_O of vortex line segment
   (4) $j_{le} = l_m + 1$

C. wake age loop: $\phi = k\Delta\psi$ (at leading edge), k = 0 to $\max(K_{FW},K_{\Delta W}) - 1$
   (1) $j_{le} = j_{le} - 1$ ($j_{le} = j_{le} + J$ if $j_{le} \le 0$)

($j_{le} = l_m - k$; so $j_{le} = l_m$ at $\phi = 0$, and decrease j_{le} by 1 when increase k by 1; j in range 1 to J)

(2) $j_{te} = j_{le} - 1$ ($j_{te} = j_{te} + J$ if $j_{te} \leq 0$)

(3) wake geometry at panel leading edge: $r_{le} = r_{te}$

(4) evaluate wake geometry r_{te} at trailing edge at ψ_m and $\phi + \Delta\psi$)

(5) if m = 0 and $k < K_{NW}$ (near wake), then $M_{RO} = M_L + 1$; else (not near wake) $M_{RO} = 1$

D. if $k \geq K_{RW}$ or $\phi \geq \phi_{RU}$, then: far wake

(1) dual peak model: calculate ρ_{GI} (single wake model if absent); interpolate wake geometry to ρ_{GI}

(2) field point: $k_r = M_{RO}$ to M_R

a. model parameters: rolling up wake if $k < K_{RW}$; far wake if $k \geq K_{RW}$ (on this rotor if $k_r \leq M_L$, off this rotor if $k_r > M_L$)

b. dual peak model: model parameters for rolled up inboard trailed wake

c. ΔC_0 of vortex line segment

d. ΔC_0 of vortex sheet element (0 to 1, or ρ_{GI} to 1); dual peak model, ΔC_I

e. dual peak model, ΔC_I of vortex sheet element (0 to ρ_{GI})

else: rolling up wake

(1) calculate f, ρ_{RU}

(2) dual peak model: calculate ρ_{GI} (single wake model if absent); interpolate wake geometry to ρ_{GI}

(3) interpolate wake geometry to ρ_{RU}

(4) field point: $k_r = M_{RO}$ to M_R

a. ΔC_0 of vortex line segment

b. ΔC_0 of vortex sheet element (ρ_{RU} to 1)

c. ΔC_0 of vortex sheet element (0 to ρ_{RU}, or ρ_{GI} to ρ_{RU}); dual peak model, ΔC_I

d. dual peak model, ΔC_I of vortex sheet element (0 to ρ_{GI})

E. if m = 0 and $k < K_{NW}$: near wake

(1) $j_{NWle} = K_{NW} + 1 - k$, $j_{NWte} = K_{NW} - k$ ($k = 0$ to $K_{NW} - 1$)

(2) calculate position vector at end points of trailed and shed line segments; calculate core radius

(3) field points: $k_r = 1$ to M_L

a. panels: $i_i = 1$ to $M_L + 1$

(i) ΔC_{NW} of trailed vortex line segment

(ii) ΔC_{NW} of shed vortex line segment

F. axisymmetric wake: only if $k \geq (K_{FW} - J)$ or $(K_{DW} - J)$ (last spiral)

(1) if $k < (K_{FW} - J)$, then $M_{R0} = M_L + 1$; else $M_{R0} = 1$

(2) if $k < (K_{DW} - J)$, then $M_{R1} = M_L$; else $M_{R1} = M_R$

(3) field point: $k_r = M_{R0}$ to M_{R1}

a. ΔC_0 of wake boundary vortex sheet elements

b. ΔC_0 of shed wake vortex sheet element

c. ΔC_0 of root vortex line segment

G. end wake age loop

end blade loop

end azimuth loop

H. axisymmetric wake: complete for $I = 2$ to J

3.1.7 Finite length vortex line element

Consider a straight vortex line segment of length s, as shown in Figure 3-12. The vortex segment has linearly varying circulation, between Γ_1 and Γ_2 at the end points (Γ_1 is the circulation at ϕ and Γ_2 is the circulation at $\phi + \Delta\psi$). The induced velocity is required at the point P, defined by the position vectors $\vec{r}_1$ and $\vec{r}_2$ from the ends of the segment. The vectors $\vec{r}_1$ and $\vec{r}_2$ can be in any convenient coordinate frame; the components of the induced velocity will be obtained in the same coordinate frame. The Biot-Savart law gives the induced velocity due to this line segment:

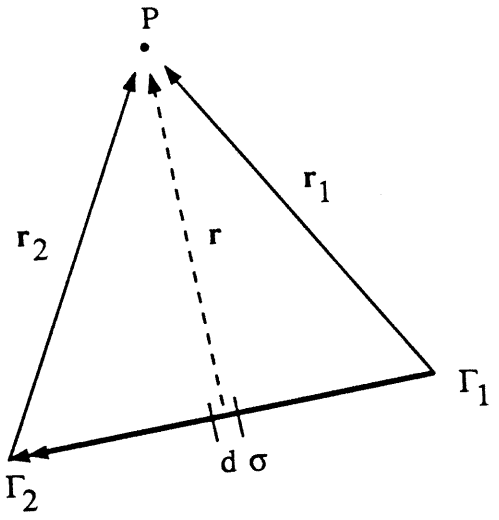

Figure 3-12. Finite length vortex line element.

$$\Delta\vec{v} = -\frac{1}{4\pi}\int \Gamma \frac{\vec{r}\times d\vec{\sigma}}{r^3}$$

where $\vec{r}$ is the vector from the element $d\sigma$ on the segment, to the point P; and $r = |\vec{r}|$. The coordinate σ is measured along the vortex segment, from s_1 to s_2:

$$s_1 = \frac{\vec{r}_1\cdot\vec{r}_2 - r_1^2}{s}$$

$$s_2 = \frac{r_2^2 - \vec{r}_1\cdot\vec{r}_2}{s} = s_1 + s$$

where s is the length of the segment:

$$s^2 = |\vec{r}_1 - \vec{r}_2|^2 = r_1^2 + r_2^2 - 2\vec{r}_1\cdot\vec{r}_2$$

Write $\vec{r} = \vec{r}_m - \sigma\hat{e}$, where $\vec{r}_m$ is the minimum distance from the vortex line (including its extension beyond the end points of the segment) to the point P, and $\hat{e}$ is the unit vector in the direction of the vortex:

$$\vec{r}_m = \frac{\vec{r}_1(r_2^2 - \vec{r}_1\cdot\vec{r}_2) + \vec{r}_2(r_1^2 - \vec{r}_1\cdot\vec{r}_2)}{s^2} = \frac{\vec{r}_1 s_2 - \vec{r}_2 s_1}{s}$$

$$\hat{e} = \frac{\vec{r}_1 - \vec{r}_2}{s}$$

The vectors $\vec{r}_m$ and $\hat{e}$ are perpendicular, and

$$r_m^2 s^2 = r_1^2 r_2^2 - (\vec{r}_1 \cdot \vec{r}_2)^2$$

The vortex strength varies linearly along the segment:

$$\Gamma = \frac{\Gamma_1 (s_2 - \sigma) + \Gamma_2 (\sigma - s_1)}{s}$$

$$= \frac{\Gamma_1 s_2 - \Gamma_2 s_1}{s} + \sigma \frac{\Gamma_2 - \Gamma_1}{s} = \Gamma_m + \sigma \Gamma_s$$

It follows that

$$\Delta \vec{v} = \frac{\vec{r}_1 \times \vec{r}_2}{4\pi s} \int_{s_1}^{s_2} \frac{\Gamma_m + \sigma \Gamma_s}{(r_m^2 + \sigma^2)^{3/2}} \, d\sigma$$

$$= \frac{\vec{r}_1 \times \vec{r}_2}{4\pi s} \left[\frac{\Gamma_m \sigma / r_m^2 - \Gamma_s}{(r_m^2 + \sigma^2)^{1/2}} \right] \Bigg|_{\sigma = s_1}^{\sigma = s_2}$$

$$= \frac{\vec{r}_1 \times \vec{r}_2}{4\pi s r_m^2} \left[\Gamma_m \left(\frac{s_2}{r_2} - \frac{s_1}{r_1} \right) - \Gamma_s r_m^2 \left(\frac{1}{r_2} - \frac{1}{r_1} \right) \right]$$

$$= \frac{\vec{r}_1 \times \vec{r}_2}{4\pi s r_m^2} \left[\Gamma_1 \left\{ \frac{s_2}{s} \left(\frac{s_2}{r_2} - \frac{s_1}{r_1} \right) + \frac{r_m^2}{s} \left(\frac{1}{r_2} - \frac{1}{r_1} \right) \right\} \right.$$

$$\left. + \Gamma_2 \left\{ \frac{s_1}{s} \left(\frac{s_1}{r_1} - \frac{s_2}{r_2} \right) + \frac{r_m^2}{s} \left(\frac{1}{r_1} - \frac{1}{r_2} \right) \right\} \right]$$

for the induced velocity of the vortex line segment with linearly varying circulation.

Consider also the induced velocity of a line vortex segment with a stepped circulation distribution. The distance from the midpoint of the segment to the point P is

$$\vec{r}_3 = \frac{1}{2}(\vec{r}_1 + \vec{r}_2)$$

and the midpoint is located at

$$s_3 = \frac{1}{2}(s_1 + s_2) = \frac{1}{2s}(r_2^2 - r_1^2)$$

The line segment has constant strength Γ_1 from s_1 to s_3, and constant strength Γ_2 from s_3 to s_2. Applying the above result (with $\Gamma_s = 0$) to both values of the line segment gives

$$\Delta\vec{v} = \frac{\vec{r}_1 \times \vec{r}_3}{4\pi(s/2)r_m^2}\Gamma_1\left(\frac{s_3}{r_3} - \frac{s_1}{r_1}\right) + \frac{\vec{r}_3 \times \vec{r}_2}{4\pi(s/2)r_m^2}\Gamma_2\left(\frac{s_2}{r_2} - \frac{s_3}{r_3}\right)$$

$$= \frac{\vec{r}_1 \times \vec{r}_2}{4\pi s r_m^2}\left[\Gamma_1\left\{\frac{s_3}{r_3} - \frac{s_1}{r_1}\right\} + \Gamma_2\left\{\frac{s_2}{r_2} - \frac{s_3}{r_3}\right\}\right]$$

The influence of the vortex core is accounted for by multiplying the induced velocity of the line segment by the factor

$$\min\left(r_m^2/r_c^2,\ 1\right)$$

for concentrated vorticity (solid body rotation) or by

$$\frac{r_m^2}{r_m^2 + r_c^2}$$

for distributed vorticity (from ref. 35). The core radius r_c is the location of the maximum tangential velocity.

In references 44 and 45 a lifting-surface theory solution was developed for the vortex induced loads on an infinite aspect-ratio, nonrotating wing encountering a straight, infinite vortex at an angle Λ with the wing (Fig. 3-13). The vortex lies in a plane parallel to the wing, a distance h below it, and is convected past the wing by the free stream. The distortion of the vortex line by interaction with the wing is not considered. In linear lifting-surface theory, the blade and wake are represented by a planar distribution of vorticity. This model problem was solved for the case of a sinusoidal-induced velocity distribution, with wave fronts parallel to the vortex line. An approximate solution was obtained by fitting analytical expressions to the numerical solution for sinusoidal loading. The vortex-induced velocity distribution can be obtained by a suitable combination of sinusoidal waves of various wavelengths, and the same superposition gives the vortex-induced loading from the sinusoidal loading solution. The approximate solution is not valid for extremely small wavelengths, but the range of validity is sufficient to handle the cases arising in rotary wing applications. For the velocity induced along the wing span by a vortex of strength Γ:

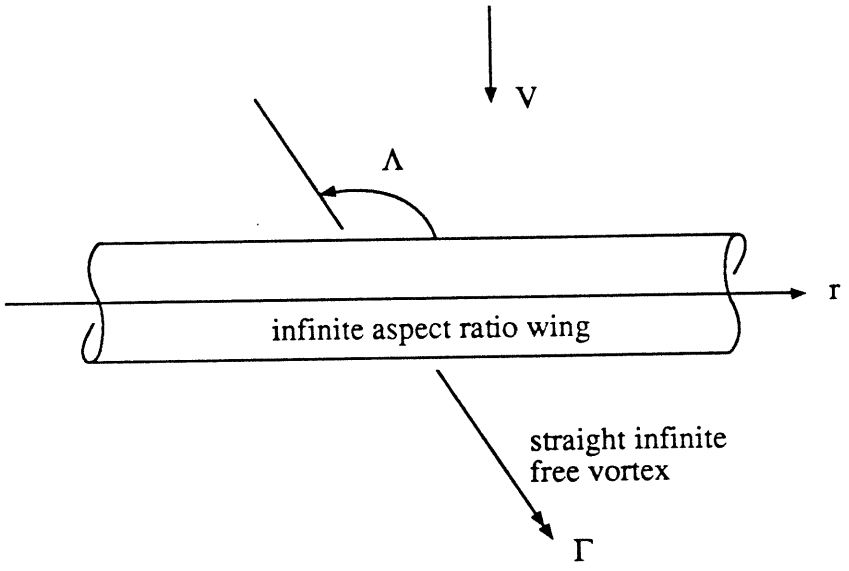

Figure 3-13. Lifting-surface theory solution for vortex-induced loads.

$$w = \frac{\Gamma}{2\pi(c/2)} \frac{-r\sin\Lambda}{(r\sin\Lambda)^2 + h^2}$$

(where r and h are here divided by the wing semichord) the approximate lifting-surface solution (from ref. 44) for the section lift is:

$$L_{2s} = \rho V \Gamma \left\{ \frac{r\sin\Lambda}{(r\sin\Lambda)^2 + (h+c_0)^2} \right.$$

$$- a_0' \frac{b_0\left(-(r\sin\Lambda)^2 + (h+c_0')^2 + b_0^2\right)}{\left(-(r\sin\Lambda)^2 + (h+c_0')^2 + b_0^2\right)^2 + 4(r\sin\Lambda)^2(h+c_0')^2}$$

$$\left. - \sum_{n=1}^{2} a_n \left(\frac{d}{2r\sin\Lambda}\right)^{2n} \left[\frac{-(r\sin\Lambda + b_1)\cos b_2 + (h+c_n)\sin b_2}{(r\sin\Lambda + b_1)^2 + (h+c_n)^2} \right] \right\}$$

For the incompressible case, the coefficients in this expression are functions of the vortex angle Λ:

$$b_0 = 8.88 - 1.88(\Lambda/90^\circ)$$

$$b_1 = -\cos\Lambda$$

$$b_2 = \frac{\pi}{4}(\Lambda/90^\circ - 1)$$

$$a_0' = .544(-\cos\Lambda) + .07\sin 2\Lambda$$

$$a_1 = -.434 - 1.09(1 - \sin\Lambda)^{.94} + .607(1 - \sin\Lambda)^{2.46}$$

$$a_2 = .0084 + .0069(-\cos\Lambda)^{1.8}$$

$$c_0' = 5.9$$

$$c_0 = 1.683 + .27(1 - \sin\Lambda)^{.90} - .154(1 - \sin\Lambda)^{2.9}$$

$$c_1 = 1.417 + .366(1 - \sin\Lambda)^{.84} - .392(1 - \sin\Lambda)^{2.0}$$
$$c_2 = .91 + .93(1 - \sin\Lambda)^{1.0} - 1.025(1 - \sin\Lambda)^{1.45}$$

(Λ is in the range 90° to 180°; the solution for Λ from 0 to 90° is obtained by symmetry considerations). The corresponding first-order lifting-line theory solution for the vortex-induced loading is obtained using:

$$c_0 = 1.571$$
$$a_1 = (1.25 + 0.5\sin\Lambda)\ (a_1)_{ls}$$
$$a_2 = (0.25 + \sin\Lambda)\ (a_1)_{ls}$$
$$a_0' = 0.75(a_0')_{ls}$$
$$b_1 = 0.5(b_1)_{ls}$$
$$b_2 = 0$$

with the other constants equal the lifting-surface values. This result is based on the lifting-line wing loading produced by a sinusoidal gust, assuming a vortex lattice wake with a line spacing of about 60% chord.

This lifting-surface solution will be used in the present analysis in the following manner. For each line segment it will be determined whether it is close enough to the blade for lifting-surface effects to be important (it is more economical to apply such a test than to always use the correction). If so, the induced velocity contribution of the line segment, as calculated above, will be multiplied by the ratio L_{ls}/L_{ll}. This lifting surface correction is intended to be applied to first-order lifting-line theory, i.e., with the collocation point at the quarter-chord. It should not be used when the collocation point is at the three-quarter-chord.

The parameters required to apply this lifting-surface correction for vortex-induced loads are h, rsinΛ, and Λ. From the minimum distance r_m between the point P and the vortex segment (in the tip-path-plane

coordinate frame), and including the influence of the viscous core on the induced velocity, the vortex/blade separation is

$$h = \frac{2}{c}\sqrt{(\vec{k}_T \cdot \vec{r}_m)^2 + r_c^2}$$

Let $\vec{i}^* = (\vec{r}_1 - \vec{r}_2)/s$ be the unit vector along the vortex segment; and $\vec{j}^* = \vec{i}_T \cos\psi + \vec{j}_T \sin\psi$ the unit vector along the blade. Then the intersection angle is

$$\Lambda = 180^\circ - \sin^{-1}\sqrt{1 - (\vec{j}^* \cdot \vec{t}^*)^2}$$

$$\sin\Lambda = \sqrt{1 - (\vec{j}^* \cdot \vec{t}^*)^2}$$

$$\cos\Lambda = -|\vec{j}^* \cdot \vec{t}^*|$$

Finally, the distance from the vortex line is

$$r\sin\Lambda = \frac{2}{c}\sqrt{(\vec{t}_T \cdot \vec{r}_m)^2 + (\vec{j}_T \cdot \vec{r}_m)^2}\ \mathrm{sign}(\vec{j}^* \cdot \vec{r}_m)\,\mathrm{sign}(\vec{j}^* \cdot \vec{t}^*) + \frac{1}{2}\cos\Lambda$$

The lifting-surface correction will be used if the distance from the segment midpoint is less than a specified distance d_{ls}:

$$r_3 = \frac{1}{2}|\vec{r}_1 + \vec{r}_2| < d_{ls}$$

Typically d_{ls} should be around 10 chords (see ref. 45).

The use of a larger viscous core radius for inboard collocation points on the blade will be allowed in order to model the various effects that evidently limit the induced loads (see section 3.1.1). The tip vortex core radius r_{c0} will be used for the radial stations outboard of r_2, and a larger value r_{cI} will be used inboard of r_1, with linear interpolation between. Hence, for a collocation point at the aerodynamic radial station r_{Ai}, the core radius is:

$$r_c = \begin{cases} r_{c0} & r \geq r_2 \\ r_{cI} & r \leq r_1 \\ \dfrac{r_{cI}(r_2 - r) + r_{c0}(r - r_1)}{r_2 - r_1} & r_1 < r < r_2 \end{cases}$$

While there are other approaches (for example, see ref. 35), increasing the core radius for inboard collocation points is the simplest, although nothing is being said about the physics of the phenomenon.

3.1.8 Vortex sheet element.

Consider a nonplanar, quadrilateral vortex sheet element, as shown in Figure 3-14. The induced velocity is required at an arbitrary point P in the flow field, defined by vectors from the four corners. The strength of the sheet is defined by the blade bound circulation values associated with the four corners (Γ_1 and Γ_3 at ϕ_k, Γ_2 and Γ_4 at ϕ_{k+1}; Γ_1 and Γ_2 at the outside edge, Γ_3 and Γ_4 at the inside edge; see Figure 3-2). It follows that the element induced velocity is a linear combination of these circulations:

$$\Delta v = \Gamma_1 \Delta v_1 + \Gamma_2 \Delta v_2 + \Gamma_3 \Delta v_3 + \Gamma_4 \Delta v_4$$

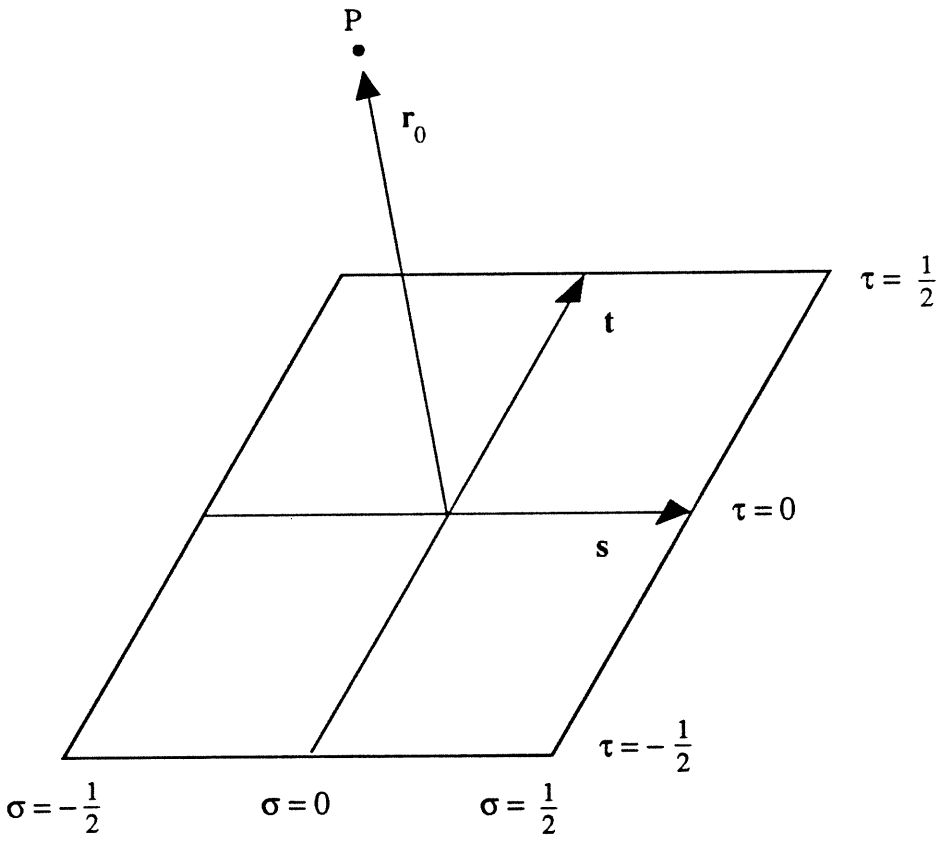

Figure 3-14. Quadrilateral vortex sheet element.

for the shed and trailed vorticity (see section 3.1.6). For the general case of a nonplanar quadrilateral element, the induced velocity will be evaluated by numerical integration. For the case of a planar rectangular element the integrations can be performed analytically. The planar rectangular element can be used as an approximation for the general element. The edges of adjacent elements will not join with this approximation, but the amount of computation required is much reduced. As a further approximation, the sheet can be replaced by trailed and shed line segments, with large core-radii to avoid high induced velocities near the lines.

The sheet geometry is defined by the vectors $\vec{s}$ and $\vec{t}$ joining the midpoints of the sides (Figure 3-14). These vectors always intersect; the vector from the intersection to P is $\vec{r}_o$. In terms of the vectors from the four corners to P:

$$\vec{r}_o = \frac{1}{4}(\vec{r}_1 + \vec{r}_2 + \vec{r}_3 + \vec{r}_4)$$

$$\vec{t} = \frac{1}{2}(\vec{r}_2 + \vec{r}_4 - \vec{r}_1 - \vec{r}_3)$$

$$\vec{s} = \frac{1}{2}(\vec{r}_3 + \vec{r}_4 - \vec{r}_1 - \vec{r}_2)$$

$$\vec{u} = \frac{1}{2}(\vec{r}_2 + \vec{r}_3 - \vec{r}_1 - \vec{r}_4)$$

where $\vec{u}$ is the vector between the midpoints of the diagonals. The sheet surface is described by the coordinates σ and t, each varying from -1/2 to 1/2; the origin $\sigma = \tau = 0$ is at $\vec{r}_o$. Then the vector from (σ,τ) on the sheet to P is

$$\vec{r} = \vec{r}_o - \sigma\vec{s} - \tau\vec{e}_t = \vec{r}_o - \tau\vec{t} - \sigma\vec{e}_s$$

$$= \vec{r}_o - \sigma\vec{e}_s - \tau\vec{e}_t + 2\sigma\tau\vec{u}$$

where the vectors in the trailed and shed directions are

$$\vec{e}_t = \vec{t} + 2\sigma\vec{n}$$

$$\vec{e}_s = \vec{s} + 2\tau\vec{n}$$

The bound circulation corresponding to the four corners is known, but not the actual vorticity distribution over the sheet. A linear variation of the trailed vorticity $\delta(\tau)$ and shed vorticity $\gamma(\sigma)$ is assumed:

$$\delta = -\frac{1}{|\vec{e}_s|}\left(\Gamma_t + 2\tau\Gamma_n\right)$$

$$\gamma = -\frac{1}{|\vec{e}_t|}\left(\Gamma_s + 2\sigma\Gamma_n\right)$$

where

$$\Gamma_t = \frac{1}{2}\left(\Gamma_3 + \Gamma_4 - \Gamma_1 - \Gamma_2\right)$$

$$\Gamma_s = \tfrac{1}{2}(\Gamma_2 + \Gamma_4 - \Gamma_1 - \Gamma_3)$$

$$\Gamma_n = \tfrac{1}{2}(\Gamma_2 + \Gamma_3 - \Gamma_1 - \Gamma_4)$$

and

$$\Gamma_t + 2\tau\Gamma_n = -(\Gamma_1 - \Gamma_3)(\tfrac{1}{2}+\tau) - (\Gamma_2 - \Gamma_4)(\tfrac{1}{2}-\tau)$$

$$\Gamma_s + 2\sigma\Gamma_n = -(\Gamma_1 - \Gamma_2)(\tfrac{1}{2}+\sigma) - (\Gamma_3 - \Gamma_4)(\tfrac{1}{2}-\sigma)$$

So the differential vorticity on the sheet is

$$\vec{\omega}\, dA = \left(\gamma \frac{\vec{e}_s}{|\vec{e}_s|} + \delta \frac{\vec{e}_t}{|\vec{e}_t|}\right) |\vec{e}_s|\, d\sigma\, |\vec{e}_t|\, d\tau$$

$$= \left[(\Gamma_s + 2\sigma\Gamma_n)\vec{e}_s - (\Gamma_t + 2\tau\Gamma_n)\vec{e}_t\right] d\sigma\, d\tau$$

The Biot-Savart law gives the induced velocity:

$$\Delta\vec{v} = -\frac{1}{4\pi}\int \frac{\vec{r}\times\vec{\omega}}{r^3}\, dA$$

$$= \frac{1}{4\pi}\int_{-\frac{1}{2}}^{\frac{1}{2}}\int_{-\frac{1}{2}}^{\frac{1}{2}} \left[-(\Gamma_s + 2\sigma\Gamma_n)(\vec{r}\times\vec{e}_s) + (\Gamma_t + 2\tau\Gamma_n)(\vec{r}\times\vec{e}_t)\right] \frac{d\sigma\, d\tau}{r^3}$$

and hence

$$\Delta v_{t_1} = \frac{1}{4\pi} \iint -\left(\tfrac{1}{2}+\tau\right)\left(\vec{r}\times\vec{e}_t\right) \frac{d\sigma\, d\tau}{r^3}$$

$$\Delta v_{t_2} = \frac{1}{4\pi} \iint -\left(\tfrac{1}{2}-\tau\right)\left(\vec{r}\times\vec{e}_t\right) \frac{d\sigma\, d\tau}{r^3}$$

$$\Delta v_{s_1} = \frac{1}{4\pi} \iint \left(\tfrac{1}{2}+\sigma\right)\left(\vec{r}\times\vec{e}_s\right) \frac{d\sigma\, d\tau}{r^3}$$

$$\Delta v_{s_3} = \frac{1}{4\pi} \iint \left(\tfrac{1}{2}-\sigma\right)\left(\vec{r}\times\vec{e}_s\right) \frac{d\sigma\, d\tau}{r^3}$$

The velocity from an infinitesimally thin vortex sheet has a logarithmic singularity near the edges. To avoid this singularity, r^3 in the integrand denominator is replaced by

$$\left(r^2 + d_{vs}^2\right)^{3/2}$$

The parameter d_{vs} may be considered a viscous core size (compare with the role of a core radius for a line segment, section 3.1.7). The introduction of d_{vs} also improves the convergence of the numerical integration when the collocation point is close to the sheet surface.

For a planar rectangular element, the velocity integrals can be evaluated analytically. The planar assumption means $\vec{u} = 0$; the rectangular assumption means $\vec{s} \cdot \vec{t} = 0$. Hence define

$$\vec{\rho} = \vec{r}_0 - \sigma\vec{s} - \tau\vec{t}$$
$$= \vec{r}_m - (\sigma - \sigma_m)\vec{s} - (\tau - \tau_m)\vec{t}$$

where the minimum distance between P and the plane of the sheet gives

$$\sigma_m = \vec{r}_0 \cdot \vec{s} \,/\, |s|^2$$
$$\tau_m = \vec{r}_0 \cdot \vec{t} \,/\, |t|^2$$
$$\vec{r}_m = \vec{r}_0 - \sigma_m \vec{s} - \tau_m \vec{t}$$

(note $\vec{r}_m \cdot \vec{s} = 0$ and $\vec{r}_m \cdot \vec{t} = 0$). So

$$\rho^2 = \rho_m^2 + (\sigma - \sigma_m)^2 s^2 + (\tau - \tau_m)^2 t^2$$
$$\rho_m^2 = r_m^2 + d_{vs}^2$$
$$\vec{\rho} \times \vec{s} = \vec{r}_m \times \vec{s} - (\tau - \tau_m)\vec{t} \times \vec{s}$$
$$\vec{\rho} \times \vec{t} = \vec{r}_m \times \vec{t} - (\sigma - \sigma_m)\vec{s} \times \vec{t}$$

Then, the induced velocity can be written as the planar-rectangular result plus a correction term:

$$\Delta v_{t_1} = (\Delta v_{t_1})_{PR} + \frac{1}{4\pi}\iint\left(-\tfrac{1}{2}-\tau\right)\left(\frac{\vec{r}\times\vec{e}_t}{r^3} - \frac{\vec{\rho}\times\vec{t}}{\rho^3}\right)d\sigma\,d\tau$$

and similarly for Δv_{t2}, Δv_{s1}, and Δv_{s3}. If the element is actually a planar rectangle, then the correction term is zero ($\vec{r} \times \vec{e}_t/r^3 - \vec{\rho} \times \vec{t}/\rho^3$). If the element is a nonplanar quadrilateral, the expressions given for $\vec{\rho}$, $\vec{\rho} \times \vec{s}$, and $\vec{\rho} \times \vec{t}$ are still used, and the correction term is evaluated by numerical integration. As an approximation, the correction term can be neglected.

The integrated expressions for the velocity induced by a planar rectangular element are:

$$(\Delta v_{t_{1,2}})_{PR} = \frac{1}{4\pi}\iint -\left(\tfrac{1}{2}\pm\tau\right)(\vec{\rho}\times\vec{t})\,\frac{d\sigma\,d\tau}{\rho^3}$$

$$= -\frac{\vec{r}_m\times\vec{t}}{4\pi}\left[\left(\tfrac{1}{2}\pm\tau_m\right)I_1 \pm I_2\right] + \frac{\vec{s}\times\vec{t}}{4\pi}\left[\left(\tfrac{1}{2}\pm\tau_m\right)I_3 \pm I_4\right]$$

$$(\Delta v_{s_{1,3}})_{PR} = \frac{1}{4\pi}\iint\left(\tfrac{1}{2}\pm\sigma\right)(\vec{\rho}\times\vec{s})\,\frac{d\sigma\,d\tau}{\rho^3}$$

$$= \frac{\vec{r}_m\times\vec{s}}{4\pi}\left[\left(\tfrac{1}{2}\pm\sigma_m\right)I_1 \pm I_3\right] - \frac{\vec{t}\times\vec{s}}{4\pi}\left[\left(\tfrac{1}{2}\pm\sigma_m\right)I_2 \pm I_4\right]$$

where

$$I_1 = \iint \frac{d\sigma\, d\tau}{\rho^3} = \frac{1}{\rho_m s t} \tan^{-1} \frac{(\sigma-\sigma_m)(\tau-\tau_m)\, st}{\rho_m \rho}$$

$$I_2 = \iint \frac{(\tau-\tau_m)\, d\sigma\, d\tau}{\rho^3} = \frac{1}{s t^2} \ln \left(\rho - s(\sigma-\sigma_m) \right)$$

$$I_3 = \iint \frac{(\sigma-\sigma_m)\, d\sigma\, d\tau}{\rho^3} = \frac{1}{s^2 t} \ln \left(\rho - t(\tau-\tau_m) \right)$$

$$I_4 = \iint \frac{(\sigma-\sigma_m)(\tau-\tau_m)\, d\sigma\, d\tau}{\rho^3} = - \frac{\rho}{s^2 t^2}$$

(each evaluated for σ = -1/2 to 1/2 and τ = -1/2 to 1/2).

For the general case of a nonplanar quadrilateral, the correction terms of the form

$$I = \int_{-\frac{1}{2}}^{\frac{1}{2}} \int_{-\frac{1}{2}}^{\frac{1}{2}} f(\sigma, \tau)\, d\sigma\, d\tau$$

are evaluated numerically. Using trapezoidal integration with M equally spaced intervals in σ and τ gives

$$I_M = \frac{1}{M^2} \sum_{i=0}^{M} \sum_{k=0}^{M} f(e_i^M, e_k^M)\, w_i^M\, w_k^M$$

where

$$e_i^M = \frac{i}{M} - \frac{1}{2}$$

$$w_i^M = \begin{cases} 1/2 & i = 0 \text{ or } M \\ 1 & \text{otherwise} \end{cases}$$

Now

$$\sum_{i=0}^{2M} f(e_i^{2M})\, w_i^{2M} = \sum_{i=0}^{M} f(e_i^M)\, w_i^M + \sum_{i=1}^{M} f(o_i^M)$$

where

$$o_i^M = \frac{2i-1}{2M} - \frac{1}{2}$$

Then doubling the number of integration steps gives

$$I_{2M} = \frac{1}{4M^2} \sum_{i=0}^{2M} \sum_{k=0}^{2M} f(e_i^{2M}, e_k^{2M})\, w_i^{2M}\, w_k^{2M}$$

$$= \frac{1}{4M^2} \sum_{i=0}^{2M} \left[\sum_{k=0}^{M} f(e_i^{2M}, e_k^{2M})\, w_k^M + \sum_{k=1}^{M} f(e_i^{2M}, o_k^M) \right] w_i^{2M}$$

$$= \frac{1}{4M^2}\left[\sum_{i=0}^{M}\sum_{k=0}^{M} f(e_i^M, e_k^M)\, w_i^M\, w_k^M + \sum_{i=1}^{M}\sum_{k=0}^{M} f(o_i^M, e_k^M)\, w_k^M + \sum_{i=0}^{M}\sum_{k=1}^{M} f(e_i^M, o_k^M)\, w_i^M + \sum_{i=1}^{M}\sum_{k=1}^{M} f(o_i^M, o_k^M)\right]$$

$$= \frac{1}{4} I_M + J_M$$

$$J_M = \frac{1}{4M^2}\sum_{i=1}^{M}\left[\sum_{k=0}^{M}\left(f(o_i^M, e_k^M) + f(e_k^M, o_i^M)\right) w_k^M + \sum_{k=1}^{M} f(o_i^M, o_k^M)\right]$$

The process is started with M = 1, and repeated until the velocity converges:

$$|I_{2M} - I_M|^2 < \epsilon^2$$

(ϵ is an input tolerance), or until the number of steps reaches a limit (such as M = 512). An unconverged result can be very wrong, so it is important that ϵ be small enough. The need for a very small value of ϵ, and the possibility of reaching the limit on M, can be controlled to some extent by the choice of d_{vs}.

An economical approximation is to replace the vortex sheet by a line segment, with either a linear or a stepped circulation

distribution, and a large core size to eliminate the high induced velocity near the line. The strength and position of the line segments are determined from the circulation and position of the four corners of the sheet:

$$\Gamma_{2\,line} = \Gamma_1 - \Gamma_3$$

$$\Gamma_{1\,line} = \Gamma_2 - \Gamma_4$$

$$\vec{r}_{2\,line} = \frac{1}{2}\left(\vec{r}_1 + \vec{r}_3\right)$$

$$\vec{r}_{1\,line} = \frac{1}{2}\left(\vec{r}_2 + \vec{r}_4\right)$$

for the trailed vorticity, and

$$\Gamma_{2\,line} = \Gamma_2 - \Gamma_1$$

$$\Gamma_{1\,line} = \Gamma_4 - \Gamma_3$$

$$\vec{r}_{2\,line} = \frac{1}{2}\left(\vec{r}_1 + \vec{r}_2\right)$$

$$\vec{r}_{1\,line} = \frac{1}{2}\left(\vec{r}_3 + \vec{r}_4\right)$$

for the shed vorticity (see Figure 3-15). Hence the line segment velocity increments Δv_1 and Δv_2 give for the trailed sheet vorticity

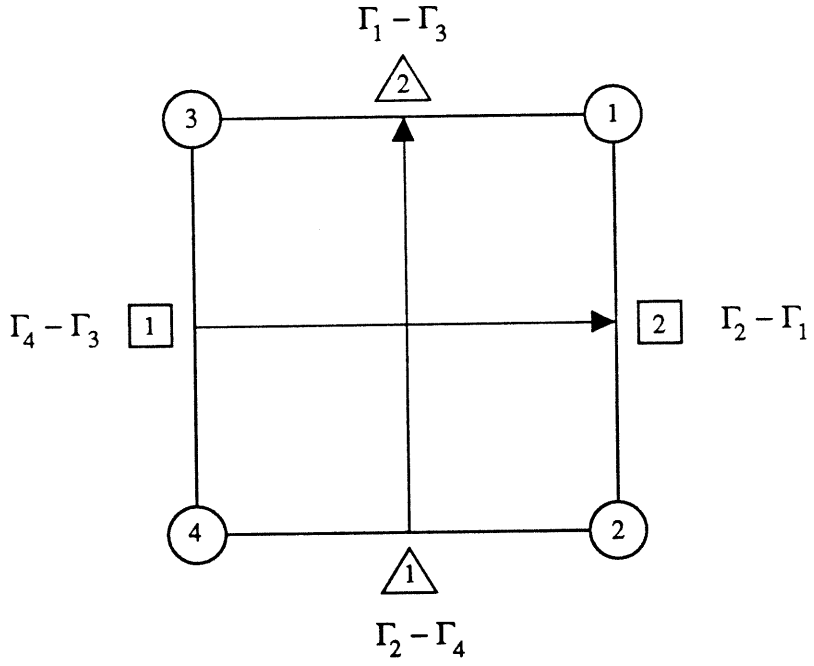

Figure 3-15. Large-core line approximation for vortex sheet element.

$$\Delta v_{t_1} = \Delta v_2$$

$$\Delta v_{t_2} = \Delta v_1$$

and for the shed sheet vorticity

$$\Delta v_{s_1} = -\Delta v_2$$

$$\Delta v_{s_3} = -\Delta v_1$$

The core radius can be specified arbitrarily; or $r_c = |\vec{s}|/2$ can be used for the trailed vorticity and $r_c = |\vec{t}|/2$ for the shed vorticity.

3.2 Free Wake Geometry

A method was developed in reference 35 for calculating the free wake geometry of a single rotor in steady state flight out of ground effect, which will be adapted for use in the present analysis. The wake model for the free wake calculation consists of line segments for the tip vortices; and rectangular sheets or line segments for the inboard shed and trailed wake (similar to the far wake model used here for the induced velocity calculation, see section 3.1.2). The near wake or rolling up wake as described above are not considered.

Only the distorted geometry of the tip vortices is calculated in the analysis of reference 35. The rigid or prescribed wake geometry is thus still used for the inboard vorticity. The distortion of the tip vortex geometry from the basic helix is defined in reference 35 as a vector $\vec{D}_s(\psi,\delta)$, giving the displacement of the wake element with current age δ which was created when the blade was at azimuth angle ψ. A

tip-path-plane coordinate frame is used, with the x axis to the right (the advancing side), the y axis aft, and the z axis down. The procedure for calculating the wake geometry consists basically of integrating the induced velocity at each wake element. The outer loop in the calculation is an iteration on the wake age δ. The induced velocity $\vec{q}(\psi)$ are calculated at all wake elements for a given age δ, and all azimuth angles ψ. Then the increment in the distortion as the wake age increases by $\Delta\psi$ is:

$$\vec{D}_s(\psi, \delta) = \vec{D}_s(\psi, \delta - \Delta\psi) + \Delta\psi\, \vec{q}(\psi)$$

An efficient calculation of the wake geometry requires many variations in this basic procedure. Reference 35 adapted the near-wake and far-wake scheme for reducing the computation. The first time the induced velocity is evaluated at a point in the wake, the contributions from all wake elements must be found. For subsequent evaluations of the induced velocity at that point, only the induced velocity due to the nearby wake elements are recalculated. The other major consideration for minimizing the computation is the matter of updating the induced velocity calculation. At a given point in the wake geometry calculation, there is a boundary in the wake between the distorted geometry and the initial, rigid geometry. The distortion has been calculated between the rotor disk and the boundary; downstream of the boundary the wake is undistorted. As time increases by $\Delta\psi$, the entire wake is convected downstream, and the rotor blades move forward by $\Delta\psi$, adding new trailed and shed vorticity at the beginning of the wake. If there were no distortion of the wake during the time $\Delta\psi$, then the induced velocity at a given wake element would not change except for the contributions from the newly created wake vorticity just behind the blade. Thus the normal calculation procedure consists of calculating

the induced velocity at the boundary, by just adding at each step the contribution from the new wake directly behind the blade. Of course, the wake does distort as it is convected and as the estimate of the distortion improves, thus it is necessary to update the calculation of the induced velocity in the wake. In boundary updating, the induced velocity is calculated at the boundary still, by summing the contributions from all elements in the wake. In general updating, the induced velocity is recalculated at all points in the wake upstream of the boundary. Boundary updating is typically done every 90° on the front and rear portions of the helices, and every 45° along the sides where the distortion is greater. General updating is typically done every 180°. General updating cannot be done often if the amount of computation is to be kept low, but it does improve the accuracy and convergence. Numerous techniques for secondary improvements in the efficiency and accuracy were also included. The distorted wake geometry is required for m revolutions, where m decreases with forward speed. A single iteration of the free wake analysis consists of calculating the distortion $\vec{D}_s(\psi,\delta)$ for $\psi = 0$ to 2π and $\delta = 0$ to $2\pi m$. Usually two iterations are sufficient to obtain the converged solution for the wake geometry.

The present analysis requires the wake geometry in the form of $\vec{D}(\psi,\phi)$ where ψ is the current azimuth angle of the blade and ϕ is the wake age ($\phi + \delta$ and δ, respectively, in the notation of ref. 35). The present analysis uses a tip-path-plane coordinate system with x aft, y to the right, and z upward. Hence

$$\vec{D}(\psi,\phi) = \left[\vec{i}_T\vec{j}_T + \vec{j}_T\vec{i}_T - \vec{k}_T\vec{k}_T\right]\vec{D}_s(\psi-\phi,\phi)$$

is the distortion as used in section 3.1.3. The rotor velocity components μ_x and μ_z are required relative to the tip path plane. The

hub motion and gust velocity at the hub can be included in these velocity components. Ground effect, rotor/rotor interference, and rotor/body interference can be accounted for by using an effective normal velocity:

$$\mu_{z_{eff}} = \mu_{z_{TPP}} + \left(1 - f_{GE}^{-1}\right)\lambda_i + \lambda_{int}$$

where f_{GE} is the ground effect factor defined in section 2.4.3, and λ_{int} is the interference induced velocity. The total uniform induced velocity

$$\lambda = \mu_{z_{TPP}} + \lambda_i + \lambda_{int}$$

is required to define the wake geometry at the start of the calculation.

3.3 CFD Interface

The methods of computational fluid dynamics (CFD) allow the calculation of rotor aerodynamic phenomenon that are beyond the scope of lifting-line theory. An example is the calculation of the shocks on the advancing blade tip, which involves transonic, unsteady, three-dimensional flow. Such calculations are so expensive that it is generally impractical to include the entire rotor flow field, or include the rotor structural dynamics. Yet the influence of the rotor wake and blade motion is essential for a complete, consistent solution.

For an efficient solution, computationally intensive operations must be moved outside the innermost loops (i.e., the circulation and motion iterations). This approach will converge well if the code is

operated in a manner such that the coupling is weak. An example is the influence coefficient and wake geometry calculation, which has been moved outside the trim iteration. Now an additional outer loop is introduced, an iteration between some CFD calculation of the blade loading and the CAMRAD/JA solution for the rotor wake and blade motion. The CFD code is not incorporated in the CAMRAD/JA code, however, but remains a separate analysis. What has been provided in CAMRAD/JA is the interface with an external analysis, implemented using input and output files.

The CFD calculation is coupled with CAMRAD/JA in terms of the angle-of-attack and blade loading (section lift, drag, and moment coefficients). CAMRAD/JA calculates the blade angle-of-attack, including the blade motion and rotor wake. The CFD analysis uses this angle-of-attack distribution (radial and azimuthal) to calculate the blade loading, perhaps on only part of the rotor disk. Then CAMRAD/JA uses the CFD blade loading to solve for the rotor and wake response. The CFD computational domain will include some wake, however, at least the wake directly behind the blade and perhaps even some tip vortices from preceding blades. This wake must not be used twice. Hence CAMRAD/JA calculates for the CFD analysis a partial angle-of-attack, obtained by excluding the wake inside the CFD domain when evaluating the nonuniform induced velocity.

Following sections 2.4.1 and 2.4.2, the partial angle-of-attack is:

$$\alpha_P = \theta + \theta_{TL} - \phi_P$$

$$\phi_P = \tan^{-1}\left(u_P - \Delta u_P\right) / \left(u_T - \Delta u_T\right)$$

where

$$\Delta u_p = \Delta\lambda_z$$

$$\Delta u_T = \Delta\lambda_x \sin\psi + \Delta\lambda_y \cos\psi$$

are the velocity components produced by the wake inside the CFD domain (neglecting some higher order terms). This partial angle-of-attack is calculated after the CAMRAD/JA solution (wake, trim, circulation, and motion iterations) has converged.

Simply setting the lift coefficient in CAMRAD/JA to the value calculated by the CFD analysis would not account for changes in the angle-of-attack as the blade motion and wake effects are revised. Hence the difference between the lifting-line theory lift coefficient from the current and previous executions of CAMRAD/JA ($c_{l_{tab}}$ and $c_{l_{old}}$, respectively) is added to the externally calculated value:

$$c_l(\alpha) = c_{l_{ext}}(\alpha_{old}) + c_{l_\alpha}(\alpha - \alpha_{old})$$

$$= c_{l_{ext}} + c_{l_{tab}} - c_{l_{old}}$$

$$= c_{l_{tab}} + (c_{l_{ext}} - c_{l_{old}})$$

When $(c_{l_{tab}} - c_{l_{old}}) = 0$, the result of the CAMRAD/JA solution is the externally calculated loading, and the solution has converged. If the externally calculated loading is available for only part of the rotor disk (radially or azimuthally, e.g., just on the advancing tip), then $(c_{l_{ext}} - c_{l_{old}}) = 0$ on the rest of the disk. In such a case $c_{l_{ext}}$ will be used on part of the disk and $c_{l_{tab}}$ on the rest, and there likely will be jumps in the loading at the boundaries. Such jumps are not physically meaningful, and may cause convergence problems. Similarly,

$$c_d = c_{d_{tab}} + c_{d_{ext}} - c_{d_{old}}$$

$$c_m = c_{m_{tab}} + c_{m_{ext}} - c_{m_{old}}$$

are used for the drag and moment coefficients.

The iteration between CAMRAD/JA and the external CFD code proceeds as follows.

(1) CAMRAD/JA calculates the partial angle of attack α_p, and saves $c_{l_{tab}}(\alpha_{old})$.

(2) The external analysis calculates $c_{l_{ext}}(\alpha_p)$.

(3) CAMRAD/JA uses $c_{l_{ext}}$ and $c_{l_{old}} = c_{l_{tab}}(\alpha_{old})$ to calculate c_l.

These steps are repeated to convergence ($c_l = c_{l_{ext}}$). Steps 3 and 1 are combined for the second and succeeding CAMRAD/JA executions. The rotor trim iteration essentially constrains the mean and once-per-revolution aerodynamic loading, so the lift coefficients will not vary much in successive CAMRAD/JA executions. Consequently, convergence of this method can be rapid, sometimes requiring only two executions of the CFD analysis.

The velocity induced by the wake inside the CFD domain is calculated as described in section 3.1. The influence coefficients are evaluated only for those wake elements inside the domain. It is not necessary to repeat the wake geometry calculation. The following possibilities for the wake accounted for in the CFD analysis are considered:

(a) the shed and trailed wake behind the reference blade, for wake ages $\phi < \phi_{bound}$;

(b) the shed and trailed wake behind the reference blade, for wake ages $\phi < \phi_{bound}$, plus tip vortices from the preceding blades;

(c) all wake elements.

The parameter ϕ_{bound} is used to limit the extent of the wake that must be tested. It is assumed that the following wake elements are never

included in the CFD analysis: bound vortices of other blades; the axisymmetric far wake; and wake from the other rotor.

Each wake line segment is tested to determine whether it is inside or outside the CFD domain. If a line segment intersects the boundary of the CFD domain, the end point outside the domain is replaced with the intersection point. Only line segments in the wake model are tested, so the wake model cannot include sheet elements inside the CFD domain.

The CFD computation domain used is a box defined by six planes. Each plane is described by a normal $\vec{n}_i$ (directed outside), and one point $\vec{o}_i$ on the plane. The plane is the locus of points $\vec{r}$ such that $(\vec{r} - \vec{o}) \cdot \vec{n} = 0$. An arbitrary point $\vec{r}$ then is outside the plane if $(\vec{r} - \vec{o}) \cdot \vec{n} > 0$, and inside it if $(\vec{r} - \vec{o}) \cdot \vec{n} < 0$. The box will be defined relative to the tip of the blade, in rotating tip-path-plane axes. The tip of the blade is $\vec{r}_b$ (tip-path-plane axes, relative to the hub; see section 3.1.3), and the unit vectors are:

$$\vec{i} = \begin{pmatrix} \cos\Psi \\ \sin\Psi \\ 0 \end{pmatrix} \qquad \vec{j} = \begin{pmatrix} -\sin\Psi \\ \cos\Psi \\ 0 \end{pmatrix} \qquad \vec{k} = \begin{pmatrix} 0 \\ 0 \\ 1 \end{pmatrix}$$

The six planes are located relative the tip: chordwise, x_B aft and x_F forward; radially, r_I inward and r_O outward; and vertically, z_L downward and z_U upward. Hence

	$\vec{n}$	d
back	$-\vec{j}$	x_B
front	$\vec{j}$	x_F
inboard	$-\vec{I}$	r_I
outboard	$\vec{I}$	r_O
lower	$-\vec{k}$	z_L
upper	$\vec{k}$	z_u

with $\vec{o} = \vec{r}_b + \vec{n}d$. A wake line segment is defined by the endpoints $\vec{r}_1$ and $\vec{r}_2$. This line or its extension intersects a plane at

$$\vec{r}_H = \vec{r}_1 (1 - \sigma) + \vec{r}_2 \sigma$$

where

$$\sigma = \frac{\vec{n} \cdot (\vec{o} - \vec{r}_1)}{\vec{n} \cdot (\vec{r}_2 - \vec{r}_1)}$$

(which gives $(\vec{r}_I - \vec{o}) \cdot \vec{n} = 0$; the line and plane are parallel if $\vec{n} \cdot (\vec{r}_2 - \vec{r}_1) = 0$). This intersection lies within the line segment if $0 \le \sigma \le 1$, and on the CFD domain boundary if $\vec{r}_I$ is on or inside the other five planes.

CFD domains of other shape can be similarly analyzed. Note that all that is required for use in CAMRAD/JA is that the domain boundary be correct where it intersects the rotor wake, and probably the partial angle-of-attack is not too sensitive to small errors in this intersection. Hence the box considered here may be sufficient.

4. AIRCRAFT MODEL

A general two-rotor aircraft is considered, with rigid body and elastic motion of the airframe. The model is applicable to the case of a rotor or helicopter on a flexible support in a wind tunnel as well. An arbitrary, nonlinear representation of the aircraft geometry and trim orientation is included, since all that requires is properly defined rotation matrices. An orthogonal mode representation of the body elastic motion is used. The modal approach is efficient, yet allows a completely general representation of the airframe. The airframe structural vibration modes must be obtained from a separate analysis. The linearized equations of motion for the rigid body degrees of freedom are used in the calculation of the aircraft vibration and transient motion. Linearized equations are consistent with the assumption in the rotor analysis that the perturbation shaft motion is small. The trim orientation of the helicopter can be large, however.

Aerodynamic forces on the wing-body, horizontal tail, and vertical tail are modeled, including control surfaces. Static aircraft aerodynamic characteristics are used, which must be defined based on experimental results. The aerodynamic characteristics are specified separately for the tail surfaces since the angle-of-attack and dynamic pressure may be different at the tail because of interference effects. An empirical model for the interference between the rotors and the airframe is included in the present analysis. It is also possible to calculate the mean rotor-induced velocity at the airframe components as part of the nonuniform inflow analysis. The generalized aerodynamic damping and control forces on the airframe elastic modes are included; these terms should be estimated for the frequency of the principal excitation of the mode. The airframe aerodynamic representation is basically a quasistatic model, however.

The rotational speed degrees of freedom of the two rotors, coupled through the drive system, can be important factors in the helicopter

dynamics. To complete the equations of motion for these degrees of freedom, a model for the drive train is required, including the engine dynamics and a rotor speed governor. An elementary model of the transmission and engine dynamics is used in the present analysis, so that at least the principal features may be included in the calculations.

4.1 Aircraft Configuration Definition

A general two-rotor aircraft is considered, with rigid body and elastic motion of the airframe. Aerodynamic forces on the wing/body, horizontal tail, and vertical tail are modeled, including aerodynamic control surfaces. The drive train connecting the rotors is modeled, with engine dynamics and a rotor speed governor. The case of a rotor or helicopter on a flexible support in a wind tunnel is included in the model.

4.1.1 Aircraft orientation: flight path and trim Euler angles.

The aircraft flight path is specified by the velocity magnitude V, and the orientation of the velocity vector with respect to earth axes (Fig. 4-1). The velocity vector has a yaw angle ψ_{FP} (positive to the right), and a pitch angle θ_{FP} (positive upward). Thus the climb and side velocities of the aircraft are $V_{climb} = V\sin\theta_{FP}$ and $V_{side} = V\sin\psi_{FP}\cos\theta_{FP}$. The aircraft attitude with respect to earth axes is specified by the trim Euler angles, first pitch θ_{FT} (positive nose up), then roll ϕ_{FT} (positive to the right). Airplane convention is followed here for the coordinate systems -- x positive forward, y positive to the right, and z positive downward (see reference 46). Between the earth axes (E system) and the velocity axes (V system) there are the rotations ψ_{FP} and θ_{FP}. Between the earth axes and the body axes (F system) there are the rotations θ_{FT} and θ_{FT}. Thus the rotation matrices from the earth axes are

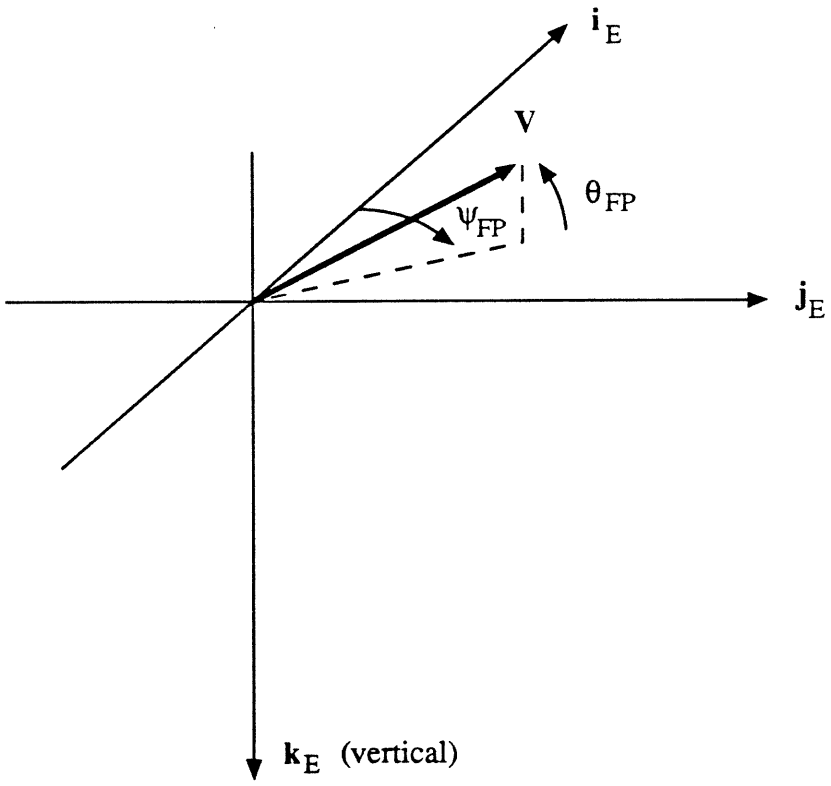

Figure 4-1. Earth axes and aircraft flight path definition.

$$R_{FE} = X_{\phi_{FT}} Y_{\theta_{FT}}$$

$$R_{VE} = Y_{\theta_{FP}} Z_{\psi_{FP}}$$

where

$$X_{\phi} = \begin{bmatrix} 1 & 0 & 0 \\ 0 & \cos\phi & \sin\phi \\ 0 & -\sin\phi & \cos\phi \end{bmatrix}$$

$$Y_{\theta} = \begin{bmatrix} \cos\theta & 0 & -\sin\theta \\ 0 & 1 & 0 \\ \sin\theta & 0 & \cos\theta \end{bmatrix}$$

$$Z_{\psi} = \begin{bmatrix} \cos\psi & \sin\psi & 0 \\ -\sin\psi & \cos\psi & 0 \\ 0 & 0 & 1 \end{bmatrix}$$

and the rotation matrix between the V system and the F system is

$$R_{FV} = R_{FE} \overline{R_{VE}}^{T}$$

The flight path angles and Euler angles are either prescribed or determined by the trim analysis.

For aircraft flight dynamics analyses, it may be desirable to express the airframe rigid body motion in stability axes (A system). The stability axes are equivalent to the wind axis system here (V axes). The trim Euler angles relative to the A axes give the rotation matrix relative to earth:

$$R_{VE} = X_{\phi_{VT}} Y_{\theta_{VT}} Z_{\psi_{VT}}$$

so $\phi_{VT} = 0$, $\theta_{VT} = \theta_{FP}$, and $\psi_{VT} = \psi_{FP}$. Note that if all roll and yaw angles are zero ($\phi = \psi = 0$), then

$$R_{FV} = Y_{\theta_{FT} - \theta_{FP}} = Y_{\alpha}$$

The velocity of the aircraft is $\vec{V} = V\vec{i}_V$, so the components in the body axes are:

$$\begin{pmatrix} V_x \\ V_y \\ V_z \end{pmatrix} = V R_{FV} \vec{i}_V$$

The acceleration due to gravity is $\vec{g} = g\vec{k}_E$ or in body axes

$$\vec{g} = g\vec{k}_E = g \begin{pmatrix} -\sin\theta_{FP} \\ \cos\theta_{FP} \sin\phi_{FP} \\ \cos\theta_{FP} \cos\phi_{FP} \end{pmatrix}$$

4.1.2. Rotor position and orientation.

The rotor hub position is specified in the body axes relative to the aircraft center of gravity position, $\vec{r}_{hub} = (x\vec{i}_F + y\vec{j}_F + z\vec{k}_F)_{hub}$. The rotor orientation is defined by the rotation matrix between the shaft axes (S system) and the aircraft body axes (F system).

$$\begin{pmatrix} \vec{\imath}_S \\ \vec{\jmath}_S \\ \vec{k}_S \end{pmatrix} = R_{SF} \begin{pmatrix} \vec{\imath}_F \\ \vec{\jmath}_F \\ \vec{k}_F \end{pmatrix}$$

The position and orientation of the rotors relative to the body axes are fixed geometric parameters. The aircraft velocity is $\vec{V} = -\mu_x\vec{i}_S + \mu_y\vec{j}_S + \mu_z\vec{k}_S = V\vec{i}_V$, so the shaft axes components of the velocity seen by the rotor are

$$\begin{pmatrix} -\mu_x \\ \mu_y \\ \mu_z \end{pmatrix} = R_{SF} R_{FV} \begin{pmatrix} V \\ 0 \\ 0 \end{pmatrix}$$

The hub plane angle-of-attack and yaw angle may then be obtained from

$$\alpha_{HP} = \tan^{-1} \mu_z / \sqrt{\mu_x^2 + \mu_y^2}$$

$$\psi_{HP} = \tan^{-1} \mu_y / \mu_x$$

and the advancing tip Mach number from

$$M_{adv} = M_{tip}\sqrt{\left(1+\sqrt{\mu_x^2+\mu_y^2}\right)^2+\mu_z^2}$$

The sign of the lateral velocity μ_y must be changed for a clockwise rotating rotor; and for rotor #2 the velocity components must be multiplied by $\Omega R_1/\Omega R_2$. The quasistatic hub motion and the gust velocity at the rotor hub will be included in the advance ratio components:

$$\begin{pmatrix} -\mu_x \\ \mu_y \\ \mu_z \end{pmatrix} = R_{SF}\,k_{FV}\begin{pmatrix} V+u_G \\ v_G \\ w_G \end{pmatrix} + \begin{pmatrix} \dot{x}_{cg} \\ \dot{y}_{cg} \\ \dot{z}_{cg} \end{pmatrix}_{static}$$

For a helicopter main rotor, the orientation with respect to the body axes will be specified by a shaft angle-of-attack θ_R (positive for rearward tilt), and a roll angle ϕ_R (positive to the right). Thus:

$$R_{SF} = \begin{bmatrix} -c\theta & 0 & s\theta \\ s\phi s\theta & c\phi & s\phi c\theta \\ -c\phi s\theta & s\phi & -c\phi c\theta \end{bmatrix}$$

The orientation of a tail rotor will be specified by a cant angle ϕ_R (positive upward), and a shaft angle-of-attack θ_R (positive rearward). The tail rotor thrust is to the right for a counterclockwise rotating main rotor, and to the left for clockwise rotation. Thus the definition of the tail rotor shaft axes depends on the main rotor rotation direction. Let Ω_{mr} have the value +1 for a counterclockwise rotating main rotor, and Ω_{mr} = -1 for a clockwise rotation. Then the rotation matrix for the tail rotor is:

$$R_{SF} = \begin{bmatrix} -C_\theta & -\Omega_{mr} C_\phi S_\theta & S_\phi S_\theta \\ 0 & S_\phi & \Omega_{mr} C_\phi \\ -S_\theta & \Omega_{mr} C_\phi C_\theta & -S_\phi C_\theta \end{bmatrix}$$

The nacelle and rotor of a tilting proprotor aircraft can be tilted by an angle α_p, where α_p = 0 for axial flow (airplane configuration), and α_p = 90° for edgewise flow (helicopter configuration). The rotor orientation is also described by a cant angle ϕ_R (positive inward in helicopter mode, zero in airplane mode), and a pitch angle θ_R (positive nose upward) which is the angle-of-attack of the shaft with respect to the body axes when α_p = 0. Thus the rotation matrix is:

$$R_{SF} = \begin{bmatrix} -C_\phi S_\alpha C_\theta - C_\alpha S_\theta & -S_\phi S_\alpha & C_\phi S_\alpha S_\theta - C_\alpha C_\theta \\ -C_\phi S_\phi (1-C_\alpha) C_\theta - S_\phi S_\alpha S_\theta & C_\phi^2 + S_\phi^2 C_\alpha & C_\phi S_\phi (1-C_\alpha) S_\theta - S_\phi S_\alpha C_\theta \\ (C_\phi^2 C_\alpha + S_\phi^2) C_\theta - C_\phi S_\alpha S_\theta & -C_\phi S_\phi (1-C_\alpha) & -(C_\phi^2 C_\alpha + S_\phi^2) S_\theta - C_\phi S_\alpha C_\theta \end{bmatrix}$$

The rotor hub location $\vec{r}_{hub}$ for the tilting proprotor aircraft is defined by the pivot location $\vec{r}_{pivot}$ and the mast height h, so

$$\vec{r}_{hub} = \vec{r}_{pivot} + h \begin{pmatrix} (c_\phi^2 c_\alpha + s_\phi^2) c_\theta - c_\phi s_\alpha s_\theta \\ -c_\phi s_\phi (1 - c_\alpha) \\ -(c_\phi^2 c_\alpha + s_\phi^2) s_\theta - c_\phi s_\alpha c_\theta \end{pmatrix}$$

4.1.3 Wind tunnel case.

For the case of a rotor or rotorcraft in a wind tunnel, the forces and moments on the body are reacted by the model support system, so trim of the body forces is no longer a concern. The flight path and trim Euler angles can be set to zero ($\theta_{FT} = \phi_{FT} = \theta_{FP} = \psi_{FP} = 0$), so the wind, earth, and body axes coincide ($R_{FV} = I$). The wind axes and body axes are therefore the tunnel axes system, with the x axis directed upstream, the y axis to the right, and the z axis vertically downward. The rotor orientation is specified by the matrix R_{SF} as above. To accommodate the case of a wind tunnel with a turntable, the R_{SF} matrices can be post-multiplied by the matrix

$$R_{FT} = \begin{bmatrix} c_\theta c_\psi & c_\theta s_\psi & -s_\theta \\ -s_\psi & c_\psi & 0 \\ s_\theta c_\psi & s_\theta s_\psi & c_\theta \end{bmatrix}$$

where ψ_T is the turntable yaw angle, positive to the right, and θ_T is the test module pitch angle, positive rearward.

4.1.4. Gust velocity.

The aerodynamic gust velocity will be defined relative to the velocity axes, with longitudinal component u_G positive rearward, lateral component v_G positive from the right, and vertical component w_G positive upward ($\vec{V}gust = - u_G\vec{i}_V - v_G\vec{j}_V - w_G\vec{k}_V$). The components in the body axes are then

$$\begin{Bmatrix} u_G \\ v_G \\ w_G \end{Bmatrix}_F = R_{FV} \begin{Bmatrix} u_G \\ v_G \\ w_G \end{Bmatrix}_V$$

The components in the rotor shaft axes are

$$\begin{Bmatrix} u_G \\ -v_G \\ w_G \end{Bmatrix}_S = R_{SF} R_{FV} \begin{Bmatrix} -u_G \\ -v_G \\ -w_G \end{Bmatrix}_V$$

For the clockwise rotating rotor, the sign of v_G is changed; for rotor #2 the gust velocities must be multiplied by $\Omega R_1/\Omega R_2$. Hence define

$$R_G = \begin{bmatrix} -1 & 0 & 0 \\ 0 & 1 & 0 \\ 0 & 0 & -1 \end{bmatrix} R_{SF} R_{FV}$$

including also the factor $\Omega R_1/\Omega R_2$ and the sign change for a clockwise rotating rotor as appropriate.

4.1.5 Aircraft description and auxiliary forces.

The aircraft geometrical description consists of the location of the following relative to the center of gravity: rotor #1; rotor #2; the point of application of airframe aerodynamic forces, for the wing/body, the horizontal tail, and the vertical tail; and the point of application of auxiliary forces. The orientation and position of the aircraft components will be defined in a body axis system (the F frame) with origin at an arbitrary reference point, as in Figure 4-2. The position data will be input in terms of fuselage station (FS, positive aft), buttline (BL, positive to the right), and waterline (WL, positive upward) relative to this arbitrary reference point. Given the dimensional positions relative to the reference point, for example

center of gravity: FSCG, BLCG, WLCG
rotor #1: FSR1, BLR1, WLR1

then the coordinates of the location of rotor #1 relative to the center of gravity (in the F frame) are

x = (FSCG - FSR1)/R
y = (BLR1 - BLCG)/R
z = (WLCG - WLR1)/R

and similarly for the other locations required.

The mode shapes of the airframe elastic motion are described by the six components of linear and angular hub motion, in the F frame: $\vec{\xi}_k$ and $\vec{\gamma}_k$ at $\vec{r}_{hub}$ (for each rotor). Assuming that the generalized coordinate q_k has dimensions of m or ft, it follows that the generalized mass M_k

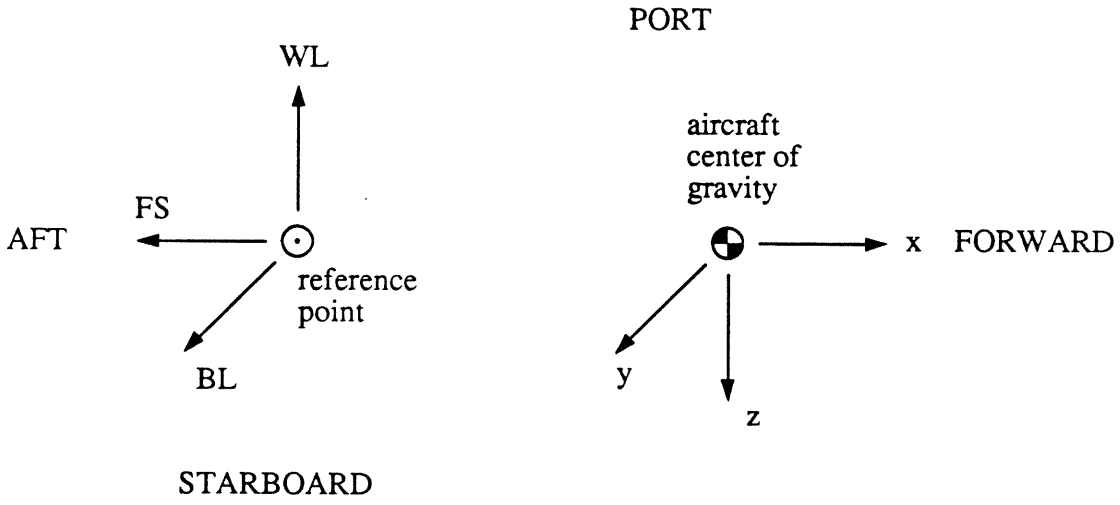

Figure 4-2. Definition of aircraft geometry.

has dimensions of kg or slug; that the hub linear motion ξ_k is dimensionless (i.e., m/m or ft/ft); and that the hub angular motion γ_k has dimensions of rad/m or rad/ft. These elastic vibration modes can be arbitrarily scaled; if ξ_k and γ_k are multiplied by a factor S, then M_k should be multiplied by S^2 and the solutions for q_k will be divided by S.

Airframe finite element analyses (such as NASTRAN) typically use inches for length dimensions. To convert to feet, as required here, the mode shapes for angular motion, γ_k, and the generalized mass, M_k, must then be multiplied by 12. The typical coordinate system for the finite element analysis has the x axis positive aft, the y axis positive to the right, and the z axis positive upward. Then to convert to the F frame used here, the signs of the x and z components of the linear and angular modes shapes, ξ_k and γ_k, must be changed.

For the case of a wind tunnel with a turntable, the geometry will be defined for zero yaw angle, relative to a reference point at the center of the rotation. Then

$$\begin{Bmatrix} x \\ y \\ z \end{Bmatrix} = R_{TF} \begin{Bmatrix} x \\ y \\ z \end{Bmatrix}_{\Psi_T = \Theta_T = 0}$$

where R_{TF} is defined in section 4.1.3. The airframe elastic mode shapes are also defined for zero pitch and yaw angle of the wind tunnel support, hence ξ_k and γ_k must be premultiplied by R_{TF}.

A set of auxiliary forces acting on the airframe, f_1, will be included. There are no dynamics (no degrees of freedom) involved in these forces. The auxiliary forces may therefore be treated as airframe control variables, that directly generate generalized forces on the airframe. The power required to generate the auxiliary forces is not calculated. The magnitude of the auxiliary force consists of a constant

term and a term proportional to the pilot's control input (see section 4.1.6), plus higher harmonic terms:

$$(f_\ell) = (f_\ell)_{control} + \left[(f_\ell)_{pc} \cos pN\Psi + (f_\ell)_{ps} \sin pN\Psi\right]_{rotor\ \#1} + \left[(f_\ell)_{pc} \cos pN\Psi + (f_\ell)_{ps} \sin pN\Psi\right]_{rotor\ \#2}$$

The constant term can represent a fixed auxiliary lift or propulsive force. The control term can be used to trim the aircraft, and as a perturbation for the transient, flight dynamics, and flutter analyses. The higher harmonic terms can represent effects such as fuselage loads produced by rotor wake impingement. The higher harmonic control terms may be associated with either or both rotors (which may have different rotational rates or phases).

The position of the auxiliary force point of application is defined by its fuselage station, buttline, and waterline (as for other fuselage positions). Thus the position vector $\mathbf{r}_f$ can be calculated for each force, as described above. The orientation of the force vector is defined by the azimuth angle ψ_f and elevation angle θ_f. These angles are measured relative to the fuselage axis system (F frame): ψ_f is in the x-y plane, positive counterclockwise from the negative x axis; θ_f is from the x-y plane, positive upward. For example, a propulsive force would be obtained with $\psi_f = 180$ and $\theta_f = 0$. These angles define a unit vector in the direction of the force:

$$\hat{e}_f = -\cos\theta_f \cos\psi_f \vec{i}_F + \cos\theta_f \sin\psi_f \vec{j}_F - \sin\theta_f \vec{k}_F$$

To determine the generalized force for the elastic airframe modes, the linear mode shape ξ_k is required at the point of application of the auxiliary force. For the wind tunnel case, all these vectors should actually be multiplied by R_{TF}, but that will be done after constructing the derivative matrix (see section 4.2.8).

4.1.6 Pilot's controls.

The control variables included in the rotorcraft model are collective and cyclic pitch of the two rotors; the aircraft controls, which consist of engine throttle θ_t, wing flaperon angle δ_f, wing aileron angle δ_a, elevator angle δ_e, and rudder angle δ_r; and the airframe auxiliary forces, f_l. The control vector is thus

$$\underset{\sim}{v}^T = \left[(\theta_0\ \theta_{1c}\ \theta_{1s})_1\ (\theta_0\ \theta_{1c}\ \theta_{1s})_2\ \delta_f\ \delta_e\ \delta_a\ \delta_r\ \theta_t\ (f_l) \right]$$

Except for the auxiliary forces, the units of v are radians internally, and degrees for input/output. The units of the auxiliary forces f_l are lb or N.

The pilot's controls consist of collective stick δ_0 (positive upward), lateral cyclic stick δ_c (positive to the right), longitudinal cyclic stick δ_s (positive forward), pedal δ_p (positive yaw right), and the throttle δ_t:

$$v_p^T = \left[\delta_0\ \delta_c\ \delta_s\ \delta_p\ \delta_t \right]$$

For the purpose of trimming the helicopter, a linear relation between the pilot's control inputs and the rotor and aircraft control variables is assumed:

$$\vec{v} = T_c \vec{v}_p + \vec{v}_o$$

where $\vec{v}_o$ is the control input and auxiliary forces with all sticks centered ($\vec{v}_p = 0$), and T_C is a transformation matrix defined by the control system geometry.

For trim, it is not intended that the matrix T_C account for the true coupling between the pilot's control and the rotor/aircraft controls. For modern helicopters that coupling is often quite complex, and may involve some nonlinear functions and gain scheduling with flight condition. All that is necessary for the present purposes is that the matrix T_C correctly account for the coupling between the redundant rotor and aircraft controls. Then the trim solution will produce the correct positions of the individual controls, and the true position of the pilot's sticks can be determined from the actual control system geometry if necessary.

For the most general case, the matrix T_C can be input directly. Alternatively, standard forms for T_C can be defined in terms of gain factors and swashplate phase angles. The control transformation matrices are given below for the following configurations: single main-rotor and tail-rotor, tandem main-rotor, side-by-side main-rotor, and coaxial main-rotor. The main rotor, front rotor, right rotor, or lower rotor, respectively, is assumed to be rotor #1; and the tail rotor, rear rotor, left rotor, or upper rotor is rotor #2. The K's are gain factors in the control system, and the $\Delta\psi$'s are swashplate azimuth lead angles. The parameter Ω here takes the value +1 for counterclockwise rotation of the rotor, and Ω = -1 for clockwise rotation. The control matrix is split into the top six rows (T_{CR}, for rotor controls) and the remainder (T_{CA}, for aircraft controls and

auxiliary forces). The top part is defined as follows for the configurations considered.

(a) single main-rotor and tail-rotor

$$T_{CR} = \begin{bmatrix} K_0 & 0 & 0 & 0 & 0 \\ 0 & -\Omega_{mr} K_c \cos\Delta\Psi_c & -K_s \sin\Delta\Psi_s & 0 & 0 \\ 0 & -\Omega_{mr} K_c \sin\Delta\Psi_c & -K_s \cos\Delta\Psi_s & 0 & 0 \\ 0 & 0 & 0 & -\Omega_{mr} K_p & 0 \\ 0 & 0 & 0 & 0 & 0 \\ 0 & 0 & 0 & 0 & 0 \end{bmatrix}$$

(b) tandem main-rotors

$$T_{CR} = \begin{bmatrix} K_{FO} & 0 & -K_{FS} & 0 & 0 \\ 0 & -\Omega_1 K_{FC} \cos\Delta\Psi_{FC} & 0 & -\Omega_1 K_{FP} \cos\Delta\Psi_{FP} & 0 \\ 0 & \Omega_1 K_{FC} \sin\Delta\Psi_{FC} & 0 & \Omega_1 K_{FP} \sin\Delta\Psi_{FP} & 0 \\ K_{RO} & 0 & K_{RS} & 0 & 0 \\ 0 & -\Omega_2 K_{RC} \cos\Delta\Psi_{RC} & 0 & -\Omega_2 K_{RP} \cos\Delta\Psi_{FP} & 0 \\ 0 & \Omega_2 K_{RC} \sin\Delta\Psi_{RC} & 0 & \Omega_2 K_{RP} \sin\Delta\Psi_{FP} & 0 \end{bmatrix}$$

(c) side-by-side main-rotors

$$T_{CR} = \begin{bmatrix} K_o & -K_c & 0 & 0 & 0 \\ 0 & 0 & -K_s \sin\Delta\Psi_s & K_p \sin\Delta\Psi_p & 0 \\ 0 & 0 & -K_s \cos\Delta\Psi_s & K_p \cos\Delta\Psi_p & 0 \\ K_o & K_c & 0 & 0 & 0 \\ 0 & 0 & -K_s \sin\Delta\Psi_s & -K_p \sin\Delta\Psi_p & 0 \\ 0 & 0 & -K_s \cos\Delta\Psi_s & -K_p \cos\Delta\Psi_p & 0 \end{bmatrix}$$

(d) coaxial main-rotors

$$T_{CR} = \begin{bmatrix} K_o & 0 & 0 & \Omega_1 K_p & 0 \\ 0 & -\Omega_1 K_c \cos\Delta\Psi_c & -K_s \sin\Delta\Psi_s & 0 & 0 \\ 0 & -\Omega_1 K_c \sin\Delta\Psi_c & -K_s \cos\Delta\Psi_s & 0 & 0 \\ K_o & 0 & 0 & \Omega_2 K_p & 0 \\ 0 & -\Omega_2 K_c \cos\Delta\Psi_c & -K_s \sin\Delta\Psi_s & 0 & 0 \\ 0 & -\Omega_2 K_c \sin\Delta\Psi_c & -K_s \cos\Delta\Psi_s & 0 & 0 \end{bmatrix}$$

The bottom part of T_C is defined identically for all the configurations:

$$T_{CA} = \begin{bmatrix} K_f & 0 & 0 & 0 & 0 \\ 0 & 0 & K_e & 0 & 0 \\ 0 & -K_a & 0 & 0 & 0 \\ 0 & 0 & 0 & K_r & 0 \\ K_t & 0 & 0 & 0 & K_{tt} \\ 0 & 0 & 0 & 0 & 57.3\ K_{at} \\ 0 & 0 & 0 & 57.3\ K_{ap} & 0 \end{bmatrix}$$

The matrix elements for the auxiliary forces make f_1 available for propulsion and f_2 for torque balance (the rows of T_C are zero for f_n, $n \geq 3$). With the pilot's controls considered angles, the units of the gain factors (K's) are deg/deg for the rotor and aircraft controls, and N/deg or lb/deg for the auxiliary forces.

4.2 Aircraft Analysis

The aircraft motion consists of the six rigid body degrees of freedom and the elastic free vibration modes. A body axis coordinate frame with origin at the aircraft center of gravity (the F system) is used for the description of the motion. Airplane practice is followed for these axes--x is forward, y is to the right, and z is downward (ref.

46). The coordinate frame used is not a principal axis system however; moreover, the airplane practice of aligning the x axis with the trim velocity is not followed, since for rotorcraft it is necessary to consider the hovering case (V = 0).

The parameters of rotor #1 are used in making quantities dimensionless and in normalizing the aircraft equations of motion. It is assumed that rotor #1 is the main-rotor of a single main rotor and tail rotor helicopter; the front rotor of a tandem rotor helicopter; or the right rotor of a side-by-side rotor helicopter. With the hub forces in rotor coefficient form it is convenient to normalize the equations by dividing by the characteristic inertia $(\frac{1}{2}NI_b)_1$.

4.2.1 Degrees of freedom.

The linear and angular rigid body motion of the aircraft is defined in the body axes (F system). The linear degrees of freedom are x_F (positive forward), y_F (positive to the right), and z_F (positive downward). These variables are dimensionless based on the rotor radius R; thus the velocity perturbations are normalized using the rotor tip speed ΩR rather than the forward speed V as is airplane practice. The angular degrees of freedom are the Euler angles ψ_F (yaw to the right), θ_F (pitch nose up), and ϕ_F (roll right). Then the linear and angular velocity perturbations are

$$\vec{v}_F = \dot{x}_F \vec{i}_F + \dot{y}_F \vec{j}_F + \dot{z}_F \vec{k}_F$$

$$\vec{\omega}_F = R_e \left(\dot{\phi}_F \vec{i}_F + \dot{\theta}_F \vec{j}_F + \dot{\psi}_F \vec{k}_F \right)$$

where $R_e = X_\phi E_\theta$, with

$$E_\theta = \begin{bmatrix} 1 & 0 & -\sin\theta \\ 0 & 1 & 0 \\ 0 & 0 & \cos\theta \end{bmatrix}$$

(the matrices X, Y, and Z are defined in section 4.1.1), so

$$R_e = \begin{bmatrix} 1 & 0 & -\sin\theta_{FT} \\ 0 & \cos\phi_{FT} & \cos\theta_{FT}\sin\phi_{FT} \\ 0 & -\sin\phi_{FT} & \cos\theta_{FT}\cos\phi_{FT} \end{bmatrix}$$

The inverse of R_e is

$$R_e^{-1} = \begin{bmatrix} 1 & \frac{\sin\theta_{FT}\sin\phi_{FT}}{\cos\theta_{FT}} & \frac{\sin\theta_{FT}\cos\phi_{FT}}{\cos\theta_{FT}} \\ 0 & \cos\phi_{FT} & -\sin\phi_{FT} \\ 0 & \frac{\sin\phi_{FT}}{\cos\theta_{FT}} & \frac{\cos\phi_{FT}}{\cos\theta_{FT}} \end{bmatrix}$$

The results are similar for R_e relative to stability (wind) axes, with $\phi_{VT} = 0$ and $\theta_{VT} = \theta_{FP}$.

The rotation matrix R transforms the linear and angular velocity between fuselage (F) and stability (V) axes:

$$\begin{pmatrix} \dot{x} \\ \dot{y} \\ \dot{z} \end{pmatrix}_F = R_{FV} \begin{pmatrix} \dot{x} \\ \dot{y} \\ \dot{z} \end{pmatrix}_V$$

$$\begin{pmatrix} p \\ q \\ r \end{pmatrix}_F = R_{FV} \begin{pmatrix} p \\ q \\ r \end{pmatrix}_V$$

Then the transformation of the perturbation Euler angles from V to F axes is:

$$\begin{pmatrix} \phi \\ \theta \\ \psi \end{pmatrix}_F = R_{eF}^{-1} R_{FV} R_{eV} \begin{pmatrix} \phi \\ \theta \\ \psi \end{pmatrix}_V = R_{FVe} \begin{pmatrix} \phi \\ \theta \\ \psi \end{pmatrix}_V$$

where

$$\begin{aligned} R_{FVe} &= R_{eF}^{-1} R_{FV} R_{eV} \\ &= E_{\theta FT}^{-1} X_{-\phi FT} R_{FV} E_{\theta FP} \\ &= E_{\theta FT}^{-1} Y_{\theta FT} Z_{-\psi FP} Y_{-\theta FP} E_{\theta FP} \end{aligned}$$

or

$$R_{FV_e} = \begin{bmatrix} \frac{\cos\psi_{FP}\cos\theta_{FP}}{\cos\theta_{FT}} & -\frac{\sin\psi_{FP}}{\cos\theta_{FT}} & 0 \\ \sin\psi_{FP}\cos\theta_{FP} & \cos\psi_{FP} & 0 \\ -\sin\theta_{FP} + \frac{\cos\psi_{FP}\cos\theta_{FP}\sin\theta_{FT}}{\cos\theta_{FT}} & -\frac{\sin\psi_{FP}\sin\theta_{FT}}{\cos\theta_{FT}} & 1 \end{bmatrix}$$

Similarly, the transformation of the perturbation Euler angles from F to V axes requires:

$$R_{VF_e} = \begin{bmatrix} \frac{\cos\psi_{FP}\cos\theta_{FT}}{\cos\theta_{FP}} & \frac{\sin\psi_{FP}}{\cos\theta_{FP}} & 0 \\ -\sin\psi_{FP}\cos\theta_{FT} & \cos\psi_{FP} & 0 \\ -\sin\theta_{FT} + \frac{\cos\psi_{FP}\cos\theta_{FT}\sin\theta_{FP}}{\cos\theta_{FP}} & \frac{\sin\psi_{FP}\sin\theta_{FP}}{\cos\theta_{FP}} & 1 \end{bmatrix}$$

Then the substitution

$$\begin{pmatrix} \phi \\ \theta \\ \psi \\ x \\ y \\ z \end{pmatrix}_F = \begin{bmatrix} R_{FV_e} & 0 \\ 0 & R_{FV} \end{bmatrix} \begin{pmatrix} \phi \\ \theta \\ \psi \\ x \\ y \\ z \end{pmatrix}_V = \mathcal{R}_{FV} \begin{pmatrix} \phi \\ \theta \\ \psi \\ x \\ y \\ z \end{pmatrix}_V$$

transforms the rigid body degrees of freedom from fuselage (F) axes to stability (V) axes.

For the elastic motion of the aircraft in flight, the displacement $\vec{u}$ and rotation $\vec{\theta}$ at an arbitrary point r are expanded in a series of the orthogonal free vibration modes:

$$\vec{u}(\vec{r},t) = \sum_{k=1}^{\infty} q_{Sk}(t)\,\vec{\xi}_k(\vec{r})$$

$$\vec{\theta}(\vec{r},t) = \sum_{k=1}^{\infty} q_{Sk}(t)\,\vec{\gamma}_k(\vec{r})$$

The first six degrees of freedom are the rigid body motions: $q_{S1}\cdots q_{S6}$ are, respectively, ϕ_F, θ_F, ψ_F, x_F, y_F, and z_F. The generalized coordinates q_{Sk} for $k \geq 7$ are the elastic modes of the aircraft. Orthogonality implies that the elastic vibration modes produce no net displacement of the aircraft center of gravity, or rotation of the principal axes.

For the rigid body motions the mode shapes are simply

$$[\vec{\xi}_1 \cdots \vec{\xi}_6] = [(-\vec{r}_x)R_e \quad I]$$

$$[\vec{\gamma}_1 \cdots \vec{\gamma}_6] = [R_e \quad 0]$$

since

$$\vec{v} = \vec{x}_F + \vec{\alpha}_F \times \vec{r} = \vec{x}_F - (\vec{r}_\times) R_e \vec{\alpha}_e$$
$$\vec{\omega} = \vec{\alpha}_F = R_e \vec{\alpha}_e$$

4.2.2 Hub motion.

The rotor equations of motion require the six components of the hub linear and angular motion in the shaft axis system:

$$\begin{pmatrix} x_h \\ y_h \\ z_h \\ \alpha_x \\ \alpha_y \\ \alpha_z \end{pmatrix} = \begin{bmatrix} \cdots & R_{SF}\vec{\xi}_k(\vec{r}_{hub}) & \cdots \\ & R_{SF}\vec{\gamma}_k(\vec{r}_{hub}) & \end{bmatrix} \{q_{sk}\}$$

or

$$\alpha = \begin{bmatrix} R_{SF}(-\vec{r}_{hub\times})R_e & R_{SF} & \cdots R_{SF}\vec{\xi}_k \cdots \\ R_{SF}R_e & 0 & \cdots R_{SF}\vec{\gamma}_k \cdots \end{bmatrix} x_s = C x_s$$

The matrix R_{SF} transforms the motion from body to shaft axes. The moment arm of the rotor hub about the aircraft center of gravity is in body axes, $\vec{r}_{hub} = x\vec{i}_F + y\vec{j}_F + z\vec{k}_F$.

The total velocity of a point is the sum of the trim and perturbation velocities, $\vec{u} = \vec{V} + \Sigma \dot{q}_{sk}\vec{\xi}_k$, in body axes. The rotor equations require the velocity components at the hub in an inertial frame however (the S system), and the Euler angle rotations between the

body and inertial axes introduce perturbations of the trim velocity $\vec{V}$. So the perturbation velocity becomes $\vec{u} = \vec{\alpha}_F \times \vec{V} + \Sigma \dot{q}_{sk} \vec{\xi}_k$, where in the S system

$$\vec{\alpha}_F \times \vec{V} = \begin{pmatrix} \mu_z \alpha_y - \mu_y \alpha_z \\ -\mu_z \alpha_x - \mu_x \alpha_z \\ \mu_x \alpha_y + \mu_y \alpha_x \end{pmatrix}$$

These contributions to the hub velocities ($\dot{x}_h$, $\dot{y}_h$, $\dot{z}_h$) cancel the terms in the blade velocity due to the Euler angle rotation of the inertial axes relative to the trim velocity (the $\mu\alpha$ terms in u_T, u_P, and u_R). Thus the evaluation of the hub rotation (α_x, α_y, α_z) for the aerodynamic analysis should not include the body Euler angle contributions, as discussed in section 2.4.2.

Finally, the rotor hub acceleration is $\ddot{\vec{u}} = \vec{\omega}_F \times \vec{V} + \Sigma \ddot{q}_{sk} \vec{\xi}_k$, where the first term is the inertial acceleration due to the rotation of the trim velocity vector by the body axes angular velocity. This additional contribution of the Euler angle velocity to the hub linear acceleration, in the shaft axes system, is

$$\Delta \begin{pmatrix} \ddot{x}_h \\ \ddot{y}_h \\ \ddot{z}_h \end{pmatrix} = \vec{\omega}_F \times \vec{V} = R_{SF}(-\vec{V}\times) R_e \begin{pmatrix} \dot{\phi}_f \\ \dot{\theta}_f \\ \dot{\psi}_f \end{pmatrix}$$

which can be written $\Delta\ddot{\alpha} = \bar{c} x_S$ with

$$\bar{c} = \begin{bmatrix} R_{SF}(-\vec{v}\times)R_e & 0 \\ 0 & 0 \end{bmatrix}$$

Note that

$$-(\vec{v}\times)R_e = \begin{bmatrix} 0 & v_z & -v_y \\ -v_z & 0 & v_x \\ v_y & -v_x & 0 \end{bmatrix} R_e$$

$$= \begin{bmatrix} 0 & v_z\cos\phi_{FT} + v_y\sin\phi_{FT} & v_z\sin\phi_{FT}\cos\theta_{FT} \\ & & -v_y\cos\phi_{FT}\cos\theta_{FT} \\ -v_z & -v_x\sin\phi_{FT} & v_z\sin\theta_{FT} \\ & & +v_x\cos\phi_{FT}\cos\theta_{FT} \\ v_y & -v_x\cos\phi_{FT} & -v_y\sin\theta_{FT} \\ & & -v_x\sin\phi_{FT}\cos\theta_{FT} \end{bmatrix}$$

and similarly for $(-\vec{r}x)R_e$.

For rotor #2 the linear hub displacement (x_h, y_h, z_h) must be multiplied by R_1/R_2 to account for the differences in normalization, c being based on rotor #1 parameters while α is based on rotor #2 parameters in this case. For a clockwise rotating rotor it is necessary to change the signs of y_h, α_x, and α_z. These conversions will be included in the definition of c and $\bar{c}$, by

a. multiplying rows 1, 2, and 3 by R_1/R_2

b. changing the signs of rows 2, 4, and 6

as appropriate. In addition, the derivatives of the hub motion of rotor #2 must be corrected for the different time base, by multiplying the velocities by Ω_1^2/Ω_2^2:

$$\dot{\alpha} = \frac{\Omega_1}{\Omega_2} c \dot{x}_s$$

$$\ddot{\alpha} = \left(\frac{\Omega_1}{\Omega_2}\right)^2 (c \ddot{x}_s + \bar{c} \dot{x}_s)$$

(See section 5.1.5 for the time scale correction in the case of harmonic body motion.)

4.2.3 Pitch/mast-bending coupling.

Flexibility between the rotor swashplate and hub will produce a blade pitch change due to elastic motion of the airframe. This coupling between the rotor pitch and mast bending is accounted for by introducing kinematic feedback of the following form:

$$\Delta\theta_{\substack{mast \\ bend}} = -\sum_{i=7}^{\infty} q_{si} \left(k_{MC_i} \cos\psi_m + k_{MS_i} \sin\psi_m\right)$$

4.2.4 Equations of motion.

Following the usual steps of airplane flight dynamics analysis (see ref. 46), the linearized rigid body equations of motion are obtained by equating the angular and linear acceleration to the net moments and

forces on the aircraft: $I\dot{\vec{\omega}}_F - \Sigma\vec{M}$ and $M(\dot{\vec{u}}_F + \vec{\omega}_F \times \vec{V}) - \Sigma\vec{F}$. In terms of the body axis degrees of freedom, including the gravitational forces, the equations are:

$$R_e^T I^* R_e \begin{pmatrix} \phi_F \\ \theta_F \\ \psi_F \end{pmatrix}^{\cdot\cdot} = \begin{pmatrix} \omega_1^* \\ \omega_2^* \\ \omega_3^* \end{pmatrix}$$

$$M^* \begin{pmatrix} x_F \\ y_F \\ z_F \end{pmatrix}^{\cdot\cdot} - M^* (\vec{V}\times) R_e \begin{pmatrix} \phi_F \\ \theta_F \\ \psi_F \end{pmatrix}^{\cdot}$$

$$= \begin{pmatrix} \omega_4^* \\ \omega_5^* \\ \omega_6^* \end{pmatrix} + M^* g \vec{k}_E - G \begin{pmatrix} \phi_F \\ \theta_F \\ \psi_F \end{pmatrix}$$

where

$$G = -M^* g \left[\frac{\partial \vec{k}_E}{\partial \phi_F} \; \frac{\partial \vec{k}_E}{\partial \theta_F} \; \frac{\partial \vec{k}_E}{\partial \psi_F} \right]$$

$$= M^* g \begin{bmatrix} 0 & \cos\theta_{FT} & 0 \\ -\cos\theta_{FT}\cos\phi_{FT} & \sin\theta_{FT}\sin\phi_{FT} & 0 \\ \cos\theta_{FT}\sin\phi_{FT} & \sin\theta_{FT}\cos\phi_{FT} & 0 \end{bmatrix}$$

Here M is the aircraft mass, including the rotors, and I is the moment of inertia matrix:

$$I = \begin{bmatrix} I_x & -I_{xy} & -I_{xz} \\ -I_{xy} & I_y & -I_{yz} \\ -I_{xz} & -I_{yz} & I_z \end{bmatrix}$$

($I_{xy} = I_{yz} = 0$ if lateral symmetry is assumed). These equations are dimensionless, and have been normalized by dividing by the characteristic inertia $(\frac{1}{2}NI_b)_1$. Thus $M^* = M/(\frac{1}{2}NI_b/R^2)$ and $I^* = I/(\frac{1}{2}NI_b)$. Note that the gravitational constant g is also dimensionless, based on the acceleration $\Omega^2 R$; and $M^*g = \gamma 2C_W/\sigma a$, where $W = Mg$ is the gross weight.

For the elastic degrees of freedom, since orthogonal free vibration modes are used the equations of motion are simply

$$M_k^* (\ddot{q}_{sk} + g_s \omega_k \dot{q}_{sk} + \omega_k^2 q_{sk}) = Q_k^* \quad (k \geq 7)$$

where M_k is the generalized mass including the rotors (in normalized form $M_k^* = M_k/(\frac{1}{2}NI_b/R^2)$), ω_k is the natural frequency of the mode, and g_s is the structural damping coefficient.

The generalized forces Q_k^* are due to the hub reactions of the two rotors, and the auxiliary and aerodynamic forces on the aircraft. Since the rotor mass is included in the aircraft inertia, the hub linear acceleration terms should not be included in the evaluation of the hub forces for these equations of motion. The aircraft aerodynamic forces are considered in section 4.2.6.

Similarly, the rotor gravitational forces are not included in the rotor hub forces, since the rotor weight is included in the aircraft gross weight.

4.2.5 Hub forces.

The aircraft generalized force due to the rotor hub reactions is

$$Q_k = \vec{\xi}_k(\vec{r}_{hub}) \cdot \vec{F}_{hub} + \vec{\gamma}_k(\vec{r}_{hub}) \cdot \vec{M}_{hub}$$

Normalizing Q_k by dividing by $\frac{1}{2}NI_b$ gives then

$$\{Q_k^*\} = \begin{bmatrix} \vdots & \vdots \\ (R_{SF}\vec{\xi}_k)^T & (R_{SF}\vec{\gamma}_k)^T \\ \vdots & \vdots \end{bmatrix} \gamma \frac{2}{\sigma a} \begin{pmatrix} C_H \\ C_Y \\ C_T \\ C_{Mx} \\ C_{My} \\ -C_Q \end{pmatrix}$$

or $Q = c^T F$, with c defined above for the hub motion.

For rotor #2 it is also necessary to account for the differences in normalization, Q and c being based on rotor #1 parameters while F is based on rotor #2 parameters. Thus the force coefficients of rotor #2 must be multiplied by

$$\frac{(NI_b\Omega^2/R)_2}{(NI_b\Omega^2/R)_1}$$

and the moment coefficients by

$$\frac{(NI_b\Omega^2)_2}{(NI_b\Omega^2)_1}$$

For a clockwise rotating rotor it is also necessary to change the signs of C_Y, C_Q, and C_{Mx}. Using c corrected for rotor #2 normalization and the rotor rotation direction as required for the hub motion, it is then only necessary to multiply the matrix by

$$\frac{(NI_b\Omega^2)_2}{(NI_b\Omega^2)_1}$$

to obtain c^T for rotor #2.

4.2.6 Aircraft aerodynamic forces.

The aerodynamic environment of the airframe is defined by the helicopter trim velocity, perturbation linear and angular velocity, gust velocity, rotor-induced interference velocity, and the aircraft controls. The generalized forces for the aircraft rigid body degrees of freedom, produced by the aerodynamic forces and moments, are $Q^* = Q_{NL}^* + Q_L^*$. There are six components: three moments and three forces. The generalized forces are dimensionless (based on ρ, Ω, and R), and divided by $\frac{1}{2}NI_b = (2\gamma)/(\sigma a\pi)$ to obtain rotor coefficient form. The nonlinear term Q_{NL}^* will be evaluated from simple equations and possibly tables. The linearized term Q_L^* will be evaluated from stability derivatives. For the trim analysis, or generally in the absence of input stability derivatives, only the nonlinear term is used: $Q^* = Q_{NL}^*$. For the flutter, flight dynamics, and transient analyses, the nonlinear term is evaluated with the trim motion and the linearized term is evaluated with

the difference between the current and trim motion: $Q^* = Q_{NLtrim}{}^* + Q_L{}^*$.

The nonlinear aerodynamic model considers the aircraft aerodynamic forces acting on the wing-body (WB), horizontal tail (HT), and vertical tail (VT). Specifically, the aerodynamic loads needed are the wing-body lift, drag, and side forces (L, D, and Y) and the roll, pitch, and yaw moments (M_x, M_y, and M_z); the horizontal tail lift and drag; and the vertical tail lift and drag. These loads are defined in terms of the force or moment divided by dynamic pressure q. The forces are multiplied by the dynamic pressure, and by the appropriate arm for the moments; they are rotated by the angle-of-attack to transform from wind axes to the body axes; they are rotated by the tail cant angles as necessary; and they are divided by $\frac{1}{2} NI_b$. The generalized force is then:

$$Q^*_{NL} = \frac{2\gamma}{\sigma a \pi} \sum \begin{bmatrix} R_e^T & R_e^T(\vec{r}x) \\ 0 & I \end{bmatrix} \begin{bmatrix} R_{FA} q \begin{pmatrix} M_x/q \\ M_y/q \\ M_z/q \end{pmatrix} \\ R_\phi R_{FA} q \begin{pmatrix} -D/q \\ Y/q \\ -L/q \end{pmatrix} \end{bmatrix}$$

The summation is over the three components wing-body, horizontal tail, and vertical tail). The tail terms have only lift and drag (no side force or moments). The matrix transforming from stability axes to F axes is:

$$R_{FA} = \begin{bmatrix} \cos\alpha & 0 & -\sin\alpha \\ 0 & 1 & 0 \\ \sin\alpha & 0 & \cos\alpha \end{bmatrix}$$

The matrices accounting for the tail cant angles are:

$$R_{\phi_{HT}} = \begin{bmatrix} 1 & 0 & 0 \\ 0 & \cos\phi & \sin\phi \\ 0 & -\sin\phi & \cos\phi \end{bmatrix}$$

$$R_{\phi_{VT}} = \begin{bmatrix} 1 & 0 & 0 \\ 0 & -\sin\phi & \cos\phi \\ 0 & \cos\phi & \sin\phi \end{bmatrix}$$

where ϕ_{HT} is positive to the left, and ϕ_{VT} is positive to the right. The moment arms of the aerodynamic centers of action about the aircraft center of gravity are in the fuselage axes, $\vec{r} = x\vec{i}_F + y\vec{j}_F + z\vec{k}_F$.

The aerodynamic forces depend on the air velocity seen by the components, and on the aircraft control positions. The air velocity consists of the trim aircraft velocity, the perturbation linear and angular rigid body contributions, the gust velocity, and the rotor-induced aerodynamic interference velocity. In fuselage axes (the F system) the total velocity is thus:

$$\begin{Bmatrix} u \\ v \\ w \end{Bmatrix} = \begin{Bmatrix} V_x \\ V_y \\ V_z \end{Bmatrix} + \begin{Bmatrix} \dot{x}_F \\ \dot{y}_F \\ \dot{z}_F \end{Bmatrix} - (\vec{r}_x) R_e \begin{Bmatrix} \dot{\phi}_F \\ \dot{\theta}_F \\ \dot{\psi}_F \end{Bmatrix} + R_{FV} \begin{Bmatrix} u_G \\ v_G \\ w_G \end{Bmatrix} - \vec{\lambda}$$

which must be evaluated at the wing/body, at the horizontal tail, and at the vertical tail. The aerodynamic interference velocity produced by

each rotor is required. With a nonuniform induced velocity calculation, $\vec{\lambda}$ is the mean value of the wake velocity calculated at the position of the fixed aerodynamic surface (see section 3.1). The angular velocity of the aircraft is

$$\begin{pmatrix} p \\ q \\ r \end{pmatrix} = R_e \begin{pmatrix} \dot{\phi}_F \\ \dot{\theta}_F \\ \dot{\psi}_F \end{pmatrix}$$

The rate of change of angle-of-attack is also required ($\dot{\alpha} = \ddot{z}_F/V_X$). The aircraft controls consist of flaperon, elevator, aileron, and rudder (δ_f, δ_e, δ_a, δ_r).

From the velocity components at the wing-body, the angle-of-attack and sideslip angle are:

$$\alpha_{WB} = \tan^{-1} w/u$$

$$\beta_{WB} = \sin^{-1} v/\sqrt{u^2+v^2+w^2}$$

and the dynamic pressure is

$$q = \frac{1}{2}(u^2+v^2+w^2)$$

The aircraft aerodynamic interference at the tail will be accounted for by an angle-of-attack change ϵ and a sideslip angle σ (positive when decreasing α and β at the tail), so the net velocity components are

$$\begin{vmatrix} u + \epsilon w + \sigma v \\ v - \sigma u \\ w - \epsilon u \end{vmatrix}$$

Then the horizontal tail angle-of-attack and dynamic pressure are

$$\alpha_{HT} = \tan^{-1} \frac{(w - \epsilon u)\cos\phi_{HT} + (v - \sigma u)\sin\phi_{HT}}{u + \epsilon w + \sigma v}$$

$$q_{HT} = \tfrac{1}{2}(u + \epsilon w + \sigma v)^2 + (v - \sigma u)^2 + (w - \epsilon u)^2$$

$$\cong \tfrac{1}{2}(u^2 + v^2 + w^2)$$

and the vertical tail angle-of-attack and dynamic pressure are

$$\alpha_{VT} = \tan^{-1} \frac{(v - \sigma u)\cos\phi_{VT} + (w - \epsilon u)\sin\phi_{VT}}{u + \epsilon w + \sigma v}$$

$$q_{VT} \cong \tfrac{1}{2}(u^2 + v^2 + w^2)$$

where ϕ_{HT} and ϕ_{VT} are the tail surface cant angles. The time-varying nonuniform inflow will increase the mean dynamic pressure in the wake:

$$q = \tfrac{1}{2}(u^2 + v^2 + w^2) + \tfrac{1}{2}\sigma_v^2$$

where $\sigma_\lambda^2 = \overline{\lambda^2} - \bar{\lambda}^2$ is the mean-square wake velocity perturbation, at the wing-body or tail as appropriate.

For best results, experimental data should be used to define the aircraft aerodynamic characteristics, including the airframe interference effects. The following loads are required.

(a) The wing-body lift, drag, and pitch moment (L/q, D/q, and M_y/q) as a function of angle-of-attack α and of flaperon deflection δ_f. The flaperon deflection is positive down, increasing the lift.

(b) The wing-body side force, roll moment and yaw moment (Y/q, M_x/q, and M_z/q) as a function of sideslip angle β and of aileron deflection δ_a. The sideslip angle β is positive for an aircraft velocity change to the right. The aileron deflection is positive down on the right wing, causing a negative roll moment.

(c) The horizontal tail lift and drag (L_{HT}/q and D_{HT}/q) as a function of angle-of-attack α and elevator deflection δ_e. The elevator deflection is positive down, increasing the tail lift.

(d) The vertical tail lift and drag (L_{VT}/q and D_{VT}/q) as a function of angle-of-attack α and rudder deflection δ_r. The vertical tail lift is positive to the left for zero cant angle. The rudder deflection is positive down, increasing the tail lift.

The force and moment characteristics have dimensions of length-squared and length-cubed, respectively (divided by R^2 and R^3 for dimensionless equations).

The following expressions are used to evaluate the wing-body aerodynamic loads.

$$\begin{pmatrix} M_x/q \\ M_z/q \\ Y/q \end{pmatrix} = \begin{bmatrix} N_{x\beta}/q & VN_{xp}/q & VN_{xr}/q & N_{x\delta_a}/q \\ N_{z\beta}/q & VN_{zp}/q & VN_{zr}/q & N_{z\delta_a}/q \\ Y_\beta/q & VY_p/q & VY_r/q & Y_{\delta_a}/q \end{bmatrix} \begin{pmatrix} \beta_{WB} \\ p/V \\ r/V \\ \delta_a \end{pmatrix}$$

$$\begin{pmatrix} M_y/q \\ D/q \\ L/q \end{pmatrix} = \begin{pmatrix} M_o/q \\ f_{wb} + f_{vert}\sin^2(\alpha_{wb} + i_D) + (L/q)^2/(\pi e Q_w^2) \\ 0 \end{pmatrix} + \begin{pmatrix} ScC_M \\ SC_D \\ SC_L \end{pmatrix}$$

$$+ \begin{bmatrix} M_\alpha/q & M_{\delta_t}/q & M_{\delta_F}/q \\ 0 & D_{o\delta_t}/q & D_{o\delta_F}/q \\ L_\alpha/q & L_{\delta_t}/q & L_{\delta_F}/q \end{bmatrix} \begin{pmatrix} \alpha_{wb} + i_{wb} \\ \delta_t \\ \delta_F \end{pmatrix}$$

and for the horizontal tail and vertical tail loads:

$$L_{HT}/q = (L_\alpha/q)(\alpha_{HT} + i_{HT}) + (L_{\delta_e}/q)\delta_e$$

$$L_{VT}/q = (L_\alpha/q)(\alpha_{VT} + i_{VT}) + (L_{\delta_r}/q)\delta_r$$

To account for stall, $\alpha = \text{sign}(\alpha)\min(|\alpha|, \alpha_{max})$ is used in the wing-body lift and pitch moment, and in the tail forces. Here δ_F is a wing flap angle. Note that both the second and third terms in D/q (vertical and induced drag) give an α^2 dependence. The zero lift angles relative to the fuselage axis system are $-i_{WB}$, $-i_{HT}$, and $-i_{VT}$; M_o/q is the moment at zero lift; and $-i_D$ is the angle of minimum parasite drag.

The wing/tail interference is evaluated from

$$\epsilon = (L/q)_{wb}/f_\epsilon + \Delta\epsilon$$

The area f_ϵ can be estimated from the wing area, span, and chord (S_w, l_w, c_w) and the horizontal tail length (l_{HT}) by

$$f_\epsilon = 2.2\, S_w \left(\ell_w^2 / S_w\right)^{.725} \left(\ell_{HT} / c_w\right)^{.25}$$

(from ref. 47). A lag in the wake velocity at the tail is also included:

$$\Delta\epsilon = -\frac{\partial\epsilon}{\partial\alpha}\frac{\ell_{HT}}{V}\dot{\alpha}_{wB} = -\frac{(L_\alpha/q)_{wB}}{f_\epsilon}\frac{\ell_{HT}}{V}\dot{\alpha}_{wB}$$

(ref. 46). The wing-induced velocity could be obtained from the first order differential equation

$$\tau\dot{\epsilon} + \epsilon = \frac{\partial\epsilon}{\partial\alpha}\alpha_{wB}$$

The usual approach for airplane flight dynamics analysis is to write this equation as

$$\epsilon = \frac{\frac{\partial\epsilon}{\partial\alpha}\alpha_{wB}}{1+\tau s} \cong (1-\tau s)\frac{\partial\epsilon}{\partial\alpha}\alpha_{wB} = \frac{\partial\epsilon}{\partial\alpha}\alpha_{wB} - \tau\frac{\partial\epsilon}{\partial\alpha}\dot{\alpha}_{wB}$$

Using $\tau = l_{HT}/V$ for the time lag gives the above result. From reference 46, the sideslip interference angle is approximately

$$\sigma = \frac{\partial\sigma}{\partial\beta}\beta + \left(\frac{V}{x_{VT}}\frac{\partial\sigma}{\partial r}\right)\frac{x_{VT}\, r}{V} + \left(\frac{V}{z_{VT}}\frac{\partial\sigma}{\partial p}\right)\frac{z_{VT}\, p}{V}$$

$$\cong \frac{z_{VT}}{V}\, p$$

where z_{VT} is the vertical tail position (positive upward).

The airframe aerodynamic characteristics could be defined by three force coefficient and three moment coefficient tables, as functions of angle-of-attack, sideslip angle, Mach number, and control positions. A less general option is provided here. The wing-body lift, drag, and pitch moment include coefficients (C_L, C_D, and C_M) that are evaluated from tables, as functions of angle-of-attack (α_{WB}, measured relative to the fuselage axes), Mach number ($M = V/c_S$), and elevator angle (δ_e). These coefficients are based on a reference area S and chord c. By using tables for the entire aircraft aerodynamics, a more complex variation of the coefficients can be included, but the capability of distinguishing between the wing-body and tail environment is lost. The tables are linearly interpolated, with no extrapolation. Given the coefficient C(j) and angle-of-attack α(j) arrays, j is found such that $\alpha_j \le \alpha \le \alpha_{j+1}$. Then

$$a_j = \frac{\alpha_{j+1} - \alpha}{\alpha_{j+1} - \alpha_j} = 1 - a_{j+1}$$

and the interpolated coefficient value is

$$C = a_j C(j) + a_{j+1} C(j+1)$$

The algorithm is similar for interpolating in Mach number and elevator angles. The table will have a full angle-of-attack and Mach number array for each elevator angle; but the (α,M) values are not necessarily the same for all elevator angles. Hence the table is first interpolated in (α,M), and then in δ_e.

The linearized aerodynamic model considers the forces acting on the entire aircraft. The forces are perturbations from trim, evaluated in terms of stability derivatives. The stability derivative coefficients are defined in stability (wind) axes, relative the aircraft center of gravity. It is assumed that the longitudinal and lateral motions are separable. The coefficients are functions of angle-of-attack and Mach number. Specifically, the aerodynamic loads needed are the longitudinal, side, and vertical forces (X, Y, and Z) and the roll, pitch, and yaw moments (L, M, and N). These loads are defined in terms of the force or moment divided by dynamic pressure q. The forces are multiplied by the dynamic pressure; they are transformed from wind axes to the body axes; and they are divided by $\frac{1}{2}NI_b$. The generalized force is then:

$$Q_L^* = \frac{2\gamma}{\sigma a \pi} \begin{bmatrix} R_e^T R_{FA}\, q \begin{pmatrix} L/q \\ M/q \\ N/q \end{pmatrix} \\ R_{FA}\, q \begin{pmatrix} X/q \\ Y/q \\ Z/q \end{pmatrix} \end{bmatrix}$$

The dimensionless dynamic pressure is $q = \frac{1}{2}V^2$. The matrix transforming from stability axes (A) to fuselage (F) axes is $R_{FA} = R_{FV}$ (see section 4.1.1). Both q and R_{FA} are based only on the free stream velocity, which is the trim velocity of the center of gravity (neglecting rotor-induced flow).

The linearized aerodynamic forces depend on the perturbation of the current motion from the trim motion. In stability axes, the motion is:

$$\ddot{z}_A = R_{FA_{33}} \left[\ddot{z}_F - (\ddot{z}_F)_{trim} \right]$$

$$\begin{pmatrix} \ddot{x} \\ \ddot{y} \\ \ddot{z} \end{pmatrix}_A = R_{FA}^T \left[\begin{pmatrix} \ddot{x} \\ \ddot{y} \\ \ddot{z} \end{pmatrix}_F + R_{FV} \begin{pmatrix} u_G \\ v_G \\ w_G \end{pmatrix} - \vec{\lambda} \right.$$

$$\left. - \left(\begin{pmatrix} \ddot{x} \\ \ddot{y} \\ \ddot{z} \end{pmatrix}_F + R_{FV} \begin{pmatrix} u_G \\ v_G \\ w_G \end{pmatrix} - \vec{\lambda} \right)_{trim} \right]$$

$$\begin{pmatrix} p \\ q \\ r \end{pmatrix}_A = R_{FA}^T R_e \left[\begin{pmatrix} \dot{\phi} \\ \dot{\theta} \\ \dot{\psi} \end{pmatrix}_F - \begin{pmatrix} \dot{\phi} \\ \dot{\theta} \\ \dot{\psi} \end{pmatrix}_{F\,trim} \right]$$

$$\begin{pmatrix} \delta_e \\ \delta_f \\ \delta_a \\ \delta_r \end{pmatrix}_A = \begin{pmatrix} \delta_e \\ \delta_f \\ \delta_a \\ \delta_r \end{pmatrix} - \begin{pmatrix} \delta_e \\ \delta_f \\ \delta_a \\ \delta_r \end{pmatrix}_{trim}$$

The force and moment characteristics have dimensions of length-squared and length-cubed respectively (divided by R^2 and R^3 for dimensionless equations). The following expressions are used to evaluate the aerodynamic loads in terms of stability derivatives.

$$\begin{pmatrix} M/q \\ -X/q \\ -Z/q \end{pmatrix} = \begin{bmatrix} VM_{\dot{\alpha}}/q & 2M/q+VM_u/q & M_\alpha/q & VM_q/q & M_{\delta_e}/q & M_{\delta_f}/q \\ VD_{\dot{\alpha}}/q & 2D/q+VD_u/q & D_\alpha/q-L/q & VD_q/q & D_{\delta_e}/q & D_{\delta_f}/q \\ VL_{\dot{\alpha}}/q & 2L/q+VL_u/q & L_\alpha/q+D/q & VL_q/q & L_{\delta_e}/q & L_{\delta_f}/q \end{bmatrix} \begin{pmatrix} \ddot{z}_A/V^2 \\ \dot{x}_A/V \\ \dot{z}_A/V \\ q_A/V \\ \delta_e \\ \delta_f \end{pmatrix}$$

$$= \begin{bmatrix} \frac{1}{2}Sc^2C_{M_{\dot\alpha}} & Sc(2C_M+MC_{M_M}) & ScC_{M_\alpha} & \frac{1}{2}Sc^2C_{M_q} & ScC_{M_{\delta e}} & ScC_{M_{\delta_f}} \\ \frac{1}{2}ScC_{D_{\dot\alpha}} & S(2C_D+MC_{D_M}) & S(C_{D_\alpha}-C_L) & \frac{1}{2}ScC_{D_q} & SC_{D_{\delta e}} & SC_{D_{\delta_f}} \\ \frac{1}{2}ScC_{L_{\dot\alpha}} & S(2C_L+MC_{L_M}) & S(C_{L_\alpha}+C_D) & \frac{1}{2}ScC_{L_q} & SC_{L_{\delta e}} & SC_{L_{\delta_f}} \end{bmatrix} \begin{pmatrix} \ddot z_A/V^2 \\ \dot x_A/V \\ \dot z_A/V \\ p_A/V \\ \delta e \\ \delta_f \end{pmatrix}$$

$$\begin{pmatrix} L/q \\ N/q \\ Y/q \end{pmatrix} = \begin{bmatrix} N_{x_\beta}/q & VN_{x_p}/q & VN_{x_r}/q & N_{x_{\delta_a}}/q & N_{x_{\delta_r}}/q \\ N_{z_\beta}/q & VN_{z_p}/q & VN_{z_r}/q & N_{z_{\delta_a}}/q & N_{z_{\delta_r}}/q \\ Y_\beta/q & VY_p/q & VY_r/q & Y_{\delta_a}/q & Y_{\delta_r}/q \end{bmatrix} \begin{pmatrix} \dot y_A/V \\ p_A/V \\ r_A/V \\ \delta_a \\ \delta_r \end{pmatrix}$$

$$= \begin{bmatrix} SbC_{l_\beta} & \frac{1}{2}Sb^2C_{l_p} & \frac{1}{2}Sb^2C_{l_r} & SbC_{l_{\delta a}} & SbC_{l_{\delta r}} \\ SbC_{n_\beta} & \frac{1}{2}Sb^2C_{n_p} & \frac{1}{2}Sb^2C_{n_r} & SbC_{n_{\delta a}} & SbC_{n_{\delta r}} \\ SC_{y_\beta} & \frac{1}{2}SbC_{y_p} & \frac{1}{2}SbC_{y_r} & SC_{y_{\delta a}} & SC_{y_{\delta r}} \end{bmatrix} \begin{pmatrix} \dot y_A/V \\ p_A/V \\ r_A/V \\ \delta_a \\ \delta_r \end{pmatrix}$$

The coefficients are based on a reference area S, chord c, and span b: C_L = lift/qS, C_D = drag/qS, C_M = pitch-moment/qSc; C_y = side-force/qS, C_l = roll-moment/qSb, C_n = yaw-moment/qSb. The dimensionless rate derivatives are $(C)_{\dot\alpha} = \partial C/\partial(\dot\alpha c/2V)$, $(C)_q = \partial C/\partial(qc/2V)$; $(C)_p = \partial C/\partial(pb/2V)$, $(C)_r = \partial C/\partial(rb/2V)$. The total aircraft lift, drag, and pitch moment coefficients are obtained from the trim (nonlinear) generalized forces:

$$M_y/q = \frac{\sigma a \pi}{2\gamma}\left(Q_z^*/q\right)$$

$$\begin{pmatrix} -D/q \\ -L/q \end{pmatrix} = \frac{\sigma a \pi}{2\gamma} \begin{bmatrix} \cos\alpha & \sin\alpha \\ -\sin\alpha & \cos\alpha \end{bmatrix}_{WB} \begin{pmatrix} Q_4^*/q \\ Q_6^*/q \end{pmatrix}$$

If the derivatives with respect to angle-of-attack, sideslip, and control angle have units of per-degree, the coefficients are multiplied by 57.3 for use here.

The stability derivative coefficients are either constants, or are evaluated from tables as functions of angle-of-attack (α_{WB}, measured relative to the fuselage axes), and Mach number ($M = V/c_s$). These coefficients are based on a reference area S, chord c, and span b. The tables are linearly interpolated, with no extrapolation. The interpolation algorithm was described above for the airframe aerodynamic coefficient tables.

The default sign conventions for the controls are as follows: δ_a positive for right aileron down; δ_e positive for elevator down; δ_r positive for rudder down (vertical tail lift increased to left). Hence the following signs are expected for the control derivatives.

(a) Nonlinear equations: $N_{x_{\delta a}}/q$ negative, L_{HT_δ}/q positive, L_{VT_δ}/q positive.

(b) Stability derivatives: $C_{l_{\delta a}}$ negative, $C_{M_{\delta e}}$ negative, $C_{n_{\delta r}}$ positive.

It is not necessary that these sign conventions be followed, but it is essential that a consistent convention be used for all input parameters (including the definition of the coupling of the aircraft and rotor controls to the pilot's controls, defined in section 4.1.6).

4.2.7 Aircraft aerodynamics - high frequency.

The aerodynamic model described in the preceding section deals with the steady forces on the aircraft, and the stability derivatives for the rigid body motions involved in flight dynamics. Such a model would not be appropriate however for the high frequencies of rotor-induced

vibration, for either rigid body or elastic motions of the airframe. An accurate analytical evaluation of the generalized forces at high frequencies would require a sophisticated model of the wing/body and tail aerodynamics, including the effects of the rotor wake-induced flow field, for the normal modes of elastic vibration of the airframe. Such an analysis is not attempted in the present investigation.

The only generalized aerodynamic forces considered for the airframe elastic modes are the direct damping and control forces. In dimensional form, the equations of motion are then

$$M_k\left(\ddot{q}_{fsk} + g_s\omega_k\dot{q}_{fsk} + \omega_k^2 q_{fsk}\right) = (Q_k)_{rotors} + \tfrac{1}{2}\rho V^2\left[-F_{q_{fk}\dot{q}_{fk}}\frac{\dot{q}_{fsk}}{V} + F_{q_{fk}\delta}\begin{pmatrix}\delta_t\\ \delta_e\\ \delta_a\\ \delta_r\end{pmatrix}\right] + (Q_k)_f$$

where $F_{q_k\dot{q}_k}$ and $F_{q_k\delta}$ are constants (with dimensions of length-squared and length-squared per radian respectively) that depend only on the airframe characteristics; $F_{q_k\dot{q}_k}$ is the damping force divided by $\frac{1}{2}\rho V$:

$$F_{q_{fk}\dot{q}_{fk}} = \frac{\partial Q_k / \frac{1}{2}\rho V^2}{\partial \dot{q}_{fsk}/V}$$

and $F_{q_k\delta}$ is the control force derivative divided by $\frac{1}{2}\rho V^2$:

$$F_{q_{fk}\delta} = \frac{\partial Q_k / \frac{1}{2}\rho V^2}{\partial \delta}$$

The dimensionless form, normalized by dividing by $\frac{1}{2}NI_b$, is then

$$M_k^* \ddot{q}_{fsk} + \left(M_k^* g_s \omega_k + \frac{2\gamma}{\sigma a A} \frac{q}{V} F_{q_{fk}\dot{q}_k} \right) \dot{q}_{fsk} + M_k^* \omega_k^2 q_{fsk}$$

$$= (Q_k^*)_{rotors} + (Q_k^*)_f$$

$$+ \frac{2\gamma}{\sigma a A} q \left[F_{q_{fk}\delta} \begin{pmatrix} \delta_f \\ \delta_e \\ \delta_a \\ \delta_r \end{pmatrix} \right]$$

4.2.8 Auxiliary forces.

The auxiliary forces, f_l, produce the following generalized forces in the airframe equations of motion:

$$(Q_k^*)_f = \frac{1}{\frac{1}{2}NI_b\Omega^2/R} \sum_l \begin{bmatrix} \vec{r}_f \times \hat{e}_f \\ \hat{e}_f \\ \vec{\zeta}_k \cdot \hat{e}_f \end{bmatrix} f_l$$

$$= b_f (f_l)$$

The position vector r_f and orientation vector $\hat{e}_f$ are defined in section 4.1.5. These forces are in the F axis system, normalized to ($\gamma 2C/\sigma a$) form. For the wind tunnel case, the rigid body forces and moments (the

first six generalized forces) must be multiplied by R_{TF} (see section 4.1.5).

4.2.9 Airframe sensors.

The response can be calculated for a number of airframe sensors. Each sensor is located at a point on the airframe, which is specified as described in section 4.1.5 (and multiplied by R_{TF} for the wind tunnel case). The sensors respond to rigid body and elastic airframe motion. The mode shapes for the rigid body motion are defined in section 4.2.1, and the elastic mode shapes are specified as described in section 4.1.5 (and multiplied by R_{TF} for the wind tunnel case). The air sensors also respond to gust velocities. Hence the sensor equations take the form

$$y = C_2 \ddot{q}_s + C_1 \dot{q}_s + C_0 q_s + D_0 g$$

where q_s is a vector of the airframe degrees of freedom, and g is a vector of the wind axis gust components. The three components of motion are derived below for each sensor; the orientation of the sensor axes can be arbitrarily specified, including a choice of fuselage (F) axis or wind (V) axis orientation. Then each element of y is one component of a particular sensor.

The following six types of airframe sensors are considered.

(a) Accelerometer. Following section 4.2.2, the linear acceleration of an airframe point is:

$$g\vec{n} = \vec{a} = \left[(-\vec{r}_x) R_e \quad I \quad \cdots \vec{\xi}_k \cdots \right] \ddot{q}_s + \left[(-\vec{v}_x) R_e \quad 0 \quad 0 \right] \dot{q}_s$$

(inertial acceleration, in the F coordinate frame). With g the dimensionless acceleration of gravity, n is the acceleration in g's.

(b) Angular velocity. Following section 4.2.1, the angular velocity of an airframe point is:

$$\vec{\omega} = \left[R_e \quad 0 \quad \cdots \vec{\delta}_k \cdots \right] \dot{q}_s$$

(in the F coordinate frame).

(c) Body angular displacement. Following section 4.2.1, the perturbation Euler angle displacements of an airframe point are:

$$\begin{pmatrix} \phi_F \\ \theta_F \\ \psi_F \end{pmatrix} = R_e^{-1} \left[R_e \quad 0 \quad \cdots \vec{\delta}_k \cdots \right] q_s$$

(in the F coordinate frame).

(d) Body angular rate. The perturbation Euler angle rates of an airframe point are:

$$\begin{pmatrix} \phi_F \\ \theta_F \\ \psi_F \end{pmatrix}^{\bullet} = R_e^{-1} \left[R_e \quad 0 \quad \cdots \vec{\delta}_k \cdots \right] \dot{q}_s$$

(in the F coordinate frame).

(e) Body angular acceleration. The perturbation Euler angle accelerations of an airframe point are:

$$\begin{pmatrix} \phi_F \\ \theta_F \\ \psi_F \end{pmatrix}^{\cdot\cdot} = R_e^{-1} \left[R_e \quad 0 \quad \cdots \vec{\gamma}_k \cdots \right] \ddot{q}_s$$

(in the F coordinate frame).

(f) Air sensor. A sensor of the perturbation air velocity relative to an airframe point gives:

$$\begin{pmatrix} \delta u/V \\ \delta\beta \\ \delta\omega \end{pmatrix} = \frac{1}{V} \begin{pmatrix} \delta v_x \\ \delta v_y \\ \delta v_z \end{pmatrix}_V = \frac{1}{V} \left\{ R_{FV}^T \left[(-\vec{r}_\times) R_e \quad I \quad \cdots \vec{\gamma}_k \cdots \right] \dot{q}_s + \begin{pmatrix} u_G \\ v_G \\ w_G \end{pmatrix}_V \right\}$$

(in wind axes, the V coordinate frame). Here $\delta\alpha$ is the perturbation angle-of-attack; $\delta\beta$ is the perturbation sideslip angle; and $\delta u/V$ is the perturbation speed. This sensor responds to gust velocities, but it is assumed to be placed so that it does not respond to rotor-induced velocities. For the rotorcraft case it is necessary to include the option of normalizing the sensor output by dividing by the rotor tip speed ΩR instead of by the flight speed V (which can be zero); then the sensor measures the three components of the perturbation aircraft speed, rather than angle-of-attack and sideslip.

The equation for each sensor can be transformed to stability (V) axes if required: the acceleration and angular velocity are multiplied by R_{FV}^T, and the body angular motions are multiplied by R_{VFe} (see section 4.2.1). The air sensor is always in wind (V) axes. The

baseline orientation of the sensor coordinates has the x axis forward, the y axis to the right, and the z axis down. Then the orientation of the sensor axes is specified by an azimuth angle ψ_s, rotating the coordinates about the x axis; and an elevation angle θ_s, rotating the coordinates about the new y axis. So the sensor equation is multiplied by the matrix:

$$\begin{bmatrix} \cos\Psi_s \cos\Theta_s & -\sin\Psi_s & \cos\Psi_s \sin\Theta_s \\ \sin\Psi_s \cos\Theta_s & \cos\Psi_s & \sin\Psi_s \sin\Theta_s \\ -\sin\Theta_s & 0 & \cos\Theta_s \end{bmatrix}$$

Finally, the response of one of the three axes of the sensor is specified, as an element of y.

4.3 Transmission and Engine Analysis

The rotor rotational speed degree of freedom can be an important factor in the helicopter dynamics, and the rotor torque perturbations can produce significant drive train loads. A model is required which accounts for the coupling of the two rotors through the flexible drive-train, and for the engine damping and inertia. The drive train dynamics will be described by the rotor speed, the interconnect shaft torsion, and the engine shaft torsion degrees of freedom. The equations of motion are derived from the balance of rotor and engine torques (in the nonrotating frame). A model for a governor with throttle or collective feedback of the rotor speed error is also considered.

4.3.1 Engine model.

The engine model includes the inertia, damping, and control torques:

$$I_E \dot{\Omega}_E = Q_E - Q_\Omega \Omega_E + Q_t \theta_t$$

The engine speed is Ω_E, and Q_E is the torque on the engine. The engine rotary inertia is I_E. Q_Ω is the engine speed damping coefficient, i.e., the torque per unit speed change at constant throttle setting:

$$Q_\Omega = \left. \frac{\partial Q_E}{\partial \Omega_E} \right|_{\theta_t = \text{constant}}$$

The variable θ_t is the engine throttle control position. Q_t is the torque applied due to a throttle change at constant speed:

$$Q_t = \frac{\partial Q_E}{\partial \theta_t} = \frac{1}{\Omega_E} \left. \frac{\partial P_E}{\partial \theta_t} \right|_{\Omega_E = \text{constant}}$$

Thus Q_t and Q_Ω can be obtained from data on the engine power as a function of throttle position and engine speed.

The engine damping may be related to the engine trim operating condition by

$$Q_\Omega = \frac{\partial Q_E}{\partial \Omega_E} \cong K \frac{Q_{E_{trim}}}{\Omega_{E_{trim}}} = K \frac{P_{trim}}{\Omega^2_{E_{trim}}}$$

where κ is a constant depending on the engine type. This approximation is applicable to a wide variety of engines. The constant takes the value $\kappa = 1$ for a turboshaft engine (ref. 48) or for a series DC electric motor (ref. 49). It takes a value $\kappa = 1/(1 - \eta)$ for an induction electric motor or an armature controlled shunt DC electric motor (ref. 49; η is the motor efficiency). For a field controlled shunt DC motor, the only damping is mechanical and the damping of the load, so $\kappa = 0$ (ref. 49). For a synchronous electric motor there is a spring on the rotational speed due to the motor, so the above model is not applicable (ref. 49). Generally, the inertia of the engine or motor is more of a factor in the dynamics than the damping.

The normalized engine damping and throttle coefficients are:

$$r_E^2 Q_\Omega^* = \frac{r_E^2 Q_\Omega}{(N I_b \Omega)_1} \cong \frac{r_E^2 \kappa Q_E / \Omega_E}{(N I_b \Omega)_1} = \frac{r_E^2 \kappa P_E}{(N I_b \Omega)_1 \Omega_E^2} = \frac{\kappa P_E}{(N I_b \Omega^3)_1}$$

$$r_E Q_t^* = \frac{r_E Q_t}{(N I_b \Omega^2)_1} = \frac{r_E \partial P_E / \partial \theta_t}{(N I_b \Omega^2)_1 \Omega_E} = \frac{\partial P_E / \partial \theta_t}{(N I_b \Omega^3)_1}$$

where r_E is the ratio of the engine speed to the rotor speed. When the throttle control is only involved in the governor, the parameters required for Q_t^* is not really $\partial P_E / \partial \theta_t$, but rather just over all loop gain of the governor -- the torque perturbation due to a rotor speed error.

The transmission losses may be viewed as a viscous damping source, with a coefficient equal to

$$\frac{\partial Q}{\partial \Omega} = \frac{(1-\eta) P_E}{\Omega^2}$$

where η is the transmission efficiency. This loss can be included in the engine damping coefficient $r_E^2 Q_\Omega^*$, by increasing the factor κ by $\Delta\kappa = 1 - \eta$. In the equations for interconnect shaft torsion and engine shaft torsion, structural damping can be included as well.

4.3.2 Equations of motion.

Figure 4-3 is a schematic of the transmission/engine model considered for asymmetric drive train configurations, such as for a single main and tail rotor helicopter. The two rotors are connected by a shaft, and the engine is geared to one rotor (rotor #1 in Fig. 4-3). The torsional flexibility of the drive train is represented by the rotor shaft springs K_{M1} and K_{M2}, the interconnect shaft spring K_I, and the engine shaft spring K_E. The transmission gear ratios are r_E (the ratio of the engine speed to rotor #1 speed), and r_{I1} and r_{I2} (the ratio of the interconnect shaft speed to the rotor speeds). Thus $r_{I1}/r_{I2} = \Omega_2/\Omega_1$ is the ratio of the trim rotational speeds of rotor #2 and rotor #1.

The degrees of freedom are the rotational speed perturbations of the two rotors ($\dot{\psi}_{s1}$ and $\dot{\psi}_{s2}$), and the engine speed perturbation $\dot{\psi}_e$. The engine shaft azimuth perturbation ψ_e is defined relative to rotor #1 rotation, so the total engine speed perturbation with respect to space is $r_E(\dot{\psi}_{s1} + \dot{\psi}_e)$. With the rotation of the two rotors coupled by the drive system, it is more appropriate to use the following degrees of freedom:

$$\psi_s = \psi_{s1}$$

$$\psi_I = \psi_{s2} - (r_{I1}/r_{I2})\psi_{s1}$$

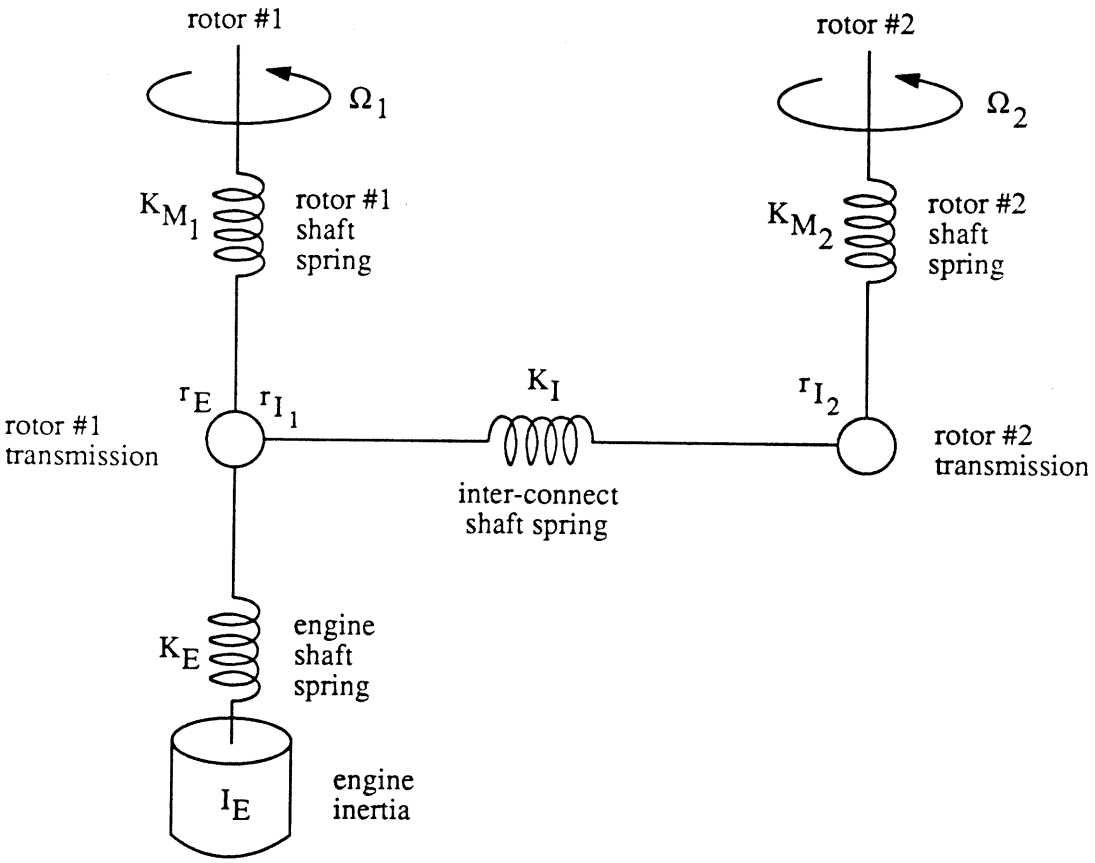

Figure 4-3. Schematic of rotorcraft transmission and engine dynamics model (asymmetric configuration).

Here ψ_I is the differential azimuth perturbation between the two rotors. The degrees of freedom ψ_I and ψ_e therefore involve elastic torsion in the drive train. The degree of freedom $\dot{\psi}_s$ is the rotational speed perturbation of the drive system as a whole: both rotors, the engine, and the transmission.

The differential equation of motion for the rotor speed dynamics are obtained from equilibrium of the torques on the two rotors and the engine. The resulting equations for ψ_s, ψ_I, and ψ_e are as follows:

$$\left(\gamma\frac{C_Q}{\sigma a}\right)_1 + \frac{r_{I_1}}{r_{I_2}}\frac{(NI_b\Omega^2)_2}{(NI_b\Omega^2)_1}\left(\gamma\frac{C_Q}{\sigma a}\right)_2 + r_E^2 I_E^*(\ddot{\psi}_s + \ddot{\psi}_e) + r_E^2 Q_\Omega^*(\dot{\psi}_s + \dot{\psi}_e) = r_E Q_t^* \theta_t + \left(\gamma\frac{C_{P_E}}{\sigma a}\right)_{trim}$$

$$-k_{MI_1}\left(\gamma\frac{C_Q}{\sigma a}\right)_1 + \frac{(NI_b\Omega^2)_2}{(NI_b\Omega^2)_1}\left(\gamma\frac{C_Q}{\sigma a}\right)_1 + k_{MR} r_E^2 I_E^* \ddot{\psi}_I + k_{MR} r_E^2 Q_\Omega^* \dot{\psi}_I + k_{MI_2}^* \psi_I = 0$$

$$r_E^2 I_E^*(\ddot{\psi}_s + \ddot{\psi}_e) + r_E^2 Q_\Omega^*(\dot{\psi}_s + \dot{\psi}_e) + k_{ME_1}^* \psi_e - k_{ME_2}^* \psi_I = r_E Q_t^* \theta_t + \left(\gamma\frac{C_{A_E}}{\sigma a}\right)_{trim}$$

where $\psi_{s1} = \psi_s$ and $\psi_{s2} = (r_{I1}/r_{I2})\,\psi_s + \psi_I$; and with the engine by rotor #1 as in Figure 4-3, the constants are:

$$K_{MI_1} = \frac{(r_{I_1}/r_{I_2})\,K_{M_2}\,r_{I_2}^2\,K_I}{K_{M_1}\,(K_{M_2} + r_{I_2}^2\,K_I)}$$

$$K_{MI_2} = \frac{K_{M_2}\,r_{I_2}^2\,K_I}{K_{M_2} + r_{I_2}^2\,K_I}$$

$$K_{ME_1} = \frac{r_E^2\,K_E\,K_{MM}}{r_E^2 K_E\,(K_{M_2} + r_{I_2}^2 K_I) + K_{MM}}$$

$$K_{ME_2} = \frac{r_E^2 K_E\; r_{I_1} K_{M_2} r_{I_2} K_I}{r_E^2 K_E\,(K_{M_2} + r_{I_2}^2 K_I) + K_{MM}}$$

$$K_{MM} = K_{M_1} K_{M_2} + K_I\,(r_{I_2}^2 K_{M_1} + r_{I_1}^2 K_{M_2})$$

$$K_{MR} = 0$$

The spring constants are normalized by dividing by $(NI_b\Omega^2)_1$; and $I_E^* = I_E/(NI_b)_1$. When evaluating the derivatives of ψ_{s2} for use in the analysis of rotor #2, it is necessary to account for the difference in time scales:

$$\dot{\psi}_{s_2} = \frac{\Omega_1}{\Omega_2}\left(\frac{r_{I_1}}{r_{I_2}}\,\dot{\psi}_s + \dot{\psi}_I\right)$$

In these equations the gear ratio r_{I1}/r_{I2} between the two rotors is a positive number, regardless of the rotor direction of rotation. Therefore here the sign of C_Q is not changed for a clockwise rotating rotor.

With the engine by rotor #2, the constants in the equations of motion are:

$$K_{MI_1} = \frac{(r_{I_1}/r_{I_2})\, K_{M_2}\, (K_{M_1} + r_{I_1}^2 K_I)}{K_{M_1}\, r_{I_1}^2\, K_I}$$

$$K_{MI_2} = K_{M_2}$$

$$K_{ME_1} = \frac{(r_{I_1}/r_{I_2})^2\, r_E^2\, K_E\, K_{MM}}{r_E^2 K_E (K_{M_1} + r_{I_1}^2 K_I) + (r_{I_1}/r_{I_2})^2 K_{MM}}$$

$$K_{ME_2} = \frac{(r_{I_1}/r_{I_2})\, r_E^2\, K_E\, K_{M_2}\, (K_{M_1} + r_{I_1}^2 K_I)}{r_E^2 K_E (K_{M_1} + r_{I_1}^2 K_I) + (r_{I_1}/r_{I_2})^2 K_{MM}}$$

Figure 4-4 sketches a symmetric drive train configuration, as might be used for a side-by-side main rotor helicopter. The two rotors are connected by a cross-shaft, and there are two engines, one geared to each rotor. The degrees of freedom of this system are symmetric and antisymmetric rotor speed perturbations, and symmetric and antisymmetric engine speed perturbations. Dropping the antisymmetric engine speed perturbation and antisymmetric throttle input, the system has three degrees of freedom as for the asymmetric configurations above. Let

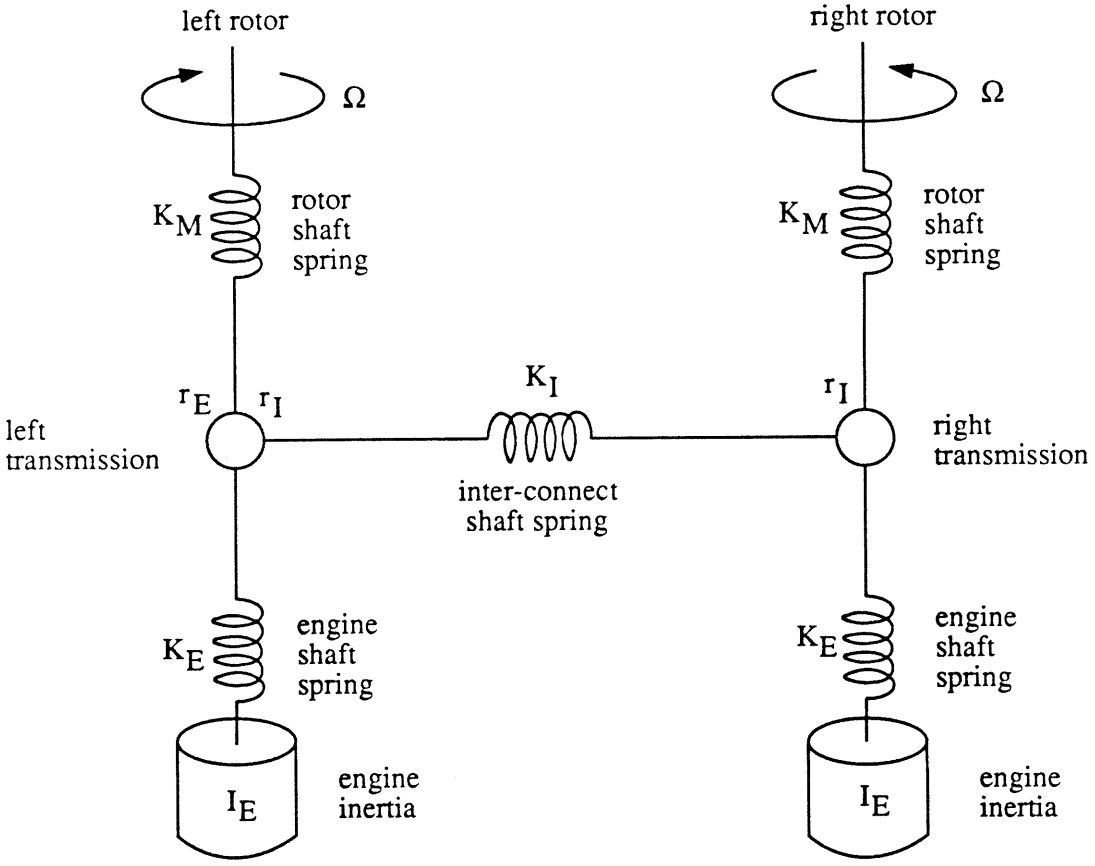

Figure 4-4. Schematic of rotorcraft transmission and engine dynamics model (symmetric configuration).

$$\Psi_{s_1} = \Psi_s$$
$$\Psi_{s_2} = (r_{I_1}/r_{I_2})\Psi_s + \Psi_I$$

again, where here $r_{I1}/r_{I2} = 1$. The constants in the equations of motion are:

$$k_{MI_1} = 1$$
$$k_{MR} = \frac{1}{2}\,\frac{k_M}{k_M + 2r_I^2 k_I}$$
$$k_{MI_2} = \frac{k_M 2r_I^2 k_I}{k_M + 2r_I^2 k_I}$$
$$k_{ME_1} = 2\,\frac{r_E^2 k_E k_M}{k_M + r_E^2 k_E}$$
$$k_{ME_2} = \frac{r_E^2 k_E k_M}{k_M + r_E^2 k_E}$$

Here the engine inertia I_E is for both engines, as are the damping and throttle coefficients (Q_Ω and Q_t). The resulting symmetric and antisymmetric drive train motions can then be obtained from

$$\Psi_{sym} = \Psi_s + \frac{1}{2}\Psi_I$$
$$\Psi_{anti} = -\frac{1}{2}\Psi_I$$
$$\Psi_{eng} = \Psi_e - \frac{1}{2}\Psi_I$$

as required.

With just one rotor (as in a wind tunnel), the equations of motion for the rotor and engine speed perturbations reduce to:

$$\gamma \frac{C_Q}{\sigma a} + r_E^2 I_E^* (\ddot{\psi}_s + \ddot{\psi}_e) + r_E^2 Q_\Omega^* (\dot{\psi}_s + \dot{\psi}_e) = r_E Q_t^* \theta_t + \left(\gamma \frac{C_{P_E}}{\sigma a}\right)_{trim}$$

$$r_E^2 I_E^* (\ddot{\psi}_s + \ddot{\psi}_e) + r_E^2 Q_\Omega^* (\dot{\psi}_s + \dot{\psi}_e) + K_{ME_1}^* \psi_e = r_E Q_t^* \theta_t + \left(\gamma \frac{C_{P_E}}{\sigma a}\right)_{trim}$$

where here

$$K_{ME_1} = \frac{r_E^2 K_E K_M}{K_M + r_E^2 K_E}$$

Hence the equations for the asymmetric drive train configuration can be used, dropping the ψ_I degree of freedom and the rotor #2 torque.

The case of a rotorcraft in autorotation can be treated with this model by dropping the engine speed degree of freedom ($\dot{\psi}_e$), dropping the engine terms from the ψ_s and ψ_I equations (helicopters usually have an over-running clutch to disconnect the rotors from the engine at zero torque), and dropping the throttle governor control input (θ_t). The

engine out case (engine and rotors still connected) requires dropping the engine damping term (or reducing it to just the transmission losses contribution) and dropping the throttle governor control input. The case of constant rotor speed is modeled by dropping the rotor and engine speed degrees of freedom and equations from the system.

Note that the inertia terms in the rotor torques are:

$$\Delta\left(\gamma \frac{C_Q}{\sigma a}\right)_1 = I_{01}^{*} \ddot{\psi}_{s1}$$

$$\Delta\left(\gamma \frac{C_Q}{\sigma a}\right)_2 = I_{02}^{*} \ddot{\psi}_{s2}$$

so the total inertia term of the ψ_S equation is

$$\frac{\left(N_1 I_{01} + (r_{I_1}/r_{I_2})^2 N_2 I_{02} + r_E^2 I_E\right)}{N_1 I_{01}} \ddot{\psi}_s$$

4.3.3 Rotor speed governor.

When the rotor rotational speed perturbation is included in the dynamics analysis, it is usually necessary to also include the rotor speed governor for a consistent calculation of the rotor and aircraft behavior. The governor model considered is integral and proportional feedback of the rotor speed to the throttle, and to the collective pitch of rotors #1 and #2. The governor dynamics are represented by a second order lag. The control equations are thus:

$$\tau_{2e}\,\Delta\ddot{\theta}_t + \tau_{1e}\,\Delta\dot{\theta}_t + \Delta\theta_t = -K_{Pe}\,\dot{\psi}_s - K_{Ie}\,\psi_s$$

$$\tau_{21}\,\Delta\ddot{\theta}_{govr_1} + \tau_{1_1}\,\Delta\dot{\theta}_{govr_1} + \Delta\theta_{govr_1} = K_{P_1}\,\dot{\psi}_s + K_{I_1}\,\psi_s$$

$$\tau_{22}\,\Delta\ddot{\theta}_{govr_2} + \tau_{12}\,\Delta\dot{\theta}_{govr_2} + \Delta\theta_{govr_2} = K_{P_2}\,\dot{\psi}_s + K_{I_2}\,\psi_s$$

Note that $\epsilon = \dot{\psi}_s$ is the rotor speed error, and ψ_s is the integral of the error. The integral gains are dimensionless (with θ and ψ_s both in radians or both in degrees), and the proportional gains have units of seconds (K_P/K_I is the lead in the integral control). When the throttle control is only used for this governor model, it is only necessary that the product of $\partial P_E/\partial\theta_t$ and the governor gains be correct:

$$K_{Pe}\,\frac{\partial P_E}{\partial \theta_t} = -\frac{\partial P}{\partial \dot{\psi}_s}$$

$$K_{Ie}\,\frac{\partial P_E}{\partial \theta_t} = -\frac{\partial P}{\partial \psi_s}$$

($P = \Omega_R Q_R = \Omega_E Q_E$), or in terms of the dimensionless parameters

$$K_{Pe}\,(r_E\,\Omega_t^*) = -\frac{\partial C_Q/\sigma a}{\partial \dot{\psi}_s/\Omega}$$

$$K_{Ie}\,(r_E\,\Omega_t^*) = -\frac{\partial C_Q/\sigma a}{\partial \psi_s}$$

4.4 Airframe/Rotor Aerodynamic Interference

The analysis will include interference velocities at the rotor disk, caused by the airframe aerodynamics. The interference velocities can be either externally calculated and read from a file, or internally calculated using a simplified representation of the airframe. The external calculation is typically based on a panel method with a detailed representation of the airframe geometry. With the internal calculation, changes in the rotor position as the solution converges are automatically accounted for, but for reasonable efficiency the model consists of a set of wings and nonlifting bodies.

The airframe can produce significant high frequency content of the velocity at the rotor. In such a case, the rotor analysis must include unsteady aerodynamics. The rotor shed and trailed wake, which will reduce the interference-generated airloads, are included by using the nonuniform inflow model (section 3.1).

The internally calculated interference velocity will be updated once per trim iteration, to allow for changes in the blade position relative to the airframe as the solution converges. Since the blade motion change is generally small during the last stages of a trim iteration, updating less often could be acceptable (Ref. 50), but would require a more complicated algorithm. In the absence of trim however, the interference velocities should be updated more often (once per circulation iteration perhaps).

4.4.1. Interference velocities.

The rotor aerodynamics analysis (section 2.4.2) requires the perturbation velocities of the air relative to the blade, in rotating shaft axes and divided by the tip speed of the rotor: Δu_R, Δu_T, and Δu_P. The input or calculated quantities will be perturbation velocities relative to the body, divided by the flight speed: $\Delta\vec{v}/V$. Various axes can be used:

(a) Airframe (F) axes, $\Delta\vec{v}_F/V$ (x positive forward, y positive right, and z positive down).

(b) Nonrotating shaft (S) axes, $\Delta\vec{v}_S/V$ (x positive aft, y positive to the advancing side, and z positive up).

(c) Rotating shaft axes, $\Delta\vec{v}_R/V$ ($x = u_R$, $y = u_T$, and $z = u_P$). Then the velocities are transformed as required:

$$\frac{\Delta\vec{v}_S}{V} = R_{SF}\,\frac{\Delta\vec{v}_F}{V}$$

$$\frac{\Delta\vec{v}_R}{V} = \begin{bmatrix} \cos\Psi & \sin\Psi & 0 \\ \sin\Psi & -\cos\Psi & 0 \\ 0 & 0 & -1 \end{bmatrix} \frac{\Delta\vec{v}_S}{V}$$

$$\begin{pmatrix} \Delta u_R \\ \Delta u_T \\ \Delta u_P \end{pmatrix} = \frac{V}{\Omega R_{ref}}\,\frac{\Omega R_{ref}}{\Omega R}\,\frac{\Delta\vec{v}_R}{V}$$

For a clockwise rotating rotor, the sign of the $\vec{j}_S$ component of $\vec{v}_S$ is changed.

4.4.2. Geometry.

The interference velocities are required at a set of (r_i, ψ_j) points on the rotor disk. The radial stations r_i are the midpoints of

the aerodynamic panels (see section 2.4.1). The azimuth stations are $\psi_j = j2\pi/J$, for j = 1 to J.

The vector from a point on the airframe to a point on a rotor blade is

$$\vec{r} = \vec{r}_P - \vec{r}_A = \left(\vec{r}_R + \frac{R}{R_{ref}} R_{SF}^T \vec{r}_b \right) - \vec{r}_A$$

in F axes, scaled with the radius of rotor #1. Here $\vec{r}_P$ and $\vec{r}_A$ are the vectors from the aircraft center-of-gravity to the rotor blade and the airframe point respectively (F axes); $\vec{r}_R$ is the vector from the center-of-gravity to the rotor hub (F axes); and $\vec{r}_b$ is the vector from the rotor hub to the blade point (S axes). Section 4.1.5 describes the calculation of $\vec{r}_A$ and $\vec{r}_R$; section 3.1.3 describes the calculation of $\vec{r}_b$. For a clockwise rotating rotor, the sign of the $\vec{j}_s$ component of $\vec{r}_b$ is changed.

4.4.3. Wing-induced velocity.

The airframe lifting surfaces will be represented by a set of simplified wings. The model for each wing consists of a constant strength horseshoe vortex for lift, and a constant strength dipole line for thickness. Such a model is correct in the far field, but will require calibration for reasonable results in the near field.

To allow for sweep and dihedral, the wing will be defined by the quarter-chord in two straight segments (Figure 4-5). The circulation and thickness lines will be placed a distance xc_w behind the leading edge, to allow calibration of the velocity field near the wing. The trailed vortices extend from the wing tips to 10 wing spans downstream. Hence the geometry is defined by the following points:

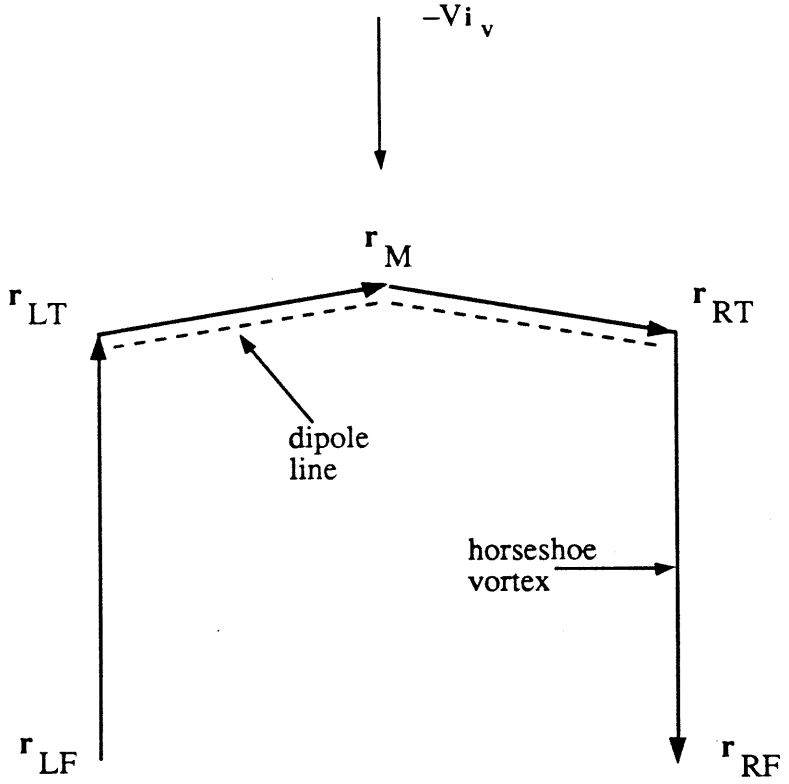

Figure 4-5. Geometry of the wing vortex and dipole lines.

$$\vec{r}_{LT} = (\vec{r}_{LT})_{QC} - (x - \tfrac{1}{4})\frac{c_W}{R} R_{FV}\vec{i}_V$$

$$\vec{r}_{M} = (\vec{r}_{M})_{QC} - (x - \tfrac{1}{4})\frac{c_W}{R} R_{FV}\vec{i}_V$$

$$\vec{r}_{RT} = (\vec{r}_{RT})_{QC} - (x - \tfrac{1}{4})\frac{c_W}{R} R_{FV}\vec{i}_V$$

$$\vec{r}_{LF} = \vec{r}_{LT} - 10\frac{b_W}{R} R_{FV}\vec{i}_V$$

$$\vec{r}_{RF} = \vec{r}_{RT} - 10\frac{b_W}{R} R_{FV}\vec{i}_V$$

where c_W is the wing chord and b_W is the wing span. The induced velocity is calculated at the points $\vec{r}_p$ on the rotor blade. The velocity of the air relative to the wing is $-VR_{FV}\vec{i}_V$.

The induced velocity of a straight line vortex with unit strength is $(\Delta\vec{v}_1 + \Delta\vec{v}_2)$, in the notation of section 3.1.7. Then the circulation-produced interference velocity is obtained by summing over all four segments of the horseshoe vortex:

$$\frac{\Delta\vec{v}}{V} = \frac{\Gamma/V}{R} \sum_{\text{wing}} (\Delta\vec{v}_1 + \Delta\vec{v}_2)$$

where $\Gamma/V = L/(q2b_W) = c_W C_L/2$ is the wing circulation strength. For generality, the circulation is obtained from a combination of an input value and the wing/body, horizontal tail, and vertical tail lifts:

$$\frac{\Gamma}{V} = \frac{\Gamma_0}{V} + \frac{(f_w L_{wB}/q + f_H L_{HT}/q + f_v L_{VT}/q)}{2 b_w}$$

The f factors may be used to calibrate the model, and to account for the effects of wing sweep.

It is assumed that the wing thickness is also concentrated into a line. The geometry is similar to the horseshoe vortex, except that there are no trailed lines. Ignoring sweep, the dipole strength is obtained from the wing airfoil cross-section area: $A_{XS} \simeq 0.68 \tau_W c_W^2$ (τ_W is the wing thickness ratio). The induced velocity of a straight dipole line segment is derived in section 4.4.4. Then the thickness-produced interference velocity is obtained by summing over the two segments:

$$\frac{\Delta \vec{V}}{V} = - \frac{A_{XS}}{R^2} \sum_{\text{wing}} S R_{FV} \vec{l}_V$$

Two dimensional airfoil theory provides guidance for the placement of the circulation and thickness lines such that the correct velocity will be obtained at the rotor position. Consider a symmetric Joukowski airfoil, with chord, thickness ratio, and leading edge position as follows:

$$\ell = 3 + 2\epsilon + \frac{1}{1+2\epsilon}$$

$$\tau = (3\sqrt{3}/4)\,\epsilon$$

$$x_L = -\left(1 + 2\epsilon + \frac{1}{1+2\epsilon}\right)$$

For the airfoil with circulation but no thickness ($\epsilon = 0$), a point vortex at $z = x + iy = -\mu$ with

$$\mu = 1 - \frac{1}{\zeta}$$

matches the airfoil velocity exactly at ζ, where $z = \zeta + 1/\zeta$. In the far field, the requirement is that the vortex be at the quarter-chord ($\mu = 1$). In the near field, the vortex position can be obtained for the velocity matched in the plane of the wing: $y = 0$, and

$$\zeta = \frac{x}{2} - \sqrt{\left(\frac{x}{2}\right)^2 - 1}$$

($x < -2$ forward of the leading edge).

For an airfoil with thickness but no circulation, a doublet (cylinder) at $z = -\mu$ with

$$\mu = \frac{(\zeta + \epsilon)\sqrt{1 + \epsilon/2}}{\sqrt{\frac{\zeta}{\zeta + 1} + \frac{\epsilon}{2}}} - z$$

matches the airfoil velocity exactly at ζ. In the far field, the requirement is that the doublet be at 3/8 chord ($\mu = 1/2$).

For a point in the plane of the wing, a distance $c_W \Delta x$ forward of the leading edge, $x = x_L - 1\Delta x$. The position of the vortex or doublet

required to match the velocity is then $-(x_L + \mu)/l$, as a fraction of the chord aft of the leading edge. This is the parameter required in the present definition of the wing geometry. The parameter is not very sensitive to Δx for points more than a quarter-chord ahead of the leading edge. As an example, to match the velocity 1/2 chord ahead of the leading edge, the vortex should be placed about 3/16 chord aft of the leading edge, and the doublet about 1/4 chord aft of the leading edge.

4.4.4. Straight dipole line segment.

The following analysis gives the basis for representing the wing thickness by a dipole line, and derives the induced velocity. Consider a thin, planar wing. The air has speed V relative to the wing (in the x direction; with x positive aft and z positive up). The velocity potential of a source distribution represents a wing with thickness but no lift:

$$\phi(\vec{x}) = \int_{wing} \frac{\sigma \, dS(\vec{y})}{4\pi r} = -\iint \frac{V \, dt/d\xi}{4\pi r} \, d\eta \, d\xi$$

where $\vec{r} = \vec{x} - \vec{y}$, $\vec{x} = (x, y, z)$, $\vec{y} = (\xi, \eta, 0)$, and t(x) is the wing chordwise thickness distribution. Integrating by parts gives

$$\phi = \iint \frac{Vt}{4\pi} \frac{d}{d\xi} \frac{1}{r} \, d\eta \, d\xi$$

which is a distribution of dipoles in the ξ direction (i.e., the direction of V). The doublet line approximation follows by evaluating the integrand at the wing mean line:

$$\phi \cong \int \frac{V}{4\pi} \left(\frac{\partial}{\partial \xi} \frac{1}{r}\right)_{\xi_m} d\eta \int t\, d\xi = \int \frac{VA}{4\pi} \frac{\partial}{\partial \xi} \frac{1}{r} d\eta$$

where $A = \int t\, d\xi$ is the wing cross-section area. This approximation implies far field, large-aspect ratio assumptions. The corresponding two-dimensional result shows that in the far field the thin wing is equivalent to a cylinder with area equal to one-half the wing cross-section area.

The dipole line result is generalized to an arbitrary direction of V (the velocity of the air relative to the wing):

$$\phi = \left[\int \frac{A}{4\pi} \vec{\nabla}_\eta \frac{1}{r} d\eta \right] \cdot \vec{V}$$

Then the velocities are

$$\vec{v} = \vec{\nabla}_x \phi = A\, S \cdot \vec{V}$$

The dyadic (matrix) S is evaluated following the geometry and notation of section 3.1.7 for the vortex line segment:

$$S = \frac{1}{4\pi} \int \vec{\nabla}_x \vec{\nabla}_y \frac{1}{r} \, d\sigma$$

$$= \frac{1}{4\pi} \int \left(\frac{1}{r^3} - \frac{3\vec{r}\vec{r}}{r^5} \right) d\sigma$$

$$= \frac{1}{4\pi} \left[(\vec{\imath}\vec{\imath} + \vec{\jmath}\vec{\jmath} + \vec{k}\vec{k}) I_1 + \vec{r}_m \vec{r}_m I_2 + (\vec{r}_m \hat{e} + \hat{e} \vec{r}_m) I_3 + \hat{e}\hat{e} I_4 \right]$$

where $\vec{r} = \vec{r}_m - \sigma\hat{e}$, $r^2 = r_m^2 + \sigma^2$, and

$$I_1 = \int \frac{d\sigma}{r^3} = \frac{\sigma}{r_m^2 r}$$

$$I_2 = -3 \int \frac{d\sigma}{r^5} = -\frac{\sigma}{r_m^4 r} \left(\frac{r_m^2}{r^2} + 2 \right)$$

$$I_3 = 3 \int \frac{\sigma d\sigma}{r^5} = -\frac{1}{r^3}$$

$$I_4 = -3 \int \frac{\sigma^2 d\sigma}{r^5} = -\frac{\sigma^3}{r_m^2 r^3}$$

evaluated from $\sigma = s_1$ to $\sigma = s_2$.

4.4.5 Nonlifting body-induced velocity.

The airframe nonlifting components will be represented by a set of bodies of revolution. The interference velocities are obtained from the potential flow solution (no separation), at arbitrary angle-of-attack. The following configurations are considered.

(a) An ovary ellipsoid, created by revolving an ellipse about its major axis (exact solution).

(b) A sphere (exact solution).

(c) An airfoil-shaped body, created by revolving the NACA 4-digit airfoil thickness distribution about the chord line (modified slender-body theory solution).

The body of revolution is analyzed in a coordinate system with the origin at the body center, the x axis directed aft along the axis of symmetry, and the z axis up. The body length is scaled to *1*. The orientation of these body analysis coordinates (A axes) relative to the fuselage coordinates (F axes) is specified by a yaw to the right by ψ_A, and then pitch up by θ_A, so the transformation matrix is:

$$R_{AF} = \begin{bmatrix} -1 & 0 & 0 \\ 0 & 1 & 0 \\ 0 & 0 & -1 \end{bmatrix} Y_{\Theta_A} Z_{\Psi_A}$$

$$= \begin{bmatrix} -\cos\Theta_A \cos\Psi_A & -\cos\Theta_A \sin\Psi_A & \sin\Theta_A \\ -\sin\Psi_A & \cos\Psi_A & 0 \\ -\sin\Theta_A \cos\Psi_A & -\sin\Theta_A \sin\Psi_A & -\cos\Theta_A \end{bmatrix}$$

The position of the body is specified by the vector $\vec{r}_A$ from the aircraft center-of-gravity to the body center. The induced velocity is calculated at the points $\vec{r}_b$ on the rotor blade, defining the vector $\vec{r}$ in

F axes, relative the body center. Then the position vector in the body analysis axes, scaled so the body length is *1*, is:

$$(\vec{r})_A = \frac{\ell}{L/R} R_{AF} \vec{r} = (x \; y \; z)^T$$

where L is the actual body length. The velocity of the air relative to the body is $-VR_{FV}\vec{i}_v$, or in body analysis axes

$$\vec{e}_v = - R_{AF} R_{FV} \vec{i}_v$$

The result of the aerodynamic analysis will be the perturbation velocity $\Delta\vec{v}/V = B\vec{e}_v$ in body analysis axes, so

$$\frac{\Delta\vec{v}}{V} = R_{AF}^T \left(\frac{\Delta\vec{v}}{V}\right)_A = R_{AF}^T B \vec{e}_v$$

is the required perturbation in fuselage axes.

The induced velocity of a sphere is derived following references 50 and 51. The length (diameter) of the sphere is *1* = 1. The interference velocity is

$$\frac{\Delta\vec{v}}{V} = \frac{1}{16\,s^5}\begin{bmatrix} y^2+z^2-2x^2 & -3xy & -3xz \\ -3xy & x^2+z^2-2y^2 & -3yz \\ -3xz & -3yz & x^2+y^2-2z^2 \end{bmatrix}\vec{e}_v$$

where $s^2 = x^2 + y^2 + z^2$.

The induced velocity of an ovary ellipsoid is derived following references 50 and 51. The length (major axis) of the ellipsoid is $l = 2/\sqrt{1 - \tau^2}$, where τ is the thickness ratio. The ellipsoid is analyzed using coordinates ν and μ

$$x = \mu\nu$$

$$r^2 = y^2 + z^2 = (1-\mu^2)(\nu^2-1)$$

or

$$\nu^2 = \frac{1+x^2+r^2}{2} + \sqrt{\left(\frac{1+x^2+r^2}{2}\right)^2 - x^2}$$

$$\mu = x/\nu$$

The coordinate ν ranges from $\nu_o = l/2$ on the surface of the ellipsoid, to infinity. The coordinate μ ranges from -1 to 1. With

$$A = \left[\frac{\nu_o}{\nu_o^2-1} - \frac{1}{2}\ln\frac{\nu_o+1}{\nu_o-1}\right]^{-1}$$

$$B = \left[\frac{1}{2} \ln \frac{\nu_0 + 1}{\nu_0 - 1} - \frac{\nu_0^2 - 2}{\nu_0 (\nu_0^2 - 1)} \right]^{-1}$$

the interference velocity is

$$\frac{\Delta \vec{v}}{V} = \left\{ \begin{bmatrix} A & 0 & 0 \\ 0 & -B & 0 \\ 0 & 0 & -B \end{bmatrix} \left(\frac{1}{2} \ln \frac{\nu + 1}{\nu - 1} - \frac{\nu}{\nu^2 - 1} \right) + \frac{\nu}{(\nu^2 - \mu^2)(\nu^2 - 1)} \begin{bmatrix} (1-\mu^2)A & -\frac{2xy}{\nu^2} B & -\frac{2xz}{\nu^2} B \\ -\frac{xy}{\nu^2} A & -\frac{2y^2}{\nu^2 - 1} B & -\frac{2yz}{\nu^2 - 1} B \\ -\frac{xz}{\nu^2} A & -\frac{2yz}{\nu^2 - 1} B & -\frac{2z^2}{\nu^2 - 1} B \end{bmatrix} \right\} \vec{e}_v$$

The induced velocity of an airfoil shaped body of revolution is calculated using the modified slender-body theory developed in reference 50. The length of the body is $l = 1$. Slender-body theory approximates the axial flow about the body by a line of sources on the axis of revolution, and the cross flow by a line of doublets. The interference velocity is

$$\frac{\Delta \vec{v}}{V} = \begin{bmatrix} A & -Cy & -Cz \\ yB & E - Dy^2 & -Dyz \\ zB & -Dyz & E - Dz^2 \end{bmatrix} \vec{e}_v$$

where

$$A = \frac{1}{4\pi} \int \frac{q(x-\xi)}{s^3} d\xi$$

$$B = \frac{1}{4\pi} \int \frac{q}{s^3} d\xi$$

$$C = \frac{3}{4\pi} \int \frac{\mu(x-\xi)}{s^5} d\xi$$

$$D = \frac{3}{4\pi} \int \frac{\mu}{s^5} d\xi$$

$$E = \frac{1}{4\pi} \int \frac{\mu}{s^3} d\xi$$

with $s^2 = (x - \xi)^2 + r^2$. Slender-body theory (ref. 52) gives limits of integration from -1/2 to 1/2, and the source and doublet strengths as

$$q_{SB} = S' = 2\pi r_0 r_0'$$

$$\mu = 2S = 2\pi r_0^2$$

where S is the cross-section area. The modifications developed in reference 50 (for zero angle-of-attack) include (a) offset of the limits of integration from the nose and tail by a distance equal to one-half the radius of curvature, so the stagnation points occur at the actual nose and tail; (b) multiplication of the source strength by a constant K, to match the actual maximum thickness point; and (c) a tail

correction for bodies with pointed tails. Hence the source strength used here is:

$$q(\xi) = K q_{SB}(\xi^*) + \{(\xi^*)(\xi^* - 1)(1 - K\xi^{*\prime}) q'_{SB}(1)$$

where

$$\xi^* = \frac{\xi - x_{Ne}}{x_{Te} - x_{Ne}}$$

$$\xi^{*\prime} = \frac{1}{x_{Te} - x_{Ne}}$$

$$q'_{SB}(1) = 2\pi (r'_o(1))^2$$

with $x_{Te} = \frac{1}{2}(1 - R_T)$ and $x_{Ne} = -\frac{1}{2}(1 - R_N)$ the limits of integration. Reference 50 gives the requirements for the tail correction, which are satisfied by $f(\xi^*)$ piecewise linear from $(\xi^{*\prime}f, \xi^*) = (0,0)$ to $(-a_o, \xi_1)$, to $(1, \xi_2)$, to $(1,1)$. The requirement that the body be closed gives a_o as a function of ξ_1 and ξ_2. The multiplicative constant K needed to match the maximum thickness is obtained from the expression for the dividing streamline:

$$2\pi r_m^2 = \int \frac{q(x_m - \xi)}{((x_m - \xi)^2 + r_m^2)^{\frac{1}{2}}} \, d\xi$$

where $q = Kc(\xi) + d(\xi)$ is given above; and (x_m, r_m) is the maximum thickness point.

The NACA 4-digit airfoil thickness distribution gives the body radius:

$$r_o = 5\tau\,(.2969\sqrt{x} - .1260x - .3516x^4 + .2843x^3 - .1036x^4)$$

with x = 0 to 1, and the maximum thickness at x = 0.3 (the last constant should be .1015, but is changed here so the radius is zero at the tail). The radius of curvature of the nose is $R_N = (r_o r_o')_N = \frac{1}{2}a^2$, where $r \sim ax^{\frac{1}{2}}$ near x = 0 ($a = 1.4845\tau$). So the limits of integration are $-\frac{1}{2}(1 - 1.1019\tau^2)$ to $\frac{1}{2}$. The tail correction parameters are $\xi_1 = 0.1$, $\xi_2 = 0.95$, and $a_o = 0.4629$ (ref. 50), so

$$\xi^{*\,1}\,f = \begin{cases} -4.628880\,\xi^* & 0 \le \xi^* \le .1 \\ 1.721045\,\xi^* - 0.6349925 & .1 \le \xi^* \le .95 \\ 1 & .95 \le \xi^* \le 1 \end{cases}$$

The integrals over ξ are evaluated by numerical integration, with about 100 steps required. The cross flow strength and integration limits are not modified.

5. SOLUTION FOR THE ROTORCRAFT MOTION

It is now necessary to develop the solution procedures for the problem defined above. The first task is the trim analysis, in which the equations are solved for the case of a steady state flight condition. After the blade motion solution has been obtained, the rotor performance, loads, and noise can be evaluated. The aeroelastic stability, flight dynamics, and transient analyses begin from the trim solution.

The trim solution is the steady state condition achieved by the system as time increases without bound with the controls fixed and no external input. Steady state means either unaccelerated flight, including climbs and descents as well as level flight, or a steady turn. Usually it is the inverse problem that is to be solved: determining the control settings necessary to achieve a specified flight condition. The system considered here has nonrotating and rotating components, the latter consisting of N identical, equally spaced blades attached to a central hub. The equations of motion for such a system are not in general time invariant, but rather have periodic coefficients. It follows that the steady state solution will also be periodic. The trim problem is concerned with the average values of the periodic state variables. Unaccelerated motion implies that the net force and moment on the entire aircraft are zero. Setting to zero the six components of the forces and moments provides algebraic equations that must be satisfied in the trimmed state. Unaccelerated flight also implies that the aircraft linear velocity is constant and that the angular velocity is zero (except for the Euler yaw rate in a steady turn). The velocity vector can be specified by its magnitude, and the pitch and yaw flight path angles. Zero angular velocity implies that the pitch and roll Euler angles are constant (and the yaw angle also, except in a turn). Some of the flight path angles, Euler angles, and aircraft controls may be specified by the definition of the trim flight state. The remaining

angles and controls constitute the set of trim variables to be determined in the solution. These variables are adjusted so that the relevant trim criteria are satisfied. The procedure is readily generalized to other cases, such as trim in a wind tunnel or specification of the power. The trim problem therefore naturally separates into two parts: the periodic rotor motion and airframe vibration, described by differential equations; and the steady state flight criteria, described by algebraic equations. The trim procedure used in the present analysis consists of an inner loop in which the solution for the periodic motion is obtained with fixed values of the trim variables; and an outer loop in which the solution for the trim variables is obtained. The two parts of the problem could be dealt with simultaneously, but by treating them separately it is possible to use procedures that match the individual characteristics of the two parts.

The rotor and airframe equations are solved for the periodic motion by a harmonic analysis method, which directly calculates the harmonics of a Fourier series representation of the motion. Basically the procedure advances the rotor around the azimuth, calculating the forcing functions in the time domain and then updating the harmonics of the response. By working in the frequency domain it is possible to use directly the information that the solution is periodic, by assuming a Fourier series. Also the time step can be kept large since the step size is determined by the frequency content of the Fourier series representation, not by the frequency content of the system dynamics. The alternative is to solve for the motion entirely in the time domain, by numerically integrating until the periodic motion is obtained. Such procedures generally require a small time increment, both for accuracy and for stability of the integration algorithm. Time domain methods also require some modification to obtain a trim solution when the system is actually unstable, or even marginally stable, which is typical of rotorcraft. The frequency domain method used in the present analysis was formulated so that the interharmonic coupling is contained in the

forcing function. The forcing function is nonlinear, so must be evaluated in time domain and harmonically analyzed, and the solution procedure is necessarily iterative. Hence leaving the interharmonic coupling in the forcing function does not add any new steps to the procedure, and it minimizes the dimensions of the matrix operations. The rotor motion and airframe vibration are calculated separately. The rotor motion solution is obtained for a single blade in the rotating frame, assuming all the blades have identical motion. All the time-varying and nonlinear terms are contained in the forcing function, but the rotor blade degrees of freedom are coupled, particularly by inertial forces. Thus a vector equation must be solved for each harmonic of the motion. The airframe vibration is evaluated separately from the rotor solution. If the rotor and airframe motion were calculated simultaneously, the harmonics of the rotor motion would be coupled by the action through the nonrotating frame. Such a separate, iterative approach is possible because the coupling is generally weak (although no doubt there are exceptions).

Several important limitations are introduced by this procedure. The assumption that the system and hence the trim solution are periodic is true for a helicopter with twin, contrarotating main rotors, but not for the single main rotor and tail rotor configuration, since the two rotors have different periods in the latter case. (The rotational speeds are a rational fraction when the two rotors are geared through a mechanical transmission. So there is some single period for the system, but it will normally be too long to be of practical use.) Hence with this solution procedure it is not possible to calculate the vibratory dynamic or aerodynamic interaction between the main and tail rotors. Only the static or mean interaction can be accounted for. The assumption that all the blades are identical and have the same motion is made so that only the equations for a single blade need by solved (the system would still be periodic if these assumptions were relaxed, although more harmonics of the airframe motion would be excited).

Finally, every numerical solution procedure introduces its own stability, accuracy and convergence characteristics.

For the trim problem, the solution of the equations of motion has been separated into two parts, based on the frequency content of the motion. The first part is the solution for the rotor motion and the airframe vibration, which are periodic with fundamental frequencies Ω and $N\Omega$ respectively. The second part is the solution for the steady state airframe motion, which gives the steady values of the Euler angles and control positions. In transient flight states, the airframe motion normally still occurs slowly relative to the rotor rotational frequency. By assuming that the aircraft rigid body motion is quasistatic, the same procedures developed to calculate the rotor motion and airframe vibration for the trim solution can be used as well for the analysis of the aircraft flight dynamics or transient motion. One approach is to use the analysis of the periodic rotor motion for specified mean shaft motion to calculate stability derivatives. By using prescribed perturbations of the body motions and controls, a linear expansion of the rotor and airframe generalized forces is obtained. Another approach is to numerically integrate the rigid body equations of motions with quasistatic rotor motion. A non-equilibrium flight path is produced by a prescribed control or gust input. At each time step, periodic rotor motion is calculated for the current shaft motion. Neither of these approaches allows the calculation of the transient motion of the aircraft for cases in which the assumption of quasistatic airframe motion is not applicable. The solution for general transient motions would require a direct time integration solution procedure for the rotor motion, in place of the harmonic analysis method used in the present analysis.

While the details of the solution procedure remain to be defined, an overview can be given at this point. The job begins with data input and initial calculations. Next the trim solution is obtained. Then the aeroelastic stability analysis, flight dynamics analysis, or transient

analysis is performed as required. In the trim analysis the aircraft controls and orientation are incremented until the equilibrium of forces and moments required for the specified operating state is achieved. Since the nonuniform inflow influence coefficients depend on the rotor thrust (through the wake geometry) it is necessary to iterate between the influence coefficient calculation and the trimmed motion and forces calculation (unless the rotor thrust is specified as part of the definition of the trim operating state). The trim analysis is performed first for uniform inflow, then the nonuniform inflow with a prescribed wake, and finally for nonuniform inflow with a free wake geometry (the analysis can stop at any of these three stages). After obtaining the trim solution, the aircraft performance and loads can be calculated. In the transient analysis, the rigid body equations of motion are numerically integrated for a prescribed gust or control input. In the flight dynamics analysis, the stability derivatives are calculated and the matrices are constructed that describe the linear differential equations of motion. For each motion or control increment in the stability derivative calculation there is an iteration between the influence coefficient calculation and the calculation of the rotor motion and forces. Finally the system of linear differential equations is analyzed (optionally including a numerical integration as for the transient analysis). In the flutter analysis the matrices are constructed that describe the linear differential equations of motion, and the constant coefficient or periodic coefficient equations are analyzed. Optionally the equations are reduced to just the aircraft rigid body degrees of freedom by assuming quasistatic response to the other degrees of freedom, and the equations are analyzed as for the flight dynamics task.

The periodic rotor motion and airframe vibration are calculated for an operating state defined by the control positions; the aircraft velocity, orientation and flight path; the linear and angular hub motion due to quasistatic aircraft rigid body motions; and any gust velocity

components. The solution procedure begins with the calculation of the blade bending and torsion modes. If nonuniform inflow is to be used, the rotor wake influence coefficients are calculated, which also requires a calculation of the prescribed or free wake geometry. The outermost loop in the solution procedure is an iteration on the rotor induced velocity and bound circulation. An iteration begins with an evaluation of the uniform or nonuniform induced velocity from the rotor thrust or bound circulation. The next loop is an iteration on the motion calculation, for a fixed induced velocity distribution. The motion calculation procedure consists of a number of cycles of successive evaluation of the rotor and airframe motion. First the hub motion harmonics are evaluated. Next there is an azimuth loop for the rotor. At each azimuth step the rotor blade motion harmonics and the aerodynamic hub reactions are updated. After the rotor motion has been updated over a number of steps (typically one rotor revolution), the total hub reactions are evaluated, and the aircraft equations are solved to update the harmonics of the body motion. Within the azimuth loop of the motion-calculation there are the following steps. At a given azimuth the hub motion and blade motion are evaluated from the current estimate of the harmonics. At each radial station the blade section pitch, velocity, angle of attack and Mach number are evaluated; the lift, drag and moment coefficients are evaluated; and the section aerodynamic forces are evaluated. The generalized aerodynamic forces of the blade modes are calculated by integrating the section forces over the blade span, and then the rotor equations are solved to update the blade motion harmonics. After each iteration of the motion calculation, the convergence is tested by comparing the blade and airframe motion harmonics with the values at the beginning of the iteration. After the converged motion is obtained, the circulation convergence is determined by comparing the rotor thrust or bound circulation used to calculate the induced velocity with the values resulting at the end of the iteration. When the solution has converged, it is possible to evaluate the

generalized forces produced by the mean hub reactions of the rotors; the body aerodynamic generalized forces; and various performance parameters of the rotor and aircraft.

5.1 Rotor Motion and Airframe Vibration

The equations of motion for the rotor and aircraft will be solved for the periodic motion by a harmonic analysis method, which obtains directly the harmonics of a Fourier series representation of the motion. After a converged solution for the blade motion and airframe vibration is obtained, the rotor performance is evaluated, including the mean aerodynamic hub reactions (in particular the rotor thrust and power). The hub motion includes the static or quasistatic contributions from the aircraft rigid body motion.

The helicopter state is determined by the control positions; the flight path angles and trim Euler angles (or test module pitch and yaw for the wind tunnel case); the quasisteady linear and angular velocity perturbations of the airframe; the quasisteady rotor speed perturbation; and the aerodynamic gust velocities. The rotor motion and airframe vibration are calculated for this state. Then the generalized forces acting on the rotor and airframe can be evaluated, as well as the various performance parameters of the aircraft.

5.5.1 Fourier series representation.

For the case of steady state flight, all the rotor blades execute the same periodic motion. It follows that the blade motion in the rotating frame can be written as a Fourier series:

$$q_k = \sum_{n=-\infty}^{\infty} \beta_n^{(k)} e^{in\psi_m}$$

$$= \beta_0^{(k)} + \sum_{n=1}^{\infty} \left(\beta_{nc}^{(k)} \cos n\psi_m + \beta_{ns}^{(k)} \sin n\psi_m \right)$$

$$p_k = \sum_{n=-\infty}^{\infty} \theta_n^{(k)} e^{in\psi_m}$$

$$= \theta_0^{(k)} + \sum_{n=1}^{\infty} \left(\theta_{nc}^{(k)} \cos n\psi_m + \theta_{ns}^{(k)} \sin n\psi_m \right)$$

where $\psi_m = \psi + m\Delta\psi$ is the azimuth angle of the mth blade ($\Delta\psi = 2\pi/N$, m = 1 to N), and $\psi = \Omega t$ is the dimensionless time variable. The complex and real Fourier coefficients are related by $\beta_n = (\beta_{nc} - i\beta_{ns})/2$ and $\theta_n = (\theta_{nc} - i\theta_{ns})/2$ for $n \geq 1$. The complex representation is most convenient for solving the equations of motion, while the real representation is best for interpreting the motion. The notation $\beta_n^{(k)}$ is used for the harmonics of the kth bending mode. With the modes ordered according to natural frequency, $\beta_n^{(1)}$ is usually the fundamental lag mode and $\beta_n^{(2)}$ the fundamental flap mode. Similarly $\theta_n^{(k)}$ are the harmonics of the kth torsion mode, with $\theta_n^{(0)}$ rigid pitch and the remaining modes elastic motion of the blade. The Fourier representation of the gimbal or teeter motion is discussed in the next section.

The degrees of freedom in the nonrotating frame are the aircraft rigid body and elastic motion, and the rotor speed perturbations. These degrees of freedom are excited by the net rotor hub reactions, obtained by summing the root forces and moments from all N blades. Ideally, the rotor hub acts as a filter, transmitting to the nonrotating frame only those harmonics at multiples of N/rev. The vibratory motion in the nonrotating frame is then also periodic, with fundamental frequency $N\Omega$, and can be written as a Fourier series:

$$q_{sk} = \sum_{p=-\infty}^{\infty} \phi_{pN}^{(k)} e^{ipN\psi}$$

for the body motion, and

$$\psi_s = \sum_{p=-\infty}^{\infty} \psi_{spN} \, e^{ipN\psi}$$

for the rotor azimuth perturbation (similarly for ψ_I and ψ_e). The static or mean terms are obtained from the low frequency solution of the airframe equation.

5.1.2 Gimbal and teeter motion.

The rotor gimbal motion (if present) is in the nonrotating frame, but it is most convenient to solve an equation in the rotating frame for the gimbal motion, along with the other rotor blade equations. From section 2.2.18, the gimbal equations of motion are given by equilibrium of the net longitudinal and lateral moments on the rotor hub:

$$-\frac{1}{2} \sum_{m=1}^{2} 2\cos\psi_m \, \gamma \frac{C_{mx}}{\sigma a} + C_{GC}^{*} \dot{\beta}_{GC} + I_0^{*} (\nu_{GC}^2 - 1)\beta_{GC} = 0$$

$$-\frac{1}{2} \sum_{m=1}^{2} 2\sin\psi_m \, \gamma \frac{C_{mx}}{\sigma a} + C_{GS}^{*} \dot{\beta}_{GS} + I_0^{*} (\nu_{GS}^2 - 1)\beta_{GS} = 0$$

where C_{mx} is the flap moment at the blade root. All harmonics of the longitudinal and lateral hub moments cancel within the hub, except those at multiples of N/rev. The pN harmonics of the gimbal equations of motion are:

$$-\left[\left(\gamma\frac{C_{mx}}{\sigma a}\right)_{pN-1}+\left(\gamma\frac{C_{mx}}{\sigma a}\right)_{pN+1}\right]$$
$$+C_{GC}^{*}\,ipN\,(\beta_{GC})_{pN}+I_{o}^{*}(\nu_{GC}^{2}-1)(\beta_{GC})_{pN}=0$$

$$i\left[\left(\gamma\frac{C_{mx}}{\sigma a}\right)_{pN-1}+\left(\gamma\frac{C_{mx}}{\sigma a}\right)_{pN+1}\right]$$
$$+C_{GS}^{*}\,ipN\,(\beta_{GS})_{pN}+I_{o}^{*}(\nu_{GS}^{2}-1)(\beta_{GS})_{pN}=0$$

where $(C_{mx})_n$ is the nth complex harmonic of C_{mx}.

The flap motion in the rotating frame due to the gimbal tilt is $\beta_G = \beta_{GC}\cos\psi + \beta_{GS}\sin\psi$. Only the pN harmonics of B_{GC} and β_{GS} are excited, hence only the pN $\pm$ 1 harmonics of β_G:

$$(\beta_G)_{pN+1} = \frac{1}{2}\left[(\beta_{GC})_{pN} - i\,(\beta_{GS})_{pN}\right]$$

$$(\beta_G)_{pN-1} = \frac{1}{2}\left[(\beta_{GC})_{pN} + i\,(\beta_{GS})_{pN}\right]$$

so

$$(\beta_{GC})_{pN} = (\beta_G)_{pN-1} + (\beta_G)_{pN+1}$$

$$(\beta_{GS})_{pN} = -i\left[(\beta_G)_{pN-1} - (\beta_G)_{pN+1}\right]$$

for $p \neq 0$, and

$$(\beta_{GC})_0 = 2\,\mathrm{Re}\,(\beta_G)_1$$

$$(\beta_{GS})_0 = -2\,\mathrm{Im}\,(\beta_G)_1$$

Note that with the restriction that only the pN $\pm$ harmonics of β_G exist, this is equivalent to the relation

$$\beta_{GC} = \frac{2}{2} \sum_{m=1}^{2} \cos\psi_m \; \beta_G^{(m)}$$

$$\beta_{GS} = \frac{2}{2} \sum_{m=1}^{2} \sin\psi_m \; \beta_G^{(m)}$$

Substituting for the harmonics of β_{GC} and β_{GS} in terms of the harmonics of β_G, the gimbal equations of motion give

$$-\left[\left(\delta \frac{C_{mx}}{\sigma a}\right)_{pN-1} + \left(\gamma \frac{C_{mx}}{\sigma a}\right)_{pN+1}\right] + C_{GC}^{*}\, ipN\left[(\beta_G)_{pN-1} + (\beta_G)_{pN+1}\right] + I_0^{*}(\gamma_{GC}^2 - 1)\left[(\beta_G)_{pN-1} + (\beta_G)_{pN+1}\right] = 0$$

$$-\left[\left(\gamma \frac{C_{mx}}{\sigma a}\right)_{pN-1} - \left(\gamma \frac{C_{mx}}{\sigma a}\right)_{pN+1}\right] + C_{GS}^{*}\, ipN\left[(\beta_G)_{pN-1} - (\beta_G)_{pN+1}\right] + I_0^{*}(\gamma_{GS}^2 - 1)\left[(\beta_G)_{pN-1} - (\beta_G)_{pN+1}\right] = 0$$

or

$$-\left(\gamma\frac{C_{mx}}{\sigma a}\right)_{pN-1} + \tfrac{1}{2}(C_{GC}^{*}+C_{GS}^{*})\,ipN\,(\beta_G)_{pN-1}$$
$$+ I_0^{*}\left(\tfrac{1}{2}(\nu_{GC}^{2}+\nu_{GS}^{2})-1\right)(\beta_G)_{pN-1} + \tfrac{1}{2}(C_{GC}^{*}-C_{GS}^{*})\,ipN\,(\beta_G)_{pN+1}$$
$$+ I_0^{*}\,\tfrac{1}{2}(\nu_{GC}^{2}-\nu_{GS}^{2})\,(\beta_G)_{pN+1} = 0$$

$$-\left(\gamma\frac{C_{mx}}{\sigma a}\right)_{pN+1} + \tfrac{1}{2}(C_{GC}^{*}+C_{GS}^{*})\,ipN\,(\beta_G)_{pN+1}$$
$$+ I_0^{*}\left(\tfrac{1}{2}(\nu_{GC}^{2}+\nu_{GS}^{2}-1)(\beta_G)_{pN+1} + \tfrac{1}{2}(C_{GC}^{*}-C_{GS}^{*})\,ipN\,(\beta_G)_{pN-1}\right.$$
$$+ I_0^{*}\,\tfrac{1}{2}(\nu_{GC}^{2}-\nu_{GS}^{2})\,(\beta_G)_{pN-1} = 0$$

which we note are just the pN ± 1 harmonics of the equation

$$-\gamma\frac{C_{mx}}{\sigma a} + C_G^{*}\dot{\beta}_G + I_0^{*}(\nu_G^{2}-1)\beta_G = 0$$

(except for the effects of asymmetric gimbal springs or dampers, and the fact that the damping is in the nonrotating frame).

The equation for the teeter motion of a two-bladed rotor is

$$-\tfrac{1}{2}\sum_{m=1}^{2}(-1)^{m}\gamma\frac{C_{mx}}{\sigma a} + C_T^{*}\dot{\beta}_T + I_0^{*}(\nu_T^{2}-1)\beta_T$$

All the even harmonics of the root flap moments cancel within the rotor hub. The summation operator only transmits the odd harmonics to produce teeter motion. Hence the solution for the teeter motion can be obtained by solving the equation

$$-\gamma \frac{C_{mx}}{\sigma a} + C_T^* \dot{\beta}_T + I_0^* (\nu_T^2 - 1)\beta_T = 0$$

for the odd harmonics (i.e., for the pN $\pm$ 1 harmonics, just as for the gimbal motion).

Thus the gimbal or teeter motion can be obtained by solving the rigid flapping equation in the rotating frame:

$$-\gamma \frac{C_{mx}}{\sigma a} + C_G^* \dot{\beta}_G + I_0^* (\nu_G^2 - 1)\beta_G = 0$$

for just the pN $\pm$ 1 harmonics of β_G. Then the harmonics of the gimbal motion are

$$(\beta_{GC})_{pN} = (\beta_G)_{pN-1} + (\beta_G)_{pN+1}$$

$$(\beta_{GS})_{pN} = -i\left[(\beta_G)_{pN-1} - (\beta_G)_{pN+1}\right]$$

from which the gimbal motion can be evaluated

$$\beta_{GC} = \sum_{p=-\infty}^{\infty} (\beta_{GC})_{pN} \, e^{ipN\psi}$$

$$\beta_{GS} = \sum_{p=-\infty}^{\infty} (\beta_{GS})_{pN} \, e^{ipN\psi}$$

and so

$$\beta_G = \beta_{GC}\cos\psi + \beta_{GS}\sin\psi = \sum_{n=pN\pm1} (\beta_G)_n e^{in\psi}$$

The harmonics of the teetering motion are

$$(\beta_T)_n = (\beta_G)_n$$

for the odd harmonics, from which

$$\beta_G = \beta_T = \sum_{n \text{ odd}} (\beta_G)_n \, e^{in\psi}$$

5.1.3. Rigid pitch motion.

In the limit of infinite control stiffness, the equation of motion for the blade rigid pitch degree of freedom reduces to $M_{FAE} = 0$ (see section 2.2.9), with the solution

$$p_o = p_r = \theta_{1c} \cos(\psi + \psi_s) + \theta_{1s} \sin(\psi + \psi_s) - \Sigma K_{P_i} q_i - K_{P_G} \beta_G + \Delta\theta_{govr} + \Delta\theta_{\substack{manual \\ bend}} + \theta_{HHC}$$

Write the total root pitch motion p_o as the sum of p_r and the motion due to elastic distortion of the control system: $p_o = p_r + p_d$. Substituting for p_o, the rotor equations of motion will be solved for the harmonics of p_d. The case of infinite control system stiffness then requires only that the equations for p_d be dropped from the solution procedure. Writing $p_o = p_r + p_d$ introduces terms due to p_r, $\dot{p}_r$, and $\ddot{p}_r$ in the equations of motion.

Allowance will be made for different stiffnesses in the collective and cyclic control systems by using different natural frequencies for the collective motion ($\theta_0^{(d)}$, cyclic motion ($\theta_1^{(d)}$), and the reactionless motion ($\theta_n^{(d)}$, $n \geq 2$). Given the collective, cyclic, and reactionless control stiffnesses, the dimensionless natural frequencies are obtained from

$$\omega_\theta^2 = \frac{k_\theta}{\Omega^2 \int_{r_{FA}}^{R} I_\theta \, dr}$$

or the natural frequencies can be specified directly.

The control system damping will be specified for the collective motion, the cyclic motion, and for the rotating frame motion. The total damping is then $c_{\theta coll} + C_{\theta rot}$ for the collective mode, $C_{\theta cyc} + C_{\theta rot}$ for the cyclic modes, and $C_{\theta rot}$ for the reactionless modes ($n \geq 2$).

5.1.4 Harmonic analysis solution.

A harmonic analysis method will be used to integrate the differential equations of motion, solving directly for the harmonics of the motion. Consider equations of the form

$$M\ddot{\beta} + K\beta = g(\beta, \dot{\beta}, \Psi)$$

where β is the degree of freedom, K and M are the appropriate stiffness and mass, and g is the forcing function (usually nonlinear). To avoid the singularity of the resonant response at harmonics near the natural frequency, it is necessary to include the damping terms of the left-hand-side of this equation. Thus the term $C\dot{\beta}$ is added to both sides, giving

$$M\ddot{\beta} + C\dot{\beta} + K\beta = g + C\dot{\beta} = F$$

where C is the damping coefficient. For good convergence the damping coefficient used should be close to the actual damping of the particular degree of freedom, including structural, mechanical, and aerodynamic

damping sources. The damping estimate does not have to be exact however, since it is added to both sides of the equation. In fact the actual damping in the forcing function g will often be time varying and even nonlinear, so the viscous damping coefficient has to be an approximation. The sole function of this damping term is to avoid divergence of the solution near resonance, and the value of C has no influence on the final converged solution.

Now the function F is evaluated at J points around the rotor azimuth:

$$F_j = F(\Psi_j) = g(\Psi_j) + C\dot{\beta}(\Psi_j)$$

where $\psi_j = j\Delta\psi$ (j = 1 to J and $\Delta\psi = 2\pi/J$). Then the harmonics of a complex Fourier series representation of F are

$$F_n = \frac{1}{J} \sum_{j=1}^{J} f_j \, e^{-in\Psi_j} \, K_n$$

where

$$K_n = \left(\frac{J}{\pi n} \sin \frac{\pi n}{J} \right)^2$$

With $K_n = 1$ these harmonics would give a Fourier interpolation representation of $F(\psi)$. While it matches the function exactly at the known points $F(\psi_j)$ (or with least squared-error if the number of harmonics used is less than (J-1)/2), the Fourier interpolation gives a poor representation elsewhere, with large excursions due to the higher harmonics. In particular, poor estimates of the derivatives of the function F are obtained. With the above values for K_n (which reduce the magnitude of the higher harmonics), and an infinite number of harmonics ($n = -\infty$ to ∞), a linear interpolation between the known points $F(\psi_j)$ is obtained. By truncating the Fourier series (n = -L to L) the representation of F is smoothed, the corners of the linear interpolation being rounded off. Usually L = J/3 is satisfactory, that is the number of azimuth stations should be about 3 times the maximum harmonic of interest. The azimuth step thus should be $\Delta\psi = 2\pi/J \simeq 120/n_{max}$ degrees. Then the solution of the equation of motion for the harmonics of β is obtained from the harmonics of F by

$$\beta_n = \frac{F_n}{H_n}$$

where $H_n = K - Mn^2 + Cin$.

The interactive solution, required because the nonlinear forcing function F depends on β and $\dot{\beta}$, proceeds as follows. At a given azimuth ψ_j, the blade motion is calculated using the current estimates of the harmonics:

$$\beta = \sum_{n=-L}^{L} \beta_n e^{in\psi_j}$$

$$\dot{\beta} = \sum_{n=-L}^{L} \beta_n \, in \, e^{in\psi_j}$$

The forcing function F_j is evaluated next. The estimates of the flapping harmonics are then updated to account for the difference between the current value of F_j and that found in the last revolution:

$$\Delta\beta_n = \left[F_j - (F_j)_{\substack{\text{last} \\ \text{rev}}} \right] \frac{k_n}{J} \frac{e^{-in\psi_j}}{H_n}$$

After adding $\Delta\beta_n$ to the flap harmonics β_n, the azimuth angle is incremented to $\psi_j + 1$. The calculation proceeds around the azimuth in this fashion until the solution converges. The test for convergence is performed once each revolution. Requiring that the root-mean-squared change in the blade motion for one revolution to the next be below a specified tolerance, the criterion is $(\Delta\beta)_{rms} < \epsilon$ for all degrees of freedom, where

$$\Delta\beta_{rms}^2 = \frac{1}{2\pi} \int_0^{2\pi} (\Delta\beta)^2 \, d\psi$$

$$= (\Delta\beta_0)^2 + \frac{1}{2} \sum_n \left((\Delta\beta_{nc})^2 + (\Delta\beta_{ns})^2 \right)$$

and

$$\Delta\beta = \beta - \beta_{\substack{\text{last}\\\text{rev}}}$$

This test is applied to all degrees of freedom, for both the rotor and the airframe.

To improve the convergence of the motion iteration, a relaxation factor is introduced. The motion iteration can be viewed as a successive substitution solution procedure, $x_{n+1} = G(x_n)$, with x_n the generalized forces of all rotor coordinates over one revolution (F_j, from which the harmonics of the motion are evaluated; x should actually also include the thrust and mean bending deflection, which appear in the rotor transfer function matrix). Convergence of the successive substitution method can often be improved (but also slowed) by use of a relaxation factor, i.e. a lag in the iteration. Hence the lagged quantity

$$\overline{F_j} = \zeta F_j + (1-\zeta)\left(\overline{F_j}\right)_{\substack{\text{last}\\\text{rev}}}$$

is used in place of F_j to calculate the blade motion. Then

$$\Delta F_j = \overline{F_j} - \left(\overline{F_j}\right)_{\substack{\text{last}\\\text{rev}}}$$

$$= \zeta F_j + (1-\zeta)\left(\overline{F_j}\right)_{\substack{\text{last}\\\text{rev}}} - \left(\overline{F_j}\right)_{\substack{\text{last}\\\text{rev}}}$$

$$= \zeta\left(F_j - \left(\overline{F_j}\right)_{\substack{\text{last}\\\text{rev}}}\right)$$

The motion relaxation factor is similar to that used for the circulation iteration, where $f < 1$ is always needed, and $f = 0.1$ to 0.2 is common. For the motion iteration it is found that the relaxation is frequently not needed, i.e. $f = 1$ often converges. This suggests that over-relaxation ($f > 1$) might even be used, to speed the motion convergence.

In the present problem, the system of equations and degrees of freedom can be separated into two sets: the rotor motion, consisting of flap/lag bending, rigid pitch/elastic torsion, and gimbal or teeter flapping; and the aircraft rigid body and elastic motion, with the engine/transmission as an independent subset. The coupling between these sets is accounted for in the nonlinear forcing functions. As long as the coupling is weak, it is possible to solve the two sets of equations separately, in parallel. Within each of these subsystems, it is necessary to solve all the equations simultaneously, including in particular the inertial coupling on the left-hand side. Thus a vector equation must be solved for each harmonic of the motion. The solution proceeds as follows.

(1) At a given azimuth station, the blade motion and hub motion are evaluated using the current estimates of the harmonics.

(2) The generalized forces are evaluated, and the rotor equations are solved to update the harmonics of the blade motion.

(3) The rotor hub reactions are evaluated, and the aircraft are equations solved for the harmonics of the body motion.

(4) The calculation is repeated until a converged solution is obtained.

For further details of the iteration between the rotor and body motion calculations, see sections 5.1.11 and 5.1.13. The relaxation factor is also needed to improve the convergence of the body motion. Hence the lagged quantity

$$\bar{F}_j = f F_j + (1-f)(\bar{F}_j)_{old}$$

is used in place of F_j to calculate the vibratory airframe and drive train motion.

5.1.5 Motion evaluation.

To begin the solution at a new azimuth station, the deflection, velocity, and acceleration of each degree of freedom must be evaluated from the harmonics. For the rotor blade bending:

$$q_k = \sum_{n=-\infty}^{\infty} \beta_n^{(k)} e^{in\psi} = \beta_0^{(k)} + \sum_{n=1}^{\infty} (\beta_{nc}^{(k)} \cos n\psi + \beta_{ns}^{(k)} \sin n\psi)$$

$$\dot{q}_k = \sum_{n=-\infty}^{\infty} in\,\beta_n^{(k)} e^{in\psi} = \sum_{n=1}^{\infty} n(-\beta_{nc}^{(k)} \sin n\psi + \beta_{ns}^{(k)} \cos n\psi)$$

$$\ddot{q}_k = \sum_{n=-\infty}^{\infty} (-n^2)\beta_n^{(k)} e^{in\psi} = \sum_{n=1}^{\infty} n^2(-\beta_{nc}^{(k)} \cos n\psi - \beta_{ns}^{(k)} \sin n\psi)$$

Similarly for the blade pitch/torsion, p_k, $\dot{p}_k$, and $\ddot{p}_k$ are obtained from the harmonics $\theta_n^{(k)}$. Note that for rotor #2 these time derivatives are based on Ω_2. For the gimbal/teeter motion, recall from section above

$$\beta_G = \sum_{n=pN\pm 1} (\beta_G)_n e^{in\psi}$$

and similarly for $\dot{\beta}_G$ and $\ddot{\beta}_G$.

Recalling that only the pN harmonics are excited in the nonrotating frame, the rigid body and elastic airframe motion of the aircraft is

$$q_{sk} = \sum_{n=pN} \phi_n^{(k)} e^{in\psi} + (q_{sk})_{static}$$

$$\dot{q}_{sk} = \sum_{n=pN} in\,\phi_n^{(k)} e^{in\psi} + (\dot{q}_{sk})_{static}$$

$$\ddot{q}_{sk} = \sum_{n=pN} (-n^2)\,\phi_n^{(k)} e^{in\psi}$$

where $q_{s1} \cdots q_{s6}$ are the six rigid body degrees of freedom, and q_{sk} for $k \geq 7$ are the airframe elastic modes. The steady state or slowly varying rigid body motion contributes the static velocity terms $(\dot{q}_{sk})_{static}$ ($k \leq 6$; this motion is static compared to the high frequency rotor motion and airframe vibration). The static elastic airframe deflection gives $(q_{sk})_{static}$ ($k \geq 7$). The rotor hub motion is then

$$\alpha = \begin{pmatrix} x_h \\ y_h \\ z_h \\ \alpha_x \\ \alpha_y \\ \alpha_z \end{pmatrix} = c \left\{ q_{sk} \right\}$$

where c is given in section 4.2.2. Recall that in the evaluation of α_x, α_y, and α_z (for the aerodynamic analysis) the contributions of the rigid body Euler angles ϕ_F, θ_F and ψ_F (q_{s1} to q_{s3}) are not included; also the

linear hub displacements (x_h, y_h, and z_h) are not used in the rotor analysis. Hence α is evaluated due to the elastic airframe modes only (q_{sk}, $k \geq 7$). The velocity and acceleration of the hub are

$$\dot{\alpha} = c \{ \dot{q}_{sk} \}$$

$$\ddot{\alpha} = c \{ \ddot{q}_{sk} \} + \bar{c} \{ \dot{q}_{sk} \}$$

For rotor #2, $\dot{\alpha}$ and $\ddot{\alpha}$ are multiplied by Ω_1/Ω_2 and $(\Omega_1/\Omega_2)^2$ respectively. Also for rotor #2, the aircraft motion harmonics are at n = pN Ω_2/Ω_1 (relative to the time scale of the nonrotating frame, Ω_1). We can write the hub velocity as follows therefore:

$$(\dot{\alpha})_{\text{rotor \#2}} = \frac{\Omega_1}{\Omega_2} c \left\{ \sum in \, \phi_n^{(k)} e^{in\psi} \right\}$$

$$= \frac{\Omega_1}{\Omega_2} c \left\{ \sum ipN \frac{\Omega_2}{\Omega_1} \phi_{pN}^{(k)} e^{ipN(\Omega_2/\Omega_1)\psi} \right\}$$

$$= c \left\{ \sum ipN \, \phi_{pN}^{(k)} e^{ipN\psi_2} \right\}$$

Hence by evaluating the hub motion as a sum of harmonics at n = pN, with the azimuth angle of rotor #2, the time scale will be automatically accounted for. Similarly for the acceleration

$$(\ddot{\alpha})_{\text{rotor \#2}} = c \left\{ - \sum (pN)^2 \phi_{pN}^{(k)} e^{ipN\psi_2} \right\}$$

$$+ \frac{\Omega_1}{\Omega_2} \bar{c} \left\{ \sum ipN \, \phi_{pN}^{(k)} e^{ipN\psi_2} \right\}$$

A factor of Ω_1/Ω_2 is still required in the second term of $\ddot{\alpha}$, to account for the scaling of the aircraft velocity in $\bar{c}$.

The acceleration due to gravity, considered as an equivalent linear acceleration, is

$$\Delta \begin{pmatrix} \ddot{x}_s \\ \ddot{y}_s \\ \ddot{z}_s \end{pmatrix} = -g k_{SF} \vec{k}_E$$

For rotor #2, the factor $(\Omega^2 R)_1/(\Omega^2 R)_2$ is also required.

The rotor shaft angular motion perturbation is evaluated from

$$\Psi_S = \sum_{n=pN} \Psi_{S_n} e^{in\Psi}$$

$$\dot{\Psi}_S = \sum_{n=pN} in\Psi_{S_n} e^{in\Psi} + (\dot{\Psi}_S)_{steady}$$

$$\ddot{\Psi}_S = \sum_{n=pN} (-n)^2 \Psi_{S_n} e^{in\Psi}$$

$$\Psi_I = \sum_{n=pN} \Psi_{I_n} e^{in\Psi} + (\Psi_I)_{steady}$$

$$\dot{\Psi}_I = \sum_{n=pN} in\Psi_{I_n} e^{in\Psi}$$

$$\ddot{\Psi}_I = \sum_{n=pN} (-n^2) \Psi_{I_n} e^{in\Psi}$$

From section 4.3.2, the angular motion perturbations of the two rotors are then obtained from

$$\Psi_{S_1} = \Psi_S$$

$$\Psi_{S_2} = \frac{r_{I_1}}{r_{I_2}} \Psi_S + \Psi_I$$

As for the airframe motion, the time scales of the velocity and acceleration perturbations for rotor #2 are accounted for without additional factors of Ω_1/Ω_2.

The static (or quasistatic) displacement and velocity of the airframe motion is obtained as follows:

	static displacement	static velocity
rigid body	zero	prescribed
elastic airframe	calculated	zero
ψ_s	zero	prescribed
ψ_I, ψ_e	calculated	zero

The solution for the helicopter trim or transient motion (section 5.3) supplies the static motion of the airframe rigid body degrees of freedom ($\dot{q}_{sk}$ for k = 1 to 6) and of the rotational speed degree of freedom ($\dot{\psi}_s$). The solution for the static elastic deflection of the airframe and drive train (q_{sk} for $k \geq 7$, ψ_I, and ψ_e) is given in section 5.1.10.

The dimensionless time variable is ψ, the azimuth angle of rotor #1. The azimuth angle of rotor #2 is

$$\Psi_2 = \frac{\Omega_2}{\Omega_1} \Psi + \Delta\Psi_{21}$$

where $\Delta\psi_{21}$ is the angle when $\psi = 0$ at rotor #1. Hence the analysis of rotor #2 must account for this phase difference of the two rotors, by evaluating the blade motion, the airloads, and the hub reactions of

rotor #2 at $\psi + \Delta\psi_{21}$. The phase of the time variable for the airframe motion is the same as that for rotor #1. Note that if $\Omega_2/\Omega_1 \neq 1$ the rotors will effectively be analyzed separately however, so $\Delta\psi_{21} = 0$ can be used.

Hence the harmonics of the rotor hub motion are obtained from the harmonics of the aircraft degrees of freedom by the following expressions:

$$\alpha_n = c\{\phi_n^{(k)}\}$$

$$\dot{\alpha}_n = in\, c\{\phi_n^{(k)}\}$$

$$\ddot{\alpha}_n = -n^2 c\{\phi_n^{(k)}\} + in\,\bar{c}\{\phi_n^{(k)}\}$$

for n a nonzero multiple of N; and the "static" components are

$$\alpha_{static} = c\{q_{sk}\}_{static}$$

$$\dot{\alpha}_{static} = c\{\dot{q}_{sk}\}_{static}$$

$$\ddot{\alpha}_{static} = \bar{c}\{\dot{q}_{sk}\}_{static} + \begin{bmatrix} -gR_{SF}\vec{k}_E \\ 0 \end{bmatrix}$$

for the displacement (α_n and α_{static}) the summation is over the elastic airframe modes only; also, only the angular displacement components are required (α_x, α_y, α_z). For rotor #2, a factor of $(\Omega^2 R)_1/(\Omega^2 R)_2$ is required in the gravity term, $(\dot{q}_{sk})_{static}$ is multiplied by Ω_1/Ω_2, and

the matrix $\bar{c}$ is multiplied by Ω_1/Ω_2. Also, for rotor #2 the harmonics are multiplied by

$$e^{-in\Delta\psi_{21}}$$

since for the azimuth angle of rotor #2 equal to ψ, the hub motion at $\psi - \Delta\psi_{21}$ is required (only if $\Omega_1 = \Omega_2$). The harmonics of the rotor azimuth perturbation are obtained from the harmonics of the drive train degrees of freedom by the following expressions:

$$(\psi_{s_1})_n = (\psi_s)_n$$

$$(\psi_{s_2})_n = \frac{\Omega_2}{\Omega_1}(\psi_s)_n + (\psi_I)_n$$

or

$$\begin{pmatrix} \psi_{s_1} \\ \psi_{s_2} \end{pmatrix} = \begin{bmatrix} 1 & 0 \\ \frac{\Omega_2}{\Omega_1} & 1 \end{bmatrix} \begin{pmatrix} \psi_s \\ \psi_I \end{pmatrix}_n = \begin{bmatrix} c_{\psi_1} \\ c_{\psi_2} \end{bmatrix} \begin{pmatrix} \psi_s \\ \psi_I \end{pmatrix}_n$$

for n a nonzero multiple of N; and the "static" components are

$$(\Psi_{s_1})_{static} = 0$$

$$(\Psi_{s_2})_{static} = (\Psi_z)_{static}$$

$$(\dot{\Psi}_{s_1})_{static} = (\dot{\Psi}_s)_{static}$$

$$(\dot{\Psi}_{s_2})_{static} = (\dot{\Psi}_s)_{static}$$

For rotor #2, $(\dot{\psi}_s)_{static}$ has been multiplied by Ω_1/Ω_2; also for rotor #2 the harmonics are multiplied by

$$e^{-in\Delta\Psi_{z1}}$$

The blade rigid pitch motion p_r requires the pitch increment due to the governor and due to the rotor mast bending. The harmonics of the governor pitch increment are obtained by summing the contributions from the two rotors; and for rotor #2 multiplying by

$$e^{-in\Delta\Psi_{z1}}$$

The pitch increment due to mast bending is

$$\Delta\theta_{\substack{mast \\ bend}} = -\sum_{k=1}^{\infty} q_{s_k}(K_{Mc_k}\cos\Psi + K_{Ms_k}\sin\Psi)$$

$$= -\sum_{k=7}^{\infty} \left((q_{sk})_{static} + \sum_n \phi_n^{(k)} e^{in\psi} \right) \left(k_{mc_k} \cos\psi + k_{ms_k} \sin\psi \right)$$

$$= \sum_n \left[-\sum_{k=7}^{\infty} \phi_n^{(k)} \frac{k_{mc_k} - i k_{ms_k}}{2} e^{i(n+1)\psi} - \sum_{k=7}^{\infty} \phi_n^{(k)} \frac{k_{mc_k} + i k_{ms_k}}{2} e^{i(n-1)\psi} \right]$$

So the harmonics are obtained from the harmonics of the airframe elastic motion by the following expression:

$$\left(\Delta\theta_{\substack{mast \\ bend}} \right)_n = -\sum_{k=7}^{\infty} \phi_{n-1}^{(k)} \frac{k_{mc_k} - i k_{ms_k}}{2} - \sum_{k=7}^{\infty} \phi_{n+1}^{(k)} \frac{k_{mc_k} + i k_{ms_k}}{2}$$

where $\phi_n^{(k)}$ is zero except when n is a nonzero multiple of N, and the convention $\phi_o^{(k)} = (q_{sk})_{static}$ is used here. For rotor #2, the harmonics $\phi_n^{(k)}$ are multiplied by

$$e^{-in\Delta\psi_{21}}$$

in this calculation.

Finally, the complete expressions for the rigid pitch and its derivatives are as follows.

$$\begin{aligned}\beta_r = \; & \theta_{1c}\cos(\psi+\psi_s) + \theta_{1s}\sin(\psi+\psi_s) \\ & - \Sigma K_{\beta_i} q_i - K_{\beta_G}\beta_G \\ & + \Delta\theta_{govr} + \Delta\theta_{\substack{mast\\bend}} + \theta_{HHC}\end{aligned}$$

$$\begin{aligned}\dot{\beta}_r = \; & (-\theta_{1c}\sin(\psi+\psi_s) + \theta_{1s}\cos(\psi+\psi_s))(1+\dot{\psi}_s) \\ & - \Sigma K_{\beta_i}\dot{q}_i - K_{\beta_G}\dot{\beta}_G \\ & + \Delta\dot{\theta}_{govr} + \Delta\dot{\theta}_{\substack{mast\\bend}} + \dot{\theta}_{HHC}\end{aligned}$$

$$\begin{aligned}\ddot{\beta}_r = \; & (-\theta_{1c}\cos(\psi+\psi_s) - \theta_{1s}\sin(\psi+\psi_s))(1+\dot{\psi}_s)^2 \\ & + (-\theta_{1c}\sin(\psi+\psi_s) + \theta_{1s}\cos(\psi+\psi_s))\ddot{\psi}_s \\ & - \Sigma K_{\beta_i}\ddot{q}_i - K_{\beta_G}\ddot{\beta}_G \\ & + \Delta\ddot{\theta}_{govr} + \Delta\ddot{\theta}_{\substack{mast\\bend}} + \ddot{\theta}_{HHC}\end{aligned}$$

5.1.6 Rotor equations

The differential equations of motion for the rotor degrees of freedom are given in section 2.2.18. For the nth harmonic, these equations take the form

$$H_n \begin{pmatrix} \beta_n^{(1)} \\ \vdots \\ \beta_n^{(i)} \\ \theta_n^{(d)} \\ \theta_n^{(1)} \\ \vdots \\ \theta_n^{(i)} \\ \beta_{Gn} \end{pmatrix} = F_n$$

where $\theta_n^{(d)}$ is the nth harmonic of p_d, and β_{Gn} is only present for the n = pN $\pm$ 1 harmonics for gimballed or teetering rotors. From the equations of section 2.2.18, the transfer functions matrix H_n and the forcing function F are as follows. The forcing function F consists of the aerodynamic forces (minus the corresponding estimate of the aerodynamic forces included in H_n); the inertial forces produced by the use of p_d as a degree of freedom); and the nonlinear lag damper moment.

$H_n =$

$I^*_{q_k}(-n^2+g_s\nu_k in+\nu_k^2)$ $+2(I^*_{q_k q_i}\dot{q}_i+\sum_j I^*_{q_k q_i q_j}\dot{q}_i q_j)in$ $+g_{eq}\vec{F}_B\cdot\vec{\eta}'_k(e)\vec{F}_B\cdot\vec{\eta}'_i(e)in$ $-\gamma M_{q_k\dot{q}_i}in+\gamma M_{q_k p_0}k_{p_i}$	$(S^*_{q_k\ddot{p}_i}+\sum_j S^*_{q_k\ddot{p}_i q_j}q_j)n^2$ $-(S^*_{q_k p_i}+\sum_j S^*_{q_k p_i q_j}q_j)$	$I^*_{q_k\alpha}\cdot\vec{t}_B(-n^2+1)$ $-(I^*_{q_k\dot{\beta}}+\sum_j I^*_{q_k\dot{\beta}q_j}q_j)iD_{G1}$ $-\gamma M_{q_k\dot{\beta}}in+\gamma M_{q_k p_0}k_{p_G}$
$(S^*_{p_k\ddot{q}_i}+\sum_j S^*_{p_k\ddot{q}_i q_j}q_j)n^2$ $-(S^*_{p_k q_i}+\sum_j S^*_{p_k q_i q_j}q_j)$ $-\gamma M_{p_k\dot{q}_i}in$	$I^*_{p_k}(-n^2+g_s\mu_k in+\mu_k^2)$ $-I^*_{p_k\ddot{p}_i}n^2+I^*_{p_k p_i}$ $-\gamma M_{p_k\dot{p}_i}in-\gamma M_{p_k p_i}$	$-(I^*_{p_k\alpha}+\sum_j I^*_{p_k\alpha}q_j)\cdot\vec{F}_B(-n^2+1)$
$I^*_{q_i\alpha}\cdot\vec{t}_B(-n^2+1)$ $+2(I^*_{q_0\dot{q}_i}+\sum_j I^*_{q_0\dot{q}_i q_j}\dot{q}_j)\cdot\vec{t}_B in$ $-\gamma M_{\dot{q}_i}in+\gamma M_{p_0}k_{p_i}$	$-(S^*_{q_0\ddot{p}_i}+\sum_j S^*_{q_0\ddot{p}_i q_j}q_j)\cdot\vec{t}_B(-n^2+1)$	$I^*_0(-n^2+\frac{1}{2}(\nu_{GC}^2+\nu_{GS}^2))$ $+\frac{1}{2}(C^*_{GC}+C^*_{GS})iD_{G2}$ $-\gamma M_{\dot{\beta}}in+\gamma M_{p_0}k_{p_G}$

$$F =$$

$$
\begin{aligned}
& I^*_{q_0} - I^*_{q_k\alpha}\cdot\vec{k}_B\,(\ddot{\psi}_s + \ddot{\alpha}_z) - 2\,(I^*_{q_k\dot{\psi}} + \sum_j I^*_{q_k\dot{\psi}q_j}\,q_j)(\dot{\psi}_s + \dot{\alpha}_z) \\
& \quad - S^*_{q_k}\cdot\vec{i}_B\,\ddot{z}_h + S^*_{q_k}\cdot\vec{k}_B\,(\ddot{x}_h \sin\psi - \ddot{y}_h \cos\psi) \\
& \quad - I^*_{q_k\alpha}\cdot\vec{i}_B\,((\ddot{\alpha}_x + 2\dot{\alpha}_y)\sin\psi - (\ddot{\alpha}_y - 2\dot{\alpha}_x)\cos\psi) \\
& \quad + (S^*_{q_k\ddot{p}_0} + \sum_j S^*_{q_k p_0 q_j}\,q_j)\,\ddot{p}_r + (S^*_{q_k p_0} + \sum_j S^*_{q_k p_0 q_j}\,q_j)\,p_r \\
& \quad + \gamma\,\frac{M_{q_k\,aero}}{ac} + \vec{k}_B\cdot\vec{\eta}'_k(e)\,(g_{leg}\,\dot{\zeta} - M_{leg}) \\
& \quad - \gamma\Big[\sum_i M_{q_k\dot{q}_i}\,\dot{q}_i + M_{q_k\dot{\beta}}\,\dot{\beta}_G - M_{q_k p_0}\,(\sum_i K_{p_i} q_i + K_{p_G}\beta_G)\Big]
\end{aligned}
$$

$$
\begin{aligned}
& I^*_{p_k 0} - (I^*_{p_k\alpha} + \sum_j I^*_{p_k\alpha q_j}\,q_j)\cdot\vec{i}_B\,(\ddot{\psi}_s + \ddot{\alpha}_z) \\
& \quad + (S^*_{p_k} + \sum_j S^*_{p_k q_j}\,q_j)\cdot(\vec{k}_B\,\ddot{z}_h + \vec{i}_B\,(\ddot{x}_h \sin\psi - \ddot{y}_h \cos\psi)) \\
& \quad + (I^*_{p_k\alpha} + \sum_j I^*_{p_k\alpha q_j}\,q_j)\cdot\vec{k}_B\,((\ddot{\alpha}_x + 2\dot{\alpha}_y)\sin\psi - (\ddot{\alpha}_y - 2\dot{\alpha}_x)\cos\psi) \\
& \quad + \gamma\,\frac{M_{p_k\,aero}}{ac} - I^*_{p_0}\,\xi_k(r_{FA})\,\ddot{p}_r - I^*_{p_k\ddot{p}_0}\,\ddot{p}_r - I^*_{p_k p_0}\,p_r \\
& \quad - \gamma\Big[\sum_i M_{p_k\dot{q}_i}\,\dot{q}_i + M_{p_k\dot{\beta}}\,\dot{\beta}_G + \sum_i M_{p_k\dot{p}_i}\,(\dot{p}_i - \xi_i(r_{FA})\,\dot{p}_r) \\
& \qquad\qquad + \sum_i M_{p_k p_i}\,(p_i - \xi_i(r_{FA})\,p_r)\Big]
\end{aligned}
$$

$$
\begin{aligned}
& - I^*_0\,((\ddot{\alpha}_x + 2\dot{\alpha}_y)\sin\psi - (\ddot{\alpha}_y - 2\dot{\alpha}_x)\cos\psi) \\
& + \left(\gamma\,\frac{C_{mx}}{\sigma a}\right)_{aero} + (S^*_{q_0\ddot{p}_0} + \sum_j S^*_{q_0\ddot{p}_0 q_j}\,q_j)\cdot\vec{i}_B\,(\ddot{p}_r + p_r) \\
& - \gamma\Big[\sum_i M_{\dot{q}_i}\,\dot{q}_i + M_{\dot{\beta}}\,\dot{\beta}_G - M_{p_0}\,(\sum_i K_{p_i} q_i + K_{p_G}\beta_G)\Big] \\
& - \sum_{n=pN}\Big[\tfrac{1}{2}(C^*_{GC} - C^*_{GS})\,in + \tfrac{1}{2}I^*_0(\nu^2_{GC} - \nu^2_{GS})\Big]\Big[\beta_{G_{n-1}}\,e^{i(n+1)\psi} \\
& \qquad\qquad + \beta_{G_{n+1}}\,e^{i(n-1)\psi}\Big]
\end{aligned}
$$

where

$$D_{G1} = \begin{cases} -(n-1)^2 & \text{gimbal, } n = pN+1 \\ (n+1)^2 & \text{gimbal, } n = pN-1 \\ 2n & \text{teeter} \end{cases}$$

$$D_{G2} = \begin{cases} (n-1) & \text{gimbal, } n = pN+1 \\ (n+1) & \text{gimbal, } n = pN-1 \\ n & \text{teeter} \end{cases}$$

Note that estimates of the aerodynamic spring and damping forces have been added to both sides of the equations. In the matrix H_n these terms must be multiplied by $((J/n\pi)\sin(n\pi/J))^2$, to be consistent with the Fourier analysis of the forcing function F (see section 5.1.4).

The derivation of H_n and F requires

$$\beta_G = \beta_{GC}\cos\Psi + \beta_{GS}\sin\Psi + \beta_T$$

$$\ddot{\theta}_G - \theta_G + 2\dot{\beta}_G = -\ddot{\beta}_{GC}\sin\Psi + \ddot{\beta}_{GS}\cos\Psi + 2\dot{\beta}_T$$

so

$$(\ddot{\theta}_G - \theta_G + 2\dot{\beta}_G)_n = D_{G1}\, i\beta_{Gn}$$

and

$$\sum_{\rho N} \left[(\rho N)^2 (\beta_{\rho N-1} + \beta_{\rho N+1}) \sin\psi - \frac{1}{i} (\rho N)^2 (\beta_{\rho N-1} - \beta_{\rho N+1}) \cos\psi \right] e^{i\rho N\psi}$$

$$= \sum_{\rho N} \left[-(\rho N)^2 i \beta_{\rho N+1} e^{i(\rho N+1)\psi} + (\rho N)^2 i \beta_{\rho N-1} e^{i(\rho N-1)\psi} \right]$$

The solution for the blade motion requires the inverse of H_n for each harmonic. One approach is to invert H_n every azimuth step. A more efficient approach is to invert H_n once and store the result. It will still be necessary to update H_n^{-1} occasionally however, because it depends on the bending solution (q_j terms). The blade motion harmonics should be completely recalculated whenever H_n^{-1} is updated.

Hence at each azimuth step ψ_j the forcing function F_j is evaluated. Then the blade motion harmonics are updated by adding the following increment:

$$\Delta \begin{pmatrix} \beta_n^{(c)} \\ \vdots \\ \beta_n^{(s)} \\ \theta_n^{(d)} \\ \theta_n^{(c)} \\ \vdots \\ \theta_n^{(s)} \\ \beta_{0n} \end{pmatrix} = f H_n^{-1} \left(F_j - (\bar{F}_j)_{\text{last rev}} \right) \frac{K_n e^{-in\psi_j}}{J}$$

5.1.7 Hub reactions.

The generalized aircraft forces due to the rotor hub reactions are $Q = c^T F$, where c is given in section 4.2.2 and

$$F^T = \left[\gamma \frac{2C_H}{\sigma a} \quad \gamma \frac{2C_Y}{\sigma a} \quad \gamma \frac{2C_T}{\sigma a} \quad \gamma \frac{2C_{M_x}}{\sigma a} \quad \gamma \frac{2C_{M_y}}{\sigma a} \quad -\gamma \frac{2C_Q}{\sigma a} \right]$$

From the results of section 2.2.18, the required hub reactions are as follows.

$$\gamma \frac{2C_H}{\sigma a} = \frac{1}{2} \sum_{m=1}^{2} \left(2 \sin\psi_m \gamma \frac{C_{fx}}{\sigma a} + 2 \cos\psi_m \gamma \frac{C_{fr}}{\sigma a} \right)_{aero} + \sum_i \zeta_{qi}^* \cdot \vec{k}_B \left[\sum_{n=pN} e^{in\psi} in^2 \left(\beta_{n-1}^{(i)} - \beta_{n+1}^{(i)} \right) \right]$$

$$\gamma \frac{2C_Y}{\sigma a} = \frac{1}{2} \sum_{m=1}^{2} \left(-2 \cos\psi_m \gamma \frac{C_{fx}}{\sigma a} + 2 \sin\psi_m \gamma \frac{C_{fr}}{\sigma a} \right)_{aero} + \sum_i \zeta_{qi}^* \cdot \vec{k}_B \left[\sum_{n=pN} e^{in\psi} n^2 \left(\beta_{n-1}^{(i)} + \beta_{n+1}^{(i)} \right) \right]$$

$$\gamma \frac{2C_T}{\sigma a} = \frac{1}{2} \sum_{m=1}^{2} \left(2 \gamma \frac{C_{fz}}{\sigma a} \right)_{aero} + 2 \sum_i \zeta_{qi}^* \cdot \vec{k}_B \left[\sum_{n=pN} e^{in\psi} n^2 \beta_n^{(i)} \right]$$

$$\gamma \frac{2C_{mx}}{\sigma a} = \frac{1}{2} \sum_{m=1}^{2} \left(2 \sin\Psi_m \gamma \frac{C_{mx}}{\sigma a} \right)_{\text{zero}}$$

$$- I_o^* \left[(\ddot{\alpha}_x + 2\dot{\alpha}_y) \frac{2}{2} \sum_{m=1}^{2} \sin^2\Psi_m \right.$$

$$\left. - (\ddot{\alpha}_y - 2\dot{\alpha}_x) \frac{2}{2} \sum_{m=1}^{2} \sin\Psi_m \cos\Psi_m \right]$$

$$- I_o^* \left[\sum_{n=pN} e^{in\Psi} \, i \left((n^2 - 2n) \beta_{G_{n-1}} - (n^2 + 2n) \beta_{G_{n+1}} \right) \right]$$

$$- \sum_i I_{q_i a}^* \cdot \vec{\iota_B} \left[\sum_{n=pN} e^{in\Psi} \, i \left((n^2 - 2n) \beta_{n-1}^{(i)} - (n^2 + 2n) \beta_{n+1}^{(i)} \right) \right]$$

$$- 2 \sum_i \left(I_{q_0 \dot{q}_i}^* + \sum_j I_{q_0 \dot{q}_i q_j}^* q_j \right) \cdot \vec{\iota_B} \left[\sum_{n=pN} e^{in\Psi} \left((n-1) \beta_{n-1}^{(i)} \right. \right.$$

$$\left. \left. - (n+1) \beta_{n+1}^{(i)} \right) \right]$$

$$\gamma \frac{2C_{my}}{\sigma a} = \frac{1}{2} \sum_{m=1}^{2} \left(-2 \cos\Psi_m \gamma \frac{C_{mx}}{\sigma a} \right)_{\text{zero}}$$

$$- I_o^* \left[-(\ddot{\alpha}_x + 2\dot{\alpha}_y) \frac{2}{2} \sum_{m=1}^{2} \sin\Psi_m \cos\Psi_m \right.$$

$$\left. + (\ddot{\alpha}_y - 2\dot{\alpha}_x) \frac{2}{2} \sum_{m=1}^{2} \cos^2\Psi_m \right]$$

$$- I_o^* \left[\sum_{n=pN} e^{in\Psi} \left((n^2 - 2n) \beta_{G_{n-1}} + (n^2 + 2n) \beta_{G_{n+1}} \right) \right]$$

$$- I_{q_i a}^* \cdot \vec{\iota_B} \left[\sum_{n=pN} e^{in\Psi} \left((n^2 - 2n) \beta_{n-1}^{(i)} + (n^2 + 2n) \beta_{n+1}^{(i)} \right) \right]$$

$$+ 2 \sum_i \left(I_{q_0 \dot{q}_i}^* + \sum_j I_{q_0 \dot{q}_i q_j}^* q_j \right) \cdot \vec{\iota_B} \left[\sum_{n=pN} e^{in\Psi} \, i \left((n-1) \beta_{n-1}^{(i)} \right. \right.$$

$$\left. \left. + (n+1) \beta_{n+1}^{(i)} \right) \right]$$

$$\gamma \frac{2Q}{\rho a} = \frac{1}{2} \sum_{m=1}^{2} \left(2\gamma \frac{C_{mz}}{\sigma_0}\right)_{hero}$$

$$+ 2 I_o^* \ddot{\psi}_s$$

$$- 2 \sum_i I_{q;\alpha}^* \cdot \vec{k}_B \left[\sum_{n=\rho N} e^{in\psi} n^2 \beta_n^{(i)} \right]$$

$$+ 4 \sum_i \left(I_{q_0 q_i}^* + \sum_j I_{q_0 q_i; q_j}^* q_j \right) \cdot \vec{k}_B \left[\sum_{n=\rho N} e^{in\psi} in \beta_n^{(i)} \right]$$

where

$$\frac{2}{2} \sum_{m=1}^{2} \cos^2 \psi_m = \begin{cases} 1 & N \geq 3 \\ 1 + \cos 2\psi & N = 2 \end{cases}$$

$$\frac{2}{2} \sum_{m=1}^{2} \sin^2 \psi_m = \begin{cases} 1 & N \geq 3 \\ 1 - \cos 2\psi & N = 2 \end{cases}$$

$$\frac{2}{2} \sum_{m=1}^{2} \cos \psi_m \sin \psi_m = \begin{cases} 0 & N \geq 3 \\ \sin 2\psi & N = 2 \end{cases}$$

These hub reactions are harmonically analyzed in the evaluation of the vibratory airframe motion. The effect of the summation over all N

blades then is to suppress the harmonics not at multiples of N/rev. An equivalent approach therefore is to omit the summation operator and only evaluate the pN/rev harmonics. Hence the aerodynamic forces are only evaluated for one blade at azimuth angle ψ.

The mean hub reactions, required in the solution for the steady state or slowly varying aircraft motion (section 5.3), are obtained by averaging the above results over one period. Note that only the aerodynamic terms contribute to the mean values of the hub forces and torque.

The hub forces due to the linear acceleration of the rotor mass

$$\Delta \begin{pmatrix} \gamma \frac{2C_H}{\sigma a} \\ \gamma \frac{2C_Y}{\sigma a} \\ \gamma \frac{2C_T}{\sigma a} \end{pmatrix} = -2M_b^* \begin{pmatrix} \ddot{x}_s \\ \ddot{y}_s \\ \ddot{z}_s \end{pmatrix}$$

have not been included here, since the airframe inertias include the rotor mass. Also, the torque produced by the angular acceleration of the rotor:

$$\Delta \left(-\gamma \frac{2C_Q}{\sigma a}\right) = -2I_0^* \ddot{\alpha}_z$$

has been omitted; this term will be included on the left-hand-side of the airframe equations. For the static elastic airframe deflection,

evaluated from the mean hub reactions, the "static" hub acceleration must be included:

$$\Delta F = -2M_b^* \ddot{\alpha}_{static}$$

which consists of the gravitational force, and the centrifugal force due to the angular velocity of the body axes.

To solve the equations of motion for the engine and drive train, the rotor torque is required in the following form:

$$\gamma \frac{\tilde{C}_Q}{\sigma_0} = \frac{1}{2} \sum_{m=1}^{N} \left(\gamma \frac{c_{m^2}}{\sigma a}\right)_{base}$$
$$+ I_0^* \ddot{\alpha}_z - \sum_i I_{q_i\alpha}^* \cdot \vec{k}_B \left[\sum_{n=pN} e^{in\psi} n^2 \beta_n^{(i)}\right]$$
$$+ 2 \sum_i \left(I_{q\dot{q}_i}^* + \sum_j I_{q\dot{q}_i q_j}^* q_j\right) \cdot \vec{k}_B \left[\sum_{n=pN} e^{in\psi} in\beta_n^{(i)}\right]$$
$$- \gamma \left[Q_\xi \dot{\psi}_s + Q_\theta \Delta\theta_{gov}\right.$$

(see section 5.1.9).

5.1.8 Aircraft equations.

The differential equations of motion for the aircraft degrees of freedom are given in section 4.2.4. For the nth harmonics, these equations take the form

$$H_n \left\{ \Phi_n^{(k)} \right\} = \left\{ Q_k^* \right\} = c^T F_n + b_f (f_g)_n$$

where Q_k^* is the generalized force produced by the hub reactions of the two rotors, and by the higher harmonic auxiliary forces. From the equations of section 4.2.4, the transfer matrix H_n is as follows.

$$H_n = \begin{bmatrix} - R_e^T I^* R_e n^2 & 0 & 0 \\ - M^* (\vec{V} \times) R_e in + G & - M^* n^2 & 0 \\ 0 & 0 & H_e \end{bmatrix}$$

$$- 2 n^2 (I_o^* c_6^T c_6)_{\text{rotor \#1}} \quad - 2 n^2 (I_o^* c_6^T c_6)_{\text{rotor \#2}}$$

The last two terms account for the rotational inertia for the two rotors, which have been omitted from the rotor torques. The subscript "6" refers to the 6th row of c (corresponding to α_z), or the 6th column of c^T (corresponding to C_Q). The transfer matrix for the elastic airframe modes ($k \geq 7$) is:

$$H_e = - M_k^* n^2 + \left(M_k^* g_s \omega_k + \frac{2\gamma}{\sigma a} \frac{q}{AV} F_{q_k \dot{q}_k} \right) in + M_k^* \omega_k^2$$

The only aircraft aerodynamic forces included in the high frequency response are the damping coefficients of the elastic modes (see section 4.2.7).

Only the harmonics of N/rev are excited in the nonrotating frame. The aircraft response to each of the two rotors is evaluated separately. For the response to the rotor #1 hub reactions, the harmonics at $n = N_1$, $2N_1$, $3N_1$, etc., are required. The time scale of the aircraft equations is the rotational speed of rotor #1, so the harmonics of motion due to rotor #2 are at $n = (\Omega_2/\Omega_1)n_2$. For the response to rotor #2 hub reactions the harmonics at $n = (\Omega_2/\Omega_1)N_2$, $(\Omega_2/\Omega_1)2N_2$, $(\Omega_2/\Omega_1)3N_2$, etc. are required. The equations of the airframe motion are not solved here for the static response ($n = 0$). The hub reactions of rotor #2 are evaluated as a function of its azimuth angle, ψ_2; to obtain the response of the airframe these hub reactions must be used at $\psi = \psi_2 - \Delta\psi_{21}$.

The hub reactions are evaluated at azimuth stations ψ_j as the rotor equations are being solved. The harmonics of the rotor hub reactions are:

$$F_n = \sum_{j=1}^{J} f_j \left(\frac{k_n}{J} e^{-in\psi_j} \right)$$

The harmonics of the auxiliary forces are:

$$(f_\ell)_n = \frac{1}{2} \left[(f_\ell)_{pc} - i (f_\ell)_{ps} \right]$$

Then the airframe vibratory motion obtained from

$$\left\{\phi_n^{(k)}\right\} = H_n^{-1}\left\{Q_k^*\right\}_n = H_n^{-1} c^T F_n + H_n^{-1} b_f (f_g)_n$$

for n a nonzero multiple of N. The motion $\phi_n^{(k)}$ is evaluated for excitation from rotor #1 and for excitation from rotor #2. For rotor #2 the harmonics must be multiplied by

$$e^{in\Delta\psi_{21}}$$

since for the airframe motion at ψ, the hub reactions at $\psi + \Delta\psi_{21}$ are required (only if $\Omega_1 = \Omega_2$).

5.1.9 Transmission and engine equations.

The differential equations of motion for the rotor and engine speed perturbations are given in section 4.3.2. The equations for the nth harmonics are

$$H_n \begin{pmatrix} \psi_s \\ \psi_I \\ \psi_e \\ \theta_{govr_e} \\ \theta_{govr_1} \\ \theta_{govr_2} \end{pmatrix}_n = F_n$$

with the forcing function and transfer function matrix as follows.

$$F = C_{D_1}\left(\gamma \frac{\tilde{c}_\theta}{c_a}\right)_1 + C_{D_2}\left(\gamma \frac{\tilde{c}_\theta}{c_a}\right)_2$$

with

$$[C_{D_1}, C_{D_2}] = \begin{bmatrix} -1 & -\ell_3 \\ K_{MI_1} & -\ell_2 \\ 0 & 0 \\ 0 & 0 \\ 0 & 0 \\ 0 & 0 \end{bmatrix}$$

and

$$H_n = -Mn^2 + Cin + K$$

with

$$M = \begin{bmatrix} r_E^2 I_E^* + I_{o_1}^* + \ell_2 I_{o_2}^* & \ell_1 I_{o_2}^* & r_E^2 I_E^* & 0 & 0 & 0 \\ -K_{MI_1} I_{o_1}^* + \ell_1 I_{o_2}^* & \ell_0 I_{o_2}^* + K_{MR} r_E^2 I_E^* & 0 & 0 & 0 & 0 \\ r_E^2 I_E^* & 0 & r_E^2 I_E^* & 0 & 0 & 0 \\ 0 & 0 & 0 & \tau_{22} & 0 & 0 \\ 0 & 0 & 0 & 0 & \tau_{21} & 0 \\ 0 & 0 & 0 & 0 & 0 & \tau_{12} \end{bmatrix}$$

$$C = \begin{bmatrix} r_\varepsilon^2 Q_\Omega^* + \gamma_1 Q_{\zeta_1} + \zeta_3 \gamma_2 Q_{\zeta_2} & \zeta_2 \gamma_2 Q_{\zeta_2} & r_\varepsilon^2 Q_\Omega^* & 0 & 0 & 0 \\ -k_{MI_1} \gamma_1 Q_{\zeta_1} + \zeta_2 \gamma_2 Q_{\zeta_2} & \zeta_1 \gamma_2 Q_{\zeta_2} + k_{MR} r_\varepsilon^2 Q_\Omega^* + \sqrt{M_{22} K_{22}}\, g_s & 0 & 0 & 0 & 0 \\ r_\varepsilon^2 Q_\Omega^* & r_\varepsilon^2 Q_\Omega^* + \sqrt{M_{33} K_{33}}\, g_s & 0 & 0 & 0 & 0 \\ k_{P_e} & 0 & 0 & \tau_e & 0 & 0 \\ -k_{P_1} & 0 & 0 & 0 & \tau_1 & 0 \\ -k_{P_2} & 0 & 0 & 0 & 0 & \tau_2 \end{bmatrix}$$

$$K = \begin{bmatrix} 0 & 0 & 0 & -r_\varepsilon Q_t^* & \gamma_1 Q_{\theta_1} & \zeta_3 \gamma_2 Q_{\theta_2} \\ 0 & k_{MI_2}^* & 0 & 0 & -k_{MI_1} \gamma_1 Q_{\theta_1} & \zeta_2 \gamma_2 Q_{\theta_2} \\ 0 & -k_{ME_2}^* & k_{ME_1}^* & -r_\varepsilon Q_t^* & 0 & 0 \\ k_{Ie} & 0 & 0 & 1 & 0 & 0 \\ -k_{I_1} & 0 & 0 & 0 & 1 & 0 \\ -k_{I_2} & 0 & 0 & 0 & 0 & 1 \end{bmatrix}$$

where

$$\zeta_n = \frac{(N I_b \Omega^n)_2}{(N I_b \Omega^n)_1}$$

The torque C_Q is defined in section 5.1.7. In summing over all N blades, all the harmonics of the torque cancel except those at N/rev. Hence the drive train equations are only solved for the n = N, 2N, 3N, etc., harmonics.

The rotor torque ($\gamma \bar{C}_Q/\sigma a$) is evaluated at the azimuth stations ψ_j as the rotor equations are being solved. Then the transmission vibratory motion is obtained from

$$\begin{pmatrix} \Psi_s \\ \Psi_I \\ \Psi_e \\ \theta_{gov_e} \\ \theta_{gov_1} \\ \theta_{gov_2} \end{pmatrix}_n = H_n^{-1} C_D \left(\gamma \frac{\tilde{C}_Q}{\sigma a} \right)_n$$

for n a nonzero multiple of N; where

$$\left(\gamma \frac{\tilde{C}_Q}{\sigma a} \right)_n = \sum_{j=1}^{J} \left(\gamma \frac{\tilde{C}_Q}{\sigma a} \right)_j \frac{k_n e^{-in\psi_j}}{J}$$

are the harmonics of the torque. For rotor #2 the harmonics are multiplied by

$$e^{in\Delta\psi_{21}}$$

The transmission motion is evaluated for excitation from rotor #1 and for excitation from rotor #2.

5.1.10 Static elastic deflection

The equations of motion for the static elastic deflection of the airframe and drive train are

$$M_k^* \omega_k^2 q_{sk} = (Q_k^*)_{rotors} + \frac{2\gamma}{\sigma a} \frac{q}{A} \left[f_{qk\delta} \begin{pmatrix} \delta_f \\ \delta_e \\ \delta_a \\ \delta_r \end{pmatrix} \right]$$

$$- K_{MI_1} \left(\gamma \frac{C_Q}{\sigma a} \right)_1 + \frac{(NI_b \Omega^2)_2}{(NI_b \Omega^2)_1} \left(\gamma \frac{C_Q}{\sigma a} \right)_2 + K_{MI_2}^* \Psi_I = 0$$

$$K_{ME_1}^* \Psi_e - K_{ME_2}^* \Psi_I = \left(\gamma \frac{C_Q}{\sigma a} \right)_1 + \frac{(NI_b \Omega^3)_2}{(NI_b \Omega^3)_1} \left(\gamma \frac{C_Q}{\sigma a} \right)_2$$

(from sections 4.2.4 and 4.3.2). Here Q_k^* is the mean generalized force due to the two rotors, and C_Q is the mean rotor torque.

Hence the solution for the static elastic airframe motion ($k \geq 7$) is

$$(q_{sk})_{static} = \frac{1}{M_k^* \omega_k^2} \left[(C_k^T F_o)_{rotor\ \#1} + (C_k^T f_o)_{rotor\ \#2} + (Q_k^*)_f + \frac{2\gamma}{\sigma a A} q f_{qk\delta} \begin{pmatrix} \delta_f \\ \delta_e \\ \delta_a \\ \delta_r \end{pmatrix} \right]$$

where c_k^T is the k-th row of c^T; and

$$F_o = \frac{1}{J} \sum_{j=1}^{J} F_j - 2M_b^* \ddot{\alpha}_{static}$$

is the mean hub reaction including the rotor mass inertial reaction. The static elastic drive train motion is

$$\begin{pmatrix} \Psi_I \\ \Psi_e \end{pmatrix}_{static} = H_o^{-1} \begin{pmatrix} (\gamma \frac{C_Q}{\sigma a})_1 \\ (\gamma \frac{C_Q}{\sigma a})_2 \end{pmatrix}$$

where

$$H_o^{-1} = \begin{bmatrix} \frac{K_{MI_1}}{K^*_{MI_2}} & -\frac{(NI_b\Omega^2)_2}{(NI_b\Omega^2)_1} \frac{1}{K^*_{MI_2}} \\ \frac{K^*_{MI_2} + K^*_{ME_2} K_{MI_1}}{K^*_{ME_1} K^*_{MI_2}} & \frac{(NI_b\Omega^2)_2}{(NI_b\Omega^2)_1} \frac{K^*_{MI_2} r_{I_1}/r_{I_2} - K^*_{ME_2}}{K^*_{ME_1} K^*_{MI_2}} \end{bmatrix}$$

and $\gamma C_Q/\sigma a$ is the mean torque.

5.1.11 Two-rotor aircraft

In the present model, the two rotors of a helicopter can influence each other through excitation of vibratory airframe motion. The analysis proceeds as follows (see Fig. 5-1). The rotor analysis calculates the hub reactions of each of the two rotors. From these hub reactions, the aircraft equations of motion are solved for the harmonics of the airframe rigid body and elastic motion. Then the hub motion can be evaluated at each rotor, due to the forces of each rotor. The motion at each hub due to the two rotors is summed. Then the rotor equations are solved for the rotor motion and for the hub reactions again.

It is useful to be able to suppress the feedback of the nonrotating frame vibration to either or both rotors. The coupling can be suppressed by omitting the summation of the two hub motion components at one or both hubs (the dotted line in Fig. 5-1). The entire vibratory hub motion can be suppressed by setting it to zero at one or both hubs (the static or low frequency hub motion and the acceleration due to gravity should be retained however). Suppressing the entire vibratory hub motion is equivalent to dropping the aircraft degrees of freedom as far as the rotor analysis is concerned, but it still may be useful to evaluate the aircraft vibration due to the hub reactions.

It should also be possible in a similar fashion to suppress the hub motion due to the static elastic deflection of the airframe and drive train.

The procedure described above is based on the assumption that the entire system is periodic, which in fact is true only if both rotors have the same rotational speed ($\Omega_2/\Omega_1 = 1$). When the two rotors do not turn at the same speed, the motion in the nonrotating frame is not periodic even in steady flight. The most important example is the single main-rotor and the tail-rotor configuration. In order to analyze a periodic system still, it is necessary to neglect the mutual interference of the two rotors. The analysis proceeds as described above, except that the hub motion of one rotor due to the vibratory

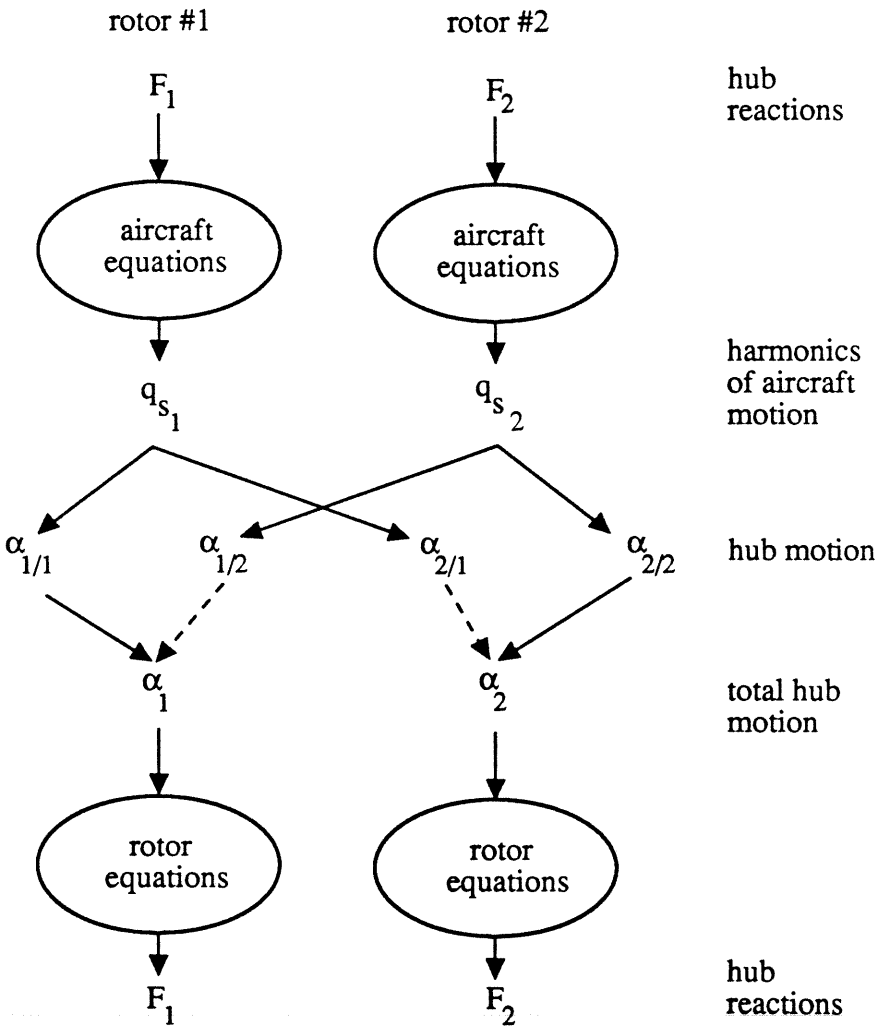

Figure 5-1. Outline of dynamic interaction of the two rotors.

airframe motion produced by the other rotor is always suppressed (the dotted line in Fig. 5-1). Effectively the helicopter is then being analyzed as two single rotor systems, except for the coupling through the aircraft "static" motion (steady state of slowly varying, including the airframe static elastic deflection).

5.1.12 Circulation convergence.

The blade motion will be calculated for a given induced velocity distribution over the rotor disk, uniform or nonuniform. When the converged solution for the blade motion is obtained, the rotor loading (C_T or bound circulation) is re-evaluated. Then the induced velocity estimate can be updated, and the blade motion solution repeated. This procedure continues until the root-mean-squared change in the bound circulation from one iteration to the next is less than a specified tolerance level:

$$\frac{1}{J} \sum_{j=1}^{J} (\Delta\Gamma_j)^2 < \left(\epsilon \frac{2\pi\sigma}{N}\right)^2$$

where Γ_j is the maximum bound circulation, the outboard peak, or the inboard peak as appropriate (see section 3.1.4); and the summation is over the azimuth. When uniform inflow is used, the criterion is

$$(\Delta C_T)^2 + 8\left(\Delta C_{M_y}^2 + \Delta C_{M_x}^2\right) < (\epsilon\sigma)^2$$

To improve the convergence of the iterative calculation of the rotor loading and wake induced velocity, a lag is introduced in the thrust coefficient and used to calculate λ_i:

$$C_T = f\,C_{T_{new}} + (1-f)\,C_{T_{old}}$$

where $C_{T_{old}}$ is the thrust used to calculate λ_i in the last iteration, and $C_{T_{new}}$ is the thrust calculated using that value of λ_i. Similarly, for a nonuniform inflow calculation, a lag is introduced in the blade bound circulation used to evaluate the induced velocity. It is not unusual for a value as low as f = 0.1 to be needed to achieve convergence. This relaxation factor improves convergence at the expense of increasing the number of iterations required. Note that the tolerance defining convergence should be decreased with f, since the relaxation factor reduces the differences between success iterations.

Representing the circulation iteration as the operation $C_{Tn+1} = A(\bar{C}_{Tn})$, and requiring that the solution be converged $(C_{Tn+1} - \bar{C}_{Tn}) = A(\bar{C}_{Tn}) - \bar{C}_{Tn} = 0)$ defines a nonlinear function of $\bar{C}_{Tn}$ with the Newton-Raphson solution $\bar{C}_{Tn} = (A(\bar{C}_{Tn-1}) - A'\bar{C}_{Tn-1})/(1-A') = (C_{Tn} - A'\bar{C}_{Tn-1})/(1-A')$, or $f = 1/(1-A')$. This f is the ideal lag for convergence of the circulation iteration by the successive substitution method. With $A' = \partial A/\partial C_T = (\partial A/\partial\lambda)(\partial\lambda/\partial C_T) \simeq (-\sigma a/4)(\partial\lambda/\partial C_T)$, f can also be identified as a lift deficiency function:

$$f \simeq \frac{1}{1 + \frac{\sigma a}{4}\frac{\partial \lambda}{\partial C_T}}$$

A difficulty with the circulation iteration occurs for a hovering rotor at low thrust, for which $A' \sim C_T^{-1/2}$. Then f approaches zero as C_T approaches zero. In this case, the solution converges to an oscillation

between $C_T = \delta$ and $C_T = -\delta$, where δ approaches zero as f approaches zero. For f = 0 there would be no iteration at all however. Hence the solution $C_T = 0$ cannot be reached exactly, but can be approached as closely as desired, at the cost of many iterations (using small f). This problem can be avoided by fixing the wake geometry in the calculation of the hover induced velocity: $\lambda = \kappa^2 C_T/2\lambda_o$, where λ_o is a fixed, nominal value of the wake vertical convection rate. Then A' = constant/λ_o is independent of the thrust, and the circulation iteration will always converge with a small enough (nonzero) value of f. The exact expression used to calculate the induced velocity for this option is given in section 2.4.3. Note that the resulting induced velocity is not accurate, but it is acceptable for cases of small thrust, particularly if a reasonable value of λ_o is used.

For the nonuniform inflow calculation of a hovering rotor at low thrust, the wake geometry can be fixed by simply using input values of the constants K_1, K_2, K_3, and K_4. A more serious problem exists however. The wake model obtains the induced velocity produced by the far wake by using the maximum bound circulation Γ_{max}. With twisted blades, the bound circulation will not be zero even at zero net rotor thrust, hence a nonzero value of the mean induced velocity will be obtained. So the vortex wake configuration used here is not applicable to the case of a hovering rotor at zero thrust.

5.1.13 Calculation procedure.

In summary, the calculation of the rotor motion and airframe vibration proceeds as follows. The input quantities are the linear and angular velocity perturbations of the rigid body motion; the rotational speed perturbation; the collective and cyclic pitch control angles of the two rotors; the aircraft aerodynamic control positions; and the gust velocity components at the two rotors. The output quantities are the generalized forces due to the mean hub reactions of the two rotors; and the converged solution for the blade motion and aircraft vibration.

The outermost loop is an iteration on the rotor induced velocity and bound circulation evaluation. The next loop is an iteration on the rotor and aircraft motion calculation.

One cycle of the blade and aircraft motion calculation consists of the following steps. First the transfer matrices H_n^{-1} are evaluated. Then there are a number of cycles of successive evaluation of the rotor and airframe motion by the following procedure. First the hub motion harmonics are evaluated. Next there is an azimuth loop for the rotor. At each azimuth step the rotor blade motion harmonics and the aerodynamic hub reactions are updated. Next the total hub reactions are evaluated; the aircraft vibration and drive train vibration harmonics are updated from the hub reactions; and the static elastic deflection is evaluated.

Within the azimuth loop of the rotor motion calculation there are the following steps. First the hub motion and blade motion are evaluated from the harmonics. Then there is an integration over the radial station. Within the radial station loop the blade section pitch, velocity, angle-of-attack, and Mach number are evaluated; the lift, drag, and moment coefficients are evaluated; and the section aerodynamic forces are evaluated. The generalized aerodynamic forces of the blade modes are evaluated by integrating the section forces over the blade radius, and then the blade motion harmonics are updated. The aerodynamic hub forces and moments are also updated.

After each cycle of the blade motion calculation, the convergence is tested by comparing the blade and airframe motion harmonics with the values at the beginning of the cycle.

Finally, after the converged blade motion is obtained, the induced velocity and circulation convergence is tested by comparing the rotor bound circulation with the values at the beginning of the iteration.

This procedure is outlined below, with indentation designating subordination (loops and iterations). The generalized forces for the rotor equations are designated F, and the root hub reactions are

designated C (both a function of azimuth). The number of azimuth steps per revolution is MPSI, the number of revolutions between tests for motion convergence is MREV, and the number of azimuth steps between update of the body motion is MPSIR. The circulation, motion, and rotor/body iterations take the following form:

I) input: shaft motion (quasistatic), gusts, controls
II) initialize F and C to zero
III) circulation iteration
    A) calculate inflow from circulation
    B) motion iteration
        i) evaluate rotor transfer function H
        ii) recalculate blade motion from F
        iii) MREV*MPSI/MPSIR cycles
            a) hub motion harmonics from body vibration
            b) rotor #1 (MPSIR azimuthal steps)
            c) rotor #2 (MPSIR azimuthal steps)
            d) total hub reactions from C
            e) body vibration harmonics
            f) drive train vibration harmonics
            g) static elastic deflection
    C) test motion convergence
IV) test circulation convergence
V) output: converged motion, rotor generalized forces

The procedure for rotor #1 (III.B.iii.b) or rotor #2 (III.B.iii.c) is as follows:

I) input: inflow, gust, hub motion harmonics
II) azimuth loop (MPSIR steps)
    A) hub motion from harmonics
    B) blade motion from harmonics

C) initialize F_{new}, C_{new} to zero

D) radial station loop

i) section aerodynamics

ii) section forces and circulation

iii) sum F_{new}, C_{new} (radial integration)

E) update blade motion harmonics from (F_{new} - F)

F) F = F_{new}

G) C = C_{new}

5.2 Rotor Performance, Loads, and Noise

Once the solution for the periodic motion of the helicopter has been obtained, the performance, loads, and noise of the rotor can be evaluated. The rotor loads of interest include the tension and shear forces, bending moments, and torsion moment at various blade radial stations; the control loads; the blade root forces and moments; and the net rotor hub reactions. The rotor-induced vibration can be evaluated at various points in the aircraft. From the rotor aerodynamic loading the rotational noise can be calculated. The rotor and hub loads are calculated by integrating the aerodynamic and inertial forces acting on the blade. The blade bending and torsion moments can also be evaluated directly from the product of the stiffness and the modal deflection.

All output quantities that are functions of the rotor azimuth can be harmonically analyzed. As in section 5.1.4, the complex harmonics of a function $F(\psi_j)$ evaluated at azimuth stations $\psi_j = j\Delta\psi$ ($j = 1$, $\Delta\psi = 2\pi/J$), are:

$$F_n = \frac{1}{J} K_n \sum_{j=1}^{J} F_j e^{-in\psi_j}$$

The factor K_n,

$$K_n = \left(\frac{J}{\pi n} \sin \frac{\pi n}{J} \right)^2$$

makes these the harmonics of a function that is piecewise linear between the known points $F(\psi_j)$, smoothed by the truncation to a finite number of harmonics. Note that application of this harmonic analysis to the rotor and airframe motion will not therefore reproduce the original harmonics of the solution.

All quantities that are functions of radial station and azimuth can be radially integrated:

$$\bar{F}(\psi) = \int_0^R F(r,\psi)\,dr = \sum_i F(r_i,\psi)\,\Delta r_i$$

(and similarly for the radial averages of the harmonics). The result is the net quantity for a single blade, which is useful for the blade thrust and power in particular. Note that the radial integration of the zeroth harmonic should give the average over the entire rotor disk, i.e. the total rotor quantity. An azimuthal average can also be calculated:

$$\bar{\bar{F}}(r) = \frac{1}{2\pi} \int_0^{2\pi} F(r,\psi)\,d\psi = \frac{1}{J} \sum_j F(r,\psi_j)$$

(which is the same as the zeroth harmonic).

5.2.1 Rotor performance.

To evaluate the rotor performance, the mean rotor hub reactions are required:

$$\begin{pmatrix} T/\rho \\ H/\rho \\ Y/\rho \\ C_{mx}/\rho \\ C_{my}/\rho \\ -Q/\rho \end{pmatrix} = \frac{1}{n} \sum_{j=1}^{n} \begin{pmatrix} \sin\psi_j \frac{C_{fx}}{\sigma} + \cos\psi_j \frac{C_{fy}}{\sigma} \\ -\cos\psi_j \frac{C_{fx}}{\sigma} + \sin\psi_j \frac{C_{fy}}{\sigma} \\ \frac{C_{fz}}{\sigma} \\ \sin\psi_j \frac{C_{mx}}{\sigma} \\ -\cos\psi_j \frac{C_{mx}}{\sigma} \\ -\frac{C_{mz}}{\sigma} \end{pmatrix}$$

where the summation operator averages the forces and moments over the azimuth. These quantities are directly available from the rotor analysis (see section 5.1.7), where they are used also to calculate the generalized forces acting on the aircraft.

The rotor performance is determined in particular by the thrust and torque. The power delivered to the rotor through the shaft is $P = \Omega Q$. The propulsive force is the component of the net rotor force in the direction of the aircraft velocity:

$$PF = -X = \frac{-\mu_x H + \mu_y Y + \mu_z T}{\sqrt{\mu_x^2 + \mu_y^2 + \mu_z^2}}$$

and then the rotor lift, normal to the aircraft velocity, is

$$L = \sqrt{T^2 + H^2 + Y^2 - X^2}$$

So L and X are the wind axis components of the net aerodynamic force of the rotor.

The hub reactions relative to the tip-path plane are obtained by multiplying the force vector by the rotation matrix

$$R_{TS} = \begin{bmatrix} 1 & 0 & \beta_c \\ 0 & 1 & \beta_s \\ -\beta_c & -\beta_s & 1 \end{bmatrix}$$

where β_c and β_s are the tip-path plane tilt angles. Also of interest are the magnitude of the net force of the rotor, and its tilt angles relative to the reference plane: $\theta = \tan^{-1}(H/T)$ and $\phi = \tan^{-1}(Y/T)$.

It is useful to split the rotor power according to the type of energy loss. The induced, interference, profile, parasite, and climb power losses are obtained as follows.

$$C_{P_i} = \int \lambda_i \, dC_T = \int \lambda_i \, \sigma a \left(\frac{F_z}{ac}\right) dr$$

$$C_{P_{int}} = \int \lambda_{int} \, dC_T = \int \lambda_{int} \, \sigma a \left(\frac{F_z}{ac}\right) dr$$

$$C_{P_c} = V_c W / \rho A (\Omega R)^3$$

$$C_{P_p} + C_{P_c} = -VX/\rho A(\Omega R)^3 = -C_x(V/\Omega R)$$
$$= -\mu_x C_H + \mu_y C_Y + \mu_z C_T$$

$$C_{P_p} = (C_{P_p} + C_{P_c}) - C_{P_c}$$

$$C_{P_o} + C_{P_i} + C_{P_{mt}} = C_P - (C_{P_p} + C_{P_c})$$

$$C_{P_o} = (C_{P_o} + C_{P_i} + C_{P_{mt}}) - C_{P_i} - C_{P_{mt}}$$

The induced and interference power losses are obtained by integrating the inflow velocities over the rotor disk.

The ideal power loss, consisting of the parasite, climb, interference, and minimum induced losses, is defined as follows:

$$C_{P_{ideal}} = (\lambda_{ideal} + \mu_z) C_T - \mu_x C_H + \mu_y C_Y + C_{P_{mt}}$$

where

$$\lambda_{ideal} = \frac{C_T}{2\sqrt{\mu_x^2 + \mu_y^2 + (\lambda_{ideal} + \mu_z)^2}}$$

The equation for λ_{ideal} is solved by a Newton-Raphson iteration (see section 2.4.3). For axial flight, the following equations are used:

$$\lambda_{ideal} = \begin{cases} -\frac{\mu_z}{2} + s\sqrt{\left(\frac{\mu_z}{2}\right)^2 + \lambda_h^2} & s\mu_z > -\lambda_h \\ \mu_z\left(.373\left(\frac{\mu_z}{\lambda_h}\right)^2 - 1.991\right) & -2\lambda_h < s\mu_z < -\lambda_h \\ -\frac{\mu_z}{2} - s\sqrt{\left(\frac{\mu_z}{2}\right)^2 - \lambda_h^2} & s\mu_z < -2\lambda_h \end{cases}$$

where $s = \text{sign}\,(C_T)$ and $\lambda_h = (|C_T/2|)^{1/2}$. Then the nonideal power loss, consisting of the profile and excess induced losses, is defined as

$$\begin{aligned} C_{P_n} &= C_P - C_{P_{ideal}} \\ &= (C_{P_0} + C_{P_i}) - \lambda_{ideal} C_T \end{aligned}$$

A measure of the rotor efficiency is the figure of merit, defined for hover as

$$M = \frac{C_T^{3/2}/\sqrt{2}}{C_P}$$

This will be generalized for axial and forward flight to

$$M = \frac{C_{P_{ideal}}}{C_P} = 1 - \frac{C_{P_n}}{C_P}$$

The ratios C_{Pi}/C_T and C_{Pint}/C_T may be considered equivalent induced velocities. A measure of the excess induced losses is the ratio

$$K = \frac{C_{Pi}}{\lambda_{ideal} C_T}$$

and the profile losses can be expressed in terms of an equivalent section drag coefficient:

$$C_{d_0} = 8 \frac{C_{P_0}}{\sigma}$$

$$C_{d_n} = 8 \frac{C_{P_n}}{\sigma}$$

In forward flight, the rotor drag is defined by

$$D_r = \frac{P}{V} + X = \frac{P_0 + P_i + P_{wt}}{V}$$

or in terms of an equivalent drag area $f = D_r/\frac{1}{2}\rho V^2$. A measure of the rotor efficiency in forward flight is the rotor lift to drag ratio, L/D_r.

The section power loading can be split into components in a similar fashion:

$$\frac{dC_P/\sigma}{dr} = r\frac{F_x}{c}$$

$$\frac{dC_{P_i}/\sigma}{dr} = \lambda_i \frac{F_z}{c}$$

$$\frac{dC_{P_{int}}/\sigma}{dr} = \lambda_{int} \frac{F_z}{c}$$

$$\frac{dC_{P_o}/\sigma}{dr} = \mu_T \frac{F_{xo}}{c} + \mu_R \frac{F_{ro}}{c}$$

$$= \frac{1}{2}\mu\left(\mu^2 C_d + \mu_R^2 C_{d_{nodrag}}\right)\frac{c}{C_m}$$

The interference power (total and section) is calculated for the rotor/rotor interference, with $\lambda_{int} = \lambda_z$; and for the airframe/rotor interference, with $\lambda_{int} = \Delta u_p$. Note that the section profile power is defined on the basis of the blade element aerodynamics, while the rotor profile power is the total power minus all other losses (so the sum of the power losses always equals the total). Hence dC_{P_o}/dr may not integrate to exactly C_{P_o}.

5.2.2 Section forces.

The rotor loads at radial station r are calculated by integrating the aerodynamic and inertial forces acting on the blade outboard of r. The root loads are calculated by integrating the forces over the entire blade. The section force and moment coefficients are defined as:

$$\frac{C_f}{\sigma} = \frac{F}{\rho(\Omega R)^2 R c_m} = \frac{F}{\rho(\Omega R)^2 A\sigma/N}$$

$$\frac{C_m}{\sigma} = \frac{M}{\rho(\Omega R)^2 R^2 c_m} = \frac{M}{\rho(\Omega R)^2 A R \sigma / N}$$

where c_m is the blade mean chord, $\sigma = Nc_m/\pi R$ the rotor solidity, and A the rotor disk area.

The total tension and shear forces on the blade section at radial station r are $\vec{F}(r) = \vec{F}_A - \vec{F}_I$, where

$$\vec{F}_I = \int_r^1 \vec{a}\, m\, d\eta$$

$$\vec{F}_A = \int_r^1 (F_x \vec{i}_B + \tilde{F}_r \vec{j}_B + F_z \vec{k}_B)\, d\eta$$

(see section 2.22.10; here a includes the gravitational acceleration). Hence

$$\vec{F}_{shear} = \frac{\vec{F}}{I_b \Omega^2 / R}$$

$$= \gamma \left(\frac{C_{fx}}{\sigma a} \vec{i}_B + \frac{C_{fr}}{\sigma a} \vec{j}_B + \frac{C_{fz}}{\sigma a} \vec{k}_B \right)$$

$$= \gamma \int_r^1 \left(\frac{f_x}{ac} \vec{i}_B + \frac{\tilde{F}_r}{ac} \vec{j}_B + \frac{F_z}{ac} \vec{k}_B \right) d\eta - \frac{1}{I_b} \int_r^1 \vec{a}\, m\, d\eta$$

Substituting for $\vec{a}$ from section 2.2.4, the inertial term becomes

$$
\begin{aligned}
-\int_r^1 \vec{a}\, m\, d\rho \;=\; \vec{\imath}_B \Big[& -\int_r^1 m\, d\rho \,(\ddot{x}_{Bh}\sin\psi - \ddot{y}_{Bh}\cos\psi) \\
& + \int_r^1 \rho m\, d\rho \,(\ddot{\alpha}_z + \ddot{\Psi}_s - \psi_s) \\
& + \sum_i \vec{\imath}_B \cdot \int_r^1 \vec{\eta}_i\, m\, d\rho \,(\ddot{q}_i - q_i) \\
& + \int_r^1 (x_I\cos\theta - x_{FA} + (\rho - r_{FA})\delta_{FA_3})\, m\, d\rho \Big]
\end{aligned}
$$

$$
\begin{aligned}
+ \vec{\jmath}_B \Big[& -\int_r^1 m\, d\rho \,(\ddot{x}_{Bh}\cos\psi + \ddot{y}_{Bh}\sin\psi) \\
& + 2\int_r^1 \rho m\, d\rho \,(\dot{\alpha}_z + \dot{\Psi}_s) \\
& + \sum_i 2\vec{\imath}_B \cdot \int_r^1 \vec{\eta}_i\, m\, d\rho\, \dot{q}_i \\
& + \int_r^1 \rho m\, d\rho \Big]
\end{aligned}
$$

$$
\begin{aligned}
+ \vec{k}_B \Big[& -\int_r^1 m\, d\rho\, \ddot{z}_{Bh} \\
& -\int_r^1 \rho m\, d\rho \,((\ddot{\alpha}_x + 2\dot{\alpha}_y)\sin\psi \\
& \qquad - (\ddot{\alpha}_y - 2\dot{\alpha}_x)\cos\psi) \\
& - \sum_i \vec{\imath}_B \cdot \int_r^1 \vec{\eta}_i\, m\, d\rho\, \ddot{q}_i \\
& - \int_r^1 \rho m\, d\rho\, \ddot{\beta}_G \Big]
\end{aligned}
$$

or

$$
-\frac{1}{I_b}\int_r^1 \vec{a}\, m\, d\rho = \vec{i}_B \left[\begin{array}{l} -M_b^* \left(\ddot{x}_h \sin\psi - \ddot{y}_h \cos\psi \right) \\ + S_b^* \left(\ddot{\alpha}_z + \ddot{\psi}_s - \psi_s \right) \\ + \sum_i \vec{k}_B \cdot S_{q_i}^* \left(\ddot{q}_i - q_i \right) \\ + I_{f_{x_0}}^* \end{array} \right.
$$

$$
+ \vec{j}_B \left[\begin{array}{l} -M_b^* \left(\ddot{x}_h \cos\psi + \ddot{y}_h \sin\psi \right) \\ + 2 S_b^* \left(\dot{\alpha}_z + \dot{\psi}_s \right) \\ + \sum_i 2 \vec{k}_B \cdot S_{q_i}^* \dot{q}_i \\ + S_b^* \end{array} \right.
$$

$$
+ \vec{k}_B \left[\begin{array}{l} -M_b^* \ddot{z}_h \\ - S_b^* \left(\left(\ddot{\alpha}_x + 2\dot{\alpha}_y \right) \sin\psi \right. \\ \qquad \left. - \left(\ddot{\alpha}_y - 2\dot{\alpha}_x \right) \cos\psi \right) \\ - \sum_i \vec{i}_B \cdot S_{q_i}^* \ddot{q}_i \\ - S_b^* \ddot{\beta}_G \end{array} \right.
$$

The above gives the forces acting on the inboard face of the section at r, in the rotating shaft axes (B axes). Note that the $S_b^* \vec{j}_B$ term is the centrifugal force.

The components of the tension and shear forces in the section principal axes are

$$\vec{F}_P = R_B R_{XS} \vec{F}_B$$

or with the centrifugal force omitted from $\vec{F}_B$:

$$\vec{F}_P = R_B R_{XS} \left[\vec{F}_B + \begin{pmatrix} 0 \\ S_b^* \\ 0 \end{pmatrix} \right] = R_B \left[R_{XS} \vec{F}_B + \begin{pmatrix} \phi_z S_b^* \\ 0 \\ -\phi_x S_b^* \end{pmatrix} \right] + \begin{pmatrix} 0 \\ S_b^* \\ 0 \end{pmatrix}$$

The matrix R_{XS}, which transforms the force to the local (bent) blade axes, is:

$$R_{XS} = \begin{bmatrix} 1 & \vec{k}_B \cdot \vec{\phi} & 0 \\ -\vec{k}_B \cdot \vec{\phi} & 1 & \vec{\imath}_B \cdot \vec{\phi} \\ 0 & -\vec{\imath}_B \cdot \vec{\phi} & 1 \end{bmatrix}$$

where

$$\vec{\phi} = \vec{\imath}_B (\beta_0 + \delta_{FA_1} - \delta_{FA_2}) + \vec{k}_B (\psi_S - \delta_{FA_3}) + (z_0 \vec{\imath} - x_0 \vec{k})'$$

The force is multiplied by R_B to obtain the components in the section principal axes, where

$$R_B = \begin{bmatrix} \cos\theta & 0 & -\sin\theta \\ 0 & 1 & 0 \\ \sin\theta & 0 & \cos\theta \end{bmatrix}$$

The integrals of the aerodynamic forces will be evaluated as follows:

$$\int_r^1 f(\rho)\,d\rho = \int_r^{r_I + \frac{1}{2}\Delta r_I} f\,d\rho + \sum_{i=I+1}^{M} \int_{r_i - \frac{1}{2}\Delta r_i}^{r_i + \frac{1}{2}\Delta r_i} f\,d\rho$$

$$= f_I\left(r_I + \tfrac{1}{2}\Delta r_I - r\right) + \sum_{i=I+1}^{M} f_i\,\Delta r_i$$

$$= \sum_{i=I}^{M} f(r_i)\,h_i$$

where I is the maximum index (over i = 1 to M) such that $r_I - \frac{1}{2}\Delta r_I < r$ (I = 1 if $r_1 - \frac{1}{2}\Delta r_1 \geq r$); and $h_i = \Delta r_i$ for i = I + 1 to M, except

$$h_I = r_I + \tfrac{1}{2}\Delta r_I - r \qquad \text{if } r_I - \tfrac{1}{2}\Delta r_I < r$$

$$= \Delta r_I + \min\left(r_I - \tfrac{1}{2}\Delta r_I - r,\ 0\right)$$

The inertia constants are evaluated by trapezoidal integration over the blade properties defined at r = (j - 1)Δr (j = 1 to M + 1, Δr = 1/M):

$$\int_r^1 f(\rho)\,d\rho = \int_r^{r_I} f(\rho)\,d\rho + \sum_{i=I}^{M} \int_{r_i}^{r_{i+1}} f(\rho)\,d\rho$$

$$= f_{I-1}\,\frac{(r_I - r)^2}{2\Delta r} + f_I\left[\frac{(r_I - r)(r + 2\Delta r - r_I)}{2\Delta r} + \frac{\Delta r}{2}\right]$$

$$+ \sum_{i=I+1}^{M} f_i\,\Delta r + f_{M+1}\,\frac{\Delta r}{2}$$

$$= \sum_{i=I-1}^{M+1} f(r_i)\,h_i$$

where I is the index (i = 2 to M + 1) such that $r_{I-1} \le r < r_I$; and $h_i = \Delta r$, except

$$h_{I-1} = \frac{(r_I - r)^2}{2\Delta r}$$

$$h_I = \frac{(r_I - r)(r + 2\Delta r - r_I)}{2\Delta r} + \frac{\Delta r}{2}$$

$$h_{M+1} = h_{M+1} - \frac{\Delta r}{2}$$

Similarly

$$\int_0^r f(\rho)\,d\rho = \sum_{i=1}^{I-2} \int_{r_i}^{r_{i+1}} f(\rho)\,d\rho + \int_{r_{I-1}}^{r} f(\rho)\,d\rho$$

$$= f_1 \frac{\Delta r}{2} + \sum_{i=2}^{I-2} f_i \Delta r + f_{I-1} \frac{\Delta r}{2} + \left[f_{I-1} + \frac{f_{I-1}(r_I - r) + f_I (r - r_{I-1})}{\Delta r} \right] \frac{r - r_{I-1}}{2}$$

$$= \sum_{i=1}^{I} f(r_i) h_i$$

with I as defined above; and $h_i = \Delta r$, except

$$h_I = \frac{(r - r_I + \Delta r)^2}{2\Delta r}$$

$$h_{I-1} = \frac{\Delta r}{2} + \frac{(r_I - r + \Delta r)(r - r_I + \Delta r)}{2\Delta r}$$

$$h_1 = h_1 - \frac{\Delta r}{2}$$

5.2.3 Section bending moment.

The bending moment on the blade section at radial station r is

$$\vec{M}^*_{bend} = \frac{\vec{M}^{(2)}}{I_b \Omega^2} = \gamma \frac{\vec{M}^{(2)}_A}{ac} - \frac{\vec{M}^{(2)}_I}{I_b}$$

where $\vec{M}^{(2)} = M_x\vec{i} + M_z\vec{k} = (\vec{i}\vec{i}_{xs} + \vec{k}\vec{k}_{xs})\vec{M}$. As in section 2.2.7, the aerodynamic and inertial moments are as follows.

$$\frac{\vec{M}^{(2)}_A}{ac} = \int_r^1 (\xi - r)\left(\frac{F_z}{ac}\vec{i}_s - \frac{F_x}{ac}\vec{k}_s\right) d\xi$$

$$\frac{\vec{M}^{(2)}_I}{ac} = \frac{1}{I_b}(\vec{i}\vec{i}_{xs} + \vec{k}\vec{k}_{xs}) \int_r^1 \int (\vec{r}|_{\xi+z} - \vec{r}|_{r=0}) \times \vec{a}\, dm\, d\xi$$

$$\cong \frac{1}{I_b}(\vec{i}\vec{i} + \vec{k}\vec{k}) \int_r^1 \begin{bmatrix} (\xi - r)\vec{j} + (x_0 + x_2)\vec{i} + z_0\vec{k} \\ -(x_0\vec{i} + z_0\vec{k})|_r \end{bmatrix} \times \vec{a}\, m\, d\xi$$

$$= \frac{1}{I_b}\left\{ \begin{array}{l} \int_r^1 (\xi - r)\vec{j} \times \vec{a}\, m\, d\xi \\ + \int_r^1 \begin{bmatrix} -(z_0\vec{i} - x_0\vec{k} - x_2\vec{k}) \\ +(z_0\vec{i} - x_0\vec{k})|_r \end{bmatrix} \begin{bmatrix} -\xi - z_\xi \dot{\psi}_s \\ -z\vec{k}_s \cdot (z_0\vec{i} - x_0\vec{k})\cdot \end{bmatrix} m\, d\xi \\ - \int_r^1 \Sigma \rho_k \left(\vec{j} \times \vec{X}_k(\xi) - \vec{j} \times \vec{X}_k(r) \right. \\ \qquad \left. + \xi_k x_2 \vec{i}|_r\right) \xi\, m\, d\xi \end{array} \right.$$

Substituting for the acceleration from section 2.2.4, the inertial moment becomes:

$$
\begin{aligned}
\vec{M}_I^{(2)} = \quad & \sum_i \ddot{q}_i \int_r^1 (\rho - r)\, \vec{\eta}_i\, m\, d\rho \\
& + \sum_i q_i \int_r^1 \left[\rho \left(\vec{\eta}_i' - \vec{\eta}_i'(r) \right) - \vec{k}_B \vec{k}_B \cdot \vec{\eta}_i' (\rho - r) \right] m\, d\rho \\
& + \sum_i \dot{q}_i \Bigg[\begin{aligned}[t]
& (\delta_{FA_1} - \delta_{FA_2}) \int_r^1 (\rho - r)\, (\vec{J} \times \vec{\eta}_i')\, m\, d\rho \\
& + \int_r^1 \left[(z_0 \vec{\imath} - x_0 \vec{k} - x_I \vec{k}) \right. \\
& \qquad \left. - (z_0 \vec{\imath} - x_0 \vec{k})\big|_r \right] \vec{k}_B \cdot \vec{\eta}_i'\, m\, d\rho \\
& - \vec{k}_B \left(\vec{\eta}_i' \cdot \vec{k}\, x_I \right)\big|_{r=0} \int_r^1 (\rho - r)\, m\, d\rho \\
& + \vec{k}_B \int_0^r \vec{\eta}_i'' \cdot (z_0 \vec{\imath} - x_0 \vec{k} - x_I \vec{k})\, d\rho \int_r^1 (\rho - r)\, m\, d\rho \\
& + \vec{k}_B \int_r^1 (z_0 \vec{\imath} - x_0 \vec{k} - x_I \vec{k}) \cdot \left\{ \vec{\eta}_i'' \int_\rho^1 (\rho^* - r)\, m\, d\rho^* \right. \\
& \qquad \left. - \vec{\eta}_i' (\rho - r)\, m \right\} d\rho
\end{aligned} \Bigg] \\
& + \left((\ddot{\beta}_G + \beta_G) \vec{\imath}_B + \ddot{\psi}_S \vec{k}_B \right) \int_r^1 (\rho - r)\, \rho\, m\, d\rho \\
& + (\ddot{\theta}_G - \theta_G + z \dot{\beta}_G) \vec{k}_B \int_r^1 (\rho - r) \left[z_{CA} - \rho\, \delta_{FA_1} \right. \\
& \qquad \left. + (\rho - r_{FA})\, \delta_{FA_2} - \vec{\imath}_B \cdot (z_0 \vec{\imath} - x_0 \vec{k} - x_I \vec{k}) \right] m\, d\rho \\
& - \sum_i \ddot{\rho}_i \int_r^1 (\rho - r)\, \vec{J} \times \vec{X}_i\, m\, d\rho \\
& - \sum_i \rho_i \int_r^1 \left\{ \vec{k}_B \vec{\imath}_B \cdot \vec{X}_i' (\rho - r) + \rho\, \vec{\jmath}_k x_I \vec{\imath}\,\big|_r \right. \\
& \qquad \left. + \rho\, \vec{J} \times \left(\vec{X}_i - \vec{X}_i\big|_r \right) \right\} m\, d\rho
\end{aligned}
$$

$$+2\dot{\psi}_s \Bigg[\int_r^1 (\rho - r)\left[\rho(\delta_{FA_1} - \delta_{FA_2})\vec{\imath}_B - (x_{FA} + r_{FA}\delta_{FA_3})\vec{k}_B\right] m\, d\rho$$
$$+ \int_r^1 \Big\{ \vec{\imath}_B \rho\, \vec{\imath}_B \cdot (z_0\vec{\imath} - x_0\vec{k} - x_I\vec{k}) + \vec{k}_B r\, \vec{k}_B \cdot (z_0\vec{\imath} - x_0\vec{k} - x_I\vec{k}) - \rho(z_0\vec{\imath} - x_0\vec{k})\Big|_r \Big\} m\, d\rho \Bigg]$$

$$+ \left[\vec{\imath}_B \ddot{z}_{cm} - \vec{k}_B(\ddot{x}_{cm}\sin\psi - \ddot{y}_{cm}\cos\psi)\right] \int_r^1 (\rho - r) m\, d\rho$$

$$+ \left[\vec{\imath}_B((\ddot{\alpha}_x + 2\dot{\alpha}_y)\sin\psi - (\ddot{\alpha}_y - 2\dot{\alpha}_x)\cos\psi) + \vec{k}_B \ddot{\alpha}_z\right] \int_r^1 (\rho - r)\rho m\, d\rho$$

$$+ \int_r^1 (\rho - r)\left[\vec{\imath}_B(\delta_{FA_1} - \delta_{FA_2})\rho + \vec{k}_B(x_I\cos\theta - x_{FA} - r_{FA}\delta_{FA_3})\right] m\, d\rho - \int_r^1 \rho x_I \vec{k} m\, d\rho$$

or

$$\frac{\vec{M}_I^{(2)}}{I_b} = \sum_i (I^*_{q_i\alpha} - r S^*_{q_i})\ddot{q}_i + \sum_i (\vec{\imath}_B \vec{\imath}_B \cdot I^*_{q_i\alpha} + r\vec{k}_B\vec{k}_B \cdot S^*_{q_i} - \vec{\eta}_i(r) S^*_{b_i})q_i$$
$$+ \sum_i 2 I^*_{q_i q_i}\dot{q}_i$$
$$+ (I^*_0 - r S^*_b)(\vec{\imath}_B(\ddot{\beta}_G + \beta_G) + \vec{k}_B \ddot{\psi}_s)$$

$$+ I^*_{q_0\dot{\beta}} \vec{k}_B \left(\ddot{\vartheta}_G - \vartheta_G + 2\dot{\beta}_G\right)$$
$$+ 2 I^*_{q_0\dot{\psi}} \dot{\psi}_S$$

$$- \sum_i S^*_{q_0 p_i} \ddot{p}_i$$
$$- \sum_i S^*_{q_0 p_i} p_i$$
$$+ \left(S^*_b - r M^*_b\right)\left(\vec{i}_B \ddot{z}_h - \vec{k}_B\left(\ddot{x}_h \sin\psi - \ddot{y}_h \cos\psi\right)\right)$$
$$+ \left(I^*_o - r S^*_b\right)\left(\vec{i}_B\left(\left(\ddot{\alpha}_x + 2\dot{\alpha}_y\right)\sin\psi - \left(\ddot{\alpha}_y - 2\dot{\alpha}_x\right)\cos\psi\right) + \vec{k}_B \ddot{\alpha}_z\right)$$
$$+ I^*_{m_{x^0}}$$

The components of the bending moment in the principal axes of the section are then obtained by

$$\begin{pmatrix} M_x \\ M_z \end{pmatrix}_{xS} = \begin{bmatrix} \cos\vartheta & -\sin\vartheta \\ \sin\vartheta & \cos\vartheta \end{bmatrix} \begin{pmatrix} M_x \\ M_z \end{pmatrix}_B$$

The integrals are evaluated as described in section 5.2.2.

The above gives the moments acting on the inboard face of the section at r, about the section elastic axis. To obtain the moments about the tension center (a distance x_c aft of the elastic axis), the chordwise moment produced by the tension force must be subtracted:

$$\vec{M}_{P_{TC}} = \vec{M}_{P_{EA}} - \begin{pmatrix} 0 \\ x_c F_{r_p} \end{pmatrix}$$

Then the moment in shaft axes, approximating the tension force by just the centrifugal force, is:

$$\begin{aligned} \vec{M}_{B_{TC}} &= R_B^T \vec{M}_{P_{TC}} \\ &= \vec{M}_{B_{EA}} - \begin{pmatrix} \sin\theta \\ \cos\theta \end{pmatrix} x_c F_{r_p} \\ &= \vec{M}_{B_{EA}} - \vec{k}\, x_c S_b^* \end{aligned}$$

This effect can be included by introducing the following term in the inertial moment:

$$\Delta I_{m_{x_0}} = (\vec{k} x_c)|_r \int_r^1 \rho m \, dy$$

Alternatively, the bending moments can be calculated directly from the product of the bending stiffness and the curvature. Recall from section 2.1.5 that the bending moment is

$$\vec{M}_E^{(z)} = \left(EI_{zz}\,\vec{\imath}\vec{\imath} + EI_{xx}\,\vec{k}\vec{k} \right)\left(z_o\vec{\imath} - x_o\vec{k} \right)''$$

$$= EI \sum_i \vec{\eta}_i'' q_i$$

where $\vec{\imath}$ and $\vec{k}$ are the section principal axes. The required coefficient form (C_M/σ) is obtained by dividing the dimensional EI by ($\rho\Omega^2 R^5 c_m$), with the curvature already dimensionless. In shaft axes, the moment is:

$$\vec{M}_{BTC} = \begin{bmatrix} EI_{zz}c^2 + EI_{xx}s^2 & (EI_{xx} - EI_{zz})sc \\ (EI_{xx} - EI_{zz})sc & EI_{zz}s^2 + EI_{xx}c^2 \end{bmatrix} \sum \vec{\eta}_i'' q_i$$

with $S = \sin\theta$ and $c = \cos\theta$. The stiffness and modal curvature are linearly interpolated to the required radial station r.

Each of the two methods of calculating the bending moments has potential sources of computational errors. The integrated force method obtains the structural bending moment as the difference between the inertial and aerodynamic loads. Since these nearly cancel on a rotor blade, the bending moment calculation is sensitive to small errors in the inertial and aerodynamic loads. The modal deflection method will not be accurate near a step change in the stiffness distribution (requiring a step change in the curvature, so the moment is continuous) or near a lag damper (requiring a non-zero curvature near the blade hinge).

5.2.4 Section torsion moment.

The torsion moment on the blade section at radial station r is

$$M^{*}_{tors} = \frac{M_r}{I_b \Omega^2} = \gamma \frac{M_{rA}}{ac} - \frac{M_{rI}}{I_b}$$

where $M_r = \vec{j}_{xs} \cdot \vec{M} = (\vec{j} + (x_o\vec{i} + z_o\vec{k})') \cdot \vec{M}$. As in section 2.2.8, the aerodynamic and inertial moments are as follows.

$$\frac{M_{rA}}{ac} = \int_r^1 \frac{M_a}{ac}\, d\xi + \vec{j}_{xs} \cdot \int_r^1 \left[(\xi - r)\vec{j} + (x_o\vec{i} + z_o\vec{k}) - (x_o\vec{i} + z_o\vec{k})|_r \right] \times \left(\frac{F_x}{ac}\vec{i}_B + \frac{F_z}{ac}\vec{k}_B \right) d\xi$$

$$= \int_r^1 \frac{M_a}{ac}\, d\xi + \int_r^1 \left(\frac{F_x}{ac}\vec{i}_B + \frac{F_z}{ac}\vec{k}_B \right) \cdot \left[(z_o\vec{i} - x_o\vec{k}) - (z_o\vec{i} - x_o\vec{k})|_r - (\xi - r)(z_o\vec{i} - x_o\vec{k})'|_r \right] d\xi$$

$$\frac{M_{rI}}{I_b} = \frac{1}{I_b}\vec{J}_{xs}\cdot\int_r^1\Big[\big[(\rho-r)\vec{J}+(x_0+x)\vec{i}+(z_0+z)\vec{k} - (x_0\vec{i}+z_0\vec{k})\big|_r\big]\times\vec{a}\,dm\,d\rho$$

$$= \frac{1}{I_b}\Bigg[\int_r^1\big[(z_0\vec{i}-x_0\vec{k}-x_I\vec{k})-(z_0\vec{i}-x_0\vec{k})\big|_r - (\rho-r)(z_0\vec{i}-x_0\vec{k})'\big|_r\big]\cdot\vec{a}\,dm\,d\rho + \int_r^1\ddot{\theta}\,I_\theta\,d\rho + \int_r^1 I_\theta\cos\theta\sin\theta\,d\rho + \int_r^1 I_\theta\,\tilde{\theta}\,(\cos^2\theta-\sin^2\theta)\,d\rho + (x_0\vec{i}+z_0\vec{k})'\cdot\int_r^1\big[(z_0\vec{i}-x_0\vec{k}-x_I\vec{k}) - (z_0\vec{i}-x_0\vec{k})\big|_r\big]\rho\,dm\,d\rho$$

Then substituting for the acceleration from section 2.2.4 gives for the inertial term:

$$M_{rI} = \sum_i \ddot{\rho}_i\int_r^1\xi_i I_\theta\,d\rho + \sum_i \rho_i\int_r^1 I_\theta\,\xi_i(\cos^2\theta-\sin^2\theta)\,d\rho + \big((\ddot{\beta}_G+\beta_G)\vec{k}_B - \ddot{\psi}_S\vec{i}_B\big)\cdot\int_r^1\vec{X}\,\rho\,dm\,d\rho + \sum_i\ddot{q}_i\int_r^1\vec{X}\cdot(-\vec{J}\times\vec{\eta}_i)\,dm\,d\rho + \int_r^1\big[I_\theta\cos\theta\sin\theta - \cos\theta\,\rho\,(\delta_{FA_1}-\delta_{FA_2})x_I m\big]d\rho$$

$$
+ \sum_i q_i \left[\begin{array}{l}
\int_r^1 [\vec{\eta}_i - \vec{\eta}_i(r) - (\rho - r)\vec{\eta}_i'(r)] \cdot \\
\quad [\vec{\imath}_B (x_{FA} + r_{FA}\,\delta f A_3 - x_2 \cos\theta) \\
\qquad + \vec{k}_B\, \rho\, (\delta f A_1 - \delta f A_2)]\, m\, d\rho \\
+ \int_r^1 x_2 [-\vec{\eta}_i'(r) \cdot \vec{\imath}\, \rho - \vec{\eta}_i \cdot \vec{k}_B \sin\theta]\, m\, d\rho \\
+ \frac{1}{2} \int_r^1 \{ [\vec{\eta}_i - \vec{\eta}_i(r) \\
\qquad - (\rho - r)\vec{\eta}_i'(r)] \cdot \vec{\imath}_B \vec{k}_B \cdot (z_0 \vec{\imath} - x_0 \vec{k}) \\
\qquad + [(z_0 \vec{\imath} - x_0 \vec{k}) - (z_0 \vec{\imath} - x_0 \vec{k})|_r \\
\qquad - (\rho - r)(z_0 \vec{\imath} - x_0 \vec{k})'|_r] \cdot \vec{\imath}_B \vec{k}_B \cdot \vec{\eta}_i \\
\qquad - \vec{\jmath} \times \vec{\eta}_i'(r) \cdot [(z_0 \vec{\imath} - x_0 \vec{k}) \\
\qquad\qquad - (z_0 \vec{\imath} - x_0 \vec{k})|_r]\, \rho \\
\qquad - \vec{\jmath} \times (z_0 \vec{\imath} - x_0 \vec{k})'|_r \cdot [\vec{\eta}_i \\
\qquad\qquad - \vec{\eta}_i(r)]\, \rho \quad \}\, m\, d\rho
\end{array} \right]
$$

$$
+ [\vec{k}_B \ddot{z}_{cm} + \vec{\imath}_B (\ddot{x}_{cm} \sin\psi - \ddot{y}_{cm} \cos\psi)] \cdot \int_r^1 \vec{X}\, m\, d\rho
$$

$$
+ [\vec{k}_B ((\ddot{\alpha}_x + 2\dot{\alpha}_y)\sin\psi - (\ddot{\alpha}_y - 2\dot{\alpha}_x)\cos\psi) \\
- \vec{\imath}_B \ddot{\alpha}_z\,] \cdot \int_r^1 \vec{X}\, \rho\, m\, d\rho
$$

---

where

$$
\vec{X} = (z_0 \vec{\imath} - x_0 \vec{k} - x_2 \vec{k}) - (z_0 \vec{\imath} - x_0 \vec{k})|_r \\
- (\rho - r)(z_0 \vec{\imath} - x_0 \vec{k})'|_r
$$

or

$$\frac{M_{r_x}}{I_b} = \sum_i I^*_{p_0 p_i} \ddot{p}_i + \sum_i I^*_{p_0 p_i} p_i + I^*_{p_0 \alpha} \cdot \left(\vec{k}_B \left(\ddot{\beta}_G + \beta_G \right) - \vec{\iota}_B \ddot{\psi}_s \right) + \sum_i S^*_{p_0 q_i} \ddot{q}_i + \sum_i S^*_{p_0 q_i} q_i + S^*_{p_0} \cdot \left(\vec{k}_B \ddot{z}_h + \vec{\iota}_B \left(\ddot{x}_h \sin\psi - \ddot{y}_h \cos\psi \right) \right) + I^*_{p_0 \alpha} \cdot \left(\vec{k}_B \left((\ddot{\alpha}_x + 2\dot{\alpha}_y)\sin\psi - (\ddot{\alpha}_y - 2\dot{\alpha}_x)\cos\psi \right) - \vec{\iota}_B \ddot{\alpha}_z \right) + I^*_{p_0}$$

The integrals are evaluated as described in section 5.2.2.

Alternatively, the torsion moment can be calculated directly from the product of the torsion stiffness and the slope. Recall from section 2.1.5 that the torsion moment is

$$M_r = GJ\, \theta'_e + k_p^2\, T \left(\theta'_e + \theta'_{tw} \right)$$

The required coefficient form (C_M/σ) is obtained by dividing the dimensional GJ by ($\rho\Omega^2 R^5 c_m$), with k_p^2 and the twist rates already dimensionless, and the tension force (C_{fr}/σ) from section 5.2.2. The stiffness and model slope are linearly interpolated to the required radial station r.

5.2.5 Control load.

The control load at the blade root is given by the moment about the feathering axis:

$$M_{con} = \frac{M_{FA}}{I_b \Omega^2} = \gamma \frac{M_{FA_A}}{ac} - \frac{M_{FA_I}}{I_b}$$

where $M_{FA} = \hat{e}_{FA} \cdot \vec{M}$. From section 2.2.9, the equation of motion for rigid pitch is

$$M_{FA_A} - M_{FA_I} = \left(\int_{r_{FA}}^{1} I_\beta \, dr \right) \left[\omega_0^2 (\beta_0 - \beta_T) + g_s \omega_0 (\dot{\beta}_0 - \dot{\beta}_T) \right]$$

Hence the control load can be evaluated from

$$\begin{aligned} -M_{con} = {} & I^*_{\beta_0} \ddot{\beta}_0 + \sum_i I^*_{\beta_0 \beta_i} \ddot{\beta}_i + \sum_i I^*_{\beta_0 \beta_i} \beta_i \\ & - \sum_i \left(S^*_{\beta_0 q_i} + \sum_j S^*_{\beta_0 \dot{q}_i q_j} q_j \right) \ddot{q}_i \\ & - \sum_i \left(S^*_{\beta_0 q_i} + \sum_j S^*_{\beta_0 q_i q_j} \dot{q}_j \right) q_i \\ & + \left(I^*_{\beta_0 \alpha} + \sum_j I^*_{\beta_0 \alpha q_j} q_j \right) \cdot \left(\vec{r}_B (\ddot{\nu}_s + \ddot{\alpha}_z) - \vec{k}_B (\ddot{\beta}_G + \beta_G) \right. \\ & \left. - \vec{k}_B \left((\ddot{\alpha}_x + 2\dot{\alpha}_y) \sin\psi - (\ddot{\alpha}_y - 2\dot{\alpha}_x) \cos\psi \right) \right) \\ & + \left(S^*_{\beta_0} + \sum_j S^*_{\beta_0 q_j} q_j \right) \cdot \left(-\vec{k}_B \ddot{z}_h - \vec{i}_B (\ddot{x}_h \sin\psi - \ddot{y}_h \cos\psi) \right) \\ & - I^*_{\beta_0 \Omega} - \gamma \frac{M_{\beta_0 \text{aero}}}{ac} \end{aligned}$$

The inertial constants are defined in section 2.2.19.

Alternatively, the control load can be calculated directly from the product of the control system stiffness and the rigid pitch motion. From section 2.2.9:

$$M_{con} = k_\theta (\beta_0 - \beta_r) + c_\theta (\beta_0 - \beta_r)$$
$$= k_\theta \beta_d + c_\theta \dot{\beta}_d$$
$$= I_{\beta_0}^* (\omega_\theta^2 \beta_d + g_s \omega_\theta \dot{\beta}_d)$$

The required coefficient form is $C_M/\sigma = (a/\gamma)M_{con}$. The collective frequency and damping values will be used.

5.2.6 Root forces and moments.

The following section 2.2.18, the forces and moments at the blade root are

$$\vec{F}_{root} = \frac{\vec{F}}{I_b \Omega^2 / R} = \gamma \left(\frac{C_{f_x}}{\sigma a} \vec{i}_B + \frac{C_{f_r}}{\sigma a} \vec{j}_B + \frac{C_{f_z}}{\sigma a} \vec{k}_B \right)$$
$$= \gamma \int_0^1 \left(\frac{f_x}{ac} \vec{i}_B + \frac{\tilde{f}_r}{ac} \vec{j}_B + \frac{f_z}{ac} \vec{k}_B \right) dr - \frac{1}{I_b} \int_0^1 \vec{a}\, m\, dr$$

$$\vec{M}_{root} = \frac{\vec{M}}{I_b \Omega^2} = \gamma \left(\frac{C_{m_x}}{\sigma a} \vec{i}_B - \frac{C_{m_z}}{\sigma a} \vec{k}_B \right)$$
$$= \gamma \int_0^1 \left(\frac{f_z}{ac} \vec{i}_B - \frac{f_x}{ac} \vec{k}_B \right) r\, dr - \frac{1}{I_b} \int_0^1 \vec{r} \times \vec{a}\, m\, dr$$

Substituting for the acceleration from section 2.2.4 gives the components of the blade root force and moment in the rotating frame:

$$\gamma \frac{C_{fx}}{\sigma a} = \left(\gamma \frac{C_{fx}}{\sigma a}\right)_{aero} - M_b^* (\ddot{x}_{eh} \sin\psi_m - \ddot{y}_{eh} \cos\psi_m) + S_b^* (\ddot{\alpha}_z + \ddot{\psi}_s) - S_b^* \psi_s + \sum_i S_{q_i}^* \cdot \vec{k}_B (\ddot{q}_i - q_i) + I_{fx^o}^*$$

$$\gamma \frac{C_{fr}}{\sigma a} = \left(\gamma \frac{C_{fr}}{\sigma a}\right)_{aero} - M_b^* (\ddot{x}_{eh} \cos\psi_m + \ddot{y}_{eh} \sin\psi_m) + 2 S_b^* (\dot{\alpha}_z + \dot{\psi}_s) + \sum_i 2 S_{q_i}^* \cdot \vec{k}_B \dot{q}_i + S_b^*$$

$$\gamma \frac{C_{mx}}{\sigma a} = \left(\gamma \frac{C_{mx}}{\sigma a}\right)_{aero} - S_b^* \ddot{z}_{eh} - I_o^* ((\ddot{\alpha}_x + 2\dot{\alpha}_y)\sin\psi_m - (\ddot{\alpha}_y - 2\dot{\alpha}_x)\cos\psi_m) - I_o^* (\ddot{\beta}_G + \beta_G) - \sum_i I_{q_i\alpha}^* \cdot \vec{t}_B (\ddot{q}_i + q_i) - 2 \sum_i (I_{q_i\dot{q}_i}^* + \sum_j I_{q_i q_i q_j}^* q_j) \cdot \vec{t}_B \dot{q}_i - 2 (I_{q_i\dot{\psi}}^* + \sum_j I_{q_i\dot{\psi} q_j} q_j)(\dot{\psi}_s + \dot{\alpha}_z) - I_{m_{x^o}}^*$$

$$\gamma \frac{C_{f_z}}{\sigma a} = \left(\gamma \frac{C_{f_z}}{\sigma a}\right)_{aero} - M_b^* \ddot{z}_h$$
$$- S_b^* \left((\ddot{\alpha}_x + 2\dot{\alpha}_y) \sin\psi_m - (\ddot{\alpha}_y - 2\dot{\alpha}_x) \cos\psi_m \right)$$
$$- S_b^* \ddot{\beta}_G - \sum_i S_{q_i}^* \cdot \vec{k}_B \ddot{q}_i$$

$$\gamma \frac{C_{m_z}}{\sigma a} = \left(\gamma \frac{C_{m_z}}{\sigma a}\right)_{aero} - S_b^* \left(\ddot{x}_h \sin\psi_m - \ddot{y}_h \cos\psi_m \right)$$
$$+ I_0^* (\ddot{\alpha}_z + \ddot{\psi}_s) + \sum_i I_{q_i \alpha}^* \cdot \vec{k}_B \ddot{q}_i$$
$$+ 2 \sum_i \left(I_{q_i \dot{q}_i}^* + \sum_j I_{q_i \dot{q}_i q_j}^* q_j \right) \cdot \vec{k}_B \dot{q}_i$$
$$- \left(I_{q_i \dot{\beta}}^* + \sum_j I_{q_i \dot{\beta} q_j}^* q_j \right) (\ddot{\theta}_G - \theta_C + 2\dot{\beta}_G)$$

The inertial constants are defined in section 2.2.19. Here the gravitational forces are included in the linear acceleration terms, and the root reaction forces due to the blade mass and weight are retained.

To be consistent with the Fourier analysis used in the equations of motion, the aerodynamic forces must be operated on as follows. Let F_j be the aerodynamic force evaluated at $\psi_j = j\Delta\psi$ (j = 1 to J, $\Delta\psi = 2\pi/J$). The function F is harmonically analyzed as in section 2.1.4, and then the function is re-evaluated (at $\psi_k = k\Delta\psi$) using those harmonics:

$$\tilde{F}_k = \sum_n F_n e^{in\psi_k}$$
$$= \sum_n \left(\frac{1}{J} K_n \sum_{j=1}^{J} F_j e^{-in\psi_j} \right) e^{in\psi_k}$$
$$= \sum_{j=1}^{J} F_j \left(\frac{1}{J} \sum_n K_n e^{in(\psi_k - \psi_j)} \right)$$
$$= \sum_{j=1}^{J} F_j S_{kj}$$

where

$$S_{kj} = \frac{1}{J} \sum_n k_n e^{in(k-j)\Delta\Psi}$$

This operation is applied to the aerodynamic load used to evaluate the section force, the section bending moment, the section torsion moment, the control load, and the root forces and moments.

5.2.7 Hub reactions.

Following section 2.2.18, the total force and moment acting on the rotor hub, resolved in the nonrotating frame (the S system) are

$$\vec{F}_{hub} = \frac{\vec{F}}{N I_b \Omega^2 / R} = \gamma \left(\frac{C_H}{\sigma a} \vec{i}_s + \frac{C_Y}{\sigma a} \vec{j}_s + \frac{C_T}{\sigma a} \vec{k}_s \right)$$

$$\vec{M}_{hub} = \frac{\vec{M}}{N I_b \Omega^2} = \gamma \left(\frac{C_{Mx}}{\sigma a} \vec{i}_s + \frac{C_{My}}{\sigma a} \vec{j}_s - \frac{C_Q}{\sigma a} \vec{k}_s \right)$$

The hub reactions are obtained from the root forces and moments by resolving the rotating components into the nonrotating frame and summing over all the blades:

$$\begin{pmatrix} \gamma \frac{C_{H_b}}{\sigma a} \\ \gamma \frac{C_{Y_b}}{\sigma a} \\ \gamma \frac{C_{T_b}}{\sigma a} \\ \gamma \frac{C_{M_{x_b}}}{\sigma a} \\ \gamma \frac{C_{M_{y_b}}}{\sigma a} \\ -\gamma \frac{C_{Q_b}}{\sigma a} \end{pmatrix} = \frac{1}{2} \sum_{m=1}^{N} \begin{pmatrix} \sin\psi_m \, \gamma \frac{C_{f_x}}{\sigma a} + \cos\psi_m \, \gamma \frac{C_{f_r}}{\sigma a} \\ -\cos\psi_m \, \gamma \frac{C_{f_x}}{\sigma a} + \sin\psi_m \, \gamma \frac{C_{f_r}}{\sigma a} \\ \gamma \frac{C_{f_z}}{\sigma a} \\ \sin\psi_m \, \gamma \frac{C_{m_x}}{\sigma a} \\ -\cos\psi_m \, \gamma \frac{C_{m_x}}{\sigma a} \\ -\gamma \frac{C_{m_z}}{\sigma a} \end{pmatrix}$$

Applying the summation operator gives directly the hub reactions in the time domain, over a period $2\pi/N$. Alternatively, the rotating frame forces and moments can be harmonically analyzed, and then the harmonics of the rotor hub reactions obtained from the harmonics of the root forces and moments, by

$$\begin{pmatrix} C_H \\ C_Y \\ C_T \\ C_{M_x} \\ C_{M_y} \\ -C_Q \end{pmatrix} = \sum_{n=pN} e^{in\psi} \begin{pmatrix} \frac{1}{2}\left((C_{f_r})_{n-1} + (C_{f_r})_{n+1}\right) - \frac{i}{2}\left((C_{f_x})_{n-1} - (C_{f_x})_{n+1}\right) \\ -\frac{i}{2}\left((C_{f_r})_{n-1} - (C_{f_r})_{n+1}\right) - \frac{1}{2}\left((C_{f_x})_{n-1} + (C_{f_x})_{n+1}\right) \\ (C_{f_z})_n \\ -\frac{i}{2}\left((C_{m_x})_{n-1} - (C_{m_x})_{n+1}\right) \\ -\frac{1}{2}\left((C_{m_x})_{n-1} + (C_{m_x})_{n+1}\right) \\ -(C_{m_z})_n \end{pmatrix}$$

Only the harmonics at multiples of N/rev are transmitted by the hub to the nonrotating frame. In the present analysis, the hub reactions are evaluated in the time domain by summing the blade rotating frame reactions. The harmonics of the hub reactions are evaluated from the

harmonics of the blade rotating frame reactions (not by harmonic analysis of the nonrotating frame time histories).

5.2.8 Airframe sensor vibratory response.

From section 4.2.9, the airframe sensor equation is

$$y = C_2 \ddot{q}_s + C_1 \dot{q}_s + C_0 q_s + D_0 g$$

where q_s is the airframe rigid body and elastic motion, and g is the gust velocity. The harmonics of the sensor response are calculated from the harmonics of the airframe motion, at multiples of the number of blades (n = pN, p = integer). There are no gust harmonics in the analysis. Hence the harmonics of y are

$$y_n = \left[-(pN\Omega/\Omega_1)^2 C_2 + i(pN\Omega/\Omega_1) C_1 + C_0 \right] \left\{ \phi_{pN}^{(k)} \right\}$$

(see section 5.1.5). For rotor #2, y is multiplied by

$$e^{-ipN\Delta\psi_{21}}$$

The response produced by each rotor is calculated, and the total response is calculated if $\Omega_2 = \Omega_1$. The root-mean-squared response (summed over all harmonics) is also calculated.

5.2.9 Rotational noise.

The rotational noise due to the blade aerodynamic loads and thickness will be calculated using the following equations for the far field harmonics of the sound pressure disturbance. Consider a rotor moving through the air with velocity components

$$(V_x \quad V_y \quad V_z) = (M_x \quad M_y \quad M_z) C_S$$

Using the tip-path plane coordinate frame, these velocity components are

$$V_x = (\mu_x - \beta_c \mu_z) \Omega R$$

$$V_y = (\mu_y + \beta_s \mu_z) \Omega R$$

$$V_z = (\mu_z + \beta_c \mu_x - \beta_s \mu_y) \Omega R$$

An observer position relative to the hub, moving with the rotor, is defined by the components x_o, y_o, and z_o (positive aft, to the right, and upward); or in terms of a range S_o, an elevation angle θ_o (positive above the tip-path plane), and an azimuth angle ψ_o (defined as for the rotor azimuth):

$$x_o = S_o \cos\theta_o \cos\psi_o$$

$$y_o = S_o \cos\theta_o \sin\psi_o$$

$$z_o = S_o \sin\theta_o$$

Write the blade section forces as

$$\Delta p_z = F_{z_{TPP}}\, l_z(x)$$
$$\Delta p_x = F_{x_{TPP}}\, l_x(x)$$
$$\Delta p_r = F_{r_{TPP}}\, l_r(x)$$

where F_{zTPP}, F_{xTPP}, and F_{rTPP} are the section aerodynamic forces; and l_z, l_x, and l_r are chordwide loading distribution functions. The section forces relative to the tip-path plane are obtained from the forces relative to the shaft axes as follows:

$$F_{z_{TPP}} = F_z - \tilde{F}_r\,(\beta_c \cos\Psi + \beta_s \sin\Psi) + F_x\,(\beta_s \cos\Psi - \beta_c \sin\Psi)$$

$$F_{x_{TPP}} = F_x - F_z\,(\beta_s \cos\Psi - \beta_c \sin\Psi)$$

$$F_{r_{TPP}} = \tilde{F}_r + F_z\,(\beta_c \cos\Psi + \beta_s \sin\Psi)$$

This loading can be written as Fourier series:

$$F_{z_{TPP}} = \sum_{n=-\infty}^{\infty} F_{zn}(r)\, e^{in\Omega t}$$

$$F_{x_{TPP}} = \sum_{n=-\infty}^{\infty} F_{xn}(r)\, e^{in\Omega t}$$

$$F_{r_{TPP}} = \sum_{n=-\infty}^{\infty} F_{rn}(r)\, e^{in\Omega t}$$

The blade thickness distribution is written as

$$t(x) = A_{xs}\, a(x)$$

where A_{xs} is the section area, and a(x) is a chordwise distribution function. The velocity normal to the section, $V_T = \Omega r + V_x \sin\Omega t$, can also be expanded as a Fourier series

$$V_T = \Omega r \sum_{n=-1}^{1} V_n(r)\, e^{in\Omega t}$$

where $V_o = 1$, $V_1 = (V_y - iV_x)/(2\Omega r)$, and $V_{-1} = (V_y + iV_x)/(2\Omega r)$.

The sound pressure at the observer has a periodic component, which is the rotor rotational noise:

$$p = \sum_{m=-\infty}^{\infty} p_m\, e^{imN\Omega t}$$

for t = 0 to $2\pi/N\Omega$. Then the harmonics of the far field rotational noise due to the rotor blade lift, drag, and thickness are:

$$p_m = -\frac{(mN\Omega)^2 N\rho}{4\pi\sigma_0 (1-M\cos\delta_r)^2} e^{-imN\Omega\sigma_0/c_s} \sum_{n=-1}^{1} \left[e^{-i(mN-n)(\psi_r-\frac{\pi}{2})} \right.$$

$$\left. (1-\tfrac{n}{mN}) \int_0^R A_{xs} a_{mN-n} V_n J_{mN-n} dr \right]$$

$$-\frac{imN^2\Omega \sin\theta_r}{4\pi c_s \sigma_0 (1-M\cos\delta_r)^2} e^{-imN\Omega\sigma_0/c_s} \sum_{n=-\infty}^{\infty} \left[e^{-i(mN-n)(\psi_r-\frac{\pi}{2})} \right.$$

$$\left. \int_0^R \ell_{mN-n} F_{zn} J_{mN-n} dr \right]$$

$$+\frac{imN^2}{4\pi\sigma_0 (1-M\cos\delta_r)} e^{-imN\Omega\sigma_0/c_s} \sum_{n=-\infty}^{\infty} \left[e^{-i(mN-n)(\psi_r-\frac{\pi}{2})} \right.$$

$$\left. (1-\tfrac{n}{mN}) \int_0^R \ell_{mN-n} \frac{f_{xn}}{r} J_{mN-n} dr \right]$$

$$-\frac{mN^2\Omega\cos\theta_r}{4\pi c_s \sigma_0 (1-M\cos\delta_r)^2} e^{-imN\Omega\sigma_0/c_s} \sum_{n=-\infty}^{\infty} \left[e^{-i(mN-n)(\psi_r-\frac{\pi}{2})} \right.$$

$$\left. \int_0^R \ell_{mN-n} f_{rn} J'_{mN-n} dr \right]$$

where the argument of the Bessel function J_{mN-n} is

$$\frac{mN\Omega r}{c_s} \qquad \frac{\cos\theta r}{1-M\cos\delta r}$$

and

$$\psi_r = \tan^{-1}\frac{y_0 - M_y\sigma_0}{x_0 - M_x\sigma_0}$$

$$\sigma_0 = \frac{1}{\beta^2}\left(S_0 - M_x x_0 + M_y y_0 + M_z z_0\right)$$

$$S_0^2 = \beta^2(x_0^2 + y_0^2 + z_0^2) + (M_x x_0 - M_y y_0 - M_z z_0)^2$$

$$\beta^2 = 1 - M_x^2 - M_y^2 - M_z^2$$

$$\frac{\cos\theta_r}{1-M\cos\delta r} = \frac{1}{S_0}\sqrt{(x_0 - M_x\sigma_0)^2 + (y_0 + M_y\sigma_0)^2}$$

$$\sigma_0(1-M\cos\delta r)^2 = S_0^2/\sigma_0$$

$$\sigma_0(1-M\cos\delta r) = S_0$$

$$\frac{\sin\theta r}{\sigma_0(1-M\cos\delta r)^2} = \frac{z_0 + M_z\sigma_0}{S_0^2}$$

The derivative of the Bessel function (required for the radial force noise) is

$$J_n'(z) = \frac{n}{z} J_n(z) - J_{n+1}(z)$$

$$J_n'(0) = \begin{cases} 1/2 & n = 1 \\ -1/2 & n = -1 \\ 0 & \text{otherwise} \end{cases}$$

The radial integration is performed as follows.

$$\int_0^R f(r)\,dr \cong \int_{r_1}^R f(r)\,dr \cong \sum_{i=1}^{M} f(r_i)\,\Delta r$$

where $r_i = r_1 + (i - \frac{1}{2})\,\Delta r$, $\Delta r = R(1 - r_1/R)$. Often a large number of radial increments (M) are required, because the Bessel functions oscillate rapidly along the span for higher harmonics. The inboard integration limit r_1 is introduced to reduce the computation in cases where the noise is dominated by the tip loading. The aerodynamic forces are available at the aerodynamic radial stations. These forces are assumed to be constant over the aerodynamic panels, in order to evaluate them at the required radial stations r_i.

The time history of the rotational noise can be evaluated over a period from the harmonics, and the maximum and minimum pressure values found. The sound pressure harmonics can be presented in dB:

$$SPL_m = 10 \log\left(2\,|p_m|^2 / p_{ref}^2\right)$$

for a single-sided spectrum. The overall sound pressure level is

$$OSPL = 10 \log(p_{rms}^2 / p_{ref}^2) = 10 \log \sum_{m=1}^{\infty} \frac{2|p_m|^2}{p_{ref}^2}$$

The reference pressure is $p_{ref} = 0.00002$ N/m^2, hence dB = $10 \log(p_{rms}^2/p_{ref}^2) = 80 + 10 \log(25\ p_{ref}^2)$. The noise level in dBA can be obtained by correcting the octave band spectrum:

n	center frequency, Hz	correction Δ_n, dB
1	31.25	-39.4
2	62.5	-26.2
3	125	-16.1
4	250	-8.6
5	500	-3.2
6	1000	0.0
7	2000	1.2
8	4000	1.0
9	8000	-1.1

The center frequency of the nth octave band is $15.625*2^n$ Hz, with a frequency range of $15.625*2^{n\pm\frac{1}{2}}$. Hence for a given frequency ω, the corresponding octave band is

$$n = \text{integer part} \left[\frac{\log(\sqrt{2}\ \omega / 15.625)}{\log 2} \right]$$

$$= \text{integer part} \left[3.321928 \log(0.09050967\ \omega) \right]$$

Then

$$dBA = 10 \log \left(\sum_n 10^{\log(25\, p_n^2) + 8 + \Delta_n/10} \right)$$

where $p_n^2 = \Sigma_i |p_i|^2$ for all harmonics with ω_i in the nth band.

The chordwise distribution functions for lift and thickness gives

$$l_n = \int_{x_{le}}^{x_{te}} l(x)\, e^{-inx/r}\, dx$$

$$a_n = \int_{x_{le}}^{x_{te}} a(x)\, e^{-inx/r}\, dx$$

A simple and generally conservative approximation is impulsive lift and thickness, for which $l_n = a_n = 1$. Thin airfoil type loading

$$l(x) = \frac{2}{\pi c} \sqrt{\frac{1-\xi}{1+\xi}}$$

gives

$$l_n = e^{-in\frac{x_m}{r}} \left[J_0\left(\frac{nc}{2r}\right) + i\, J_1\left(\frac{nc}{2r}\right) \right]$$

where x_m is the midchord distance from the spanwise axis of the blade. For NACA 4- and 5-digit airfoil series, $A_{xs} = .685\tau c^2$ where τ is the thickness to chord ratio. For these airfoils

$$a_n = e^{-in\left(\frac{x_m}{c}-\frac{1}{2}\right)\frac{c}{r}} \int_0^1 ca\, e^{-in\frac{c}{r}\zeta}\, d\zeta$$

where

$$ac = \frac{tc}{A_{xs}} = 14.597\left[.2969\sqrt{\zeta} - .1260\zeta - .3516\zeta^2 + .2843\zeta^3 - .1015\zeta^4\right]$$

So

$$\int_0^1 ac\, e^{-in\frac{c}{r}\zeta}\, d\zeta = 14.597\left(0.2969\,\hat{I}_0 - 0.1260\,I_1 - 0.3516\,I_2 + 0.2843\,I_3 - 0.1015\,I_4\right)$$

where ($\alpha = nc/r$)

$$I_m = \int_0^1 \zeta^m e^{-i\alpha\zeta}\, d\zeta = \frac{i}{\alpha}\left[e^{-i\alpha} - m I_{m-1}\right]$$

$$I_0 = \frac{i}{\alpha}\left(e^{-i\alpha} - 1\right)$$

and ($z = (2\alpha/\pi)^{1/2}$)

$$\hat{I}_0 = \int_0^1 \sqrt{\zeta}\, e^{-i\alpha\zeta}\, d\zeta$$

$$= \frac{i}{\alpha}\left[e^{-i\alpha} - \sqrt{\frac{\pi}{2\alpha}}\int_0^{\sqrt{\frac{2\alpha}{\pi}}} e^{-i\frac{\pi}{2}t^2}\,dt\right]$$

$$= \frac{i}{\alpha}\left[e^{-i\alpha} - \sqrt{\frac{\pi}{2\alpha}}\,(C(z) - iS(z))\right]$$

$$= \frac{i}{\alpha}\left[e^{-i\alpha} - \sqrt{\frac{\pi}{2\alpha}}\left(\left(\tfrac{1}{2} - i\tfrac{1}{2}\right) - (g(z) - if(z))e^{-i\alpha}\right)\right]$$

(C and S are Fresnel integrals; g and f are approximated by polynomials; $\hat{I}_o$ is evaluated for $|a|$, and replaced by its complex conjugate if $\alpha<0$). A rectangular loading distribution gives

$$l_n = e^{-in x_m/r}\,\frac{2r}{cn}\sin\frac{cn}{2r}$$

which will be used for the drag. In each of these chordwise distribution functions, $x_m = cR/4$ is used, where c is the local dimensionless chord.

5.3 Steady State or Slowly Varying Aircraft Motion

The linearized equations of motion for the rotorcraft rigid body degrees of freedom are

$$\left[R_e^T I^* R_e + 2I_{o1}^*\vec{\xi}_1\vec{g}_1^T + 2I_{o2}^*\left(\frac{\Omega_1}{\Omega_2}\right)^2\vec{\xi}_2\vec{g}_2^T\right]\begin{pmatrix}\phi_F\\ \theta_F\\ \psi_F\end{pmatrix}^{\cdot\cdot}$$

$$= \vec{Q}_{\substack{\text{moment}\\ \text{rotor \#1}}} + \vec{Q}_{\substack{\text{moment}\\ \text{rotor \#2}}} + \vec{Q}_{\substack{\text{moment}\\ \text{aero}}}$$

$$M^* \begin{pmatrix} x_F \\ y_F \\ z_F \end{pmatrix}'' - M^* (\vec{V}_x) R_e \begin{pmatrix} \phi_F \\ \theta_F \\ \psi_F \end{pmatrix}'$$

$$= \vec{\omega}_{\substack{force \\ rotor\#1}} + \vec{\omega}_{\substack{force \\ rotor\#2}} + \vec{\omega}_{\substack{force \\ aero}}$$

$$+ M^* g \vec{k}_E - G \begin{pmatrix} \phi_F \\ \theta_F \\ \psi_F \end{pmatrix}$$

from section 4.2.4. Here

g^T = first 3 elements of 6th row of c

f = first 3 elements of 6th column of c^T

with the matrices c and c^T defined in section 4.2. The terms involving $I_{01}{}^*$ and $I_{02}{}^*$ account for the rotational moments of inertia of the two rotors. The rotor mass is included in the aircraft gross weight and moments of inertia. Note that $M^*g = \gamma 2C_W/\sigma a$. Hence if these equations are divided by $2\gamma/a$ (rotor #1 parameters), they will be in the form of rotor coefficient to solidity ratio, with the components in the body axes (F system). When the rotor speed perturbation is included, the equations of motion become

$$L \begin{vmatrix} \phi_F \\ \theta_F \\ \psi_F \\ x_F \\ y_F \\ z_F \\ \psi_S \end{vmatrix} = \begin{vmatrix} \vec{\omega}_{\substack{moment \\ rotor\#1}} + \vec{\omega}_{\substack{moment \\ rotor\#2}} + \vec{\omega}_{\substack{moment \\ aero}} + \vec{\omega}_{\substack{moment \\ aux}} \\ \vec{\omega}_{\substack{force \\ rotor\#1}} + \vec{\omega}_{\substack{force \\ rotor\#2}} + \vec{\omega}_{\substack{force \\ aero}} + \vec{\omega}_{\substack{force \\ aux}} \\ -\left(\gamma \frac{C_Q}{\sigma a}\right)_1 - \frac{(NI_b \Omega^3)_2}{(NI_b \Omega^3)_1} \left(\gamma \frac{C_Q}{\sigma a}\right)_2 \end{vmatrix}$$

$$+ \begin{vmatrix} 0 \\ M^* (\vec{V}_x) R_e \begin{pmatrix} \phi_F \\ \theta_F \\ \psi_F \end{pmatrix}' + M^* g \vec{k}_E - G \begin{pmatrix} \phi_F \\ \theta_F \\ \psi_F \end{pmatrix} \\ -r_E^2 \Omega_\Omega^* \dot{\psi}_S + r_E \Omega_t^* \theta_t + \left(\gamma \frac{C_{A_E}}{\sigma a}\right)_{trim} \end{vmatrix}$$

(see section 4.3.2). The inertia matrix is as follows:

$$J = \begin{bmatrix} R_e^T I^* R_e + 2 I_{o1}^* \vec{\zeta}_1 \vec{q}_1^T + 2 I_{o2}^* \left(\frac{\Omega_1}{\Omega_2}\right)^2 \vec{\zeta}_2 \vec{q}_2^T & 0 & 2 I_{o1}^* \vec{\zeta}_1 + 2 I_{o2}^* \frac{\Omega_1}{\Omega_2} \vec{\zeta}_2 \\ 0 & M^* & 0 \\ I_{o1}^* \vec{q}_1^T + \frac{(N I_b \Omega)_2}{(N I_b \Omega)_1} I_{o2}^* \vec{q}_2^T & 0 & I_R^* \end{bmatrix}$$

where I_R^* includes the rotational moments of inertia of the two rotors:

$$I_R^* = \frac{1}{N I_b} \left(r_E^2 I_E + I_{o1} + \left(\frac{r_{I_1}}{r_{I_2}}\right)^2 I_{o2} \right)$$

$$= r_E^2 I_E^* + I_{o1}^* + \frac{(N I_b \Omega^2)_2}{(N I_b \Omega^2)_1} I_{o2}^*$$

The solution for the generalized forces produced by the two rotors is described in section 4.2.5. The solution for the generalized forces produced by the airframe aerodynamics is described in section 4.2.6. The solution for the generalized forces produced by the auxiliary forces is described in section 4.2.8.

In the trim analysis, these equations are solved for the case of steady state flight. The controls are adjusted until the desired operating condition is achieved.

In the transient analysis, these equations are numerically integrated in time. A non-equilibrium flight path is produced by a prescribed control or gust input.

In the flight dynamics analysis, the stability derivatives in a linear expansion of the rotor and airframe generalized forces are obtained by prescribed perturbations of the body motion and controls.

5.3.1 Trim analysis.

The helicopter trim calculation determines the control positions and aircraft orientation for the specified flight condition. Both free flight and wind tunnel trim options are considered. In the free flight cases, the helicopter is trimmed to force and moment equilibrium. In the wind tunnel cases the rotor is trimmed to prescribed loading or flapping values (or perhaps the sum of the loading of the two rotors). The trim option can be specified independently of the rotorcraft configuration and degrees of freedom. Hence it is possible to use a wind tunnel trim option for a complete aircraft. For each trim option, it is necessary to identify a set of trim quantities, and an equal number of trim variables which are adjusted to achieve the target values of the trim quantities.

The trim iteration can also be omitted. In this case the helicopter or rotor behavior is evaluated for a specified control setting.

In steady state flight, the perturbation rigid body motion is zero, so the net force and moment on the aircraft must be zero. Thus the rigid body equations of motion give six equations to be solved for the six trim variables, such as the four pilot's controls (δ_o, δ_c, δ_s, and δ_p) and the two trim Euler angles (θ_{FT} and ϕ_{FT}). The controls are adjusted until equilibrium flight is achieved for the specified flight condition. For level flight ($\theta_{FP} = 0$) or a specified climb velocity, it is assumed that the engine can supply whatever power is required to maintain the rotor rotational speed. Alternatively, the aircraft power

available can be specified (for example, zero for power-off descent or an autogyro). Then there is an additional trim variable (the flight path angle or the throttle connected to auxiliary propulsion) and an additional equation to be solved (the rotor power required equal the power available). The aircraft can also be trimmed in a steady turn by prescribing the rate $\dot{\psi}_F$. A coordinated turn is obtained if zero sideslip ($\psi_{FP} = 0$) is specified. In forward flight the resultant bank angle should be

$$\tan \phi_{FT} = \sqrt{n^2 - 1} = \dot{\psi}_F V / g$$

where n is the normal load factor.

Hence the trim analysis solves the equations of motion for a specified steady flight speed and rotor speed (and possibly a specified turn rate). Setting the perturbation rigid body motion and rotational speed to zero gives the following equations.

$$\frac{a}{2\gamma} (\vec{\Omega})_{moment} = 0$$

$$\frac{a}{2\gamma} (\vec{\Omega})_{force} + \frac{C_w}{\sigma} \vec{k}_E + \frac{1}{g} \frac{C_w}{\sigma} (\vec{V} \times) R_c \vec{k}_F \dot{\psi}_F = 0$$

$$(C_Q/\sigma)_{rotor\,\#1} + \frac{(\gamma N I_b \Omega^3)_2}{(\gamma N I_b \Omega^3)_1} (C_Q/\sigma)_{rotor\,\#2} = (C_P/\sigma)_{available}$$

There are contributions to the force and moment (Q) from the two rotors, the airframe aerodynamics, and the auxiliary forces. The force

equations also include the acceleration produced by the turn rate, and the aircraft weight.

The pilot's controls are the collective stick δ_o, lateral cyclic stick δ_c, longitudinal cyclic stick δ_s pedal δ_p, and throttle δ_t. The controls of the rotors and aircraft are related to the pilot's controls by

$$\vec{v} = T_c \vec{v}_p + \vec{v}_o$$

where $\vec{v}_o$ is the control input and auxiliary forces with all sticks centered (see section 4.1.6). Note possible uses of the auxiliary forces in trim include a propulsive force (f_1) proportional to the throttle input, or an antitorque force (f_2) proportional to the pedal input.

For some rotorcraft configurations, the pilot's collective stick (δ_o) does not control the rotor collective pitch, rotor trim being handled by a rotor speed governor using collective pitch feedback. In such a case the static component of the blade pitch governor, $(\Delta\theta_{govr})_{static}$ for either or both rotors, can be used as the trim variable in place of δ_o. Hence $\Delta\theta_{govr}$ is added to the rotor collective pitch θ_{75} obtained from $\vec{v}_p$ and $\vec{v}_o$.

The free flight trim options include the following. The potential trim variables are the five pilot's controls, the trim pitch and roll angles, the flight path pitch angle (climb or descent), and the flight path yaw angle (sideslip). Those variables not adjusted to achieve trim are part of the prescribed operating condition.

a) Force and moment equilibrium (six degrees of freedom trim): Five trim variables are the pilot's collective, longitudinal cyclic, lateral cyclic, and pedal controls, and the aircraft pitch angle. The sixth trim variable can be either roll attitude (for fixed sideslip), or

flight path yaw angle (for fixed roll). The operating condition can be level flight, climb or descent, or turning.

b) Force and moment equilibrium, at specified rotor power (seven degrees of freedom trim): Another trim variable is added to each of the two options for six degrees of freedom trim. This trim variable can be either flight path angle (climb or descent rate), or auxiliary propulsion (through the throttle). Note that these options do not apply to vertical flight (where the vertical speed would have to be adjusted, or the auxiliary force directed vertically).

c) Trim of longitudinal variables only (vertical and horizontal force, pitch moment, and perhaps power): The corresponding lateral trim variables are excluded from the above options. For a laterally symmetric aircraft in a symmetric operating condition, longitudinal trim is exact. It is also a useful approximation that may converge better than a full trim analysis, or allow the tail rotor to be ignored in the analysis.

For a rotor in a wind tunnel, the potential trim quantities include the rotor thrust or lift, drag force, side force, power, longitudinal flapping, and lateral flapping. These quantities are trimmed to specified target values. The rotor tip-path plane tilt (relative to the shaft) is defined as the first harmonics of the tip deflection:

$$z_{tp} = \beta_0 + \sum_i q_i \vec{r}_B \cdot \vec{\eta}_i \quad (1)$$

The rotor lift and drag are defined in wind axes. The thrust and side force are in shaft axes. The target for the drag can be specified as either the rotor drag coefficient to solidity ratio C_X/σ, or the equivalent drag area X/q (so $C_X/\sigma = (X/q)(V/\Omega R)^2/(2A_b)$.

For wind tunnel cases with two main rotors, the option to add the forces and power from the two rotors is allowed. The coefficients for

rotor #2 are converted to rotor #1 normalization (and the sign of the side force changed if the two rotors rotate in opposite directions), but the actual orientation of the rotor forces (defined by R_{SF}) is not considered. This summation is correct for the power and drag force, and for the thrust and side force if the shaft axes coincide for the two rotors.

The wind tunnel trim options include the following. The potential trim variables are the three pilot's controls (δ_o, δ_c, and δ_s), and the test module pitch and yaw angles (θ_T and ψ_T). Those variables not adjusted to achieve trim are part of the prescribed operating condition. The free flight parameters (aircraft Euler angles and flight path angles) are zero.

a) There are five longitudinal trim quantities: lift, thrust, power, drag, and longitudinal flapping. Any one, two, or three of these five quantities can be trimmed, using an equal number of the longitudinal trim variables: collective, longitudinal cyclic, and test module pitch. It is appropriate to trim the drag and lift, but not the drag and thrust.

b) There are two lateral trim quantities: side force and lateral flapping. One of these can be trimmed using lateral cyclic. It is appropriate to trim the longitudinal and lateral flapping, but not the longitudinal flapping and side force.

In the free flight cases, the criterion for the convergence of the trim iteration is that the net force and moment be less than a certain tolerance level as specified by the parameter ϵ:

$$\left[(C_{F_x}/\sigma)^2 + (C_{F_y}/\sigma)^2 + (C_{F_z}/\sigma)^2 \right] < \epsilon \ (C_w/\sigma)$$

$$\left[(C_{M_x}/\sigma)^2 + (C_{M_y}/\sigma)^2 + (C_{M_z}/\sigma)^2 \right] < \epsilon \ (.05\, C_w/\sigma)$$

$$\left| \left(C_P/\sigma - (C_P/\sigma)_{target} \right) \right|$$

$$< \epsilon \max\left(.001, (C_P/\sigma)_{target} \right)$$

For the wind tunnel cases, the following criterion is used:

$$\frac{\left| f - f_{target} \right|}{\max\left(\left| f_{target} \right|, f_{min} \right)} < \epsilon$$

where $f = C_T/\sigma$, C_P/σ, C_L/σ, C_X/σ, or C_Y/σ as appropriate (with f_{min} = .01, .001, .01, .001, .001, respectively). The criterion for the flapping is

$$\left| \left(\beta_c - (\beta_c)_{target} \right) \right| < \epsilon$$

$$\left| \left(\beta_s - (\beta_s)_{target} \right) \right| < \epsilon$$

with β_c and β_s in radians.

The trim problem is solved using a modified Newton-Raphson technique. The task is to find the values of the trim variables $\vec{v}$ such that the target values of certain trim criteria $\vec{M}$ are achieved. The complex, nonlinear equations involved require an iterative solution procedure. A first order expansion of $\vec{M}(\vec{v})$ gives

$$\vec{M}_{target} = \vec{M}_{n+1} \cong \vec{M}_n + \frac{\partial M}{\partial v}\left(\vec{v}_{n+1} - \vec{v}_n\right)$$

or

$$\vec{v}_{n+1} = \vec{v}_n + D^{-1}\left(\vec{M}_{target} - \vec{M}_n\right) F$$

The partial derivative matrix required is

$$D = \frac{\partial M}{\partial v} = \left[\cdots \frac{\partial \vec{M}}{\partial v_i} \cdots\right] = \left[\cdots \frac{\vec{M}(v_i) - \vec{M}(v_i + \Delta v_i)}{\Delta v_i} \cdots\right]$$

The factor $F \leq 1$ is included to avoid overshoot oscillations in the trim iteration by reducing the step size.

The matrix D^{-1} is constructed as follows. First $\vec{M}_{old}$ is calculated using the initial values of $\vec{v}$. Then each control v_i is decreased by the increment Δv_i, and $\vec{M}_{new}$ is calculated; then the i-th column of D is given by

$$\left(\vec{M}_{new} - \vec{M}_{old}\right) / \Delta v_i$$

and the control is restored to its initial value. Finally the matrix D is inverted, and all elements multiplied by the factor F. The partial derivative matrix can be recalculated occasionally as the iteration

proceeds, to improve the convergence. Generally a step size of about Δ = 1 degree is satisfactory for all control variables.

In addition to using this perturbation identification method, the matrix D can be recursively updated as the trim iteration proceeds. An exponential window method is used (see section 5.4). After each trim iteration, the trim criterion change ΔM_n, corresponding to the control increment Δv_n, is calculated. Then:

$$a = P_{n-1} \Delta v_n / \alpha$$

$$k_n = a/(1 + \Delta v_n^T a)$$

$$P_n = P_{n-1} / \alpha - a k_n^T$$

$$D_n = D_{n-1} + (\Delta M_n - D_{n-1} \Delta v_n) k_n^T$$

This is a weighted-least-squares estimate of D using information from all control increments, with α equal to the ratio of the weight for the previous step to the weight for the current step ($0 < \alpha < 1$). The variance matrix P is initially set after the perturbation identification procedure to:

$$P_0 = \begin{bmatrix} \ddots & & \\ & \frac{1}{\Delta v_i^2} & \\ & & \ddots \end{bmatrix}$$

where Δv_i is the control perturbation.

5.3.2 Transient analysis.

The helicopter transient analysis involves numerically integrating the equations of motion for the rigid body and rotor speed degrees of

freedom. A non-equilibrium flight path is produced by a prescribed control or gust input as a function of time. The assumptions of this analysis are that the aircraft motion is slow compared to the rotor speed, and that the perturbed rigid body motion is small. The assumption of quasistatic body motion allows the periodic rotor motion solution to be used with the transient analysis. The small motion assumption arises because it was assumed that the perturbation rotor hub motion is small; it is consistent therefore to integrate the linearized equations for the rigid body motion.

The degrees of freedom considered are the six linear and angular rigid body motions (x_F, y_F, z_F, ϕ_F, θ_F, ψ_F) and the rotor speed perturbation ($\dot{\psi}_s$). The input parameters are the aircraft controls (δ_o, δ_c, δ_s, δ_p δ_t) and aerodynamic gusts. Optionally any of these degrees of freedom can be held constant. The transient analysis with all seven degrees of freedom fixed produces the rotor response to control and gust inputs. The equations to be integrated are:

$$J\begin{pmatrix} \phi_F \\ \theta_F \\ \psi_F \\ x_F \\ y_F \\ z_F \\ \psi_s \end{pmatrix}^{\bullet\bullet} = \begin{pmatrix} \Delta\vec{Q}_{moment} \\ \Delta\vec{Q}_{force} \\ -\Delta\left(\gamma\frac{C_Q}{\sigma a}\right)_1 - \frac{(NI_b\Omega^3)_2}{(NI_b\Omega^3)_1}\Delta\left(\gamma\frac{C_Q}{\sigma a}\right)_2 \end{pmatrix}$$

$$+ \begin{pmatrix} 0 \\ M^*(\vec{V}_x)\,Re\begin{pmatrix} \phi_F \\ \theta_F \\ \Delta\psi_F \end{pmatrix}^{\bullet} - G\begin{pmatrix} \phi_F \\ \theta_F \\ \psi_F \end{pmatrix} \\ -r_E^2 Q_\Omega^* \dot{\psi}_s + r_E Q_t^* \theta_t \end{pmatrix}$$

where $\Delta\vec{Q}$ is the sum of the rotor, aerodynamic, and auxiliary generalized forces, less the trim value; and ΔC_Q is the rotor torque, less the trim value. The initial conditions are zero (except for $\dot{\psi}_F$ when the helicopter is trimmed in a steady turn). These equations are used in the form of increments from trim because the trim solution (obtained by numerical procedures, to within a certain prescribed tolerance) is probably not exact. So there will be small residual forces and moments on the aircraft in the trim state, that if retained would produce spurious transient motions.

The transient rotor speed perturbations will produce throttle and rotor collective pitch increments due to the governor:

$$\Delta\theta_t = -K_{P_e}\dot{\psi}_s - K_{I_e}\psi_s$$

and

$$(\Delta\theta_{govr})_{static} = (\Delta\theta_{govr})_{trim} + K_P\dot{\psi}_s + K_I\psi_s$$

for rotor #1 and rotor #2. The rotor azimuth perturbation ψ_s will also produce cyclic pitch increments due to the trim swash-plate tilt:

$$\begin{pmatrix} \Delta\theta_{1c} \\ \Delta\theta_{1s} \end{pmatrix} = \psi_s \begin{pmatrix} \theta_{1s} \\ -\theta_{1c} \end{pmatrix}_{trim}$$

For rotor #2 these cyclic pitch increments must be multiplied by Ω_2/Ω_1.

The pilot's control positions consist of the trim setting and the transient changes. The options available for the transient changes are described in section 5.3.4. In addition, the self-tuning regulator may be active during the transient (see section 5.4), and a quasistatic feedback system may be implemented. The individual rotor and airframe controls are thus obtained from:

$$v = T_c \left(v_{p_{trim}} + v_{p_{transient}} \right) + v_0 + v_{STR} + v_{SAS}$$

with the governor contributions added as required. No specific feedback system is considered here, but v_{SAS} is included for general use. Note that the flight dynamics analysis can also produce a time history of the aircraft response to Vp_{trans} by numerical integration, but the flight dynamics analysis does not include v_{SAS} or v_{STR} (the self-tuning regulator would be included in the stability derivatives).

From section 4.2.9, the equations for the airframe sensors are:

$$y = C_2 \ddot{q}_s + C_1 \dot{q}_s + C_0 q_s + D_0 g$$

where here q_s is the quasistatic, rigid body motion of the airframe. The gust velocities at the wing-body are used to evaluate the sensor response.

Optionally the airframe rigid body motion can be transformed from fuselage (F) axes to stability (V) axes. The generalized forces are still evaluated in the fuselage (F) axes, and multiplied by J^{-1}. Then the airframe accelerations are multiplied by $\mathfrak{R}_{VF}$ (see section 4.2.1), and integrated in stability (V) axes. The rigid body motion (displacements and rates) is transformed from V to F axes as required

for calculating the generalized forces. The initial conditions of the quasistatic motion are all zero, except for $\psi_{Ftrim} = \psi_{Vtrim}$.

The transient calculation begins with the trim solution, at time t = 0. The pilot's controls or gust input are specified as a function of t. The equations of motion above are in the form

$$\ddot{y} = f(t, y, \dot{y})$$

A fourth order Runge-Kutta method will be used to numerically integrate these equations from time t_n to time $t_{n+1} = t_n + h$:

$$k_1 = f(t_n, y_n, \dot{y}_n)$$

$$k_2 = f(t_n + \tfrac{1}{2}h, y_n + \tfrac{h}{2}\dot{y}_n + \tfrac{h^2}{8}k_1, \dot{y}_n + \tfrac{h}{2}k_1)$$

$$k_3 = f(t_n + \tfrac{1}{2}h, y_n + \tfrac{h}{2}\dot{y}_n + \tfrac{h^2}{8}k_1, \dot{y}_n + \tfrac{h}{2}k_2)$$

$$k_4 = f(t_n + h, y_n + h\dot{y}_n + \tfrac{h^2}{2}k_3, \dot{y}_n + hk_3)$$

$$y_{n+1} = y_n + h\dot{y}_n + \frac{h^2}{6}(k_1 + k_2 + k_3)$$

$$\dot{y}_{n+1} = \dot{y}_n + \frac{h}{6}(k_1 + 2k_2 + 2k_3 + k_4)$$

Note that it is necessary to solve for the periodic rotor motion four times per integration step.

5.3.3 Flight dynamics analysis.

The flight dynamics analysis here consists of a calculation of the helicopter stability derivatives and an analysis of the resulting linear differential equations. As for the transient analysis it is assumed

that the body motion will be slow (compared to the rotor rotational speed), so the quasistatic rotor solution can be used. The assumption that the perturbation body motion has small magnitude is here consistent with the stability derivative representation of the rotor.

The equations of motion are the same as considered for the transient analysis (section 5.3.2). Here the rotor hub forces and the aircraft aerodynamic forces are expanded in terms of the stability derivatives. By making successive perturbations to the inputs for the rotor and aircraft analysis, the generalized forces can be expanded as follows:

$$\Delta\vec{Q} = a_2 \ddot{\vec{z}}_F + a_1 \begin{pmatrix} \phi_F \\ \theta_F \\ \psi_F \\ x_F \\ y_F \\ z_F \\ \psi_S \end{pmatrix}^{\bullet} + b_1 \begin{pmatrix} \theta^{con}_{rotor\#1} \\ \theta^{con}_{rotor\#2} \\ \delta_t \\ \delta_e \\ \delta_a \\ \delta_r \end{pmatrix}$$

$$+ b_G \begin{pmatrix} u_G \\ v_G \\ w_G \end{pmatrix} + b_f (f_n)$$

The coefficients of the matrices are the aircraft stability derivatives. There are contributions from each rotor from auxiliary forces, and from the wing/body, horizontal tail, and vertical tail. The airframe terms include the effects of the rotor-induced interference velocities. The result for ΔC_Q is similar (rotor contributions only). The gust velocity here is uniform throughout space.

The rotor speed governor, defined by the following control laws

$$\Delta\Theta_t = -K_{P_e}\dot{\Psi}_s - K_{I_e}\Psi_s$$
$$(\Delta\Theta_{govr})_1 = K_{P_1}\dot{\Psi}_s + K_{I_1}\Psi_s$$
$$(\Delta\Theta_{govr})_2 = K_{P_2}\dot{\Psi}_s + K_{I_2}\Psi_s$$

will be directly included in the stability derivatives. It is also necessary to account for the cyclic pitch perturbations due to the rotor azimuth perturbation:

$$\begin{pmatrix}\Delta\Theta_{1c}\\ \Delta\Theta_{1s}\end{pmatrix} = \Psi_s \begin{pmatrix}\Theta_{1s}\\ -\Theta_{1c}\end{pmatrix}_{trim}$$

For rotor #2 these cyclic pitch increments must be multiplied by Ω_2/Ω_1.

The result is a set of linear differential equations of the form

$$A_2\ddot{x} + A_1\dot{x} + A_0 x = B v + B_p v_p + B_G g$$

describing the flight dynamics of the aircraft. The state vector x consists of the rigid body and rotor speed degrees of freedom:

$$x = [\,\Phi_F\ \Theta_F\ \Psi_F\ x_F\ y_F\ z_F\ \Psi_s\,]^T$$

The control and gust vectors are defined as follows

$$v = [(\theta_0\ \theta_{1c}\ \theta_{1s})_{\text{rotor \#1}}\ (\theta_0\ \theta_{1c}\ \theta_{1s})_{\text{rotor \#2}}\ \delta_f\ \delta_e\ \delta_a\ \delta_r\ \theta_t\ (\delta_n)]^T$$

$$= T_c\, v_p$$

$$v_p = [\delta_0\ \delta_c\ \delta_s\ \delta_p\ \delta_t]^T$$

$$g = [u_G\ v_G\ w_G]^T$$

(the gust components are in wind axes). Optionally any of the degrees of freedom can be omitted from the analysis. From section 4.2.9, the equations for the airframe sensors are:

$$y = C_2 \ddot{q}_s + C_1 \dot{q}_s + C_0 q_s + D_0 g$$

where here q_s is just the rigid body motion of the airframe (in the state vector x).

Optionally the airframe rigid body motion can be transformed from fuselage (F) axes to stability (V) axes, by substituting

$$x_F = \begin{bmatrix} \mathcal{R}_{FV} & 0 \\ 0 & 1 \end{bmatrix} x_V$$

(see section 4.2.1), and multiplying the equations of motion by the transpose of the transform.

Using these equations, the helicopter flying qualities can be examined, in terms of the eigenvalues and eigenvectors. The transfer

function (pole-zero set or frequency respor.. or the transient response to a prescribed control or gust input can a:so be obtained. The transient response can be calculated by numerically integrating the equations

$$\ddot{x} = A_2^{-1} \left[-A_1 \dot{x} - A_0 x + B_p v_p + B_G g \right]$$

in a manner similar to the transient analysis (see section 5.3.2). In this case only a gust that is uniform throughout space can be considered.

The stability derivatives are obtained in body axes (the F system) relative to the aircraft center of gravity. There are contributions from each of the rotors, and the aircraft aerodynamic components (wing/body, horizontal tail, and vertical tail). The following notation is used for the stability derivatives.

Equation	Notation	Variable	Subscript
roll moment	$I_x^* L$	$\dot{\phi}_F$	p
pitch moment	$I_y^* M$	$\dot{\theta}_F$	q
yaw moment	$I_z^* N$	$\dot{\psi}_F$	r
longitudinal force	$M^* X$	$\dot{x}_F$	u
lateral force	$M^* Y$	$\dot{y}_F$	v
vertical force	$M^* Z$	$\dot{z}_F$	w
torque	$I_R^* Q$	$\dot{\psi}_S$	Ω

The aircraft inertias are introduced so that the coefficient of the highest time derivative in an equation is unity. The derivatives are defined with positive signs on the right-hand side of the equation of motion.

5.3.4 Transient gust and control.

Transient gust and control inputs are required when the equations of motion are integrated for the transient or flight dynamics analysis. The pilot's control increment $\Delta\vec{v}_p$ is required at time t. A simple form is

$$\Delta\vec{v}_p = \vec{v}_{po}\, C(t)$$

where $\vec{v}_{po}$ is a constant vector and C is a scaler function of time. More generally, the control input can be a function of the aircraft motion as well.

The gust velocity $\vec{g} = (u_G\ v_G\ w_G)^T$ (in wind axes) is required at the time t, at the location of both rotors and the airframe aerodynamic components. Consider a convected gust field, defined by a function $G(x_g, y_g, z_g)$. The gust coordinates have origin at the center of gravity when t = 0. The aircraft velocity in V_a, in the x (wind axis) direction. The gust field has velocity V_g in the negative x_g direction; the gust is coming from azimuth angle ψ_g relative to the aircraft (see Fig. 5-2). Hence given the position r (in wind axes), the location in the gust field is

$$\begin{pmatrix} x_g \\ y_g \\ z_g \end{pmatrix} = \begin{pmatrix} -x\cos\psi_g + y\sin\psi_g + (V_g - V_a\cos\psi_g)t \\ -x\sin\psi_g - y\cos\psi_g - (V_a\sin\psi_g)t \\ z \end{pmatrix}$$

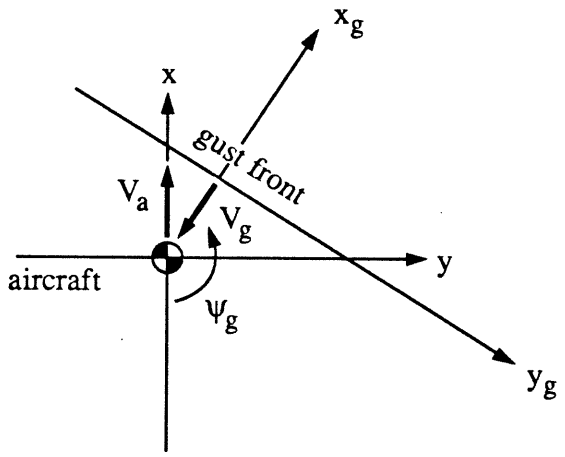

Figure 5.2. Convected gust description.

The position vector for the wing/body is

$$\vec{r} = R_{FV}^{T} \vec{r}_{WB}$$

with $\vec{r}_{WB}$ in the F frame, relative to the aircraft center of gravity; the position vectors for the horizontal tail, vertical tail, and rotor hub are obtained in a similar manner. The positions on the rotor disk are

$$\vec{r} = R_{FV}^{T} \left(\vec{r}_{hub} + R_{SF}^{T} \left(r \cos\Psi \, \vec{i}_s + r \sin\Psi \, \vec{j}_s \right) \right)$$

(neglecting the tilt of the tip-path plane relative to the hub; the sign of the $\vec{j}_s$ component is changed for a clockwise rotating rotor). A one-dimensional convected gust field is defined by

$$\vec{g} = \vec{g}_0 \, G(x_g)$$

Note that the gust is convected at the rate V_g relative to the aircraft if V_a is not used, and at a rate V_g relative to the fixed frame if V_a is used. With $V_g = 0$ the gust field is stationary (relative to the aircraft or the earth if V_a is not or is used).

Alternatively, a uniform gust field can be used, which is a function of time only. A simple form is

$$\vec{g} = \vec{g}_0 \, G(t)$$

where $\vec{g}_o$ is a constant vector and G is a scaler function of time.

For the control and gust amplitude factors, C and G, eight options are implemented:

(a) step response, $C = 1$

(b) impulse response, $C = 1/T$, $0 < t < T$

(c) cosine impulse, $C = \frac{1}{2}(1 - \cos 2\pi t/T)$, $0 < t < T$

(d) sine doublet, $C = \sin 2\pi t/T$, $0 < t < T$

(e) square impulse, $C = 1$, $0 < t < T$

(f) square doublet, $C = 1$ for $0 < t < T/2$, $C = -1$ for $T/2 < t < T$

(g) ramp response, $C = t$

(h) triangular impulse, $C = 2t/T$ for $0 < t \leq T/2$, $C = 2(1 - t/T)$ for $T/2 < t < T$

5.3.5 Calculation procedure.

The solution for the rotorcraft aerodynamics and dynamics proceeds as follows. The job begins with data input and initial calculations. Next the trim solution is obtained. Then the aeroelastic stability analysis, flight dynamics analysis, or transient analysis is performed as required.

In the trim analysis the controls are iterated until the required operating state is achieved. Since the nonuniform inflow influence coefficients depend on the rotor thrust (through the wake geometry) it is necessary to iterate between the influence coefficient calculation and the trimmed motion and forces calculation (unless the rotor thrust is specified as part of the definition of the required operating state). The trim analysis is performed first for uniform inflow, then for nonuniform inflow with a prescribed wake, and finally for nonuniform inflow with a free wake geometry. After obtaining the trim solution, the aircraft performance and loads can be calculated.

In the transient analysis, the rigid body equations of motion are numerically integrated. At each time step there is an iteration between the nonuniform inflow influence coefficient calculation, and the calculation of the rotor and airframe motion and forces.

In the flight dynamics analysis, the stability derivatives are calculated and the matrices are constructed that describe the linear differential equations of motion. At each motion or control increment in the stability derivative calculation there is an iteration between the influence coefficient calculation and the calculation of the motion and forces. Finally the system of linear differential equations is analyzed (optionally including a numerical integration as for the transient analysis).

In the flutter analysis the matrices are constructed that describe the linear differential equations of motion, and the constant coefficient or periodic coefficient equations are analyzed. Optionally the equations are reduced to just the aircraft rigid body degrees of freedom by assuming quasistatic response of the other degrees of freedom, and the equations are analyzed as for the flight dynamics task.

5.4 Self-Tuning Regulator

The rotorcraft model provides controls that can be used to optimize or change the system behavior: higher harmonic control; higher harmonic auxiliary forces; and airframe and rotor primary controls, and mean auxiliary forces (section 4.1.6). The analysis implements a self-tuning regulator to automatically adjust selected controls to minimize a cost function. The cost function is a weighted sum of the squares of selected rotor measurements. Typical uses of the regulator are multicyclic control of vibration or loads; and cyclic pitch feedback to control flapping. The regulator solution is iterative, and is obtained inside the trim iteration, and outside the circulation and motion iterations. The regulator can also be used as part of the quasistatic

rotor analysis of the flight dynamics and transient analyses, but is not considered for the flutter analysis.

The trim iteration adjusts selected pilot's controls to achieve a desired flight state. The pilot's controls are connected to the airframe and rotor primary controls, and the mean auxiliary forces, by a matrix that depends on the aircraft configuration (see section 4.1.6). Controls that are not being used by the trim iteration are available for use by the self-tuning regulator. The analysis does not check that the controls selected for trim and for the regulator are independent. Erroneous specification of the same control for both iterations would probably result in the trim solution not converging. Similarly, the controls perturbed to obtain stability derivatives in the flight dynamics analysis should be independent of the regulator controls.

A self-tuning regulator is a system that combines recursive parameter estimation with linear feedback. Specifically, control systems are considered that are characterized by:

(a) a linear, quasi-static, frequency-domain model of the rotor craft response to control;

(b) identification of the rotorcraft model by least-squared-error or Kalman-filter methods;

(c) a minimum variance or quadratic performance-function controller.

A complete derivation of the algorithms for several regulator configurations is given in reference 53. A typical but not completely general regulator configuration is used here. For the trim and flight dynamics analyses, the regulator is iterated until a converged solution is obtained. So the regulator algorithm represents a solution procedure, rather than an actual control system of the aircraft. For the transient analysis, the regulator is executed for a specified number of iterations per time step, and it would be appropriate to model the actual control system.

5.4.1 Rotorcraft model.

Consider a vector of measurements z, and a vector of controls θ. It is assumed that the number of measurements is equal to or greater than the number of controls. These parameters are selected from the output and input for the periodic solution of the rotor behavior in a steady-state flight condition (or quasi-steady, for the flight dynamics and transient analyses). The measurement and control variables are both in the frequency domain, hence are constant (or slowly varying) parameters that describes the periodic solution. The rotorcraft analysis represents a nonlinear algebraic relation between the input and output: $z = f(\theta)$. To develop the regulator algorithm, a local linearization of this relation is considered:

$$z_n = z_{n-1} + T(\theta_n - \theta_{n-1})$$

where the subscript refers to the regulator iteration. This is a linear, quasistatic, frequency-domain model of the measurement response to control changes.

The following quantities can be selected for the control vector θ:

(a) higher harmonic rotor control, in the rotating or nonrotating frame (section 2.2.21);

(b) higher harmonic auxiliary forces (section 4.1.5);

(c) airframe and rotor primary controls, and mean auxiliary forces (section 4.1.6).

Hence the control equation of section 4.1.6 becomes:

$$V = T_c v_p + v_o + v_{STR}$$

If there are two rotors, then the control parameter used can be that of rotor #1 or rotor #2; or can be symmetric or antisymmetric control (the same magnitude of control to each rotor, with same or opposite signs respectively).

The following quantities can be selected for the measurement vector z:

(a) rotor lateral or longitudinal flapping;

(b) rotor power;

(c) airframe sensor vibratory response (section 5.2.8);

(d) nonrotating frame hub loads (section 5.2.7);

(e) rotating frame blade root loads (sections 5.2.5, 5.2.6);

(f) blade section loads, rotating shaft axes or principal axes (sections 5.2.2, 5.2.3, 5.2.4);

(g) far field rotational noise (section 5.2.9).

If there are two rotors, then the measurement parameter used can be that of rotor #1 or rotor #2; or can be the symmetric or antisymmetric measurement (one-half the sum or difference respectively). For the power and airframe sensor vibratory response, the total from both rotors can be used. For each measurement it is necessary to identify the specific quantity being used (mean, half peak-to-peak, sine or cosine harmonic, etc.).

5.4.2 Feedback control.

The control equation is obtained by minimizing a quadratic cost function J:

$$J = (z_n - z_{targ})^T W_z (z_n - z_{targ}) + \Delta\theta_n^T W_{\Delta\theta} \Delta\theta_n$$

where z_{targ} is a target value of the measurements (often zero). The last term serves to limit the rate of change of the control, improving

stability without changing the converged value of the response. The weighting matrices W_z and $W_{\Delta\theta}$ will be diagonal here; note that these matrices must account for the different units of the measurements and controls. Substituting $z_n = z_{n-1} + T\Delta\theta_n$, the control that minimizes J is:

$$\theta_n - \theta_{n-1} = \Delta\theta_n = -C\left(z_{n-1} - z_{tan}\right)$$

which is linear feedback of the current measurement. The gain matrix C is:

$$C = \left(T^T W_z T + W_{\Delta\theta}\right)^{-1} T^T W_z \, f$$

(f is a relaxation factor, introduced to provide further improvement of the convergence by reducing the magnitude of the control applied).

Consider several special cases. If the number of measurements equals the number of controls (T is square), then:

$$C = T^{-1}\left(I + W_z^{-1} T^{-T} W_{\Delta\theta} T^{-1}\right)^{-1} f$$

which shows that $W_{\Delta\theta}$ and f produce similar effects. If $W_{\Delta\theta} = 0$, then:

$$C = \left(T^T W_z T\right)^{-1} T^T W_z \, f$$

which is a weighted generalized inverse (CT = I). If T is square and $W_{\Delta\theta} = 0$, then:

$$\theta_n = \theta_{n-1} - T^{-1}(z_{n-1} - z_{targ})$$

which is the Newton-Raphson solution (used for the trim iteration, see section 5.3.1).

The two tests for convergence of the regulator iteration are considered:

a) $\sqrt{J} < \epsilon$

b) $\sqrt{\Delta J} < \epsilon$

The first criterion (with ϵ a small number) is appropriate if J = 0 is achievable. It can also be used with ϵ representing a nonzero target value of J. The second criterion (ΔJ the difference between J for two successive regulator iterations, and ϵ a small number) is appropriate if the minimum achievable J is nonzero.

For the transient analysis, the regulator is executed for a specified number of iterations (M), with no test for convergence. The Runge-Kutta numerical integration requires four evaluations of the aircraft forces per time step, hence there will be 4*M regulator iterations per time step.

5.4.3 T-matrix identification.

The linear relation between the measurement and control changes must be known in order to construct the feedback gain. The T-matrix can

be obtained in several ways: prescribed input; perturbation identification; and recursive update.

For the perturbation identification, the elements of the control vector are successively perturbed from a starting point ($\Delta\theta_i$), and the corresponding measurement changes (Δz_i) obtained. These perturbations are combined into a single equation:

$$[\cdots \ \Delta z \ \cdots] = T\,[\cdots \ \Delta\theta \ \cdots]$$

or

$$Z = T\,\Theta$$

The weighted-least-squares solution for T is:

$$T = Z W \Theta^T (\Theta W \Theta^T)^{-1}$$

If Θ is square then:

$$T = Z\,\Theta^{-1}$$

Finally if Θ is also diagonal then:

$$T = \left[\cdots \quad \frac{\Delta z}{\Delta \theta_j} \quad \cdots \right]$$

which is the approach to be used here (as for the identification of the derivative matrix for trim, section 5.3.1).

A recursive weighted-least-squares method is obtained by adding one measurement (with weight $1/\alpha$) to the above solution:

$$T_n = \left(Z_{n-1} W_{n-1} \Theta_{n-1}^T + \Delta z_n \Delta \theta_n^T / \alpha \right) \left(\Theta_{n-1} W_{n-1} \Theta_{n-1}^T + \Delta \theta_n \Delta \theta_n^T / \alpha \right)^{-1}$$

Let

$$P_{n-1} = \left(\Theta_{n-1} W_{n-1} \Theta_{n-1}^T \right)^{-1}$$

$$M_n = P_{n-1} / \alpha$$

then

$$P_n = \left(M_n^{-1} + \Delta \theta_n \Delta \theta_n^T \right)^{-1}$$

$$= M_n - M_n \Delta \theta_n \Delta \theta_n^T M_n / (1 + \Delta \theta_n^T M_n \Delta \theta_n)$$

and so

$$k_n = P_n \Delta \theta_n$$

$$T_n = T_{n-1} + (\Delta z_n - T_{n-1} \Delta \theta_n) k_n^T$$

With $\alpha = 1$, a least-squares solution is obtained, in which every measurement has equal weight; hence eventually the recursive identification will turn itself off. With $\alpha < 1$, an exponential window solution is obtained, in which the ratio of the weight for a measurement to the weight for the next measurement is α; hence the most recent measurements always dominate the identification. Note also that the initial value of P is

$$P_0 = \left(\Theta W \Theta^T\right)^{-1} = \begin{bmatrix} \ddots & & \\ & \frac{1}{\Delta\theta^2} & \\ & & \ddots \end{bmatrix}$$

where $\Delta\theta$ is the control increment in the perturbation identification process.

A similar recursive algorithm is obtained using a Kalman filter, which provides a minimum error-variance estimate (see reference 53). Assume that the measurement equation is

$$\Delta z_n = T \Delta\theta_n + \text{noise}$$

with r_n the mean-square measurement noise; and that the T-matrix varies according to the equation

$$T_{n+1} = T_n + \text{noise}$$

with Q'_n the variance of the process noise. In practice, Q'_n may be considered simply a parameter that forces the estimate to be updated.

Let $\alpha = r_n/r_{n-1}$, and $Q_n = Q'_n$; so Q is the ratio of the process noise and measurement noise, with units of $1/\theta^2$. Then the Kalman filter algorithm is identical to that for the exponential window, except that

$$M_n = (P_{n-1} + Q_{n-1})/\alpha$$

Note that α and Q_n have similar effects (equivalent for $P/\alpha = P + Q$).

In summary, the recursive identification algorithm (either exponential window or Kalman-filter) is:

$$a = M_n \Delta\Theta_n = (P_{n-1} + Q_{n-1}) \Delta\Theta_n / \alpha$$

$$k_n = P_n \Delta\Theta_n = a/(1 + \Delta\theta_n^T a)$$

$$P_n = M_n - a\, a^T/(1 + \Delta\theta_n^T a)$$

$$= (P_{n-1} + Q_{n-1})/\alpha - a\, k_n^T$$

$$T_n = T_{n-1} + (\Delta z_n - T_{n-1} \Delta\Theta_n)\, k_n^T$$

with P_0 set after the perturbation identification.

The present analysis implements the following identification options.

(a) Initialize the T-matrix to input values (perhaps representing off-design conditions), or to zero.

(b) Perturbation identification as follows.

(i) Trim analysis: never (use the input T-matrix); at the beginning of trim; or at each trim iteration.

(ii) Flight dynamics analysis: never (use the T-matrix from trim); or at each stability derivative iteration.

(iii) Transient analysis: never (use the T-matrix from trim); or at the start of the transient.

The perturbation identification can be periodically repeated during the regulator iteration.

(c) Recursive identification used, or not.

6. AEROELASTIC STABILITY

The objective of the aeroelastic analysis is to derive a set of linear differential equations describing the perturbed motion of the helicopter from the trim flight condition. The stability of the system is defined by the eigenvalues of these equations. To construct the equations it is necessary to derive a perturbation form of the rotor and airframe model described in the previous sections, by linearizing the aerodynamic and inertial forces about the trim solution. For the most general case, the linear differential equations describing the helicopter motion have periodic coefficients, and must be analyzed by the methods of Floquet-Liapunov theory. With axial flow aerodynamics (and usually other restrictions if the rotor has two blades) the equations have constant coefficients, and the more powerful techniques for analyzing time-invariant systems are applicable. For low and moderate advance ratios, it is often possible to describe the helicopter dynamics by a set of constant coefficient differential equations that represent an adequate approximation to the true dynamics for many applications. The present analysis can treat all three cases: periodic coefficient equations, constant coefficient equations in axial flow, and a constant coefficient approximation.

6.1 Rotor Model

The differential equations of motion for the rotor blade have been derived in section 2.2.18. Here it is necessary to linearize the inertial and aerodynamic forces in these equations.

6.1.1 Rotor degrees of freedom.

The rotor blade motion is described by coupled flap/lag bending, rigid pitch and elastic torsion, and optionally the gimbal pitch and roll motion (or teeter motion for the two-bladed rotor case). The blade

degrees of freedom are written as the sum of trim terms and perturbation terms. The trim solution is described in section 5.1; the perturbation motions are the degrees of freedom for the aeroelastic analysis. In particular, the generalized coordinate of the ith blade bending mode is written

$$q_i = q_{i_{trim}} + \delta q_i$$

or for the bending deflection

$$(z_o\vec{i} - x_o\vec{k}) = (z_o\vec{i} - x_o\vec{k})_{trim} + \sum_{i=1}^{\infty} \delta q_i \vec{\eta}_i$$

After substituting for q_i, the delta notation indicating the perturbed motion can be omitted.

The rotor equations of motion have been obtained in the rotating frame, with degrees of freedom describing the motion of each blade separately. In fact, however, the rotor responds as a whole to excitation from the nonrotating frame -- shaft motion, aerodynamic gusts, or control inputs. It is desirable to work with degrees of freedom that reflect this behavior. Such a representation of the rotor motion simplifies both the analysis and the understanding of the behavior.

The appropriate transformation to obtain the degrees of freedom and equations of motion in the nonrotating frame is of the Fourier type. There are many similarities between this coordinate change and Fourier series, discrete Fourier transforms, and Fourier interpolation; the common factor is the periodic nature of the system. A Fourier series representation of the blade motion is appropriate for dealing with the

steady-state solution (section 5.1.1). Here we are considering the general dynamic behavior, including transient motions; hence the Fourier coordinate transformation is required. This coordinate transformation has been widely used in the classical literature, although often with only a heuristic basis. For example, it has been used in ground resonance analyses to represent the rotor lag motion (ref. 54) and in helicopter stability and control analyses for the rotor flap motion (ref. 55). More recently, there have been applications of the Fourier coordinate transformation with a sounder mathematical basis (e.g., ref. 56).

Consider a rotor with N blades equally spaced around the azimuth, at $\psi_m = \psi + m\Delta\psi$ (where $\Delta\psi = 2\pi/N$ and the blade index m ranges from 1 to N). Hence $\psi = \Omega t$ is the dimensionless time variable. Let $q^{(m)}$ be the degree of freedom in the rotating frame for the mth blade, m = 1 to N. The Fourier coordinate transformation is a linear transform of the degrees of freedom from the rotating to the nonrotating frame. Thus the following new degrees of freedom are introduced:

$$\beta_0 = \frac{1}{2} \sum_{m=1}^{N} q^{(m)}$$

$$\beta_{nc} = \frac{2}{N} \sum_{m=1}^{N} q^{(m)} \cos n\psi_m$$

$$\beta_{ns} = \frac{2}{N} \sum_{m=1}^{N} q^{(m)} \sin n\psi_m$$

$$\beta_{N/2} = \frac{1}{N} \sum_{m=1}^{N} q^{(m)} (-1)^m$$

Here β_0 is a collective mode, β_{1C} and β_{1S} are cyclic modes, and $\beta_{N/2}$ is the reactionless mode. For example, for the rotor flap motion, β_0 is

the coning degree of freedom, which β_{1C} and β_{1S} are the tip-path plane tilt degrees of freedom. The inverse transformation is

$$q^{(m)} = \beta_0 + \sum_n \left(\beta_{nc} \cos n\psi_m + \beta_{ns} \sin n\psi_m \right) + \beta_{\frac{N}{2}} (-1)^m$$

which gives the motion of the individual blades again. The summation over n goes from 1 to (N-1)/2 for N odd and from 1 to (N-2)/2 for N is even. The corresponding transformation for the velocity and acceleration are

$$\dot{q}^{(m)} = \dot{\beta}_0 + \sum_n \left[\left(\dot{\beta}_{nc} + n\beta_{ns} \right) \cos n\psi_m + \left(\dot{\beta}_{ns} - n\beta_{nc} \right) \sin n\psi_m \right] + \dot{\beta}_{\frac{N}{2}} (-1)^m$$

$$\ddot{q}^{(m)} = \ddot{\beta}_0 + \sum_n \left[\left(\ddot{\beta}_{nc} + 2n\beta_{ns} - n^2\beta_{nc} \right) \cos n\psi_m + \left(\ddot{\beta}_{ns} - 2n\beta_{nc} - n^2\beta_{ns} \right) \sin n\psi_m \right] + \ddot{\beta}_{\frac{N}{2}} (-1)^m$$

Note that transformation to the nonrotating frame introduces Coriolis and centrifugal terms.

The variables β_0, β_{nc}, β_{ns}, $\beta_{N/2}$ are degrees of freedom, that is, functions of time, just as the variables $q^{(m)}$ are. These degrees of freedom describe the rotor motion as a whole, in the nonrotating frame, while $q^{(m)}$ described the motion of an individual blade in the rotating frame. Thus we have a linear, reversible transformation between the N degrees of freedom $q^{(m)}$ in the rotating frame (m = 1, ..., N) and the N degrees of freedom (β_0, β_{nc}, β_{ns}, $\beta_{N/2}$) in the nonrotating frame. Compare this coordinate transformation with a Fourier series

representation of the steady-state solution. In that case, $q^{(m)}$ is a periodic function of ψ_m, so the motions of all the blades are identical. It follows that the motion in the rotating frame may be represented by a Fourier series, the coefficients of which are steady in time but infinite in number. Thus there are similarities between the Fourier coordinate transformation and the Fourier series, but they are by no means identical.

This coordinate transform must be accompanied by a conversion of the equations of motion for $q^{(m)}$ from the rotating to the nonrotating frame. This conversion is accomplished by operating on the equations of motion with the following summation operations:

$$\frac{1}{N}\sum_m (\cdots) \quad \frac{2}{N}\sum_m (\cdots)\cos n\psi_m \quad \frac{2}{N}\sum_m (\cdots)\sin n\psi_m \quad \frac{1}{N}\sum_m (\cdots)(-1)^m$$

The result is equations for the β_0, β_{nc}, β_{ns}, and $\beta_{N/2}$ degrees of freedom, respectively. Note that these are the same operations as are involved in transforming the degrees of freedom from the rotating to the nonrotating frame. Since the operators are linear, constants may be factored out. Thus with constant coefficients in the equations of motion, the operators act only on the degrees of freedom. By making use of the definition of the degrees of freedom in the nonrotating frame, and the corresponding results for the time derivatives, the conversion of the equations of motion is then straightforward. Complexities arise when it is necessary to consider periodic coefficients, such as due to the aerodynamics of the rotor in nonaxial flow.

The total force and moment on the hub have been obtained by summing the contributions from the individual blades. The result is operators exactly of the form above, for obtaining the total hub reaction in the nonrotating frame from the root reaction of the individual blades in the rotating frame. The origin of the summation operation is clear, and the

$\sin\psi_m$ or $\cos\psi_m$ factors arise when the rotating forces are resolved into the nonrotating frame. In fact, the equation conversion operators in general may be viewed as simply resolving the moments on the individual blades into the nonrotating frame.

The Fourier coordinate transformation is often associated in rotor dynamics with the generalized Floquet analysis. The latter is a stability analysis for linear differential equations with periodic coefficients. Indeed, there is a fundamental link between these topics because both are associated with the rotation of the system. They are, however, truly separate subjects -- either can be required in the rotor analysis without the other. For example, a rotor in axial flow on a flexible support (or with some other relation to the nonrotating frame) requires the Fourier coordinate transformation to represent the blade motion, but is then a constant coefficient system. Alternatively, for the shaft-fixed dynamics of a rotor in forward flight, a single-blade representation in the rotating frame is appropriate, but there are periodic coefficients due to the forward flight aerodynamics which require the Floquet analysis to determine the system stability.

For the present investigation, the degrees of freedom to be transformed to the nonrotating frame are blade bending, blade pitch, and gimbal motion. The nomenclature for the corresponding degrees of freedom in the rotating and nonrotating frames are as follows:

	rotating	nonrotating
bending	$q_i^{(m)}$	$\beta_0^{(i)}$ $\beta_{nc}^{(i)}$ $\beta_{ns}^{(i)}$ $\beta_{N/2}^{(i)}$
torsion	$p_i^{(m)}$	$\theta_0^{(i)}$ $\theta_{nc}^{(i)}$ $\theta_{ns}^{(i)}$ $\theta_{N/2}^{(i)}$
gimbal	β_G θ_G	β_{Gc} β_{Gs}

The notation $\beta^{(i)}$ is used for the ith bending mode in the nonrotating frame. With the modes ordered according to frequency, $\beta^{(1)}$ is thus

usually the fundamental lag mode, and $\beta^{(2)}$ the fundamental flap mode. Similarly, $\theta^{(i)}$ is the ith torsion mode, with $\theta^{(0)}$ rigid pitch and the remaining modes elastic torsion. The collective and cyclic modes (0, 1C, 1S) are particularly important because of their fundamental role in the coupled motion of the rotor and the nonrotating system. When the transformation of the equations and degrees of freedom is accomplished, for axial flow there is a complete decoupling of the variables into the following sets:

(a) the collective and cyclic (0, 1C, 1S) rotor degrees of freedom together with the gimbal tilt and rotor speed degrees of freedom and the rotor shaft motion;

(b) the 2C, 2S, ..., nc, ns, and N/2 rotor degrees of freedom (as present).

Thus the rotor motion in the first set is coupled with the fixed system, while the second set consists of purely internal rotor motion. Nonaxial flow couples, to some extent, all the rotor degrees of freedom and the fixed system variables, primarily due to the aerodynamic terms; still the above separation of the degrees of freedom remains a dominant feature of the rotor dynamic behavior.

For a two-bladed rotor, the blade bending degrees of freedom are coning and teetering type modes:

$$\beta_0 = \frac{1}{2} \sum_{m=1}^{2} q^{(m)} = \frac{1}{2} \left(q^{(2)} + q^{(1)} \right)$$

$$\beta_1 = \frac{1}{2} \sum_{m=1}^{2} q^{(m)} = \frac{1}{2} \left(q^{(2)} - q^{(1)} \right)$$

The pitch/torsion degrees of freedom θ_0 and θ_1 are similarly defined. The teetering degree of freedom β_T is also included for the two-bladed rotor (in place of the gimbal degrees of freedom). The teetering motion is defined in the rotating frame, hence

$$\beta_G = \beta_T (-1)^m$$
$$\vartheta_G = 0$$

The special characteristics of the two-bladed rotor dynamics are reflected in the appearance of the teetering-type degrees of freedom (β_1, θ_1, and β_T), rather than the cyclic motions (1C and 1S) as for $N \geq 3$. The coning and teetering equations of motion are obtained by applying to the rotating frame equations the following operators:

$$\frac{1}{2} \sum_m (\ldots) \qquad \frac{1}{2} \sum_m (\ldots)(-1)^m$$

6.1.2 Rotor equations and hub reactions.

The equations of motion for the coupled flap/lag bending and for elastic torsion/rigid pitch motion of the blade in the rotating frame (section 2.2.18) are linearized for the aeroelastic analysis. The result is:

$$I^*_{q_k} (\ddot{q}_k + g_s \nu_k \dot{q}_k + \nu_k^2 q_k) + 2 \sum_i I^*_{q_k q_i} \dot{q}_i - \sum_i S^*_{q_k \ddot{p}_i} \ddot{p}_i - \sum_i S^*_{q_k p_i} p_i$$

$$+ I^*_{q_k\alpha} \cdot \vec{k}_B (\ddot{\psi}_S + \ddot{\alpha}_Z) + I^*_{q_k\alpha} \cdot \vec{\iota}_B (\ddot{\beta}_G + \beta_G)$$
$$+ 2 I^*_{q_k\dot{\psi}} (\dot{\psi}_S + \dot{\alpha}_Z) - I^*_{q_k\beta} (\ddot{\theta}_G - \theta_G + 2\dot{\beta}_G)$$
$$+ S^*_{q_k} \cdot \vec{\iota}_B \ddot{z}_h - S^*_{q_k} \cdot \vec{k}_B (\ddot{x}_h \sin\psi_m - \ddot{y}_h \cos\psi_m)$$
$$+ I^*_{q_k\alpha} \cdot \vec{\iota}_B ((\ddot{\alpha}_x + 2\dot{\alpha}_y)\sin\psi_m - (\ddot{\alpha}_y - 2\dot{\alpha}_x)\cos\psi_m)$$
$$= \gamma \frac{M_{q_k aero}}{ac}$$

$$I^*_{p_k} (\ddot{p}_k + g_s \mu_k \dot{p}_k + \omega_k^2 p_k)$$
$$+ \sum_i I^*_{p_k \ddot{p}_i} \ddot{p}_i + \sum_i I^*_{p_k p_i} p_i$$
$$- \sum_i S^*_{p_k \ddot{q}_i} \ddot{q}_i - \sum_i S^*_{p_k q_i} q_i$$
$$+ I^*_{p_k\alpha} \cdot \vec{\iota}_B (\ddot{\psi}_S + \ddot{\alpha}_Z) - I^*_{p_k\alpha} \cdot \vec{k}_B (\ddot{\beta}_G + \beta_G)$$
$$- S^*_{p_k} \cdot \vec{k}_B \ddot{z}_h - S^*_{p_k} \cdot \vec{\iota}_B (\ddot{x}_h \sin\psi_m - \ddot{y}_h \cos\psi_m)$$
$$- I^*_{p_k\alpha} \cdot \vec{k}_B ((\ddot{\alpha}_x + 2\dot{\alpha}_y)\sin\psi_m - (\ddot{\alpha}_y - 2\dot{\alpha}_x)\cos\psi_m)$$
$$= \gamma \frac{M_{p_k aero}}{ac} + S^*_{p_k \Omega} p_\Omega$$

where

$$p_r = \theta_{1c}\cos\psi_m + \theta_{1s}\sin\psi_m + \Delta\theta_{gov} + \Delta\theta_{\substack{mast\\bend}}$$
$$- \sum K_{p_i} q_i - K_{p_G}\beta_G + (\theta_{1s}\cos\psi_m - \theta_{1c}\sin\psi_m)\psi_s$$

The inertia constants are defined in section 6.1.3. Only linear lag damping has been considered here, and for convenience the lag damper term is included in the coefficient $I_{q_k\dot{q}_i}{}^*$. Introducing the Fourier coordinate transformation for the blade degrees of freedom, the rotor hub forces and moments derived in section 2.2.18 become:

$$\gamma\frac{2C_H}{\sigma a} = \gamma\left(\frac{2C_H}{\sigma a}\right)_{aero} - 2M_b^*\ddot{x}_h + \sum_i S_{q_i}^*\cdot\vec{k}_B\,\ddot{\beta}_{1s}^{(i)}$$

$$\gamma\frac{2C_Y}{\sigma a} = \gamma\left(\frac{2C_Y}{\sigma a}\right)_{aero} - 2M_b^*\ddot{y}_h - \sum_i S_{q_i}^*\cdot\vec{k}_B\,\ddot{\beta}_{1c}^{(i)}$$

$$\gamma\frac{2C_T}{\sigma a} = \gamma\left(\frac{2C_T}{\sigma a}\right)_{aero} - 2M_b^*\ddot{z}_h - \sum_i S_{q_i}^*\cdot\vec{i}_B\,\ddot{\beta}_0^{(i)}$$

$$\gamma\frac{2C_{Mx}}{\sigma a} = \gamma\left(\frac{2C_{Mx}}{\sigma a}\right)_{aero} - I_0^*(\ddot{\alpha}_x + 2\dot{\alpha}_y) - I_0^*(\ddot{\beta}_{GS} - 2\dot{\beta}_{GC})$$
$$- \sum_i I_{q_i a}^*\cdot\vec{i}_B\,(\ddot{\beta}_{1s}^{(i)} - 2\dot{\beta}_{1c}^{(i)})$$
$$+ \sum_i S_{q_0\ddot{p}_i}^*\cdot\vec{i}_B\,(\ddot{\theta}_{1s}^{(i)} - 2\dot{\theta}_{1c}^{(i)})$$
$$- \sum_i 2I_{q_0\dot{q}_i}^*\cdot\vec{i}_B\,(\dot{\beta}_{1s}^{(i)} - \beta_{1c}^{(i)})$$

$$\gamma \frac{2C_{My}}{\sigma a} = \gamma \left(\frac{2C_{My}}{\sigma a}\right)_{aero} - I_o^* (\ddot{\alpha}_y - 2\dot{\alpha}_x) + I_o^* (\ddot{\beta}_{Gc} + 2\dot{\beta}_{Gs})$$
$$+ \sum_i I^*_{q_i\alpha} \cdot \vec{i}_B \left(\ddot{\beta}_{1c}^{(i)} + 2\dot{\beta}_{1s}^{(i)}\right)$$
$$- \sum_i S^*_{q_o p_i} \ddot{\vec{i}}_B \left(\ddot{\theta}_{1c}^{(i)} + 2\dot{\theta}_{1s}^{(i)}\right)$$
$$+ \sum_i 2 I^*_{q_o q_i} \cdot \dot{\vec{i}}_B \left(\dot{\beta}_{1c}^{(i)} + \beta_{1s}^{(i)}\right)$$

$$\gamma \frac{2C_Q}{\sigma a} = \gamma \left(\frac{2C_Q}{\sigma a}\right)_{aero} + 2 I_o^* (\ddot{\psi}_s + \ddot{\alpha}_z)$$
$$+ 2 \sum_i I^*_{q_i\alpha} \cdot \vec{k}_B \ddot{\beta}_o^{(i)}$$
$$- 2 \sum_i S^*_{q_o p_i} \cdot \vec{k}_B \ddot{\theta}_o^{(i)}$$
$$+ 2 \sum_i 2 I^*_{q_o q_i} \cdot \vec{k}_B \dot{\beta}_o^{(i)}$$

The equations of motion for gimbal tilt and roll, or for the teeter motion of a two-bladed rotor, are obtained from

$$\gamma \frac{2C_{My}}{\sigma a} + I_o^* C^*_{Gc} \dot{\beta}_{Gc} + I_o^* (\nu^2_{Gc} - 1) \beta_{Gc} = 0$$
$$- \gamma \frac{2C_{Mx}}{\sigma a} + I_o^* C^*_{Gs} \dot{\beta}_{Gs} + I_o^* (\nu^2_{Gs} - 1) \beta_{Gs} = 0$$

or

$$- \gamma \frac{C_{MT}}{\sigma a} + I_o^* C^*_T \dot{\beta}_T + I_o^* (\nu^2_T - 1) \beta_T = 0$$

where

$$\gamma \frac{C_{M_T}}{\sigma a} = \frac{1}{2} \sum_{m=1}^{2} (-1)^m \gamma \frac{C_{mx}}{\sigma a}$$

$$= \gamma \left(\frac{C_{M_T}}{\sigma a}\right)_{zero}$$
$$- I_0^* \left((\ddot{\alpha}_x + 2\dot{\alpha}_y) \sin\Psi - (\ddot{\alpha}_y - 2\dot{\alpha}_x) \cos\Psi \right)$$
$$- I_0^* \left(\ddot{\beta}_T + \beta_T \right)$$
$$- \sum_i I_{q_i\alpha}^* \cdot \vec{r}_B \left(\ddot{\beta}_1^{(i)} + \beta_1^{(i)} \right)$$
$$+ \sum_i S_{q_i\beta}^* \cdot \vec{r}_B \left(\ddot{\theta}_1^{(i)} + \theta_1^{(i)} \right)$$
$$- 2 \sum_i I_{q_i\dot{q}_i}^* \cdot \vec{r}_B \dot{\beta}_1^{(i)}$$

(section 2.2.18). Also, for a two-bladed rotor, the hub reactions take a somewhat different form:

$$\gamma \frac{2C_H}{\sigma a} = \gamma \left(\frac{2C_H}{\sigma a}\right)_{zero} - 2M_b^* \ddot{x}_h$$
$$+ \sum_i S_{q_i}^* \cdot \vec{r}_B \left(2\sin\Psi \ddot{\beta}_1^{(i)} + 4\cos\Psi \dot{\beta}_1^{(i)} - 2\sin\Psi \beta_1^{(i)} \right)$$

$$\gamma \frac{2C_Y}{\sigma a} = \gamma \left(\frac{2C_Y}{\sigma a}\right)_{zero} - 2M_b^* \ddot{y}_h$$
$$- \sum_i S_{q_i}^* \cdot \vec{r}_B \left(2\cos\Psi \ddot{\beta}_1^{(i)} - 4\sin\Psi \dot{\beta}_1^{(i)} - 2\cos\Psi \beta_1^{(i)} \right)$$

$$\gamma \frac{2C_{Mx}}{\sigma a} = 2 \sin\Psi \left(\gamma \frac{C_{MT}}{\sigma a} \right)$$

$$\gamma \frac{2C_{My}}{\sigma a} = -2 \cos\Psi \left(\gamma \frac{C_{MT}}{\sigma a} \right)$$

The aerodynamic forces required are

$$\frac{2C_H}{\sigma a} = \frac{N}{2} \sum_m \left(\sin\Psi_m \int_0^1 \frac{F_x}{ac} dr + \cos\Psi_m \int_0^1 \frac{\tilde{F}_r}{ac} dr \right)$$

$$\frac{2C_Y}{\sigma a} = \frac{N}{2} \sum_m \left(-\cos\Psi_m \int_0^1 \frac{F_x}{ac} dr + \sin\Psi_m \int_0^1 \frac{\tilde{F}_r}{ac} dr \right)$$

$$\frac{C_T}{\sigma a} = \frac{1}{2} \sum_m \int_0^1 \frac{F_z}{ac} dr$$

$$\frac{2C_{Mx}}{\sigma a} = \frac{N}{2} \sum_m \sin\Psi_m \int_0^1 \frac{F_z}{ac} r\, dr$$

$$\frac{2C_{My}}{\sigma a} = \frac{N}{2} \sum_m (-\cos\Psi_m) \int_0^1 \frac{F_z}{ac} r\, dr$$

$$\frac{C_Q}{\sigma a} = \frac{1}{2} \sum_m \int_0^1 \frac{F_x}{ac} dr$$

$$\frac{M_{q_k}^{aero}}{ac} = \int_0^1 \vec{r}_k \cdot \left(\frac{F_z}{ac} \vec{k}_B - \frac{F_x}{ac} \vec{i}_B \right) dr$$

$$\frac{M_{pk}^{aero}}{ac} = \int_{r_{FA}}^{1} \xi_k \frac{M_a}{ac} - \int_{r_{FA}}^{1} \left(\frac{f_x}{ac} \vec{i}_B + \frac{f_z}{ac} \vec{k}_B \right) \cdot \vec{\chi}_{Ak} \, dr$$

and

$$\frac{C_{M_T}}{ra} = \frac{1}{N} \sum_m (-1)^m \int_0^1 \frac{f_z}{ac} r \, dr$$

6.1.3 Inertial constants.

The inertial constants for these linearized equations of motion are obtained from the constants defined in section 2.2.19 as follows:

$$(I^*_{q_k})_{\substack{lin \\ eqs}} = I^*_{q_k}$$

$$(I^*_{q_k \dot{q}_i})_{\substack{lin \\ eqs}} = I^*_{q_k \dot{q}_i} + \sum_j I^*_{q_k \dot{q}_i q_j} q_{j_{trim}} + \frac{1}{2} g_{earg} \vec{k}_B \cdot \vec{\gamma}'_k(e) \vec{k}_B \cdot \vec{\gamma}'_i(e)$$

$$(S^*_{q_k \ddot{p}_i})_{\substack{lin \\ eqs}} = S^*_{q_k \ddot{p}_i} + \sum_j S^*_{q_k \ddot{p}_i q_j} q_{j_{trim}}$$

$$(S^*_{q_k p_i})_{\substack{lin \\ eqs}} = S^*_{q_k p_i} + \sum_j S^*_{q_k p_i q_j} q_{j_{trim}}$$

$$(I^*_{q_k \alpha})_{\substack{lin \\ eqs}} = I^*_{q_k \alpha}$$

$$(I^*_{q_k \dot{\psi}})_{\substack{lin \\ eqs}} = I^*_{q_k \dot{\psi}} + \sum_j I^*_{q_k \dot{\psi} q_j} q_{j_{trim}}$$

$$(I^*_{q_k \dot{\beta}})_{\substack{lin \\ eqs}} = I^*_{q_k \dot{\beta}} + \sum_j I^*_{q_k \dot{\beta} q_j} q_{j_{trim}}$$

$$(S^*_{q_k})_{\substack{lin\\eqs}} = S^*_{q_k}$$

$$(I^*_{p_k})_{\substack{lin\\eqs}} = I^*_{p_k}$$

$$(I^*_{p_k \ddot{p}_i})_{\substack{lin\\eqs}} = I^*_{p_k \ddot{p}_i}$$

$$(I^*_{p_k p_i})_{\substack{lin\\eqs}} = I^*_{p_k p_i}$$

$$(S^*_{p_k \ddot{q}_i})_{\substack{lin\\eqs}} = S^*_{p_k \ddot{q}_i} + \sum_j S^*_{p_k \ddot{q}_i q_j} q_{j\,trim}$$

$$(S^*_{p_k q_i})_{\substack{lin\\eqs}} = S^*_{p_k q_i} + \sum_j \left(S^*_{p_k q_i q_j} + S^*_{p_k q_j q_i}\right) q_{j\,trim}$$

$$(I^*_{p_k \alpha})_{\substack{lin\\eqs}} = I^*_{p_k \alpha} + \sum_j I^*_{p_k \alpha q_j} q_{j\,trim}$$

$$(S^*_{p_k})_{\substack{lin\\eqs}} = S^*_{p_k} + \sum_j S^*_{p_k q_j} q_{j\,trim}$$

$$(M^*_b)_{\substack{lin\\eqs}} = M^*_b$$

$$(I^*_o)_{\substack{lin\\eqs}} = I^*_o$$

$$(S^*_{q_o \ddot{p}_i})_{\substack{lin\\eqs}} = S^*_{q_o \ddot{p}_i} + \sum_j S^*_{q_o \ddot{p}_i q_j} q_{j\,trim}$$

$$(I^*_{q_o \dot{q}_i})_{\substack{lin\\eqs}} = I^*_{q_o \dot{q}_i} + \sum_j I^*_{q_o \dot{q}_i q_j} q_{j\,trim}$$

$$(S_{p_k o})_{\substack{lin\\eqs}} = I^*_{p_o} \omega_o^2 \xi_k(r_{FA})$$

6.1.4 Aerodynamic forces

The aerodynamic forces are defined in terms of integrals of the section forces over the blade span. A linearized form of the aerodynamic forces is obtained as follows: the velocity and blade pitch are written as a trim term plus a perturbation term; the angle of attack and Mach number perturbations are defined in terms of the velocity perturbations; and the derivatives of the section aerodynamic coefficients with respect to angle of attack and Mach number are evaluated (by making finite increments in α and M). Hence the section loading is expressed in terms of the perturbation of the pitch and velocity components are linear functions of the rotor degrees of freedom, shaft motion, and gust velocity, with the coefficients depending on the rotor mean velocity and the blade azimuth angle. A perturbation induced velocity is included in the normal velocity u_p, for use with a dynamic inflow model. Combining the expansion for the section loads in terms of the velocity perturbations, and the velocity in terms of the motion of the rotor, the linearized form of the integrated aerodynamic forces is obtained. The aerodynamic coefficients are constant in axial flow, but for nonaxial flow they are periodic functions of ψ_m.

The blade section forces and pitch moment as derived in section 2.4.1 are:

$$\frac{F_z}{ac} = U\left(u_T \frac{c_l}{2a} - u_P \frac{c_d}{2a}\right)\frac{c}{c_m}$$

$$\frac{F_x}{ac} = U\left(u_P \frac{c_l}{2a} + u_T \frac{c_d}{2a}\right)\frac{c}{c_m}$$

$$\frac{F_r}{ac} = \left(U u_R \frac{c_d}{2a}\right)\frac{c}{c_m}$$

$$\frac{M_a}{ac} = \left(-x_A U^2 \frac{c_l}{2a} + U^2 c \frac{c_m}{2a} + \frac{M_{us}}{ac}\right)\frac{c}{c_m}$$

Each component of the velocity seen by the blade has a trim term and a small perturbation term, so we write

$$\theta \Rightarrow \theta + \delta\theta$$

$$u_T \Rightarrow u_T + \delta u_T$$

$$u_P \Rightarrow u_P + \delta u_P$$

$$u_R \Rightarrow u_R + \delta u_R$$

It follows that the perturbation of angle of attack, resultant velocity, and Mach number are:

$$\delta\alpha = \delta\theta - (u_T \delta u_P - u_P \delta u_T)/U^2$$

$$\delta M = M_{mp}\, \delta U$$

$$\delta U = (u_T \delta u_T + u_P \delta u_P)/U$$

and the perturbations of the aerodynamic coefficients are

$$\delta c_\ell = \frac{\partial c_\ell}{\partial \alpha}\delta\alpha + \frac{\partial c_\ell}{\partial M}\delta M = c_{\ell_\alpha}\delta\alpha + c_{\ell_M}\delta M$$

with similar results for c_m and c_d. The perturbations of the section aerodynamic forces may then be obtained by carrying out the differential operation on the expressions for F_z, F_x, F_r, and M_a, using the above results to express the perturbations in terms of $\delta\theta$, δu_T, δu_P, and δu_R. The coefficients of the perturbation quantities are evaluated at the trim state. The results for the perturbation forces are:

$$\delta\frac{F_z}{ac} = \left(U u_T \frac{c_{\ell_\alpha}}{2a} - U u_P \frac{c_{d_\alpha}}{2a}\right)\frac{c}{c_m}\delta\theta$$

$$+\left[-\frac{u_T}{U}\left(u_T \frac{c_{\ell_\alpha}}{2a} - u_P \frac{c_{d_\alpha}}{2a}\right) + \left(\frac{c_\ell}{2a} + M\frac{c_{\ell_M}}{2a}\right)\frac{u_T u_P}{U}\right.$$

$$\left. - \left(\frac{c_d}{2a} + M\frac{c_{d_M}}{2a}\right)\frac{u_P^2}{U} - \frac{c_d}{2a}U\right]\frac{c}{c_m}\delta u_P$$

$$+\left[\frac{u_P}{U}\left(u_T \frac{c_{\ell_\alpha}}{2a} - u_P \frac{c_{d_\alpha}}{2a}\right) + \left(\frac{c_\ell}{2a} + M\frac{c_{\ell_M}}{2a}\right)\frac{u_T^2}{U}\right.$$

$$\left. + \frac{c_\ell}{2a}U - \left(\frac{c_d}{2a} + M\frac{c_{d_M}}{2a}\right)\frac{u_T u_P}{U}\right]\frac{c}{c_m}\delta u_T$$

$$= F_{z_\theta}\delta\theta + F_{z_P}\delta u_P + F_{z_T}\delta u_T$$

$$\delta\frac{F_x}{ac} = \left(U u_P \frac{C_{L\alpha}}{2a} + U u_T \frac{C_{d\alpha}}{2a}\right)\frac{c}{c_m}\delta\theta$$

$$+\left[-\frac{u_T}{U}\left(u_P\frac{C_{L\alpha}}{2a}+u_T\frac{C_{d\alpha}}{2a}\right)+\left(\frac{C_L}{2a}+M\frac{C_{LM}}{2a}\right)\frac{u_P^2}{U}\right.$$

$$\left.+\frac{C_L}{2a}U+\left(\frac{C_d}{2a}+M\frac{C_{dM}}{2a}\right)\frac{u_T u_P}{U^2}\right]\frac{c}{c_m}\delta u_P$$

$$+\left[\frac{u_P}{U}\left(u_P\frac{C_{L\alpha}}{2a}+u_T\frac{C_{d\alpha}}{2a}\right)+\left(\frac{C_L}{2a}+M\frac{C_{LM}}{2a}\right)\frac{u_P u_T}{U}\right.$$

$$\left.+\left(\frac{C_d}{2a}+M\frac{C_{dM}}{2a}\right)\frac{u_T^2}{U}+\frac{C_d}{2a}U\right]\frac{c}{c_m}\delta u_T$$

$$= F_{x_\theta}\delta\theta + F_{x_P}\delta u_P + F_{x_T}\delta u_T$$

$$\delta\frac{M_a}{ac} = \left[U^2\left(-x_A\frac{C_{L\alpha}}{2a}+c\frac{C_{m\alpha}}{2a}\right)\right]\frac{c}{c_m}\delta\theta$$

$$+\left[u_P\left(-x_A\frac{C_{L\alpha}}{2a}+c\frac{C_{m\alpha}}{2a}\right)-x_A u_T\left(2\frac{C_L}{2a}+M\frac{C_{LM}}{2a}\right)\right.$$

$$\left.+cu_T\left(2\frac{C_m}{2a}+M\frac{C_{mM}}{2a}\right)\right]\frac{c}{c_m}\delta u_P$$

$$+\left[-u_T\left(-x_A\frac{C_{L\alpha}}{2a}+c\frac{C_{m\alpha}}{2a}\right)-x_A u_P\left(2\frac{C_L}{2a}+M\frac{C_{LM}}{2a}\right)\right.$$

$$\left.+cu_P\left(2\frac{C_m}{2a}+M\frac{C_{mM}}{2a}\right)\right]\frac{c}{c_m}\delta u_T$$

$$+\frac{M_{us}}{ac}\frac{c}{c_m}$$

$$= M_{a_\theta}\delta\theta + M_{a_P}\delta u_P + M_{a_T}\delta u_T + \frac{M_{us}}{ac}\frac{c}{c_m}$$

$$\delta \frac{F_r}{ac} = \left(U u_R \frac{c_{d_\alpha}}{2a}\right) \frac{c}{c_m} \delta\theta$$
$$+ \left[-\frac{u_T u_R}{U} \frac{c_{d_\alpha}}{2a} + \left(\frac{c_d}{2a} + M \frac{c_{d_M}}{2a}\right) \frac{u_R u_P}{U} \right] \frac{c}{c_m} \delta u_P$$
$$+ \left[\frac{u_P u_R}{U} \frac{c_{d_\alpha}}{2a} + \left(\frac{c_d}{2a} + M \frac{c_{d_M}}{2a}\right) \frac{u_R u_T}{U} \right] \frac{c}{c_m} \delta u_T$$
$$+ \left(U \frac{c_d}{2a}\right) \frac{c}{c_m} \delta u_R$$
$$= F_{r_\theta} \delta\theta + F_{r_P} \delta u_P + F_{r_T} \delta u_T + F_{r_R} \delta u_R$$

The blade trim velocity components are defined in section 2.4.2. The perturbation velocity components are due to the blade degrees of freedom, the shaft motion, and the aerodynamic gust velocity:

$$\delta u_T = (\mu_x \alpha_x + \dot{y}_h + v_G)\cos\Psi_m + (\mu_z \alpha_y - \dot{x}_h + u_G)\sin\Psi_m$$
$$+ (\mu_x \cos\Psi_m - \mu_y \sin\Psi_m)(\alpha_z + \Psi_s) + r(\dot{\alpha}_z + \dot{\Psi}_s)$$
$$+ \sum_i \dot{q}_i \vec{r}_B \cdot \vec{\eta}_i + u_R \sum_i q_i \vec{r}_B \cdot \vec{\eta}_i'$$

$$\delta u_R = -(\mu_z \alpha_x + \dot{y}_h + v_G)\sin\Psi_m + (\mu_z \alpha_y - \dot{x}_h + u_G)\cos\Psi_m$$
$$- (\mu_x \sin\Psi_m + \mu_y \cos\Psi_m)(\alpha_z + \Psi_s) - \mu_z \beta_G$$
$$+ \sum_i q_i \left[\vec{r}_B \cdot (\vec{\eta}_i - u_T \vec{\eta}_i') - \mu_z \vec{r}_B \cdot \vec{\eta}_i' \right]$$

$$\delta u_P = (\dot{z}_h - \mu_x \alpha_y - \mu_y \alpha_x - w_G + \lambda_u) + u_R \beta_G$$
$$+ r(\dot{\beta}_G + \dot{\alpha}_x \sin\Psi_m - \dot{\alpha}_y \cos\Psi_m + \lambda_x \cos\Psi_m + \lambda_y \sin\Psi_m)$$
$$+ \sum_i \dot{q}_i \vec{r}_B \cdot \vec{\eta}_i + u_R \sum_i q_i \vec{r}_B \cdot \vec{\eta}_i'$$

$$\delta\Theta = \sum_i p_i \xi_i$$

The gust velocity components are here assumed to be uniform throughout space. Perturbation inflow components λ_u, λ_x, and λ_y have been included in δu_P (see section 6.1.5). Recall that the body Euler angle contributions are not included in the evaluation of α_x, α_y, and α_z here. The perturbation quantities required for the unsteady pitch moment are

$$B = \sum_i \dot{p}_i \xi_i + u_R \sum_i p_i \xi_i' + \beta_G + \sum_i q_i \tau_B \cdot \vec{\eta}_i'$$

$$\dot{w} + u_R w' = V \sum_i \dot{p}_i \xi_i + u_R V \sum_i p_i \xi_i'$$
$$- 2u_R \cos\theta \dot{\beta}_G - \dot{u}_R \cos\theta \beta_G$$
$$+ 2u_R \sin\theta (\dot{\alpha}_z + \dot{\psi}_s) + \dot{u}_R \sin\theta (\alpha_z + \psi_s)$$
$$- 2u_R \sum_i \dot{q}_i \tau \cdot \vec{\eta}_i'$$
$$+ \sum_i q_i (-\dot{u}_R \tau \cdot \vec{\eta}_i' - u_R^2 \tau \cdot \vec{\eta}_i'')$$

(see section 2.4.8). The derivatives of the blade section aerodynamic coefficients with respect to angle of attack and Mach number are obtained from steady, two-dimensional airfoil characteristics with corrections for tip flow, yawed flow, and dynamic stall effects, as described in sections 2.4.4 and 2.4.7.

Combining the expansion for the section forces and moment in terms of the velocity perturbations, and the velocity in terms of the motion of the rotor and shaft, the perturbation aerodynamic blade forces expanded linearly in the degrees of freedom are obtained. Giving names to the aerodynamic coefficients at this point in the analysis, the results for the required aerodynamic forces on the rotating blade are as follows. The aerodynamic force for flap/lag banding is:

$$\int_0^1 \vec{\eta}_k \cdot \left(\frac{F_z}{ac} \vec{i}_B - \frac{F_x}{ac} \vec{k}_B\right) dr$$
$$= M_{q_k \mu} \left[(\mu_z \alpha_x + \dot{\lambda}_m + v_G) \cos\psi_m + (\mu_z \alpha_y - \dot{x}_m + u_G) \sin\psi_m \right]$$

$$+ M_{q_k \dot{\zeta}} \left(\dot{\alpha}_z + \dot{\Psi}_s \right) + M_{q_k \zeta} \left(\alpha_z + \Psi_s \right)$$
$$+ M_{q_k \lambda} \left(\dot{z}_h - \mu_x \alpha_y - \mu_y \alpha_x - w_G + \lambda_u \right)$$
$$+ M_{q_k \dot{\beta}} \left(\dot{\beta}_G + \dot{\alpha}_x \sin\Psi_m - \dot{\alpha}_y \cos\Psi_m + \lambda_x \cos\Psi_m + \lambda_y \sin\Psi_m \right)$$
$$+ M_{q_k \beta} \beta_G + \sum_i M_{q_k \dot{q}_i} \dot{q}_i + \sum_i M_{q_k q_i} q_i$$
$$+ \sum_i M_{q_k p_i} p_i$$

The radial force is

$$\int_0^1 \frac{\tilde{F}_r}{ac} d\bar{r} = R_\mu \left[-(\mu_z \alpha_x + \dot{y}_h + v_G) \sin\Psi_m + (\mu_z \alpha_y - \dot{x}_h + u_G) \cos\Psi_m \right]$$
$$+ R_r \left[(\mu_z \alpha_x + \dot{y}_h + v_G) \cos\Psi_m + (\mu_z \alpha_y - \dot{x}_h + u_G) \sin\Psi_m \right]$$
$$+ R_{\dot{\zeta}} \left(\dot{\alpha}_z + \dot{\Psi}_s \right) + R_\zeta \left(\alpha_z + \Psi_s \right)$$
$$+ R_\lambda \left(\dot{z}_h - \mu_x \alpha_y - \mu_y \alpha_x - w_G + \lambda_u \right)$$
$$+ R_{\dot{\beta}} \left(\dot{\beta}_G + \dot{\alpha}_x \sin\Psi_m - \dot{\alpha}_y \cos\Psi_m + \lambda_x \cos\Psi_m + \lambda_y \sin\Psi_m \right)$$
$$+ R_\beta \beta_G + \sum_i R_{\dot{q}_i} \dot{q}_i + \sum_i R_{q_i} q_i + \sum_i R_{p_i} p_i$$

The aerodynamic force for blade torsion and pitch is:

$$\int_0^1 \bar{\zeta}_k \frac{M_a}{ac} d\bar{r} - \int_0^1 \left(\frac{F_x}{ac} \vec{i}_B + \frac{F_z}{ac} \vec{k}_B \right) \cdot \vec{X}_{A_k} d\bar{r}$$
$$= M_{p_k \mu} \left[(\mu_z \alpha_x + \dot{y}_h + v_G) \cos\Psi_m + (\mu_z \alpha_y - \dot{x}_h + u_G) \sin\Psi_m \right]$$

$$+ M_{p_k \dot{\zeta}} (\dot{\alpha}_z + \dot{\psi}_s) + M_{p_k \zeta} (\alpha_z + \psi_s)$$

$$+ M_{p_k \lambda} (\dot{z}_h - \mu_x \alpha_y - \mu_y \alpha_x - w_G + \lambda_h)$$

$$+ M_{p_k \dot{\beta}} (\dot{\beta}_G + \dot{\alpha}_x \sin\psi_m - \dot{\alpha}_y \cos\psi_m + \lambda_x \cos\psi_m + \lambda_y \sin\psi_m)$$

$$+ M_{p_k \beta} \beta_G + \sum_i M_{p_k \dot{q}_i} \dot{q}_i + \sum_i M_{p_k q_i} q_i$$

$$+ \sum_i M_{p_k \dot{p}_i} \dot{p}_i + \sum_i M_{p_k p_i} p_i$$

Finally, the aerodynamic hub forces and moments are similar to the result for the blade bending, but with the following changes in the integrands and notation:

	Integrand	Coefficient Notation
Flap moment	rF_z	M
Torque	rF_x	Q
Blade drag force	F_x	H
Thrust	F_z	T

Combining the results for the expansion of the aerodynamic forces and the expansions of the velocities, the aerodynamic coefficients can be evaluated. The aerodynamic coefficients are constant for axial flow, but for nonaxial flow they are periodic functions of ψ_m. The coefficients for flap/lag bending are:

$$M_{q_k \mu} = \int_0^1 \vec{\eta}_k \cdot (F_{z_T} \vec{i}_B - F_{x_T} \vec{k}_B) \, dr$$

$$M_{q_k \dot{\zeta}} = \int_0^1 \vec{\eta}_k \cdot (F_{z_T} \vec{i}_B - F_{x_T} \vec{k}_B) r \, dr$$

$$M_{q_k \zeta} = (\mu_x \cos\psi_m - \mu_y \sin\psi_m) M_{q_k \mu}$$

$$M_{q_k \lambda} = \int_0^1 \vec{\eta}_k \cdot (F_{z_p} \vec{i}_B - F_{x_p} \vec{k}_B)\, dr$$

$$M_{q_k \dot{\beta}} = \int_0^1 \vec{\eta}_k \cdot (F_{z_p} \vec{i}_B - F_{x_p} \vec{k}_B)\, r\, dr$$

$$M_{q_k \beta} = u_R M_{q_k \lambda}$$

$$M_{q_k \dot{q}_i} = \int_0^1 \vec{\eta}_k \cdot (F_{z_T} \vec{i}_B - F_{x_T} \vec{k}_B) \vec{k}_B \cdot \vec{\eta}_i\, dr + \int_0^1 \vec{\eta}_k \cdot (F_{z_p} \vec{i}_B - F_{x_p} \vec{k}_B) \vec{i}_B \cdot \vec{\eta}_i\, dr$$

$$M_{q_k q_i} = u_R \int_0^1 \vec{\eta}_k \cdot (F_{z_T} \vec{i}_B - F_{x_T} \vec{k}_B) \vec{k}_B \cdot \vec{\eta}_i'\, dr + u_R \int_0^1 \vec{\eta}_k \cdot (F_{z_p} \vec{i}_B - F_{x_p} \vec{k}_B) \vec{i}_B \cdot \vec{\eta}_i'\, dr$$

$$M_{q_k p_i} = \int_0^1 \vec{\eta}_k \cdot (F_{z_\theta} \vec{i}_B - F_{x_\theta} \vec{k}_B) \xi_i\, dr$$

The aerodynamic coefficients for the flap moment are

$$M_\mu = \int_0^1 F_{z_T}\, r\, dr$$

$$M_{\dot{\zeta}} = \int_0^1 F_{z_T}\, r^2\, dr$$

$$M_5 = (\mu_x \cos\psi_m - \mu_y \sin\psi_m) M_\mu$$

$$M_\lambda = \int_0^1 F_{zp}\, r\, dr$$

$$M_{\dot\beta} = \int_0^1 F_{zp}\, r^2\, dr$$

$$M_\beta = u_R M_\lambda$$

$$M_{\dot q_i} = \int_0^1 (F_{z_T} \vec{k}_B \cdot \vec{\eta}_i + F_{zp} \vec{i}_B \cdot \vec{\eta}_i)\, r\, dr$$

$$M_{q_i} = u_R \int_0^1 (F_{z_T} \vec{k}_B \cdot \vec{\eta}_i' + F_{zp} \vec{i}_B \cdot \vec{\eta}_i')\, r\, dr$$

$$M_{p_i} = \int_0^1 F_{z_\theta} \xi_i\, r\, dr$$

The aerodynamic coefficients for the other hub forces and moments follow the pattern of the flap moment, with the following changes in the notation and integrands:

	Integrand	Coefficient
Flap moment	rF_z	M
Torque	rF_x	Q
Blade drag force	F_x	H
Thrust	F_z	T

The radial force coefficients are

$$R_\mu = \int_0^1 F_{r_R}\, dr$$

$$R_r = \int_0^1 \tilde{F}_{r_T}\, dr$$

$$R_5 = \int_0^1 \tilde{F}_{r_T}\, r\, dr$$

$$R_S = (\mu_x \cos\Psi_m - \mu_y \sin\Psi_m) R_T - (\mu_x \sin\Psi_m + \mu_y \cos\Psi_m) R_M - \int_0^1 \frac{F_x}{ac}\, d\tau$$

$$R_\lambda = \int_0^1 \tilde{F}_{r_P}\, d\tau$$

$$R_\beta = \int_0^1 \tilde{F}_{r_P}\, r\, d\tau$$

$$R_\beta = u_R R_\lambda - \mu_z R_M - \int_0^1 \frac{F_z}{ac}\, d\tau$$

$$R_{q_i} = \int_0^1 (\tilde{F}_{r_T} \vec{k}_B \cdot \vec{\eta}_i + \tilde{F}_{r_P} \vec{\iota}_B \cdot \vec{\eta}_i)\, d\tau$$

$$R_{q_i} = u_R \int_0^1 (\tilde{F}_{r_T} \vec{k}_B \cdot \vec{\eta}_i' + \tilde{F}_{r_P} \vec{\iota}_B \cdot \vec{\eta}_i')\, d\tau + \int_0^1 F_{r_R} [\vec{k}_B \cdot (\vec{\eta}_i - u_T \vec{\eta}_i') - \mu_z \vec{\iota}_B \cdot \vec{\eta}_i']\, d\tau - \int_0^1 \left(\frac{F_z}{ac} \vec{\iota}_B \cdot \vec{\eta}_i' + \frac{F_x}{ac} \vec{k}_B \cdot \vec{\eta}_i'\right) d\tau$$

$$R_{p_i} = \int_0^1 \tilde{F}_{r_\Theta} \xi_i\, d\tau$$

where

$$\tilde{F}_{r_T} = F_{r_T} - F_{z_T} [\beta_G + \delta_{fA_1} - \delta_{fA_2} + \vec{k}_B \cdot (x_0 \vec{\iota} + z_0 \vec{k})'] - F_{x_T} [\delta_{fA_3} + \vec{\iota}_B \cdot (x_0 \vec{\iota} + z_0 \vec{k})']$$

and F_{rp} and $F_{r\theta}$ are similarly defined. Finally, the aerodynamic coefficients for the blade pitch and torsion are

$$M_{P_k\mu} = \int_{r_{FA}}^{1} \left[\xi_k M_{a_T} - (F_{x_T}\vec{i}_B + F_{z_T}\vec{k}_B)\cdot\vec{Y}_{A_k} \right] dr$$

$$M_{P_k\zeta} = \int_{r_{FA}}^{1} \left[\xi_k M_{a_T} - (F_{x_T}\vec{i}_B + F_{z_T}\vec{k}_B)\cdot\vec{Y}_{A_k} \right] r\, dr$$
$$- \int_{r_{FA}}^{1} \xi_k \frac{c^2}{32}\left(1+4\frac{x_{Ac}}{c}\right) 2u_R \sin\theta \operatorname{sign} V \frac{c}{c_m}\, dr$$

$$M_{F_k\zeta} = (\mu_x \cos\psi_m - \mu_y \sin\psi_m) M_{P_k\mu}$$
$$- \int_{r_{FA}}^{1} \xi_k \frac{c^2}{32}\left(1+4\frac{x_{Ac}}{c}\right) \dot{u}_R \sin\theta \operatorname{sign} V \frac{c}{c_m}\, dr$$

$$M_{P_k\lambda} = \int_{r_{FA}}^{1} \left[\xi_k M_{a_P} - (F_{x_P}\vec{i}_B + F_{z_P}\vec{k}_B)\cdot\vec{Y}_{A_k} \right] dr$$

$$M_{P_k\dot{\beta}} = \int_{r_{FA}}^{1} \left[\xi_k M_{a_P} - (F_{x_P}\vec{i}_B + F_{z_P}\vec{k}_B)\cdot\vec{Y}_{A_k} \right] r\, dr$$
$$+ \int_{r_{FA}}^{1} \xi_k \frac{c^2}{32}\left(1+4\frac{x_{Ac}}{c}\right) 2u_R \cos\theta \operatorname{sign} V \frac{c}{c_m}\, dr$$

$$M_{P_k\beta} = u_R M_{P_k\lambda}$$
$$- \int_{r_{FA}}^{1} \xi_k \frac{c^2}{32} |V| \left(1+4\frac{x_{Ac}}{c}\right)^2 \frac{c}{c_m}\, dr$$
$$+ \int_{r_{FA}}^{1} \xi_k \frac{c^2}{32}\left(1+4\frac{x_{Ac}}{c}\right) \dot{u}_R \cos\theta \operatorname{sign} V \frac{c}{c_m}\, dr.$$

$$M_{A\dot{q}_i} = \int_{r_{FA}}^{1} [\xi_k M_{aT} - (F_{xT}\vec{\imath}_B + F_{zT}\vec{k}_B)\cdot\vec{X}_{Ak}]\vec{k}_B\cdot\vec{\eta}_i\, dr$$
$$+ \int_{r_{FA}}^{1} [\xi_k M_{aP} - (F_{xP}\vec{\imath}_B + F_{zP}\vec{k}_B)\cdot\vec{X}_{Ak}]\vec{\imath}_B\cdot\vec{\eta}_i\, dr$$
$$+ \int_{r_{FA}}^{1} \xi_k \frac{c^2}{32}\left(1+4\frac{x_{Ac}}{c}\right) 2\mu_R \vec{\tau}\cdot\vec{\eta}_i' \operatorname{sign} V \frac{c}{c_m}\, dr$$

$$M_{P\dot{q}_i} = \mu_R \int_{r_{FA}}^{1} [\xi_k M_{aT} - (F_{xT}\vec{\imath}_B + F_{zT}\vec{k}_B)\cdot\vec{X}_{Ak}]\vec{k}_B\cdot\vec{\eta}_i'\, dr$$
$$+ \mu_R \int_{r_{FA}}^{1} [\xi_k M_{aP} - (F_{xP}\vec{\imath}_B + F_{zP}\vec{k}_B)\cdot\vec{X}_{Ak}]\vec{\imath}_B\cdot\vec{\eta}_i'\, dr$$
$$- \int_{r_{FA}}^{1} \left(\frac{F_x}{ac}\vec{\imath}_B + \frac{F_z}{ac}\vec{k}_B\right)\cdot\vec{X}_{Ak}q_i\, dr$$
$$- \int_{r_{FA}}^{1} \xi_k \frac{c^2}{32} |V| \left(1+4\frac{x_{Ac}}{c}\right)^2 \vec{\imath}_B\cdot\vec{\eta}_i' \frac{c}{c_m}\, dr$$
$$+ \int_{r_{FA}}^{1} \xi_k \frac{c^2}{32}\left(1+4\frac{x_{Ac}}{c}\right)[\mu_R \vec{\tau}\cdot\vec{\eta}_i' + \mu_R^2 \vec{\tau}\cdot\vec{\eta}_i''] \operatorname{sign} V \frac{c}{c_m}\, dr$$

$$M_{P\dot{P}_i} = \int_{r_{FA}}^{1} [\xi_k M_{a\theta} - (F_{x\theta}\vec{\imath}_B + F_{z\theta}\vec{k}_B)\cdot\vec{X}_{Ak}]\xi_i\, dr$$
$$- \int_{r_{FA}}^{1} \xi_k \frac{c^2}{16}\mu_R \xi_i' |V| \left(1+4\frac{x_{Ac}}{c}\right)\left(1+2\frac{x_{Ac}}{c}\right)\frac{c}{c_m}\, dr$$

$$M_{P\dot{P}_i} = -\int_{r_{FA}}^{1} \xi_k \xi_i \frac{c^2}{16} |V| \left(1+4\frac{x_{Ac}}{c}\right)\left(1+2\frac{x_{Ac}}{c}\right)\frac{c}{c_m}\, dr$$

where

$$\vec{X}_{Akq_i} = -\int_{r_{FA}}^{r} \xi_k \vec{\eta}_i''(r-\xi)\,d\xi$$

$$\vec{X}_{Akq_0} = -\vec{\eta}_i + \vec{\eta}_i(r_{FA}) + \vec{\eta}_i'(r_{FA})(r-r_{FA})$$

$$V = u_T \cos\theta + u_P \sin\theta$$

$$x_{Ae} = \begin{cases} x_{AC} & \text{normal flow} \\ -(x_{AC} + \frac{c}{2}) & \text{reverse flow} \end{cases}$$

$$u_R = \mu_x \cos\psi - \mu_z \sin\psi$$

$$i_R = -\mu_x \sin\psi - \mu_z \cos\psi$$

and

$$\vec{X}_{Ak} = \xi_k(r_{FA})\left[(\delta_{FA_2} - \delta_{FA_4})\vec{i}_B + (\delta_{FA_3} - \delta_{FA_5})\vec{k}_B\right](r-r_{FA}) + \sum_j \vec{X}_{kj} q_j$$

6.1.5 Inflow dynamics.

The aerodynamic forces on the rotor result in wake-induced inflow velocities at the desk, for both the trim and transient loadings. The wake-induced velocity perturbations can be a significant factor in the rotor aeroelastic behavior; an extreme case is the influence of the shed

wake on rotor blade flutter. The rotor inflow dynamics should therefore be included in the aeroelastic analysis. However, the relationship between the inflow perturbations and the transient loading is likely more complex even than for the steady problem (nonuniform wake-induced inflow calculation), and models for the perturbation inflow dynamics are still under development. In the present analysis, an elementary representation of the inflow dynamics is used. The basic assumption is that the rotor total forces vary slowly enough (compared to the wake response) that the classical actuator disk results are applicable to the perturbation as well as the trim velocities.

A contribution to the velocity normal to the rotor disk of the following form has been included in δu_p:

$$\delta u_p = \lambda_u + \lambda_x r \cos\psi_m + \lambda_y r \sin\psi_m$$

where λ_u is the inflow perturbation component uniform over the disk, while the λ_x and λ_y components vary linearly over the disk. The inflow dynamics model must relate these inflow components to the transient aerodynamic forces on the rotor, specifically to the thrust, pitch moment, and roll moment; and to the transient rotor velocity perturbations $\delta\mu_x$, $\delta\mu_y$, and $\delta\mu_z$.

Including a time lag in the inflow response to loading changes, the dynamic inflow equations are:

$$LM \begin{Bmatrix} \lambda_u \\ \lambda_x \\ \lambda_y \end{Bmatrix}^{\bullet} + \begin{Bmatrix} \lambda_u \\ \lambda_x \\ \lambda_y \end{Bmatrix} = L \begin{Bmatrix} \tilde{C}_T \\ -C_{M_y} \\ C_{M_x} \end{Bmatrix}$$

where

$$\tilde{C}_T = C_T - \frac{C_{T_{trim}}}{(\mu^2/k_f^2 + \lambda^2/k_2^4)} \left(\frac{\mu_x}{k_f^2} \delta\mu_x + \frac{\mu_y}{k_f^2} \delta\mu_y + \frac{\lambda}{k_2^4} \delta\mu_z \right)$$

includes the effect of the velocity perturbations (references 57 and 58). The time lag matrix M is diagonal:

$$M = \begin{bmatrix} \frac{8}{3\pi} & 0 & 0 \\ 0 & \frac{16}{45\pi} & 0 \\ 0 & 0 & \frac{16}{45\pi} \end{bmatrix}$$

(references 59 to 61). For the matrix L relating quasistatic inflow changes to quasistatic loading changes, the following two models are used:

a) A perturbation form of the empirical inflow model used for trim.

$$L = \begin{bmatrix} \frac{\partial \lambda}{\partial T} & 0 & 0 \\ K_x \frac{\partial \lambda}{\partial T} & \frac{\partial \lambda}{\partial M} & 0 \\ K_y \frac{\partial \lambda}{\partial T} & 0 & \frac{\partial \lambda}{\partial M} \end{bmatrix}$$

where κ_x and κ_y are defined in section 2.4.3; and

$$\frac{\partial \lambda}{\partial T} = \left[2\sqrt{\mu^2/\lambda_f^2 + \lambda^2/k_e^4} + \frac{C_T \lambda / k_e^4}{\mu^2/k_f^2 + \lambda^2/k_e^4} \right]^{-1}$$

$$\frac{\partial \lambda}{\partial M} = \frac{2 f_M}{\sqrt{\mu^2/\lambda_f^2 + \lambda^2/k_e^4}}$$

b) The Pitt and Peters actuator disk model (reference 58), generalized to include the effects of sideward velocity.

$$L = \begin{bmatrix} \frac{\partial \lambda}{\partial T} & -K_x \frac{\partial \lambda}{\partial T} & -K_y \frac{\partial \lambda}{\partial T} \\ K_x \frac{\partial \lambda}{\partial T} & \frac{\partial \lambda}{\partial M} & \frac{\partial \lambda}{\partial N} \\ K_y \frac{\partial \lambda}{\partial T} & \frac{\partial \lambda}{\partial N} & \frac{\partial \lambda}{\partial L} \end{bmatrix}$$

where

$$V = \frac{\mu^2 + (\lambda + \lambda_i)\lambda}{\sqrt{\mu^2 + \lambda^2}}$$

$$\frac{\partial \lambda}{\partial T} = \frac{1}{2V}$$

$$K_x = \frac{\mu_x}{\sqrt{\mu^2+\lambda^2} + |\lambda|}$$

$$K_y = \frac{-\mu_y}{\sqrt{\mu^2+\lambda^2} + |\lambda|}$$

$$\frac{\partial \lambda}{\partial M} = \frac{1}{V}\left[\frac{4\lambda}{\sqrt{\mu^2+\lambda^2} + |\lambda|} + \frac{4\mu_y^2}{(\sqrt{\mu^2+\lambda^2} + |\lambda|)^2}\right]$$

$$\frac{\partial \lambda}{\partial L} = \frac{1}{V}\left[\frac{4\sqrt{\mu^2+\lambda^2}}{\sqrt{\mu^2+\lambda^2} + |\lambda|} - \frac{4\mu_y^2}{(\sqrt{\mu^2+\lambda^2} + |\lambda|)^2}\right]$$

$$\frac{\partial \lambda}{\partial N} = \frac{1}{V}\frac{4\mu_x\mu_y}{(\sqrt{\mu^2+\lambda^2} + |\lambda|)^2}$$

The effect of the ground on the inflow dynamics is to add a perturbation due to changes in the rotor height above the ground:

$$\delta\lambda = \frac{\partial \lambda}{\partial z}\delta z$$

As for the trim inflow analysis, the result of reference 21 for the ratio of the induced velocity in and out of ground effect is used:

$$\frac{v_\infty}{v} = \frac{T}{T_\infty} = \frac{1}{1 - \left(\frac{\cos\epsilon}{4z}\right)^2}$$

which gives

$$\frac{\partial\lambda}{\partial z} = \frac{\lambda_i \cos^2\epsilon}{8z^3}$$

Expressions for $\cos\epsilon$ and z are derived in section 2.4.3. Since $\partial\lambda/\partial z > 0$, ground effect introduces a positive spring to the rotorcraft flight dynamics. A decrease in the rotor height above the ground produces a decrease in the induced velocity, hence a rotor thrust increase that acts as a spring against the vertical height change.

For the side-by-side helicopter configuration, the antisymmetric dynamics exhibit an unstable roll oscillation due to interaction of the rotor wake and ground. Such behavior can be included in the ground effect model derived here by using a negative value for $\partial\lambda/\partial z$ (a negative roll spring), which must be obtained from experimental data. In this case the inflow perturbations of the two rotors are related to the symmetric and antisymmetric height perturbations:

$$\delta\lambda_1 = \frac{\partial\lambda}{\partial z_S}\delta z_S + \frac{\partial\lambda}{\partial z_A}\delta z_A$$

$$= \frac{1}{2}\left(\frac{\partial\lambda}{\partial z_S} + \frac{\partial\lambda}{\partial z_A}\right)\delta z_1 + \frac{1}{2}\left(\frac{\partial\lambda}{\partial z_S} - \frac{\partial\lambda}{\partial z_A}\right)\delta z_2$$

$$\delta\lambda_2 = \frac{\partial\lambda}{\partial z_s}\delta z_s - \frac{\partial\lambda}{\partial z_A}\delta z_A$$

$$= \frac{1}{2}\left(\frac{\partial\lambda}{\partial z_s} - \frac{\partial\lambda}{\partial z_A}\right)\delta z_1 + \frac{1}{2}\left(\frac{\partial\lambda}{\partial z_s} - \frac{\partial\lambda}{\partial z_A}\right)\delta z_2$$

where δz_1 and δz_2 are the height perturbations at the two rotor hubs. Hence for the tiltrotor configuration, it will be possible as an option to use:

$$\frac{\partial\lambda}{\partial z_s} = \lambda_i \frac{1}{8}\left(\frac{\cos\epsilon}{z}\right)^2$$

$$\frac{\partial\lambda}{\partial z_A} = \min\left(\lambda_i \frac{1}{8}\left(\frac{\cos\epsilon}{z}\right)^2, \frac{\partial\lambda}{\partial z_{TR}}\right)$$

where the antisymmetric term is

$$\frac{\partial\lambda}{\partial z_{TR}} = \lambda_i\left[1.722 - 2.726\,(z/\cos\epsilon) + 1.216\,(z/\cos\epsilon)^2 - .1649\,(z/\cos\epsilon)^3\right]$$

which gives a negative (unstable) value for about $1 < z < 3$, with a minimum of $-.21\lambda_i$ at about $z = 1.7$. A form applicable in general is:

$$\delta\lambda_1 = \frac{\partial\lambda}{\partial z_1}\delta z_1 + \frac{\partial\lambda}{\partial z_{12}}\delta z_2$$

$$\delta\lambda_2 = \frac{R_1}{R_2}\frac{\partial\lambda}{\partial z_{21}}\delta z_1 + \frac{R_1}{R_2}\frac{\partial\lambda}{\partial z_2}\delta z_2$$

including the factor R_1/R_2 since the hub motion is normalized using R_1.

Finally, the rotor/rotor interference is included in the inflow dynamics model, using the same interference factors κ_{12} and κ_{21} as for the trim induced velocity model (see section 2.4.3).

In summary, the differential equations for the inflow perturbations are:

$$L M \begin{Bmatrix} \lambda_u \\ \lambda_x \\ \lambda_y \end{Bmatrix}^{\circ} + \begin{Bmatrix} \lambda_u \\ \lambda_x \\ \lambda_y \end{Bmatrix} + \left(\frac{\sigma a}{2\gamma}\right) L \begin{Bmatrix} -\gamma \frac{2\tilde{C}_T}{\sigma a} \\ \gamma \frac{2C_{My}}{\sigma a} \\ -\gamma \frac{2C_{Mx}}{\sigma a} \end{Bmatrix}_{\text{cero}}$$

$$+ \begin{Bmatrix} k_{12} \frac{(\Omega R)_2}{(\Omega R)_1} \left(\frac{\sigma a}{2\gamma} \frac{\partial \lambda}{\partial \tau}\right)_2 \left(-\gamma \frac{2\tilde{C}_T}{\sigma a}\right)_2 + \frac{\partial \lambda}{\partial z_1} \delta z_{\text{emb\#1}} + \frac{\partial \lambda}{\partial z_{12}} \delta z_{\text{emb\#2}} \\ 0 \\ 0 \end{Bmatrix}$$

$$= 0$$

for rotor #1; and

$$\left(\frac{\Omega_1}{\Omega_2}\right)^2 L M \begin{Bmatrix} \lambda_u \\ \lambda_x \\ \lambda_y \end{Bmatrix}^{\circ} + \left(\frac{\Omega_1}{\Omega_2}\right) \begin{Bmatrix} \lambda_u \\ \lambda_x \\ \lambda_y \end{Bmatrix} + \left(\frac{\sigma a}{2\gamma}\right) L \begin{Bmatrix} -\gamma \frac{2\tilde{C}_T}{\sigma a} \\ \gamma \frac{2C_{My}}{\sigma a} \\ -\gamma \frac{2C_{Mx}}{\sigma a} \end{Bmatrix}_{\text{cero}}$$

$$+\begin{pmatrix} k_{21}\dfrac{(\Omega R)_1}{(\Omega R)_2}\left(\dfrac{\sigma a}{2\gamma}\dfrac{\partial\lambda}{\partial T}\right)_1\left(-\gamma\dfrac{2\tilde{C}_T}{\sigma a}\right)_1 + \dfrac{\partial\lambda}{\partial z_{21}}\dfrac{R_1}{R_2}\delta z_{hub\#1} + \dfrac{\partial\lambda}{\partial z_2}\dfrac{R_1}{R_2}\delta z_{hub\#2} \\ 0 \\ 0 \end{pmatrix}$$

$$= 0$$

for rotor #2. The velocity perturbations $\delta\mu_x$, $\delta\mu_y$, and $\delta\mu_z$ are required for C_T. In shaft axes, the shaft motion and gusts give:

$$\begin{aligned} \delta\mu_x &= -\dot{x}_h + u_G \\ \delta\mu_y &= \dot{y}_h + v_G \\ \delta\mu_z &= \dot{z}_h - w_G \end{aligned}$$

The rotor height perturbation δz is obtained from the vertical component of the displacement at the rotor hub:

$$\begin{aligned} \delta z &= -\vec{\zeta}_E \cdot (x_h \vec{i}_s + y_h \vec{j}_s + z_h \vec{k}_s) \\ &= -\vec{\zeta}_E \cdot \left(\sum_k \vec{\zeta}_k(\vec{r}_{hub})\, q_{sk}\right) \end{aligned}$$

expressing the hub motion in terms of airframe degrees of freedom. For the rigid body degrees of freedom the mode shapes are:

$$[\vec{\zeta}_1 \cdots \vec{\zeta}_6] = [(-\vec{r}_{lmk} \times) R_e \quad I]$$

(section 4.2.1). Hence

$$\begin{aligned}
-\delta z = {} & (-z_{lmk}\cos\theta_{FT}\sin\phi_{FT} + y_{lmk}\cos\theta_{FT}\cos\phi_{FT})\,\phi_F \\
& + (-z_{lmk}\sin\theta_{FT}\cos\phi_{FT} - y_{lmk}\sin\theta_{FT}\sin\phi_{FT} \\
& \qquad - x_{lmk}\cos\theta_{FT})\,\theta_F \\
& + (-\sin\theta_{FT})x_F + (\cos\theta_{FT}\sin\phi_{FT})y_F \\
& + (\cos\theta_{FT}\cos\phi_{FT})z_F \\
& + \sum_{k=7}^{\infty} \psi_E \cdot \vec{\zeta}_k(\vec{r}_{lmk})\, q_{sk}
\end{aligned}$$

Note that a spring is introduced into the z_F equation (if $\cos\theta_{FT}\cos\phi_{FT} \neq 0$), and also possibly into the y_F and x_F equations.

The time lag is often not an important factor, so a quasistatic model for the inflow dynamics is generally sufficient. Dropping the time lag terms, the equations for λ_u, λ_x, and λ_y reduce to linear algebraic equations. Hence in the quasistatic case the inflow perturbations do not increase the order of the system. The wake influence reduces to an algebraic substitution relation, which if incorporated analytically would lead to lift deficiency functions; with large-order systems, it is more practical to accomplish the substitution numerically.

6.1.6 Rotor equations of motion.

The linear differential equations of motion for the rotor model can be constructed now. The equations of motion are in the nonrotating frame, that is the Fourier coordinate transformation has been applied to the bending and torsion degrees of freedom of the blade. For now only a three-bladed rotor is considered; the equations are extended to an arbitrary number of blades below. The equations of motion for the rotor, and the hub reactions, take the following form:

$$A_2 \ddot{x}_R + A_1 \dot{x}_R + A_0 x_R + \tilde{A}_2 \ddot{\alpha} + \tilde{A}_1 \dot{\alpha} = B v_R + M_{aero}$$

$$F = C_2 \ddot{x}_R + C_1 \dot{x}_R + C_0 x_R + \tilde{C}_2 \ddot{\alpha} + \tilde{C}_1 \dot{\alpha} + f_{aero}$$

The coefficient matrices are constructed from the results of section 6.1.2. Here the matrices only include the structural and inertial terms; M_{aero} and F_{aero} are the aerodynamic forces. The vectors of the rotor degrees of freedom (x_R), shaft motion (α), rotor blade pitch input (v_R) aerodynamic gust (g_s, in shaft axes), and the hub forces and moments (F) are defined as:

$$x_R = \left[\beta_0^{(k)} \; \beta_{1c}^{(k)} \; \beta_{1s}^{(k)} \; \vartheta_0^{(k)} \; \vartheta_{1c}^{(k)} \; \vartheta_{1s}^{(k)} \; \beta_{Gc} \; \beta_{Gs} \; \Psi_s \; \lambda_w \; \lambda_x \; \lambda_y \right]^T$$

$$v_R = \left[\vartheta_0^{com} \; \vartheta_{1c}^{com} \; \vartheta_{1s}^{com} \right]^T$$

$$g_s = \left[u_G \; v_G \; w_G \right]^T$$

$$\alpha = \left[x_{en} \; y_{en} \; z_{en} \; \alpha_x \; \alpha_y \; \alpha_z \right]^T$$

$$F = \left[\gamma \frac{2C_H}{\sigma a} \quad \gamma \frac{2C_Y}{\sigma a} \quad \gamma \frac{2C_T}{\sigma a} \quad \gamma \frac{2C_{M_x}}{\sigma a} \quad \gamma \frac{2C_{M_y}}{\sigma a} \quad -\gamma \frac{2C_Q}{\sigma a} \right]^T$$

Note that in the rotor degrees of freedom x_R, the notation $\beta^{(k)}$ and $\theta^{(k)}$ is intended to cover as many bending and torsion modes as the analysis requires. Also, the degrees of freedom used for the inflow dynamics model are Λ_u, Λ_x, and Λ_y defined by $\mathring{\Lambda} = \lambda$ (in order that the highest order derivatives will be $\ddot{\Lambda}$, in the acceleration matrix). The inertial matrices are defined in section 6.4.1.

The aerodynamic terms M_{aero} and F_{aero} are required to complete the differential equations of the rotor model. They are obtained by summing over all N blades the aerodynamic forces in the rotating frame (section 6.1.4) and introducing the fourier coordinate transformation for the blade bending and torsion degrees of freedom as required. The result for the required aerodynamic forces is

$$-M_{aero} = A_1 \dot{x}_R + A_0 x_R + \tilde{A}_1 \dot{\alpha} + \tilde{A}_0 \alpha - B_G g_s$$

$$F_{aero} = C_1 \dot{x}_R + C_0 x_R + \tilde{C}_1 \dot{\alpha} + \tilde{C}_0 \alpha + D_G g_s$$

For the case of a rotor operating in axial flow ($\mu = 0$) the aerodynamic coefficients for the blade forces in the rotating frame are constants, independent of the blade azimuth angle ψ_m. The coefficients are also then entirely independent of the blade index (m); hence the summation over the N blades operates only on the system degrees of freedom, not on the aerodynamic coefficients themselves (which factor out of the summation). The resulting coefficient matrices, which are constant for axial flow, are defined in section 6.4.2.

For the case of a rotor operating in nonaxial flow ($\mu > 0$) the aerodynamic coefficients of the rotating blade forces are periodic functions of ψ_m because of the periodically varying aerodynamics of the edgewise moving rotor. It follows that the rotor in nonaxial flight is described by a system of differential equations with periodic coefficients. It is possible to express the aerodynamic coefficient of the rotating blade forces as Fourier series, and then to obtain the coefficients of the nonrotating equations in terms of these harmonics. However, the simplest approach for numerical work with large-order systems is to leave the coefficients of the nonrotating equations in terms of the summation over the N blades of the rotor. The summation is easily performed numerically, and it is found that this form is also appropriate for a constant coefficient approximation to the system. For nonaxial flow, the coefficient matrices are periodic functions of the blade azimuth angle $\psi_m = \psi + m\Delta\psi$, $\Delta\psi = 2\pi/N$. The period is $\Delta\psi = 120^\circ$ for the N = 3 case considered here. The coefficient matrices for nonaxial flow are defined in section 6.4.3.

The rotor equations as constructed here are not entirely complete. First, the rotor aerodynamic thrust and hub moments:

$$-\gamma \frac{2\tilde{C}_T}{\sigma a} = -\left(\gamma \frac{2C_T}{\sigma a}\right)_{aero} + \frac{\partial \lambda}{\partial \mu}\left[\frac{\mu_x}{k_f^2}\left(-\dot{x}_m + u_G\right) + \frac{\mu_y}{k_f^2}\left(\dot{y}_m + v_G\right) + \frac{\lambda}{k_m^4}\left(\dot{z}_m - w_G\right)\right]$$

$$\left(\gamma \frac{2C_{My}}{\sigma a}\right)_{aero}$$

$$\left(\gamma \frac{2C_{Mx}}{\sigma a}\right)_{aero}$$

where

$$\frac{\partial \lambda}{\partial \mu} = \frac{(a\, 2C_T/\sigma a)_{trim}}{\mu^2/k_s^2 + \lambda^2/k_m^4}$$

have been put in place for the λ_u, λ_x, and λ_y equations. Because of the rotor/rotor interference and ground effect, it is appropriate to finish the construction of these equations at a later stage (section 6.3.1).

Secondly, we have substituted in the equation of motion for rigid pitch:

$$p_r = \theta_{con} - \sum_i k_{p_i} q_i - k_{p_G} \beta_G + (\theta_{1s} \cos\psi_m - \theta_{1c} \sin\psi_m)\, \psi_s$$

However, the rotor pitch control θ_{con} here still includes the governor and mast bending terms, as well as external control inputs.

Thirdly, the rotor torque $\gamma C_Q/\sigma a$ has been put in place as the equations of motion for the rotational speed perturbation ψ_s. The drive train couples the rotational speed perturbations of the two rotors, so it is necessary to construct these equations at a later stage (section 6.3.1).

Consider now the case of a rotor with four or more blades. Each rotating degree of freedom of the blade (bending or torsion motion) must result in N degrees of freedom for the rotor as a whole. Thus increasing the number of blades adds degrees of freedom and equations of motion to the rotor description. In axial flow these additional degrees of freedom do not couple with the collective and cyclic degrees of freedom of the rotor. Hence the equations given above remain valid for rotors with $N > 3$ also, and we need be concerned here only with the equations of motion for the additional degrees of freedom. These additional degrees of freedom are not coupled inertially with the shaft

or gimbal motion. The additional equations of motion for bending and torsion of a rotor blade with four or more blades are then:

$$A_2 \ddot{x}_R + A_1 \dot{x}_R + A_0 x_R = B v_R + M_{aero}$$

with the vectors of the degrees of freedom and blade pitch control here defined as follows:

$$x_R = \left[\beta_{nc}^{(k)} \quad \beta_{ns}^{(k)} \quad \beta_{N/2}^{(k)} \quad \theta_{nc}^{(k)} \quad \theta_{ns}^{(k)} \quad \theta_{N/2}^{(k)} \right]^T$$

$$v_R = \left[\theta_{nc}^{con} \quad \theta_{ns}^{con} \quad \theta_{N/2}^{con} \right]^T$$

The inertial coefficient matrices are given in section 6.1.4.

The aerodynamic forces are required to complete the equations of motion. In axial flow the aerodynamic forces still do not couple the additional degrees of freedom for $N \geq 4$ with the shaft or gimbal motion. Hence the aerodynamic forces for axial flow take the form

$$-M_{aero} = A_1 \dot{x}_R + A_0 x_R$$

with the coefficient matrices defined in section 6.1.5.

The aerodynamic forces in nonaxial flow ($\mu > 0$) couple all degrees of freedom of the rotor with each other and with the shaft and gimbal motion. Then not only are additional degrees of freedom and equations of motion involved if $N > 3$, but the number of blades also influences the equations and the hub reactions given above. Rather than directly

presenting the aerodynamic matrices for the general case of three or more blades in nonaxial flow, the analysis is extended by means of an observed pattern in the coefficients. In the nonaxial flow equations (section 6.4.3), note the repeated occurrence of the following submatrices:

$$P = \begin{bmatrix} 1 & c_1 & s_1 \\ 2c_1 & 2c_1^2 & 2c_1 s_1 \\ 2s_1 & 2c_1 s_1 & 2s_1^2 \end{bmatrix} = \begin{pmatrix} 1 \\ 2c_1 \\ 2s_1 \end{pmatrix} (1 \quad c_1 \quad s_1)$$

$$\Delta P = \begin{bmatrix} 0 & -s_1 & c_1 \\ 0 & -2c_1 s_1 & 2c_1^2 \\ 0 & -2s_1^2 & 2c_1 s_1 \end{bmatrix} = \begin{pmatrix} 1 \\ 2c_1 \\ 2s_1 \end{pmatrix} (0 \quad -s_1 \quad c_1)$$

(using the notation $S_n = \sin n\psi_m$ and $C_n = \cos n\psi_m$). These matrices are a direct result of the introduction of the Fourier coordinate transformation (columns) and the application of the summation operators to obtain the nonrotating equations (rows). The matrix DP arises from application of the Fourier transformation to the time derivatives ($\dot{q}_i$ or $\dot{p}_i$). In the B_G and $\bar{A}$ matrices, only some columns of P and DP appear, while in the C matrices only some rows appear. The extension to an arbitrary number of blades ($N \geq 3$) is then simply

$$P = \begin{pmatrix} 1 \\ 2c_1 \\ 2s_1 \\ \vdots \\ 2c_n \\ 2s_n \\ (-1)^m \end{pmatrix} (1 \quad c_1 \quad s_1 \quad \cdots \quad c_n \quad s_n \quad (-1)^m)$$

$$\Delta P = \begin{pmatrix} 1 \\ 2C_1 \\ 2S_1 \\ \vdots \\ 2C_n \\ 2S_n \\ (-1)^m \end{pmatrix} \begin{pmatrix} 0 & -S_1 & C_1 & \cdots & -nS_n & nC_n & 0 \end{pmatrix}$$

Rotors with three or more blades may be analyzed within the same general framework, but the two-bladed rotor is a special case. The rotor with $N \geq 3$ has axisymmetric inertial and structural properties and hence the nonrotating frame equations have constant coefficients in axial flow. In contrast, the lack of axisymmetry with two blades leads to periodic coefficient differential equations, even in the inertial terms and in axial flow. Only in special cases are the dynamics of a two-bladed rotor described by constant coefficient equations. The equations of motion again take the form

$$A_2\ddot{x}_R + A_1\dot{x}_R + A_0 x_R + \tilde{A}_2\ddot{\alpha} + \tilde{A}_1\dot{\alpha} = Bv_R + M_{aero}$$

$$F = C_2\ddot{x}_R + C_1\dot{x}_R + C_0 x_R + \tilde{C}_2\ddot{\alpha} + \tilde{C}_1\alpha + F_{aero}$$

with now for N = 2 the rotor degrees of freedom and pitch input defined as follows:

$$x_R = \left[\beta_0^{(k)} \; \beta_1^{(k)} \; \theta_0^{(k)} \; \theta_1^{(k)} \; \beta_T \; \psi_s \; \lambda_n \; \lambda_x \; \lambda_y \right]^T$$

$$v_R = \left[\theta_0^{com} \; \theta_1^{com} \right]^T$$

The inertial coefficient matrices are defined in section 6.4.6. Note that there are periodic coefficients in the matrices coupling the rotor and shaft motion ($\bar{A}$, C, $\bar{C}$).

The required aerodynamic forces for the two-bladed rotor case again take the form

$$-M_{aero} = A_1 \dot{x}_R + A_0 x_R + \tilde{A}_1 \dot{v} + \tilde{A}_0 \alpha - B_G g_s$$

$$f_{aero} = C_1 \dot{x}_R + C_0 x_R + \tilde{C}_1 \dot{\alpha} + \tilde{C}_0 \alpha + D_G g_s$$

The aerodynamic coefficient matrices are defined in section 6.4.7.

An independent blade analysis is useful for problems not involving the shaft motion or other excitation from the nonrotating frame. The only rotor blade degrees of freedom involved are the bending and torsion motion. The shaft motion, gimbal motion, and the rotor speed perturbation are dropped from the system. Only a single blade need by analyzed, in the rotating frame. The equations of motion for the bending and torsion modes are then:

$$I^*_{q_k}\left(\ddot{q}_k + g_s\nu_k\dot{q}_k + \nu_k^2 q_k\right) + 2\sum_i I^*_{q_k q_i}\dot{q}_i - \sum_i S^*_{q_k p_i}\ddot{p}_i - \sum_i S^*_{q_k p_i} p_i - \sum_i \gamma M_{q_k q_i}\dot{q}_i - \sum_i \gamma M_{q_k q_i} q_i - \sum_i \gamma M_{q_k p_i} p_i = 0$$

$$I^*_{p_k}\left(\ddot{p}_k + g_s\omega_k\dot{p}_k + \omega_k^2 p_k\right) + \sum_i I^*_{p_k p_i}\ddot{p}_i + \sum_i I^*_{p_k p_i} p_i - \sum_i S^*_{p_k q_i}\ddot{q}_i - \sum_i \left(S^*_{p_k q_i} - k_{p_i} S^*_{p_k 0}\right) q_i - \sum_i \gamma M_{p_k q_i}\dot{q}_i - \sum_i \gamma M_{p_k q_i} q_i - \sum_i \gamma M_{p_k p_i}\dot{p}_i - \sum_i \gamma M_{p_k p_i} p_i = S^*_{p_k 0}\theta_{con}$$

or

$$A_2\ddot{x}_R + A_1\dot{x}_R + A_0 x_R = B v_R$$

with $x_R = (q_k\ p_k)^T$ and $v_R = \theta_{con}$. These equations can also be obtained by dropping all degrees of freedom except the collective modes from the analysis above; a separate construction for the independent blade case is more efficient however.

6.1.7 Constant coefficient approximation.

The rotor dynamics in nonaxial flow are described by a set of linear differential equations with periodic coefficients. A constant coefficient approximation for nonaxial flow is desirable (if it is demonstrated to be accurate enough) because the calculation required to analyze the dynamic behavior is reduced considerably compared to that

for the periodic coefficient equations, and because the powerful techniques for analyzing time-invariant linear differential equations are then applicable. However, such a model is only an approximation to the correct aeroelastic behavior. The accuracy of the approximation must be determined by comparison with the correct periodic coefficient solutions. The constant coefficient approximation derived here used the mean values of the periodic coefficients of the differential equations in the nonrotating frame.

To find the mean value of the coefficients, the operator

$$\frac{1}{2\pi}\int_0^{2\pi}(\ldots)\,d\psi$$

is applied to the periodic aerodynamic coefficients (given in section 6.4.3), resulting in terms of the following form for the N = 3 case:

$$\frac{1}{2\pi}\int_0^{2\pi}\frac{1}{2}\sum_m \begin{pmatrix} 1 \\ \cos\psi_m \\ \sin\psi_m \\ 2\cos^2\psi_m \\ 2\sin^2\psi_m \\ 2\sin\psi_m\cos\psi_m \end{pmatrix} M(\psi_m)\,d\psi$$

$$= \frac{1}{2}\sum_m \frac{1}{2\pi}\int_0^{2\pi} \begin{pmatrix} 1 \\ \cos\psi_m \\ \sin\psi_m \\ 2\cos^2\psi_m \\ 2\sin^2\psi_m \\ 2\sin\psi_m\cos\psi_m \end{pmatrix} M(\psi_m)\,d\psi_m = \begin{pmatrix} M^0 \\ \frac{1}{2}M^{1c} \\ \frac{1}{2}M^{1s} \\ M^0 + \frac{1}{2}M^{2c} \\ M^0 - \frac{1}{2}M^{2c} \\ \frac{1}{2}M^{2s} \end{pmatrix}$$

Here M^{nc} and M^{ns} are the harmonics of a Fourier series representation of the rotating blade aerodynamic coefficient M:

$$M(\psi_m) = M^0 + \sum_{n=1}^{\infty} M^{nc} \cos n\psi_m + M^{ns} \sin n\psi_m$$

In the present case, these harmonics must be evaluated numerically. The aerodynamic coefficient M is calculated at J points, equally spaced around the azimuth. Then the harmonics are calculated using the Fourier interpolation formulas:

$$M^0 = \frac{1}{J} \sum_j M(\psi_j)$$
$$M^{nc} = \frac{1}{J} \sum_j M(\psi_j) \cos n\psi_j$$
$$M^{ns} = \frac{1}{J} \sum_j M(\psi_j) \sin n\psi_j$$

where $\psi_i = j\Delta\psi = j(2\pi/J)$ (j = 1, ..., J). The number of harmonics required is n = N - 1 for N odd and n = N - 2 for N even (N is the number of blades). Good accuracy from the Fourier interpolation requires at least that J = 6n. Using these Fourier interpolation expressions, the required harmonics are

$$\begin{pmatrix} M^0 \\ \frac{1}{2}M^{1c} \\ \frac{1}{2}M^{1s} \\ M^0 + \frac{1}{2}M^{2c} \\ M^0 - \frac{1}{2}M^{2c} \\ \frac{1}{2}M^{2s} \end{pmatrix} = \frac{1}{J} \sum_j \begin{pmatrix} 1 \\ \cos\psi_j \\ \sin\psi_j \\ 2\cos^2\psi_j \\ 2\sin^2\psi_j \\ 2\sin\psi_j \cos\psi_j \end{pmatrix} M(\psi_j)$$

It follows then that the constant coefficient approximation is obtained from the periodic coefficient expressions by the simple transformation:

$$\frac{1}{2}\sum_{m=1}^{2}(\ldots)M(\psi_m) \Rightarrow \frac{1}{J}\sum_{j=1}^{J}(\ldots)M(\psi_j)$$

The summation over N blades (m = 1, ..., N; $\Delta\psi = 2\pi/N$) for a periodic coefficient is replaced by a summation over the rotor azimuth (j = 1, ..., J; $\Delta\psi = 2\pi/J$) for the constant coefficient approximation. This is quite convenient since the same procedure may be used to evaluate the coefficients for the two cases, with simply a change in the azimuth increment. The periodic coefficients must be evaluated throughout the period of $\psi = 0$ to $2\pi/N$; the constant coefficient approximation (mean values only) is evaluated only once.

With the above substitution, the results given in section 6.4.3 for the periodic coefficient matrices are directly applicable to the constant coefficient approximation as well.

For the case of a rotor with four or more blades, the constant coefficient approximation involves the transformation of higher order harmonics:

$$\frac{1}{2}\sum_{m=1}^{2}\begin{Bmatrix} 1 \\ C_m \\ S_m \\ C_m C_\ell \\ C_m S_\ell \\ S_m S_\ell \end{Bmatrix} M(\psi_m) \Rightarrow \frac{1}{J}\sum_{j=1}^{J}\begin{Bmatrix} 1 \\ C_m \\ S_m \\ C_m C_\ell \\ C_m S_\ell \\ S_m S_\ell \end{Bmatrix} M(\psi_j)$$

$$\frac{1}{N}\sum_{m=1}^{N}\begin{pmatrix}(-1)^m\\ C_m(-1)^m\\ S_m(-1)^m\end{pmatrix} M(\psi_m) \Rightarrow \quad 0$$

So the periodic coefficient results are still applicable to the constant coefficient approximation if the summation over the N blades is replaced by a summation around the rotor azimuth.

This transformation is also applicable to the case of a two-bladed rotor, but the constant coefficient approximation is not as useful or as accurate for N = 2 as for N $\geq$ 3. With three or more blades, the source of the periodic coefficients is nonaxial flow, hence the periodicity is order μ or smaller. At low advance ratio then, the constant coefficient approximation may be expected to be a good representation of the correct dynamics. Two two-bladed rotor has also periodic coefficients due to the inherent lack of axisymmetry of the rotor. This periodicity is large even for axial flow, and neglecting it in the constant coefficient approximation may be a poor representation of the dynamics. In particular, it is not possible to use the constant coefficient approximation as formulated here for the flight dynamics analysis of a two-bladed rotor helicopter, since this averaging eliminates the coupling between the rotor and the shaft motion.

6.2 Aircraft Model

6.2.1. Aircraft degrees of freedom.

The aircraft motion is described by the rigid body and elastic airframe degrees of freedom:

$$x_s = \{q_{sk}\} = \left[\phi_F\ \theta_F\ \psi_F\ x_F\ y_F\ z_F\ q_{sk}\ (k \geq 7)\right]^T$$

as defined in section 4.2.1. The aircraft controls consist of flaperon, elevator, aileron, and rudder deflections; and the auxiliary forces:

$$v_s = [\delta_f \; \delta_e \; \delta_a \; \delta_r \; (f_g)^T]$$

The rotor hub motion is obtained from

$$\alpha = c x_s$$

where c is defined in section 4.2.2, including the sign changes for a clockwise rotating rotor and scaling for rotor #2. Recall that the Euler angles do not contribute to α_x, α_y, and α_z however. In addition there is a linear acceleration due to the rotation of the velocity vector in body axes by the Euler angular velocities, written

$$\Delta\ddot{\alpha} = \bar{c}\dot{x}_s$$

(see section 4.2.2).

The feedback of the airframe elastic motion to the rotor cyclic pitch is

$$\Delta\theta_{\substack{mast \\ Bend}} = -\sum_{i=7}^{\infty} q_{si}\left[k_{MC_i}\cos\psi_m + k_{MS_i}\sin\psi_m\right]$$

as defined in section 4.2.3.

6.2.2 Aircraft equations of motion.

The linearized equations of motion for the aircraft rigid body and elastic motion are:

$$\begin{bmatrix} R_e^T I^* R_e & 0 & 0 \\ 0 & M^* & 0 \\ 0 & 0 & M_k^* \end{bmatrix} \ddot{x}_s + \begin{bmatrix} 0 & 0 & 0 \\ -M^*(\vec{V}_x) R_e & 0 & 0 \\ 0 & 0 & M_k^* g_s \omega_k \end{bmatrix} \dot{x}_s$$

$$+ \begin{bmatrix} 0 & 0 & 0 \\ G & 0 & 0 \\ 0 & 0 & M_k^* \omega_k^2 \end{bmatrix} x_s = \begin{Bmatrix} Q_k^* \end{Bmatrix}$$

(see section 4.2.4). The generalized forces due to the rotor hub reactions are:

$$\{Q_k^*\}_{rotor} = c^T F$$

where c^T is defined in section 4.2.5, including the sign changes for a clockwise rotating rotor and the scaling for rotor #2.

The generalized forces due to the aircraft aerodynamics can be linearized by successively perturbing the inputs to the analysis described in section 4.2.6. Hence for the rigid body degrees of freedom we obtain:

$$\{Q_k^*\}_{aero} = a_2 \ddot{z}_F + a_1 \begin{pmatrix} \dot{\phi}_F \\ \dot{\theta}_F \\ \dot{\psi}_F \\ \dot{x}_F \\ \dot{y}_F \\ \dot{z}_F \end{pmatrix} + b \begin{pmatrix} \delta_f \\ \delta_e \\ \delta_a \\ \delta_r \end{pmatrix} + b_G \begin{pmatrix} u_G \\ v_G \\ w_G \end{pmatrix} + b_\lambda \begin{pmatrix} \lambda_{w_1} \\ \lambda_{w_2} \end{pmatrix}$$

(The coefficients of the matrices are the aircraft stability derivatives, due to the wing/body, horizontal tail, and vertical tail.) A gust velocity uniform throughout space is considered; hence the gust velocity components are the same at the wing/body and tail. The mean inflow perturbations influence the airframe through the rotor-induced aerodynamic interference, which is modeled as described in section 4.2.6. So the interference velocities at the wing and tail are obtained from

$$\begin{pmatrix} \vec{\lambda}_W \\ \vec{\lambda}_H \\ \vec{\lambda}_V \end{pmatrix} = \begin{bmatrix} K_{W1} C_{W1} R_{SF}^T(-\vec{k}_S) & K_{W2} C_{W2} R_{SF}^T(-\vec{k}_S) \\ K_{H1} C_{H1} R_{SF}^T(-\vec{k}_S) & K_{H2} C_{H2} R_{SF}^T(-\vec{k}_S) \\ K_{V1} C_{V1} R_{SF}^T(-\vec{k}_S) & K_{V2} C_{V2} R_{SF}^T(-\vec{k}_S) \end{bmatrix} \begin{pmatrix} \lambda_{w_1} \\ \lambda_{w_2} \end{pmatrix}$$

From section 4.2.7, the generalized forces for the airframe elastic degrees of freedom ($k \geq 7$) are:

$$(Q_k^*)_{aero} = \frac{2\gamma}{\sigma a} \frac{q}{\Lambda} \left[-\frac{F_{q_k} \dot{q}_k}{V} \dot{q}_k + F_{q_k \delta} \begin{pmatrix} \delta_f \\ \delta_e \\ \delta_a \\ \delta_r \end{pmatrix} \right]$$

Finally, from section 4.2.8, the generalized forces produced by the airframe auxiliary forces are:

$$(Q_k^*)_f = \beta_f (f_n)$$

Hence the aeroelastic motion of the helicopter airframe is described by a set of linear, constant coefficient differential equations of the form:

$$a_2 \ddot{x}_s + a_1 \dot{x}_s + a_0 x_s = \beta_{v_s} + \beta_g g + \beta_\lambda \begin{pmatrix} \lambda_{u_1} \\ \lambda_{u_2} \end{pmatrix} + c_1^T F_1 + c_2^T F_2$$

where x_s is the vector of aircraft degrees of freedom, v_s is the vector of aircraft control variables, g is the vector of gust velocity components (in wind axes), and F_1 and F_2 are the hub reactions of the two rotors.

6.2.3 Drive train equations of motion.

A model for the transmission and engine dynamics was derived in section 4.3.2. The degrees of freedom involved are the rotational speed perturbations of the two rotors ($\dot{\psi}_{s1}$ and $\dot{\psi}_{s2}$) and the engine speed perturbation (degree of freedom ψ_e, defined relative to the rotation of rotor #1). With the coupling of the rotors by the drive train, it is more appropriate to use the degrees of freedom defined by

$$\Psi_{s_1} = \Psi_s$$

$$\Psi_{s_2} = (r_{I_1}/r_{I_2})\Psi_s + \Psi_I$$

or

$$\psi_S = \psi_{S1}$$

$$\psi_I = \psi_{S2} - (r_{I1}/r_{I2})\,\psi_{S1}$$

where $r_{I1}/r_{I2} = \Omega_2/\Omega_1$ is the ratio of the trim rotational speeds of the two rotors. So ψ_s is the rotational speed perturbation of the rotors and drive train as a whole, while ψ_I represents differential rotation of the two rotors. The degrees of freedom ψ_I and ψ_e therefore involve elastic deflection of the drive train. The engine model introduces the throttle control variable θ_t. The linearized equations of motion for the drive train are then:

$$\left(\gamma \frac{C_Q}{\sigma a}\right)_1 + \frac{(N I_b \Omega^3)_2}{(N I_b \Omega^3)_1} \left(\gamma \frac{C_Q}{\sigma a}\right)_2 + r_E^2 I_E^* (\ddot{\psi}_S + \ddot{\psi}_e) + r_E^2 Q_\Omega^* (\dot{\psi}_S + \dot{\psi}_e) = r_E Q_t^* \theta_t$$

$$-K_{MI_1} \left(\gamma \frac{C_Q}{\sigma a}\right)_1 + \frac{(N I_b \Omega^2)_2}{(N I_b \Omega^2)_1} \left(\gamma \frac{C_Q}{\sigma a}\right)_2 + K_{MR} (r_E^2 I_E^* \ddot{\psi}_I + r_E^2 Q_\Omega^* \dot{\psi}_I) + K_{MI_2}^* \psi_I = 0$$

$$r_E^2 I_E^* (\ddot{\psi}_S + \ddot{\psi}_e) + r_E^2 Q_\Omega^* (\dot{\psi}_S + \dot{\psi}_e) + K_{ME_1}^* \psi_e - K_{ME_2}^* \psi_I = r_E Q_t^* \theta_t$$

The constants appearing in these equations are defined in section 4.3.2 for several drive train configurations.

For the autorotation case the ψ_e degree of freedom is dropped, and the Q_Ω, Q_t, and I_E engine terms in the ψ_s and ψ_I equations are omitted.

For the engine out case, with the engine and rotors still connected, the engine terms Q_Ω and Q_t are omitted. The case of constant rotor speed is treated by dropping the ψ_s and ψ_I degrees of freedom from the system.

The rotor speed governor, consisting of $\dot{\psi}_s$ and ψ_s feedback to the engine throttle and to the collective pitch of each rotor, is described by the following equations:

$$\tau_{2e}\,\Delta\ddot{\theta}_t + \tau_{1e}\,\Delta\dot{\theta}_t + \Delta\theta_t = -k_{P_e}\dot{\psi}_s - k_{I_e}\psi_s$$

$$\tau_{21}\,\Delta\ddot{\theta}_{govr_1} + \tau_{11}\,\Delta\dot{\theta}_{govr_1} + \Delta\theta_{govr_1} = k_{P_1}\dot{\psi}_s + k_{I_1}\psi_s$$

$$\tau_{22}\,\Delta\ddot{\theta}_{govr_2} + \tau_{12}\,\Delta\dot{\theta}_{govr_2} + \Delta\theta_{govr_2} = k_{P_2}\dot{\psi}_s + k_{I_2}\psi_s$$

(see section 4.3.3). For the tilting proprotor configuration, the variable ψ_s is replaced by the symmetric variable $\psi_{sym} = \psi_s + 1/2\ \psi_I$.

6.3 Coupled Rotor and Aircraft

6.3.1 Coupled equations of motion.

The equations of motion have been derived for the two rotors and the aircraft body. The rotor equations of motion take the form

$$A_2\ddot{x}_R + A_1\dot{x}_R + A_0 x_R + \tilde{A}_2\ddot{\alpha} + \tilde{A}_1\dot{\alpha} + \tilde{A}_0\alpha = B v_R + B_G g_s$$

$$f = C_2\ddot{x}_R + C_1\dot{x}_R + C_0 x_R + \tilde{C}_2\ddot{\alpha} + \tilde{C}_1\dot{\alpha} + \tilde{C}_0\alpha + D_G g_s$$

(see section 6.1.6). The rotor degrees of freedom vector x_R consists of flap/lag bending, rigid pitch and elastic torsion, gimbal or teeter motion, rotational speed, and inflow perturbations. The rotor control

vector v_R consists of the blade pitch control. The gust vector in shaft axes is related to the gust vector in velocity axes by

$$g_s = R_G g$$

(section 4.1.4). The hub motion is related to the aircraft degrees of freedom by

$$\alpha = c x_s$$
$$\dot{\alpha} = c \dot{x}_s$$
$$\ddot{\alpha} = c \ddot{x}_s + \bar{c} \dot{x}_s$$

(section 4.2.2; only the 3 x 3 submatrix in the upper left corner of $\bar{c}$ is nonzero). For rotor #2 it is necessary to change the time scale to the rotational speed of rotor #1.

$$\frac{\partial}{\partial \Omega_2 t} = \frac{\Omega_1}{\Omega_1} \frac{\partial}{\partial \Omega_1 t}$$

So the matrices A_1, $\bar{A}_1$, C_1, and $\bar{C}_1$ are multiplied by (Ω_1/Ω_2); and the matrices A_2, $\bar{A}_2$, C_2, $\bar{C}_2$ are multiplied by $(\Omega_1/\Omega_2)^2$.

The aircraft equations of motion take the form

$$a_2 \ddot{x}_s + a_1 \dot{x}_s + a_0 x_s = b v_s + b_c g + B_\lambda \begin{pmatrix} \dot{\lambda}_{m_1} \\ (\Omega_1/\Omega_2)\dot{\lambda}_{m_2} \end{pmatrix} + C_{R1}^T F_{R1} + C_{R2}^T F_{R2}$$

(see section 6.2.2). The vector x_s consists of the aircraft rigid body and elastic airframe degrees of freedom. The vector v_s consists of the aircraft controls.

The equations for the rotor and aircraft can now be combined to construct the set of linear differential equations that describe the dynamics of the complete system. These equations take the following form:

$$A_2 \ddot{x} + A_1 \dot{x} + A_0 x = B_v + B_p v_p + B_G g$$

The state vector x, control vectors v and v_p, and the gust vector g are defined as:

$$x = [\ (\beta^{(k)}\ \theta^{(k)}\ \beta_{GC}\ \beta_{GS})_{rotor\#1}\ \psi_s\ \lambda_{u_1}\ \lambda_{x_1}\ \lambda_{y_1}$$
$$(\beta^{(k)}\ \theta^{(k)}\ \beta_{GC}\ \beta_{GS})_{rotor\#2}\ \psi_z\ \lambda_{u_2}\ \lambda_{x_2}\ \lambda_{y_2}$$
$$\phi_F\ \theta_F\ \psi_F\ x_F\ y_F\ z_F\ q_{s_k}(k \geq 7)\ \psi_e\ \Delta\theta_t\ \Delta\theta_{gov_1}\ \Delta\theta_{gov_2}\ ]^T$$

$$v = [\ \theta^{con}_{rotor\#1}\ \theta^{con}_{rotor\#2}\ \delta_f\ \delta_e\ \delta_a\ \delta_r\ \theta_t\ (\Omega)\ ]^T$$

$$v_p = [\ \delta_0\ \delta_c\ \delta_s\ \delta_p\ \delta_t\ ]^T$$

$$g = [\ u_G\ v_G\ w_G\ ]^T$$

The vector of the degrees of freedom for the entire system (x) consists of the degrees of freedom of the two rotors and the aircraft. The rotational speed degrees of freedom of the two rotors are replaced by the coupled degrees of freedom ψ_s and ψ_I; and the engine speed degree of freedom ψ_e is added. The governor dynamics introduce the degrees of freedom $\Delta\theta_t$, $\Delta\theta_{govr1}$, $\Delta\theta_{govr2}$. The vector of control variables for the entire system (v) consists of the blade pitch of the two rotors, the aircraft controls, and the engine throttle. The vector of the pilot's controls (v_p) is related to the individual control inputs by the linear transformation

$$v = T_c v_p$$

where T_{CFE} is defined in section 4.1.6. The aerodynamic gust vector (g) is in velocity axes.

The coupled equations of motion are obtained by substituting the hub motion into the rotor equations and hub reactions, and then the hub reactions into the body equations of motion. The resulting coefficient matrices for the coupled system are:

$$A_2 = \begin{bmatrix} A_{2R1} & & \tilde{A}_{2R1} C_{R1} & \\ & \left(\frac{\Omega_1}{\Omega_2}\right)^2 A_{2R2} & \left(\frac{\Omega_1}{\Omega_2}\right)^2 \tilde{A}_{2R2} C_{R2} & \\ -C_{R1}^T C_{2R1} & -\left(\frac{\Omega_1}{\Omega_2}\right)^2 C_{R2}^T C_{2R2} & a_2 - C_{R1}^T \tilde{C}_{2R1} C_{R1} - \left(\frac{\Omega_1}{\Omega_2}\right)^2 C_{R2}^T \tilde{C}_{2R2} C_{R2} & \\ & & & \end{bmatrix}$$

$$A_1 = \begin{bmatrix} A_{1R1} & & \tilde{A}_{1R1} C_{R1} + \tilde{A}_{2R1} \bar{C}_{R1} \\ & \left(\frac{\Omega_1}{\Omega_2}\right) A_{1R2} & \left(\frac{\Omega_1}{\Omega_2}\right) \tilde{A}_{1R2} C_{R2} + \left(\frac{\Omega_1}{\Omega_2}\right)^2 \tilde{A}_{2R2} \bar{C}_{R2} \\ -C_{R1}^T C_{1R1} & -\left(\frac{\Omega_1}{\Omega_2}\right) C_{R2}^T C_{1R2} & \begin{array}{l} a_1 - C_{R1}^T \tilde{C}_{1R1} C_{R1} - \left(\frac{\Omega_1}{\Omega_2}\right) C_{R2}^T \tilde{C}_{1R2} C_{R2} \\ -C_{R1}^T \tilde{C}_{2R1} \bar{C}_{R1} - \left(\frac{\Omega_1}{\Omega_2}\right)^2 C_{R2}^T \tilde{C}_{2R2} \bar{C}_{R2} \end{array} \\ & & \end{bmatrix}$$

$$A_o = \begin{bmatrix} A_{oR1} & & \tilde{A}_{oR1} C_{R1} \\ & A_{oR2} & \tilde{A}_{oR2} C_{R2} \\ -C_{R1}^T C_{oR1} & -C_{R2}^T C_{oR2} & a_o - C_{R1}^T \tilde{C}_{oR1} C_{R1} - C_{R2}^T \tilde{C}_{oR2} C_{R2} \\ & & \end{bmatrix}$$

$$B = \begin{bmatrix} B_{R1} & & \\ & B_{R2} & \\ & & b \\ & & \end{bmatrix}$$

$$B_G = \begin{bmatrix} B_{GR1} R_{GR1} \\ B_{GR2} R_{GR2} \\ b_G + C_{R1}^T D_{GR1} R_{GR1} + C_{R2}^T D_{GR2} R_{GR2} \\ \end{bmatrix}$$

Recall that the Euler angle contributions are not to be included in α_x, α_y, and α_z. Hence in constructing A_o it is necessary to skip the

angular hub motion (α_x, α_y, α_z) columns of $\bar{A}_o$ and $\bar{C}_o$ for the Euler angle (ϕ_F, θ_F, ψ_F) columns of c (and A_o) when evaluating $\bar{A}_o c$ and $\bar{C}_o c$.

The rotor mass will be included in the helicopter gross weight. Hence in constructing A_2 it is necessary to skip the linear hub motion (x_h, y_h, z_h) columns of $\bar{C}_2$ for the rigid body (ϕ_F, θ_F, ψ_F, x_F, y_F, z_F) columns of c (and A_2) when evaluating $\bar{C}_2 c$. Also the rotor mass is included in the generalized mass of the airframe free vibration modes; so the linear hub motion columns of $\bar{C}_2$ will be skipped for all the body degrees of freedom columns of c when evaluating $\bar{C}_2 c$. This approach is also required for the $c^T \bar{C}_2 c$ term in A_1. Since the term involving $\bar{c}$ is the linear hub acceleration due to Euler angle velocities, which has already been included in a_1 if the gross weight includes the rotor mass, it follows that the entire $c^T \bar{C}_2 \bar{c}$ term is to be dropped.

The construction of the coupled equations of motion is still incomplete. The matrices defined above basically account for the coupling of the rotors and aircraft through the rotor hubs. It remains to account for the coupling which occurs through other paths.

Frequently the rotor is modeled as having a rigid control system. This option requires some restructuring of the equations of motion, since the rotor equations have been derived assuming that the blade rigid pitch degrees of freedom are present in the model and that the blade pitch control inputs enter through these degrees of freedom. In the limit of infinite control system stiffness, the solution of the rigid pitch equation of motion reduces to

$$\beta_0 = \beta_r = \theta_{com} - \sum \dot{k}_{\beta_i} \dot{q}_i - k_{\beta_G} \beta_G + (\theta_{1s} \cos\psi_m - \theta_{1c} \sin\psi_m)\dot{\psi}_s$$

or in the nonrotating frame

$$\begin{pmatrix} \theta_0 \\ \theta_{1c} \\ \theta_{1s} \\ \theta_{nc} \\ \theta_{ns} \\ \theta_{N/2} \end{pmatrix}_0 = \begin{pmatrix} \theta_0 \\ \theta_K \\ \theta_{1s} \\ \theta_{nc} \\ \theta_{ns} \\ \theta_{N/2} \end{pmatrix}_{con} - \sum_i k_{P_i} \begin{pmatrix} \beta_0 \\ \beta_{1c} \\ \beta_{1s} \\ \beta_{nc} \\ \beta_{ns} \\ \beta_{N/2} \end{pmatrix}_i$$

$$- k_{P_G} \begin{pmatrix} 0 \\ \beta_{Gc} \\ \beta_{Gs} \\ 0 \\ 0 \\ 0 \end{pmatrix} + \begin{pmatrix} 0 \\ \theta_{1s} \\ -\theta_{1c} \\ 0 \\ 0 \\ 0 \end{pmatrix} \psi_s$$

for $N \geq 3$; and

$$\begin{pmatrix} \theta_0 \\ \theta_1 \end{pmatrix}_0 = \begin{pmatrix} \theta_0 \\ \theta_1 \end{pmatrix}_{con} - \sum_i k_{P_i} \begin{pmatrix} \beta_0 \\ \beta_1 \end{pmatrix}_i - k_{P_G} \begin{pmatrix} 0 \\ \beta_T \end{pmatrix} + \begin{pmatrix} 0 \\ \theta_{1s}\cos\psi - \theta_{1c}\sin\psi \end{pmatrix} \psi_s$$

for $N = 2$. The blade rigid pitch motion in this limit consists of the commanded control input, feedback of the bending and gimbal motion due to the kinematic coupling, and a pitch change due to the azimuth perturbation with a fixed swashplate. Substituting for p_0, the pitch/bending, pitch/gimbal, and pitch/azimuth coupling requires operations on the columns of A_0, as defined by the above equations. Next the rotor terms in the control matrix B are reconstructed from the rigid pitch columns of A_0 since the blade pitch motion becomes a control

variable rather than a degree of freedom. Then the equations of motion for the rigid pitch degrees of freedom are dropped from the system.

So far the aerodynamic hub forces have been put in place for the λ_u, λ_x, and λ_y equations of the two rotors; $\alpha = cx_s$ has been substituted for the hub motion; and the time scale for rotor #2 has been changed to Ω_1. Completion of the equations of motion for the inflow dynamics requires the following steps:

a. Multiply the equations by the matrix $(\sigma a/2\gamma)L$.

b. Account for the coupling of the λ_{u1} and λ_{u2} equations by the rotor/rotor interference.

c. Construct the diagonal (1.0) terms in A_1, and the LM terms in A_2 (times (Ω_1/Ω_2) and $(\Omega_1/\Omega_2)^2$ for rotor #2).

d. Construct the ground effect terms (body motion contributions to $(\partial\lambda/\partial z)\delta z$) in the λ_{u1} and λ_{u2} equations.

e. Construct the aerodynamic interference terms

$$\rho_\lambda \begin{pmatrix} \dot{\lambda}_{u_1} \\ (\Omega_1/\Omega_2)\,\dot{\lambda}_{u_2} \end{pmatrix}$$

in the aircraft equations.

So far the torque has been put in place for the rotational speed equations of the two rotors; $\alpha = cx_s$ has been substituted for the hub motion; and the time scale for rotor #2 has been changed to Ω_1. Completion of the equations of motion for the drive train dynamics requires the following steps.

a. Transform the ψ_{s1} and ψ_{s2} columns of the matrices according to

$$\Psi_{s_1} = \Psi_s$$

$$\Psi_{s_2} = \frac{r_{I_1}}{r_{I_2}}\Psi_s + \Psi_I$$

to convert from ψ_{s1} and ψ_{s2} degrees of freedom to ψ_s and ψ_I degrees of freedom.

b. Combine C_{Q1} and C_{Q2} as required for the ψ_s and ψ_I equations.

c. Construct the equation of motion for ψ_e and complete construction of the ψ_s and ψ_I equation by adding inertial, damping, and spring terms. Construct throttle control terms in ψ_s and ψ_e equations.

d. Construct the governor equations, and the governor degree of freedom terms in the other equations of motion.

It is still necessary to account for the mast bending and governor feedback terms in the pitch control θ_{con}. The pitch/mast bending coupling is (for each rotor)

$$\begin{pmatrix} \Delta\theta_c \\ \Delta\theta_s \end{pmatrix} = -\sum_{i=7}^{\infty} \begin{pmatrix} K_{MC_i} \\ K_{MS_i} \end{pmatrix} q_{s_i}$$

for $N \geq 3$, and

$$\Delta\theta_1 = -\sum_{i=7}^{\infty} \left(K_{MC_i} \cos\psi + K_{MS_i} \sin\psi \right) q_{s_i}$$

for $N = 2$.

For a two-bladed rotor the pitch control degrees of freedom are θ_0 and θ_1. It is also useful to consider conventional cyclic control, which gives

$$\Delta\theta_1 = \theta_{1c} \cos\psi + \theta_{1s} \sin\psi$$

The θ_{1c} and θ_{1s} columns of the control matrix can be constructed from the θ_1 column according to this equation.

Next, the pilot's control matrix is constructed from the individual control matrix by the linear transformation $B_P = BT_C$.

From section 4.2.9, the equations for the airframe sensors have the form

$$y = c_2 \ddot{x}_s + c_1 \dot{x}_s + c_0 x_s + d_0 g$$

or

$$y = C_2 \ddot{x} + C_1 \dot{x} + C_0 x + D_0 g$$

or in terms of the state vector of the complete system.

Optionally the airframe rigid body motion can be transformed from fuselage (F) axes to stability (V) axes, by substituting

$$\begin{pmatrix} \phi \\ \theta \\ \psi \\ x \\ y \\ z \end{pmatrix}_F = \mathcal{R}_{FV} \begin{pmatrix} \phi \\ \theta \\ \psi \\ x \\ y \\ z \end{pmatrix}_V$$

(see section 4.2.1), and multiplying the equations of motion by the transpose of the transform.

Finally, the unused equations of motion and degrees of freedom are eliminated from the model by deleting the appropriate rows and columns from the coefficient matrices. Note that a number of the degrees of

freedom are first order (no spring terms): all the inflow perturbation variables; the rigid body degrees of freedom ψ_F, x_F, y_F (except possibly in ground effect); and perhaps the rotational speed degree of freedom (in axial flow with no integral governor).

6.3.2 Quasistatic approximation.

It is frequently possible to reduce the order of the system of equations describing the rotorcraft dynamics by considering a quasistatic approximation for certain of the degrees of freedom. The equations of motion and the output equation are:

$$A_2 \ddot{x} + A_1 \dot{x} + A_0 x = B_0 v$$

$$y = C_2 \ddot{x} + C_1 \dot{x} + C_0 x + D_0 v$$

Assume that the degrees of freedom have been reordered so that the quasistatic variables (x_0) appear last in the vector:

$$x = \begin{pmatrix} x_1 \\ x_0 \end{pmatrix}$$

The quasistatic approximation consists of neglecting the acceleration and velocity terms of the quasistatic variables. Thus the equations take the form:

$$\begin{bmatrix} A_2^{11} & 0 \\ A_2^{01} & 0 \end{bmatrix} \begin{pmatrix} x_1 \\ x_0 \end{pmatrix}^{\cdot\cdot} + \begin{bmatrix} A_1^{11} & 0 \\ A_1^{01} & 0 \end{bmatrix} \begin{pmatrix} x_1 \\ x_0 \end{pmatrix}^{\cdot} + \begin{bmatrix} A_0^{11} & A_0^{10} \\ A_0^{01} & A_0^{00} \end{bmatrix} \begin{pmatrix} x_1 \\ x_0 \end{pmatrix} = \begin{pmatrix} B_0^{1} \\ B_0^{0} \end{pmatrix} v$$

$$y = \begin{bmatrix} C_2^{1} & 0 \end{bmatrix} \begin{pmatrix} x_1 \\ x_0 \end{pmatrix}^{\cdot\cdot} + \begin{bmatrix} C_1^{1} & 0 \end{bmatrix} \begin{pmatrix} x_1 \\ x_0 \end{pmatrix}^{\cdot} + \begin{bmatrix} C_0^{1} & C_0^{0} \end{bmatrix} \begin{pmatrix} x_1 \\ x_0 \end{pmatrix} + D_0 v$$

The quasistatic variables now are not described by differential equations but rather by linear algebraic equations. The solution for x_0 then is simply

$$x_0 = (A_0^{00})^{-1} \left[B_0^0 v - A_2^{01} \ddot{x}_1 - A_1^{01} \dot{x}_1 - A_0^{01} x_1 \right]$$

Substituting for x_0 in the x_1 equations of motion and in the output equations, gives the reduced-order equations for the quasistatic approximation:

$$\left[A_2^{11} - A_0^{10} (A_0^{00})^{-1} A_2^{01} \right] \ddot{x}_1 + \left[A_1^{11} - A_0^{10} (A_0^{00})^{-1} A_1^{01} \right] \dot{x}_1$$
$$+ \left[A_0^{11} - A_0^{10} (A_0^{00})^{-1} A_0^{01} \right] x_1 = \left[B_0 - A_0^{10} (A_0^{00})^{-1} B_0^0 \right] v$$

$$y = \left[C_2^1 - C_0^0 (A_0^{00})^{-1} A_2^{01} \right] \ddot{x}_1 + \left[C_1^1 - C_0^0 (A_0^{00})^{-1} A_1^{01} \right] \dot{x}_1$$
$$+ \left[C_0^1 - C_0^0 (A_0^{00})^{-1} A_0^{01} \right] x_1 + \left[D_0 + C_0^0 (A_0^{00})^{-1} B^0 \right] v$$

For any first-order quasistatic variables, the columns of A_0 and C_0 are replaced by the columns of A_1 and C_1.

In the present analysis, the quasistatic approximation can be applied to the inflow dynamics of either or both rotors; to the rigid pitch/elastic torsion degrees of freedom of either or both rotors; to all the degrees of freedom for either or both rotors; or even to all the degrees of freedom except the rigid-body motions of the aircraft.

The quasistatic approximation retains the low-frequency dynamics of the eliminated degrees of freedom. Whether that is a satisfactory representation of the elastic behavior must be established by comparison with the results of the higher order model.

The quasistatic approximation as implemented here does not give the low frequency response when applied to a two-bladed rotor. The source of this difficulty is the fact that the teetering equations of motion ($\beta_1^{(k)}$, $\theta_1^{(k)}$, β_T) are really still in the rotating frame, so the response of the teetering modes to low frequency inputs from the nonrotating frame is not at low frequency also, but rather at frequencies around 1/rev.

6.3.3 Symmetric aircraft.

With lateral symmetry of both the aircraft and flight state, the symmetric and antisymmetric motions are completely decoupled. Hence it is possible to analyze the dynamics by considering two sets of equations, each of half the order as the whole system. This case is applicable to side-by-side or tilting proprotor aircraft configuration in a trim flight condition with no sideward velocity or turn rate.

The equations of motion must be restructured in terms of symmetric and antisymmetric degrees of freedom. The motions of the right and left sides of the aircraft are given by respectively the sum and difference of the symmetric and antisymmetric degrees of freedom:

$$q_{rotor\,\#1} = q_{sym} + q_{anti}$$

$$q_{rotor\,\#2} = q_{sym} - q_{anti}$$

These conversions apply to the rotor bending, torsion, gimbal, and inflow degrees of freedom, and to the rotor pitch control variables. The columns of the coefficient matrices are reconstructed according to

these definitions of the symmetric and antisymmetric degrees of freedom. The symmetric and antisymmetric equations of motion are obtained by operating on the rows of the matrices as follows:

$$(\text{sym eq}_i) = \frac{1}{2}(\text{rotor \#1 eq}_i) + \frac{1}{2}(\text{rotor \#2 eq}_i)$$

$$(\text{antisym eq}_i) = \frac{1}{2}(\text{rotor \#1 eq}_i) - \frac{1}{2}(\text{rotor \#2 eq}_i)$$

Finally, the symmetric and antisymmetric drive train motions are obtained from

$$\Psi_s = \Psi_{sym} + \Psi_{anti}$$

$$\Psi_I = -2\Psi_{anti}$$

$$\Psi_e = \Psi_{sym} - \Psi_{anti}$$

(from section 4.3.3); the columns of the matrices are reconstructed according to these equations. Now the symmetric and antisymmetric degrees of freedom are completely decoupled, and may be analyzed separately. The state vector, control vectors, and gust vector for the symmetric system are:

$$x = [\, \beta^{(k)} \; \theta^{(k)} \; \beta_{GC} \; \beta_{bs} \; \Psi_s \; l_u \; l_x \; l_y \; \theta_f \; x_F \; z_F \; q_{sk} \; \Psi_e \; \Delta\theta_t \; \Delta\theta_{govr} \,]^T$$

$$v = [\, \theta^{con} \; \delta_f \; \delta_e \; \theta_t \; (f_l)_{sym} \,]^T$$

$$v_p = [\delta_0 \; \delta_s \; \delta_t]^T$$

$$g = [u_G \; w_G]^T$$

The state vector, control vectors, and gust vector for the antisymmetric system are:

$$x = [\beta^{(k)} \; \partial^{(k)} \; \beta_{GC} \; \beta_{GS} \; \psi_I \; l_u \; l_v \; l_y \; \phi_F \; \psi_F \; y_F \; \gamma_{SK}]^T$$

$$v = [\theta^{com} \; \delta_a \; \delta_r \; (f_\Omega)_{anti}]^T$$

$$v_p = [\delta_c \; \delta_e]^T$$

$$g = [v_G]^T$$

Note that it is necessary to designate symmetric and antisymmetric elastic airframe vibration modes.

6.4 Matrices of Rotor Equations of Motion

6.4.1 Inertial matrices for rotor equations.

The inertial matrices for the rotor equations of motion in the nonrotating frame are given below. For clarity, the superscript * denoting the normalization of the inertial coefficients has been omitted.

$$A_2 = \begin{bmatrix}
I_{q_k} & & & -S_{q_k}\ddot{p}_i & & & & & I_{q_k\alpha}\cdot\vec{k}_B & & & \\
& I_{q_k} & & & -S_{q_k}\ddot{p}_i & & I_{q_k\alpha}\cdot\vec{I}_B & -I_{q_k}\dot{\beta} & & & & \\
& & I_{q_k} & & & -S_{q_k}\ddot{p}_i & I_{q_k}\dot{\beta} & I_{q_k\alpha}\cdot\vec{I}_B & & & & \\
-S_{p_k}\ddot{q}_i & & & I_{p_k} & & & & & I_{p_k\alpha}\cdot\vec{I}_B & & & \\
& -S_{p_k}\ddot{q}_i & & & I_{p_k} & & -I_{p_k\alpha}\cdot\vec{k}_B & & & & & \\
& & -S_{p_k}\ddot{q}_i & & & I_{p_k} & & -I_{p_k\alpha}\cdot\vec{k}_B & & & & \\
& I_{q_i\alpha}\cdot\vec{I}_B & & & -S_{q_o}\ddot{p}_i\cdot\vec{I}_B & & I_o & & & & & \\
& & I_{q_i\alpha}\cdot\vec{I}_B & & & -S_{q_o}\ddot{p}_i\cdot\vec{I}_B & & I_o & & & & \\
I_{q_i\alpha}\cdot\vec{k}_B & & & -S_{q_o}\ddot{p}_i\cdot\vec{k}_B & & & & & I_o & & & \\
& & & & & & & & & & & \\
& & & & & & & & & & & \\
& & & & & & & & & & &
\end{bmatrix}$$

$$
A_1 =
\begin{bmatrix}
I_{q_k} g_s^{\nu_k} + 2I_{q_k} \dot{q}_1 & 2I_{q_k} & I_{q_k} g_s^{\nu_k} + 2I_{q_k} \dot{q}_1 & & -2S_{q_k} \ddot{p}_1 & & 2I_{q_k} \cdot \dot{i}_B & 2I_{q_k} \dot{\psi} \\
-2I_{q_k} & & 2S_{q_k} \ddot{p}_1 & & & -2I_{q_k \alpha} \cdot \dot{i}_B & & \\
& I_{p_k} g_s^{\omega_k} & & & & & & \\
2S_{p_k} \ddot{q}_1 & -2S_{p_k} \ddot{q}_1 & & I_{p_k} g_s^{\omega_k} & 2I_{p_k} + 2I_{p_k} \ddot{p}_1 & & -2I_{p_k \alpha} \cdot \dot{k}_B & \\
2I_{q_o} \dot{q}_1 \cdot \dot{I}_B & 2I_{q_1 \alpha} \cdot \dot{I}_B & & -2I_{p_k} - 2I_{p_k} \ddot{p}_1 & & 2I_{p_k \alpha} \cdot \dot{k}_B & & \\
-2I_{q_1 \alpha} \cdot \dot{i}_B & 2I_{q_o} \dot{q}_1 \cdot \dot{I}_B & 2S_{q_o} \ddot{p}_1 \cdot \dot{I}_B & & 2S_{q_o} \ddot{q}_o p_1 \cdot \dot{I}_B & I_o C_G & 2I_o & \\
2I_{q_o} \dot{q}_1 \cdot \dot{k}_B & & & & -2I_o & I_o C_G & & \\
& & & & & & & \\
& & & & & & & \\
& & & & & & &
\end{bmatrix}
$$

$$
A_o = \begin{bmatrix}
{}^{1}q_k \bar{v}_k & & & -S_{q_k p_i} & & & & & & & & \\
& {}^{1}q_k (\bar{v}_k^2 - 1) & {}^{1}q_k g_s \nu_k + 2 {}^{1}q_k \dot{q}_i & & S_{q_k \ddot{p}_i} - S_{q_k p_i} & & & & & & & \\
& -{}^{1}q_k g_s \nu_k - 2 {}^{1}q_k \dot{q}_i & {}^{1}q_k (\bar{v}_k^2 - 1) & & & S_{q_k \ddot{p}_i} - S_{q_k p_i} & & & & & & \\
-S_{p_k q_i} + S_{p_k o^K p_i} & & & {}^{1}p_k \bar{v}_k + {}^{1}p_k p_i & & & & & & & & \\
& S_{p_k \ddot{q}_i} - S_{p_k q_i} + S_{p_k o^K p_i} & & & {}^{1}p_k (\omega_k^2 - 1) + {}^{1}p_k p_i - {}^{1}p_k \ddot{p}_i & {}^{1}p_k g_s \nu_k & S_{p_k o^K p_G} & & -S_{p_k o^{\theta_{1s}}} & & & \\
& & S_{p_k \ddot{q}_i} - S_{p_k q_i} + S_{p_k o^K p_i} & & -{}^{1}p_k g_s \nu_k & {}^{1}p_k (\omega_k^2 - 1) + {}^{1}p_k p_i - {}^{1}p_k \ddot{p}_i & & S_{p_k o^K p_G} & S_{p_k o^{\theta_{1c}}} & & & \\
& & 2 {}^{1}q_o \dot{q}_i \cdot \bar{I}_B & & & & I_o (\bar{v}_G^2 - 1) & & & & & \\
& -2 {}^{1}q_o \dot{q}_i \cdot \bar{I}_B & & & & & & I_o (\bar{v}_G^2 - 1) & & & & \\
& & & & & & & & & & & \\
& & & & & & & & & & & \\
& & & & & & & & & & & \\
& & & & & & & & & & &
\end{bmatrix}
$$

$$\tilde{A}_2 = \begin{bmatrix}
 & & S_{q_k}\cdot\vec{i}_B & & & I_{q_k\alpha}\cdot\vec{k}_B \\
 & S_{q_k}\cdot\vec{k}_B & & & -I_{q_k\alpha}\cdot\vec{i}_B & \\
-S_{q_k}\cdot\vec{k}_B & & & I_{q_k\alpha}\cdot\vec{i}_B & & \\
 & & -S_{p_k}\cdot\vec{k}_B & & & I_{p_k\alpha}\cdot\vec{i}_B \\
 & S_{p_k}\cdot\vec{i}_B & & & I_{p_k\alpha}\cdot\vec{k}_B & \\
-S_{p_k}\cdot\vec{i}_B & & & -I_{p_k\alpha}\cdot\vec{k}_B & & \\
 & & & & -I_o & \\
 & & & I_o & & \\
 & & & & & I_o \\
 & & & & & \\
 & & & & & \\
 & & & & &
\end{bmatrix}$$

$$\tilde{A}_1 = \begin{bmatrix} & & & & & 2I_{q_k}\dot{\psi} \\ & & & 2I_{q_k\alpha}\cdot\vec{i}_B & & \\ & & & & 2I_{q_k\alpha}\cdot\vec{i}_B & \\ & & & & & \\ & & & -2I_{p_k\alpha}\cdot\vec{k}_B & & \\ & & & & -2I_{p_k\alpha}\cdot\vec{k}_B & \\ & & & 2I_o & & \\ & & & & 2I_o & \\ & & & & & \\ & & & & & \\ & & & & & \\ & & & & & \end{bmatrix}$$

$$B = \begin{bmatrix} & & \\ & & \\ & & \\ S_{p_k^o} & & \\ & S_{p_k^o} & \\ & & S_{p_k^o} \\ & & \\ & & \\ & & \\ & & \\ & & \\ & & \end{bmatrix}$$

$$
C_2 \equiv
\begin{bmatrix}
 & & & & & \\
 & & & & & \\
 & & & & & \\
 & & & & & -2I_o \\
 & & & I_o & & \\
 & & & & I_o & \\
 & & & S_{q_o \ddot{p}_i} \cdot \hat{i}_B & & \\
 & & & & -S_{q_o \ddot{p}_i} \cdot \hat{i}_B & \\
 & & & & & 2S_{q_o \ddot{p}_i} \cdot \hat{k}_B \\
S_{q_1} \cdot \hat{k}_B & & & -I_{q_1 \alpha} \cdot \hat{i}_B & & \\
 & -S_{q_1} \cdot \hat{k}_B & & & I_{q_1 \alpha} \cdot \hat{i}_B & \\
 & & -2S_{q_1} \cdot \hat{i}_B & & & -2I_{q_1 \alpha} \cdot \hat{k}_B
\end{bmatrix}
$$

$$
C_1 = \begin{bmatrix}
 & & & & & \\
 & & & & & \\
 & & & & & \\
 & & & & & \\
 & & & & 2I_o & \\
 & & & 2I_o & & \\
 & & & & -2S_{q_o\ddot{p}_1}\cdot\vec{i}_B & \\
 & & & -2S_{q_o\ddot{p}_1}\cdot\vec{i}_B & & \\
 & & & -2I_{q_o\dot{q}_1}\cdot\vec{i}_B & 2I_{q_1\alpha}\cdot\vec{i}_B & \\
 & & & 2I_{q_1\alpha}\cdot\vec{i}_B & 2I_{q_o\dot{q}_1}\cdot\vec{i}_B & -4I_{q_o\dot{q}_1}\cdot\vec{k}_B
\end{bmatrix}
$$

$$
C_o = \begin{bmatrix}
 & & & & & \\
 & & & & & \\
 & & & & & \\
 & & & & & \\
 & & & & & \\
 & & & & & \\
 & & & & & \\
 & & & & & \\
 & & & & & \\
 & & & & & \\
 & & & 2I_{q_o}\dot{q}_1 \cdot \hat{i}_B & 2I_{q_o}\dot{q}_1 \cdot \hat{i}_B & \\
 & & & & & \\
\end{bmatrix}
$$

$$\tilde{C}_2 = \begin{bmatrix} -2M_b & & & & & \\ & -2M_b & & & & \\ & & -2M_b & & & \\ & & & -I_o & & \\ & & & & -I_o & \\ & & & & & -2I_o \end{bmatrix}$$

$$\tilde{C}_1 = \begin{bmatrix} & & & & & \\ & & & & & \\ & & & & & \\ & & & & -2I_o & \\ & & & 2I_o & & \\ & & & & & \end{bmatrix}$$

6.4.2 Aerodynamic matrices for rotor equations in axial flow.

The aerodynamic matrices for the rotor equations of motion in axial flow are given below.

$$A_1 = \begin{bmatrix}
-\gamma M_{q_k \dot{q}_i} & & & & & & & & -\gamma M_{q_k \dot{\zeta}} & -\gamma M_{q_k \lambda} & & \\
& -\gamma M_{q_k \dot{q}_i} & & & & & -\gamma M_{q_k \dot{\beta}} & & & & -\gamma M_{q_k \dot{\beta}} & \\
& & -\gamma M_{q_k \dot{q}_i} & & & & & -\gamma M_{q_k \dot{\beta}} & & & & -\gamma M_{q_k \dot{\beta}} \\
-\gamma M_{p_k \dot{q}_i} & & & -\gamma M_{p_k \dot{p}_i} & & & & & -\gamma M_{p_k \dot{\zeta}} & -\gamma M_{p_k \lambda} & & \\
& -\gamma M_{p_k \dot{q}_i} & & & -\gamma M_{p_k \dot{p}_i} & & -\gamma M_{p_k \dot{\beta}} & & & & -\gamma M_{p_k \dot{\beta}} & \\
& & -\gamma M_{p_k \dot{q}_i} & & & -\gamma M_{p_k \dot{p}_i} & & -\gamma M_{p_k \dot{\beta}} & & & & -\gamma M_{p_k \dot{\beta}} \\
& -\gamma M^{\bullet}_{q_i} & & & & & -\gamma M^{\bullet}_{\beta} & & & & -\gamma M^{\bullet}_{\beta} & \\
& & -\gamma M^{\bullet}_{q_i} & & & & & -\gamma M^{\bullet}_{\beta} & & & & -\gamma M^{\bullet}_{\beta} \\
\gamma Q^{\bullet}_{p_i} & & & & & & & & \gamma Q^{\bullet}_{\zeta} & \gamma Q_{\lambda} & & \\
-2\gamma T^{\bullet}_{q_i} & & & & & & & & -2\gamma T^{\bullet}_{\zeta} & -2\gamma T_{\lambda} & & \\
& -\gamma M^{\bullet}_{q_i} & & & & & -\gamma M^{\bullet}_{\beta} & & & & -\gamma M^{\bullet}_{\beta} & \\
& & -\gamma M^{\bullet}_{q_i} & & & & & -\gamma M^{\bullet}_{\beta} & & & & -\gamma M^{\bullet}_{\beta}
\end{bmatrix}$$

$$
A_o = \begin{bmatrix}
-\gamma M_{q_k q_i} & & -\gamma M_{q_k p_i} & & & & & -\gamma M_{q_k \zeta} & & & \\
 & -\gamma M_{q_k q_i} & & -\gamma M_{q_k p_j} & & -\gamma M_{q_k \beta} & -\gamma M_{q_k \dot{\beta}} & & & & \\
 & \gamma M_{q_k \dot{q}_i} & -\gamma M_{q_k q_i} & & -\gamma M_{q_k p_i} & \gamma M_{q_k \dot{\beta}} & -\gamma M_{q_k \beta} & & & & \\
-\gamma M_{p_k q_i} & & -\gamma M_{p_k p_i} & & & & & -\gamma M_{p_k \zeta} & & & \\
 & -\gamma M_{p_k q_i} & & -\gamma M_{p_k p_j} & & -\gamma M_{p_k \beta} & -\gamma M_{p_k \dot{\beta}} & & & & \\
 & \gamma M_{p_k \dot{q}_i} & -\gamma M_{p_k q_i} & & -\gamma M_{p_k \dot{p}_i} & \gamma M_{p_k \dot{\beta}} & -\gamma M_{p_k \beta} & & & & \\
 & -\gamma M_{q_i} & -\gamma M_{\dot{q}_i} & & -\gamma M_{p_i} & -\gamma M_{\beta} & -\gamma M_{\dot{\beta}} & & & & \\
 & \gamma M_{\dot{q}_i} & -\gamma M_{q_i} & & -\gamma M_{\dot{p}_i} & \gamma M_{\dot{\beta}} & -\gamma M_{\beta} & & & & \\
\gamma Q_{q_i} & & \gamma Q_{p_i} & & & & & \gamma Q_{\zeta} & & & \\
-2\gamma T_{q_i} & & -2\gamma T_{p_i} & & & & & -2\gamma T_{\zeta} & & & \\
 & -\gamma M_{q_i} & -\gamma M_{\dot{q}_i} & & -\gamma M_{p_i} & -\gamma M_{\beta} & -\gamma M_{\dot{\beta}} & & & & \\
 & \gamma M_{\dot{q}_i} & -\gamma M_{q_i} & & -\gamma M_{\dot{p}_i} & \gamma M_{\dot{\beta}} & -\gamma M_{\beta} & & & &
\end{bmatrix}
$$

$$\tilde{A}_1 = \begin{bmatrix}
 & & -\gamma M_{q_k\lambda} & & & -\gamma M_{q_k\dot{\zeta}} \\
 & -\gamma M_{q_k\mu} & & & \gamma M_{q_k\dot{\beta}} & \\
\gamma M_{q_k\mu} & & & -\gamma M_{q_k\dot{\beta}} & & \\
 & & -\gamma M_{p_k\lambda} & & & -\gamma M_{p_k\dot{\zeta}} \\
 & -\gamma M_{p_k\mu} & & & \gamma M_{p_k\dot{\beta}} & \\
\gamma M_{p_k\mu} & & & -\gamma M_{p_k\dot{\beta}} & & \\
 & -\gamma M_{\mu} & & & \gamma M_{\dot{\beta}} & \\
\gamma M_{\mu} & & & -\gamma M_{\dot{\beta}} & & \\
 & & \gamma Q_{\lambda} & & & \gamma Q_{\dot{\zeta}} \\
-\frac{\mu_x}{\kappa_f^2}\frac{\partial\lambda}{\partial\mu} & +\frac{\mu_y}{\kappa_f^2}\frac{\partial\lambda}{\partial\mu} & -2\gamma T_{\lambda} + \frac{\lambda}{\kappa_h^4}\frac{\partial\lambda}{\partial\mu} & & & -2\gamma T_{\dot{\zeta}} \\
 & -\gamma M_{\mu} & & & \gamma M_{\dot{\beta}} & \\
\gamma M_{\mu} & & & -\gamma M_{\dot{\beta}} & &
\end{bmatrix}$$

$$\tilde{A}_o = \begin{bmatrix} & & & \gamma\mu_y M_{q_k\lambda} & \gamma\mu_{\ddot{x}} M_{q_k\lambda} & -\gamma M_{q_k\zeta} \\ & & & -\gamma\mu_z M_{q_k\lambda} & & \\ & & & & -\gamma\mu_z M_{q_k\mu} & \\ & & & -\gamma\mu_y M_{p_k\lambda} & -\gamma\mu_x M_{p_k\lambda} & -\gamma M_{p_k\zeta} \\ & & & -\gamma\mu_z M_{p_k\mu} & & \\ & & & & -\gamma\mu_z M_{p_k\mu} & \\ & & & -\gamma\mu_z M_{\mu} & & \\ & & & & -\gamma\mu_z M_{\mu} & \\ & & & -\gamma\mu_y Q_{\lambda} & -\gamma\mu_x Q_{\lambda} & \gamma Q_{\zeta} \\ & & & 2\gamma\mu_y T_{\lambda} & 2\gamma\mu_x T_{\lambda} & -2\gamma T_{\zeta} \\ & & & -\gamma\mu_z M_{\mu} & & \\ & & & & -\gamma\mu_z M_{\mu} & \end{bmatrix}$$

$$
B_G = \begin{bmatrix}
 & & -\gamma M_{q_k{}^\lambda} \\
 & \gamma M_{q_k{}^\mu} & \\
\gamma M_{q_k{}^\mu} & & \\
 & & -\gamma M_{p_k{}^\lambda} \\
 & \gamma M_{p_k{}^\mu} & \\
\gamma M_{p_k{}^\mu} & & \\
 & \gamma M_\mu & \\
\gamma M_\mu & & \\
 & & \gamma Q_\lambda \\
-\frac{\mu_x}{\kappa_f{}^2}\frac{\partial\lambda}{\partial\mu} & -\frac{\mu_y}{\kappa_f{}^2}\frac{\partial\lambda}{\partial\mu} & \begin{matrix}-2\gamma T_\lambda \\ +\frac{\lambda}{\kappa_h{}^4}\frac{\partial\lambda}{\partial\mu}\end{matrix} \\
 & \gamma M_\mu & \\
\gamma M_\mu & &
\end{bmatrix}
$$

$$C_1 = \begin{bmatrix}
 & \gamma R^{\bullet}_{q_i} & \gamma H^{\bullet}_{q_i} & & & & \gamma R^{\bullet}_{\beta} & \gamma H^{\bullet}_{\beta} & & & \gamma R^{\bullet}_{\beta} & \gamma H^{\bullet}_{\beta} \\
 & -\gamma H^{\bullet}_{q_i} & \gamma R^{\bullet}_{q_i} & & & & -\gamma H^{\bullet}_{\beta} & \gamma R^{\bullet}_{\beta} & & & -\gamma H^{\bullet}_{\beta} & \gamma R^{\bullet}_{\beta} \\
2\gamma T^{\bullet}_{q_i} & & & & & & & & 2\gamma T^{\bullet}_{\zeta} & 2\gamma T_{\lambda} & & \\
 & & \gamma M^{\bullet}_{q_i} & & & & & \gamma M^{\bullet}_{\beta} & & & & \gamma M^{\bullet}_{\beta} \\
 & -\gamma M^{\bullet}_{q_i} & & & & & -\gamma M^{\bullet}_{\beta} & & & & -\gamma M^{\bullet}_{\beta} & \\
-2\gamma Q^{\bullet}_{q_i} & & & & & & & & -2\gamma Q^{\bullet}_{\zeta} & -2\gamma Q_{\lambda} & &
\end{bmatrix}$$

$$
C_o = \begin{bmatrix}
 & \gamma R_{q_i} - \gamma H_{\dot{q}_i} & \gamma H_{q_i} + \gamma R_{\dot{q}_i} & & \gamma R_{p_i} & \gamma H_{q_i} & \gamma R_{\beta} - \gamma H_{\dot{\beta}} & \gamma H_{\beta} + \gamma R_{\dot{\beta}} & & & & \\
 & -\gamma H_{q_i} - \gamma R_{\dot{q}_i} & \gamma R_{q_i} - \gamma H_{\dot{q}_i} & & -\gamma H_{p_i} & \gamma R_{p_i} & -\gamma H_{\beta} - \gamma R_{\dot{\beta}} & \gamma R_{\beta} - \gamma H_{\dot{\beta}} & & & & \\
2\gamma T_{q_i} & & & 2\gamma T_{p_i} & & & & & 2\gamma T_{\zeta} & & & \\
 & -\gamma M_{\dot{q}_i} & \gamma M_{q_i} & & & \gamma M_{p_i} & -\gamma M_{\dot{\beta}} & \gamma M_{\beta} & & & & \\
 & -\gamma M_{q_i} & -\gamma M_{\dot{q}_i} & & -\gamma M_{p_i} & & -\gamma M_{\beta} & -\gamma M_{\dot{\beta}} & & & & \\
-2\gamma Q_{q_i} & & & -2\gamma Q_{p_i} & & & & & -2\gamma Q_{\zeta} & & &
\end{bmatrix}
$$

$$\tilde{C}_1 = \begin{bmatrix} -\gamma(H_\mu + R_\mu) & \gamma R_r & & \gamma H_{\dot{\beta}} & -\gamma R_{\dot{\beta}} & \\ -\gamma R_r & -\gamma(H_\mu + R_\mu) & & \gamma R_{\dot{\beta}} & \gamma H_{\dot{\beta}} & \\ & & 2\gamma T_\lambda & & & 2\gamma T_{\dot{\zeta}} \\ -\gamma M_\mu & & & \gamma M_{\dot{\beta}} & & \\ & -\gamma M_\mu & & & \gamma M_{\dot{\beta}} & \\ & & -2\gamma Q_\lambda & & & -2\gamma Q_{\dot{\zeta}} \end{bmatrix}$$

$$\tilde{C}_o = \begin{bmatrix} & & & \gamma\mu_z R_r & -\gamma\mu_z(H_\mu+R_\mu) & \\ & & & -\gamma\mu_z(H_\mu+R_\mu) & \gamma\mu_z R_r & \\ & & & -2\gamma\mu_y T_\lambda & -2\gamma\mu_x T_\lambda & 2\gamma T_\zeta \\ & & & & \gamma\mu_z M_\mu & \\ & & & -\gamma\mu_z M_\mu & & \\ & & & 2\gamma\mu_y Q_\lambda & 2\gamma\mu_x Q_\lambda & -2\gamma Q_\zeta \end{bmatrix}$$

$$D_G = \begin{bmatrix} \gamma(H_\mu+R_\mu) & \gamma R_r & \\ \gamma R_r & -\gamma(H_\mu+R_\mu) & \\ & & -2\gamma T_\lambda \\ \gamma M_\mu & & \\ & -\gamma M_\mu & \\ & & 2\gamma Q_\lambda \end{bmatrix}$$

6.4.3 Aerodynamic matrices for rotor equations in nonaxial flow.

The aerodynamic matrices for the rotor equations of motion in nonaxial flow are given below. Note that each matrix is a summation over all the blades (m = 1 to N). The notation $C = \cos\psi_m$ and $S = \sin\psi_m$ is used in these matrices.

$$A_1 = \gamma \frac{1}{N} \sum_m$$

$-M_{q_k \dot{q}_i}$	$-M_{q_k \dot{q}_i}\, C$	$-M_{q_k \dot{q}_i}\, S$					$-M_{q_k \dot{\rho}}\, C$	$-M_{q_k \dot{\rho}}\, S$	$-M_{q_k \dot{\zeta}}$	$-M_{q_k \lambda}$	$-M_{q_k \dot{\rho}}\, C$	$-M_{q_k \dot{\rho}}\, S$	$-M_{q_k \dot{\rho}}\, S$	
$-M_{q_k \dot{q}_i}\, 2C$	$-M_{q_k \dot{q}_i}\, 2C^2$	$-M_{q_k \dot{q}_i}\, 2CS$					$-M_{q_k \dot{\rho}}\, 2C^2$	$-M_{q_k \dot{\rho}}\, 2CS$	$-M_{q_k \dot{\zeta}}\, 2C$	$-M_{q_k \lambda}\, 2C$	$-M_{q_k \dot{\rho}}\, 2C^2$	$-M_{q_k \dot{\rho}}\, 2CS$	$-M_{q_k \dot{\rho}}\, 2S^2$	
$-M_{q_k \dot{q}_i}\, 2S$	$-M_{q_k \dot{q}_i}\, 2CS$	$-M_{q_k \dot{q}_i}\, 2S^2$					$-M_{q_k \dot{\rho}}\, 2CS$	$-M_{q_k \dot{\rho}}\, 2S^2$	$-M_{q_k \dot{\zeta}}\, 2S$	$-M_{q_k \lambda}\, 2S$	$-M_{q_k \dot{\rho}}\, 2CS$	$-M_{q_k \dot{\rho}}\, 2S^2$		
$-M_{p_k \dot{q}_i}$	$-M_{p_k \dot{q}_i}\, C$	$-M_{p_k \dot{q}_i}\, S$	$-M_{p_k \dot{p}_i}$	$-M_{p_k \dot{p}_i}\, C$	$-M_{p_k \dot{p}_i}\, S$	$-M_{p_k \dot{p}_i}\, S$	$-M_{p_k \dot{\rho}}\, C$	$-M_{p_k \dot{\rho}}\, S$	$-M_{p_k \dot{\zeta}}$	$-M_{p_k \lambda}$	$-M_{p_k \dot{\rho}}\, C$	$-M_{p_k \dot{\rho}}\, S$	$-M_{p_k \dot{\rho}}\, S$	
$-M_{p_k \dot{q}_i}\, 2C$	$-M_{p_k \dot{q}_i}\, 2C^2$	$-M_{p_k \dot{q}_i}\, 2CS$	$-M_{p_k \dot{p}_i}\, 2C$	$-M_{p_k \dot{p}_i}\, 2C^2$	$-M_{p_k \dot{p}_i}\, 2CS$	$-M_{p_k \dot{p}_i}\, 2CS$	$-M_{p_k \dot{\rho}}\, 2C^2$	$-M_{p_k \dot{\rho}}\, 2CS$	$-M_{p_k \dot{\zeta}}\, 2C$	$-M_{p_k \lambda}\, 2C$	$-M_{p_k \dot{\rho}}\, 2C^2$	$-M_{p_k \dot{\rho}}\, 2CS$	$-M_{p_k \dot{\rho}}\, 2CS$	
$-M_{p_k \dot{q}_i}\, 2S$	$-M_{p_k \dot{q}_i}\, 2CS$	$-M_{p_k \dot{q}_i}\, 2S^2$	$-M_{p_k \dot{p}_i}\, 2S$	$-M_{p_k \dot{p}_i}\, 2CS$	$-M_{p_k \dot{p}_i}\, 2S^2$	$-M_{p_k \dot{p}_i}\, 2S^2$	$-M_{p_k \dot{\rho}}\, 2CS$	$-M_{p_k \dot{\rho}}\, 2S^2$	$-M_{p_k \dot{\zeta}}\, 2S$	$-M_{p_k \lambda}\, 2S$	$-M_{p_k \dot{\rho}}\, 2CS$	$-M_{p_k \dot{\rho}}\, 2S^2$	$-M_{p_k \dot{\rho}}\, 2S^2$	
$-M_{\dot{q}_i}\, 2C$	$-M_{\dot{q}_i}\, 2C^2$	$-M_{\dot{q}_i}\, 2CS$					$-M_{\dot{\rho}}\, 2C^2$	$-M_{\dot{\rho}}\, 2CS$	$-M_{\dot{\zeta}}\, 2C$	$-M_{\lambda}\, 2C$	$-M_{\dot{\rho}}\, 2C^2$	$-M_{\dot{\rho}}\, 2CS$	$-M_{\dot{\rho}}\, 2CS$	
$-M_{\dot{q}_i}\, 2S$	$-M_{\dot{q}_i}\, 2CS$	$-M_{\dot{q}_i}\, 2S^2$					$-M_{\dot{\rho}}\, 2CS$	$-M_{\dot{\rho}}\, 2S^2$	$-M_{\dot{\zeta}}\, 2S$	$-M_{\lambda}\, 2S$	$-M_{\dot{\rho}}\, 2CS$	$-M_{\dot{\rho}}\, 2S^2$	$-M_{\dot{\rho}}\, 2S^2$	
$Q_{\dot{q}_i}$	$Q_{\dot{q}_i}\, C$	$Q_{\dot{q}_i}\, S$					$Q_{\dot{\rho}}\, C$	$Q_{\dot{\rho}}\, S$	$Q_{\dot{\zeta}}$	Q_{λ}	$Q_{\dot{\rho}}\, C$	$Q_{\dot{\rho}}\, S$	$Q_{\dot{\rho}}\, S$	
$-2T_{\dot{q}_i}$	$-2T_{\dot{q}_i}\, C$	$-2T_{\dot{q}_i}\, S$					$-2T_{\dot{\rho}}\, C$	$-2T_{\dot{\rho}}\, S$	$-2T_{\dot{\zeta}}$	$-2T_{\lambda}$	$-2T_{\dot{\rho}}\, C$	$-2T_{\dot{\rho}}\, S$	$-2T_{\dot{\rho}}\, S$	
$-M_{\dot{q}_i}\, 2C$	$-M_{\dot{q}_i}\, 2C^2$	$-M_{\dot{q}_i}\, 2CS$					$-M_{\dot{\rho}}\, 2C^2$	$-M_{\dot{\rho}}\, 2CS$	$-M_{\dot{\zeta}}\, 2C$	$-M_{\lambda}\, 2C$	$-M_{\dot{\rho}}\, 2C^2$	$-M_{\dot{\rho}}\, 2CS$	$-M_{\dot{\rho}}\, 2CS$	
$-M_{\dot{q}_i}\, 2S$	$-M_{\dot{q}_i}\, 2CS$	$-M_{\dot{q}_i}\, 2S^2$					$-M_{\dot{\rho}}\, 2CS$	$-M_{\dot{\rho}}\, 2S^2$	$-M_{\dot{\zeta}}\, 2S$	$-M_{\lambda}\, 2S$	$-M_{\dot{\rho}}\, 2CS$	$-M_{\dot{\rho}}\, 2S^2$	$-M_{\dot{\rho}}\, 2S^2$	

$$A_o = \gamma \frac{1}{N} \sum_m$$

$-M_{q_k q_l}$	$M_{q_k \dot{q}_l} \dot{q}_l^S$ $-M_{q_k q_l} q_l^C$	$-M_{q_k \dot{q}_l} \dot{q}_l^C$ $-M_{q_k q_l} q_l^S$	$-M_{q_k P_l}$	$-M_{q_k P_l} C$	$-M_{q_k P_l} S$	$M_{q_k \beta} S$ $-M_{q_k \beta} C$	$-M_{q_k \beta} C$ $-M_{q_k \beta} S$	$-M_{q_k \zeta}$			
$-M_{q_k q_l} 2C$	$M_{q_k \dot{q}_l} 2CS$ $-M_{q_k q_l} 2C^2$	$-M_{q_k \dot{q}_l} 2C^2$ $-M_{q_k q_l} 2CS$	$-M_{q_k P_l} 2C$	$-M_{q_k P_l} 2C^2$	$-M_{q_k P_l} 2CS$	$M_{q_k \beta} 2CS$ $-M_{q_k \beta} 2C^2$	$-M_{q_k \beta} 2C^2$ $-M_{q_k \beta} 2CS$	$-M_{q_k \zeta} 2C$			
$-M_{q_k q_l} 2S$	$M_{q_k \dot{q}_l} 2S^2$ $-M_{q_k q_l} 2CS$	$-M_{q_k \dot{q}_l} 2CS$ $-M_{q_k q_l} 2S^2$	$-M_{q_k P_l} 2S$	$-M_{q_k P_l} 2CS$	$-M_{q_k P_l} 2S^2$	$M_{q_k \beta} 2S^2$ $-M_{q_k \beta} 2CS$	$-M_{q_k \beta} 2CS$ $-M_{q_k \beta} 2S^2$	$-M_{q_k \zeta} 2S$			
$-M_{p_k q_l}$	$+M_{p_k \dot{q}_l} S$ $-M_{p_k q_l} C$	$-M_{p_k \dot{q}_l} C$ $-M_{p_k q_l} S$	$-M_{p_k P_l}$	$-M_{p_k P_l} C$ $M_{p_k \dot{P}_l} S$	$-M_{p_k P_l} S$ $-M_{p_k \dot{P}_l} C$	$+M_{p_k \beta} S$ $-M_{p_k \beta} C$	$-M_{p_k \beta} C$ $-M_{p_k \beta} S$	$-M_{p_k \zeta}$			
$-M_{p_k q_l} 2C$	$+M_{p_k \dot{q}_l} 2CS$ $-M_{p_k q_l} 2C^2$	$-M_{p_k \dot{q}_l} 2C^2$ $-M_{p_k q_l} 2CS$	$-M_{p_k P_l} 2C$	$-M_{p_k P_l} 2C^2$ $M_{p_k \dot{P}_l} 2CS$	$-M_{p_k P_l} 2CS$ $-M_{p_k \dot{P}_l} 2C^2$	$+M_{p_k \beta} 2CS$ $-M_{p_k \beta} 2C^2$	$-M_{p_k \beta} 2C^2$ $-M_{p_k \beta} 2CS$	$-M_{p_k \zeta} 2C$			
$-M_{p_k q_l} 2S$	$+M_{p_k \dot{q}_l} 2S^2$ $-M_{p_k q_l} 2CS$	$-M_{p_k \dot{q}_l} 2CS$ $-M_{p_k q_l} 2S^2$	$-M_{p_k P_l} 2S$	$-M_{p_k P_l} 2CS$ $M_{p_k \dot{P}_l} 2S^2$	$-M_{p_k P_l} 2S^2$ $-M_{p_k \dot{P}_l} 2CS$	$+M_{p_k \beta} 2S^2$ $-M_{p_k \beta} 2CS$	$-M_{p_k \beta} 2CS$ $-M_{p_k \beta} 2S^2$	$-M_{p_k \zeta} 2S$			
$-M_{q_l} 2C$	$+M_{q_l} 2CS$ $-M_{q_l} 2C^2$	$-M_{q_l} 2C^2$ $-M_{q_l} 2CS$	$-M_{P_l} 2C$	$-M_{P_l} 2C^2$	$-M_{P_l} 2CS$	$+M_{\beta} 2CS$ $-M_{\beta} 2C^2$	$-M_{\beta} 2C^2$ $-M_{\beta} 2CS$	$-M_{\zeta} 2C$			
$-M_{q_l} 2S$	$+M_{q_l} 2S^2$ $-M_{q_l} 2CS$	$-M_{q_l} 2CS$ $-M_{q_l} 2S^2$	$-M_{P_l} 2S$	$-M_{P_l} 2CS$	$-M_{P_l} 2S^2$	$+M_{\beta} 2S^2$ $-M_{\beta} 2CS$	$-M_{\beta} 2CS$ $-M_{\beta} 2S^2$	$-M_{\zeta} 2S$			
Q_{q_l}	$Q_{q_l} C$ $-Q_{q_l} S$	$Q_{q_l} S$ $Q_{q_l} C$	Q_{P_l}	$Q_{P_l} C$	$Q_{P_l} S$	$-Q_{\beta} S$ $Q_{\beta} C$	$Q_{\beta} C$ $Q_{\beta} S$	Q_{ζ}			
$-2T_{q_l}$	$-2T_{q_l} C$ $2T_{q_l} S$	$-2T_{q_l} S$ $-2T_{q_l} C$	$-2T_{P_l}$	$-2T_{P_l} C$	$-2T_{P_l} S$	$2T_{\beta} S$ $-2T_{\beta} C$	$-2T_{\beta} C$ $-2T_{\beta} S$	$-2T_{\zeta}$			
$-M_{q_l} 2C$	$-M_{q_l} 2C^2$ $M_{q_l} 2CS$	$-M_{q_l} 2CS$ $-M_{q_l} 2C^2$	$-M_{P_l} 2C$	$-M_{P_l} 2C^2$	$-M_{P_l} 2CS$	$M_{\beta} 2CS$ $-M_{\beta} 2C^2$	$-M_{\beta} 2C^2$ $-M_{\beta} 2CS$	$-M_{\zeta} 2C$			
$-M_{q_l} 2S$	$-M_{q_l} 2CS$ $M_{q_l} 2S^2$	$-M_{q_l} 2C^2$ $-M_{q_l} 2CS$	$-M_{P_l} 2S$	$-M_{P_l} 2CS$	$-M_{P_l} 2S^2$	$M_{\beta} 2S^2$ $-M_{\beta} 2CS$	$-M_{\beta} 2CS$ $-M_{\beta} 2S^2$	$-M_{\zeta} 2S$			

$$\tilde{A}_1 = \gamma \frac{1}{N} \sum_m$$

$M_{q_k\mu}S$	$-M_{q_k\mu}C$	$-M_{q_k\lambda}$	$-M_{q_k\dot{\beta}}S$	$M_{q_k\dot{\beta}}C$	$-M_{q_k\dot{\zeta}}$
$M_{q_k\mu}2CS$	$-M_{q_k\mu}2C^2$	$-M_{q_k\lambda}2C$	$-M_{q_k\dot{\beta}}2CS$	$M_{q_k\dot{\beta}}2C^2$	$-M_{q_k\dot{\zeta}}2C$
$M_{q_k\mu}2S^2$	$-M_{q_k\mu}2CS$	$-M_{q_k\lambda}2S$	$-M_{q_k\dot{\beta}}2S^2$	$M_{q_k\dot{\beta}}2CS$	$-M_{q_k\dot{\zeta}}2S$
$M_{p_k\mu}S$	$-M_{p_k\mu}C$	$-M_{p_k\lambda}$	$-M_{p_k\dot{\beta}}S$	$M_{p_k\dot{\beta}}C$	$-M_{p_k\dot{\zeta}}$
$M_{p_k\mu}2CS$	$-M_{p_k\mu}2C^2$	$-M_{p_k\lambda}2C$	$-M_{p_k\dot{\beta}}2CS$	$M_{p_k\dot{\beta}}2C^2$	$-M_{p_k\dot{\zeta}}2C$
$M_{p_k\mu}2S^2$	$-M_{p_k\mu}2CS$	$-M_{p_k\lambda}2S$	$-M_{p_k\dot{\beta}}2S^2$	$M_{p_k\dot{\beta}}2CS$	$-M_{p_k\dot{\zeta}}2S$
$M_\mu 2CS$	$-M_\mu 2C^2$	$-M_\lambda 2C$	$-M_{\dot{\beta}}2CS$	$M_{\dot{\beta}}2C^2$	$-M_{\dot{\zeta}}2C$
$M_\mu 2S^2$	$-M_\mu 2CS$	$-M_\lambda 2S$	$-M_{\dot{\beta}}2S^2$	$M_{\dot{\beta}}2CS$	$-M_{\dot{\zeta}}2S$
$-Q_\mu S$	$Q_\mu C$	Q_λ	$Q_{\dot{\beta}}S$	$-Q_{\dot{\beta}}C$	$Q_{\dot{\zeta}}$
$2T_\mu S - \frac{\mu_x}{\kappa_f{}^2}\frac{\partial\lambda}{\partial\mu}$	$-2T_\mu C + \frac{\mu_y}{\kappa_f{}^2}\frac{\partial\lambda}{\partial\mu}$	$-2T_\lambda + \frac{\lambda}{\kappa_h{}^4}\frac{\partial\lambda}{\partial\mu}$	$-2T_{\dot{\beta}}S$	$2T_{\dot{\beta}}C$	$-2T_{\dot{\zeta}}$
$M_\mu 2CS$	$-M_\mu 2C^2$	$-M_\lambda 2C$	$-M_{\dot{\beta}}2CS$	$M_{\dot{\beta}}2C^2$	$-M_{\dot{\zeta}}2C$
$M_\mu 2S^2$	$-M_\mu 2CS$	$-M_\lambda 2S$	$-M_{\dot{\beta}}2S^2$	$M_{\dot{\beta}}2CS$	$-M_{\dot{\zeta}}2S$

$$\tilde{A}_o = \gamma \frac{1}{N} \sum_m \left[\begin{array}{c|c|c|c|c|c}
 & & & \mu_y M_{q_k \lambda} - \mu_z M_{q_k \mu} C & \mu_x M_{q_k \lambda} - \mu_z M_{q_k \mu} S & -M_{q_k \zeta} \\ \hline
 & & & \mu_y M_{q_k \lambda} 2C - \mu_z M_{q_k \mu} 2C^2 & \mu_x M_{q_k \lambda} 2C - \mu_z M_{q_k \mu} 2CS & -M_{q_k \zeta} 2C \\ \hline
 & & & \mu_y M_{q_k \lambda} 2S - \mu_z M_{q_k \mu} 2CS & \mu_x M_{q_k \lambda} 2S - \mu_z M_{q_k \mu} 2S^2 & -M_{q_k \zeta} 2S \\ \hline
 & & & \mu_y M_{p_k \lambda} - \mu_z M_{p_k \mu} C & \mu_x M_{p_k \lambda} - \mu_z M_{p_k \mu} S & -M_{p_k \zeta} \\ \hline
 & & & \mu_y M_{p_k \lambda} 2C - \mu_z M_{p_k \mu} 2C^2 & \mu_x M_{p_k \lambda} 2C - \mu_z M_{p_k \mu} 2CS & -M_{p_k \zeta} 2C \\ \hline
 & & & \mu_y M_{p_k \lambda} 2S - \mu_z M_{p_k \mu} 2CS & \mu_x M_{p_k \lambda} 2S - \mu_z M_{p_k \mu} 2S^2 & -M_{p_k \zeta} 2S \\ \hline
 & & & \mu_y M_\lambda 2C - \mu_z M_\mu 2C^2 & \mu_x M_\lambda 2C - \mu_z M_\mu 2CS & -M_\zeta 2C \\ \hline
 & & & \mu_y M_\lambda 2S - \mu_z M_\mu 2CS & \mu_x M_\lambda 2S - \mu_z M_\mu 2S^2 & -M_\zeta 2S \\ \hline
 & & & -\mu_y Q_\lambda \quad \mu_z Q_\mu C & -\mu_x Q_\lambda \quad \mu_z Q_\mu S & Q_\zeta \\ \hline
 & & & 2\mu_y T_\lambda - 2\mu_z T_\mu C & 2\mu_x T_\lambda - 2\mu_z T_\mu S & -2T_\zeta \\ \hline
 & & & \mu_y M_\lambda 2C - \mu_z M_\mu 2C^2 & \mu_x M_\lambda 2C - \mu_z M_\mu 2CS & -M_\zeta 2C \\ \hline
 & & & \mu_y M_\lambda 2S - \mu_z M_\mu 2CS & \mu_x M_\lambda 2S - \mu_z M_\mu 2S^2 & -M_\zeta 2S
\end{array} \right]$$

$$B_G = \gamma \frac{1}{N} \sum_m$$

$$\begin{bmatrix}
M_{q_k\mu} S & M_{q_k\mu} C & -M_{q_k\lambda} \\
M_{q_k\mu} 2CS & M_{q_k\mu} 2C^2 & -M_{q_k\lambda} 2C \\
M_{q_k\mu} 2S^2 & M_{q_k\mu} 2CS & -M_{q_k\lambda} 2S \\
M_{p_k\mu} S & M_{p_k\mu} C & -M_{p_k\lambda} \\
M_{p_k\mu} 2CS & M_{p_k\mu} 2C^2 & -M_{p_k\lambda} 2C \\
M_{p_k\mu} 2S^2 & M_{p_k\mu} 2CS & -M_{p_k\lambda} 2S \\
M_\mu 2CS & M_\mu 2C^2 & -M_\lambda 2C \\
M_\mu 2S^2 & M_\mu 2CS & -M_\lambda 2S \\
-Q_\mu S & -Q_\mu C & Q_\lambda \\
2T_\mu S - \frac{\mu_x}{\kappa_f^2}\frac{\partial\lambda}{\partial\mu} & 2T_\mu C - \frac{\mu_y}{\kappa_f^2}\frac{\partial\lambda}{\partial\mu} & -2T_\lambda + \frac{\lambda}{\kappa_h^4}\frac{\partial\lambda}{\partial\mu} \\
M_\mu 2CS & M_\mu 2C^2 & -M_\lambda 2C \\
M_\mu 2S^2 & M_\mu 2CS & -M_\lambda 2S
\end{bmatrix}$$

$$C_1 =$$

$H_{q_i} 2S$ $R_{q_i} 2C$	$H_{q_i} 2CS$ $R_{q_i} 2C^2$	$H_{q_i} 2S^2$ $R_{q_i} 2CS$				$H_\beta 2CS$ $R_\beta 2C^2$	$H_\beta 2S^2$ $R_\beta 2CS$	$H_\zeta 2S$ $R_\zeta 2C$	$H_\lambda 2S$ $R_\lambda 2C$	$H_\beta 2CS$ $R_\beta 2C^2$	$H_\beta 2S^2$ $R_\beta 2CS$
$-H_{q_i} 2C$ $+R_{q_i} 2S$	$-H_{q_i} 2C^2$ $+R_{q_i} 2CS$	$-H_{q_i} 2CS$ $+R_{q_i} 2S^2$				$-H_\beta 2C^2$ $+R_\beta 2CS$	$-H_\beta 2CS$ $+R_\beta 2S^2$	$-H_\zeta 2C$ $+R_\zeta 2S$	$-H_\lambda 2C$ $+R_\lambda 2S$	$-H_\beta 2C^2$ $+R_\beta 2CS$	$-H_\beta 2CS$ $+R_\beta 2S^2$
$2T_{q_i}$	$2T_{q_i} C$	$2T_{q_i} S$				$2T_\beta C$	$2T_\beta S$	$2T_\zeta$	$2T_\lambda$	$2T_\beta C$	$2T_\beta S$
$M_{q_i} 2S$	$M_{q_i} 2CS$	$M_{q_i} 2S^2$				$M_\beta 2CS$	$M_\beta 2S^2$	$M_\zeta 2S$	$M_\lambda 2S$	$M_\beta 2CS$	$M_\beta 2S^2$
$-M_{q_i} 2C$	$-M_{q_i} 2C^2$	$-M_{q_i} 2CS$				$-M_\beta 2C^2$	$-M_\beta 2CS$	$-M_\zeta 2C$	$-M_\lambda 2C$	$-M_\beta 2C^2$	$-M_\beta 2CS$
$-2Q_{q_i}$	$-2Q_{q_i} C$	$-2Q_{q_i} S$				$-2Q_\beta C$	$-2Q_\beta S$	$-2Q_\zeta$	$-2Q_\lambda$	$-2Q_\beta C$	$-2Q_\beta S$

$$C_o = \gamma \frac{1}{N} \sum_m$$

$$\begin{bmatrix}
H_{q_i}2S \; R_{q_i}2C & -H_{q_i}2S^2 \; H_{q_i}2CS \; -R_{q_i}2CS \; R_{q_i}2C^2 & H_{q_i}2CS \; H_{q_i}2S^2 \; R_{q_i}2C^2 \; R_{q_i}2CS & H_{p_i}2S \; R_{p_i}2C & H_{p_i}2CS \; R_{p_i}2C^2 & H_{p_i}2S^2 \; R_{p_i}2CS & -H_{\beta}2S^2 \; H_{\beta}2CS \; -R_{\beta}2CS \; R_{\beta}2C^2 & H_{\beta}2CS \; H_{\beta}2S^2 \; R_{\beta}2C^2 \; R_{\beta}2CS & H_{\zeta}2S \; R_{\zeta}2C & & & \\
-H_{q_i}2C \; +R_{q_i}2S & H_{q_i}2CS \; -H_{q_i}2C^2 \; -R_{q_i}2S^2 \; +R_{q_i}2CS & -H_{q_i}2C^2 \; -H_{q_i}2CS \; +R_{q_i}2CS \; +R_{q_i}2S^2 & -H_{p_i}2C \; +R_{p_i}2S & -H_{p_i}2C^2 \; +R_{p_i}2CS & -H_{p_i}2CS \; +R_{p_i}2S^2 & H_{\beta}2CS \; -H_{\beta}2C^2 \; -R_{\beta}2S^2 \; +R_{\beta}2CS & -H_{\beta}2C^2 \; -H_{\beta}2CS \; +R_{\beta}2CS \; +R_{\beta}2S^2 & -H_{\zeta}2C \; +R_{\zeta}2S & & & \\
2T_{q_i} & -2T_{q_i}S \; 2T_{q_i}C & 2T_{q_i}C \; 2T_{q_i}S & 2T_{p_i} & 2T_{p_i}C & 2T_{p_i}S & -2T_{\beta}S \; 2T_{\beta}C & 2T_{\beta}C \; 2T_{\beta}S & 2T_{\zeta} & & & \\
M_{q_i}2S & -M_{q_i}2S^2 \; +M_{q_i}2CS & M_{q_i}2CS \; +M_{q_i}2S^2 & M_{p_i}2S & M_{p_i}2CS & M_{p_i}2S^2 & -M_{\beta}2S^2 \; +M_{\beta}2CS & M_{\beta}2CS \; +M_{\beta}2S^2 & M_{\zeta}2S & & & \\
-M_{q_i}2C & M_{q_i}2CS \; -M_{q_i}2C^2 & -M_{q_i}2C^2 \; -M_{q_i}2CS & -M_{p_i}2C & -M_{p_i}2C^2 & -M_{p_i}2CS & M_{\beta}2CS \; -M_{\beta}2C^2 & -M_{\beta}2C^2 \; -M_{\beta}2CS & -M_{\zeta}2C & & & \\
-2Q_{q_i} & 2Q_{q_i}S \; -2Q_{q_i}C & -2Q_{q_i}C \; -2Q_{q_i}S & -2Q_{p_i} & -2Q_{p_i}C & -2Q_{p_i}S & 2Q_{\beta}S \; -2Q_{\beta}C & -2Q_{\beta}C \; -2Q_{\beta}S & -2Q_{\zeta} & & &
\end{bmatrix}$$

$$\tilde{C}_{ij} = \frac{1}{N}\sum_{m}$$

$$\begin{bmatrix}
-H_\mu 2S^2 - R_\mu 2C^2 - R_r 2CS & H_\mu 2CS - R_\mu 2CS + R_r 2C^2 & H_\lambda 2S + R_\lambda 2C & -H_\zeta 2C + R_\zeta 2S & -H_{\dot\beta} 2CS - R_{\dot\beta} 2C^2 & H_{\dot\zeta} 2S + R_{\dot\zeta} 2C \\
H_\mu 2CS - R_\mu 2CS - R_r 2S^2 & -H_\mu 2C^2 - R_\mu 2S^2 + R_r 2CS & -H_\lambda 2C + R_\lambda 2S & -H_{\dot\beta} 2CS + R_{\dot\beta} 2S^2 & H_{\dot\beta} 2C^2 - R_{\dot\beta} 2CS & H_{\dot\beta} 2S^2 + R_{\dot\beta} 2CS \\
-2T_\mu S & 2T_\mu C & 2T_\lambda & 2T_{\dot\beta} S & -2T_{\dot\beta} C & 2T_{\dot\zeta} \\
-M_\mu 2S^2 & M_\mu 2CS & M_\lambda 2S & M_{\dot\beta} 2S^2 & -M_{\dot\beta} 2CS & M_{\dot\zeta} 2S \\
M_\mu 2CS & +M_{\dot\beta} 2C^2 & -M_\lambda 2C & -M_{\dot\beta} 2CS & -M_\mu 2C^2 & -M_{\dot\zeta} 2C \\
2Q_\mu S & -2Q_\mu C & -2Q_\lambda & -2Q_{\dot\beta} S & 2Q_{\dot\beta} C & -2Q_{\dot\zeta}
\end{bmatrix}$$

$$\tilde{C}_o = \gamma \frac{1}{N} \sum_m$$

			$\mu_z H_\mu 2CS$ $-\mu_y H_\lambda 2S$ $-\mu_z R_\mu 2CS$ $-\mu_y R_\lambda 2C$ $\mu_z R_r 2C^2$	$\mu_z R_\mu 2C^2$ $-\mu_x H_\lambda 2S$ $\mu_z H_\mu 2S^2$ $-\mu_x R_\lambda 2C$ $\mu_z R_r 2CS$	$H_\zeta 2S$ $R_\zeta 2C$
			$-\mu_z H_\mu 2C^2$ $+\mu_y H_\lambda 2C$ $-\mu_z R_\mu 2S^2$ $-\mu_y R_\lambda 2S$ $+\mu_z R_r 2CS$	$\mu_z R_\mu 2CS$ $+\mu_x H_\lambda 2C$ $-\mu_z H_\mu 2CS$ $-\mu_x R_\lambda 2S$ $+\mu_z R_r 2S^2$	$-H_\zeta 2C$ $+R_\zeta 2S$
			$-2\mu_y T_\lambda$ $2\mu_z T_\mu C$	$-2\mu_x T_\lambda$ $2\mu_z T_\mu S$	$2T_\zeta$
			$-\mu_y M_\lambda 2S$ $+\mu_z M_\mu 2CS$	$-\mu_x M_\lambda 2S$ $+\mu_z M_\mu 2S^2$	$M_\zeta 2S$
			$\mu_y M_\lambda 2C$ $-\mu_z M_\mu 2C^2$	$\mu_x M_\lambda 2C$ $-\mu_z M_\mu 2CS$	$-M_\zeta 2C$
			$2\mu_y Q_\lambda$ $-2\mu_z Q_\mu C$	$2\mu_x Q_\lambda$ $-2\mu_z Q_\mu S$	$-2Q_\zeta$

$$D_G = \gamma \frac{1}{N} \sum_m \begin{bmatrix} H_\mu 2S^2 + R_\mu 2C^2 + R_r 2CS & H_\mu 2CS - R_\mu 2CS + R_r 2C^2 & -H_\lambda 2S - R_\lambda 2C \\ -H_\mu 2CS + R_\mu 2CS + R_r 2S^2 & -H_\mu 2C^2 - R_\mu 2S^2 + R_r 2CS & H_\lambda 2C - R_\lambda 2S \\ 2T_\mu S & 2T_\mu C & -2T_\lambda \\ M_\mu 2S^2 & M_\mu 2CS & -M_\lambda 2S \\ -M_\mu 2CS & -M_\mu 2C^2 & M_\lambda 2C \\ -2Q_\mu S & -2Q_\mu C & 2Q_\lambda \end{bmatrix}$$

6.4.4 Inertial matrices for rotor with four or more blades.

The inertial matrices for the equations of motion of a rotor with four or more blades are given below.

$$A_2 = \begin{bmatrix} I_{q_k} & & & -S_{q_k}\ddot{p}_i & & \\ & I_{q_k} & & & -S_{q_k}\ddot{p}_i & \\ & & I_{q_k} & & & -S_{q_k}\ddot{p}_i \\ -S_{p_k}\ddot{q}_i & & & I_{p_k}+I_{p_k}\ddot{p}_i & & \\ & -S_{p_k}\ddot{q}_i & & & I_{p_k}+I_{p_k}\ddot{p}_i & \\ & & -S_{p_k}\ddot{q}_i & & & I_{p_k}+I_{p_k}\ddot{p}_i \end{bmatrix}$$

$$A_1 = \begin{bmatrix}
I_{q_k} g_s \nu_k + 2I_{q_k} \dot{q}_i & 2nI_{q_k} & & & -2nS_{q_k} \ddot{p}_i & \\
-2nI_{q_k} & I_{q_k} g_s \nu_k + 2I_{q_k} \dot{q}_i & & 2nS_{q_k} \ddot{p}_i & & \\
 & & I_{q_k} g_s \nu_k + 2I_{q_k} \dot{q}_i & & & \\
 & -2nS_{p_k} \ddot{q}_i & & I_{p_k} g_s \omega_k & 2nI_{p_k} + 2nI_{p_k} \ddot{p}_i & \\
2nS_{p_k} \ddot{q}_i & & & -2nI_{p_k} - 2nI_{p_k} \ddot{p}_i & I_{p_k} g_s \omega_k & \\
 & & & & & I_{p_k} g_s \omega_k
\end{bmatrix}$$

$$A_o = \begin{bmatrix}
I_{q_k}(\nu_k^2-n^2) & nI_{q_k}g_s\nu_k + n2I_{q_k}\dot{q}_i & & -S_{q_kp_i} + n^2S_{q_k}\ddot{p}_i & & \\
-nI_{q_k}g_s\nu_k - n2I_{q_k}\dot{q}_i & I_{q_k}(\nu_k^2-n^2) & & & -S_{q_kp_i} + n^2S_{q_k}\ddot{p}_i & \\
 & & I_{q_k}\nu_k^2 & & & -S_{q_kp_i} \\
-S_{p_kq_i} + n\,S_{p_k}\ddot{q}_i + S_{p_ko}K_{p_i} & & & I_{p_k}(\omega_k^2-n^2) + I_{p_kp_i} - n^2I_{p_k}\ddot{p}_i & nI_{p_k}g_s\omega_k & \\
 & -S_{p_kq_i} + n\,S_{p_k}\ddot{q}_i + S_{p_ko}K_{p_i} & & -nI_{p_k}g_s\omega_k & I_{p_k}(\omega_k^2-n^2) + I_{p_kp_i} - n^2I_{p_k}\ddot{p}_i & \\
 & & -S_{p_kq_i} + S_{p_ko}K_{p_i} & & & I_{p_k}\omega_k^2 + I_{p_kp_i}
\end{bmatrix}$$

$$B = \begin{bmatrix} & & \\ & & \\ & & \\ S_{p_k^o} & & \\ & S_{p_k^o} & \\ & & S_{p_k^o} \end{bmatrix}$$

6.4.5 Aerodynamic matrices for rotor with four or more blades in axial flow.

The aerodynamic matrices for the equations of motion of a rotor with four or more blades in axial flow are given below.

$$A_1 = \begin{bmatrix} -\gamma M_{q_k \dot{q}_i} & & & & & \\ & -\gamma M_{q_k \dot{q}_i} & & & & \\ & & -\gamma M_{q_i \dot{q}_i} & & & \\ -\gamma M_{p_k \dot{q}_i} & & & -\gamma M_{p_k \dot{p}_i} & & \\ & -\gamma M_{p_k \dot{q}_i} & & & -\gamma M_{p_k \dot{p}_i} & \\ & & -\gamma M_{p_k \dot{q}_i} & & & -\gamma M_{p_k \dot{p}_i} \end{bmatrix}$$

$$A_o = \begin{bmatrix} -\gamma M_{q_k q_i} & -n\gamma M_{q_k \dot{q}_i} & & -\gamma M_{q_k p_i} & & \\ n\gamma M_{q_k \dot{q}_i} & -\gamma M_{q_k q_i} & & & -\gamma M_{q_i p_i} & \\ & & -\gamma M_{q_k q_i} & & & -\gamma M_{q_k p_i} \\ -\gamma M_{p_k q_i} & -n\gamma M_{p_k \dot{q}_i} & & -\gamma M_{p_k p_i} & -n\gamma M_{p_k \dot{p}_i} & \\ n\gamma M_{p_k \dot{q}_i} & -\gamma M_{p_k q_i} & & n\gamma M_{p_k \dot{p}_i} & -\gamma M_{p_k p_i} & \\ & & -\gamma M_{p_k q_i} & & & -\gamma M_{p_k p_i} \end{bmatrix}$$

6.4.6 Inertial matrices for two-bladed rotor.

The inertial matrices for the two-bladed rotor equations of motion are given below. The notation $C = \cos\psi_m$ and $S = \sin\psi_m$ is used, where $\psi_m = \psi + m\pi$.

$$A_2 = \frac{1}{N}\sum_m$$

I_{q_k}	I_{q_k}	$-S_{q_k}\ddot{p}_1$	$-S_{p_k}\ddot{q}_1$	$I_{q_k\alpha}\cdot\hat{k}_B$					
$-S_{p_k}\ddot{q}_1$	I_{q_k}	$I_{p_k}+I_{p_k}\ddot{p}_1$	$-S_{p_k}\ddot{q}_1$	$I_{p_k\alpha}\cdot\hat{i}_B$					
$I_{q_1\alpha}\cdot\hat{k}_B$	$-S_{q_k}\ddot{p}_1$	$I_{p_k}+I_{p_k}\ddot{p}_1$	$I_{q_1\alpha}\cdot\hat{i}_B$	$-S_{q_o}\ddot{p}_1\cdot\hat{i}_B$					
	$I_{q_k\alpha}\cdot\hat{i}_B$	$-S_{q_k}\ddot{p}_1$	$-I_{p_k\alpha}\cdot\hat{k}_B$	I_o					
$I_{q_1\alpha}\cdot\hat{k}_B$	$-S_{q_o}\ddot{p}_1$	$-S_{q_o}\ddot{p}_1\cdot\hat{k}_B$	I_o						

$$A_1 = \frac{1}{N}\sum_m$$

$I_{q_k} g_s \nu_k + 2I_{q_k} \dot{q}_1$	$I_{q_k} g_s \nu_k + 2I_{q_k} \dot{q}_1$	$I_{p_k} g_s \omega_k$	$I_{p_k} g_s \omega_k$	$2I_{q_o} \dot{q}_1 \cdot \dot{t}_B$	$2I_{q_o} \dot{q}_1 \cdot \dot{k}_B$				
	$-2I_{q_k} \dot{\beta}$			$I_o C_T$					
			$I_{p_k} g_s \omega_k$						
$2I_{q_k} \dot{\psi}$									

$$A_o = \frac{1}{N}\sum_m$$

$I_{q_k} \nu_k^2$		$-S_{p_k q_1}$ $+S_{p_k o^K p_1}$		$I_{q_1 \alpha} \cdot \dot{t}_B$					
	$I_{q_k} \nu_k^2$		$-S_{p_k q_1}$ $+S_{p_k o^K p_1}$						
$-S_{q_k p_1}$		$I_{p_k} \omega_k^2$ $+I_{p_k p_1}$							
	$-S_{q_k p_1}$		$I_{p_k} \omega_k^2$ $+I_{p_k p_1}$	$-S_{q_o \ddot{p}_1} \cdot \dot{t}_B$					
	$I_{q_k \alpha} \cdot \dot{t}_B$		$S_{p_k o^K p_T}$ $-I_{p_k \alpha} \cdot \dot{k}_B$	$I_o \nu_T^2$					
			$S_{p_k o}(\theta_{1C} S$ $-\theta_{1S} C)(-1)^m$						

$$\tilde{A}_2 = \frac{1}{N} \sum_m \Gamma$$

$-S_{q_k} \cdot \vec{k}_B S(-1)^m$	$S_{q_k} \cdot \vec{k}_B C(-1)^m$	$S_{q_k} \cdot \vec{i}_B$	$I_{q_k \alpha} \cdot \vec{i}_B S(-1)^m$	$-I_{q_k \alpha} \cdot \vec{i}_B C(-1)^m$	$I_{q_k \alpha} \cdot \vec{k}_B$
		$-S_{p_k} \cdot \vec{k}_B$			$I_{p_k \alpha} \cdot \vec{i}_B$
$-S_{p_k} \cdot \vec{i}_B S(-1)^m$	$S_{p_k} \cdot \vec{i}_B C(-1)^m$		$-I_{p_k \alpha} \cdot \vec{k}_B S(-1)^m$	$I_{p_k \alpha} \cdot \vec{k}_B C(-1)^m$	
			$I_o S(-1)^m$	$-I_o C(-1)^m$	
					I_o

$$
\begin{array}{|c|c|c|c|c|c|c|c|}
\hline
2I_{q_k}\dot{\psi} & & & & & & & \\
\hline
2I_{q_k\alpha}\cdot\vec{i}_B S(-1)^m & & -2I_{p_k\alpha}\cdot\vec{k}_B S(-1)^m & 2I_o S(-1)^m & & & & \\
\hline
2I_{q_k\alpha}\cdot\vec{i}_B C(-1)^m & & -2I_{p_k\alpha}\cdot k_B C(-1)^m & 2I_o C(-1)^m & & & & \\
\hline
 & & & & & & & \\
\hline
 & & & & & & & \\
\hline
 & & & & & & & \\
\hline
 & & & & & & & \\
\hline
 & & & & & & & \\
\hline
\end{array}
$$

$$\tilde{A}_1 = \frac{1}{N}\sum_m$$

$$B = \begin{bmatrix} & \\ & \\ S_{p_k^o} & \\ & S_{p_k^o} \\ & \\ & \\ & \\ & \\ & \end{bmatrix}$$

$$C_2 = \frac{1}{N}\sum_m \begin{bmatrix}
 & & & & & & & & & \\
 & & & & & & & & & \\
 & & & & & & & & & \\

$$
\begin{bmatrix}
 & & & & & \\
 & & & & & \\
 & & & & & \\
 & & & & & \\
 & & & & & \\
 & & & & & \\
 & & & & & \\
 & & & & -2I_o S(-1)^m & 2I_o C(-1)^m \\
 & & & & S_{q_o} \ddot{p}_1 \cdot \hat{I}_B 2S(-1)^m & -S_{q_o} \ddot{p}_1 \cdot \hat{I}_B 2C(-1)^m \\
 & & & & & \\
-S_{q_1} \cdot \hat{k}_B 2S(-1)^m & S_{q_1} \cdot \hat{k}_B 2C(-1)^m & -I_{q_1^\alpha} \cdot \hat{I}_B 2S(-1)^m & I_{q_1^\alpha} \cdot \hat{I}_B 2C(-1)^m & &
\end{bmatrix}
$$

$$
C_o = \frac{1}{N} \sum_{m}^{N}
$$

$$\tilde{C}_2 = \frac{1}{N} \sum_m \begin{bmatrix} -2M_b & & & & & \\ & -2M_b & & & & \\ & & -2M_b & & & \\ & & & -I_o 2S^2 & I_o 2CS & \\ & & & I_o 2CS & -I_o 2C^2 & \\ & & & & & -2I_o \end{bmatrix}$$

$$\tilde{C}_1 = \frac{1}{N} \sum_m \begin{bmatrix} & & & & & \\ & & & & & \\ & & & & & \\ & & & -I_o 4CS & -I_o 4S^2 & \\ & & & I_o 4C^2 & I_o 4CS & \\ & & & & & \end{bmatrix}$$

6.4.7 Aerodynamic matrices for two-bladed rotor.

The aerodynamic matrices for the two-bladed rotor equations of motion are given below. The notation $C = \cos\psi_m$ and $S = \sin\psi_m$ is used, where $\psi_m = \psi + m\pi$.

$$A_1 = \gamma \frac{1}{N} \sum_m$$

$-M_{q_k \dot{q}_1}$	$-M_{q_k \dot{q}_1}(-1)^m$			$-M_{q_k \beta}(-1)^m$	$-M_{q_k \dot{\zeta}}$	$-M_{q_k \lambda}$	$-M_{q_k \beta} C$	$-M_{q_k \beta} S$
$-M_{q_k \dot{q}_1}(-1)^m$	$-M_{q_k \dot{q}_1}$		$-M_{p_k \dot{p}_1}(-1)^m$	$-M_{q_k \beta}$	$-M_{q_k \dot{\zeta}}(-1)^m$	$-M_{q_k \lambda}(-1)^m$	$-M_{q_k \beta} C(-1)^m$	$-M_{q_k \beta} S(-1)^m$
$-M_{p_k \dot{q}_1}$	$-M_{p_k \dot{q}_1}(-1)^m$	$-M_{p_k \dot{p}_1}$		$-M_{p_k \beta}$	$-M_{p_k \dot{\zeta}}$	$-M_{p_k \lambda}$	$-M_{p_k \beta} C$	$-M_{p_k \beta} S$
$-M_{p_k \dot{q}_1}(-1)^m$	$-M_{p_k \dot{q}_1}$	$-M_{p_k \dot{p}_1}(-1)^m$	$-M_{p_k \dot{p}_1}$	$-M_{p_k \beta}(-1)^m$	$-M_{p_k \dot{\zeta}}(-1)^m$	$-M_{p_k \lambda}(-1)^m$	$-M_{p_k \beta} C(-1)^m$	$-M_{p_k \beta} S(-1)^m$
$-M_{q_1}(-1)^m$	$-M_{q_1}$			$-M_\beta$	$-M_\zeta(-1)^m$	$-M_\lambda(-1)^m$	$-M_\beta C(-1)^m$	$-M_\beta S(-1)^m$
Q_{q_1}	$Q_{q_1}(-1)^m$			$Q_\beta(-1)^m$	Q_ζ	Q_λ	$Q_\beta C$	$Q_\beta S$
$-2T_{q_1}$	$-2T_{q_1}(-1)^m$			$-2T_\beta(-1)^m$	$-2T_\zeta$	$-2T_\lambda$	$-2T_\beta C$	$-2T_\beta S$
$-M_{q_1} 2C$	$-M_{q_1} 2C(-1)^m$			$-M_\beta 2C(-1)^m$	$-M_\zeta 2C$	$-M_\lambda 2C$	$-M_\beta 2C^2$	$-M_\beta 2CS$
$-M_{q_1} 2S$	$-M_{q_1} 2S(-1)^m$			$-M_\beta 2S(-1)^m$	$-M_\zeta 2S$	$-M_\lambda 2S$	$-M_\beta 2CS$	$-M_\beta 2S^2$

$$
A_o = \gamma \frac{1}{N} \sum_m
\begin{bmatrix}
-M_{q_k q_i} & -M_{q_k q_i}(-1)^m & -M_{q_k p_i} & -M_{q_k p_i}(-1)^m & -M_{q_k \beta} & -M_{q_k \beta}(-1)^m & -M_{q_k \zeta} \\
-M_{q_k q_i}(-1)^m & -M_{q_k q_i} & -M_{q_k p_i}(-1)^m & -M_{q_k p_i} & -M_{q_k \beta}(-1)^m & -M_{q_k \beta} & -M_{q_k \zeta}(-1)^m \\
-M_{p_k q_i} & -M_{p_k q_i}(-1)^m & -M_{p_k p_i} & -M_{p_k p_i}(-1)^m & -M_{p_k \beta} & -M_{p_k \beta}(-1)^m & -M_{p_k \zeta} \\
-M_{p_k q_i}(-1)^m & -M_{p_k q_i} & -M_{p_k p_i}(-1)^m & -M_{p_k p_i} & -M_{p_k \beta}(-1)^m & -M_{p_k \beta} & -M_{p_k \zeta}(-1)^m \\
-M_{q_i}(-1)^m & -M_{q_i} & -M_{p_i} & -M_{p_i}(-1)^m & -M_{\beta} & -M_{\beta}(-1)^m & -M_{\zeta}(-1)^m \\
Q_{q_i} & Q_{q_i}(-1)^m & Q_{p_i} & Q_{p_i}(-1)^m & Q_{\beta}(-1)^m & Q_{\beta} & Q_{\zeta} \\
-2T_{q_i} & -2T_{q_i}(-1)^m & -2T_{p_i} & -2T_{p_i}(-1)^m & -2T_{\beta}(-1)^m & -2T_{\beta} & -2T_{\zeta} \\
-M_{q_i} 2C & -M_{q_i} 2C(-1)^m & -M_{p_i} 2C & -M_{p_i} 2C(-1)^m & -M_{\beta} 2C(-1)^m & -M_{\beta} 2C & -M_{\zeta} 2C \\
-M_{q_i} 2S & -M_{q_i} 2S(-1)^m & -M_{p_i} 2S & -M_{p_i} 2S(-1)^m & -M_{\beta} 2S(-1)^m & -M_{\beta} 2S & -M_{\zeta} 2S
\end{bmatrix}
$$

$$\tilde{A}_1 = \gamma \frac{1}{N} \sum_m$$

$M_{q_k \mu} S$	$-M_{q_k \mu} C$	$-M_{q_k \lambda}$	$-M_{q_k \dot{\beta}} S$	$M_{q_k \dot{\beta}} C$	$-M_{q_k \dot{\zeta}}$
$M_{q_k \mu} S(-1)^m$	$-M_{q_k \mu} C(-1)^m$	$-M_{q_k \lambda}(-1)^m$	$-M_{q_k \dot{\beta}} S(-1)^m$	$M_{q_k \dot{\beta}} C(-1)^m$	$-M_{q_k \dot{\zeta}}(-1)^m$
$M_{p_k \mu} S$	$-M_{p_k \mu} C$	$-M_{p_k \lambda}$	$-M_{p_k \dot{\beta}} S$	$M_{p_k \dot{\beta}} C$	$-M_{p_k \dot{\zeta}}$
$M_{p_k \mu} S(-1)^m$	$-M_{p_k \mu} C(-1)^m$	$-M_{p_k \lambda}(-1)^m$	$-M_{p_k \dot{\beta}} S(-1)^m$	$M_{p_k \dot{\beta}} C(-1)^m$	$-M_{p_k \dot{\zeta}}(-1)^m$
$M_\mu S(-1)^m$	$-M_\mu C(-1)^m$	$-M_\lambda(-1)^m$	$-M_{\dot{\beta}} S(-1)^m$	$M_{\dot{\beta}} C(-1)^m$	$-M_{\dot{\zeta}}(-1)^m$
$-Q_\mu S$	$Q_\mu C$	Q_λ	$Q_{\dot{\beta}} S$	$-Q_{\dot{\beta}} C$	$Q_{\dot{\zeta}}$
$2T_\mu S$ $-\frac{\mu_x}{\kappa_f^2}\frac{\partial \lambda}{\partial \lambda}$	$-2T_\mu C$ $+\frac{\mu_y}{\kappa_f^2}\frac{\partial \lambda}{\partial \mu}$	$-2T_\lambda$ $+\frac{\lambda}{\kappa_h^4}\frac{\partial \lambda}{\partial \mu}$	$-2T_{\dot{\beta}} S$	$2T_{\dot{\beta}} C$	$-2T_{\dot{\zeta}}$
$M_\mu 2CS$	$-M_\mu 2C^2$	$-M_\lambda 2C$	$-M_{\dot{\beta}} 2CS$	$M_{\dot{\beta}} 2C^2$	$-M_{\dot{\zeta}} 2C$
$M_\mu 2S^2$	$-M_\mu 2CS$	$-M_\lambda 2S$	$-M_{\dot{\beta}} 2S^2$	$M_{\dot{\beta}} 2CS$	$-M_{\dot{\zeta}} 2S$

$$\tilde{A}_o = \gamma \frac{1}{N} \sum_m$$

$-M_{q_k\zeta}$	$\mu_x M_{q_k\lambda}$ $-\mu_z M_{q_k\mu} S$	$\mu_y M_{q_k\lambda}$ $-\mu_z M_{q_k\mu} C$						
$-M_{q_k\zeta}(-1)^m$	$\mu_x M_{q_k\lambda}(-1)^m$ $-\mu_z M_{q_k\mu} S(-1)^m$	$\mu_y M_{q_k\lambda}(-1)^m$ $-\mu_z M_{q_k\mu} C(-1)^m$						
$-M_{p_k\zeta}$	$\mu_x M_{p_k\lambda}$ $-\mu_z M_{p_k\mu} S$	$\mu_y M_{p_k\lambda}$ $-\mu_z M_{p_k\mu} C$						
$-M_{p_k\zeta}(-1)^m$	$\mu_x M_{p_k\lambda}(-1)^m$ $-\mu_z M_{p_k\mu} S(-1)^m$	$\mu_y M_{p_k\lambda}(-1)^m$ $-\mu_z M_{p_k\mu} C(-1)^m$						
$-M_\zeta(-1)^m$	$\mu_x M_\lambda(-1)^m$ $-\mu_z M_\mu S(-1)^m$	$\mu_y M_\lambda(-1)^m$ $-\mu_z M_\mu C(-1)^m$						
Q_ζ	$-\mu_x Q_\lambda$ $\mu_z Q_\mu S$	$-\mu_y Q_\lambda$ $\mu_z Q_\mu C$						
$-2T_\zeta$	$2\mu_x T_\lambda$ $-2\mu_z T_\mu S$	$2\mu_y T_\lambda$ $-2\mu_z T_\mu C$						
$-M_\zeta 2C$	$\mu_x M_\lambda 2C$ $-\mu_z M_\mu 2CS$	$\mu_y M_\lambda 2C$ $-\mu_z M_\mu 2C^2$						
$-M_\zeta 2S$	$\mu_x M_\lambda 2S$ $-\mu_z M_\mu 2S^2$	$\mu_y M_\lambda 2S$ $-\mu_z M_\mu 2CS$						

$$B_G = \gamma \frac{1}{N} \sum_m \begin{bmatrix} M_{q_k\mu} S & M_{q_k\mu} C & -M_{q_k\lambda} \\ M_{q_k\mu} S(-1)^m & M_{q_k\mu} C(-1)^m & -M_{q_k\lambda}(-1)^m \\ M_{p_k\mu} S & M_{p_k\mu} C & -M_{p_k\lambda} \\ M_{p_k\mu} S(-1)^m & M_{p_k\mu} C(-1)^m & -M_{p_k\lambda}(-1)^m \\ M_\mu S(-1)^m & M_\mu C(-1)^m & -M_\lambda(-1)^m \\ -Q_\mu S & -Q_\mu C & Q_\lambda \\ 2T_\mu S - \frac{\mu_x}{\kappa_f^2}\frac{\partial\lambda}{\partial\mu} & 2T_\mu C - \frac{\mu_y}{\kappa_f^2}\frac{\partial\lambda}{\partial\mu} & -2T_\lambda + \frac{\lambda}{\kappa_h^4}\frac{\partial\lambda}{\partial\mu} \\ M_\mu 2CS & M_\mu 2C^2 & -M_\lambda 2C \\ M_\mu 2S^2 & M_\mu 2CS & -M_\lambda 2S \end{bmatrix}$$

$$C_1 = \gamma \frac{1}{N} \sum_m$$

$H_{q_1}\cdot 2S$ $R_{q_1}\cdot 2C$	$H_{q_1}\cdot 2S(-1)^m$ $R_{q_1}\cdot 2C(-1)^m$		$H_\beta 2S(-1)^m$ $R_\beta 2C(-1)^m$	$H_\zeta\cdot 2S$ $R_\zeta\cdot 2C$	$H_\lambda 2S$ $R_\lambda 2C$	$H_\beta 2CS$ $R_\beta 2C^2$	$H_\beta 2S^2$ $R_\beta 2CS$
$-H_{q_1}\cdot 2C$ $+R_{q_1}\cdot 2S$	$-H_{q_1}\cdot 2C(-1)^m$ $+R_{q_1}\cdot 2S(-1)^m$		$-H_\beta 2C(-1)^m$ $+R_\beta 2S(-1)^m$	$-H_\zeta\cdot 2C$ $+R_\zeta\cdot 2S$	$-H_\lambda 2C$ $+R_\lambda 2S$	$-H_\beta 2C^2$ $+R_\beta 2CS$	$-H_\beta 2CS$ $+R_\beta 2S^2$
$2T_{q_1}$	$2T_{q_1}\cdot(-1)^m$		$2T_\beta(-1)^m$	$2T_\zeta$	$2T_\lambda$	$2T_\beta C$	$2T_\beta S$
$M_{q_1}\cdot 2S$	$M_{q_1}\cdot 2S(-1)^m$		$M_\beta 2S(-1)^m$	$M_\zeta\cdot 2S$	$M_\lambda 2S$	$M_\beta 2CS$	$M_\beta 2S^2$
$-M_{q_1}\cdot 2C$	$-M_{q_1}\cdot 2C(-1)^m$		$-M_\beta 2C(-1)^m$	$-M_\zeta\cdot 2C$	$-M_\lambda 2C$	$-M_\beta 2C^2$	$-M_\beta 2CS$
$-2Q_{q_1}$	$-2Q_{q_1}\cdot(-1)^m$		$-2Q_\beta(-1)^m$	$-2Q_\zeta$	$-2Q_\lambda$	$-2Q_\beta C$	$-2Q_\beta S$

$$C_o = \gamma \frac{1}{N} \sum_m$$

$H_{q_i}^{\ 2S}$ $R_{q_1}^{\ 2C}$	$H_{q_i}^{\ 2S(-1)^m}$ $R_{q_1}^{\ 2C(-1)^m}$	$H_{p_1}^{\ 2S}$ $R_{p_1}^{\ 2C}$	$H_{p_i}^{\ 2S(-1)^m}$ $R_{p_i}^{\ 2C(-1)^m}$	$H_\rho 2S(-1)^m$ $R_\beta 2C(-1)^m$	$H_\zeta 2S$ $R_\zeta 2C$	
$-H_{q_1}^{\ 2C}$ $+R_{q_1}^{\ 2S}$	$-H_{q_1}^{\ 2C(-1)^m}$ $+R_{q_1}^{\ 2S(-1)^m}$	$-H_{p_1}^{\ 2C}$ $+R_{p_1}^{\ 2S}$	$-H_{p_1}^{\ 2C(-1)^m}$ $+R_{p_1}^{\ 2S(-1)^m}$	$-H_\beta 2C(-1)^m$ $+R_\beta 2S(-1)^m$	$-H_\zeta 2C$ $+R_\zeta 2S$	
$2T_{q_1}$	$2T_{q_1}^{\ (-1)^m}$	$2T_{p_1}$	$2T_{p_i}^{\ (-1)^m}$	$2T_\beta(-1)^m$	$2T_\zeta$	
$M_{q_1}^{\ 2S}$	$M_{q_1}^{\ 2S(-1)^m}$	$M_{p_1}^{\ 2S}$	$M_{p_1}^{\ 2S(-1)^m}$	$M_\beta 2S(-1)^m$	$M_\zeta 2S$	
$-M_{q_1}^{\ 2C}$	$-M_{q_1}^{\ 2C(-1)^m}$	$-M_{p_1}^{\ 2C}$	$-M_{p_1}^{\ 2C(-1)^m}$	$-M_\beta 2C(-1)^m$	$-M_\zeta 2C$	
$-2Q_{q_1}$	$-2Q_{q_1}^{\ (-1)^m}$	$-2Q_{p_1}$	$-2Q_{p_i}^{\ (-1)^m}$	$-2Q_\beta(-1)^m$	$-2Q_\zeta$	

$$\tilde{C}_1 = \gamma \frac{1}{N} \sum_m$$

$$\begin{bmatrix}
\begin{matrix} -H_\mu 2S^2 \\ -R_\mu 2C^2 \\ -R_r 2CS \end{matrix} & \begin{matrix} H_\mu 2CS \\ -R_\mu 2CS \\ R_r 2C^2 \end{matrix} & \begin{matrix} H_\lambda 2S \\ R_\lambda 2C \end{matrix} & \begin{matrix} H_{\dot\beta} 2S^2 \\ R_{\dot\beta} 2CS \end{matrix} & \begin{matrix} -H_{\dot\beta} 2CS \\ -R_{\dot\beta} 2C^2 \end{matrix} & \begin{matrix} H_{\dot\zeta} 2S \\ R_{\dot\zeta} 2C \end{matrix} \\
\hline
\begin{matrix} H_\mu 2CS \\ -R_\mu 2CS \\ -R_r 2S^2 \end{matrix} & \begin{matrix} -H_\mu 2C^2 \\ -R_\mu 2S^2 \\ +R_r 2CS \end{matrix} & \begin{matrix} -H_\lambda 2C \\ +R_\lambda 2S \end{matrix} & \begin{matrix} -H_{\dot\beta} 2CS \\ +R_{\dot\beta} 2S^2 \end{matrix} & \begin{matrix} H_{\dot\beta} 2C^2 \\ -R_{\dot\beta} 2CS \end{matrix} & \begin{matrix} -H_{\dot\zeta} 2C \\ +R_{\dot\zeta} 2S \end{matrix} \\
\hline
-2T_\mu S & 2T_\mu C & 2T_\lambda & 2T_{\dot\beta} S & -2T_{\dot\beta} C & 2T_{\dot\zeta} \\
\hline
-M_\mu 2S^2 & M_\mu 2CS & M_\lambda 2S & M_{\dot\beta} 2S^2 & -M_{\dot\beta} 2CS & M_{\dot\zeta} 2S \\
\hline
M_\mu 2CS & -M_\mu 2C^2 & -M_\lambda 2C & -M_{\dot\beta} 2CS & M_{\dot\beta} 2C^2 & -M_{\dot\zeta} 2C \\
\hline
2Q_\mu S & -2Q_\mu C & -2Q_\lambda & -2Q_{\dot\beta} S & 2Q_\mu C & -2Q_{\dot\zeta}
\end{bmatrix}$$

$$\tilde{C}_o = \gamma \frac{1}{N} \sum_m$$

			$\mu_z H_\mu 2CS$ $-\mu_z R_\mu 2CS$ $\mu_z R_r 2C^2$ $-\mu_y H_\lambda 2S$ $-\mu_y R_\lambda 2C$	$\mu_z H_\mu 2S^2$ $\mu_z R_\mu 2C^2$ $\mu_z R_r 2CS$ $-\mu_x H_\lambda 2S$ $-\mu_x R_\lambda 2C$	$H_\zeta 2S$ $R_\zeta 2C$
			$-\mu_z H_\mu 2C^2$ $-\mu_z R_\mu 2S^2$ $+\mu_z R_r 2CS$ $+\mu_y H_\lambda 2C$ $+\mu_y R_\lambda 2S$	$-\mu_z H_\mu 2CS$ $+\mu_z R_\mu 2CS$ $+\mu_z R_r 2S^2$ $+\mu_x H_\lambda 2C$ $+\mu_x R_\lambda 2S$	$-H_\zeta 2C$ $+R_\zeta 2S$
			$2\mu_z T_\mu C$ $-2\mu_y T_\lambda$	$2\mu_z T_\mu S$ $-2\mu_x T_\lambda$	$2T_\zeta$
			$\mu_z M_\mu 2CS$ $-\mu_y M_\lambda 2S$	$\mu_z M_\mu 2S^2$ $-\mu_x M_\lambda 2S$	$M_\zeta 2S$
			$-\mu_z M_\mu 2C^2$ $\mu_y M_\lambda 2C$	$-\mu_z M_\mu 2CS$ $\mu_x M_\lambda 2C$	$-M_\zeta 2C$
			$-2\mu_z Q_\mu C$ $+2\mu_y Q_\lambda$	$-2\mu_z Q_\mu S$ $+2\mu_x Q_\lambda$	$-2Q_\zeta$

$$D_G = \gamma \frac{1}{N} \sum_m \begin{bmatrix} H_\mu 2S^2 + R_\mu 2C^2 + R_r 2CS & H_\mu 2CS - R_\mu 2CS + R_r 2C^2 & -H_\lambda 2S - R_\lambda 2C \\ -H_\mu 2CS + R_\mu 2CS + R_r 2C^2 & -H_\mu 2C^2 - R_\mu 2S^2 + R_r 2CS & +H_\lambda 2C - R_\lambda 2S \\ 2T_\mu S & 2T_\mu C & -2T_\lambda \\ M_\mu 2S^2 & M_\mu 2CS & -M_\lambda 2S \\ -M_\mu 2CS & -M_\mu 2C^2 & M_\lambda 2C \\ -2Q_\mu S & -2Q_\mu C & 2Q_\lambda \end{bmatrix}$$

7. LINEAR SYSTEM ANALYSIS

The flight dynamics and aeroelastic stability analyses (sections 5.3.3 and 6) result in a set of linear differential equations describing the aircraft motion, of the form

$$A_2 \ddot{x} + A_1 \dot{x} + A_0 x = B_0 v$$

$$y = C_2 \ddot{x} + C_1 \dot{x} + C_0 x + D_0 v$$

where x is the vector of degrees of freedom, v is the vector of control and gust inputs, and y is the vector of sensors and output. A subset of (x, $\dot{x}$, $\ddot{x}$, and v) will be taken as additional output. The coefficient matrices are either constant or periodic in time. The analysis of these linear equations proceeds as follows (see reference 62).

7.1 State Variable Form.

It is convenient to transform the equations to a standard first order form. Let MX be the number of degrees of freedom. Assume that MX1 of the degrees of freedom are first order, so they zero columns in the spring matrices A_0 and C_0. Reorder the degrees of freedom so these first order states occur last in the vector x:

$$\begin{pmatrix} x_2 \\ x_1 \end{pmatrix}$$

where x_2 are the MX-MX1 second order degrees of freedom and x_1 are the MX1 first order degrees of freedom. Then

$$A_0 = \begin{bmatrix} \tilde{A}_0 & 0 \end{bmatrix}$$

$$C_0 = \begin{bmatrix} \tilde{C}_0 & 0 \end{bmatrix}$$

where $\tilde{A}_o$ and $\tilde{C}_o$ have MX-MX1 columns. The equations of motion can now be written in the form

$$\dot{x} = Ax + Bv$$
$$y = Cx + Dv$$

where

$$A = \begin{bmatrix} -A_2^{-1}A_1 & -A_2^{-1}\tilde{A}_o \\ I \quad 0 & 0 \end{bmatrix}$$

$$B = \begin{bmatrix} A_2^{-1}B_o \\ 0 \end{bmatrix}$$

$$C = \begin{bmatrix} C_1 - C_2 A_2^{-1}A_1 & \tilde{C}_o - C_2 A_2^{-1}\tilde{A}_o \end{bmatrix}$$

$$D = \begin{bmatrix} D_o + C_2 A_2^{-1}B_o \end{bmatrix}$$

with the state vector

$$x = \begin{pmatrix} \dot{x}_2 \\ \dot{x}_1 \\ x_2 \end{pmatrix}$$

There are 2*MX-MX1 states: the velocities of all degrees of freedom, plus the displacements of the second order degrees of freedom. A subset of the states or controls as output adds rows to C and D. For y equal to a displacement or velocity, the rows of C and D are zero except for 1 in the appropriate column of C (displacements of first-order states cannot be obtained as output this way). For y equal to a control, the rows of C and D are zero except for 1 in the appropriate column of D. For y equal to the acceleration of the ith degree of freedom, the rows of C and D are equal to the ith rows of A and B.

7.2 Constant Coefficient System.

7.2.1 Eigenanalysis.

The transient solution of the homogeneous equation $\dot{x} = Ax$ is:

$$x = \sum_i u_i e^{\lambda_i t} q_i(0) = M e^{\Lambda t} q(0)$$

where λ_i u_i are the eigenvalues and eigenvectors of the matrix A, and $q_i(0)$ are constants determined by the initial conditions. M is the modal matrix, with the eigenvectors as columns; and Λ is the diagonal matrix of eigenvalues. The system is unstable if $\mathrm{Re}\lambda_i > 0$ for any mode.

The frequency of a mode is $\omega = |\mathrm{Im}\lambda|$, and the natural frequency is $\omega_n = |\lambda|$. The frequency in Hz is obtained by multiplying by $\Omega/2\pi$. The period is then $T = 1/\omega$ sec, with ω the frequency in Hz. The damping ratio is $\zeta = -\mathrm{Re}\lambda/|\lambda|$ (fraction of critical damping). The time constant is $\tau = -1/(\Omega \mathrm{Re}\lambda)$ sec. The time to half-amplitude is then $t_{\frac{1}{2}} = 0.693\tau$ (or time to double-amplitude for unstable modes).

7.2.2 Static response.

The static response, obtained by setting $\dot{x} = 0$, is

$$y = (D - CA^{-1}B)v$$

7.2.3 Frequency response.

The frequency response, obtained by setting $x = x_o e^{i\omega t}$, $y = y_o e^{i\omega t}$, and $v = v_o e^{i\omega t}$ in the equations, is $y_o = Hv_o$, where from the matrices

$$H = D - C(A - i\omega)^{-1}B = D - C(A + i\omega)(A^2 + \omega^2)^{-1}B$$

or from the modes

$$H = D - CM(\Lambda - i\omega)^{-1}M^{-1}B$$

The frequency response can also be obtained from the poles and zeros by

$$y_i / v_j = k_1 \frac{\prod_m (z_m - i\omega)}{\prod_n (p_n - i\omega)}$$

where p_n are the poles (eigenvalues) and z_m are the zeros.

7.2.4 Zeros.

For each input/output pair, the response in Laplace form is

$$y_i / v_j = d - c(A-s)^{-1} b$$

where here y and v are scalars; so c is a single row, b is a single column, and d is a scalar. An equivalent equation is

$$y_i / v_j = - \frac{\det A^*}{\det (A - s)}$$

where

$$A^* = \begin{bmatrix} -d & c \\ -b & A-s \end{bmatrix}$$

The poles are defined by det(A-s) = 0, hence are the eigenvalues of the matrix A. The zeros are defined by $\det(A^*) = 0$. In A^* the diagonal elements are all of the form $(a_{kk} - s)$, except for the first element. By expanding the determinant of A^* it is possible to reduce it to a form with $(a_{kk} - s)$ for all the diagonal elements

$$- \det A^* = k_1 \det (A_1 - s)$$

Then the zeros are the eigenvalues of the matrix A_1. We have then

$$y_i / v_j = k_1 \frac{\prod_m (z_m - s)}{\prod_n (p_n - s)} = k_s \frac{\prod_m (1 - s/z_m)}{\prod_n (1 - s/p_n)}$$

and the static response is $K_s = K_1 \Pi z / \Pi p$. The partial fraction expansion of the response is

$$y_i / v_j = \sum_k \frac{A_k}{p_k - s}$$

Where

$$A_k = K_1 \frac{\prod_m (z_m - p_k)}{\prod_{n \neq k} (p_n - p_k)}$$

are the residues, which define the modal contribution to the impulse response.

7.2.5 Transient response.

The general solution of $\dot{x} = Ax + Bv$ is

$$x = M e^{\Lambda t} M^{-1} x_0 + \int_0^t M e^{\Lambda (t-\tau)} M^{-1} B v \, d\tau$$

Consider the case with zero initial conditions at $t = 0$, and control with time variation of the form $v = v_0 f(\tau)$ ($f = 0$ for $\tau < 0$). Then

$$y = [D f(t) + C M F(t) M^{-1} B] v_0$$

where

$$F = \left[\int_0^t e^{\lambda_i (t-\tau)} f(\tau)\, d\tau \right]$$

is a diagonal matrix depending on the eigenvalues and on the input function f. The cases considered are:

(a) step response, f = 1

(b) impulse response, f = $\delta(t)$

(c) cosine impulse, f = $\frac{1}{2}(1 - \cos 2\pi t/T)$, $0 < t < T$

(d) sine doublet, f = $\sin 2\pi t/T$, $0 < t < T$

(e) square impulse, f = 1, $0 < t < T$

(f) square doublet, f = 1 for $0 < t < T/2$, f = -1 for $T/2 < t < T$

(g) ramp response, f = t

(h) triangular impulse, f = $2t/T$ for $0 < t \leq T/2$, f = $2(1 - t/T)$ for $T/2 < t < T$

The function F(t) can be evaluated for these and other inputs.

7.2.6 RMS gust response.

Consider the rms gust response of the system $\dot{x} = Ax + Bg$, $y = Cx + Dg$. Here the only input considered is the vector of gust components g. Note that the rms response is not properly defined for a system with unstable modes. Two gust spectra (functions of frequency ω) will be considered:

(a) Dryden spectra

longitudinal $$S_u = \frac{\sigma^2 \tau}{\pi} \frac{1}{1 + (\tau\omega)^2}$$

lateral/vertical $$S_v = S_w = \frac{\sigma^2 \tau}{2\pi} \frac{1 + 3(\tau\omega)^2}{(1 + (\tau\omega)^2)^2}$$

(b) von Karman spectra (a = 1.339)

longitudinal $$S_u = \frac{\sigma^2 \tau}{\pi} \frac{1}{(1+(a\tau\omega)^2)^{5/6}}$$

lateral/vertical $$S_v = S_w = \frac{\sigma^2 \tau}{2\pi} \frac{1+\frac{8}{3}(a\tau\omega)^2}{(1+(a\tau\omega)^2)^{11/6}}$$

where σ is the rms gust magnitude, the time constant τ = L/V, L is the gust correlation length, and V is the aircraft speed. It is assumed that the three components of the gust are uncorrelated, so the mean-squared response can be evaluated for each component separately, and added to obtain the total mean-squared response. The rms response will be calculated by two methods.

The rms gust response can be obtained by integrating the product of the gust spectrum and the square of the frequency response:

$$\sigma_y^2 = \int_{-\infty}^{\infty} S_y \, d\omega = \int_{-\infty}^{\infty} |H|^2 S_g \, d\omega$$

where H is evaluated as in section 7.2.3. The integral will be evaluated numerically. Consider a set of frequencies, uniformly spaced from ω_1 to ω_M (either log or linear frequency scale). In addition, ω = 0 will always be used. Then by trapezoidal integration,

$$\sigma_y^2 = \sum_{i=0}^{M} S_i h_i$$

where for a linear frequency scale $h_o = \omega_1$, $h_1 = \omega_1 + \Delta\omega$, $h_i = 2\Delta\omega$, $h_M = \Delta\omega$; and for a log frequency scale $h_o = \omega_1$, $h_1 = \omega_1 + \omega_1 \Delta ln\omega$, $h_i = 2\omega_i \Delta ln\omega$, $h_M = \omega_M \Delta ln\omega$. For a system with a neutrally damped mode ($Re\lambda = 0$), the transfer function will be infinite at resonance, and the integral does not converge. For a system with unstable modes ($Re\lambda > 0$), the integrals exist but the result is not meaningful.

Alternatively, the gust can be as a Markov process: $\dot{g} = Tg + Sw$, where w is stationary Gaussian noise, with zero mean and correlation

$$E\left[w(t)\, w^T(\tau)\right] = Q_G\, \delta(t-\tau)$$

The matrices T and S can be constructed to produce the longitudinal or the lateral/vertical Dryden spectrum. For an rms gust velocity of σ, it follows that $Q_G = 2\sigma^2/t$. The aircraft and gust model are thus described by the set of

$$\begin{pmatrix} x \\ g \end{pmatrix}^{\bullet} = \begin{bmatrix} A & B \\ 0 & T \end{bmatrix} \begin{pmatrix} x \\ g \end{pmatrix} + \begin{bmatrix} 0 \\ S \end{bmatrix} w$$

$$y = \begin{bmatrix} C & D \end{bmatrix} \begin{pmatrix} x \\ g \end{pmatrix}$$

or $\dot{z} = Fz + Gw$, $y = Hz$. The correlation matrix $Z = E(zz^T)$ is then the solution of the equation

$$FZ + ZF^T + GQ_G G^T = 0$$

and the output correlation matrix is $Y = E(yy^T) = HZH^T$. The diagonal elements of Y are the mean-squared gust response. For a single gust component, the solution is

$$Y/\sigma^2 = (CM)X^*(CM)^T - (CM)L(M^{-1}b)d^T - d(M^{-1}b)^T L(CM)^T + dd^T$$

where M is the modal matrix, $L = [l_i]$ is a diagonal matrix, and the modal correlation matrix is

$$X^*_{ij} = \left[(M^{-1}b)(M^{-1}b)^T\right]_{ij} \frac{l_i + l_j}{\lambda_i + \lambda_j}$$

The matrix L depends on the gust spectrum:

longitudinal $$l = \frac{1}{\lambda - \frac{1}{\tau}}$$

lateral/vertical $$l = \frac{\lambda - \frac{1}{2\tau}}{\left(\lambda - \frac{1}{\tau}\right)^2}$$

For a system with unstable eigenvalues ($Re\lambda \geq 0$), these modes can be omitted from X^*, but the result is not meaningful.

7.3 Periodic Coefficient System

Consider the system of equations $\dot{x} = Ax + Bv$, where A is periodic with period T, $A(t + T) = A(t)$. The transient solution can be written

$$x = \sum_i u_i(t)\, e^{\lambda_i t}\, q_i(0)$$

as for the constant coefficient system, but here the modes u_i are periodic functions of time. The eigenvalues λ_i are obtained as follows.

The state transition matrix ϕ is calculated by integrating $\dot{\phi} = A\phi$ over one period, t = 0 to T, with initial conditions $\phi(0) = I$. Let $C = \phi(T)$; and let λ_c and v be the eigenvalues and eigenvectors of the matrix C. Then the system roots are

$$\lambda = \frac{1}{T} \ln \lambda_c = \frac{1}{T} \left(\ln |\lambda_c| + i \angle \lambda_c \right)$$

(the principal part - a multiple of $2\pi/T$ can be added to the frequency) and the mode shapes can be obtained from

$$u_i = e^{-\lambda_i t}\, \phi(t)\, v_i$$

The system is unstable if $\mathrm{Re}\lambda > 0$ (or $|\lambda_c| > 1$) for any mode.

It is necessary to integrate the equations $\dot{\phi} = f(t, \phi) = A(t)\phi$ numerically from t = 0 to t = T. Two methods are considered. The first method is a modified trapezoidal rule:

$$\begin{aligned} \phi_{n+1} &= \phi_n + \frac{h}{2} \left(\dot{\phi}_{n+1} + \dot{\phi}_n \right) + O(h^3) \\ &= \phi_n + \frac{h}{2} \left(A_{n+1} \phi_{n+1} + A_n \phi_n \right) \\ &= \left(1 - \frac{h}{2} A_{n+1} \right)^{-1} \left(1 + \frac{h}{2} A_n \right) \phi_n \end{aligned}$$

$$\cong \quad \left(1 + \frac{h}{2} A_{n+1} + \frac{h^2}{4} A_{n+1}^2\right)\left(1 + \frac{h}{2} A_n\right) \phi_n$$

$$= \quad \phi_n + \frac{h}{2}\left(1 + \frac{h}{2} A_{n+1}\right)\left(A_n + A_{n+1}\right) \phi_n$$

where $\phi_n = \phi(t_n)$, $\phi_{n+1} = \phi(t_{n+1})$, and $h = t_{n+1} - t_n$. The second method is the fourth order Runge-Kutta method:

$$\phi_{n+1} = \phi_n + \frac{h}{6}\left(k_1 + 2k_2 + 2k_3 + k_4\right) + O(h^5)$$

$$k_1 = A_n \phi_n$$

$$k_2 = A_{n+\frac{1}{2}}\left(\phi_n + \frac{h}{2} k_1\right)$$

$$k_3 = A_{n+\frac{1}{2}}\left(\phi_n + \frac{h}{2} k_2\right)$$

$$k_4 = A_{n+1}\left(\phi_n + h\, k_3\right)$$

7.4 Aeroservoelasticity Analysis

The flight dynamics and aeroelastic stability tasks produce linear differential equations for the rotorcraft. To perform an aeroservoelasticity analysis of the complete system, it is necessary to add a control system model to the open-loop aircraft and sensor model. Then the resulting equations will be analyzed in the frequency domain to determine the stability and response.

The control system will be defined in terms of transfer functions, so a frequency domain analysis of the closed-loop system is straightforward. The control system will include an arbitrary number of feedback loop closures, and feedforward from additional input variables

(typically pilot's controls). The closed-loop stability is determined from open-loop Bodes for each loop closure (in terms of gain and phase margins). The closed-loop response is calculated in terms of the frequency response and rms gust response.

7.4.1 Control system model.

The control system consists of a sequence of loops. Each loop has the form shown in Figure 7-1. The aircraft input variables (v and Δv), the aircraft output variables (y), and the controller pilot input (δ) may be vectors. The feedback loop quantities (c, d, e, and θ) are scalars, so that the classical stability criteria can be applied to the loop. Note the minus sign at the loop closure (negative feedback). It follows that the transfer function H is a scalar, while H_y and H_δ are row vectors:

$$H_y = [\cdots \; H_{y_i} \; \cdots]$$

$$H_\delta = [\cdots \; \sum_k H_{\delta_{kj}} \; \cdots]$$

The summation in H_δ allows several feedforward paths. The control matrix T_θ is a constant column vector, relating the actuator output θ to the aircraft controls Δv. For the first loop, H_v is the open-loop aircraft frequency response, calculated as described in section 7.2.3; and $H_p = 0$. For subsequent loop closures, H_v and H_p are the system response with the inner loops closed.

The equations describing the aircraft and controller in the frequency domain are thus:

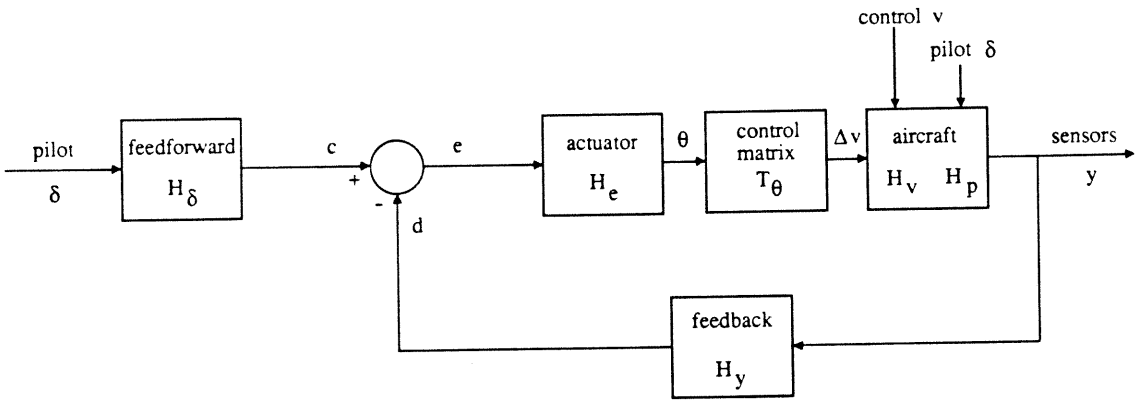

Figure 7-1. Control system model (each loop).

$$y = H_v T_\theta \Theta + H_v v + H_p \delta$$

$$\Theta = H_e (H_\delta \delta - H_y y)$$

Each transfer H can include gain factors, time lags, and poles and zeros:

$$H = K e^{-\tau s} \frac{\prod (s - z_n)}{\prod (s - p_n)}$$

where the poles and zeros can be real, or complex conjugate pairs. The frequency response is obtained from $s = i\omega$, where the frequency in rad/sec is $\omega = \Omega \omega_{\text{per rev}}$.

7.4.2 Stability evaluation.

The stability of the system after closure of a loop can be evaluated from the open-loop Bode, $d = H_{OL} e$, where

$$H_{OL} = H_y (H_v T_\Theta) H_e$$

is the scalar frequency response of the feedback path. The stability is obtained by applying the Nyquist criterion to the open-loop transfer function H_{OL} (reference 63). The gain margin (GM, in dB) and phase margin (PM, in degrees relative -180) are defined as follows:

$$GM = -20 \log |H_{OL}| \qquad \text{where} \qquad \angle H_{OL} = -180$$

$$PM = 180 + \angle H_{OL} \qquad \text{where} \qquad |H_{OL}| = 1$$

The closed loop system is stable if the gain margin is positive; and for a minimum phase system it is stable if the phase margin is positive.

Construction and interpretation of a Nyquist plot (imaginary H_{OL} vs. real H_{OL}) can involve a number of subtleties (see reference 63), but determining the stability from Bode plot is relatively straightforward if the open-loop system is stable. In such a case, the closed-loop system must be stable for sufficiently small gain. Hence the frequencies where the phase = -180° identify the gains at which the system switches between stability and instability (i.e. a change in the number of encirclements of -1 for a Nyquist plot). Then for a particular gain, the phase margin provides information about the response of the closed loop system (such as damping ratio and overshoot).

7.4.3 Closed-loop response.

The closed-loop transfer function is obtained by substituting for y in the control equation and solving for θ (a scalar):

$$\Theta = (1 + H_{OL})^{-1} H_e \left(H_\delta \delta - H_y (H_v v + H_p \delta) \right)$$

or

$$H_v T_\theta \theta = G_p \delta + G_y (H_v v + H_p \delta)$$

$$G_p = H_v T_\theta (1 + H_{OL})^{-1} H_e H_\delta$$

$$G_y = -H_v T_\theta (1 + H_{OL})^{-1} H_e H_y$$

Then substituting for θ in the aircraft equation gives:

$$y = H_{cL}\begin{pmatrix} v \\ \delta \end{pmatrix} = (I + G_y)(H_v v + H_\rho \delta) + G_\rho \delta$$

or

$$H_{cL} = H + G_y \begin{bmatrix} H_v & H_\rho \end{bmatrix} + \begin{bmatrix} 0 & G_\rho \end{bmatrix}$$

$$= H + \left[(H_v T_\theta)(1 + H_{oL})^{-1} H_e\right]\left[-H_y H_v \quad -H_y H_\rho + H_\delta\right]$$

This calculation is repeated for each loop closure.

The closed-loop system behavior that can be obtained with this frequency domain analysis includes the static response, frequency response, and rms gust response (by integrating the product of the gust spectrum and the frequency response).

REFERENCES

1. Johnson, W.: A Comprehensive Analytical Model of Rotorcraft Aerodynamics and Dynamics, Part I: Analysis Development. NASA TM-81182, June 1980.
2. Johnson, W.: A Comprehensive Analytical Model of Rotorcraft Aerodynamics and Dynamics, Part II: User's Manual. MASA TN-81183, July 1980.
3. Johnson, W.: A Comprehensive Analytical Model of Rotorcraft Aerodynamics and Dynamics, Part III: Program Manual. NASA TM-81184, June 1980.
4. Johnson, W.: Development of a Comprehensive Analysis for Rotorcraft - I. Rotor Model and Wake Analysis, Vertica, vol. 5, no. 2, 1981.
5. Johnson, W.: Development of a Comprehensive Analysis for Rotorcraft - II. Aircraft Model, Solution Procedure and Applications, Vertica, vol. 5, no. 3, 1981.
6. Johnson, W.: Assessment of Aerodynamic and Dynamic Models in a Comprehensive Analysis for Rotorcraft. Computers and Mathematics with Applications, Vol 12A, No 1, January 1986.
7. Johnson, W.: The Effect of Dynamic Stall on the Response and Airloading of Helicopter Rotor Blades. J. of the American Helicopter Soc., vol. 14, no. 2, Apr. 1969.
8. Johnson, W.: The Response and Airloading of Helicopter Rotor Blades due to Dynamic Stall. Massachusetts Institute of Technology, ASRL TR 130-1, May 1970.
9. Johnson, W.: A Lifting Surface Solution for Vortex Induced Airloads and Its Application to Rotary Wing Airloads Calculations. Massachusetts Institute of Technology, ASRL TR 153-2, Apr. 1970.
10. Johnson, W.: Application of a Lifting Surface Theory to the Calculation of Helicopter Airloads. Twenty-Seventh Ann. Nat. Forum of the American Helicopter Soc., Washington, D.C., May 1971.

11. Johnson, W.: Analytical Model for Tilting Proprotor Aircraft Dynamics, Including Blade Torsion and Coupled Bending Modes, and Conversion Mode Operation. NASA TM X-62369, Aug. 1974.

12. Johnson, W.: Analytical Modeling Requirements for Tilting Proprotor Aircraft Dynamics. NASA TN D-8013, July 1975.

13. Johnson, W.: The Influence of Engine/Transmission/Governor on Tilting Proprotor Aircraft Dynamics. NASA TM X-62455, June 1975.

14. Johnson, W.: Aeroelastic Analysis for Rotorcraft in Flight or in a Wind Tunnel. NASA TN D-8515, July 1977.

15. Johnson, W.: Predicted Dynamic Characteristics of the XV-15 Tilting Proprotor Aircraft in Flight and in the 40- by 80-Foot Wind Tunnel. NASA TM X-73158, June 1976.

16. Johnson, W.: Calculated Dynamic Characteristics of a Soft-Inplane Hingeless Rotor Helicopter. NASA TM-73262, June 1977.

17. Scully, M. P.: Computation of Helicopter Rotor Wake Geometry and Its Influence on Rotor Harmonic Airloads. Massachusetts Institute of Technology, ASRL TR 178-1, March 1975.

18. Houbolt, John C., And Brooks, George W., "Differential Equations of Motion for Combined Flapwise Banding, Chordwise Bending, and Torsion of Twisted Nonuniform Rotor Blades," NACA Report 1346, 1958.

19. Bisplinghoff, Raymond L., Mar, James W., and Pian, Theodore H. H., Statics of Deformable Solids, Addison-Wesley, Reading, Massachusetts, 1965.

20. Lang, K. W., and Nemat Nasser, S., "An Approach for Estimating Vibration Characteristics of Nonuniform Rotor Blades," AIAA Journal, Vol. 17, No. 9, September 1979.

21. Cheeseman, I. C., and Bennett, W. E., "The Effect of the Ground on a Helicopter Rotor in Forward Flight," ARC R & M 3021, September 1955.

22. Coleman, Robert P., Feingold, Arnold M., and Stempin, Carl W., "Evaluation of the Induced-Velocity Field of an Idealized Helicopter Rotor," NACA ARR L5E10, June 1945.

23. Mangler, K. W., and Squire, H. B., "The Induced Velocity Field of a Rotor," ARC R & M 2642, May 1950.

24. Drees, J. M., "A Theory of Airflow Through Rotors and its Application to Some Helicopter Problems," Journal of the Helicopter Association of Great Britain, Volume 3, Number 2, July-September 1949.

25. White, T., and Blake, B. B. "Improved Method of Predicting Helicopter Control Response and Gust Sensitivity." Annual National Forum of the American Helicopter Society, May 1979.

26. Yamauchi, G. K., and Johnson, W. "Trends of Reynolds Number Effects on Two-Dimensional Airfoil Characteristics for Helicopter Rotor Analyses." NASA TM 84363, April 1983.

27. Johnson, Wayne, "The Response and Airloading of Helicopter Rotor Blades Due to Dynamic Stall," Massachusetts Institute of Technology, ASRL TR 130-1, May 1970.

28. McCroskey, W. J., "Recent Developments in Dynamic Stall," Symposium on Unsteady Aerodynamics, Tucson, Arizona, March 1975.

29. Beddoes, T. S., "A Synthesis of Unsteady Aerodynamic Effects Including Stall Hysteresis," Vertica, Vol. 1, No. 2, 1976.

30. Ham, Norman D., and Garelick, Melvin S., "Dynamic Stall Considerations in Helicopter Rotors," Journal of the American Helicopter Society, Vol. 13, No. 2, April 1968.

31. Harris, Franklin D., Tarzanin, Frank J., Jr., and Fisher, Richard K., Jr., "Rotor High Speed Performance, Theory vs. Test," Journal of the American Helicopter Society, Vol. 15, No. 3, July 1970.

32. Tarzanin, F. J., Jr., "Prediction of Control Loads due to Blade Stall," Journal of the American Helicopter Society, Vol. 17, No. 2, April 1972.

33. Gormont, Ronald E., "A Mathematical Model of Unsteady Aerodynamics and Radial Flow for Application to Helicopter Rotors," USAAVLABS TR 72-67, May 1973.

34. Johnson, Wayne, "A Comparison Between Experimental Data and Helicopter Airloads Calculated Using a Lifting-Surface Theory," Massachusetts Institute of Technology, ASRL TR 157-1, July 1970.

35. Scully, M. P., "Computation of Helicopter Rotor Wake Geometry and its Influence on Rotor Harmonic Airloads," Massachusetts Institute of Technology, ASRL TR 178-1, March 1975.

36. Ham, Norman D., "Some Conclusions from an Investigation of Blade-Vortex Interaction," Journal of the American Helicopter Society, Vol. 20, No. 4, October 1975.

37. Johnson, W. "Recent Developments in Rotary-Wing Aerodynamic Theory." AIAA Journal, Vol. 24, No. 8, August 1986.

38. Miller, R. H., "Rotor Blade Harmonic Air Loading," AIAA Journal, Vol. 2, No. 7, July 1964.

39. Piziali, R. A., "Method for the Solution of the Aeroelastic Response Problem for Rotary Wings," Journal of Sound and Vibration, Vol. 4, No. 3, 1966.

40. Landgrebe, Anton J., "The Wake Geometry of a Hovering Helicopter Rotor and its Influence on Rotor Performance," Journal of the American Helicopter Society, Vol. 17, No. 4, October 1972.

41. Kocurek, J. David, and Tangler, James L., "A Prescribed Wake Lifting Surface Hover Performance Analysis," Journal of the American Helicopter Society, Vol. 22, No. 1, January 1977.

42. Reddy, K. R., and Gilbert, N. E. "Comparison with Flight Data of Hover Performance Using Various Rotor Wake Models." European Rotorcraft Forum, Arles, France, September 1987.

43. Landgrebe, Anton J., Moffitt, Robert C., and Clark, David R., "Aerodynamic Technology for Advanced Rotorcraft," Journal of the American Helicopter Society, Vol. 22, No. 2, April 1977.

44. Johnson, Wayne, "A Lifting-Surface Solution for Vortex-Induced Airloads," AIAA Journal, Vol. 9, No. 4, April 1971.

45. Johnson, Wayne, "Application of a Lifting-Surface Theory to the Calculation of Helicopter Airloads," American Helicopter Society Annual Forum, Washington, D.C., May 1971.

46. Etkin, Bernard, Dynamics of Flight, John Wiley and Sons, Inc., New York, 1959.

47. Dommasch, Daniel O., Sherby, Sydney S., and Connally, Thomas F., Airplane Aerodynamics, Fourth Edition, Pitman Publishing Corp., New York, 1967.

48. Kerrebrock, Jack L., Aircraft Engines and Gas Turbines, The MIT Press, Cambridge, Massachusetts, 1977.

49. Nasar, S. A., Electromagnetic Energy Conversion Devices and Systems, Prentice-Hall, Inc., Englewood Cliffs, New Jersey, 1970.

50. Yamauchi, G. K., and Johnson, W. "Development and Application of an Analysis of Axisymmetric body Effects on Helicopter Rotor Aerodynamics Using Modified Slender Body Theory." NASA TM 855934, July 1984.

51. Durand, W. F., Editor-in-Chief. Aerodynamic Theory, Volume I. Dover Publications Inc., New York, 1936.

52. Karamcheti, K. Principles of Ideal-Fluid Aerodynamics. John Wiley and Sons, New York, 1966.

53. Johnson, W. "Self-Tuning Regulators for Multicyclic Control of Helicopter Vibration." NASA TP 1996, March 1982.

54. Coleman, Robert P., and Feingold, Arnold M., "Theory of Self-Excited Mechanical Oscillations of Helicopter Rotors with Hinged Blades," NACA Report 1351, 1958.

55. Miller, R. H., "Helicopter Control and Stability in Havering Flight," Journal of the Aeronautical Sciences, Vol. 15, No. 8, August 1948.

56. Hohenemser, Kurt H., and Yin, Sheng-Kuang, "Some Applications of the Method of Multiblade Coordinates," Journal of the American Helicopter Society, Vol. 17, No. 3, July 1972.

57. Johnson, Wayne, "Aeroelastic Analysis for Rotorcraft in Flight or in a Wind Tunnel," NASA TN D-8515, July 1977.

58. Gaonkar, G. H., and Peters, D. A. "Review of Dynamic Inflow Modelling for Rotorcraft Flight Dynamics." AIAA Paper No. 86-0845, May 1986.

59. Peters, David A., "Hingeless Rotor Frequency Response with Unsteady Inflow," NASA SP-352, February 1974.

60. Carpenter, Paul J., and Fridovich, Bernard, "Effect of a Rapid Blade-Pitch Increase on the Thrust and Induced-Velocity Response of a Full-Scale Helicopter Rotor," NACA TN 3044, November 1953.

61. Hohenemser, K. H., and Crews, S. T., "Unsteady Hovering Wake Parameters Identified from Dynamic Model Tests," NASA CR 152022, June 1977.

62. DeRusso, Paul M., Roy, Rob J., and Close, Charles M., State Variables for Engineers, John Wiley and Sons, Inc., New York, 1965.

63. D'Azzo, J. J., and Houpis, C. H. Feedback Control System Analysis and Synthesis. McGraw Hill Book Co., New York, 1966.